

Electronic Thesis and Dissertation Repository

12-9-2020 3:00 PM

Reconstructing carbon dynamics of alpine and temperate zone lakes using stable isotopic analysis

Rebecca M. Doyle, *The University of Western Ontario*

Supervisor: Moser, Katrina A., *The University of Western Ontario*

Joint Supervisor: Longstaffe, Fred J., *The University of Western Ontario*

A thesis submitted in partial fulfillment of the requirements for the Doctor of Philosophy degree in Geography

© Rebecca M. Doyle 2020

Follow this and additional works at: <https://ir.lib.uwo.ca/etd>



Part of the [Biogeochemistry Commons](#), [Environmental Chemistry Commons](#), [Geochemistry Commons](#), [Hydrology Commons](#), and the [Other Plant Sciences Commons](#)

Recommended Citation

Doyle, Rebecca M., "Reconstructing carbon dynamics of alpine and temperate zone lakes using stable isotopic analysis" (2020). *Electronic Thesis and Dissertation Repository*. 7515.
<https://ir.lib.uwo.ca/etd/7515>

This Dissertation/Thesis is brought to you for free and open access by Scholarship@Western. It has been accepted for inclusion in Electronic Thesis and Dissertation Repository by an authorized administrator of Scholarship@Western. For more information, please contact wlsadmin@uwo.ca.

Abstract

Lake sediments integrate signals from the catchment, atmosphere and water column, offering a unique window through which to view changes in the carbon cycle. Carbon dynamics in lakes are changing due to nitrogen loading and anthropogenic climate warming (ACW), threatening the water quality of lakes. This thesis identifies how the carbon dynamics of lakes have responded to anthropogenically-driven forcings by comparing pre- and post- AD 1850 records preserved in lake sediments. First, the carbon dynamics of Barry Lake (Ontario, Canada), a low-elevation temperate lake, are investigated. Effective moisture (the net of water inputs and evaporation) is reconstructed using the carbon and oxygen isotope compositions of marl, carbon isotope compositions of total organic carbon and hydrogen isotope compositions of the *n*-alkane C₁₇. The isotope compositions and abundances of biomarkers are used to reconstruct changes in organic matter (OM) source and methane oxidation. These reconstructions reveal that current levels of primary production in Barry Lake are unprecedented during the last ~900 years, likely due to land use change and, perhaps, ACW. Furthermore, inferred methane oxidation and OM source, but not primary production, are closely tied to changes in effective moisture. This finding suggests that future changes in aridity driven by anthropogenic climate change may alter the sources of carbon to sediments and affect how methane is recycled by temperate lakes. A second goal of this thesis is to characterize sources of organic matter to four cold, high-elevation alpine lakes (Uinta Mountains, Utah, United States). Analyses of modern terrestrial and aquatic samples provide a baseline to improve interpretations of stable isotopes in alpine lake sediments. A database of carbon and hydrogen isotope compositions of *n*-alkanes extracted from vegetation surrounding the lakes is used to estimate the carbon isotopic composition of ancient carbon dioxide ($\delta^{13}\text{C}_{\text{CO}_2}$) and hydrogen isotopic composition of ancient precipitation ($\delta^2\text{H}_{\text{precip}}$). Finally, a comparison of Barry Lake with the Uinta Mountain lakes reveals that both systems have become more productive in the last 50-100 years. In summary, this thesis identifies recent changes in the carbon dynamics at Barry Lake and advances the ability of researchers to interpret proxies in alpine environments.

Keywords

n-alkane, southwestern Ontario, paleolimnology, climate, alpine, stable isotope

Summary for Lay Audience

Lake scientists analyze sediments, or lake mud, to reconstruct environmental conditions. To do this, they first assign ages to each layer of sediment deposited at the bottom of the lake. Next, they measure the chemical, physical and/or biological characteristics of the sediment. In the same way that paleontologists search for the bones of ancient fish to infer whether a landscape was once covered with water, lake scientists use microfossils, chemical analyses and physical characteristics of the sediment to make educated guesses about past environmental conditions. By marrying the ages of sediment layers with these inferences about past environments, lake scientists reconstruct long-term records of variables such as temperature and precipitation. These techniques are used in this thesis to reconstruct environmental change at Barry Lake, a small lake in southern Ontario (Canada). It is determined that European settler-colonizers, rather than natural changes in aridity, likely initiated an unprecedented increase in algal growth at Barry Lake upon their arrival in AD ~1850. It is also uncovered that methane recycling by the lake and, to a lesser degree, the type of vegetation entering the lake, are associated with changes in aridity (*i.e.*, dryness). This finding suggests that, at Barry Lake, increases in aridity may alter the sources of carbon to lake sediments and affect how methane, a greenhouse gas, is recycled by the lake. This thesis also presents a database of chemical signatures from modern sources of organic matter (OM) (*e.g.*, plants and algae) that are expected to occur in the sediments of alpine lakes in the Uinta Mountains, Utah (USA). This database will improve the ability of scientists to determine which OM sources have contributed most to sediments in understudied alpine regions. Reconstructing such sources is vital for determining whether lake sediments are recording environmental conditions within or outside of the lake. Without this information, it is difficult for lake scientists to accurately reconstruct paleoenvironmental change. Finally, Barry Lake is compared with the Uinta Mountain lakes. Recent increases in algal growth are detected in both systems. This finding is concerning because rapid algal growth can degrade water quality.

Epigraph

Carbon's fate is tricky to trace
As its pathways vary with place
But *n*-alkanes can see
If 'twas algae or tree
Revealing the journey through space
–RMD & FJL

Dedication

*For my parents, Glenda and Randy;
for my sister, Robin;
and for my partner, Yohann.*

Co-Authorship Statement

This thesis contains four manuscripts. The first manuscript, “Hydroclimate-Primary Production Decoupling in a Small Lake, South-Central Canada, over the last 900 years” (Chapter 2), is in preparation. This manuscript is co-authored with Zijun Liu, Jacob T. Walker, Ryan Hladyniuk, Katrina A. Moser (supervisor) and Fred J. Longstaffe (supervisor). I assisted with sample collection, conducted all the analyses of organic matter (OM) of core BL-G17-01, established a theoretical framework for interpreting the data and compared the Barry Lake hydroclimate record to other hydroclimatic records from the region. I also established the most recent age-depth model. Zijun Liu assisted with sample collection and conducted all analyses of BL-G16-01. Jacob Walker assisted with sample collection and analyzed the carbonates from core BL-G17-01. Ryan Hladyniuk assisted with sample collection, selected Barry Lake as a study site and assisted with the initial version of the age-depth model. Katrina A. Moser provided guidance on the research design and data interpretation. Fred J. Longstaffe also provided guidance on the research design and data interpretation and funded the project. Ryan Hladyniuk, Katrina A. Moser and Fred J. Longstaffe are involved in editing the manuscript.

A second manuscript titled “Uncovering the linkages between effective moisture and the carbon dynamics of a small kettle lake in Ontario, Canada” is in preparation. This manuscript is co-authored with Katrina A. Moser (supervisor) and Fred J. Longstaffe (supervisor). I collected all of the samples, conducted all analyses and established a theoretical framework for interpreting the data. Katrina A. Moser provided guidance on the research design and data interpretation. Fred J. Longstaffe also provided guidance on the research design and data interpretation and funded the project. All authors are involved in the editing of the manuscript.

A third manuscript titled “Estimating source apportionment of OM to alpine lake sediments using bulk and compound-specific stable isotopic analysis” is in preparation (Chapter 4). This manuscript is co-authored with Katrina A. Moser (supervisor) and Fred J. Longstaffe (supervisor). I assisted Katrina A. Moser (supervisor) with sample collection, conducted all analyses and established a theoretical framework for interpreting the data.

Katrina A. Moser and Fred J. Longstaffe provided guidance on the research design and data interpretation. Both provided funding for the project. All authors are involved in editing the manuscript.

A fourth manuscript titled “Strengths and limitations of stable isotopic proxies of environmental change from lake sediment archives” is in preparation (Chapter 5). This manuscript is co-authored with Katrina A. Moser (supervisor) and Fred J. Longstaffe (supervisor). I assisted with sample collection, conducted all analyses and established a theoretical framework for interpreting the data. Katrina A. Moser and Fred J. Longstaffe provided guidance on the research design and data interpretation. Both provided funding for the project. All authors are involved in editing the manuscript.

I will be the first author on all publications.

Acknowledgments

First and foremost, I wish to thank my thesis supervisors, Katrina A. Moser and Fred J. Longstaffe. How do I put into words how lucky I feel to have worked with you over these last five years? Katrina, you continue to inspire me, not only because of your intelligence and skill as an academic, but also because of your patience and integrity. I feel very fortunate to have you as a role model, somebody who has blazed a successful career in research while also working as a mother, hockey trainer, professor and environmental advocate. I truly appreciate everything you have done for me. Fred, you are one of the best teachers I have ever met. Sure, you taught me a lot about stable isotope geochemistry. But the most important lessons I learned from you are not about science. When you continued to run the LSIS lab after experiencing health complications, I learned about perseverance. When you gave me cookies after I vaporized several weeks of *n*-alkane extracts (pinhole-gate), I learned about compassion. When you managed to coordinate our large lab during the COVID-19 pandemic, I learned about leadership. I will remember these lessons wherever I go and will never forget the man who imparted them to me.

I am also thankful to my friends and co-workers at the Laboratory for Stable Isotope Science (LSIS) and Lake and Reservoir Systems (LARS) Research Facility. I would have been lost without the expert help of Kim Law, Grace Yau, Li Huang and Erika Hill. I am also grateful to the past and present Lake Podites: Jay Nijim, Fereshteh (Fere) Najafi, James Thayer, David Zilkey, Amanda Philavong, Jane Wilson, Emma-Dawn Ferguson, Jen Baron, Jess Kowalski, Zijun Liu, Ryan Hladyniuk, Maria Eloisa Sia, Uma Dhir and Nils Mann. I would especially like to thank my friend Jacob Walker for his loyalty, his expertise in the field and his encyclopedic knowledge of mass spectrometers.

I would also like to thank some non-Lake Podites: Dianna Moreiras, Jordon Munizzi, Sarah Simpson, Tessa Plint, Rachel Schwartz-Narbonne, Beth Hundey and Farnoush Tahmasebi. Everyone, I am appreciative for your expertise and great company.

A special thanks also goes out to our friends in Utah: Chris Plunkett, Mark Muir, Darlene Koerner, Helen Kempenich, Christy Oprandy, Nick Oprandy, Mike Devito (all of Ashley

National Forest). Without your hard work, I would never have been able to obtain samples from such a remote field site. I am also grateful to Matty Seegers, Nandini Thogarapalli and Jacob Walker for their field assistance in the Uinta Mountains, and for being awesome.

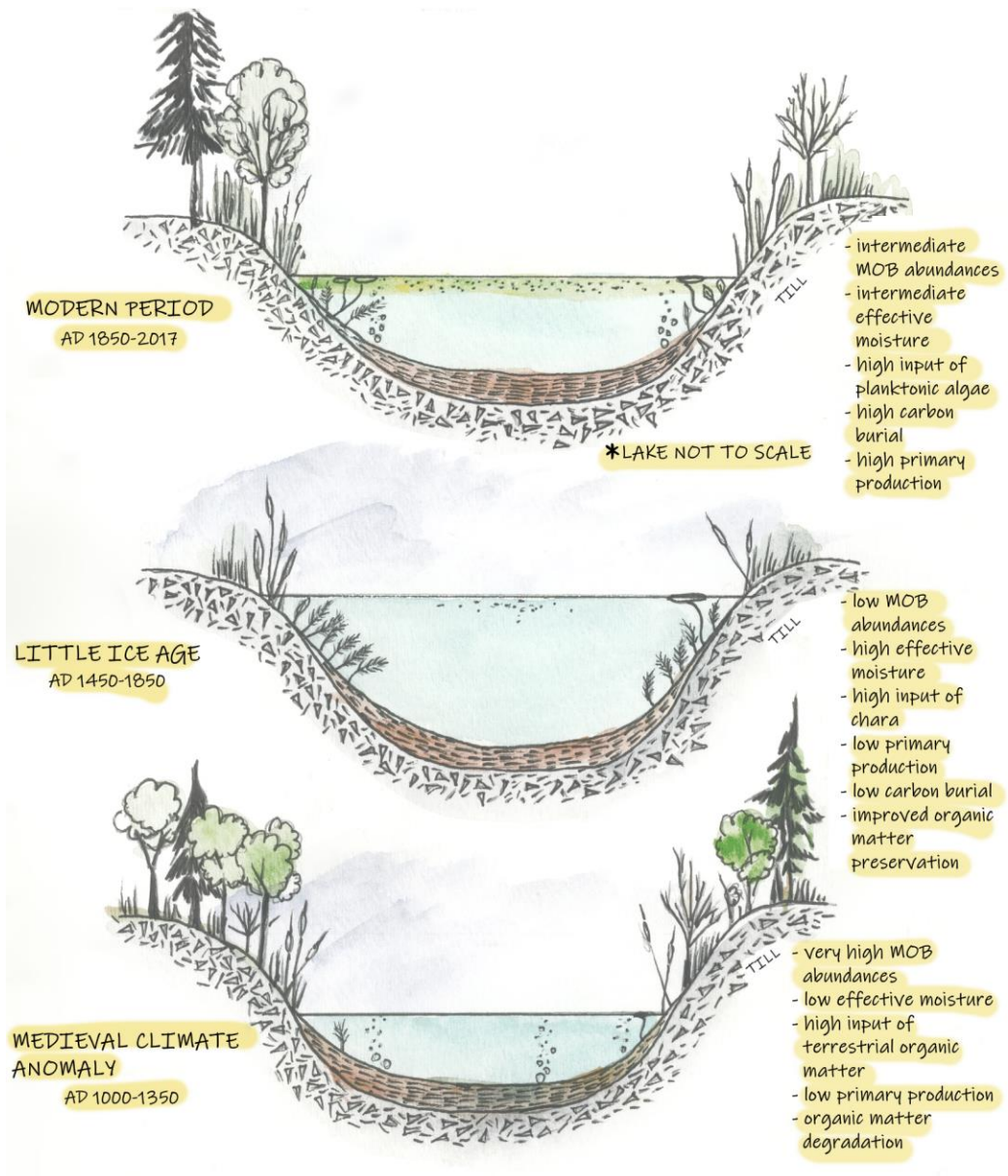
I also want to thank George and Kathy Archer for letting us study their lake, Barry Lake, and for being so kind to us students during our field visits. I feel very fortunate to know you and to work at such a beautiful lake. Thank you Maria Eloisa Sia, Amanda Philavong and Carolyn Hill for your field assistance at Barry Lake.

Thank you to Carl Zimmerman (University of Maryland, Nutrient Analytical Services Laboratory) for water chemistry analysis; the LANSET and A.E. Lalonde laboratories at the University of Ottawa for AMS and ^{210}Pb dates; and the PEARL lab at Queen's University for contributing to chlorophyll *a* analysis. I also want to give a huge thanks to Karen Van Kerkoerle for her help with my figures. I am very grateful to Dr. Liz Web, for taking the time to read my (long) thesis and for being a great listener. Thank you to my examining committee (Dr. Hugh Henry, Dr. Peter Ashmore, Dr. Brent Wolfe and Dr. Jamie Voogt) for taking the time to read my thesis and for asking such thoughtful questions.

Funding for this research was provided by a Natural Sciences and Engineering Research Council (NSERC) Discovery Grant (FJL), the Canada Research Chairs Program (FJL), the Canada Foundation for Innovation (FJL and KAM), Western Social Sciences (KAM), the Ontario Research Fund (FJL), the Ashley National Forest, and two NSERC Canada Graduate Scholarships (RMD). I especially want to thank NSERC for extending my funding in light of the COVID-19 pandemic.

Finally, I would like to thank my support system: my parents, Randy and Glenda; my sister, Robin; my partner, Yohann; and my rabbits, Miki and Stella. Mom and Dad, I could write an entire thesis about all the ways you supported me. Instead, I will say this: I couldn't have done this without you. I love you with all my heart. Robin, I know that you will go on to do amazing things – you are an awesome sister. Yohann, you are one of the only people who can calm me down when I'm anxious. Your brilliance impresses me every day. To Miki and Stella, I say this: hop, sniff, hop, hop, sniff, dig.

Preface



BARRY LAKE THROUGH THE AGES

Artistic depiction of the carbon dynamics of Barry Lake during the Medieval Climate Anomaly (AD 1000– 1350), the Little Ice Age (AD 1450–1850) and the Modern Period (AD 1850–2017). Drawing by

R. Doyle.

Table of Contents

Abstract.....	ii
Summary for Lay Audience	iv
Epigraph	v
Dedication	vi
Co-Authorship Statement	vii
Acknowledgments.....	ix
Preface	xi
Table of Contents.....	xii
List of Tables	xix
List of Figures	xxiv
List of Appendices	xxxiii
List of Abbreviations	xxxiv
List of Equations.....	xxxv
Chapter 1.....	1
1 Introduction	1
1.1 Overview	1
1.2 Background on isotope systematics	4
1.2.1 Isotopic notation.....	5
1.2.2 Controls on the carbon and oxygen isotopic compositions ($\delta^{13}\text{C}$ and $\delta^{18}\text{O}$) of carbonates in lakes	6
1.2.3 Controls on the carbon isotopic compositions ($\delta^{13}\text{C}_{\text{TOC}}$) of lake sediment OM	10
1.2.4 Controls on the nitrogen isotopic compositions ($\delta^{15}\text{N}_{\text{TN}}$) of the sediment OM	16
1.2.5 Systematics of <i>n</i> -alkane chain lengths and isotopic compositions.....	20

1.2.6	Differences in the isotope systematics of alpine and temperate lakes....	26
1.3	Study Area.....	27
1.4	Structure of the dissertation and research questions.....	32
1.5	References.....	35
Chapter 2.....		52
2	Hydroclimate-Primary Production Decoupling in a Small Lake, South-Central Canada, over the last 900 years.....	52
2.1	Materials and methods.....	54
2.1.1	Study Area.....	54
2.1.2	Sample Collection.....	55
2.1.3	Chronology.....	55
2.1.4	Isotopic and elemental analysis.....	56
2.1.5	Analysis of sedimentary chlorophyll <i>a</i> and its derivatives (Chl- <i>a</i> _(s)).....	58
2.1.6	Mass accumulation rates.....	59
2.1.7	Calculation of statistical significance.....	59
2.1.8	Breakpoint analysis.....	59
2.1.9	Data treatment of hydroclimatic records.....	60
2.2	Results.....	61
2.2.1	Chronology.....	61
2.2.2	Isotope ratios of marl.....	64
2.2.3	Isotopic and elemental ratios of organic matter (OM).....	64
2.2.4	Mass accumulation rates.....	65
2.2.5	Breakpoint analysis.....	65
2.3	Discussion.....	67
2.3.1	Sensitivity of Barry Lake to Effective Moisture.....	67

2.3.2	Proxies of primary production at Barry Lake	71
2.3.3	Primary production versus effective moisture at Barry Lake from AD ~1100-2017	74
2.3.4	A Regional Comparison of Effective moisture	81
2.4	Conclusions	87
2.5	References	88
Chapter 3.....		102
3	Uncovering the linkages between effective moisture and the carbon dynamics of a small kettle lake in Ontario, Canada	102
3.1	Introduction	102
3.2	Materials and methods.....	106
3.2.1	Study area	106
3.2.2	Core collection and sediment subsectioning.....	107
3.2.3	Analysis of sedimentary chlorophyll <i>a</i> and its derivatives (Chl- <i>a</i> _(s))	107
3.2.4	Isotopic analysis of bulk sediment, marl and shelly fauna	108
3.2.5	Isotopic analysis of dissolved inorganic carbon (DIC) in modern waters	109
3.2.6	Extraction, identification and quantification of <i>n</i> -alkanes	109
3.2.7	Isotopic analysis of <i>n</i> -alkanes	111
3.2.8	Chronology	112
3.3	Results.....	112
3.3.1	Chronology.....	112
3.3.2	Isotopic composition of biomarkers	113
3.3.3	Mass accumulation rates and relative abundances of <i>n</i> -alkanes.....	116
3.3.4	Isotopic and elemental ratios of bulk sediment from BL-G17-01	120
3.3.5	Mass accumulation rates of diploptene, lupan-3-one and C ₁₈ , and trends in $\epsilon_{\text{marl-TOC}}$	122

3.3.6	Carbon isotopic compositions of shelly fauna from BL-G11-01	122
3.4	Discussion.....	124
3.4.1	Identifying sources of OM in Barry Lake sediments using <i>n</i> -alkanes	124
3.4.2	Reconstructing MOB abundance and degradation using biomarker quantification and compound-specific isotopic analysis.....	126
3.4.3	Reconstructing variations in primary production, carbon burial and effective moisture	127
3.4.4	At Barry Lake, effective moisture exerts a stronger control on OM source than carbon availability or primary production.....	128
3.4.5	Effective moisture and OM source, rather than carbon availability or primary production, control MOB abundance at Barry Lake	130
3.4.6	Implications for greenhouse gas emissions from Barry Lake	132
3.5	Conclusions	135
3.6	References	136
Chapter 4	149
4	Estimating source apportionment of organic matter (OM) to alpine lake sediments using bulk and compound-specific stable isotopic analysis.....	149
4.1	Introduction	149
4.2	Materials and methods.....	153
4.2.1	Study area	153
4.2.2	Sample collection and storage.....	155
4.2.3	Determination of nutrient limitation in the Uinta Mountain study lakes	159
4.2.4	Dissolved oxygen measurements	160
4.2.5	Analyses of carbon and nitrogen isotope ratios of bulk organic material	160
4.2.6	Extraction, identification and quantification of <i>n</i> -alkanes	162
4.2.7	Analyses of carbon and hydrogen isotope ratios of <i>n</i> -alkanes.....	163

4.2.8	Analyses of hydrogen and oxygen isotope ratios of lake waters	163
4.2.9	Data treatment and calculations	165
4.3	Results.....	169
4.3.1	Water chemistry and dissolved oxygen in the four study lakes.....	169
4.3.2	Isotopic and elemental analyses of bulk sediments and tissues	170
4.3.3	Relative and absolute abundances of <i>n</i> -alkanes extracted from probable OM sources and littoral sediments.....	178
4.3.4	Carbon and hydrogen isotopic compositions of <i>n</i> -alkanes extracted from probable OM sources and littoral sediments	185
4.4	Discussion.....	189
4.4.1	Estimating sources of OM using TOC:TN, $\delta^{13}\text{C}_{\text{TOC}}$ and $\delta^{15}\text{N}_{\text{TN}}$	189
4.5	Estimating the sources of OM to sediments from the littoral zone of Uinta Mountain lakes	193
4.6	Unique characteristics of OM at high elevations.....	196
4.6.1	Investigating the ϵ_{bulk} , $\epsilon_{\text{atm-}n\text{-alkane}}$ and ϵ_{water} of sources of OM to Uinta Mountain lakes	198
4.7	Conclusion.....	201
4.8	References	203
Chapter 5.....		217
5	Strengths and limitations of stable isotopic proxies of environmental change from lake sediment archives.....	217
5.1	Introduction	217
5.2	Materials and methods.....	220
5.2.1	Study area	220
5.2.2	Sample collection from the Uinta Mountain lakes.....	221
5.2.3	Sample collection from Barry Lake	221
5.2.4	Chronology of cores collected from Barry Lake.....	224

5.2.5	Extraction, identification and quantification of <i>n</i> -alkanes in sediments of the Uinta Mountain lakes and Barry Lake	224
5.2.6	Analyses of carbon and nitrogen isotope ratios of modern vegetation and sediment core BL-G17-01 from Barry Lake, and modern vegetation from the Uinta Mountains.....	224
5.2.7	Analysis of sedimentary chlorophyll <i>a</i> and its derivatives (Chl- <i>a</i> _(s)) in Barry Lake sediment core BL-G17-01	226
5.2.8	Data treatment and calculations	226
5.3	Results.....	227
5.3.1	Dissolved inorganic carbon (DIC) concentrations in modern Uinta Mountain lake waters.....	227
5.3.2	The CPI of <i>n</i> -alkanes extracted from surficial sediments from the Uinta Mountains lakes and Barry Lake	227
5.3.3	Carbon and nitrogen isotope compositions, and elemental ratios, of modern vegetation around the Uinta Mountain lakes and Barry Lake..	227
5.3.4	Comparison of isotopic compositions, elemental ratios and Chl- <i>a</i> _(s) -MAR of lake sediment records from Barry Lake to Uinta Mountains	229
5.4	Discussion.....	231
5.4.1	OM is well preserved in Barry Lake and in the Uinta Mountain lakes ...	231
5.4.2	The $\delta^{13}\text{C}_{\text{TOC}}$ and $\delta^{15}\text{N}_{\text{TN}}$ of potential OM sources present in Uinta Mountain lakes and Barry Lake sediments are similar	234
5.4.3	Recent increases in primary production in the Uinta Mountain lakes and Barry Lake are not recorded by $\delta^{13}\text{C}_{\text{TOC}}$ or $\delta^{15}\text{N}_{\text{TN}}$	238
5.4.4	Are there anthropogenic drivers of recent increases in primary production in the Uinta Mountain lakes and Barry Lake?	239
5.5	Conclusion.....	241
5.6	References	241
6	Conclusion	250
6.1	Key findings of this thesis	250

6.1.1	Carbon dynamics at Barry Lake today are unique in the last ~1000 years	250
6.1.2	Human impacts contribute to recent changes to the carbon cycle at Barry Lake and in the Uinta Mountains.....	251
6.1.3	Methane oxidation in Barry Lake is closely associated with changes in dissolved oxygen and temperature that co-occur with effective moisture	252
6.1.4	Baselines of $\epsilon_{n\text{-alkane-atm}}$ and ϵ_{water} can be used to calibrate estimates of ancient $\delta^{13}\text{C}_{\text{CO}_2}$ and $\delta^2\text{H}_{\text{precipitation}}$ in the Uinta Mountains	253
6.1.5	Isotopic compositions of <i>n</i> -alkanes and bulk sediments must be interpreted differently in low-elevation environments than in remote, high-elevation environments.....	253
6.2	Suggestions for future research.....	254
6.2.1	Confirming the cause of increased primary production in Barry Lake beginning in AD ~1850	254
6.2.2	Characterizing the greenhouse gas fluxes to and from modern Barry Lake	255
6.2.3	Identifying and enumerating the community MOB and methanogens living in Barry Lake	256
6.2.4	Concurrent monitoring of diploptene abundances, dissolved oxygen concentrations and temperature	256
6.2.5	Estimating changes in $\delta^{13}\text{C}_{\text{CO}_2}$ and $\delta^2\text{H}_{\text{precipitation}}$ in the Uinta Mountains using the fractionation factors established in Chapter 4	257
6.3	References	258
	Curriculum Vitae	387

List of Tables

<p>Table 2.1 A summary of data used to generate Figure 2.7. The sites shown here were (i) located between 40-55 °N and 60-100 °W and (ii) available from the National Oceanic and Atmospheric Administration (NOAA) paleoclimate database (https://www.ncdc.noaa.gov/paleo-search/).</p>	84
<p>Table 4.1 Summary characteristics of the four study lakes. Adapted with permission from Hundey et al., 2014. The trophic status of each lake was determined by Hundey et al. (2014).</p>	154
<p>Table 4.2 Summary of nutrient measurements for water from the four Uinta Mountain lakes examined in this study and their N:P relationships. Bold text represents N limitation (DIN:TP <1.5), italic text represents uncertain limitation (DIN:TP= 1.5- 3.4), and underlined text represents P limitation (DIN:TP> 3.4). Limitation thresholds were taken from Bergström (2010). Data collected from before 2015 are from Hundey et al. (2014) (used with permission).</p>	170
<p>Table 5.1 A summary of how $\delta^{13}\text{C}_{\text{TOC}}$, $\delta^{15}\text{N}_{\text{TN}}$ and TOC:TN degrade under aerobic and anaerobic conditions. Degradation trends are typically described as a change in the original isotopic value of the sediment that occurs with age. This table also reports how this change manifests in a sediment core (<i>e.g.</i>, an increase of $\delta^{13}\text{C}$ with sediment age looks like a decrease in $\delta^{13}\text{C}$ when the core is interpreted from the past/bottom to the present/top).</p>	219
<p>Table A.1 $\delta^{13}\text{C}_{\text{DIC}}$ of modern waters collected from Barry Lake. From Liu (2016).</p>	262
<p>Table A.2 Values of $\delta^{13}\text{C}_{\text{TOC}}$, $\delta^{15}\text{N}_{\text{TN}}$, %TOC, %TN and TOC:TN from BL-G11-01. From Liu (2016).</p>	263
<p>Table A.3 Values of $\delta^{13}\text{C}_{\text{marl}}$, $\delta^{18}\text{O}_{\text{marl}}$ and %calcite from BL-G11-01. From Liu (2016).</p>	266
<p>Table A.4 Mass accumulation rates from BL-G11-01. From Liu et al. (2016).</p>	269

Table A.5 Minerology, magnetic susceptibility (MS) and grain size analysis of BL-G11-01 (Liu, 2016). Minerology was determined using powder x-ray diffraction (<i>p</i> XRD) and as a byproduct of isotope analysis.....	272
Table A.6 Values of $\delta^{13}\text{C}_{\text{marl}}$ and $\delta^{18}\text{O}_{\text{marl}}$ of shelly fauna from BL-G11-01. From Liu (2016).	275
Table A.7 Values of $\delta^{13}\text{C}_{\text{TOC}}$, $\delta^{15}\text{N}_{\text{TN}}$, %TOC, %TN and TOC:TN from BL-G17-01.	276
Table A.8 Mass accumulation rates and TOC:TN from BL-G17-01.	279
Table A.9 Values of $\delta^{13}\text{C}_{\text{marl}}$, $\delta^{18}\text{O}_{\text{marl}}$ and %calcite from BL-G17-01.	282
Table A.10 Minerology, magnetic susceptibility (MS) and grain size analysis of BL-G11-01 (Liu, 2016). Minerology was determined using powder x-ray diffraction (<i>p</i> XRD) and as a byproduct of isotope analysis.....	285
Table A.11 Mass accumulation rates of odd-chain <i>n</i> -alkanes extracted from BL-G16-01....	288
Table A.12 Mass accumulation rates of even-chain <i>n</i> -alkanes, diploptene and lupan-3-one extracted from BL-G16-01.	288
Table A.13 Hydrogen isotope ratios of C_{17} from BL-G16-01.....	289
Table A.14 Carbon isotope ratios of C_{17} and C_{19} from BL-G16-01.	289
Table A.15 Carbon isotope ratios of C_{21} and C_{23} from BL-G16-01.	290
Table A.16 Carbon isotope ratios of C_{25} and C_{27} from BL-G16-01.	290
Table A.17 Carbon isotope ratios of C_{29} and C_{31} from BL-G16-01.	291
Table A.18 Carbon isotope ratios of diploptene and lupan-3-one from BL-G16-01.	291
Table A.19 Relative abundances of odd-chain <i>n</i> -alkanes extracted from BL-G16-01.	292
Table A.20 Relative abundances of even-chain <i>n</i> -alkanes extracted from BL-G16-01.	292

Table A.21 Absolute abundances of odd-chain <i>n</i> -alkanes extracted from BI-G16-01.	293
Table A.22 Absolute abundances of even-chain <i>n</i> -alkanes, diploptene and lupan-3-one extracted from BI-G16-01.	293
Table A.23 Indices calculated using relative abundances of <i>n</i> -alkanes extracted from BI-G16- 01.	294
Table A.24 Values of $\delta^{13}\text{C}_{\text{TOC}}$ and %TOC from modern OM sources to Uinta Mountain lakes. Conif. tree = coniferous krummholz tree; Herb = herbaceous perennial; B.D. shrub = broadleaf deciduous shrub; S.E. macro = semi-emergent macrophyte; Unk = unknown; Litt sed = littoral sediment; Sub macro = submergent macrophyte.	295
Table A.25 Values of $\delta^{13}\text{C}_{\text{TOC}}$, $\delta^{15}\text{N}_{\text{TN}}$, %TOC and %TN from modern OM sources to Uinta Mountains lakes. Avg: average of plant parts.	301
Table A.26 Values of $\delta^{13}\text{C}_{\text{TOC}}$, $\delta^{15}\text{N}_{\text{TN}}$, %TOC and %TN from modern OM sources to Uinta Mountains lakes. Avg: average of plant parts.	307
Table A.27 Additional information about foliar tissue from which <i>n</i> -alkanes are extracted. Conif. tree = coniferous krummholz tree; Herb = herbaceous perennial; B.D. shrub = broadleaf deciduous shrub; S.E. macro = semi-emergent macrophyte; Unk = unknown; Litt sed = littoral sediment; Sub macro = submergent macrophyte; Sub sed = submerged sed.	312
Table A.28 Relative abundances of <i>n</i> -alkanes extracted from modern sources to Uinta Mountain lakes, and Uinta Mountain lake sediments.	314
Table A.29 Absolute abundances of <i>n</i> -alkanes extracted from modern sources to Uinta Mountain lakes, and Uinta Mountain lake sediments.	315
Table A.30 Carbon isotope ratios of C_{19} and C_{21} extracted from OM sources to Uinta Mountain lakes.	316
Table A.31 Carbon isotope ratios of C_{23} and C_{25} extracted from OM sources to Uinta Mountain lakes.	317

Table A.32 Carbon isotope ratios of C ₂₇ and C ₂₉ extracted from OM sources to Uinta Mountain lakes.	318
Table A.33 Carbon isotope ratios of C ₃₁ and C ₃₃ extracted from OM sources to Uinta Mountain lakes.	319
Table A.34 Hydrogen isotope ratios of C ₁₉ and C ₂₁ extracted from OM sources to Uinta Mountain lakes.	320
Table A.35 Hydrogen isotope ratios of C ₁₉ and C ₂₁ extracted from OM sources to Uinta Mountain lakes.	321
Table A.36 Hydrogen isotope ratios of C ₂₇ and C ₂₉ extracted from OM sources to Uinta Mountain lakes.	322
Table A.37 Hydrogen isotope ratios of C ₃₁ and C ₃₃ extracted from OM sources to Uinta Mountain lakes.	323
Table A.38 Oxygen isotope ratios of Uinta Mountain lake waters.....	324
Table A.39 Hydrogen isotope ratios of Uinta Mountain lake waters.....	326
Table B.1 Sample preparation methods in Chapter 2.	328
Table B.2 Calibrated and uncalibrated AMS ¹⁴ C (BL-G17-01) and ²¹⁰ Pb dates (BL-G11-02). Depths of BL-G17-01 are in parentheses. Depths from BL-G17-01 are 0.69 cm lower than those of BL-G11-01 to account for the 5.6-year difference between collection of the cores.	330
Table B.3 The Pearson correlation coefficient (r) between two variables, and associated p-values. All variables are derived from BL-G17-01 (see text). Values of δ ¹³ C _{TOC} and δ ¹³ C _{marl} were Suess-corrected prior to these tests according to Verburg (2007).	333
Table C.1 Sample preparation methods.	335

Table C.2 Calculated vital effects using the measured $\delta^{13}\text{C}_{\text{DIC}}$ of modern waters, and the $\delta^{13}\text{C}$ of modern <i>H. anceps</i> shells.....	337
Table C.3 Statistical comparisons of variables.....	339
Table D.1 Pairwise Wilcox tests of $\delta^{13}\text{C}_{\text{TOC}}$ of potential sources of OM in Uinta Mountain sediments. Significant <i>p</i> -values are shown in red. Sample sizes are showed in brackets. ..	346
Table D.2 Pairwise Wilcox tests of $\delta^{15}\text{N}_{\text{TN}}$ of OM sources. Significant <i>p</i> -values are shown in red. Sample sizes are shown in brackets.	347
Table D.3 Pairwise Wilcox tests of TOC:TN of potential OM sources. Significant <i>p</i> -values are shown in red. Sample sizes are shown in brackets.....	348
Table D.4 Other statistical comparisons among groups. Significant <i>p</i> -values are shown in red.	349
Table D.5 Hydrogen isotope composition of lake waters and inflows from the Uinta Mountains. Standard deviations represent the reproducibility of replicate analyses.....	350
Table D.6 Summary of the information used to generate the phylogenetic tree in the following figure.	351
Table D.7 Concentrations of DIC from the Uinta Mountain study lakes.	354
Table E.1 Measurements of pH of waters from the Uinta Mountain lakes and Barry Lake.	363
Table E.2 The <i>p</i> -values from two-tailed t-tests (normally distributed data) or Kruskal-Wallis tests (non-parametric data). Statistically significant <i>p</i> -values (<i>p</i> < 0.01) are shown in red..	363
Table F.1 Expected response in mV after injecting Ar into the Trace – Delta V IRMS system while the combustion reactor is in use.....	368
Table F.2 Expected response in mV after injecting Ar into the Trace – Delta V IRMS system while the reduction/HTC reactor is in use.	374

List of Figures

Figure 1.1 Important steps in CO₂ fixation during C₃ photosynthesis. Size of font reflects the relative concentrations of CO₂ at different stages, whereas sizes of arrows indicate the relative fluxes. Used with permission from O’Leary (1988). 11

Figure 1.2 Maps of Barry Lake: (i) Location of Barry Lake within North America; (ii) Location of Barry Lake and other well-studied lakes in southern Ontario; (iii) Local hydrology in the vicinity of Barry Lake. The direction of surface flows is indicated by blue arrows, whereas the direction of groundwater is indicated by purple arrows. Figure produced by the Cartographic Section, Department of Geography and Environment, *The University of Western Ontario*, 2020. 28

Figure 1.3 Photographs of the five study sites: (i) Denise Lake, (ii) Taylor Lake, (iii) Upper Carrol Lake, (iv) East Carrol Lake and (v) Barry Lake. Photographs (i), (ii), (iii) and (v) were taken by R.M. Doyle, while photograph (iv) was taken by K.A. Moser. 29

Figure 1.4 Map of northeastern Utah depicting (i) the location of Utah, and (iii) the location of Upper Carrol, East Carrol, Denise and Taylor lakes. Modified with permission from Hundey et al. (2014). Figure produced by the Cartographic Section, Department of Geography and Environment, *The University of Western Ontario*, 2020. 31

Figure 2.1 Age-depth model for BL-G17-01 (i) and BL-G11-01 (ii) generated using the R package “Bacon”. Light-grey circles represent ages obtained using ²¹⁰Pb dating whereas dark-grey circles represent ¹⁴C dates. The same dating information is used for both cores, with the ²¹⁰Pb originating from BL-G11-01 and the ¹⁴C originating from BL-G17-01. Grey shading indicates the overall error associated with the age-depth model. Data used to generate these models is provided in Table B.2 in Appendix B and further explanation is included in Supplementary Information..... 61

Figure 2.2 Age-dependent variation in climate proxies for cores BL-G11-01 (grey) and BL-G17-01 (black). The paleoclimatic record is subdivided into intervals (right) based on major shifts in δ¹⁸O_{marl}. Tan shading indicates below-average values of δ¹⁸O_{marl} and blue shading

indicates above-average values $\delta^{18}\text{O}_{\text{marl}}$. After AD 1850, the $\delta^{13}\text{C}_{\text{TOC}}$ and $\delta^{13}\text{C}_{\text{marl}}$ record have been corrected for the Suess Effect, following Verburg (2007). This figure should be printed in colour. 63

Figure 2.3 Breakpoint analysis of the $\delta^{18}\text{O}_{\text{marl}}$ record from BL-G17-01 compared with breakpoint analysis of the North American Drought Atlas (NADA). The NADA shown here is for a 0.5 ° latitude/longitude grid centered over 44.3, -77.9 (Cook et al., 2010). Negative values of NADA correspond to arid conditions. To facilitate comparison with the marl data, the NADA data has been smoothed using a 50-year cubic spline. Breakpoints that are similar between the two records are coloured in blue. 66

Figure 2.4 The $\delta^{18}\text{O}_{\text{marl}}$ record from BL-G17-01 compared with the North American Drought Atlas (NADA) (i) and summer (June-August) Palmer Drought Severity Index (PDSI) (ii) on a 0.5° latitude/longitude grid centered over 44.3, -77.9 (Cook et al., 2009). Negative values of NADA and PDSI correspond to arid conditions. Left – comparison between the $\delta^{18}\text{O}_{\text{marl}}$ record and NADA. To facilitate comparison with the marl data, the NADA data has been smoothed using a 50-year cubic spline. Right - comparison between the same marl record with instrumental PDSI. The instrumental PDSI data has been smoothed using a 10-year cubic spline..... 70

Figure 2.5 Comparisons between $\text{Chl-}a_{(s)\text{-MAR}}$ from Barry Lake and instrumental temperature records (Harris et al., 2014). (i) – comparison between $\text{Chl-}a_{(s)\text{-MAR}}$ and mean June, July and August temperatures. (ii) – comparison between $\text{Chl-}a_{(s)\text{-MAR}}$ and mean annual temperatures. Both temperature records were smoothed using a 9-year running mean. 78

Figure 2.6 Comparisons between $\text{Chl-}a_{(s)\text{-MAR}}$ from Barry Lake and instrumental precipitation records (Harris et al., 2014). (i) – comparison between $\text{Chl-}a_{(s)\text{-MAR}}$ and total June, July and August precipitation. (ii) – comparison between $\text{Chl-}a_{(s)\text{-MAR}}$ and total annual precipitation. Both precipitation records were smoothed using a 9-year running mean. 80

Figure 2.7 A regional view of hydroclimate across the (i) MCA (AD 1000-1350), (ii) LIA (AD 1450-1850) and (iii) the modern period (AD 1850-present). The sites shown here were lake records located between 40-55 °N and 60-100 °W and available from the National Oceanic and Atmospheric Administration (NOAA) paleoclimate database (<https://www.ncdc.noaa.gov/paleo-search/>). All records were averaged into three bins: AD 1000-1350, AD 1450-1850 and AD 1850-2005 and converted into z-scores, as described earlier. Shades of blue denote wetter-than-average conditions while shades of orange indicate more arid-than-average conditions. NWO stands for “northwestern Ontario”. 83

Figure 2.8 A comparison of (i) the $\delta^{18}\text{O}_{\text{marl}}$ record from BL-G17-01, (ii) a diatom-based reconstruction of lake level from lakes in northwestern Ontario (site 3 in Figure 2.7; Laird et al., 2012) and (iii) a reconstructed water table record from Saco Bog, Maine (site 25 in Figure 2.7), derived from testate amoebas (Clifford and Booth, 2013). Drier-than-average values are depicted in orange while wetter-than-average values are coloured blue..... 87

Figure 3.1 Age-depth model for BL-G17-01 (i) and BL-G16-01 (ii) generated using the R package “Bacon”. Light grey stippled circles represent ages obtained using ^{210}Pb dating whereas dark grey circles represent ^{14}C dates. Grey shading indicates the overall error associated with the age-depth model. Data used to generate the age-depth model for BL-G17-01 is provided in Chapter 2. More information about the age-depth model of BL-G16-01 is provided in Section C.3 in Appendix C..... 112

Figure 3.2 The $\delta^2\text{H}_{\text{C17}}$ from BL-G16-01 varies closely with $\delta^{18}\text{O}_{\text{marl}}$ from BL-G17-01, suggesting that both proxies respond to changes in effective moisture. The record is subdivided into six intervals based on variations in $\delta^{18}\text{O}_{\text{marl}}$. Brown shading indicates a dry period (defined by high $\delta^{18}\text{O}_{\text{marl}}$), whereas blue shading denotes a wet period (defined by low $\delta^{18}\text{O}_{\text{marl}}$). The grey shading around $\delta^2\text{H}_{\text{C17}}$ represents measurement error. Measurement error of $\delta^{18}\text{O}_{\text{marl}}$ is too low to visualize. 114

Figure 3.3 Carbon isotope ratios of diploptene and *n*-alkanes (BL-G16-01) compared with $\delta^{13}\text{C}_{\text{marl}}$ (BL-G17-01). The record is subdivided into six intervals based on variations in $\delta^{18}\text{O}_{\text{marl}}$. Brown shading indicates a dry period (defined by high $\delta^{18}\text{O}_{\text{marl}}$), whereas blue

shading denotes a wet period (defined by low $\delta^{18}\text{O}_{\text{marl}}$). The grey shading around $\delta^2\text{H}_{\text{C}_{17}}$ represents measurement error. Measurement error of $\delta^{18}\text{O}_{\text{marl}}$ is too low to visualize. After AD 1850, the $\delta^{13}\text{C}_{\text{marl}}$ and the $\delta^{13}\text{C}$ of each *n*-alkane were corrected for the Suess Effect, following Verburg (2007). 115

Figure 3.4 Mass accumulation rates, P_{aq} and CPI of *n*-alkanes. The record is subdivided into six intervals based on variations in $\delta^{18}\text{O}_{\text{marl}}$. Brown shading indicates a dry period (defined by high $\delta^{18}\text{O}_{\text{marl}}$), whereas blue shading denotes a wet period (defined by low $\delta^{18}\text{O}_{\text{marl}}$)... 117

Figure 3.5 Relative abundances of *n*-alkanes. The record is subdivided into six intervals based on variations in $\delta^{18}\text{O}_{\text{marl}}$. Brown shading indicates a dry period (defined by high $\delta^{18}\text{O}_{\text{marl}}$), whereas blue shading denotes a wet period (defined by low $\delta^{18}\text{O}_{\text{marl}}$). 119

Figure 3.6 The (i) hydrogen isotopic composition of C_{17} compared with (ii) indicators of microbial abundance, (iii) OM source and (iv) primary production and carbon burial. The record is subdivided into six intervals based on variations in $\delta^{18}\text{O}_{\text{marl}}$. Brown shading indicates a dry period (defined by high $\delta^{18}\text{O}_{\text{marl}}$), whereas blue shading denotes a wet period (defined by low $\delta^{18}\text{O}_{\text{marl}}$)..... 121

Figure 3.7 Estimates of the $\delta^{13}\text{C}_{\text{DIC}}$ based on measurements of the $\delta^{13}\text{C}_{\text{DIC}}$ of two shelly fauna (*Helisoma anceps* and *Pisidium* sp.), and marl. Shaded bars around *Helisoma anceps* and *Pisidium* sp. represent the variation of $\delta^{13}\text{C}$ present within a single shell. *Pisidium* sp. disappears from the sediment record around AD ~1230, while *Helisoma anceps* disappears from the record around AD ~1270. Brown shading indicates a dry period (defined by high $\delta^{18}\text{O}_{\text{marl}}$), whereas blue shading denotes a wet period (defined by low $\delta^{18}\text{O}_{\text{marl}}$). For more details regarding the estimation of $\delta^{13}\text{C}_{\text{DIC}}$, see Section C.2 in Appendix C. 123

Figure 4.1 Photos of potential sources of OM in sediments: (i) algae, (ii) broadleaf deciduous shrubs, (iii) moss, (iv) semi-emergent macrophytes, (v) coniferous krummholz trees, (vi) lichen, (vii) herbaceous perennials, (viii) submergent macrophytes, and (ix) graminoids. . 157

Figure 4.2 Scatter plot showing the $\delta^{13}\text{C}_{\text{TOC}}$ and $\delta^{15}\text{N}_{\text{TN}}$ of potential sources of OM captured by surficial sediments at the center of each study lake. 172

Figure 4.3 Standard Bayesian ellipses generated from the $\delta^{13}\text{C}_{\text{TOC}}$ and $\delta^{15}\text{N}_{\text{TN}}$ of probable OM sources sampled from the Uinta Mountain study sites. Graminoids and herbaceous perennials were excluded from this analysis due to their low sample size (<8 samples per group). Submerged and semi-emergent macrophytes were combined into one group because these groups have similar isotopic compositions. (i) – Measured $\delta^{13}\text{C}_{\text{TOC}}$ and $\delta^{15}\text{N}_{\text{TN}}$ of OM sources and sediments from the center of the lakes. (ii) – The $\delta^{13}\text{C}_{\text{TOC}}$ and $\delta^{15}\text{N}_{\text{TN}}$ of sediments from the center of the lake have been corrected for the influence of degradation (see text). 175

Figure 4.4 Atomic TOC:TN ratios of probable OM sources and surficial sediments from the center of the lake. (i): the TOC:TN of all probable sources of OM to the Uinta Mountain lakes. (ii): the TOC:TN of terrestrial plants, lichen and semi-emergent macrophytes; algae and submerged macrophytes; and sediments from the centre of the lake (Hundey et al., 2014). Each coloured box represents 50 % of the data clustered around the mean. Tails extending above and below these boxes represent the interquartile range of the data. Bold numbers represent the sample size of each group. 177

Figure 4.5 Average relative abundances of *n*-alkanes extracted from (i) coniferous krummholz trees, (ii) mosses, (iii) broadleaf deciduous shrubs, (iv) semi-emergent macrophytes, (v) littoral sediments, (vi) graminoids, (vii) herbaceous perennials and (viii) lichen. Error bars represent the standard error of the mean. 179

Figure 4.6 PCA generated using the relative abundances of *n*-alkanes extracted from semi-emergent macrophytes, graminoids, littoral sediments, broadleaf deciduous shrubs, herbaceous perennials, moss and lichen. Samples are represented as points surrounded by non-Bayesian ellipses that represent the bimodal standard deviation of each group. Eigenvectors represent odd chain lengths of *n*-alkanes. Lichen and moss samples are not surrounded by an ellipse due to their small sample sizes. 181

Figure 4.7 The same PCA as in Figure 4.7, but points are labelled and ellipses have been removed for clarity. By noting the proximity of samples to the tip of each eigenvector, one can deduce the relative abundance of chain lengths produced by each group of possible OM

sources. For instance, shrubs plot near the tip of the C₂₅ eigenvector, indicating that they produce high relative abundances of C₂₅. Groups of potential OM sources that overlap produce similar relative abundances of *n*-alkanes, while groups that plot separately produce unique relative abundances of *n*-alkanes. This plot demonstrates that broadleaf deciduous shrubs and coniferous krummholz trees produce unique distributions of *n*-alkanes. 182

Figure 4.8 Variations in (i) average chain length (ACL), (ii) absolute abundances of *n*-alkanes, and (iii) carbon preference index (CPI) of potential OM sources that may have contributed to the littoral sediments. Potential OM sources to littoral sediments include: lichen, mosses, herbaceous perennials, semi-emergent macrophytes, graminoids, broadleaf deciduous shrubs and coniferous krummholz trees. *n*-Alkanes could not be extracted from algae or submerged macrophytes. These potential sources of OM were sampled from a subset of plants analyzed to determine $\delta^{13}\text{C}_{\text{TOC}}$, $\delta^{15}\text{N}_{\text{TN}}$ and TOC:TN. Littoral sediments consisted of one sediment sample per lake..... 184

Figure 4.9 Variations in (i) $\delta^{13}\text{C}_{n\text{-alkane}}$, (ii) $\delta^2\text{H}_{n\text{-alkane}}$, (iii) $\delta^{13}\text{C}_{n\text{-alkane}}$ (corrected for the effect of senescence) and (iv) $\epsilon_{\text{atm-}n\text{-alkane}}$ of C₁₉ to C₃₃ *n*-alkanes extracted from semi-emergent macrophytes, littoral sediments, coniferous krummholz trees, lichen, moss, graminoids and herbaceous perennials sampled around Uinta Mountain lakes. Error bars represent the standard error of the mean. Sample sizes represent the number of organisms analyzed. Sample sizes of individual *n*-alkanes may differ from this total sample size. 186

Figure 4.10 A phylogenetic tree representing the phylogenetic relationships between OM sources. The phylogenetic tree shown in panel (ii) was generated using the PhyloT tool at <https://phylot.biobyte.de/>. Semi-emergent macrophytes and other graminoids are classified as monocots, a type of non-flowering angiosperm, while broadleaf deciduous shrubs and herbaceous perennials (herbs) are classified as dicots, or flowering angiosperms. 187

Figure 4.11 Variations in (i) ϵ_{bulk} from terrestrial/semi-aquatic OM sources; (ii) ϵ_{bulk} from angiosperms and gymnosperms; (iii) ϵ_{bulk} from monocots and dicots; and (iv) ϵ_{water} from terrestrial/semi-aquatic OM sources. Error bars represent the standard error of the mean.

Sample sizes represent the number of organisms analyzed. Sample sizes of individual <i>n</i> -alkanes may differ from this total sample size.	188
Figure 5.1 Photos of vegetation subgroups from Barry Lake: (i) algae (1000x magnification), (ii) floating macrophytes, (iii) submerged macrophytes, (iv) semi-emergent macrophytes, and (v) broadleaf deciduous plants.	223
Figure 5.2 40 % standard predictive ellipses surrounding the $\delta^{15}\text{N}_{\text{TN}}$ and $\delta^{13}\text{C}_{\text{TOC}}$ of probable sources to (i) the Uinta Mountain lakes, and (ii) Barry Lake. Only groups of OM sources common to the two sites were included in these plots. Algae are found at both sites, but too few algae samples from Barry Lake were analyzed to include in this figure.	228
Figure 5.3 The $\delta^{13}\text{C}_{\text{TOC}}$, $\delta^{15}\text{N}_{\text{TN}}$, TOC:TN and Chl- $\alpha_{(\text{s})}$ -MAR of sediment cores collected from (i) Barry Lake, (ii) Denise Lake, (iii) Upper Carrol Lake, (iv) Taylor Lake, and (v) East Carrol Lake. Data for plots (ii) to (v) is from Hundey et al. (2014). For plots of $\delta^{13}\text{C}_{\text{TOC}}$, grey lines represent uncorrected data while black lines represent data corrected for the Suess Effect (Verberg, 2007)	230
Figure B.1 Estimate of the sedimentation rate of Barry Lake from AD 1900– 2017.....	331
Figure B.2 Downcore activity of ^{210}Pb , ^{214}Pb , ^{137}Cs and ^{243}Am in core BL-G11-01. Shading represents the error associated with each measurement.	331
Figure B.3 Age (depth) dependent variation (from left to right) in: (i) quartz, calcite and OM contents of BL-G17-01 and BL-G11-01 (see text), (ii) quartz, calcite and aragonite contents of BL-G11-01 determined by powder x-ray diffraction (<i>p</i> XRD) (normalized to 100%), and (iii) magnetic susceptibility of BL-G17-01 (black), BL-G11-01 (grey) and BL-G11-02 (white). Time periods shaded blue are interpreted to be wetter than average, whereas yellow shading denotes drier periods.....	332
Figure C.1 Plots of depth (left) and year (right) versus $\delta^{13}\text{C}_{\text{TOC}}$ from BL-G17-01 and BL-G16-01. Cores BL-17-01 and BL-G16-01 were visually correlated so that a number of ^{210}Pb (blue dots) and AMS (red dots) dates from BL-G17-01 could be matched with depths from BL-	

G16-01. These ages, and new depths, were used to generate the age-depth model for BL-G16-01 shown in Figure 3.1. This new age-depth model, and the age-depth model for BL-G17-01, were used to create the plot of year versus $\delta^{13}\text{C}_{\text{TOC}}$ shown to the right.	338
Figure C.2 Chromatograph depicting the <i>n</i> -alkanes contained in modern <i>Chara</i> . <i>Chara</i> in Barry Lake produce predominately C ₁₉ <i>n</i> -alkanes.	339
Figure D.1 This phylogenetic tree was generated using the PhyloT tool at https://phylot.biobyte.de/ . Only terrestrial and semi-aquatic organisms were used to create the tree because it is used to help interpret variation in n-alkane data. Because of sample size limitations, n-alkanes could only be extracted from terrestrial and semi-aquatic plant samples.	352
Figure D.2 The same tree as shown in Figure D.1, except that species names have been replaced by their group names.	352
Figure D.3 Simplified phylogenetic tree used in the main text of Chapter 4.	352
Figure D.4 Dissolved oxygen concentrations for (i) Upper Carrol Lake, (ii) Taylor Lake, (iii) East Carrol Lake, and (iv) Denise Lake. Numbers in the legend (e.g., Jul-16) refer to the year of collection (July 2016).	353
Figure D.5 Comparison of the isotopic and elemental compositions of fresh (11 samples) versus senescing (7 samples) leaves from <i>Carex aquatilis</i> . There is no significant difference in the $\delta^{13}\text{C}$ (left), $\delta^{15}\text{N}$ (middle) and TOC:TN (right) of fresh versus senesced material.	355
Figure D.6 A comparison of the isotopic and elemental compositions of broadleaves (15 samples) and woody tissue (13 samples) from deciduous shrubs. There are no significant differences in the $\delta^{13}\text{C}$ (left), $\delta^{15}\text{N}$ (middle) or TOC:TN of broadleaves and woody tissue from deciduous shrubs.	355
Figure D.7 A comparison of the isotopic and elemental compositions of needles (15 samples) and woody tissue (15 samples) from coniferous krummholz trees. There are no	

significant differences in the $\delta^{13}\text{C}$ (left), $\delta^{15}\text{N}$ (middle) or TOC:TN of needles and woody tissue from coniferous krummholz trees..... 356

Figure D.8 A comparison of the isotopic and elemental compositions of *Salix* sp. leaves from Taylor Lake (5 samples) and East Carrol Lake (5 samples). There is no significant difference in the $\delta^{13}\text{C}_{\text{TOC}}$ (left) and $\delta^{15}\text{N}_{\text{TN}}$ (middle) of *Salix* from Taylor Lake and East Carrol Lake. There is a significant difference in the TOC:TN of *Salix* from Taylor Lake and East Carrol Lake..... 359

Figure D.9 Comparing the ϵ_{bulk} of broadleaf deciduous shrubs (*Salix* sp. and *Betula* sp.) across three of the four study lakes. (i) the ϵ_{bulk} of C₂₃. (ii) the ϵ_{bulk} of C₂₅. (iii) the ϵ_{bulk} of C₂₇. (iv) the ϵ_{bulk} of C₂₉. Broadleaf deciduous shrubs were not sampled from Denise Lake. Numbers beside the boxplots represent the sample size. 360

Figure E.1 Measurements of dissolved oxygen concentrations from (i) Upper Carrol Lake, (ii) Taylor Lake, (iii) East Carrol Lake, (iv) Denise Lake, and (v) Barry Lake. Numbers in the legend (e.g., Jul-16) refer to the year of collection (July 2016)..... 364

Figure F.1 Evaluating the linearity of the Trace-Delta V IRMS system by injecting the same mixture at different concentrations. These results indicate that samples should be analyzed between ~2000 to 10 000 mV to maintain a sample error of $\sim\pm 0.3$ ‰. Note that $\delta^{13}\text{C}$ is not yet relative to VPDB. 370

Figure F.2 Evaluating the linearity of the Trace-Delta V IRMS system by injecting the same mixture at different concentrations. These results indicate that samples should be analyzed between ~2000 to 10 000 mV to maintain a sample error of $\sim\pm 3$ ‰. 376

Figure F.3 This plot shows that evaporation and chromatography do not alter the $\delta^2\text{H}$ of the standard 5 α -androstane. 377

List of Appendices

Appendix A: Data tables.....	262
Appendix B: Supplementary methods for Chapter 2.....	328
Appendix C: Supplementary methods for Chapter 3.....	335
Appendix D: Supplementary methods for Chapter 4	342
Appendix E: Supplementary Methods for Chapter 5.....	363
Appendix F: Technical Memorandum for Analyzing the $\delta^{13}\text{C}$ and $\delta^2\text{H}$ of <i>n</i> -Alkanes.....	365
Appendix G: Published Manuscript Reprint Permissions	378

List of Abbreviations

ACW	Anthropogenic climate warming
Chl- $a_{(s)}$	Sedimentary chlorophyll a
DO	Dissolved oxygen
EA-IRMS	Elemental analyzer paired to an isotope ratio mass spectrometer
GC-C-IRMS	Gas chromatography combustion isotope ratio mass spectrometry
GC-FID	Gas chromatograph paired to a flame ionizing diode
LIA	Little Ice Age (AD 1450- 1850)
MAR	Mass accumulation rate
MCA	Medieval Climate Anomaly (AD 1000-1350)
MOB	Methane oxidizing bacteria
MS	Magnetic susceptibility
OM	OM
TN	Total nitrogen
TOC	Total organic carbon
TOC-MAR	Mass accumulation rate of total organic carbon
TOC:TN	The ratio of total organic carbon to total nitrogen

List of Equations

Equation 1.1
$$\delta = \left[\left(\frac{R_{\text{sample}}}{R_{\text{standard}}} \right) - 1 \right] (\text{in } \text{‰})$$

Equation 1.2
$$\alpha_{A-B} = R_A/R_B$$

Equation 1.3
$$\varepsilon = (\alpha - 1) * 1000$$

Equation 1.4
$$\varepsilon \left(\frac{R}{R_i} \right) = F^{a-1}$$

Equation 1.5
$$\varepsilon_{C_3\text{leaf}} = a + (b - a) \frac{C_i}{C_a}$$

Equation 1.6
$$\varepsilon_{\text{macrophyte}} = d + b_3 \frac{F_3}{F_1}$$

Equation 1.7
$$\text{ACL} = \frac{\sum (C_n \times n)}{\sum (C_n)}$$

Equation 1.8
$$\text{CPI} = 0.5 \left[\frac{(C_{17} + C_{19} + C_{21} + C_{23} + C_{25} + C_{27} + C_{29} + C_{31})}{(C_{18} + C_{22} + C_{24} + C_{26} + C_{28} + C_{30})} \right]$$

Equation 1.9
$$P_{\text{aq}} = \left[\frac{(C_{17} + C_{19})}{(C_{17} + C_{19} + C_{27} + C_{29} + C_{31})} \right]$$

Equation 1.10
$$\varepsilon_{\text{bulk}} = 1000 \left[\frac{(\delta^{13}\text{C}_{n\text{-alkane}} + 1000)}{(\delta^{13}\text{C}_{\text{bulk}} + 1000)} - 1 \right]$$

Equation 1.11
$$\varepsilon_{\text{water}} = 1000 \left[\frac{(\delta^2\text{H}_{n\text{-alkane}} + 1000)}{(\delta^2\text{H}_{\text{source water}} + 1000)} - 1 \right]$$

Equation 2.1 Chlorophyll *a* + derivatives = 0.0919 x peak area 650– 700 nm + 0.0011

Equation 2.2 (TOC, TN, calcite or Chl-*a*(s))-MAR = [wt. % (TOC, TN, calcite or Chl-*a*(s))] x [LSR] x [DBD] x 1000

Equation 3.1
$$\varepsilon_{\text{marl-TOC}} = 1000 * \left[\left(\frac{(1000 + \delta^{13}\text{C}_{\text{marl}})}{1000 + \delta^{13}\text{C}_{\text{TOC}}} \right) - 1 \right] (\text{in } \text{‰})$$

Equation 4.1
$$\varepsilon_{\text{atm-n-alkane}} = 1000 * \left[\left(\frac{1000 + \delta^{13}\text{C}_{\text{atm}}}{1000 + \delta^{13}\text{C}_{n\text{-alkane}}} \right) - 1 \right] (\text{in } \text{‰})$$

Equation 4.2
$$\varepsilon_{\text{water}} = 1000 * \left[\left(\frac{1000 + \delta^2\text{H}_{n\text{-alkane}}}{1000 + \delta^2\text{H}_{\text{water}}} \right) - 1 \right] (\text{in } \text{‰})$$

Chapter 1

1 Introduction

1.1 Overview

Lakes are globally important sources of freshwater for humans and other animals. Lakes also serve as hotspots of biodiversity, sinks for some greenhouse gasses, and purifiers of dissolved nutrients and toxins (Schallenberg et al., 2013). Yet, pressures such as eutrophication (excessive primary production) and anthropogenic climate warming (ACW) are acting synergistically to reduce the water quality of these important resources (Moos et al., 2009; Nazari-Sharabian et al., 2018; Watson et al., 2016). Monitoring of lakes can provide high-resolution information about such changes in water quality (*e.g.*, Dörnhöfer et al., 2018). However, monitoring is often expensive, time-intensive, logistically challenging and restricted to short temporal scales (years to decades) (Smol, 2008). Paleoenvironmental reconstructions allow scientists to gain a long-term (seasonal to millennia) perspective on how humans have impacted lakes. With this information, researchers can evaluate the magnitude of recent changes in water quality against a backdrop of natural variability. Paleoenvironmental reconstructions are not only useful for assessing changes in water quality, however; they are also used to gain insight into how conditions outside of the lake have varied over time (*e.g.*, Hladyniuk and Longstaffe, 2015; Hundey et al., 2014; Hyodo and Longstaffe, 2011). Lakes are natural archives: as they deposit sediment they continuously record changes in environmental conditions such as temperature (Colcord et al., 2015), plant/algal community composition (Chevalier et al., 2015; Mead et al., 2005) and aridity (Street et al., 2013). Understanding how these variables have changed over long time periods can provide insight into how ACW is altering the temperature and precipitation regimes, and plant community compositions, around these lakes (Castaneda et al., 2009; O'Beirne et al., 2017).

In order to conduct such paleoenvironmental investigations, limnologists measure chemical, biological and/or physical characteristics of the lake sediment. These

characteristics, or proxies, are known to vary in predictable ways when environmental conditions change. Determining how these proxies change throughout a sediment core can indicate how the environment in and around a lake has varied over time. Stable isotopic compositions of organic matter (OM) and carbonates in sediments are useful proxies that may be used to reconstruct many aspects of past environments. The carbon isotope composition of the sediment OM ($\delta^{13}\text{C}_{\text{TOC}}$), for instance, may be used to understand if the sediment is receiving inputs of OM from predominantly terrestrial (*e.g.*, tree leaves) or aquatic sources (*e.g.*, algae) (Meyers, 1994; Meyers and Ishiwatari, 1993). The $\delta^{13}\text{C}_{\text{TOC}}$ is also sensitive to changes in aridity, lake water pH, primary production and respiration, bedrock dissolution, methanogenesis, and the carbon isotopic composition of atmospheric carbon dioxide ($\delta^{13}\text{C}_{\text{CO}_2}$) (Diefendorf and Freimuth, 2017; Finlay and Kendall, 2007; Fogel and Cifuentes, 1993; Hladyniuk and Longstaffe, 2015; Hollander and McKenzie, 1991). Like the $\delta^{13}\text{C}_{\text{TOC}}$, the nitrogen isotope composition of the sediment OM ($\delta^{15}\text{N}_{\text{TN}}$) is sensitive to changes in OM source, primary production and respiration (Talbot, 2001). Values of $\delta^{15}\text{N}_{\text{TN}}$ may also, however, record changes in nitrogen speciation (*i.e.*, nitrification and denitrification) (Hornibrook et al., 2000; Meyers and Ishiwatari, 1993), inputs of nitrogenous fertilizers and changes in trophic status in the lake (Kendall, 1998). The $\delta^{18}\text{O}$ and $\delta^{13}\text{C}$ of carbonates in lakes, such as shelly fauna or marl, are also useful proxies of environmental change. The $\delta^{18}\text{O}$ of marl and shelly fauna ($\delta^{18}\text{O}_{\text{marl}}$ and $\delta^{18}\text{O}_{\text{shell}}$) are influenced by temperature, moisture source and, in closed basins, changes in effective moisture (the net of water inputs to evaporation) (Talbot, 1990). The $\delta^{13}\text{C}$ of marl and shelly fauna ($\delta^{13}\text{C}_{\text{marl}}$ and $\delta^{13}\text{C}_{\text{shell}}$) record many of the same variables as $\delta^{13}\text{C}_{\text{TOC}}$ because both are controlled by the $\delta^{13}\text{C}$ of dissolved inorganic carbon ($\delta^{13}\text{C}_{\text{DIC}}$) (Diefendorf et al., 2008). The $\delta^{18}\text{O}_{\text{shell}}$ and $\delta^{13}\text{C}_{\text{shell}}$ may also be influenced by vital effects associated with metabolic effects and/or the rate of shell formation (Fritz and Poplawski, 1974; McConnaughey, 1989a, 1989b; McConnaughey et al., 1997; Von Grafenstein et al., 1999).

The fact that stable isotopic compositions of lake sediments are sensitive to so many variables makes them difficult to interpret, however. A prerequisite for accurately interpreting stable isotope records is ascertaining whether the isotopic compositions of sediments are reflecting conditions within or outside of the lake (Meyers, 1994). The $\delta^{13}\text{C}$

and $\delta^{18}\text{O}$ of carbonates in the sediment, for instance, only reflect conditions within the lake if the carbonates themselves were produced within the lake. Fortunately, distinguishing between carbonates derived from authigenic precipitation compared with detrital inputs is relatively straightforward and involves examining the morphology of calcite crystals (Verrecchia and Verrecchia, 2003). Likewise, distinguishing between the shells of aquatic and terrestrial gastropods involves identifying the organism by its shell morphology (*e.g.*, Hladyniuk and Longstaffe, 2016). More difficult is determining whether the $\delta^{13}\text{C}_{\text{TOC}}$ and $\delta^{15}\text{N}_{\text{TN}}$ of sediments are reflecting conditions within or outside of the lake. The $\delta^{13}\text{C}_{\text{TOC}}$ and $\delta^{15}\text{N}_{\text{TN}}$ of sediments receiving predominately terrestrial OM inputs, for instance, will reflect conditions outside of the lake (Meyers, 1994; Meyers and Ishiwatari, 1993). Conversely, the $\delta^{13}\text{C}_{\text{TOC}}$ and $\delta^{15}\text{N}_{\text{TN}}$ of sediments receiving predominately aquatic OM inputs, reflect conditions within the lake (Meyers, 1994; Meyers and Ishiwatari, 1993). Further complicating interpretations of $\delta^{13}\text{C}_{\text{TOC}}$ and $\delta^{15}\text{N}_{\text{TN}}$ is that these proxies are susceptible to alteration after deposition, particularly in lakes with fully oxygenated water columns (Brahney et al., 2014; Lehmann et al., 2002).

To simplify interpretations of stable isotopic compositions of lake sediments, and to minimize the risk of post-depositional alteration, many researchers have begun analyzing the stable isotopic compositions of specific compounds extracted from the sediment OM rather than analyzing this OM in its entirety (*i.e.*, the “bulk” sediment) (Chevalier et al., 2015; Mead et al., 2005; Street et al., 2013; Zhang et al., 2020). This technique is called compound-specific isotopic analysis. Straight-chain hydrocarbons, or *n*-alkanes, extracted from the sediment OM are commonly used for this purpose. Measurements of the carbon isotope composition of *n*-alkanes (*i.e.*, $\delta^{13}\text{C}_{n\text{-alkane}}$) can be interpreted similarly to $\delta^{13}\text{C}_{\text{TOC}}$ but are more resistant to degradation (Meyers and Eadie, 1993). The hydrogen isotope composition of *n*-alkanes (*i.e.*, $\delta^2\text{H}_{n\text{-alkane}}$) is typically used to reconstruct variations in OM source, temperature and/or effective moisture (Sachse et al., 2012). Another unique aspect of *n*-alkanes is that they are source-specific (Ficken et al., 2000). Previous studies have demonstrated that different types of OM produce characteristic chain-lengths of *n*-alkanes. Terrigenous plants, for instance, typically produce *n*-alkanes with long chain lengths ($>\text{C}_{27}$) (Ficken et al., 2000). Analyzing the $\delta^{13}\text{C}$ of these individual carbon chains therefore

simplifies paleoenvironmental interpretations by clarifying whether the $\delta^{13}\text{C}$ or $\delta^2\text{H}$ of that *n*-alkane is reflecting conditions within or outside of the lake.

In low-elevation temperate lakes, the isotope systematics of lake sediments are reasonably well understood. However, in more extreme environments, such as alpine lakes, our understanding of how to interpret stable isotope results for OM from bulk sediments, and *n*-alkanes extracted from that OM, is more limited. This knowledge gap is problematic since alpine lakes are highly sensitive to environmental change and serve as bellwethers of anthropogenic impacts on freshwater resources (Moser et al., 2019). It is therefore vital that stable isotopic compositions of alpine lake sediments are interpreted correctly. Alpine lakes differ from low-elevation lakes in two ways that are germane to stable isotope science. Unlike low-elevation, temperate lakes, which typically derive most of their OM from algae, alpine lakes are comparatively unproductive and usually receive most of their OM from terrestrial sources (Zhang et al., 2020). Paleoclimate records from alpine lakes therefore tend to reflect conditions outside of the lake. Alpine lakes also tend to be more well-oxygenated than lakes at lower elevations because they are colder and less productive (Jacobsen and Dangles, 2017). Under aerobic conditions, sediments are susceptible to oxidative degradation as well as degradation by aerobic heterotrophic bacteria (Meyers and Ishiwatari, 1993). Low-elevation, temperate lakes typically develop anoxic bottom water during the summer months, which can slow the rate of oxidative degradation (Lehmann et al., 2002). Proxies derived from the sediment OM, such as $\delta^{13}\text{C}_{\text{TOC}}$ and $\delta^{15}\text{N}_{\text{TN}}$, are therefore less likely to be well-preserved in aerobic alpine waters compared with anoxic, temperate waters (Lehmann et al., 2002).

1.2 Background on isotope systematics

This thesis focuses on interpreting the stable isotopic compositions of carbon, nitrogen, oxygen and hydrogen of sediments, and OM sources to lake sediments. The isotope ratios of bulk sediments and vegetation are reported, as well as the carbon and hydrogen isotope compositions and chain lengths of *n*-alkanes extracted from these materials. This review outlines the isotope systematics of lake sediments and their OM sources, and highlights differences between alpine and temperate lake systems.

1.2.1 Isotopic notation

Isotopes are atoms with the same number of protons and electrons but different numbers of neutrons (Sharp, 2017). Stable isotopic compositions are presented as ratios of the heavy (rare) isotope to the light (common) isotope relative to a reference standard (Equation 1.1). Stable isotope compositions use the δ -notation relative to the Vienna PDB standard for C, AIR standard for N or Vienna SMOW standard for O and H.

Equation 1.1

$$\delta = \left[\left(\frac{R_{\text{sample}}}{R_{\text{standard}}} \right) - 1 \right] \text{ (in ‰)}$$

where R_{sample} and $R_{\text{standard}} = {}^{13}\text{C}/{}^{12}\text{C}$ for carbon, ${}^{15}\text{N}/{}^{14}\text{N}$ for nitrogen, ${}^{18}\text{O}/{}^{16}\text{O}$ for oxygen, or ${}^2\text{H}/{}^1\text{H}$ for hydrogen, in the sample and standard, respectively (Coplen, 2011, 1996; Mariotti, 1983). Changes in the ratios of heavy to light isotopes are the result of fractionation. Many natural processes, such as photosynthesis or evaporation/condensation, can alter the relative abundance of stable isotopes (Sharp, 2017). Measuring the stable isotopic composition of ancient materials, such as shells or lake sediments, can therefore shed light on natural processes that occurred in the past. The isotope fractionation factor, α , represents the partitioning of stable isotopes between two substances, A and B , as shown in Equation 1.2.

Equation 1.2

$$\alpha_{A-B} = R_A/R_B$$

where R is the ratio of heavy to light isotopes (Sharp, 2017). Another way of expressing the fractionation factor is by calculating ε using Equation 1.3. While the use of ε is discouraged by some (Sharp, 2017), its use has become routine in some subfields of stable isotope geochemistry, such as organic isotope geochemistry. Since organic isotope geochemistry is a focus of this thesis, ε is often used to represent stable isotope fractionations.

Equation 1.3

$$\varepsilon = (\alpha - 1) * 1000$$

1.2.2 Controls on the carbon and oxygen isotopic compositions ($\delta^{13}\text{C}$ and $\delta^{18}\text{O}$) of carbonates in lakes

Measurements of the $\delta^{13}\text{C}$ of carbonates in lakes are useful for reconstructing ancient carbon isotope compositions of dissolved inorganic carbon ($\delta^{13}\text{C}_{\text{DIC}}$) in lake water (Talbot, 1990). This information can provide insight into carbon cycling within lakes. The $\delta^{18}\text{O}$ of endogenic and biogenic carbonates are used to reconstruct variations in temperature and/or effective moisture, the latter being the net of water inputs to evaporative outputs (Talbot, 1990). The $\delta^{18}\text{O}$ of endogenic and biogenic carbonates inherit their isotopic composition from the $\delta^{18}\text{O}$ of water, which is largely controlled by the $\delta^{18}\text{O}$ of precipitation (Talbot, 1990). This review therefore begins by outlining the controls of $\delta^{18}\text{O}$ and $\delta^2\text{H}$ in precipitation and lake water.

1.2.2.1 Controls on the $\delta^{18}\text{O}$ and $\delta^2\text{H}$ of precipitation and lake water

Globally, the relationship between $\delta^{18}\text{O}$ and $\delta^2\text{H}$ is called the Global Meteoric Water Line (GMWL) and is given as: $\delta^2\text{H} = 8\delta^{18}\text{O} + 10$ (Craig, 1961). At the regional scale, local evaporation lines (LEL) deviate from the GMWL (Craig, 1961). Samples collected from lake waters, for instance, have $\delta^{18}\text{O}$ and $\delta^2\text{H}$ that fall to the right of the GMWL (*i.e.*, have slopes <8), whilst corresponding vapor samples have $\delta^{18}\text{O}$ and $\delta^2\text{H}$ that fall to the left of the GMWL (*i.e.*, have slopes <8) (Craig, 1961). This effect is due to evaporation, which concentrates ^{18}O and ^2H in the liquid phase (Gat, 1996). Spatiotemporal patterns in the $\delta^{18}\text{O}$ and $\delta^2\text{H}$ of precipitation arise in response to temperature, latitude, altitude, continental, seasonal and amount effects (Sharp, 2017).

Temperature influences the $\delta^2\text{H}$ and $\delta^{18}\text{O}$ of meteoric water through processes typically attributed to Rayleigh distillation (Dansgaard, 1964). Under Rayleigh conditions, condensate is continuously removed from the system, preventing back exchange between the water and vapor phases after their separation. The temperature-dependence stems from the fact that warmer air masses can hold more water vapor, and vice versa. Since the size of the vapour reservoir decreases with temperature, the successive removal of condensate systematically decreases the $\delta^2\text{H}$ and $\delta^{18}\text{O}$ of the remaining vapor (Dansgaard, 1964). This relationship is described in Equation 1.4.

Equation 1.4

$$\varepsilon \left(\frac{R}{R_i} \right) = F^{a-1}$$

where R is the isotopic ratio ($^2\text{H}/^1\text{H}$ or $^{18}\text{O}/^{16}\text{O}$), a is the fractionation factor between liquid and vapor, F is the fraction of vapor remaining, and i is the initial ratio (Dansgaard, 1964). Compounding this effect is the increasing fractionation between water vapor and air with lower temperatures.

Rayleigh distillation is also invoked to explain the global pattern of $\delta^2\text{H}$ and $\delta^{18}\text{O}$ of meteoric water. As warm equatorial vapor migrates towards the poles, for example, the degree of rainout increases and temperature decreases (Dansgaard, 1964). Consequently, the $\delta^2\text{H}$ and $\delta^{18}\text{O}$ of water vapor and precipitation decrease with increasing latitude (Gat, 1996). Likewise, as an air mass is pushed up a mountain, its temperature cools and it decompresses, causing rainout (Dansgaard, 1964). Again, the lower temperatures cause the fractionation between water vapor and precipitation to increase, compounding the lowering of $\delta^2\text{H}$ and $\delta^{18}\text{O}$ of the remaining vapor. The result is a decrease in $\delta^2\text{H}$ and $\delta^{18}\text{O}$ of water vapor and precipitation with increasing altitude (Gat, 1996). Furthermore, as air masses move inland, the $\delta^2\text{H}$ and $\delta^{18}\text{O}$ of precipitation decrease because the air mass has undergone more cycles of precipitation (Dansgaard, 1964). In seasonal climates, the $\delta^2\text{H}$ and $\delta^{18}\text{O}$ of precipitation decrease in the winter months relative to the summer months as a consequence of the temperature effect (Dansgaard, 1964; Gat, 1996).

Lake water inherits the $\delta^2\text{H}$ and $\delta^{18}\text{O}$ of precipitation. These values are then modified depending on the isotopic compositions of groundwater and surface flows, and the extent of lake water evaporation (Talbot, 1990). Lake water evaporation causes the $\delta^2\text{H}$ and $\delta^{18}\text{O}$ of lake water to increase, while the infiltration of groundwater typically causes the $\delta^2\text{H}$ and $\delta^{18}\text{O}$ of lake waters to decrease (Fritz and Clark, 1997). In temperate regions, groundwater is disproportionately recharged by snowmelt, which has a low $\delta^2\text{H}$ and $\delta^{18}\text{O}$ (Fritz and Clark, 1997), leading to overall lower groundwater isotopic compositions compared to annual precipitation at the locality.

It has been observed that, in tropical regions, a negative correlation exists between the mean $\delta^2\text{H}$ and $\delta^{18}\text{O}$ of precipitation and the amount of precipitation. This phenomenon is attributed in part to the lack of exchange between water droplets, and lack of re-evaporation of water droplets, during heavy rainouts. It is because mechanisms such as the amount effect only operate predominately in lower latitudes that alternatives to Rayleigh distillation are being proposed. One such alternative is that spatiotemporal patterns in $\delta^2\text{H}$ and $\delta^{18}\text{O}$ of precipitation are caused by changes in the proportion of precipitation from stratiform versus deep convective precipitation systems. Stratiform precipitation is more depleted in ^2H and ^{18}O relative to precipitation derived from deep convective precipitation (Aggarwal et al., 2016).

1.2.2.2 Controls on the $\delta^{18}\text{O}$ and $\delta^{13}\text{C}$ of marl

Marl, or endogenic calcite (CaCO_3), is naturally produced in lakes that are supersaturated with respect to Ca^{2+} (Wiik et al., 2013). Such lakes are typically situated in carbonate-rich bedrock. The precipitation of marl occurs rapidly during the summer months when water temperatures and primary production are high (Wiik et al., 2013). Unlike most salts, the saturation point of calcite decreases with increasing temperature (Wiik et al., 2013). Increasing water temperatures will therefore drive marl formation. Photosynthetic organisms also drive marl formation by removing CO_2 from the water column, a process that reduces the concentration of H^+ and increases the pH of lake water (Wiik et al., 2013). Since the saturation point of calcite decreases with increasing pH, increases in primary production also favour the formation of marl (Wiik et al., 2013).

The oxygen isotope composition of marl ($\delta^{18}\text{O}_{\text{marl}}$) reflects the $\delta^{18}\text{O}$ of lake water and the temperature at which the marl crystallizes. Higher temperatures of marl crystallization decrease $\delta^{18}\text{O}_{\text{marl}}$, given the temperature dependence of the calcite-water oxygen-isotope fractionation (Craig, 1965). However, marl likely precipitates within a narrow temperature range during the summer months (Drummond et al., 1995). Typically, therefore, $\delta^{18}\text{O}_{\text{marl}}$ increases under conditions that favour lake water evaporation. At such times, lake levels are generally low, conditions are dry, and/or temperatures are high; $\delta^{18}\text{O}_{\text{marl}}$ commonly decreases when lake levels are high, conditions are wet, and/or temperatures are low

(Henderson and Shuman, 2009; Hladyniuk and Longstaffe, 2016; Schwalb and Dean, 2002; Talbot, 1990). In short, changes in $\delta^{18}\text{O}_{\text{marl}}$ are dominated by changes in $\delta^{18}\text{O}_{\text{lake water}}$, which in hydrologically closed lakes are largely a function of changes in effective moisture.

Variations in $\delta^{13}\text{C}_{\text{marl}}$ closely reflect the $\delta^{13}\text{C}$ of dissolved inorganic carbon (DIC) (Talbot, 1990). Because the fractionation between DIC and marl is only weakly sensitive to temperature (Mook et al., 1974), changes in water temperature do not noticeably drive variations in $\delta^{13}\text{C}_{\text{marl}}$. Instead, $\delta^{13}\text{C}_{\text{DIC}}$ and, by extension, $\delta^{13}\text{C}_{\text{marl}}$ reflect several in-lake processes. As for $\delta^{18}\text{O}_{\text{lake water}}$, $\delta^{13}\text{C}_{\text{DIC}}$ is influenced by evaporation (Talbot, 1990). In hydrologically closed systems, evaporation of lake waters may outpace the recharge of lake waters by groundwater. During arid periods, the lighter stable isotope of carbon, ^{12}C , is preferentially removed from the system, enriching DIC and marl in ^{13}C (Talbot, 1990). During wet periods, $\delta^{13}\text{C}_{\text{DIC}}$ exchanges with atmospheric CO_2 , driving down $\delta^{13}\text{C}_{\text{DIC}}$ (Li and Ku, 1997).

Primary production and respiration are also important controls on $\delta^{13}\text{C}_{\text{DIC}}$ and $\delta^{13}\text{C}_{\text{marl}}$. Primary producers, such as algae and macrophytes, preferentially take up ^{12}C -rich DIC over ^{13}C -rich DIC (Hollander and McKenzie, 1991a). A fraction of these ^{12}C -rich organisms is incorporated into sediment OM, which removes ^{12}C -rich DIC from the water column and enriches the remaining DIC in ^{13}C (Hollander and McKenzie, 1991). The rest of the ^{12}C -rich algae can be returned to the water column through respiration, mitigating the increase in $\delta^{13}\text{C}_{\text{DIC}}$ (Hollander and McKenzie, 1991). In addition, ^{12}C -rich DIC can be supplied to the lake by groundwater infiltration and surface flows (Talbot, 1990).

The $\delta^{13}\text{C}_{\text{DIC}}$ and $\delta^{13}\text{C}_{\text{marl}}$ of lakes with short residence times, or unproductive lakes, are typically unchanging since ^{12}C -rich DIC is replenished at a rate faster than it can be removed from the system by evaporation and/or primary production (Talbot, 1990). Conversely, the $\delta^{13}\text{C}_{\text{DIC}}$ and $\delta^{13}\text{C}_{\text{marl}}$ of highly productive lakes and/or lakes with long residence times tend to increase in response to evaporation and/or primary production. This pattern occurs because ^{12}C -rich DIC is removed from the water column at a faster rate than it can be replenished (Talbot, 1990). The dissolution of marine carbonate bedrock,

which typically has $\delta^{13}\text{C} \approx 0\text{-}+2\text{ ‰}$, in lake water can magnify this effect (Coniglio and Williams-Jones, 1992).

Another important control on $\delta^{13}\text{C}_{\text{DIC}}$ is methanogenesis, the process by which anaerobic archaea convert CO_2 and/or acetate into methane (Borrel et al., 2011). The methane produced by methanogenesis is typically enriched in ^{13}C relative to DIC, while CO_2 produced by methanogenesis is depleted of ^{13}C relative to DIC (Teranes and Bernasconi, 2005). Methane produced in the hypolimnion may directly escape the water column via ebullition (bubbling) and/or plant-mediated transport (Borrel et al., 2011). These transport pathways are common in shallow lakes (Bastviken et al., 2004). Alternatively, methane may be stored in the hypolimnion until turnover, when almost all of it is oxidized at once (Borrel et al., 2011). This pathway is common in deep lakes (Bastviken et al., 2004). Although methanogenesis greatly influences the $\delta^{13}\text{C}_{\text{DIC}}$ of the hypolimnion, it typically has little effect on $\delta^{13}\text{C}_{\text{marl}}$ since marl forms in the epilimnion (an isotopically distinct pool of DIC) between spring and fall turnover (Teranes and Bernasconi, 2005).

1.2.3 Controls on the carbon isotopic compositions ($\delta^{13}\text{C}_{\text{TOC}}$) of lake sediment OM

Measurements of $\delta^{13}\text{C}_{\text{TOC}}$ are typically interpreted to reflect changes in primary production (e.g., Hladyniuk and Longstaffe, 2015; Hundey et al., 2014; Hyodo and Longstaffe, 2011). Because sediments receive inputs of allochthonous as well as autochthonous OM (Meyers and Ishiwatari, 1993); however, the $\delta^{13}\text{C}_{\text{TOC}}$ also offers insight into catchment-scale changes in vegetation and climate.

1.2.3.1 Watershed-scale influences on $\delta^{13}\text{C}_{\text{TOC}}$ of the sediment OM

The main watershed-scale influences on $\delta^{13}\text{C}_{\text{TOC}}$ are: (i) the $\delta^{13}\text{C}$ of atmospheric carbon dioxide (CO_2); (ii) the source of OM captured by lake sediments, and (iii) climate. The ultimate source of carbon to lakes is atmospheric carbon dioxide (CO_2) (Figure 1.1). On a global scale, the $\delta^{13}\text{C}$ of atmospheric CO_2 ($\delta^{13}\text{C}_{\text{atm}}$) varies temporally and spatially. There is a slight latitudinal gradient in $\delta^{13}\text{C}_{\text{atm}}$. The $\delta^{13}\text{C}_{\text{atm}}$ at 60°N is generally 0.2 ‰ more negative than at 60°S ; this effect is most likely due to the anthropogenic burning of fossil fuels

occurring at northern latitudes (Keeling et al., 1989). The $\delta^{13}\text{C}_{\text{atm}}$ also varies seasonally; in the spring the $\delta^{13}\text{C}_{\text{atm}}$ over the northern hemisphere is ~ 1 ‰ lower than in autumn. This change corresponds with seasonal shifts in the partial pressure of atmospheric CO_2 ($\text{CO}_{2\text{atm}}$) related to seasonal patterns of photosynthesis and respiration (Keeling et al., 1989). Another temporal change in $\delta^{13}\text{C}_{\text{atm}}$ is the “Suess Effect,” which describes the ^{13}C depletion of atmospheric CO_2 of >1.5 ‰ since pre-industrial times. This depletion is caused by the release of fossil fuel emissions, which have low $\delta^{13}\text{C}$ (Eide et al., 2017; Keeling, 1979; Verburg, 2007).

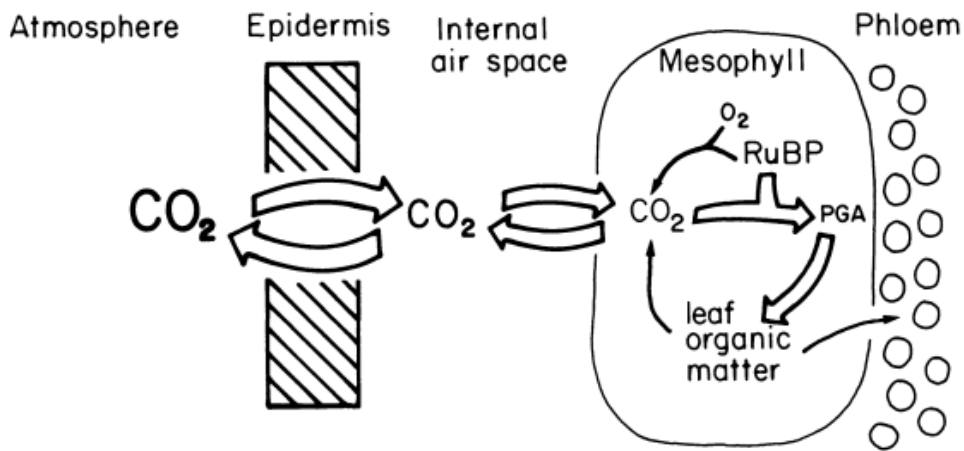


Figure 1.1 Important steps in CO_2 fixation during C_3 photosynthesis. Size of font reflects the relative concentrations of CO_2 at different stages, whereas sizes of arrows indicate the relative fluxes. Used with permission from O’Leary (1988).

Another important control on $\delta^{13}\text{C}_{\text{TOC}}$ is the source of OM present in lake sediments (Meyers, 1994). Different OM sources can have characteristic $\delta^{13}\text{C}_{\text{TOC}}$; hence, the source of OM to the lake will influence $\delta^{13}\text{C}_{\text{TOC}}$ of the sediment OM (Meyers and Ishiwatari, 1993). The $\delta^{13}\text{C}_{\text{TOC}}$ of different types of vegetation is largely controlled by the organism’s carbon concentrating mechanism and partial pressure of CO_2 ($p\text{CO}_2$) within the cell (Farquhar et al., 1982; Fogel and Cifuentes, 1993). All the organisms examined in this thesis utilize the C_3 pathway of photosynthesis, and so differences between the $\delta^{13}\text{C}_{\text{TOC}}$ of C_3 , C_4 and CAM plants are not reviewed here. First, the factors controlling $\delta^{13}\text{C}_{\text{TOC}}$ of organisms that obtain carbon from atmospheric CO_2 (*i.e.*, terrestrial plants, lichen and semi-emergent/floating macrophytes) are discussed. Then, the factors controlling the $\delta^{13}\text{C}_{\text{TOC}}$ of organisms that

obtain carbon from dissolved CO₂ and/or bicarbonate (HCO₃⁻) (*i.e.*, algae and submerged macrophytes) are reviewed.

Among terrestrial, vascular plants, CO_{2atm} enters the leaf via pores called stomata (O'Leary, 1988). So-called guard cells surrounding individual stomata (stoma) can open and close the pores. Stoma are opened to obtain CO_{2atm} for photosynthesis and to initiate transpiration (Heldt et al., 2005). The primary reason why stomata are closed is to minimize water loss. Before CO_{2atm} can enter the stoma, it must diffuse across a boundary layer caused by laminar flow of air adjacent to the leaf surface (O'Leary, 1988). Once the CO_{2atm} has diffused through the boundary layer, it must diffuse across the stoma (Fig. 1.1). These steps fractionate $\delta^{13}\text{C}_{\text{CO}_2}$. The magnitude of this fractionation depends on the aperture of the stoma (O'Leary, 1988). Once CO₂ has diffused into the stomata, it must then diffuse through the intercellular air space on route to the sites of carboxylation (Farquhar et al., 1989). Next, the gaseous CO₂ must diffuse across the cell wall of the chloroplast and dissolve in its liquid stroma (Farquhar et al., 1989). Then, the dissolved CO₂ must travel through the stroma to the sites of carboxylation.

Non-vascular plants (*e.g.*, mosses) and lichen lack stomata (Farquhar et al., 1989). The $\delta^{13}\text{C}_{\text{CO}_2}$ of mosses depend not on stomatal apertures but on the layer of water sitting on their leaves (Rice, 2000; Rundel et al., 1979; Szpak et al., 2013). The $\delta^{13}\text{C}_{\text{TOC}}$ of lichen, which are composite organisms consisting of fungi and algae, is determined by the type of algae present within the organism. Lichen with cyanobacteria as the photobiont tend to have $\delta^{13}\text{C}_{\text{TOC}}$ between -23 and -14 ‰, while lichen with green algae as the photobiont exhibit $\delta^{13}\text{C}_{\text{TOC}}$ between -35 and -17 ‰ (Huiskes et al., 2007; Lange et al., 1988; Lee et al., 2009).

In plants, mosses and lichen, the major discrimination against ¹³CO₂ during photosynthesis occurs during carboxylation in the Calvin Cycle when ribulose-1,5-bisphosphate carboxylase/oxygenase (RuBisCO) initiates the fixation of CO₂ into glyceraldehyde-3-phosphate (G3P) (Farquhar et al., 1989). The discrimination against ¹³CO₂ associated with this step is between 28 and 30 ‰ (Farquhar et al., 1989; Farquhar and Lloyd, 1993; O'Leary, 1988). Changes in environmental conditions can influence the

processes described above. To simplify their discussion the aforementioned pathways of $\text{CO}_{2\text{atm}}$ will be summarized using Equation 1.5 by Farquhar *et al.* (1989) that describes fractionation between the bulk leaf $\delta^{13}\text{C}_{\text{TOC}}$ and $\delta^{13}\text{C}_{\text{atm}}$ ($\varepsilon_{\text{C}_3\text{leaf}}$).

Equation 1.5

$$\varepsilon_{\text{C}_3\text{leaf}} = a + (b - a) \frac{c_i}{c_a}$$

In Equation 1.5, a is the isotopic fractionation resulting from differences in the rates of diffusion of $^{12}\text{CO}_2$ versus $^{13}\text{CO}_2$, b is the isotopic fractionation due to RuBisCo, c_i is the partial pressure of CO_2 within the cell and c_a is the partial pressure of atmospheric CO_2 . Since a (typically ~ 4.4 ‰) and b (29 ‰) are relatively constant, the major factor which influences discrimination between the $\delta^{13}\text{C}_{\text{atm}}$ and $\delta^{13}\text{C}_{\text{leaf}}$ is c_i/c_a (Farquhar *et al.*, 1989).

Some of the primary environmental changes that influence c_i/c_a are: changes in irradiance and temperature, shifts in nutrient availability, changes in water and osmotic stress, and changes in $p\text{CO}_2$ (Tieszen, 1991). Decreases in irradiance and temperature, for example, decrease the rate of photosynthesis because the plant is limited by photon availability and the rate of chemical reactions, respectively (Tieszen, 1991). CO_2 concentrations within the plant therefore become less limiting. As a result, c_i/c_a increases as irradiance and temperature decrease, and the $\delta^{13}\text{C}_{n\text{-alkane}}$ (and $\delta^{13}\text{C}_{\text{TOC}}$ of the bulk leaf tissue) decreases (Tieszen, 1991). Decreases in nutrient availability influence $\delta^{13}\text{C}_{n\text{-alkane}}$ in the same way. Nitrogen limitation, for example, limits the formation of enzymes needed for photosynthesis, causing a reduction in the overall rate of photosynthesis, an increase in c_i/c_a and a decrease in $\delta^{13}\text{C}_{\text{TOC}}$ of the plant (Fogel and Cifuentes, 1993; Tieszen, 1991).

Increasing water and osmotic stress, conversely, decrease c_i/c_a . Vascular plants growing in arid environments close their stomata to conserve water (Tieszen, 1991). Closing stomata means that the reservoir of $^{12}\text{CO}_2$ begins to decrease. As the intercellular concentration of CO_2 decreases, the plant must eventually take up $^{13}\text{CO}_2$ to maintain rates of photosynthesis. Thus increasing water and osmotic stress causes the $\delta^{13}\text{C}_{\text{TOC}}$ of the plant to increase (Tieszen, 1991). In theory, reduced partial pressure of $\text{CO}_{2\text{atm}}$ ($p\text{CO}_2$) (*e.g.*, with increasing elevation) should decrease the ratio of c_i/c_a and therefore increase $\delta^{13}\text{C}_{\text{TOC}}$

(Tieszen, 1991). The relationship between $p\text{CO}_2$ and $\delta^{13}\text{C}_{\text{TOC}}$ of the plant has proven difficult to validate, however, because plants likely adapt over time to lower $p\text{CO}_2$ by changing their stomatal density and/or modulating C_i to match the new value of C_a (Arens et al., 2000).

The source of carbon for submerged macrophytes and algae is dissolved inorganic carbon (DIC), which in most lakes is predominately HCO_3^- (Fogel and Cifuentes, 1993). The factors controlling $\delta^{13}\text{C}_{\text{DIC}}$ reviewed in the previous section therefore control the $\delta^{13}\text{C}_{\text{TOC}}$ of macrophytes and algae. Unlike in terrestrial plants, diffusion of DIC into submerged macrophytes and algae is commonly the rate-limiting step of photosynthesis (Fogel and Cifuentes, 1993). This behaviour occurs because CO_2 and HCO_3^- diffuse into cells more slowly in water than in air (Fogel and Cifuentes, 1993). To maintain rates of photosynthesis, some submerged macrophytes and algae (*e.g.*, Charophytes) have evolved pumps to actively transport DIC across the cell membrane (Hammarlund et al., 1997; McConnaughey, 1991). The DIC taken up by aquatic organisms must eventually be converted to CO_2 , which is the form of carbon used by RuBisCO (Fogel and Cifuentes, 1993). Converting DIC to CO_2 is energy-intensive (Fogel and Cifuentes, 1993). Thus most aquatic organisms preferentially take up CO_2 until it becomes limiting (Finlay and Kendall, 2007). Once this occurs (usually in the summer months) some organisms will begin actively transporting and concentrating HCO_3^- in their cells and converting it into CO_2 using carbonic anhydrase near the sites of carboxylation (Badger and Price, 2003).

Organisms that derive their DIC from HCO_3^- have internal DIC pools that are enriched in ^{13}C by $\sim 8\text{‰}$ relative to organisms that derive their DIC from dissolved CO_2 (Fogel and Cifuentes, 1993). Consequently, the $\delta^{13}\text{C}_{\text{TOC}}$ of bulk tissues from organisms using HCO_3^- will be $\sim 8\text{‰}$ higher than those organisms which derive their DIC directly from CO_2 . It is therefore not surprising that many algae and aquatic plants usually have tissues with $\delta^{13}\text{C}_{\text{TOC}}$ clustered around -28‰ and -20‰ (Fogel and Cifuentes, 1993). Equation 1.6, modified from Equation 1.5, describes the fractionation between the $\delta^{13}\text{C}$ of dissolved CO_2 and the $\delta^{13}\text{C}_{\text{TOC}}$ of bulk tissue.

Equation 1.6

$$\epsilon_{\text{macrophyte}} = d + b_3 \frac{F_3}{F_1}$$

In Equation 1.6, d is the equilibrium isotope fractionation between CO_2 and HCO_3^- , b_3 is the isotope fractionation associated with carboxylation by RuBisCO and F_3/F_1 is the ratio of CO_2 leaking out of the cell (Fogel and Cifuentes, 1993). In short, the $\delta^{13}\text{C}$ of OM sources delivered to sediments vary depending on environmental conditions.

1.2.3.2 Lake-scale influences on $\delta^{13}\text{C}_{\text{TOC}}$ of the sediment OM

Values of sediment $\delta^{13}\text{C}_{\text{TOC}}$ are also controlled by in-lake processes. These processes include: (i) primary production and respiration (Hollander and McKenzie, 1991); (ii) OM degradation (Lehmann et al., 2002); and (iii) methanogenesis (Teranes and Bernasconi, 2005). Primary production and respiration alter the $\delta^{13}\text{C}_{\text{TOC}}$ of sediment by changing $\delta^{13}\text{C}_{\text{DIC}}$ (Hollander and McKenzie, 1991). Increases in $\delta^{13}\text{C}_{\text{DIC}}$ caused by enhanced primary production, or decreased $\delta^{13}\text{C}$ caused by enhanced respiration, influence the $\delta^{13}\text{C}_{\text{TOC}}$ of algae and submerged macrophytes taking up this DIC (Hollander and McKenzie, 1991). When these organisms die and are incorporated into the sediment OM, the sediment $\delta^{13}\text{C}_{\text{TOC}}$ inherits these changes. Sediment $\delta^{13}\text{C}_{\text{TOC}}$ can also be affected by oxidative and microbial degradation (Gälman et al., 2009; Lehmann et al., 2002). Under aerobic conditions, $\delta^{13}\text{C}_{\text{TOC}}$ typically decreases (Lehmann et al., 2002), while under anoxic conditions, $\delta^{13}\text{C}_{\text{TOC}}$ increases (Gälman et al., 2009). Original values of $\delta^{13}\text{C}_{\text{TOC}}$ are better preserved under anoxic conditions than under aerobic conditions (Lehmann et al., 2002). Methanogenesis, which occurs under anoxic conditions, can cause $\delta^{13}\text{C}_{\text{TOC}}$ to decrease (Teranes and Bernasconi, 2005). Since the $\delta^{13}\text{C}_{\text{marl}}$ remains similar to $\delta^{13}\text{C}_{\text{DIC}}$ during methanogenesis, but $\delta^{13}\text{C}_{\text{TOC}}$ decreases, one can estimate the extent of methanogenesis by measuring $\epsilon_{\text{marl-TOC}}$, which is the fractionation between $\delta^{13}\text{C}_{\text{marl}}$ and $\delta^{13}\text{C}_{\text{TOC}}$ (Teranes and Bernasconi, 2005).

1.2.4 Controls on the nitrogen isotopic compositions ($\delta^{15}\text{N}_{\text{TN}}$) of the sediment OM

In paleolimnology, sediment $\delta^{15}\text{N}_{\text{TN}}$ is commonly used as an indicator of primary production and nitrogen source (Talbot, 2001). The $\delta^{15}\text{N}$ of total nitrogen (TN) reflects OM almost entirely except at very low OM contents. Sediment $\delta^{15}\text{N}_{\text{TN}}$ can be influenced by watershed-scale and lake-scale processes.

1.2.4.1 Watershed-scale influences on $\delta^{15}\text{N}_{\text{TN}}$ of the sediment OM

The main watershed-scale influences on $\delta^{15}\text{N}$ are: (i) the relative proportions of groundwater versus surface runoff contributing to streamflow; (ii) the presence of reducing conditions in groundwater, the riparian and hyporheic zones and sediments; (iii) land use and extent of human disturbance in the watershed and airshed; (iv) climate; and (v) source of OM (Finlay and Kendall, 2007).

Inputs of groundwater and surface water have opposing influences on the $\delta^{15}\text{N}$ of lakes and rivers. Groundwater contains low concentrations of dissolved oxygen (DO), and so rates of denitrification are high in groundwater relative to surface water (Kendall, 1998). As the product of denitrification, N_2 , leaves the system, groundwater DIN becomes increasingly enriched in ^{15}N . Enrichment factors associated with denitrification range from -40 to -5 ‰ (Kendall, 1998). Consequently, increases in groundwater inflows result in higher in-lake $\delta^{15}\text{N}$. Reducing conditions in the riparian, hyporheic zones and sediments will also result in increases in $\delta^{15}\text{N}$ due to denitrification (Kendall, 1998). The extent of these increases depends on temperature and the availability of NO_3^- , which is reduced to N_2 (Kendall, 1998).

In pristine surface waters, DO concentrations are higher, and so denitrification is rare and $\delta^{15}\text{N}$ is relatively low. Nitrification ($\epsilon = -29$ to -18 ‰) drives down values of $\delta^{15}\text{N}$. The $\delta^{15}\text{N}$ of nitrogen in surface waters may be modified, however, by anthropogenic inputs of nitrogen. The combustion of fossil fuels, for example, can result in dry and/or wet deposition of DIN in the watershed. Wet deposition refers to the processes that transfer atmospheric nitrogen to the catchment in aqueous forms, including snow, fog and rain (Finlay and Kendall, 2007). Dry deposition involves the direct transfer of gaseous and

particulate nitrogen without the aid of precipitation (Finlay and Kendall, 2007). Both types of deposition are composed of nitrogen from fossil fuel and vehicle emissions. Wet deposition is the dominant form of nitrogen deposition in temperate regions, while dry deposition is the dominant form in dry climates (Fenn et al., 2003).

The $\delta^{15}\text{N}$ of wet and dry deposition are difficult to constrain because they vary wildly with region and season. Generally, the $\delta^{15}\text{N}$ of NO_3^- and NH_4^+ in dry deposition are higher than in wet deposition (Heaton et al., 1997). The $\delta^{15}\text{N}$ of dry deposition usually reflects its sources, which commonly are vehicle fuel combustion ($\delta^{15}\text{N} = +3.7$ to $+5.7$ ‰) (Pearson et al., 2000) and coal combustion ($\delta^{15}\text{N} = +5$ to $+13$ ‰). The $\delta^{15}\text{N}$ of wet deposition increases in areas where fossil fuel emissions are more abundant (Kendall, 1998).

The contribution of fertilizers to lake basins can also change $\delta^{15}\text{N}$. Organic fertilizers have $\delta^{15}\text{N}$ that range from $+6$ to $+30$ ‰ while inorganic fertilizers have $\delta^{15}\text{N}$ that range from -4 to $+4$ ‰ (Kendall, 1998). Contributions of organic fertilizers or human waste can increase the $\delta^{15}\text{N}$ of surface waters, in turn increasing the $\delta^{15}\text{N}$ of lakes. Cole et al. (2006), for example, found that watersheds containing greater populations contributed larger nitrate loads with higher $\delta^{15}\text{N}$ to receiving waters; these higher values were detected in groundwater flows. The contribution of inorganic fertilizers to surface waters tends to lower $\delta^{15}\text{N}$ of the lake sediment (Talbot, 2001).

Climate also exerts a control on $\delta^{15}\text{N}$ by influencing the degree to which the nitrogen-cycle is open or closed. In drier sites, nitrogen availability increases because the demand for nitrogen by plants is lower (Austin and Vitousek, 1998). In this case, the nitrogen cycle is said to be more open. A more open nitrogen cycle can stimulate NH_4^+ volatilization, leading to higher plant and soil $\delta^{15}\text{N}$. Environments with closed nitrogen cycles are characterized by higher amounts of mean annual precipitation (Austin and Vitousek, 1998), lower N availability and increasing reliance on mycorrhizal association for nitrogen acquisition (Craine et al., 2009). Closed nitrogen cycles lead to lower plant and soil $\delta^{15}\text{N}$ (Austin and Vitousek, 1998). N-fixing bacteria associated with plants have $\delta^{15}\text{N}$ that

approximate atmospheric N_2 (*i.e.*, 0 ‰) (Kendall, 1998). The input of detritus generated from N-fixing plants therefore lowers the $\delta^{15}N$ of lake sediments.

Another important control on sediment $\delta^{15}N_{TN}$ is that of the OM delivered to the sediment (*e.g.*, plants and algae) from the surrounding catchment, and from the lake itself. The $\delta^{15}N_{TN}$ of organisms is largely controlled by the nitrogenous species utilized by the organism: nitrate (NO_3^-), ammonium (NH_4^+), atmospheric nitrogen (N_2) or organic nitrogen (*e.g.*, free amino acids) (Hamilton, 2009). These species exhibit different $\delta^{15}N_{TN}$; thus, the type of species utilized by the plant will influence the plant's $\delta^{15}N_{TN}$. Organisms that utilize N_2 , for instance, are characterized by $\delta^{15}N_{TN}$ of ~ 0 ‰ (Hamilton, 2009). Organisms that utilize free amino acids, commonly through mycorrhizal associations, typically have $\delta^{15}N_{TN} < 0$ ‰, while organisms utilizing soil NO_3^- and NH_4^+ exhibit $\delta^{15}N_{TN} > 0$ ‰ (Hamilton, 2009).

Vascular, terrestrial plants typically obtain nitrogen from soil NO_3^- , although they may utilize NH_4^+ in nitrogen-limited environments, or if soils are waterlogged or acidic (Hamilton, 2009). Some terrestrial plants, particularly those living in nitrogen-stressed environments, form mycorrhizal associations with fungi, allowing them to utilize free amino acids (Szpak et al., 2013; Talbot, 2001). Lichen and mosses utilize atmospheric NH_4^+ and/or free amino acids, and typically have lower $\delta^{15}N_{TN}$ than vascular plants (Lee et al., 2009). Rooted macrophytes obtain nitrogen from sediments in the littoral zone of lakes (Cloern et al., 2002). Such nitrogen typically has high $\delta^{15}N_{TN}$ due to denitrification along the margins of lakes (Cloern et al., 2002). Consequently, macrophytes commonly have higher $\delta^{15}N_{TN}$ than other OM sources (Cloern et al., 2002; Molina et al., 2011). The $\delta^{15}N_{TN}$ of algae depends on the $\delta^{15}N_{TN}$ of dissolved inorganic nitrogen and can vary widely depending on factors such as the dissolved oxygen concentration of the water column (Talbot, 1990). These factors are reviewed in detail in the next section.

1.2.4.2 Lake-scale controls on $\delta^{15}N_{TN}$

In lakes, DIN is delivered via allochthonous (outside of the lake) and autochthonous (within the lake) sources. Allochthonous sources include groundwater, detrital material from plants and soils, atmospheric deposition (including snow) and surface flows. Autochthonous

sources of DIN include detritus from algae, macrophytes and periphyton and nitrogen-fixing organisms (e.g., cyanobacteria) (Wetzel, 2001). Once DIN is delivered to the catchment, it may undergo several transformations. Compounds such as NH_4^+ and NO_3^- may be assimilated by biota (Talbot, 2001). While algae prefer to assimilate NH_4^+ , they usually take up NO_3^- due to its higher abundance (Hamilton, 2009). In anoxic waters, NH_4^+ will predominate, while in aerobic waters NO_3^- will be available in higher concentrations (Wetzel, 2001). In general, dissolved NO_3^- has a $\delta^{15}\text{N}$ ranging from +7 to +10 ‰ while atmospheric N has a $\delta^{15}\text{N}$ of 0 ‰ (Talbot, 2001; Teranes and Bernasconi, 2000).

Additional sources and transformations of nitrogen complicate this simple picture, however. For example, there is a fractionation of -27 to 0 ‰ associated with the assimilation of NH_4^+ or NO_3^- (Fogel and Cifuentes, 1993). If algae are assimilating NH_4^+ , the magnitude of the fractionation depends on whether assimilation occurs via enzyme-limited, diffusion-limited or nitrogen-limited transport (Fogel and Cifuentes, 1993). If algae are assimilating NO_3^- , the magnitude of the fractionation varies with concentration of NO_3^- in the water column (Fogel and Cifuentes, 1993). There is a negligible fractionation associated with the assimilation of atmospheric N_2 by nitrogen fixers, and so nitrogen fixers decrease the $\delta^{15}\text{N}$ of the sediment OM (Talbot, 1990). Assimilation also modifies $\delta^{15}\text{N}$ of DIN since photosynthetic organisms preferentially assimilate ^{14}N . If the DIN pool is limited, this kinetic fractionation will produce an increase in $\delta^{15}\text{N}$ of the DIN, which will be reflected in the $\delta^{15}\text{N}$ of the sediments (Fogel and Cifuentes, 1993).

Once DIN is assimilated, it may be lost from the system via sedimentation and burial, or recycled by microorganisms, which release the DIN in the form of NH_4^+ . This process, called *immobilization* or *ammonification*, does not fractionate DIN (Sharp, 2017). NH_4^+ generated by this process is quickly converted (in aerobic environments) to NO_2^- by the bacteria such as *Nitrosomonas* (Sharp, 2017). This process discriminates against ^{15}N by -29 to -18 ‰. The subsequent conversion of NO_2^- to NO_3^- by bacteria such as *Nitrobacter* is rapid and complete, and so has no associated fractionation (Sharp, 2017). This NO_3^- is taken up by biota via assimilation and the process repeats. As in the catchment, NO_3^- may be

converted to NO_2^- , N_2O and, finally, N_2 by denitrification (Sharp, 2017). As in the terrestrial system, the fractionation associated with denitrification is -40 to -5 ‰ (Sharp, 2017).

The $\delta^{15}\text{N}_{\text{TN}}$ of the sediment OM is vulnerable to microbial and oxidative degradation, which can change the $\delta^{15}\text{N}_{\text{TN}}$ of sediments after deposition, obscuring paleoenvironmental records (Gälman et al., 2009; Lehmann et al., 2002). Under aerobic conditions, nitrogen in the lake sediment is vulnerable to oxidation and to microbial reworking by aerobic bacteria (Lehmann et al., 2002). The $\delta^{15}\text{N}_{\text{TN}}$ of sediments typically experiences no net change over time under aerobic conditions (Lehmann et al., 2002). Under anaerobic conditions, nitrogen in the lake sediment is protected from oxidative degradation but is still vulnerable to reworking by anaerobic microbes (Lehmann et al., 2002). The $\delta^{15}\text{N}_{\text{TN}}$ of lake sediments is typically better preserved under anaerobic conditions than under aerobic conditions. Under anaerobic conditions, the $\delta^{15}\text{N}_{\text{TN}}$ typically decreases over time (Brahney et al., 2014).

1.2.5 Systematics of *n*-alkane chain lengths and isotopic compositions

While useful, the $\delta^{13}\text{C}_{\text{TOC}}$ and $\delta^{15}\text{N}_{\text{TN}}$ of the sediment OM are vulnerable to degradation. These proxies can also be difficult to interpret because they integrate signals from the terrestrial and aquatic environment. For this reason, many studies have shifted towards interpreting the isotopic compositions of individual compounds, such as *n*-alkanes, rather than all OM in the sediment. Interpreting the isotopic compositions of *n*-alkanes has two advantages: (i) they are more resistant to degradation than bulk OM and (ii) the chain lengths of *n*-alkanes are indicative of OM source (Meyers and Ishiwatari, 1993). The chain lengths of *n*-alkanes are interpreted as indicators of OM source but can also indicate whether the *n*-alkane has degraded (Carrizo et al., 2019). Carbon isotope ratios of *n*-alkanes ($\delta^{13}\text{C}_{n\text{-alkane}}$) extracted from the sediment OM have been used to reconstruct OM source, aridity and primary production (Diefendorf and Freimuth, 2017). Hydrogen isotope ratios of *n*-alkanes are typically used to reconstruct the hydrogen isotopic compositions of paleowater (Sachse et al., 2012).

1.2.5.1 Controls on *n*-alkane chain length

Since *n*-alkanes are produced via the decarboxylation of even-chained fatty acids, *n*-alkane distributions in fresh plants are almost always dominated by odd-chained *n*-alkanes (Bianchi and Canuel, 2011). Different functional groups reportedly produce characteristic *n*-alkane chain length distributions, with algae producing predominately C₁₇, C₁₉ and C₂₁; submergent macrophytes and mosses producing predominately C₂₃ and C₂₅; and emergent macrophytes and terrestrial plants producing mainly C₂₇, C₂₉ and C₃₁ (Ficken et al., 2000; Hockun et al., 2016; Street et al., 2013). A recent review of 2093 *n*-alkane measurements found that while terrestrial plant species cannot be distinguished by their *n*-alkane distributions, mosses can be distinguished from higher terrestrial plants using this technique (Bush and McInerney, 2013). This review also identified environmental factors that influence the distribution of chain lengths. While distributions do not change in response to canopy position or time of leaf collection (Bush and McInerney, 2013), they increase in response to aridity and temperature (Duan and He, 2011). Additional research is needed to better understand how *n*-alkane distributions change across spatial scales.

Several useful indices can be calculated using the relative abundances of individual *n*-alkanes. The average chain length (ACL), a weighted average of the abundance of each *n*-alkane, can be used to characterize OM sources. The equation for ACL is shown in Equation 1.7, where C_{*n*} is the concentration of each *n*-alkane with *n* carbon atoms (Bush and McInerney, 2013). Terrestrial organisms (*e.g.*, trees) typically exhibit higher ACL than aquatic organisms (*e.g.*, algae) (Bush and McInerney, 2013).

Equation 1.7

$$ACL = \sum (C_n \times n) / \sum (C_n)$$

The carbon preference index (CPI, Equation 1.8) is used to assess the odd to even predominance of *n*-alkanes. Samples with a CPI <1 are said to be degraded, while samples with a CPI >1 are said to be well-preserved. The formula for CPI used in this thesis is modified from the traditional formula (Marzi et al., 1993). The abundance of C₂₀ was not included in this equation since C₂₀ sometimes coeluted with the internal standard, 5 α -

androstane, used in the analytical protocol. C₂₀ was commonly also present in abundances too small to quantify.

Equation 1.8
$$\text{CPI} = 0.5 \left[\frac{(C_{17} + C_{19} + C_{21} + C_{23} + C_{25} + C_{27} + C_{29} + C_{31})}{(C_{18} + C_{22} + C_{24} + C_{26} + C_{28} + C_{30})} \right]$$

The P_{aq} index represents the ratio of short- to long-chain *n*-alkanes. As contributions of aquatic OM to the sediment rise, P_{aq} increases. Conversely, as contributions of terrestrial OM to the sediment rise, P_{aq} decreases. The original formula presented by Ficken et al. (2000) has been adjusted to reflect the *n*-alkanes examined in this thesis. This revised formula for P_{aq} is provided in Equation 1.9.

Equation 1.9
$$P_{\text{aq}} = \left[\frac{(C_{17} + C_{19})}{(C_{17} + C_{19} + C_{27} + C_{29} + C_{31})} \right]$$

1.2.5.2 Controls on the carbon isotopic compositions of *n*-alkanes extracted from plants and sediments

In this section, the controls of $\delta^{13}\text{C}_{n\text{-alkane}}$ are reviewed for C₃ plants. The controls on $\delta^{13}\text{C}_{n\text{-alkane}}$ are similar to those controlling $\delta^{13}\text{C}_{\text{TOC}}$ of bulk plant tissue; however, *n*-alkanes are also influenced by fractionations associated with their formation. Importantly, these biosynthetic fractionations are minimal compared to the fractionations associated with uptake and carboxylation of CO_{2atm} (Diefendorf and Freimuth, 2017). This section first considers: (i) factors controlling uptake and carboxylation of CO_{2atm}, and then (ii) biosynthetic fractionations associated with the synthesis of *n*-alkanes. Since *n*-alkanes are synthesized from the precursor molecules generated in step (i), they inherit signals associated with changes in environmental conditions that control delivery of CO₂ to sites of carboxylation as well as subtle source-specific differences in lipid biosynthesis (Freimuth et al., 2017).

1.2.5.3 Biosynthetic fractionations associated with *n*-alkane synthesis

Since the biosynthetic fractionations associated with lipid synthesis are small relative to the fractionations associated with the uptake and carboxylation of CO_{2atm}, shifts in $\delta^{13}\text{C}_{n\text{-alkane}}$

reflect changes in the plant's environment as well as more subtle differences between plant groups caused by heterogeneity in biochemical pathways (Diefendorf and Freimuth, 2017).

Once fixed into sugars by the Calvin Cycle, the carbon originating from CO_{2atm} is incorporated into plant waxes via the acetogenic pathway described above. Biosynthetic fractionations associated with the formation of $\delta^{13}\text{C}_{n\text{-alkane}}$ are commonly measured using ϵ_{bulk} notation, as shown in Equation 1.10.

Equation 1.10

$$\epsilon_{\text{bulk}} = 1000 \left[\frac{(\delta^{13}\text{C}_{n\text{-alkane}} + 1000)}{(\delta^{13}\text{C}_{\text{bulk}} + 1000)} - 1 \right]$$

whereby the $\delta^{13}\text{C}$ of the *n*-alkane of interest is compared to the $\delta^{13}\text{C}_{\text{TOC}}$ of the bulk leaf tissue (Chikaraishi and Naraoka, 2003; Diefendorf and Freimuth, 2017). According to a review of the literature by Diefendorf and Freimuth (2017), the average discrimination against ¹³C for the abundant C₂₉ *n*-alkane in C₃ plants is 5.2 ‰ for trees, 6.0 ‰ for graminoids, 7.3 ‰ for forbs and 7.4 ‰ for shrubs. These values have been shown to vary greatly, however, according to region (Freimuth et al., 2017). One proposed reason for this regional variation in biosynthetic fractionation is differences in carbon storage and allocation (Freeman and Pancost, 2013). The chain length of the *n*-alkane also exerts a control on $\delta^{13}\text{C}_{n\text{-alkane}}$; within the same plant shorter chain lengths (*e.g.*, C₁₉) are enriched in ¹³C relative to longer chain *n*-alkanes (*e.g.*, C₂₉) by as much as 8 ‰ (Hockun et al., 2016). It is not yet clear why this is the case.

1.2.5.4 Controls on $\delta^2\text{H}$ of *n*-alkanes in the terrestrial system

The ultimate source of hydrogen to terrestrial plants is meteoric water. Once meteoric water falls to the surface as precipitation, it can infiltrate the soil. The $\delta^2\text{H}$ of this soil water is usually higher than the $\delta^2\text{H}$ of local meteoric water due to evaporation (Thorburn et al., 1993). Plants with shallow rooting depths take up the soil water that has been most intensively evaporated. Consequently, they incorporate water with the highest $\delta^2\text{H}$ (Meinzer et al., 1999). The magnitude of this separation also varies with aridity (Sachse et al., 2006).

Plants take up soil water through their root systems without significantly changing the $\delta^2\text{H}$ of the water. Once in the roots, water is moved through the xylem to the leaves by capillary action and transpiration. While there is no fractionation associated with movement of the root water into the xylem (*i.e.*, the stem), the water becomes enriched in ^2H within the leaves (Thorburn et al., 1993). This behaviour occurs because the lighter isotopologues of water diffuse and evaporate in air faster than their heavier counterparts (*e.g.*, $^1\text{H}_2^{16}\text{O}$ versus $^1\text{H}^2\text{H}^{16}\text{O}$) (Thorburn et al., 1993). The extent of this enrichment depends on relative humidity, temperature and the isotopic composition of the water vapor surrounding the leaf (Evaristo et al., 2015; Sachse et al., 2012; Tang and Feng, 2001), but generally ranges between 20 to 80 ‰ (Leaney et al., 1985)

Since *n*-alkanes are synthesized in the leaves, their $\delta^2\text{H}$ originates from leaf water. Leaf water is water in the leaves of plants that is enriched in ^2H due to evaporation (Sessions et al., 1999). Thus, $\delta^2\text{H}_{n\text{-alkane}}$ is influenced by the processes discussed above. For example, in arid climates $\delta^2\text{H}_{n\text{-alkane}}$ should be higher than in wetter climates due to the stronger influence of evaporative enrichment on the $\delta^2\text{H}$ of soil water and transpiration (Sessions, 2016). Research has demonstrated that this relationship is not strong, however, because differences in water use efficiency between plant types and water conservation strategies (*e.g.*, closing stomata), can mitigate some of this enrichment (Liu et al., 2006).

Aside from the $\delta^2\text{H}$ of source water, the strongest control on $\delta^2\text{H}_{n\text{-alkane}}$ is biosynthetic pathway (Sachse et al., 2012). Lipids produced via the acetogenic pathway, the *n*-alkyl lipids (including *n*-alkanes), have the closest $\delta^2\text{H}$ to their source water (Sachse et al., 2012). During acetogenic biosynthesis, hydrogen undergoes exchange reactions, hydrogenations and dehydrogenations that change its $\delta^2\text{H}$ dramatically (Sessions et al., 1999). Fatty acids and alkenones, both produced in the acetogenic pathway, can differ up to 200 ‰ due to their varying degrees of saturation (Chikaraishi et al., 2004). The effect of each of these reactions on $\delta^2\text{H}$ of lipid precursors is not well understood. Acetogenic biosynthesis produces long C chains composed of H atoms inherited from acetate, NADPH and leaf water (Sachse et al., 2004). Next, acetyl-CoA units are added, forming a fatty acid.

This even-chained fatty acid is decarboxylated to form an odd-chained n -alkane (Sachse et al., 2004; Sessions et al., 1999).

Although n -alkanes are synthesized from leaf water that is enriched in ^2H relative to source water, the addition of NADPH ($\delta^2\text{H} = -200 \text{ ‰}$) lowers $\delta^2\text{H}_{n\text{-alkane}}$ so that, relative to source water, the n -alkane is depleted in ^2H (Sessions et al., 1999). It is not well understood where leaves obtain the NADPH used in lipid synthesis. It is hypothesized that differences in NADPH sources can explain the large intraspecies variability observed in different plant tissues throughout the year (Sachse et al., 2012). In plants, two processes are used to reduce NADP^+ to NADPH: (i) oxidation of sugars in the pentose-phosphate pathway in the cytosol, and (ii) reduction of NADP^+ via the electron transport chains associated with photosynthesis in the chloroplast (Heldt et al., 2005). When synthesizing heterotrophic tissues, such as buds, in the spring, plants may tend to draw on NADPH generated from the oxidation of sugars. After leaf emergence, NADPH may be drawn from an isotopically distinct compartment originating from the electron transport chain. These variations could explain why $\delta^2\text{H}_{n\text{-alkane}}$ is typically higher in the early spring than in late fall (Sessions et al., 1999)

Different groups of plants exhibit different “apparent fractionations”, or fractionations between source water and $\delta^2\text{H}_{n\text{-alkane}}$ (Sachse et al., 2012). The formula for this apparent fractionation (ϵ_{water}) is shown in Equation 1.11. A review of the literature by Sessions (2016) demonstrated that C_3 graminoids (grasses) usually have the highest separations between source water $\delta^2\text{H}$ and $\delta^2\text{H}_{n\text{-alkane}}$. Conversely, trees (particularly coniferous trees) and shrubs have the lowest separations between source water $\delta^2\text{H}$ and $\delta^2\text{H}_{n\text{-alkane}}$. The ϵ_{water} of shrubs falls between these two end-members (Sessions, 2016).

Equation 1.11

$$\epsilon_{\text{water}} = 1000 \left[\frac{(\delta^2\text{H}_{n\text{-alkane}} + 1000)}{(\delta^2\text{H}_{\text{source water}} + 1000)} - 1 \right]$$

1.2.5.5 Controls on $\delta^2\text{H}$ of n -alkanes in the aquatic system: macrophytes and algae

The $\delta^2\text{H}_{n\text{-alkane}}$ of macrophytes and algae is currently poorly understood but the subject of much active investigation. The main source of hydrogen to aquatic plants is lake water originating from meteoric water. The $\delta^2\text{H}_{n\text{-alkane}}$ of plants and algae is therefore influenced by latitude, altitude, temperature, seasonal and amount effects, as described for terrestrial plants, but is additionally affected by evaporation of the water basin. In an open lake system, the $\delta^2\text{H}$ of the lake water may differ little from the $\delta^2\text{H}$ of local precipitation (Sachse et al., 2006). In a closed lake system, in lake systems with long residence times, or in arid climates, evaporation can increase the separation between the $\delta^2\text{H}$ of the lake water and the $\delta^2\text{H}$ of precipitation (Sachse et al., 2006).

The fractionation associated with water diffusion across the membranes of algae and submerged macrophytes is small, but highly variable between species (Sachse et al., 2012). It is commonly assumed in the literature that the fractionation associated with hydrogen uptake by algae is 0 ‰, but recent research has demonstrated negative correlations between growth rate and $\delta^2\text{H}_{n\text{-alkane}}$, which are likely associated with an increased reliance on metabolic water (Sachse et al., 2012). Metabolic water is slightly enriched in ^2H relative to source water (Kreuzer-Martin et al., 2006). Salinity has also been shown to influence $\delta^2\text{H}_{n\text{-alkane}}$ (Sachse and Sachs, 2008), but such discussion extends beyond the scope of this paper. Once the source water has diffused into the cells of the algae/macrophyte, the acetogenic pathway proceeds as described above. The resulting n -alkanes have $\delta^2\text{H}$ that closely reflect source water and are in many cases isotopically distinct from terrestrial plants (Sachse et al., 2012; Sessions, 2016).

1.2.6 Differences in the isotope systematics of alpine and temperate lakes

The isotope systematics of alpine lakes differ from temperate lakes in ways that are not fully understood. The most obvious difference between alpine and temperate lakes is that alpine lakes tend to be less productive than temperate lakes (Catalan et al., 2006). This difference in primary productivity is reflected in the isotopic compositions of lake sediments. In temperate lakes, primary production can become so great that the demand for ^{12}C -rich DIC

by algae exceeds the availability of ^{12}C -rich DIC, causing the $\delta^{13}\text{C}_{\text{DIC}}$ and the $\delta^{13}\text{C}_{\text{TOC}}$ of the sediment OM to increase (Hollander and McKenzie, 1991). In oligotrophic alpine lakes, this pattern may not be observed if algae do not remove enough ^{12}C -rich DIC from the DIC pool. Instead, the $\delta^{13}\text{C}_{\text{TOC}}$ of oligotrophic systems may initially decrease during periods of high primary production as contributions of ^{12}C -rich algae to the sediment OM increase (Panizzo et al., 2008).

Interpretations of *n*-alkane abundances and isotopic compositions may also vary between low-elevation and alpine environments. At high elevations, many plants produce shorter chain lengths of *n*-alkanes than their low-elevation counterparts (Duan and He, 2011; Guo et al., 2016). It therefore cannot be assumed that a high-elevation plant will produce the same chain lengths of alkanes as a low-elevation plant. Likewise, it cannot be assumed that a high-elevation plant will have the same isotopic composition as a low-elevation plant. Increased elevation can increase the carbon isotope ratios of *n*-alkanes ($\delta^{13}\text{C}_{n\text{-alkane}}$) (Diefendorf and Freimuth, 2017) and decrease the hydrogen isotope ratios of *n*-alkanes ($\delta^2\text{H}_{n\text{-alkane}}$) (Sachse et al., 2012). Moreover, there is some evidence that carbon and hydrogen biosynthetic isotopic fractionations associated with *n*-alkane formation (ϵ_{water} and ϵ_{bulk} , respectively) are variable among environments (Freeman and Pancost, 2013; Liu and An, 2019).

1.3 Study Area

Barry Lake (44°18'28"N, 77°55'17"W) is a small, dimictic kettle lake located in southeastern Ontario, Canada, 32 km east of Peterborough, Ontario, and 40 km north of Lake Ontario (Figs. 1.2 and 1.3). Barry Lake, which has a bowl-like bathymetry, is ~7.6 m deep. The lake develops an anoxic hypolimnion in the summer months. It has two ephemeral inflows, probably derived from groundwater springs, and three ephemeral outflows. The area is characterized by hot, humid summers and cool, drier winters. The main water body is surrounded by swamp, and adjacent to the wetland is farmland. The surrounding vegetation is dominated by cedar and balsam fir. Floating (*e.g.*, *Nuphar* sp.), semi-emerged (*e.g.*, *Typha* sp.) and submerged (*e.g.*, *Chara* sp., *Potamogeton* sp.) macrophytes are abundant at Barry Lake.

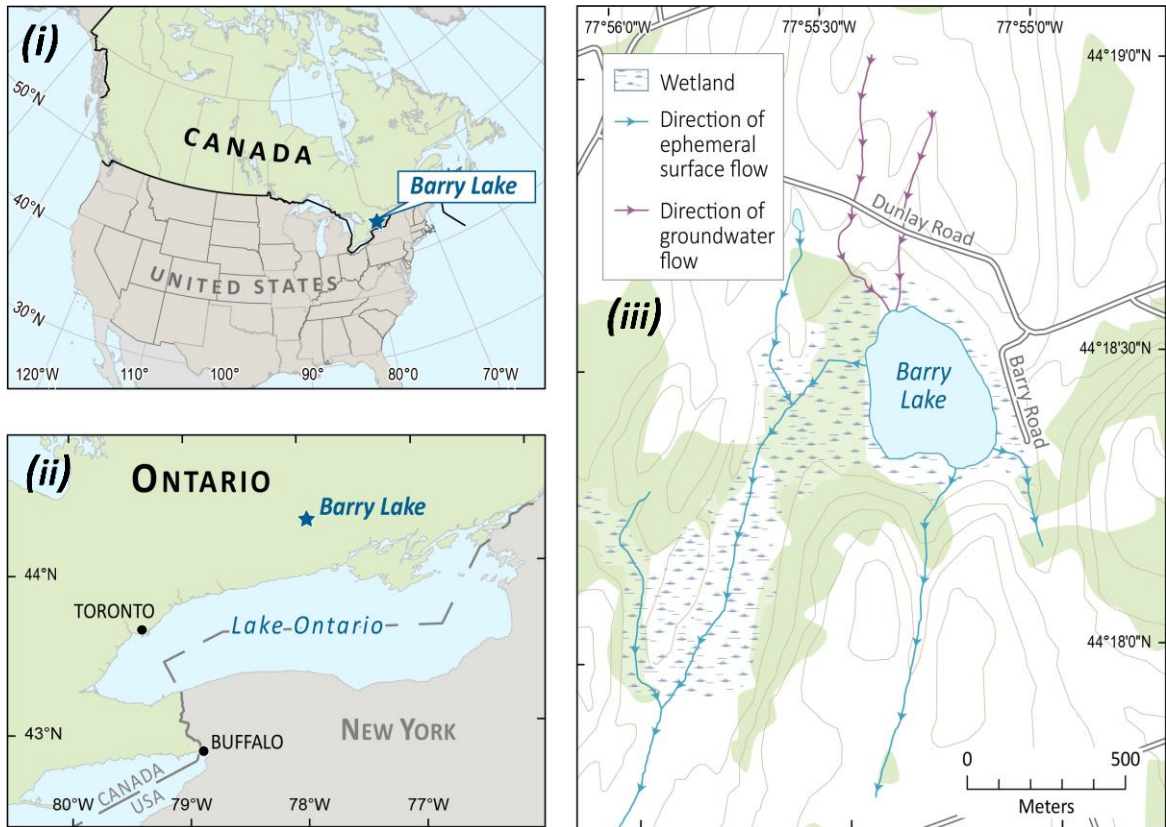


Figure 1.2 Maps of Barry Lake: (i) Location of Barry Lake within North America; (ii) Location of Barry Lake and other well-studied lakes in southern Ontario; (iii) Local hydrology in the vicinity of Barry Lake. The direction of surface flows is indicated by blue arrows, whereas the direction of groundwater is indicated by purple arrows. Figure produced by the Cartographic Section, Department of Geography and Environment, *The University of Western Ontario*, 2020.



Figure 1.3 Photographs of the five study sites: *(i)* Denise Lake, *(ii)* Taylor Lake, *(iii)* Upper Carrol Lake, *(iv)* East Carrol Lake and *(v)* Barry Lake. Photographs *(i)*, *(ii)*, *(iii)* and *(v)* were taken by R.M. Doyle, while photograph *(iv)* was taken by K.A. Moser.

The Uinta Mountains are an east-west trending mountain range that stretches from the northeastern part of Utah (40°-41° N, 109°-111° west) to northeastern Colorado (Figs. 1.3 and 1.4). The mountain range reaches elevations over 4000 m above sea level and contains hundreds of lakes with minimal exposure to direct human activity. The geology is primarily quartzite, sandstone and shale. Multiple glacial events in the Uinta Mountains have led to the formation of cirques, U-shaped valleys, and many glacial lakes (Munroe et al., 2007). There are two climate regimes in the Uinta Mountains: a summer wet/winter dry regime that impacts the eastern Uinta Mountains, and a summer dry/winter wet regime that dominates the western Uinta Mountains (MacDonald and Tingstad, 2007).

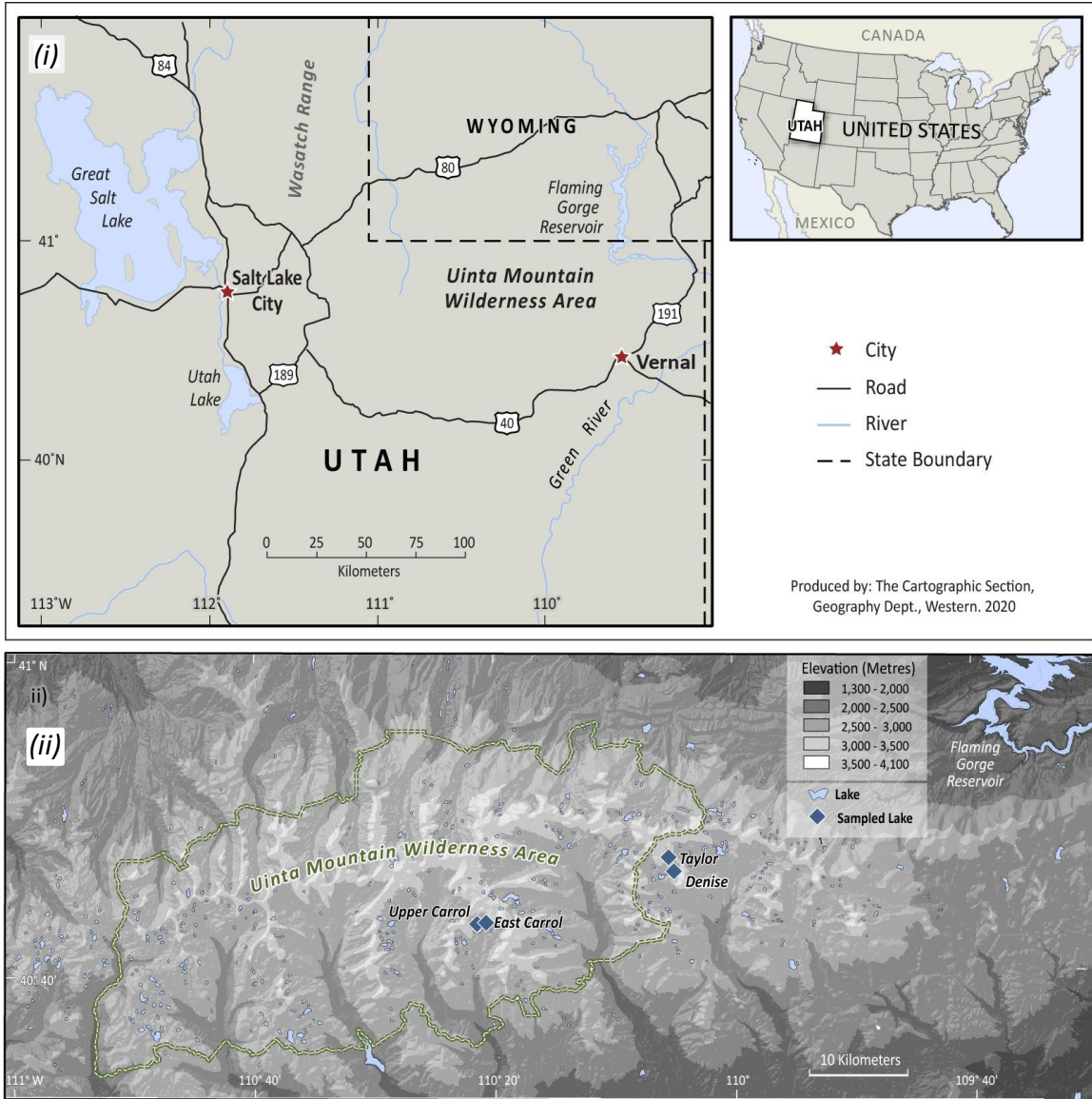


Figure 1.4 Map of northeastern Utah depicting *(i)* the location of Utah, and *(iii)* the location of Upper Carrol, East Carrol, Denise and Taylor lakes. Modified with permission from Hundey et al. (2014). Figure produced by the Cartographic Section, Department of Geography and Environment, The University of Western Ontario, 2020.

The following high elevation (> 3000 m.a.s.l.), oligotrophic lakes in the Uinta Mountains were selected as sampling locations: Denise Lake, Taylor Lake, Upper Carrol Lake, and East Carrol Lake (Fig. 1.3). These lakes were chosen from a 57-lake calibration set within the Uinta Mountains assembled by K.A. Moser. Lakes were selected to maximize variation in their catchment characteristics, including lake depth, lake to catchment area ratios, and vegetation coverage. Denise Lake and East Carrol Lake are shallow (2.4 m and 5.5 m, respectively) while Taylor Lake and Upper Carrol Lake are deeper (9.7 m and 13.8 m, respectively). Taylor and Upper Carrol lake experience thermal stratification and anoxia in the summer months; Denise and East Carrol lakes, however, do not stratify. The water columns of all four lakes are well-oxygenated throughout most of the year. Taylor and Upper Carrol lakes have permanent inflows, while Denise and East Carrol lakes have intermittent inflows. The dominant tree species at these sites is Engelmann spruce (*Picea engelmanni*), which adopts a krummholz formation at high altitudes, meaning that its growth is stunted by continual exposure to fierce, freezing winds. Other common species at these high elevation sites include the sedge *Carex aquatilis*; the prostrate shrubs *Betula glandulosa*, *Salix glauca* and *Salix plantifolia*; and various species of mosses and lichen.

1.4 Structure of the dissertation and research questions

This thesis is divided into introductory and concluding chapters (1 and 6, respectively) and four main chapters (2 to 5). Seven appendices are provided at the end of the thesis. These appendices supply supplementary information, including datasheets, technical memoranda, R codes for some types of analyses and permissions for reusing material from published manuscripts.

Chapter 2 uses stable isotope science to investigate the relationship between effective moisture and primary production at Barry Lake. Variations in effective moisture are reconstructed using $\delta^{18}\text{O}_{\text{marl}}$, $\delta^{13}\text{C}_{\text{marl}}$ and $\delta^{13}\text{C}_{\text{TOC}}$. Shifts in primary production are identified by measuring the mass accumulation rates of total organic carbon (TOC-MAR), total nitrogen (TN-MAR), calcite (calcite-MAR) and sedimentary chlorophyll-*a* (Chl-*a*_(s)-MAR). The nitrogen dynamics of Barry Lake are reconstructed using $\delta^{15}\text{N}_{\text{TN}}$. The overarching goal of this chapter is to ascertain the relationship between primary production and effective

moisture at Barry Lake across the last ~900 years, and to provide knowledge necessary to predict how primary production will change in small lakes located across Ontario, Quebec, Michigan and Minnesota. First, trends in effective moisture and primary production are reconstructed at Barry Lake across the MCA, LIA and modern periods. Then, it is determined whether changes in effective moisture are driving shifts in primary production. Lastly, the $\delta^{18}\text{O}_{\text{marl}}$ record from Barry Lake is compared with other hydroclimatic records from the region to assess whether Barry Lake is recording local or regional hydroclimatic signals. The first research question of this thesis is therefore as follows:

(1) What is the relationship between effective moisture and primary production at Barry Lake, and how have these variables changed across the last 900 years?

Chapter 3 focuses on reconstructing sources of OM to Barry Lake and microbial abundances in Barry Lake. Sources of OM are reconstructed using *n*-alkane abundances and $\delta^{13}\text{C}_{n\text{-alkane}}$. Variations in $\delta^2\text{H}_{\text{C}17}$ are used to substantiate the record of effective moisture generated using $\delta^{18}\text{O}_{\text{marl}}$, $\delta^{13}\text{C}_{\text{marl}}$ and $\delta^{13}\text{C}_{\text{TOC}}$. Microbial abundances are reconstructed using the following proxies: (i) the mass accumulation rates of diploptene (diploptene-MAR), a biomarker produced by methane oxidizing bacteria (MOB); (ii) the fractionation between $\delta^{13}\text{C}_{\text{marl}}$ and $\delta^{13}\text{C}_{\text{TOC}}$ ($\epsilon_{\text{marl-TOC}}$), an indicator of the abundance of chemoautotrophic bacteria; (iii) mass accumulation rates of lupan-3-one, an indicator of terrigenous degradation by microbes; and (iv) the mass accumulation rate of the *n*-alkane C_{18} , a broad indicator of microbial abundances. The goal of this chapter is to contextualize recent changes in the carbon dynamics of Barry Lake against a backdrop of natural variability, and to predict how these dynamics will change in future years. First, this chapter assesses how OM source and microbial abundances change across the MCA, LIA and the modern period. Next, it investigates the factors controlling microbial abundances at Barry Lake and postulate how such abundances may change in future years as ACW intensifies. The second research question of this thesis is therefore as follows:

(2) How have the carbon dynamics, and microbial abundances, of Barry Lake changed in the modern period relative to the MCA and LIA, and how might the carbon dynamics of Barry Lake change in future years?

Chapter 4 focuses on establishing a baseline of $\delta^{13}\text{C}_{\text{TOC}}$, $\delta^{15}\text{N}_{\text{TN}}$, $\delta^{13}\text{C}_{n\text{-alkane}}$, $\delta^2\text{H}_{n\text{-alkane}}$, ϵ_{bulk} and ϵ_{water} for modern sources of OM to Uinta Mountain lake sediments. The goal of this chapter is to improve current interpretations of limnological proxies by investigating how changes in OM source alter the isotopic compositions and *n*-alkane characteristics of alpine lake sediments. First, this chapter determines which proxies of OM source are most effective for reconstructing OM sources present in alpine lake sediments. Next, it investigates the environmental and phylogenetic controls on ϵ_{bulk} ¹ and ϵ_{water} ² in the Uinta Mountains. Finally, this chapter outlines several ways in which interpretations of these proxies differ in alpine regions relative to low-elevation, temperate lakes. The third research question of this thesis is therefore as follows:

(3) How do the isotopic compositions and *n*-alkane characteristics of modern vegetation surrounding Uinta Mountain lakes differ from temperate, low-elevation lakes and how do these differences affect one's ability to infer changes in OM source from proxies in alpine lake sediments?

Chapter 5 synthesizes results from the previous chapters by comparing the carbon and nitrogen isotope systematics of Barry Lake with the Uinta Mountain lakes. The goal of this chapter is to explore how interpretations of $\delta^{13}\text{C}_{\text{TOC}}$ and $\delta^{15}\text{N}_{\text{TN}}$ might differ between low-elevation, temperate lakes and alpine lakes. This chapter first compares the $\delta^{13}\text{C}_{\text{TOC}}$ and $\delta^{15}\text{N}_{\text{TN}}$ of modern vegetation around the Uinta Mountains and Barry Lake, and discusses how reconstructions of OM source differ between the two systems. Then, the degradation regimes of the two groups of lakes are compared to assess the relative preservation of

¹ ϵ_{bulk} is the carbon isotope fractionation between an *n*-alkane and bulk leaf tissue.

² ϵ_{water} is the hydrogen isotope fractionation between an *n*-alkane and its source water.

$\delta^{13}\text{C}_{\text{TOC}}$ and $\delta^{15}\text{N}_{\text{TN}}$ in both sets of lakes. Finally, this chapter compares variations in primary production in the two sites. The fourth research question of this thesis is therefore as follows:

(4) How do the carbon and nitrogen systematics of the sediment OM, and its sources, differ in Barry Lake compared with the Uinta Mountain lakes?

1.5 References

- Aggarwal, P., Romatschke, U., Araguas-Araguas, L., Belachew, D., Longstaffe, F.J., Berg, P., Schumacher, C., Funk, A., 2016. Proportions of convective and stratiform precipitation revealed in water isotope ratios. *Nat. Geosci.* 8, 624–629. <https://doi.org/10.1038/ngeo2739>
- Arens, C.N., Jahren, H. A., Amundson, R., 2000. Can C3 plants faithfully record the carbon isotopic composition of atmospheric carbon dioxide? *Paleobiol.* 26, 137–164. [https://doi.org/10.1666/0094-8373\(2000\)026<0137:CCPFRT>2.0.CO;2](https://doi.org/10.1666/0094-8373(2000)026<0137:CCPFRT>2.0.CO;2)
- Austin, A.T., Vitousek, P.M., 1998. Nutrient dynamics on a precipitation gradient in Hawai'i. *Oecologia* 113, 519–529. <https://doi.org/10.1007/s004420050405>
- Badger, M.R., Price, G.D., 2003. CO₂ concentrating mechanisms in cyanobacteria: Molecular components, their diversity and evolution. *J. Exp. Bot.* 54, 609–622. <https://doi.org/10.1093/jxb/erg076>
- Bastviken, D., Cole, J., Pace, M., Tranvik, L., 2004. Methane emissions from lakes: Dependence of lake characteristics, two regional assessments, and a global estimate. *Global Biogeochem. Cycles* 18, 1–12. <https://doi.org/10.1029/2004GB002238>
- Bianchi, T.S., Canuel, E.A., 2011. *Chemical Biomarkers in Aquatic Ecosystems*, first ed. Princeton University Press, Princeton, United States, pp. 185–206. <https://doi.org/10.1515/9781400839100>

- Borrel, G., Jézéquel, D., Biderre-Petit, C., Morel-Desrosiers, N., Morel, J.P., Peyret, P., Fonty, G., Lehours, A.C., 2011. Production and consumption of methane in freshwater lake ecosystems. *Res. Microbiol.* 162, 832–847.
<https://doi.org/10.1016/j.resmic.2011.06.004>
- Brahney, J., Ballantyne, A.P., Turner, B.L., Spaulding, S.A., Otu, M., Neff, J.C., 2014. Separating the influences of diagenesis, productivity and anthropogenic nitrogen deposition on sedimentary $\delta^{15}\text{N}$ variations. *Org. Geochem.* 75, 140–150.
<https://doi.org/10.1016/j.orggeochem.2014.07.003>
- Bush, R.T., McInerney, F.A., 2013. Leaf wax *n*-alkane distributions in and across modern plants: Implications for paleoecology and chemotaxonomy. *Geochim. Cosmochim. Acta* 117, 161–179. <https://doi.org/10.1016/j.gca.2013.04.016>
- Carrizo, D., Sánchez-García, L., Menes, R.J., García-Rodríguez, F., 2019. Discriminating sources and preservation of organic matter in surface sediments from five Antarctic lakes in the Fildes Peninsula (King George Island) by lipid biomarkers and compound specific isotopic analysis. *Sci. Total Environ.* 672, 657–668.
<https://doi.org/10.1016/j.scitotenv.2019.03.459>
- Castaneda, I.S., Werne, J.P., Johnson, T.C., 2009. Influence of climate change on algal community structure and primary productivity of Lake Malawi (East Africa) from the Last Glacial Maximum to present. *Limnol. Oceanogr.* 54, 2431–2447.
https://doi.org/10.4319/lo.2009.54.6_part_2.2431
- Catalan, J., Camarero, L., Felip, M., Pla, S., Ventura, M., Buchaca, T., Bartumeus, F., De Mendoza, G., Miró, A., Casamayor, E.O., Medina-Sánchez, J.M., Bacardit, M., Altuna, M., Bartrons, M., De Quijano, D.D., 2006. High mountain lakes: Extreme habitats and witnesses of environmental changes. *Limnetica* 25, 551–584.
<https://doi.org/10.23818/limn.25.38>
- Chevalier, N., Savoye, N., Dubois, S., Lama, M.L., David, V., Lecroart, P., Le Ménach, K., Budzinski, H., 2015. Precise indices based on *n*-alkane distribution for quantifying

- sources of sedimentary organic matter in coastal systems. *Org. Geochem.* 88, 69–77.
<https://doi.org/10.1016/j.orggeochem.2015.07.006>
- Chikaraishi, Y., Naraoka, H., 2003. Compound-specific D–C analyses of *n*-alkanes extracted from terrestrial and aquatic plants. *Phytochemistry* 63, 361–371.
[https://doi.org/10.1016/S0031-9422\(02\)00749-5](https://doi.org/10.1016/S0031-9422(02)00749-5)
- Chikaraishi, Y., Suzuki, Y., Naraoka, H., 2004. Hydrogen isotopic fractionations during desaturation and elongation associated with polyunsaturated fatty acid biosynthesis in marine macroalgae. *Phytochemistry* 65, 2293–2300.
<https://doi.org/10.1016/j.phytochem.2004.06.030>
- Cloern, J.E., Canuel, E.A., Harris, D., 2002. Stable carbon and nitrogen isotope composition of aquatic and terrestrial plants of the San Francisco Bay estuarine system. *Limnol. Oceanogr.* 47, 713–729. <https://doi.org/10.4319/lo.2002.47.3.0713>
- Colcord, D.E., Cadieux, S.B., Brassell, S.C., Castañeda, I.S., Pratt, L.M., White, J.R., 2015. Assessment of branched GDGTs as temperature proxies in sedimentary records from several small lakes in southwestern Greenland. *Org. Geochem.* 82, 33–41.
<https://doi.org/10.1016/j.orggeochem.2015.02.005>
- Cole, M.L., Kroeger, K.D., McClelland, J.W., Valiela, I., 2006. Effects of watershed land use on nitrogen concentrations and $\delta^{15}\text{N}$ in groundwater. *Biogeochem.* 77, 199–215.
<https://doi.org/10.1007/s10533-005-1036-2>
- Coniglio, M., Williams-Jones, A.E., 1992. Diagenesis of Ordovician carbonates from the north east Michigan Basin, Manitoulin Island area, Ontario: evidence from petrography, stable isotopes and fluid inclusions. *Sedimentology* 39, 813–836.
<https://doi.org/10.1111/j.1365-3091.1992.tb02155.x>
- Coplen, T.B., 2011. Guidelines and recommended terms for expression of stable-isotope ratio and gas-ratio measurement results. *Rapid Commun. Mass Spectrom.* 25, 2538–2560. <https://doi.org/10.1002/rcm.5129>

- Coplen, T.B., 1996. New guidelines for reporting stable hydrogen, carbon, and oxygen isotope ratio data. *Geochim. Cosmochim. Acta* 60, 3359–3360.
[https://doi.org/10.1016/00167037\(96\)00263-3](https://doi.org/10.1016/00167037(96)00263-3)
- Craig, H., 1965. The measurement of oxygen isotope paleotemperatures, in: Tongiorgi, E. (Ed.), *Stable Isotopes in Oceanographic Studies and Paleotemperatures*. Consiglio Nazionale delle Ricerche, Laboratorio de Geologia Nuclare, Pisa, 161–182.
- Craig, H., 1961. Isotopic variations in meteoric waters. *Science* 133, 1702–1703.
<https://doi.org/10.1126/science.133.3465.1702>
- Craine, J.M., Elmore, A.J., Aidar, M.P.M., Bustamante, M., Dawson, T.E., Hobbie, E.A., Kahmen, A., Mac, M.C., McLauchlan, K.K., Michelsen, A., Nardoto, G.B., Pardo, L.H., Peñuelas, J., Reich, P.B., Schuur, E.A.G., Stock, W.D., Templer, P.H., Virginia, R.A., Welker, J.M., Wright, I.J., 2009. Global patterns of foliar nitrogen isotopes and their relationships with climate, mycorrhizal fungi, foliar nutrient concentrations, and nitrogen availability. *New Phytol.* 183, 980–992.
<https://doi.org/10.1111/j.1469-8137.2009.02917.x>
- Dansgaard, W., 1964. Stable isotopes in precipitation. *Tellus* 16, 436–468.
<https://doi.org/10.3402/tellusa.v16i4.8993>
- Diefendorf, A.F., Freimuth, E.J., 2017. Extracting the most from terrestrial plant-derived *n* alkyl lipids and their carbon isotopes from the sedimentary record: A review. *Org. Geochem.* 103, 1–21. <https://doi.org/10.1016/j.orggeochem.2016.10.016>
- Diefendorf, A.F., Patterson, W.P., Holmden, C., Mullins, H.T., 2008. Carbon isotopes of marl and lake sediment organic matter reflect terrestrial landscape change during the late Glacial and early Holocene (16,800 to 5,540 cal yr B.P.): A multiproxy study of lacustrine sediments at Lough Inchiquin, western Ireland. *J. Paleolimnol.* 39, 101–115. <https://doi.org/10.1007/s10933-007-9099-9>

- Dörnhöfer, K., Klinger, P., Heege, T., Oppelt, N., 2018. Multi-sensor satellite and in situ monitoring of phytoplankton development in a eutrophic-mesotrophic lake. *Sci. Total Environ.* 612, 1200–1214. <https://doi.org/10.1016/j.scitotenv.2017.08.219>
- Drummond, C.N., Patterson, W.P., Walker, J.C.G., 1995. Climatic forcing of carbon-oxygen isotopic covariance in temperate-region marl lakes. *Geology* 23, 1031–1034. [https://doi.org/10.1130/0091-7613\(1995\)023<1031:cfocoi>2.3.co;2](https://doi.org/10.1130/0091-7613(1995)023<1031:cfocoi>2.3.co;2)
- Duan, Y., He, J., 2011. Distribution and isotopic composition of *n*-alkanes from grass, reed and tree leaves along a latitudinal gradient in China. *Geochem. J.* 45, 199–207. <https://doi.org/10.2343/geochemj.1.0115>
- Eide, M., Olsen, A., Ninnemann, U.S., Eldevik, T., 2017. A global estimate of the full oceanic ¹³C Suess effect since the preindustrial. *Global Biogeochem. Cycles* 31, 492–514. <https://doi.org/10.1002/2016GB005472>
- Evaristo, J., Jasechko, S., McDonnell, J.J., 2015. Global separation of plant transpiration from groundwater and streamflow. *Nature* 525, 91–93. <https://doi.org/10.1038/nature14983>
- Farquhar, G., O’Leary, M., Berry, J., 1982. On the relationship between carbon isotope discrimination and the intercellular carbon dioxide concentration in leaves. *Aust. J. Plant Physiol.* 9, 121–137. <https://doi.org/10.1071/PP9820121>
- Farquhar, G.D., Ehleringer, J.R., Hubick, K.T., 1989. Carbon isotope discrimination and photosynthesis. *Annu. Rev. Plant Physiol. Plant Mol. Biol.* 40, 503–537. <https://doi.org/10.1146/annurev.pp.40.060189.002443>
- Farquhar, G.D., Lloyd, J., 1993. Carbon and oxygen isotope effects in the exchange of carbon dioxide between terrestrial plants and the atmosphere, in: Ehleringer, J.R., Hall, A.E., Farquhar, G.D. (Eds.), *Stable Isotopes and Plant-Carbon-Water Relations*, first ed. Elsevier Inc., Amsterdam, Netherlands, pp. 47–70. <https://doi.org/10.1016/C2009-0-03312-1>

- Fenn, M.E., Haeuber, R., Tonnesen, G.S., Baron, J.S., Grossman-Clarke, S., Hope, D., Jaffe, D.A., Copeland, S., Geiser, L., Rueth, H.M., Sickman, J.O., 2003. Nitrogen emissions, deposition, and monitoring in the western United States. *Bioscience* 53, 391–403. [https://doi.org/10.1641/0006-3568\(2003\)053\[0391:NEDAMI\]2.0.CO;2](https://doi.org/10.1641/0006-3568(2003)053[0391:NEDAMI]2.0.CO;2)
- Ficken, K.J., Li, B., Swain, D.L., Eglinton, G., 2000. An *n*-alkane proxy for the sedimentary input of submerged/floating freshwater aquatic macrophytes. *Org. Geochem.* 31, 745–749. [https://doi.org/10.1016/S0146-6380\(00\)00081-4](https://doi.org/10.1016/S0146-6380(00)00081-4)
- Finlay, J.C., Kendall, C., 2007. Stable isotope tracing of temporal and spatial variability in organic matter sources to freshwater ecosystems, in: Michener, R., Lajtha, K., *Stable Isotopes in Ecology and Environmental Science*, second ed. Blackwell Publishing Ltd, Hoboken, United States, pp. 283–333. <https://doi.org/10.1002/9780470691854.ch10>
- Fogel, M.L., Cifuentes, L.A., 1993. Isotope fractionation during primary production, in: Eglinton, G., Murphy, M.T.J. (Eds.) *Organic Geochemistry*, first ed. Springer US, New York City, United States, pp. 73–94. https://doi.org/10.1007/978-1-4615-2890-6_3
- Freeman, K.H., Pancost, R.D., 2013. Biomarkers for terrestrial plants and climate, in: Turekian, K., Holland, H. (Eds.), *Treatise on Geochemistry*, second ed. Elsevier Inc., Amsterdam, Netherlands, pp. 395–416.
- Freimuth, E.J., Diefendorf, A.F., Lowell, T. V., 2017. Hydrogen isotopes of *n*-alkanes and *n* alkanolic acids as tracers of precipitation in a temperate forest and implications for paleorecords. *Geochim. Cosmochim. Acta* 206, 166–183. <https://doi.org/10.1016/j.gca.2017.02.027>
- Fritz, P., Clark, I.D., 1997. *Environmental Isotopes in Hydrogeology*, first ed. Lewis Publishers, New York, United States.

- Fritz, P., Poplawski, S., 1974. ^{18}O and ^{13}C in the shells of freshwater molluscs and their environments. *Earth Planet. Sci. Lett.* 24, 91–98. [https://doi.org/10.1016/0012-821X\(74\)90012-0](https://doi.org/10.1016/0012-821X(74)90012-0)
- Gälman, V., Rydberg, J., Bigler, C., 2009. Decadal diagenetic effects on $\delta^{13}\text{C}$ and $\delta^{15}\text{N}$ studied in varved lake sediment. *Limnol. Oceanogr.* 54, 917–924. <https://doi.org/10.4319/lo.2009.54.3.0917>
- Gat, J.R., 1996. Oxygen and hydrogen isotopes in the hydrologic cycle. *Annu. Rev. Earth Planet. Sci.* 24, 225–262. <https://doi.org/10.1146/annurev.earth.24.1.225>
- Guo, N., Gao, J., He, Y., Guo, Y., 2016. Compositae plants differed in leaf cuticular waxes between high and low altitudes. *Chem. Biodivers.* 13, 710–718. <https://doi.org/10.1002/cbdv.201500208>
- Hamilton, S.K., 2009. *Stable isotopes in ecology and environmental science*, second ed. Blackwell Publishing. Malden, MA, USA. <https://doi.org/10.1899/0887-3593028.002.0516>
- Hammarlund, D., Aravena, R., Barnekow, L., Buchardt, B., Possnert, G., 1997. Multi component carbon isotope evidence of early Holocene environmental change and carbon-flow pathways from a hard-water lake in northern Sweden. *J. Paleolimnol.* 18, 219–233. <https://doi.org/10.1023/A:1007953614927>
- Heaton, T.H.E., Spiro, B., Robertson, S.M.C., 1997. Potential canopy influences on the isotopic composition of nitrogen and sulphur in atmospheric deposition. *Oecologia* 109, 600–607. <https://doi.org/10.1007/s004420050122>
- Heldt, H.W., Piechulla, B., Heldt, F., 2005. *Plant Biochemistry*, third ed. Elsevier Inc., Amsterdam, Netherlands. <https://doi.org/10.1016/B978-0-12-088391-2.X5000-7>
- Henderson, A.K., Shuman, B.N., 2009. Hydrogen and oxygen isotopic compositions of lake water in the western United States. *Bull. Geol. Soc. Am.* 121, 1179–1189. <https://doi.org/10.1130/B26441.1>

- Hladyniuk, R., Longstaffe, F.J., 2016. Oxygen-isotope variations in post-glacial Lake Ontario. *Quat. Sci. Rev.* 134, 39–50. <https://doi.org/10.1016/J.QUASCIREV.2016.01.002>
- Hladyniuk, R., Longstaffe, F.J., 2015. Paleoproductivity and organic matter sources in Late Quaternary Lake Ontario. *Palaeogeogr. Palaeoclimatol. Palaeoecol.* 435, 13–23. <https://doi.org/10.1016/j.palaeo.2015.05.026>
- Hockun, K., Mollenhauer, G., Ho, S.L., Hefter, J., Ohlendorf, C., Zolitschka, B., Mayr, C., Lücke, A., Schefuß, E., 2016. Using distributions and stable isotopes of *n*-alkanes to disentangle organic matter contributions to sediments of Laguna Potrok Aike, Argentina. *Org. Geochem.* 102, 110–119. <https://doi.org/10.1016/j.orggeochem.2016.10.001>
- Hollander, D.J., McKenzie, J.A., 1991. CO₂ control on carbon-isotope fractionation during aqueous photosynthesis: A paleo-*p*CO₂ barometer. *Geology* 19, 929–932. [https://doi.org/10.1130/0091-7613\(1991\)019<0929:CCOCIF>2.3.CO;2](https://doi.org/10.1130/0091-7613(1991)019<0929:CCOCIF>2.3.CO;2)
- Hornibrook, E.R.C., Longstaffe, F.J., Fyfe, W.S., 2000. Evolution of stable carbon isotope compositions for methane and carbon dioxide in freshwater wetlands and other anaerobic environments. *Geochim. Cosmochim. Acta* 64, 1013–1027. [https://doi.org/10.1016/S0016-7037\(99\)00321-X](https://doi.org/10.1016/S0016-7037(99)00321-X)
- Huiskes, A.H.L., Boschker, H.T.S., Lud, D., Moerdijk-Poortvliet, T.C.W., 2007. Stable isotope ratios as a tool for assessing changes in carbon and nutrient sources in Antarctic terrestrial ecosystems, in: Rozema, J., Aerts, R., Cornelissen, H. (Eds.), *Plants and Climate Change*. Springer Netherlands, Amsterdam, Netherlands, pp. 79–88. https://doi.org/10.1007/978-1-4020-4443-4_6
- Hundey, E.J., Moser, K.A., Longstaffe, F.J., Michelutti, N., Hladyniuk, R., 2014. Recent changes in production in oligotrophic Uinta Mountain lakes, Utah, identified using paleolimnology. *Limnol. Oceanogr.* 59, 1987–2001. <https://doi.org/10.4319/lo.2014.59.6.1987>

- Hyodo, A., Longstaffe, F.J., 2011. The palaeoproductivity of ancient Lake Superior. *Quat. Sci. Rev.* 30, 2988–3000. <https://doi.org/10.1016/J.QUASCIREV.2011.07.004>
- Jacobsen, D., Dangles, O., 2017. *Ecology of High-Altitude Waters*, first ed. Oxford University Press, New York, NY.
- Keeling, C.D., 1979. The Suess effect: ¹³Carbon-¹⁴Carbon interrelations. *Environ. Int.* 2, 229–300. [https://doi.org/10.1016/0160-4120\(79\)90005-9](https://doi.org/10.1016/0160-4120(79)90005-9)
- Keeling, C.D., Bacastow, R.B., Carter, A.F., Piper, S.C., Whorf, T.P., Heimann, M., Mook, W.G., Roeloffzen, H., 1989. A three-dimensional model of atmospheric CO₂ transport based on observed winds: 1. Analysis of observational data., in: Peterson, D.H. (Ed.), *Aspects of Climate Variability in the Pacific and the Western Americas*. American Geophysical Union, Washington, United States, pp. 165–236.
- Kendall, C., 1998. Tracing nitrogen sources and cycling in catchments, in: McDonnell, J.J., Kendall, C. (Eds.), *Isotope Tracers in Catchment Hydrology*, first ed. Elsevier Science, Philadelphia, United States, pp. 519–576.
<https://doi.org/10.1016/B978-0-444-81546-0.50023-9>
- Kreuzer-Martin, H.W., Lott, M.J., Ehleringer, J.R., Hegg, E.L., 2006. Metabolic processes account for the majority of the intracellular water in log-phase *Escherichia coli* cells as revealed by hydrogen isotopes. *Biochemistry* 45, 13622–13630.
<https://doi.org/10.1021/bi0609164>
- Lange, O.L., Green, T.G.A., Ziegler, H., 1988. Water status related photosynthesis and carbon isotope discrimination in species of the lichen genus *Pseudocyphellaria* with green or blue-green photobionts and in photosymbiodemes. *Oecologia* 75, 494–501.
<https://doi.org/10.1007/BF00776410>
- Leaney, F.W., Osmond, C.B., Allison, G.B., Ziegler, H., 1985. Hydrogen-isotope composition of leaf water in C₃ and C₄ plants: its relationship to the hydrogen-isotope

- composition of dry matter. *Planta* 164, 215–220.
<https://doi.org/10.1007/BF00396084>
- Lee, Y. Il, Lim, H.S., Yoon, H. Il, 2009. Carbon and nitrogen isotope composition of vegetation on King George Island, maritime Antarctic. *Polar Biol.* 32, 1607–1615.
<https://doi.org/10.1007/s00300-009-0659-5>
- Lehmann, M.F., Bernasconi, S.M., Barbieri, A., Mckenzie, J.A., 2002. Preservation of organic matter and alteration of its carbon and nitrogen isotope composition during simulated and in situ early sedimentary diagenesis. *Geochim. Cosmochim. Acta* 66, 3573–3584. [https://doi.org/10.1016/S0016-7037\(02\)00968-7](https://doi.org/10.1016/S0016-7037(02)00968-7)
- Li, H.C., Ku, T.L., 1997. $\delta^{13}\text{C}$ - $\delta^{18}\text{O}$ covariance as a paleohydrological indicator for closed basin lakes. *Palaeogr. Palaeoclimatol. Palaeoecol.* 133, 69–80.
[https://doi.org/10.1016/S0031-0182\(96\)00153-8](https://doi.org/10.1016/S0031-0182(96)00153-8)
- Liu, J., An, Z., 2019. Variations in hydrogen isotopic fractionation in higher plants and sediments across different latitudes: Implications for paleohydrological reconstruction. *Sci. Total Environ.* 650, 470–478.
<https://doi.org/10.1016/j.scitotenv.2018.09.047>
- Liu, W., Yang, H., Li, L., 2006. Hydrogen isotopic compositions of *n*-alkanes from terrestrial plants correlate with their ecological life forms. *Oecologia* 150, 330–338.
<https://doi.org/10.1007/s00442-006-0494-0>
- Macdonald, G.M., Tingstad, A.H., 2007. Recent and multicentennial precipitation variability and drought occurrence in the Uinta Mountains region, Utah. *Arct. Antarct. Alp. Res.* 39, 549–555. [https://doi.org/10.1657/1523-0430\(06-070\)](https://doi.org/10.1657/1523-0430(06-070))
- Mariotti, A., 1983. Atmospheric nitrogen is a reliable standard for natural ^{15}N abundance measurements. *Nature* 303, 685–687. <https://doi.org/10.1038/303685a0>
- Marzi, R., Torkelson, B.E., Olson, R.K., 1993. A revised carbon preference index. *Org. Geochem.* 20, 1303–1306. [https://doi.org/10.1016/0146-6380\(93\)90016-5](https://doi.org/10.1016/0146-6380(93)90016-5)

- McConnaughey, T., 1991. Calcification in *Chara corallina*: CO₂ hydroxylation generates protons for bicarbonate assimilation. *Limnol. Oceanogr.* 36, 619–628.
<https://doi.org/10.4319/lo.1991.36.4.0619>
- McConnaughey, T., 1989a. ¹³C and ¹⁸O isotopic disequilibrium in biological carbonates: I. Patterns. *Geochim. Cosmochim. Acta* 53, 151–162. [https://doi.org/10.1016/0016-7037\(89\)90282-2](https://doi.org/10.1016/0016-7037(89)90282-2)
- McConnaughey, T., 1989b. ¹³C and ¹⁸O isotopic disequilibrium in biological carbonates: II. In vitro simulation of kinetic isotope effects. *Geochim. Cosmochim. Acta* 53, 151–162.
[https://doi.org/10.1016/0016-7037\(89\)90282-2](https://doi.org/10.1016/0016-7037(89)90282-2)
- McConnaughey, T.A., Burdett, J., Whelan, J.F., Paull, C.K., 1997. Carbon isotopes in biological carbonates: Respiration and photosynthesis. *Geochim. Cosmochim. Acta* 61, 611–622. [https://doi.org/10.1016/S0016-7037\(96\)00361-4](https://doi.org/10.1016/S0016-7037(96)00361-4)
- Mead, R., Xu, Y., Chong, J., Jaffé, R., 2005. Sediment and soil organic matter source assessment as revealed by the molecular distribution and carbon isotopic composition of *n*-alkanes. *Org. Geochem.* 36, 363–370.
<https://doi.org/10.1016/j.orggeochem.2004.10.003>
- Meinzer, F.C., Andrade, J.L., Goldstein, G., Holbrook, N.M., Cavelier, J., Wright, S.J., 1999. Partitioning of soil water among canopy trees in a seasonally dry tropical forest. *Oecologia* 121, 293. <https://doi.org/10.1007/s004420050931>
- Meyers, P.A., 1994. Preservation of elemental and isotopic source identification of sedimentary organic matter. *Chem. Geol.* 114, 289–302.
[https://doi.org/10.1016/0009-2541\(94\)90059-0](https://doi.org/10.1016/0009-2541(94)90059-0)
- Meyers, P.A., Eadie, B.J., 1993. Sources, degradation and recycling of organic matter associated with sinking particles in Lake Michigan. *Org. Geochem.* 20, 47–56.
[https://doi.org/10.1016/0146-6380\(93\)90080-U](https://doi.org/10.1016/0146-6380(93)90080-U)

- Meyers, P.A., Ishiwatari, R., 1993. Lacustrine organic geochemistry – an overview of indicators of organic matter sources and diagenesis in lake sediments. *Org. Geochem* 20, 867–900. [https://doi.org/10.1016/0146-6380\(93\)90100-P](https://doi.org/10.1016/0146-6380(93)90100-P)
- Molina, C.I., Gibon, F.M., Oberdorff, T., Dominguez, E., Pinto, J., Marín, R., Roulet, M., 2011. Macroinvertebrate food web structure in a floodplain lake of the Bolivian Amazon. *Hydrobiologia* 663, 135–153. <https://doi.org/10.1007/s10750-010-0565-4>
- Mook, W.G., Bommerson, J.C., Staverman, W.H., 1974. Carbon isotope fractionation between dissolved bicarbonate and gaseous carbon dioxide. *Earth Planet. Sci. Lett.* 22, 169–176. [https://doi.org/10.1016/0012-821X\(74\)90078-8](https://doi.org/10.1016/0012-821X(74)90078-8)
- Moos, M.T., Laird, K.R., Cumming, B.F., 2009. Climate-related eutrophication of a small boreal lake in northwestern Ontario: A palaeolimnological perspective. *The Holocene* 19, 359–367. <https://doi.org/10.1177/0959683608101387>
- Moser, K.A., Baron, J.S., Brahney, J., Oleksy, I.A., Saros, J.E., Hundey, E.J., Sadro, S.A., Kopáček, J., Sommaruga, R., Kainz, M.J., Strecker, A.L., Chandra, S., Walters, D.M., Preston, D.L., Michelutti, N., Lepori, F., Spaulding, S.A., Christianson, K.R., Melack, J.M., Smol, J.P., 2019. Mountain lakes: Eyes on global environmental change. *Glob. Planet. Change.* 178, 77–95. <https://doi.org/10.1016/j.gloplacha.2019.04.001>
- Munroe, J., 2007. Exploring relationships between watershed properties and Holocene loss on-ignition records in high-elevation lakes, southern Uinta Mountains, Utah, USA. *Arc. Antarct. Alp. Res.* 39, 556–565. [https://doi.org/10.1657/1523-0430\(06-096\)\[MUNROE\]2.0.CO;2](https://doi.org/10.1657/1523-0430(06-096)[MUNROE]2.0.CO;2)
- Nazari-Sharabian, M., Ahmad, S., Karakouzian, M., 2018. Climate change and eutrophication: A short review. *Eng. Technol. Appl. Sci. Res.* 8, 3668–3672. <https://doi.org/10.5281/zenodo.2532694>

- O'Beirne, M.D., Werne, J.P., Hecky, R.E., Johnson, T.C., Katsev, S., Reavie, E.D., 2017. Anthropogenic climate change has altered primary productivity in Lake Superior. *Nat. Commun.* 8, 15713. <https://doi.org/10.1038/ncomms15713>
- O'Leary, M.H., 1988. Carbon isotopes in photosynthesis: Fractionation techniques may reveal new aspects of carbon dynamics in plants. *BioScience* 38, 328–336. <https://doi.org/10.2307/1310735>
- Panizzo, V.N., MacKay, A.W., Ssemmanda, I., Taylor, R., Rose, N., Leng, M.J., 2008. A 140-year record of recent changes in aquatic productivity in a remote, tropical alpine lake in the Rwenzori Mountain National Park, Uganda. *J. Paleolimnol.* 40, 325–338. <https://doi.org/10.1007/s10933-007-9163-5>
- Pearson, J., Wells, D.M., Seller, K.J., Bennett, A., Soares, A., Woodall, J., Ingrouille, M.J., 2000. Traffic exposure increases natural ¹⁵N and heavy metal concentrations in mosses. *New Phytol.* 147, 317–326. <https://doi.org/10.1046/j.14698137.2000.00702.x>
- Rice, S.K., 2000. Variation in carbon isotope discrimination within and among *Sphagnum* species in a temperate wetland. *Oecologia* 123, 1–8. <https://doi.org/10.1007/s004420050983>
- Rundel, P.W., Stichler, W., Zander, R.H., Ziegler, H., 1979. Carbon and hydrogen isotope ratios of bryophytes from arid and humid regions. *Oecologia* 44, 91–94. <https://doi.org/10.1007/BF00346404>
- Sachse, D., Billault, I., Bowen, G.J., Chikaraishi, Y., Dawson, T.E., Feakins, S.J., Freeman, K.H., Magill, C.R., McInerney, F.A., van der Meer, M.T.J., Polissar, P., Robins, R.J., Sachs, J.P., Schmidt, H.-L., Sessions, A.L., White, J.W.C., West, J.B., Kahmen, A., 2012. molecular paleohydrology: Interpreting the hydrogen-isotopic composition of lipid biomarkers from photosynthesizing organisms. *Annu. Rev. Earth Planet. Sci.* 40, 221–249. <https://doi.org/10.1146/annurev-earth-042711-105535>

- Sachse, D., Radke, J., Gleixner, G., 2004. Hydrogen isotope ratios of recent lacustrine sedimentary *n*-alkanes record modern climate variability. *Geochim. Cosmochim. Acta* 68, 4877–4889. <https://doi.org/10.1016/j.gca.2004.06.004>
- Sachse, D., Radke, J., Gleixner, Gerd, Gleixner, G., 2006. $\delta^2\text{D}$ values of individual *n*-alkanes from terrestrial plants along a climatic gradient – Implications for the sedimentary biomarker record. *Org. Geochem.* 37, 469–483. <https://doi.org/10.1016/j.orggeochem.2005.12.003>
- Sachse, D., Sachs, J.P., 2008. Inverse relationship between D/H fractionation in cyanobacterial lipids and salinity in Christmas Island saline ponds. *Geochim. Cosmochim. Acta* 72, 793– 806. <https://doi.org/10.1016/j.gca.2007.11.022>
- Schallenberg, M., De Winton, M.D., Verburg, P., Kelly, D.J., Hamill, K.D., Hamilton, D.P., 2013. Ecosystem services of lakes, in: Dymond, J. (Ed.), *Ecosystem Services in New Zealand: Conditions and Trends*, first ed. Manaaki Whenua Press, Lincoln, New Zealand, pp. 203–225.
- Schwalb, A., Dean, W.E., 2002. Reconstruction of hydrological changes and response to effective moisture variations from North-Central USA lake sediments. *Quat. Sci. Rev.* 21, 1541–1554. [https://doi.org/10.1016/S0277-3791\(01\)00121-4](https://doi.org/10.1016/S0277-3791(01)00121-4)
- Sessions, A.L., 2016. Factors controlling the deuterium contents of sedimentary hydrocarbons. *Org. Geochem.* 96, 43–64. <https://doi.org/10.1016/j.orggeochem.2016.02.012>
- Sessions, A.L., Burgoyne, T.W., Schimmelmann, A., Hayes, J.M., 1999. Fractionation of hydrogen isotopes in lipid biosynthesis. *Org. Geochem.* 30, 1193–1200.
- Sharp, Z., 2017. *Principles of Stable Isotope Geochemistry*, second ed. Open Educational Resources. <https://doi.org/10.25844/h9q1-0p82>
- Smol, J.P., 2008. *Pollution of Lakes and Rivers: A Paleoenvironmental Perspective*, second ed. Wiley-Blackwell, Hoboken, United States. <https://doi.org/10.1002/aqc.571>

- Street, J.H., Anderson, R.S., Rosenbauer, R.J., Paytan, A., 2013. *n*-Alkane evidence for the onset of wetter conditions in the Sierra Nevada, California (USA) at the mid-late Holocene transition, ~3.0ka. *Quat. Res.* 79, 14–23.
<https://doi.org/10.1016/j.yqres.2012.09.004>
- Szpak, P., White, C.D., Longstaffe, F.J., Millaire, J.-F., Vásquez Sánchez, V.F., 2013. Carbon and nitrogen isotopic survey of northern Peruvian plants: Baselines for paleodietary and paleoecological studies. *PLoS One* 8, e53763.
<https://doi.org/10.1371/journal.pone.0053763>
- Talbot, M., 2001. Nitrogen isotopes in paleolimnology, in: Smol, J., Birks, H., Last, W. (Eds.), *Tracking Environmental Change Using Lake Sediments*, first ed. Springer Netherlands, Dordrecht, Netherlands, pp. 401– 439.
- Talbot, M.R., 1990. A review of the palaeohydrological interpretation of carbon and oxygen isotopic ratios in primary lacustrine carbonates. *Chem. Geol. Isot. Geosci. Sect.* 80, 261– 279. [https://doi.org/10.1016/0168-9622\(90\)90009-2](https://doi.org/10.1016/0168-9622(90)90009-2)
- Tang, K., Feng, X., 2001. The effect of soil hydrology on the oxygen and hydrogen isotopic compositions of plants' source water. *Earth Planet. Sci. Lett.* 185, 355–367.
[https://doi.org/10.1016/S0012-821X\(00\)00385-X](https://doi.org/10.1016/S0012-821X(00)00385-X)
- Teranes, J.L., Bernasconi, S.M., 2005. Factors controlling $\delta^{13}\text{C}$ values of sedimentary carbon in hypertrophic Baldeggersee, Switzerland, and implications for interpreting isotope excursions in lake sedimentary records. *Limnol. Oceanogr.* 50, 914–922.
<https://doi.org/10.4319/lo.2005.50.3.0914>
- Teranes, J.L., Bernasconi, S.M., 2000. The record of nitrate utilization and productivity limitation provided by $\delta^{15}\text{N}$ values in lake organic matter – A study of sediment trap and core sediments from Baldeggersee, Switzerland. *Limnol. Oceanogr.* 45, 801–813.
<https://doi.org/10.4319/lo.2000.45.4.0801>

- Thorburn, P.J., Walker, G.R., Brunel, J.P., 1993. Extraction of water from eucalyptus trees for analysis of deuterium and oxygen-18: laboratory and field techniques. *Plant, Cell Environ.* 16, 269–277. <https://doi.org/10.1111/j.1365-3040.1993.tb00869.x>
- Tieszen, L.L., 1991. Natural variations in the carbon isotope values of plants: Implications for archaeology, ecology, and paleoecology. *J. Archaeol. Sci.* 18, 227–248. [https://doi.org/10.1016/0305-4403\(91\)90063-U](https://doi.org/10.1016/0305-4403(91)90063-U)
- Verburg, P., 2007. The need to correct for the Suess effect in the application of $\delta^{13}\text{C}$ in sediment of autotrophic Lake Tanganyika, as a productivity proxy in the Anthropocene. *J. Paleolimnol.* 37, 591–602. <https://doi.org/10.1007/s10933-006-9056-z>
- Verrecchia, E.P., Verrecchia, K.E., 2003. Needle-fiber calcite: A critical review and a proposed classification. *SEPM J. Sediment. Res. Vol. 64A*, 650–664. <https://doi.org/10.1306/d4267e33-2b26-11d7-8648000102c1865d>
- Von Grafenstein, U., Erlenkeuser, H., Trimborn, P., 1999. Oxygen and carbon isotopes in modern fresh-water ostracod valves: assessing vital offsets and autecological effects of interest for palaeoclimate studies. *Palaeogeogr. Palaeoclimatol. Palaeoecol.* 148, 133–152. [https://doi.org/10.1016/S0031-0182\(98\)00180-1](https://doi.org/10.1016/S0031-0182(98)00180-1)
- Watson, S.B., Miller, C., Arhonditsis, G., Boyer, G.L., Carmichael, W., Charlton, M.N., Confesor, R., Depew, D.C., Höök, T.O., Ludsin, S.A., Matisoff, G., McElmurry, S.P., Murray, M.W., Peter Richards, R., Rao, Y.R., Steffen, M.M., Wilhelm, S.W., 2016. The re-eutrophication of Lake Erie: Harmful algal blooms and hypoxia. *Harmful Algae* 56, 44–66. <https://doi.org/10.1016/j.hal.2016.04.010>
- Wetzel, R., 2001. *Limnology: Lake and River Ecosystems*, third ed. Academic Press, San Diego, United States.
- Wiik, E., Bennion, H., Sayer, C.D., Willby, N.J., 2013. Chemical and biological responses of marl lakes to eutrophication. *Freshw. Rev.* 6, 35–62.

<https://doi.org/10.1608/frj6.2.630>

Zhang, Y., Yu, J., Su, Y., Du, Y., Liu, Z., 2020. A comparison of *n*-alkane contents in sediments of five lakes from contrasting environments. *Org. Geochem.* 139, 103943.

<https://doi.org/10.1016/j.orggeochem.2019.103943>

Chapter 2

2 Hydroclimate-Primary Production Decoupling in a Small Lake, South-Central Canada, over the last 900 years

Climate warming is expected to alter moisture regimes in temperate areas like southern Ontario, Canada, resulting in drier summers and wetter winters (Zhang et al., 2019). Previous studies have determined that such changes in atmospheric moisture can drive unprecedented changes in effective moisture (the net of water inputs versus evaporative loss) (Wang et al., 2018). Of interest is whether these shifts in effective moisture associated with climate warming can influence primary production. It is important that the links between effective moisture and primary production are clarified because excessive primary production can lead to eutrophication, which degrades water quality (Le Moal et al., 2018).

Previous research has suggested that changes in effective moisture can influence primary production, although the specific links between these two variables remain ambiguous. Some studies, for instance, have determined that decreases in effective moisture can lower lake levels and concentrate limiting nutrients, thereby stimulating primary production (Gąsiorowski and Hercman, 2005; Özen et al., 2010; Yuan et al., 2006). In shallow lakes, decreases in lake levels caused by a lowering of effective moisture can enhance vertical mixing (Naselli-Flores, 2003). Enhanced vertical mixing can transfer nutrients from the hypolimnion to the epilimnion, thereby stimulating primary production (Li and Ku, 1997). Other research, however, has contradicted these studies and suggested that increases in effective moisture may stimulate primary production (Fritz et al., 1991; Ho and Michalak, 2019; Reichwaldt and Ghadouani, 2012). These studies determined that increased surface flow during periods of high effective moisture delivered limiting nutrients to lakes, and these nutrients stimulated algal growth (Fritz et al., 1991; Ho and Michalak, 2019; Reichwaldt and Ghadouani, 2012).

The first goal of this study was therefore to improve our understanding of the connections between primary production and effective moisture. To accomplish this goal, the ~900-year history of effective moisture and primary production was reconstructed for a

kettle lake in central Ontario. Changes in effective moisture were reconstructed using the stable carbon and oxygen isotope ratios of marl, ($\delta^{13}\text{C}_{\text{marl}}$ and $\delta^{18}\text{O}_{\text{marl}}$, respectively), and the carbon isotope ratios of sedimentary total organic carbon ($\delta^{13}\text{C}_{\text{TOC}}$). To reconstruct the history of primary production in Barry Lake, the mass accumulation rate of total organic carbon, total nitrogen, sedimentary chlorophyll *a* and calcium carbonate (TOC-MAR, TN-MAR, Chl-*a*(_s)-MAR and calcite-MAR, respectively) were measured, as well as the ratio of total organic carbon to total nitrogen (TOC:TN).

This chapter focused on the last ~900 years because effective moisture varied considerably during this period (Booth et al., 2006; Ma et al., 2013; St. Jacques et al., 2008). The Medieval Climate Anomaly (MCA) (AD 1000– 1300), for example, was characterized by arid, warm conditions (Booth et al., 2006), while climate during the Little Ice Age (LIA) (AD 1450– 1850) was cooler, wetter and more unstable (Buhay and Edwards, 1993). Investigating how primary production changed during the MCA and LIA allowed us to gain a better understanding of how aridity influences primary production without the confounding influence of European disturbance. With this information, one can begin to target the main drivers of increased primary production.

In this first section of this study, the following research questions are addressed: *(i)* how well does the $\delta^{18}\text{O}_{\text{marl}}$ record of Barry Lake track effective moisture? *(ii)* Does primary production change with, or independently of, effective moisture? Finally, *(iii)* how have effective moisture and primary production changed in Barry Lake over the past ~900 years? Prior to conducting this study, it was expected that the $\delta^{18}\text{O}_{\text{marl}}$ of Barry Lake would track effective moisture because Barry Lake is hydrologically closed, and such lakes are often sensitive to variations in atmospheric moisture (Talbot, 1990). It was also predicted that decreasing atmospheric moisture would lower effective moisture and concentrate limiting nutrients, thereby stimulating primary production (Naselli-Flores, 2003); thus, it was anticipated that effective moisture and primary production would vary inversely. It is unlikely that an increase in effective moisture would introduce nutrients to Barry Lake via surface flows, as reported by Ho and Michalak (2019), because Barry Lake is hydrologically closed on the surface. Lastly, it was predicted that effective moisture would decrease during

the arid MCA, increase during the wetter LIA and decrease during the modern period. Since it was predicted that primary production would vary inversely with effective moisture, it was anticipated that primary production would increase during the MCA, decrease during the LIA and increase in the modern period.

The second goal of this study was to predict how lakes in central Ontario will change as climate warming accelerates. To accomplish this goal, the Barry Lake hydroclimatic record was compared with similar lake records from across the region. Future trends in effective moisture are challenging to model in this region because the climate controls in this area are complex; the region receives moist air from the Great Lakes and the Gulf of Mexico (Edwards and Fritz, 1986), and drier air from the northwest (Jasechko et al., 2014).

In this second section of this chapter, the following research questions were addressed: how does the Barry Lake hydroclimate record compare with similar records from the region? It was anticipated that the Barry Lake record would show similarities to nearby records, but not distant records, because small lakes like Barry Lake tend to integrate local signals of environmental change (*e.g.*, Lemdahl, 2000). The findings of this study improve the scientific understanding of how changes in effective moisture affect primary production while also investigating regional variations in effective moisture.

2.1 Materials and methods

2.1.1 Study Area

Barry Lake (44°18'28"N, 77°55'17"W) is a ~7.6 m-deep, small, dimictic kettle lake located in southeastern Ontario, Canada, 32 km east of Peterborough, Ontario, and 40 km north of Lake Ontario (Fig. 1.2 in Chapter 1). The main water body is immediately surrounded by wetland. Adjacent to about 1/3 of the wetland is farmland. The remaining 2/3 of the wetland is surrounded by forest. The lake has two ephemeral inflows, probably derived from groundwater springs, and three ephemeral outflows. The area is characterized by hot, humid summers and cool, drier winters.

2.1.2 Sample Collection

Three sediment cores were collected from the deepest part of Barry Lake using a Glew gravity corer (Glew et al., 2002), two in November 2011 (BL-G11-01, 41.5 cm; BL-G11-02, 41.0 cm) and one in July 2017 (BL-G17-01; 42.5 cm). All cores had an undisturbed sediment-water interface. Immediately following collection, the cores were subsampled onshore using a vertical-type extruder (Glew et al., 2002) at 0.5 cm intervals and individually sealed in Whirl-Pak bags. Samples from BL-G11-01 and BL-G17-01 were stored at 4 °C in the Laboratory for Stable Isotope Science (LSIS) at the University of Western Ontario (Canada). Samples from BL-G11-02 were stored frozen at LSIS. All data obtained from these cores are available in Appendix A. For more details about sample preparation, see Table B.1 in Appendix B.

2.1.3 Chronology

The ^{210}Pb and ^{137}Cs measurements were made at the LANCET Laboratory (Ottawa, Canada). These analyses were performed on samples from the upper 19.25 cm of BL-G11-02 and certified reference materials (International Atomic Energy Agency (IAEA), Vienna, Austria) using an Ortec® High Purity Germanium Gamma Spectrometer (Oak Ridge, TN, USA). A constant rate of supply (CRS) model was used to calculate the ^{210}Pb dates as it accounts for variations in sedimentation rates (Appleby and Oldfield, 1978). The ^{214}Pb and ^{241}Am were used to determine background ^{210}Pb . The ^{137}Cs , which typically peaks at AD 1963, was used to verify the ages determined from ^{210}Pb . The age-depth models also included five radiocarbon dates obtained from materials in core BL-G17-01 (Table B.2 in Appendix B). These analyses were performed at the A.E. Lalonde AMS Laboratory (Ottawa, Canada) using accelerator mass spectrometry (AMS). ^{210}Pb dates for BL-G11-01 were first reported in Liu (2016). For additional information about the creation of the age-depth model, see Section B.1 in Appendix B.

Age-depth models were generated using the “Bacon” package in R (Blaauw and Christen, 2011), which uses Bayesian statistics, IntCal13 (Reimer et al., 2013) and the calibration curves for each date to calculate sediment accumulation rates based on a

gamma autoregressive process (Blaauw and Christen, 2011). All default settings were unchanged, except the model thickness was reduced to 1.5 to increase flexibility of the model, and maximum and minimum depths were specified. A surface (depth= 0) date of AD 2017.5 and AD 2011.9 was assigned for BL-G17-01 and BL-G11-01, respectively, to prevent extrapolation of the model into the future. The amount of sediment deposited between the collection of the 2011 core and collection of the 2017 core was calculated to aid in correlating the cores (Figure B.1 in Appendix B). According to the age-depth models, the sediments examined in this study span the time period from AD ~1100 -2017.

2.1.4 Isotopic and elemental analysis

All measurements of BL-G11-01 were conducted by Zijun Liu and were first reported in Liu (2019). All measurements of BL-G17-01 are reported for the first time in this thesis and were made by R. Doyle, unless otherwise noted. Sample preparation methods for all analyses in Chapter 2 are provided in Table B.1 in Appendix B. The stable isotope results are reported in the standard δ -notation relative to VPDB for C, AIR for N and VSMOW for O, as shown in Equation 1.1. The amounts of total organic carbon (%TOC) and total nitrogen (%TN) in BL-G11-01 were measured using a Carlo Erba Fisons[®] 1108 elemental analyzer at LSIS, while the %TOC and %TN of BL-G17-01 were analyzed concurrently with $\delta^{13}\text{C}_{\text{TOC}}$ and $\delta^{15}\text{N}_{\text{TN}}$ at LSIS using a Costech Elemental Combustion system (EA) coupled to a Thermo Scientific[™] Delta^{PLUS} XL[™] isotope ratio mass spectrometer (IRMS) in continuous-flow (He) mode (EA-IRMS). The %TOC and %TN data were used to calculate elemental TOC:TN ratios (Meyers, 1994). Values of $\delta^{13}\text{C}_{\text{TOC}}$ and $\delta^{15}\text{N}_{\text{TN}}$ were measured in separate analytical sessions to generate reliable amplitudes, and samples designated for the analysis of $\delta^{13}\text{C}_{\text{TOC}}$ first underwent acid fumigation following Harris et al. (2001). The $\delta^{13}\text{C}_{\text{TOC}}$ of sediments deposited after AD 1850 were corrected for the Suess Effect to account for the enrichment of atmospheric $^{12}\text{CO}_2$ caused by fossil fuel emissions (Verburg, 2007).

For BL-G11-01, two standards, Low Organic Content (LOC) soil (accepted values: %TOC= 1.52 %; %TN= 0.13 wt.%) and High Organic Content (HOC) soil (accepted values: %TOC= 6.10 %; %TN= 0.46 %) were used to generate calibration curves for %TOC and %TN

measurements. The Peach Leaf standard (SRM number: 1547, accepted values: %TOC= 47.79 %; %TN= 2.94 %; ISOGEOCHEM communication, <https://list.uvm.edu/cgi-bin/wa?A2=isogeochem;b0553eee.0206>; Julia Cox, University of Arkansas, June 19, 2020) was also measured in each %TOC and %TN analytical session to evaluate accuracy and precision of carbon and nitrogen contents. The measured average value of 46.3 ± 0.19 % compares well with its accepted values for %TOC, and the measured average value of 2.92 ± 0.02 % compares well with its accepted values for %TN. Duplicates were analyzed every ~11 samples and had average reproducibilities of ± 0.3 % ($n= 10$ sample pairs) for TOC and ± 0.01 % ($n= 7$ sample pairs) for %TN.

For BL-G17-01, two standards, USGS 40 (accepted values: %TOC= 40.7 %; %TN= 9.52 %) and USGS 41a (accepted values: %TOC= 40.7 %; %TN= 9.52 %) were used to generate calibration curves for %TOC and %TN measurements. The internal standard keratin (MP Biomedicals Inc., Cat. No. 90211, Lot No. 9966H; average values: %TOC= 48.14 %; TN= 15.10 %) was used to evaluate precision and accuracy of carbon and nitrogen contents. The average %TOC and %TN of keratin was calculated by averaging over 1050 analyses of keratin at LSIS. The measured average value of 48.4 ± 1.47 % ($n= 25$) compares well with its accepted values for %TOC, and the measured average value of 14.8 ± 0.36 % ($n= 26$) compares well with its accepted values for %TN. Duplicates were analyzed every ~11 samples and had average reproducibilities of ± 0.5 % ($n= 7$ sample pairs) for %TOC and ± 0.04 % ($n= 8$ sample pairs) for %TN.

The $\delta^{13}\text{C}_{\text{TOC}}$ and $\delta^{15}\text{N}_{\text{TN}}$ of BL-G11-01 were calibrated to VPDB and AIR using USGS 40 (accepted values: $\delta^{13}\text{C} = -26.39$ ‰; $\delta^{15}\text{N} = -4.52$ ‰) and USGS 41 (accepted values: $\delta^{13}\text{C} = +37.63$ ‰; $\delta^{15}\text{N} = +47.57$ ‰). For BL-G17-01, USGS 41 was replaced by USGS 41a (accepted values: $\delta^{13}\text{C} = +36.55$ ‰; $\delta^{15}\text{N} = +47.55$ ‰). Internal standard keratin (accepted values: $\delta^{13}\text{C} = -24.04$ ‰; $\delta^{15}\text{N} = +6.35$ ‰) was used to monitor both analytical accuracy and precision. The average obtained for the keratin was -24.04 ± 0.15 ‰ ($n= 39$) for $\delta^{13}\text{C}$ and $+6.39 \pm 0.09$ ‰ ($n= 50$) for $\delta^{15}\text{N}$, which compares well with its accepted values and expected reproducibility. Sample duplicates were analyzed every 10 samples, with an average reproducibility of ± 0.09 ‰ ($n= 8$ sample pairs) for $\delta^{13}\text{C}$ and ± 0.06 ‰ ($n= 12$ sample pairs) for $\delta^{15}\text{N}$.

The $\delta^{13}\text{C}_{\text{marl}}$, $\delta^{18}\text{O}_{\text{marl}}$ and percentage of calcite (%calcite) of bulk sediments from BL-G11-01 and BL-G17-01 were obtained at LSIS by J. Walker by reaction with orthophosphoric acid (H_3PO_4) at 90 °C using a Micromass MultiPrep® device coupled to a VG Optima® dual-inlet IRMS. Calibration of $\delta^{13}\text{C}$ to VPDB was achieved using NBS-19 (accepted value: $\delta^{13}\text{C} = +1.95 \text{ ‰}$) and LSVEC (accepted value: $\delta^{13}\text{C} = -46.6 \text{ ‰}$). Accuracy and precision of analyses were evaluated using the $\delta^{13}\text{C}$ of NBS-18 (accepted value: $\delta^{13}\text{C} = -5.0 \text{ ‰}$) and laboratory standards Suprapur (accepted value: $\delta^{13}\text{C} = -35.28 \text{ ‰}$) and WS-1 (accepted value: $\delta^{13}\text{C} = +0.76 \text{ ‰}$). The $\delta^{13}\text{C}$ results for NBS-18, Suprapur and WS-1 were $-5.04 \pm 0.09 \text{ ‰}$ ($n = 27$), $-35.57 \pm 0.08 \text{ ‰}$ ($n = 13$), and $+0.80 \pm 0.04 \text{ ‰}$ ($n = 17$), respectively, which compare well with accepted values and expected reproducibility. Like $\delta^{13}\text{C}_{\text{TOC}}$, $\delta^{13}\text{C}_{\text{marl}}$ was corrected for the Suess Effect for marl deposited after AD 1850 according to Verberg (2007). Calibration of $\delta^{18}\text{O}_{\text{marl}}$ to VSMOW was achieved using NBS-19 (accepted value: $\delta^{18}\text{O} = +28.65 \text{ ‰}$) and NBS-18 (accepted value: $\delta^{18}\text{O} = +7.20 \text{ ‰}$). Analytical accuracy and precision were evaluated using Suprapur (accepted value: $\delta^{18}\text{O} = +13.25 \text{ ‰}$) and WS-1 (accepted value: $\delta^{18}\text{O} = +26.23 \text{ ‰}$). The $\delta^{18}\text{O}$ results for Suprapur and WS-1 were $+13.25 \pm 0.11 \text{ ‰}$ ($n = 13$) and $+26.29 \pm 0.10 \text{ ‰}$ ($n = 17$), respectively, which compare well with accepted values and expected reproducibility. The pressure transducer reading of the Multiprep® device, which varies directly with the amount of calcite in the sample, was used to estimate the percentage of calcite (%calcite) throughout the cores, and in some cases cross-checked using powder X-ray diffraction (*p*XRD).

2.1.5 Analysis of sedimentary chlorophyll *a* and its derivatives (Chl- $a_{(s)}$)

Sediments from BL-G17-01 were analyzed to determine the concentration of chlorophyll *a* and its derivatives using visible reflectance spectroscopy (VRS), as detailed in Michelutti et al. (2010). The 400– 2500 nm spectral range was measured for each 0.5 cm sediment interval using the spectroradiometer (Rapid Content Analyzer) at the Paleoecological Environmental Assessment and Research Laboratory (PEARL, Queen’s University). To determine the Chl- $a_{(s)}$ concentration, the area under the peak between 650-700 nm was calculated. Then, the linear relationship in Equation 2.1 was used to infer the concentration of Chl- $a_{(s)}$ (Michelutti et al., 2010).

$$\text{Equation 2.1} \quad \text{Chlorophyll } a + \text{ derivatives} = 0.0919 \times \text{peak area } 650\text{--}700 \text{ nm} + 0.0011$$

2.1.6 Mass accumulation rates

For BL-G11-01, the %calcite was calculated using *p*XRD data. The *p*XRD was performed at LSIS using a Rigaku High Brilliance Rotating Anode X-ray Diffractometer. Shell fragments (dominantly aragonite) were removed by hand-picking prior to *p*XRD. Values of %TN and %TOC were determined using a Carlo Erba Fisons® 1108 elemental analyzer at LSIS, as described above. For BL-G17-01, the %TN, %TOC and %calcite were determined using ancillary outputs from the EA-IRMS and the Multiprep® device, as described above. These values were converted into mass accumulation rates using Equation 2.2, derived from Yu et al. (2007). The mass accumulation rate of Chl-*a*_(s) (Chl-*a*_(s)-MAR) was calculated by (i) converting the concentration of Chl-*a*_(s) into a weight percentage of Chl-*a*_(s) and (ii) inputting the result from step (i) into Equation 2.2.

$$\text{Equation 2.2} \quad (\text{TOC, TN, calcite or Chl-}a_{(s)})\text{-MAR} = [\text{wt. \% (TOC, TN, calcite or Chl-}a_{(s)})] \times [\text{LSR}] \times [\text{DBD}] \times 1000$$

where LSR is the linear sedimentation rate in cm/year estimated from the age-depth model, and DBD is the dry bulk density (g/cm³).

2.1.7 Calculation of statistical significance

Linear correlations between variables were evaluated using *r*, the Pearson correlation coefficient (Derrick et al., 1994). Following the calculation of *r*, a *p*-value was calculated using a student *t* distribution. Significance was set at *p* < 0.01. All Pearson correlations were performed on data from BL-G17-01 since this core has better age-constraint than BL-G11-01, and, as such, is the primary focus of discussion below.

2.1.8 Breakpoint analysis

Breakpoint analysis was used to identify abrupt shifts in the Barry Lake δ¹⁸O_{marl} record and the North American Drought Atlas (NADA) record. All breakpoint analyses were completed using the “strucchange” package in R (R Core Development Team, 2020). These abrupt

shifts, or “breakpoints”, were identified using piecewise linear regression (Toms and Lesperance, 2003). First, generalized fluctuation tests were used to identify breakpoints (Zeileis et al., 2003). Generalized fluctuation tests test the null hypothesis that the regression coefficients remain constant against the alternative that at least one coefficient varies over time (Zeileis et al., 2003). Next, Bayesian information criteria (BIC) and the residual sum of squares (RSS) were used to determine the optional number of breakpoints (Bai and Perron, 2003; Zeileis et al., 2003). Finally, 95 % confidence intervals were calculated around each breakpoint (Bai and Perron, 2003).

2.1.9 Data treatment of hydroclimatic records

In order to contextualize the Barry Lake $\delta^{18}\text{O}_{\text{marl}}$ record, all of the reconstructions of effective moisture, precipitation, lake depth and lake salinity were downloaded from the National Oceanic and Atmospheric Administration (NOAA) paleoclimate database (<https://www.ncdc.noaa.gov/paleo-search/>) for sites located between 40-55 °N and 60-100 °W. This research focuses only on proxies derived from lake sediments because proxies in other deposits integrate climatic information across different temporal scales. Testate amoeba in bogs, for instance, record climatic information across multi-decadal timescales (Booth et al., 2012) rather than multi-centennial timescales recorded in many lake records (*e.g.*, the Barry Lake records). All records were averaged into three bins: AD 1000-1350, AD 1450-1850 and AD 1850-2005. Sites with less than three data points per bin were excluded from the dataset. Next, these averages were converted into z-scores by subtracting the mean of all values from AD 1000-2005 from the mean of each bin and dividing by the standard deviation of values from AD 1000-2005. All of these z-scores fell between -2 and +2. A colour was assigned to each z-score: shades of blue were assigned to values between -2 and 0, indicating wetter or cooler conditions, and shades of orange were assigned to values between 0 and +2, indicating drier or hotter conditions. Colour-coded sites were then plotted on a map to determine spatial patterns of hydroclimate conditions.

2.2 Results

2.2.1 Chronology

Concentrations of ^{210}Pb follow a typical exponential curve (Fig. B.2 in Appendix B). The ^{210}Pb dates generated from BL-G11-02 were correlated with BL-G11-01 using magnetic susceptibility (MS) patterns (Fig. B.3 in Appendix B). Since the trends in MS from both cores are similar, and these cores were collected at the same time, the dates from BL-G11-02 could be matched with depths from BL-G11-01 without adjustment. The two dated cores were collected several years apart (2011 and 2017). Hence, the age models for BL-G11-01 and BL-G17-01 were finalized only after adjustments to ensure age-equivalent matches between them (Figure 2.1). The peak in ^{137}Cs (expected to occur at 1963-1964) occurs at 11.25 cm (AD 1966-1967), confirming the ^{210}Pb models (Fig. B.2 in Appendix B). Data used to generate these models is provided in Table B.2 in Appendix B. and further explanation is included in Section B.1 in Appendix B.

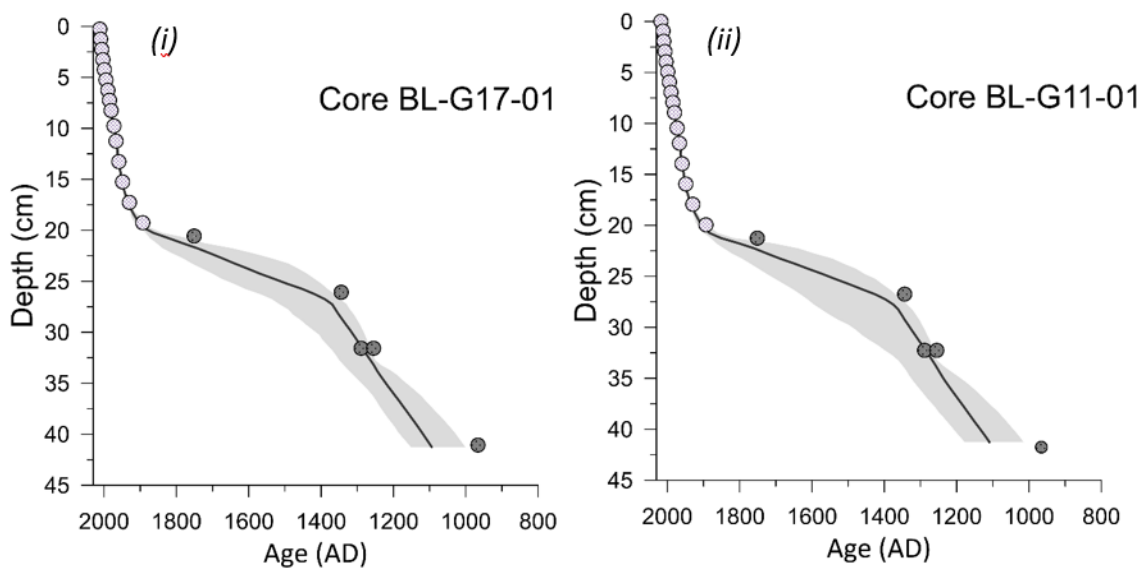


Figure 2.1 Age-depth model for BL-G17-01 (i) and BL-G11-01 (ii) generated using the R package “Bacon”. Light-grey circles represent ages obtained using ^{210}Pb dating whereas dark-grey circles represent ^{14}C dates. The same dating information is used for both cores, with the ^{210}Pb originating from BL-G11-01 and the ^{14}C originating from BL-G17-01. Grey shading indicates the overall error associated with the age-depth model. Data used to generate these models is provided in Table B.2 in Appendix B and further explanation is included in Supplementary Information.

According to the age-depth models, the sediments examined in this study span the time period from AD ~1100 to AD 2017. These sediments have been divided into six intervals, from oldest (*I*) to youngest (*VI*) (Fig. 2.2), as discussed below. The accumulation rate is unchanged from *Interval I* until *Interval V*, remaining less than 10 mg/cm²/year. During *Interval VI*, the accumulation rate increases substantially, reaching 55 mg/cm²/year (Fig. 2.2).

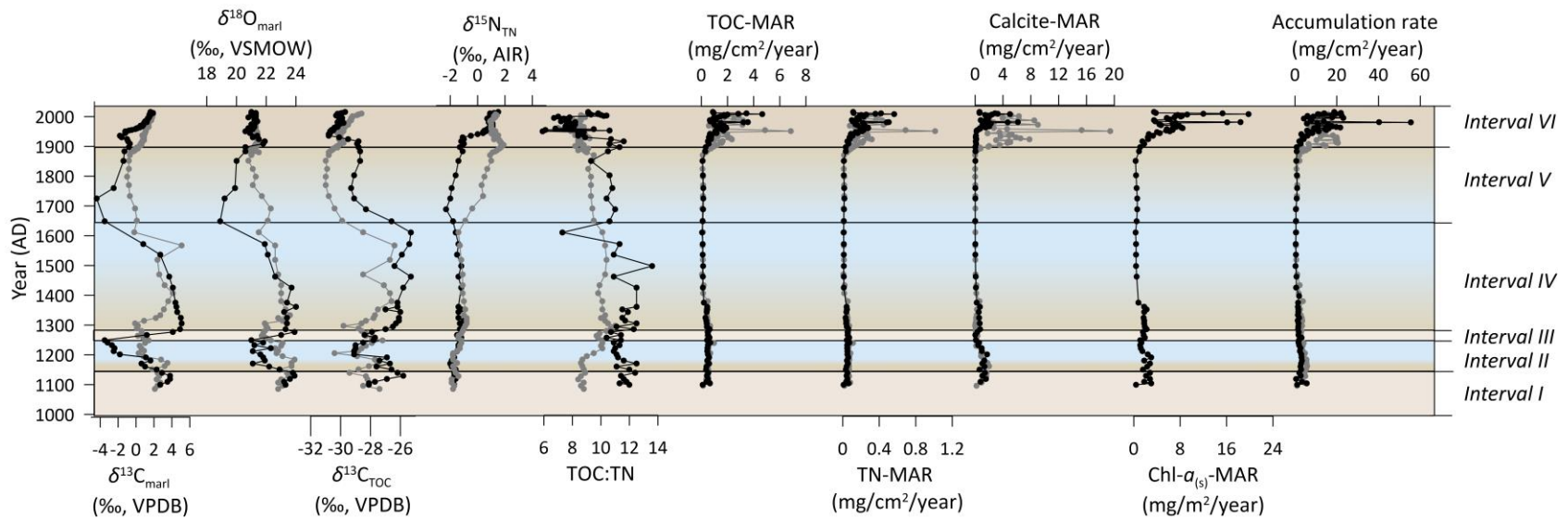


Figure 2.2 Age-dependent variation in climate proxies for cores BL-G11-01 (grey) and BL-G17-01 (black). The paleoclimatic record is subdivided into intervals (right) based on major shifts in $\delta^{18}\text{O}_{\text{marl}}$. Tan shading indicates below-average values of $\delta^{18}\text{O}_{\text{marl}}$ and blue shading indicates above-average values $\delta^{18}\text{O}_{\text{marl}}$. After AD 1850, the $\delta^{13}\text{C}_{\text{TOC}}$ and $\delta^{13}\text{C}_{\text{marl}}$ record have been corrected for the Suess Effect, following Verburg (2007). Data from BL-G11-01 (grey) was first reported in Liu (2019).

2.2.2 Isotope ratios of marl

Values of $\delta^{18}\text{O}_{\text{marl}}$ and $\delta^{13}\text{C}_{\text{marl}}$ are significantly correlated throughout the core records (Table B.3 in Appendix B). During *Interval I*, $\delta^{13}\text{C}_{\text{marl}}$ (+2 to +4 ‰) and $\delta^{18}\text{O}_{\text{marl}}$ (+22 to +23 ‰) are high relative to the mean $\delta^{13}\text{C}_{\text{marl}}$ (+0.2 ‰ for BL-G17-01; +0.6 ‰ for BL-G11-01) and $\delta^{18}\text{O}_{\text{marl}}$ (+21.6 ‰ for BL-G17-01 and +21.9 ‰ for BL-G11-01) of the entire record (Fig. 2.2). Throughout *Interval II*, $\delta^{13}\text{C}_{\text{marl}}$ decreases to between -4 ‰ (BL-G17-01) and +1 ‰ (BL-G11-01) while $\delta^{18}\text{O}_{\text{marl}}$ decreases to +20 ‰ (BL-G17-01) and +22 ‰ (BL-G11-01). During *Interval III*, $\delta^{13}\text{C}_{\text{marl}}$ and $\delta^{18}\text{O}_{\text{marl}}$ return to values observed in *Interval I*. Throughout *Interval IV*, $\delta^{13}\text{C}_{\text{marl}}$ decreases from +5 ‰ to -3 ‰, and $\delta^{18}\text{O}_{\text{marl}}$ decreases from +22 ‰ to +19 ‰. During *Interval V*, $\delta^{18}\text{O}_{\text{marl}}$ increases until it stabilizes in *Interval VI* at ~ +21 ‰. The Suess-corrected $\delta^{13}\text{C}_{\text{marl}}$ continues to increase to ~ +4 ‰. $\delta^{18}\text{O}_{\text{marl}}$ rapidly increases (≥ 1 ‰/50 years) (H.-C. Li and Ku, 1997) twice: during *Interval III* and at the end of *Interval IV*. Rapid decreases (in $\delta^{18}\text{O}_{\text{marl}} \geq 1$ ‰/50 years) occur three times: at the beginning of *Interval II*, the end of *Interval IV* and the beginning of *Interval VI*.

Values of $\delta^{13}\text{C}_{\text{marl}}$ from BL-G17-01 do not correlate significantly with TOC-MAR, TN-MAR or calcite-MAR. Values of $\delta^{18}\text{O}_{\text{marl}}$ from BL-G17-01 correlate significantly with $\delta^{13}\text{C}_{\text{marl}}$ and $\delta^{13}\text{C}_{\text{TOC}}$, but do not correlate significantly with calcite-MAR, TOC-MAR, TN-MAR or $\text{Chl-}a_{(s)}$ -MAR. When only the period AD 1950-2017 is considered, the $\delta^{18}\text{O}_{\text{marl}}$ is significantly correlated with calcite-MAR, but not TOC-MAR or TN-MAR. Values of r and p for all correlations are reported in Table B.3 in Appendix B.

2.2.3 Isotopic and elemental ratios of organic matter (OM)

Values of $\delta^{13}\text{C}_{\text{TOC}}$ correlate significantly with $\delta^{18}\text{O}_{\text{marl}}$ and $\delta^{13}\text{C}_{\text{marl}}$ (Table B.3 in Appendix B). Values of $\delta^{13}\text{C}_{\text{TOC}}$ also correlate significantly with TOC-MAR, TN-MAR and calcite-MAR after AD 1900. When data for years after AD 1900 are removed from the record, however, values of $\delta^{13}\text{C}_{\text{TOC}}$ do not correlate significantly with TOC-MAR, TN-MAR and calcite-MAR. The most distinct feature of both $\delta^{15}\text{N}_{\text{TN}}$ records is the sharp upward increase from -1 to +1 ‰ that begins in AD 1948 (BL-G11-01) and in AD 1939 (BL-G17-01) and continues until the present

(Fig. 2.2). The $\delta^{15}\text{N}_{\text{TN}}$ is significantly correlated with TOC-MAR, TN-MAR, calcite-MAR and Chl- $a_{(s)}$ -MAR. From *Interval I* to *Interval V*, shifts in TOC:TN are, on average, minimal. The average TOC:TN of BL-G11-01 is 9.1 ± 0.8 (SD) while the TOC:TN of BL-G17-01 averages 9.9 ± 1.8 (SD). During *Interval VI*, the TOC:TN of both cores noticeably decreases to <8 , except for one outlier at AD 2015 (TOC:TN= 17.1).

2.2.4 Mass accumulation rates

The TOC-MAR and TN-MAR are similar between BL-G11-01 and BL-G17-01 and follow the accumulation rate, reaching a maximum of ~ 7 mg/cm²/year and ~ 1.0 mg/cm²/year, respectively, in *Interval VI*. The calcite-MAR follows the accumulation rate and reach a maximum of ~ 20 mg/cm²/year and ~ 24 mg/cm²/year, respectively, in *Interval VI*. The Chl- $a_{(s)}$ -MAR also follows the accumulation rate and reaches a maximum of ~ 20 mg/m²/year in *Interval VI*. The calcite-MAR is significantly correlated with the TOC-MAR, TN-MAR and Chl- $a_{(s)}$ -MAR.

2.2.5 Breakpoint analysis

Five breakpoints were identified in the NADA data: AD 1300, AD 1405, AD 1600, AD 1725 and AD 1850 (Fig. 2.3). Four breakpoints were identified in the Barry Lake $\delta^{18}\text{O}_{\text{marl}}$ record: AD 1280, AD 1490, AD 1690, and AD 1850. The 95 % confidence intervals surrounding these breakpoints are shown in Figure 2.3. Both records have breakpoints around AD ~ 1300 , AD ~ 1700 and AD ~ 1850 .

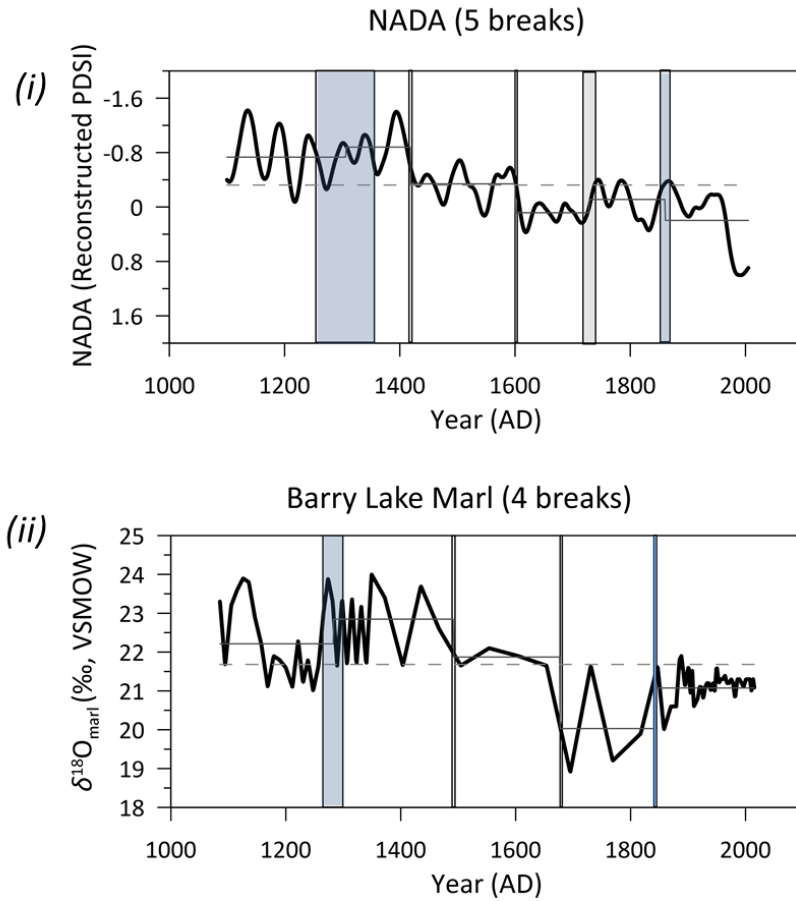


Figure 2.3 Breakpoint analysis of the $\delta^{18}\text{O}_{\text{marl}}$ record from BL-G17-01 compared with breakpoint analysis of the North American Drought Atlas (NADA). The NADA shown here is for a 0.5° latitude/longitude grid centered over $44.3, -77.9$ (Cook et al., 2010). Negative values of NADA correspond to arid conditions. To facilitate comparison with the marl data, the NADA data has been smoothed using a 50-year cubic spline. Breakpoints that are similar between the two records are coloured in blue.

2.3 Discussion

Here, the data obtained for BL-G11-01 and BL-G17-01 are used to infer the environmental/climatic history of Barry Lake since AD ~1100. In general, the proxies from the two cores match reasonably well. In the sections of sediment dated using ^{210}Pb dating (*i.e.*, *Interval VI*), proxy results from the two cores are very similar. In the sections of sediment dated using ^{14}C dating (*Interval I* to *Interval V*), however, proxy results sometimes disagree between the two cores. Such heterogeneity is to be expected given the dynamic nature of lake basins (Beaudoin and Reasoner, 1992; Downing and Rath, 1988; Hilton, 1985; Li et al., 2018; Potůčková et al., 2018). At times when proxy results from these two cores disagree, emphasis is placed on BL-G17-01 since the ^{14}C dates originated from this core.

2.3.1 Sensitivity of Barry Lake to Effective Moisture

The calcite crystals comprising Barry Lake marl vary from diamond to needle-shaped, consistent with the morphology of calcite precipitated in the epilimnion of other lakes (Verrecchia and Verrecchia, 1994). Hence geochemical signatures preserved in this marl should be reliable proxies for conditions in the epilimnion. Neither tubular structures, indicative of calcite from *Charophyte* encrustations (Diefendorf et al., 2008; Hammarlund et al., 1997), nor authigenic magnesium-carbonate minerals, were observed.

Values of $\delta^{18}\text{O}_{\text{marl}}$ reflect $\delta^{18}\text{O}_{\text{lake water}}$ and the temperature at which the marl crystallizes. The $\delta^{18}\text{O}_{\text{marl}}$ is also temperature sensitive, as is the oxygen-isotope fractionation between marl calcite and the lake water from which it crystallizes. Higher temperatures of marl crystallization are expected to decrease $\delta^{18}\text{O}_{\text{marl}}$, given the temperature dependence of the calcite-water oxygen-isotope fractionation (Craig, 1965). Yet, the observed variations in $\delta^{18}\text{O}_{\text{marl}}$ are too large to be caused solely by temperature variations. For example, between AD 1250-1276, $\delta^{18}\text{O}_{\text{marl}}$ increased by 2.9 ‰. Without the influence of evaporation on $\delta^{18}\text{O}_{\text{lake water}}$, such an increase would require a 14.5°C rise in summer water temperatures (Kim and O'Neil, 1997). This seems very unlikely, and average June, July and August temperatures derived from pollen assemblages in Clear Pond, New York (~345 km from

Barry Lake) show that, between AD 1245– 1285, average summer temperatures increased by only 0.4 °C (Paquette and Gajewski, 2013). Moreover, marl likely precipitates within a narrow temperature range during the summer months (Drummond et al., 1995). Thus, it is unlikely that temperature is a strong driver of $\delta^{18}\text{O}_{\text{marl}}$ at Barry Lake. Instead, $\delta^{18}\text{O}_{\text{marl}}$ increases under conditions that increase $\delta^{18}\text{O}_{\text{lake water}}$.

An understanding of the drivers of variation in $\delta^{18}\text{O}_{\text{lake water}}$ is therefore needed to understand the factors controlling $\delta^{18}\text{O}_{\text{marl}}$. Key to addressing this question is identifying whether Barry Lake was hydrologically open or closed over the last ~900 years. Two pieces of evidence suggest that Barry Lake was hydrologically closed throughout this period. Firstly, modern Barry Lake lacks permanent inflows/outflows and there is no evidence of ancient inflows/outflows. Secondly, the $\delta^{13}\text{C}_{\text{marl}}$ and $\delta^{18}\text{O}_{\text{marl}}$ of Barry Lake vary considerably across the entire record (4 ‰ for $\delta^{18}\text{O}_{\text{marl}}$ and 8 ‰ for $\delta^{13}\text{C}_{\text{marl}}$). Such large fluctuations are uncommon in open basins because the residence time of water is short (Talbot, 1990). Consequently, there is less time for the DIC and lake water pools to become fractionated by in-lake processes like evaporation/condensation and primary production (Talbot, 1990). In closed basins, however, $\delta^{13}\text{C}_{\text{marl}}$ and $\delta^{18}\text{O}_{\text{marl}}$ are more variable because the residence time of the water is longer and, consequently, there is more time for the DIC and lake water pools to be fractionated by in-lake processes (Talbot, 1990).

Given that Barry Lake was likely hydrologically closed throughout the last ~900 years, variations in $\delta^{18}\text{O}_{\text{marl}}$ can be interpreted using the framework established in Li and Ku (1997). In this paper, the authors propose that $\delta^{18}\text{O}_{\text{marl}}$ in closed lakes is sensitive to evaporation, increasing during arid periods when lake level decreases. Conversely, $\delta^{18}\text{O}_{\text{marl}}$ decreases during wet periods when lake level increases because evaporation slows and, consequently, less ^{16}O enters the vapour phase. Increases in precipitation and overland flow during wet periods serve to further replenish ^{16}O of the lake water (Li and Ku, 1997). Viewed through this lens, $\delta^{18}\text{O}_{\text{marl}}$ is sensitive to changes in the ratio of precipitation to evaporation (*i.e.*, effective moisture) (Li and Ku, 1997).

Strengthening this argument is the fact that the $\delta^{18}\text{O}_{\text{marl}}$ record from Barry Lake corresponds well with instrumental PDSI, a measurement of aridity (Figs. 2.4) (Cook et al., 2009). It is unsurprising that these records correspond better in recent years relative to older years because the errors of the age-depth model increase with age (for errors in the age-depth model, see Fig. 2.1). Correspondence between the North American Drought Atlas (NADA) (a tree ring-based reconstruction of PDSI) (Cook et al., 2009) and $\delta^{18}\text{O}_{\text{marl}}$ suggest that effective moisture was also an important control of $\delta^{18}\text{O}_{\text{marl}}$ in past years. Breakpoint analysis of the entire Barry Lake $\delta^{18}\text{O}_{\text{marl}}$ record and NADA record further emphasize the similarity of these data (Fig. 2.3). Two breakpoints (one around AD ~1300 and the other around AD ~1850) overlap within the error of the age-depth model, suggesting that a structural change occurred simultaneously in both records. Two other breakpoints (one at AD ~1715 and the other at AD ~1690) are not overlapping but are very close.

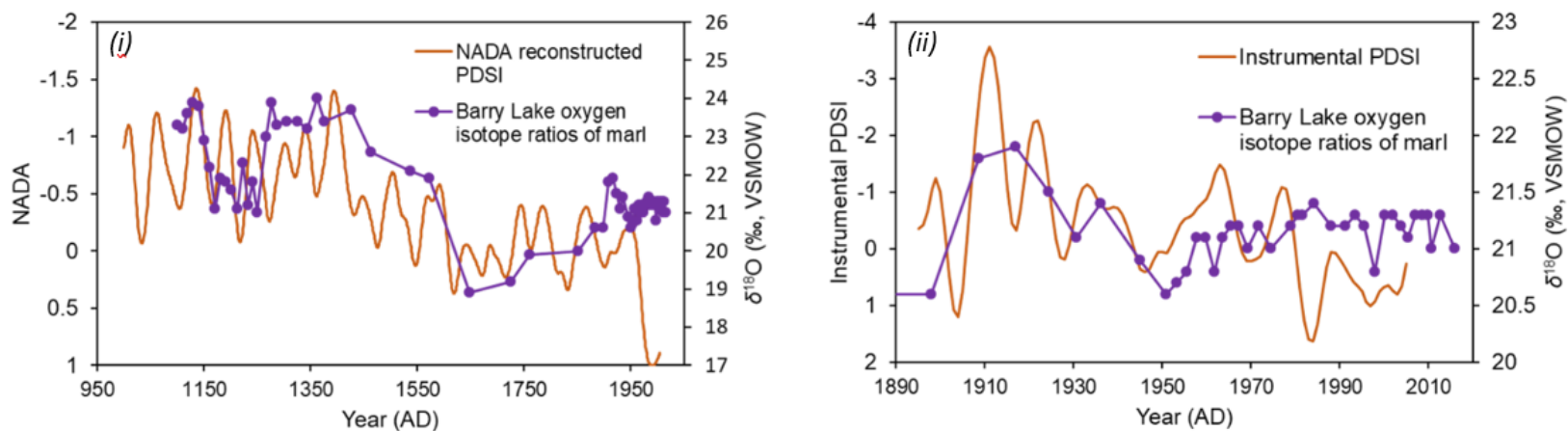


Figure 2.4 The $\delta^{18}\text{O}_{\text{marl}}$ record from BL-G17-01 compared with the North American Drought Atlas (NADA) (i) and summer (June-August) Palmer Drought Severity Index (PDSI) (ii) on a 0.5° latitude/longitude grid centered over $44.3, -77.9$ (Cook et al., 2009). Negative values of NADA and PDSI correspond to arid conditions. Left – comparison between the $\delta^{18}\text{O}_{\text{marl}}$ record and NADA. To facilitate comparison with the marl data, the NADA data has been smoothed using a 50-year cubic spline. Right - comparison between the same marl record with instrumental PDSI. The instrumental PDSI data has been smoothed using a 10-year cubic spline.

Of note is that effective moisture is not always rapidly changing; sometimes it is stable. Li and Ku (1997) define a lake as stable when $\delta^{18}\text{O}_{\text{marl}}$ changes less than 1 ‰ over 50 years. Likewise, a lake is experiencing a strong change in lake volume when $\delta^{18}\text{O}_{\text{marl}}$ is changing >1 ‰ over 50 years. This framework is adopted here when discussing the rate of change in effective moisture at Barry Lake. During periods of stability, $\delta^{18}\text{O}_{\text{lake water}}$ will increase or decrease until it equilibrates with atmospheric water vapour. Vapour exchange also occurs during periods of rapid changes in effective moisture (Li and Ku, 1997). However, compared to evaporation and dilution, vapour exchange is not an important control on $\delta^{18}\text{O}_{\text{marl}}$ during periods of rapid change in effective moisture (Li and Ku, 1997). This chapter will therefore only discuss vapour exchange during periods of relative stability.

2.3.2 Proxies of primary production at Barry Lake

Many studies have demonstrated that concentrations of sedimentary chlorophyll *a* (*i.e.*, Chl- $a_{(s)}$) are reliable proxies of primary production (Guilizzoni et al., 1983; Michelutti et al., 2010; Szymczak-Zyła et al., 2011; Yunev et al., 2002). Although Chl- $a_{(s)}$ is susceptible to degradation (Sun et al., 1991; Szymczak-Zyła et al., 2008), the measurements of Chl- $a_{(s)}$ reported here represent the concentration of chlorophyll-*a* and its degradation products (Michelutti et al., 2010); thus the mass accumulation rates of Chl- $a_{(s)}$ (*i.e.*, Chl- $a_{(s)}$ -MAR) presented should capture the original sedimentary chlorophyll *a* signal.

Variations in primary production can also be inferred from TOC-MAR and TN-MAR since the TOC:TN ratio of the sediment OM is, on average, 9.9, indicating that algae are a major source of OM to the sediment (Meyers and Ishiwatari, 1993). The TOC:TN of modern lacustrine algae measured for Barry Lake is ~8 while the TOC:TN of terrestrial OM sources are >20. The strong correlations between Chl- $a_{(s)}$ -MAR and TOC-MAR and TN-MAR further suggest that the original TOC-MAR and TN-MAR have not been noticeably impacted by post-depositional alteration.

Previous research indicates that calcite-MAR can be influenced by effective moisture and primary production (Lowe et al., 1997; Wiik et al., 2014). A decrease in effective

moisture can lead to lower water levels, which can drive marl precipitation (Murphy and Wilkinson, 1980). However, algae can also drive the precipitation of marl by taking up CO₂ during photosynthesis, which ultimately decreases the solubility of calcite in water (McConnaughey et al., 1994; Wiik et al., 2014). When the entire record is considered, calcite-MAR correlates significantly with TOC-MAR and TN-MAR, but not with $\delta^{18}\text{O}_{\text{marl}}$, suggesting that, in this system, calcite-MAR more closely reflects changes in primary production than climatic variations (Table B.3 in Appendix B). In other words, since the correlations between $\delta^{18}\text{O}_{\text{marl}}$ and TOC-MAR, TN-MAR, Chl-*a*(_s)-MAR and calcite-MAR are not significant, effective moisture is not the main driver of primary production in Barry Lake.

Changes in $\delta^{13}\text{C}_{\text{marl}}$ and $\delta^{13}\text{C}_{\text{TOC}}$ are commonly used as proxies of primary production (Drummond et al., 1995; Ekdahl et al., 2004; Hladyniuk and Longstaffe, 2015; Hundey et al., 2014). However, across the time interval studied (AD ~1100–2017), $\delta^{13}\text{C}_{\text{marl}}$ does not correlate significantly with any of the proxies of primary production, TOC-MAR, TN-MAR, Chl-*a*(_s)-MAR and calcite-MAR. Likewise, $\delta^{13}\text{C}_{\text{TOC}}$ does not correlate significantly with TOC-MAR, TN-MAR, Chl-*a*(_s)-MAR or calcite-MAR.

What then are $\delta^{13}\text{C}_{\text{marl}}$ and $\delta^{13}\text{C}_{\text{TOC}}$ tracking throughout most of the record? In Barry Lake, $\delta^{18}\text{O}_{\text{marl}}$ is significantly correlated with $\delta^{13}\text{C}_{\text{marl}}$ and $\delta^{13}\text{C}_{\text{TOC}}$, suggesting that changes in effective moisture are also influencing $\delta^{13}\text{C}_{\text{marl}}$ and $\delta^{13}\text{C}_{\text{TOC}}$. The $\delta^{13}\text{C}_{\text{marl}}$ and $\delta^{13}\text{C}_{\text{TOC}}$ are controlled by $\delta^{13}\text{C}_{\text{DIC}}$ (Diefendorf et al., 2008). Hence, any changes to $\delta^{13}\text{C}_{\text{DIC}}$ arising from variations in effective moisture would influence $\delta^{13}\text{C}_{\text{marl}}$ and $\delta^{13}\text{C}_{\text{TOC}}$. Specifically, an increase in effective moisture would lower $\delta^{13}\text{C}_{\text{DIC}}$, thereby lowering $\delta^{13}\text{C}_{\text{marl}}$ and $\delta^{13}\text{C}_{\text{TOC}}$. Conversely, a decrease in effective moisture would increase $\delta^{13}\text{C}_{\text{DIC}}$, causing $\delta^{13}\text{C}_{\text{marl}}$ and $\delta^{13}\text{C}_{\text{TOC}}$ to rise.

For closed lakes like Barry Lake, periods of low effective moisture manifest as a decrease in lake volume. A decrease in lake volume can increase $\delta^{13}\text{C}_{\text{DIC}}$ in three ways. First, a decrease in lake volume increases the partial pressure of CO₂ ($p\text{CO}_2$) in the lake, leading to outgassing of CO₂ from the system (Li and Ku, 1997). Such outgassing preferentially removes

lighter isotopologues³ of CO₂ from the water, thus increasing $\delta^{13}\text{C}_{\text{DIC}}$ and, consequently, increasing $\delta^{13}\text{C}_{\text{marl}}$ and $\delta^{13}\text{C}_{\text{TOC}}$ (Li and Ku, 1997; Talbot, 1990). Second, during periods of low effective moisture, contributions of precipitation and surface flows are diminished. Since these surface flows exhibit lower $\delta^{13}\text{C}_{\text{DIC}}$ than lake water, their absence will raise the $\delta^{13}\text{C}_{\text{DIC}}$, even if primary production remains unchanged (Li and Ku, 1997). Third, a decrease in lake volume can promote vertical mixing, transporting nutrients from the hypolimnion to the epilimnion and stimulating primary production (Li and Ku, 1997). This increase in primary production then leads to an increase in $\delta^{13}\text{C}_{\text{DIC}}$ as photosynthetic organisms preferentially incorporate ¹²C into their tissues, enriching the surrounding DIC pool in ¹³C (Hollander and McKenzie, 1991). While the first two options are plausible, this last option cannot be controlling $\delta^{13}\text{C}_{\text{DIC}}$ at Barry Lake because the proxies of primary production, Chl- $\alpha_{(s)}$ -MAR, TOC-MAR, TN-MAR and calcite-MAR are unchanging throughout most of the record.

An increase in lake volume caused by high effective moisture can lower $\delta^{13}\text{C}_{\text{DIC}}$, thereby lowering $\delta^{13}\text{C}_{\text{TOC}}$ and $\delta^{13}\text{C}_{\text{marl}}$. Increases in precipitation and surface flows during periods of high effective moisture typically lower $\delta^{13}\text{C}_{\text{DIC}}$ because the $\delta^{13}\text{C}_{\text{DIC}}$ of fresh water is lower than the $\delta^{13}\text{C}_{\text{DIC}}$ of lake water (Li and Ku, 1997). This lowering of $\delta^{13}\text{C}_{\text{DIC}}$ caused by increased freshwater inputs is amplified by reduced outgassing of CO₂ (Li and Ku, 1997). A larger pool of ¹³C also reduces the impact of photosynthesis on $\delta^{13}\text{C}_{\text{DIC}}$, even if rates of photosynthesis remain unchanged (Li and Ku, 1997). This also contributes to lower $\delta^{13}\text{C}_{\text{DIC}}$ during periods of high effective moisture.

Of note is that these factors control $\delta^{13}\text{C}_{\text{DIC}}$ (and therefore $\delta^{13}\text{C}_{\text{marl}}$ and $\delta^{13}\text{C}_{\text{TOC}}$) during periods of rapid lake volume change, or periods of rapid changes in effective moisture. When $\delta^{18}\text{O}_{\text{marl}}$ is changing at a rate lower than 1 ‰ per 50 years, it will be assumed that lake volume is stable and that $\delta^{13}\text{C}_{\text{marl}}$ and $\delta^{13}\text{C}_{\text{TOC}}$ are controlled by factors other than effective moisture, such as vapor exchange (Li and Ku, 1997). While vapour

³ Isotopologues are molecules that differ only in their isotopic composition.

exchange can also influence $\delta^{13}\text{C}_{\text{DIC}}$ (and therefore $\delta^{13}\text{C}_{\text{TOC}}$ and $\delta^{13}\text{C}_{\text{marl}}$) during periods of rapid lake volume change, the effect of this exchange on $\delta^{13}\text{C}_{\text{DIC}}$ is minimal relative to the factors discussed above (Li and Ku, 1997). Thus, the influence of vapour exchange on $\delta^{13}\text{C}_{\text{DIC}}$, $\delta^{13}\text{C}_{\text{TOC}}$ and $\delta^{13}\text{C}_{\text{marl}}$ during periods of rapid lake volume change will not be considered here.

In summary, C-MAR, N-MAR, Chl- $a_{(s)}$ -MAR and calcite-MAR serve as proxies of primary production, whereas $\delta^{13}\text{C}_{\text{TOC}}$, $\delta^{18}\text{O}_{\text{marl}}$ and $\delta^{13}\text{C}_{\text{marl}}$ are most strongly controlled by effective moisture and associated lake level change.

2.3.3 Primary production versus effective moisture at Barry Lake from AD ~1100-2017

Variations in effective moisture do not correspond with those of primary production. While primary production remains constant until the end of *Interval V*, effective moisture varies several times throughout the record. During *Interval I* (AD ~1100– 1150), effective moisture is stable and low relative to the rest of the record. *Interval II* (AD ~1150– 1250) is characterized by a sharp increase in effective moisture at the beginning of the record (AD ~1150–1160), followed by a period of stability (AD ~1160– 1250). Effective moisture at this time is high relative to the entire record. During *Interval III* (AD 1250– 1300), effective moisture sharply decreases, reaching levels that are low relative to the rest of the record. Most of *Interval IV* (AD ~1300– 1590) is characterized by climatic stability (AD ~1300– 1590) and low effective moisture relative to the entire record. At the end of this interval (AD 1590– 1650), however, effective moisture rapidly drops, reaching values that are low relative to the rest of the record. During *Interval V* (AD 1650–1900), effective moisture is stable and high. *Interval VI* is characterized by a rapid lowering of effective moisture (AD 1900– 1950) followed by a period of relative stability (AD 1950– 2017). At this time, effective moisture is neither high nor low relative to the rest of the record. Of note is that levels of effective moisture in *Interval VI* are within the range of variations observed across the last ~900 years. This finding suggests that anthropogenic climate warming has not altered effective moisture at Barry Lake beyond pre-industrial levels.

These variations in effective moisture had little impact on primary production. During the MCA (AD 1000– 1350), effective moisture fluctuated, indicating that conditions were unstable and, at times, arid. During the LIA (AD 1450– 1850), effective moisture was comparatively stable, except for one rapid increase in effective moisture, a sign of wetter climatic conditions. These pronounced shifts in effective moisture had little impact on primary production. This finding suggests that the concentration of nutrients (Gąsiorowski and Hercman, 2005; Özen et al., 2010; Yuan et al., 2006) and enhanced vertical mixing (Naselli-Flores, 2003) that occur in lakes during arid periods are not strong drivers of primary production at Barry Lake. Likewise, variations of primary production cannot be explained by the introduction of nutrients via surface flows during wetter periods (Fritz et al., 1991; Ho and Michalak, 2019; Reichwaldt and Ghadouani, 2012).

The sharp increase in primary production that occurs during the modern period, *Interval VI* (AD 1916-2017) is not related to changes in effective moisture. The most rapid increase in primary production occurs after AD 1950 when effective moisture is stable. Stable lake levels are inferred from unchanging $\delta^{18}\text{O}_{\text{marl}}$. High primary production is suggested by rapidly increasing $\delta^{13}\text{C}_{\text{TOC}}$, TOC-MAR, TN-MAR, Chl- $a_{(s)}$ -MAR and calcite-MAR. While variations in $\delta^{13}\text{C}_{\text{TOC}}$ were previously interpreted to reflect variations in effective moisture, significant correlations between the proxies of primary production and $\delta^{13}\text{C}_{\text{TOC}}$ during *Interval VI* suggest that, at this time, increases in $\delta^{13}\text{C}_{\text{TOC}}$ are related to rising primary production. Since photosynthetic organisms preferentially incorporate ^{12}C -rich DIC into their tissues, they enrich the remaining DIC, and future OM, in ^{13}C (Hollander and McKenzie, 1991). As such, it was expected that a substantial rise in primary production would increase $\delta^{13}\text{C}_{\text{TOC}}$.

The timing of increases in Chl- $a_{(s)}$ -MAR and other proxies of primary production suggests that land-use changes and/or anthropogenic climate warming may be responsible for enhancing primary production at the end of *Interval V* and throughout *Interval VI*. Census data demonstrates that European agriculture began near Barry Lake around AD 1850 (Stevenson, 2019), which is also when the proxies of primary production in Barry Lake

begin to rise. Previous studies have attributed sharp increases in primary production to the advent of European agriculture as European settlers manured their fields (Cooper and Brush, 1993; Reinhardt et al., 2005). Runoff containing manure can stimulate primary production (Cooper and Brush, 1993; Reinhardt et al., 2005). Inputs of manure could explain the rising $\delta^{15}\text{N}_{\text{TN}}$ during *Interval VI*. Manure has a high $\delta^{15}\text{N}_{\text{TN}}$ of +6 to +30 ‰ (Lake et al., 2011), so even small inputs of organic fertilizer could drive the 4 ‰ increase in $\delta^{15}\text{N}_{\text{TN}}$ observed here.

Yet, rising $\delta^{15}\text{N}_{\text{TN}}$ may also be the result of other factors, such as (i) rising primary production, (ii) OM degradation and/or (iii) denitrification. A rise in primary production would be expected to drive ^{14}N -limitation in a lake with ephemeral inlets and outlets like Barry Lake, thereby increasing $\delta^{15}\text{N}_{\text{TN}}$ (Hyodo and Longstaffe, 2011; Talbot, 2001). Indeed, $\text{Chl-}a_{(s)\text{-MAR}}$ is significantly correlated with $\delta^{15}\text{N}_{\text{TN}}$ across the entire record, suggesting a strong connection between these variables. Degradation of OM can also result in an increase in $\delta^{15}\text{N}_{\text{TN}}$ (Brahney et al., 2014). It is unlikely, however, that this possibility can explain the rising values of $\delta^{15}\text{N}_{\text{TN}}$ observed during *Interval VI* since modern Barry Lake is stratified and develops anoxic bottom waters throughout much of the year. Increasing $\delta^{15}\text{N}_{\text{TN}}$ could also reflect denitrification, since $^{14}\text{NO}_3$ is selectively utilized by bacteria, enriching the remaining nitrate in ^{15}N . Given that rates of denitrification can increase with primary production, it is possible that both factors are driving rising $\delta^{15}\text{N}_{\text{TN}}$. Without further information, it is therefore not possible to confirm whether inputs of organic fertilizer are responsible for increasing $\delta^{15}\text{N}_{\text{TN}}$ and primary production in Barry Lake.

Another possible driver of increased primary production in *Interval VI* is anthropogenic climate warming (ACW), which can increase primary production by altering temperature and precipitation regimes. Recent increases in precipitation and temperature suggest that ACW is changing effective moisture in Canada (Bonsal et al., 2019). Indeed, the instrumental record suggests that conditions at Barry Lake are slowly becoming wetter and warmer (Fig. 2.5; Harris et al., 2014). The data reported in this chapter are of a sufficiently high temporal resolution that they can be used to investigate the impacts of ACW on

production at Barry Lake from AD 1950-2017. Across this period, June, July and August (JJA) temperatures have increased at a rate of 0.04 °C/year and total JJA precipitation increased at a rate of 0.01 mm/year (Harris et al., 2014). Annual temperatures from AD 1950-2017 have increased at a rate of 0.01 °C/year while total annual precipitation increased at a rate of 0.09 mm/year across this period (Fig. 2.5; Harris et al., 2014). Comparisons between mean JJA temperatures and Chl- $a_{(s)}$ -MAR show that, from AD 1900- 2017, both variables are increasing. Mean annual temperatures also increase with Chl- $a_{(s)}$ -MAR across this period. Yet, higher frequency variations in Chl- $a_{(s)}$ -MAR do not correspond with variations in annual temperature or JJA temperature. These results suggest that rising temperatures are likely one of several factors responsible for the observed increase in primary production.

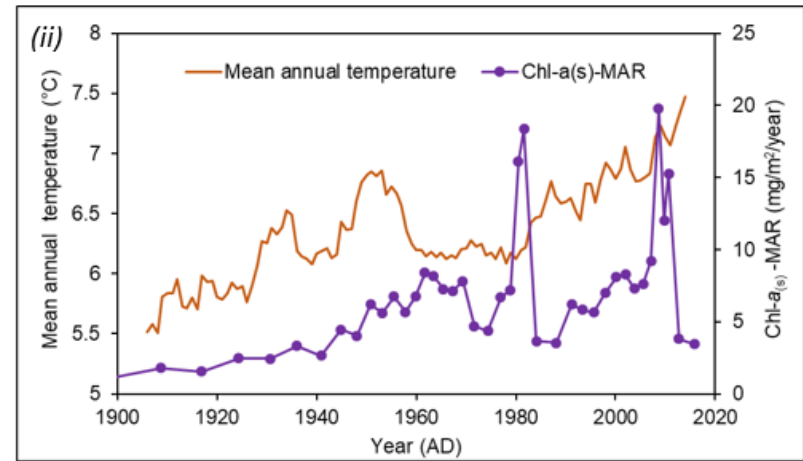
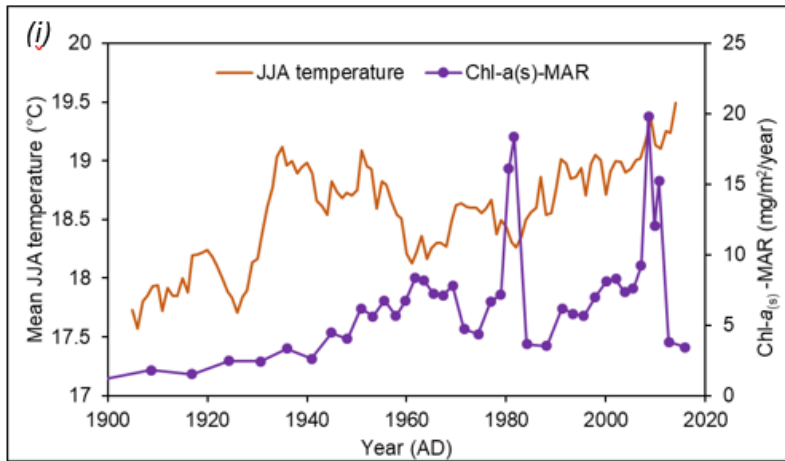


Figure 2.5 Comparisons between Chl- $a_{(s)}$ -MAR from Barry Lake and instrumental temperature records (Harris et al., 2014). *(i)* – comparison between Chl- $a_{(s)}$ -MAR and mean June, July and August temperatures. *(ii)* – comparison between Chl- $a_{(s)}$ -MAR and mean annual temperatures. Both temperature records were smoothed using a 9-year running mean.

Relative to the trends in temperature, variations in total JJA precipitation and total annual precipitation correspond more closely with variations in Chl- $a_{(s)}$ -MAR (Fig. 2.6). At times when Chl- $a_{(s)}$ -MAR peaks, for example, total JJA precipitation and total annual precipitation are also high. In theory, periods of high precipitation could increase primary production in Barry Lake by delivering nutrients to the lake from nearby agricultural fields. This interpretation is complicated by the fact that not all increases in total JJA precipitation or total annual precipitation are accompanied by an increase in Chl- $a_{(s)}$ -MAR. Likewise, if increases in precipitation were responsible for stimulating primary production from AD 1950– present, one would expect to observe significant correlations between $\delta^{18}\text{O}_{\text{marl}}$ and the proxies of primary production across this period. Instead, $\delta^{18}\text{O}_{\text{marl}}$ does not correlate significantly with TOC-MAR, nor does it correlate with TN-MAR or Chl- $a_{(s)}$ -MAR. Interestingly, $\delta^{18}\text{O}_{\text{marl}}$ does correlate significantly with calcite-MAR from AD 1950-present. This finding suggests that production of marl after AD 1950 is being driven by changes in effective moisture for reasons that are not yet clear.

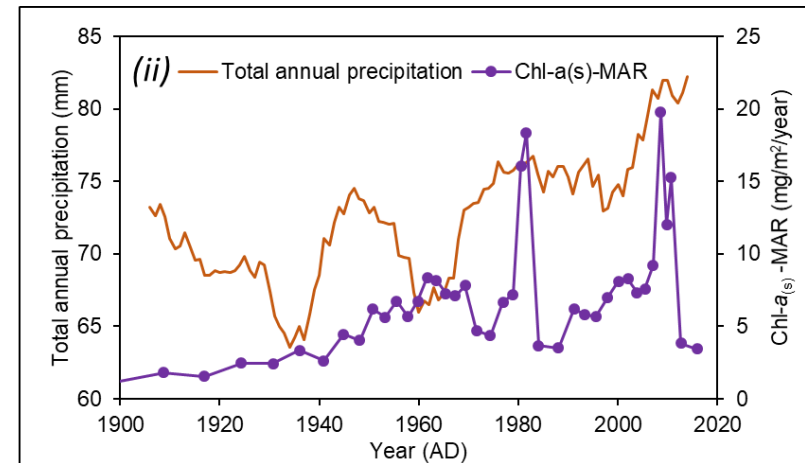
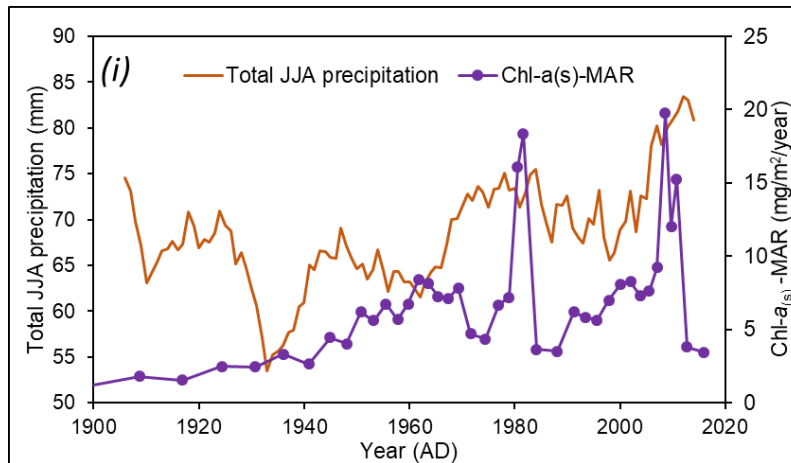


Figure 2.6 Comparisons between Chl- $a_{(s)}$ -MAR from Barry Lake and instrumental precipitation records (Harris et al., 2014). (i) – comparison between Chl- $a_{(s)}$ -MAR and total June, July and August precipitation. (ii) – comparison between Chl- $a_{(s)}$ -MAR and total annual precipitation. Both precipitation records were smoothed using a 9-year running mean.

In short, while the timing of increased primary production in *Interval VI* coincides with land-use changes and ACW, it is unclear which of these factors is the primary driver of rising primary production in Barry Lake. It is possible that each of these factors is working synergistically to stimulate primary production in Barry Lake.

2.3.4 A Regional Comparison of Effective moisture

Proxies of hydroclimate measured at Barry Lake (*i.e.*, $\delta^{13}\text{C}_{\text{TOC}}$, $\delta^{13}\text{C}_{\text{marl}}$ and $\delta^{18}\text{O}_{\text{marl}}$), and hydroclimatic records from other sites in the region, capture widespread, climatic shifts such as the MCA, LIA and the modern period. Although most researchers agree that neither the MCA nor LIA were globally synchronous events during their respective broad time periods, it is generally thought that, in North America, the MCA occurred between AD 1000– 1350, and the LIA occurred between AD 1450– 1850. The modern period spans AD 1850– present. Dry conditions in the Great Lakes region during the MCA may have been driven by an anomalously warm North Atlantic, an anomalously cold Tropical Pacific and a warm, mid-latitude North Pacific, which altered moisture transport across the continent (Booth et al., 2006; Cook et al., 2004). Drier- and wetter-than-average climatic conditions during the LIA have been attributed to movement of the polar jet stream between more southerly and more northerly positions (Buhay and Edwards, 1995). When the polar jet stream was located at higher latitudes, warm moist air moved into southern Ontario. When the polar jet stream was located at lower latitudes, the region received cooler, drier air (Buhay and Edwards, 1995).

At Barry Lake, variations in effective moisture are inferred from $\delta^{18}\text{O}_{\text{marl}}$, $\delta^{13}\text{C}_{\text{marl}}$ and $\delta^{13}\text{C}_{\text{TOC}}$. The conventional dates for the MCA overlap well with periods of especially low effective moisture during *Interval I* (AD ~1100-1139) and *Interval III* (AD 1250-1277) at Barry Lake. Likewise, dates of the LIA overlap with *Interval IV* (AD ~1450-1649), a period of relatively high effective moisture. The modern period overlaps with the latter half of *Interval V* and the entirety of *Interval VI*, a period characterized by fluctuating, but still higher-than-average, effective moisture.

A comparison of hydroclimatic records from across the region (Fig. 2.7; Table 2.1) demonstrates that many sites were indeed drier-than-average during the MCA and modern period, and wetter-than-average during the LIA. Not all sites responded in this fashion, however. Of note is that hydroclimate was more heterogeneous during the MCA and modern periods than during the LIA.

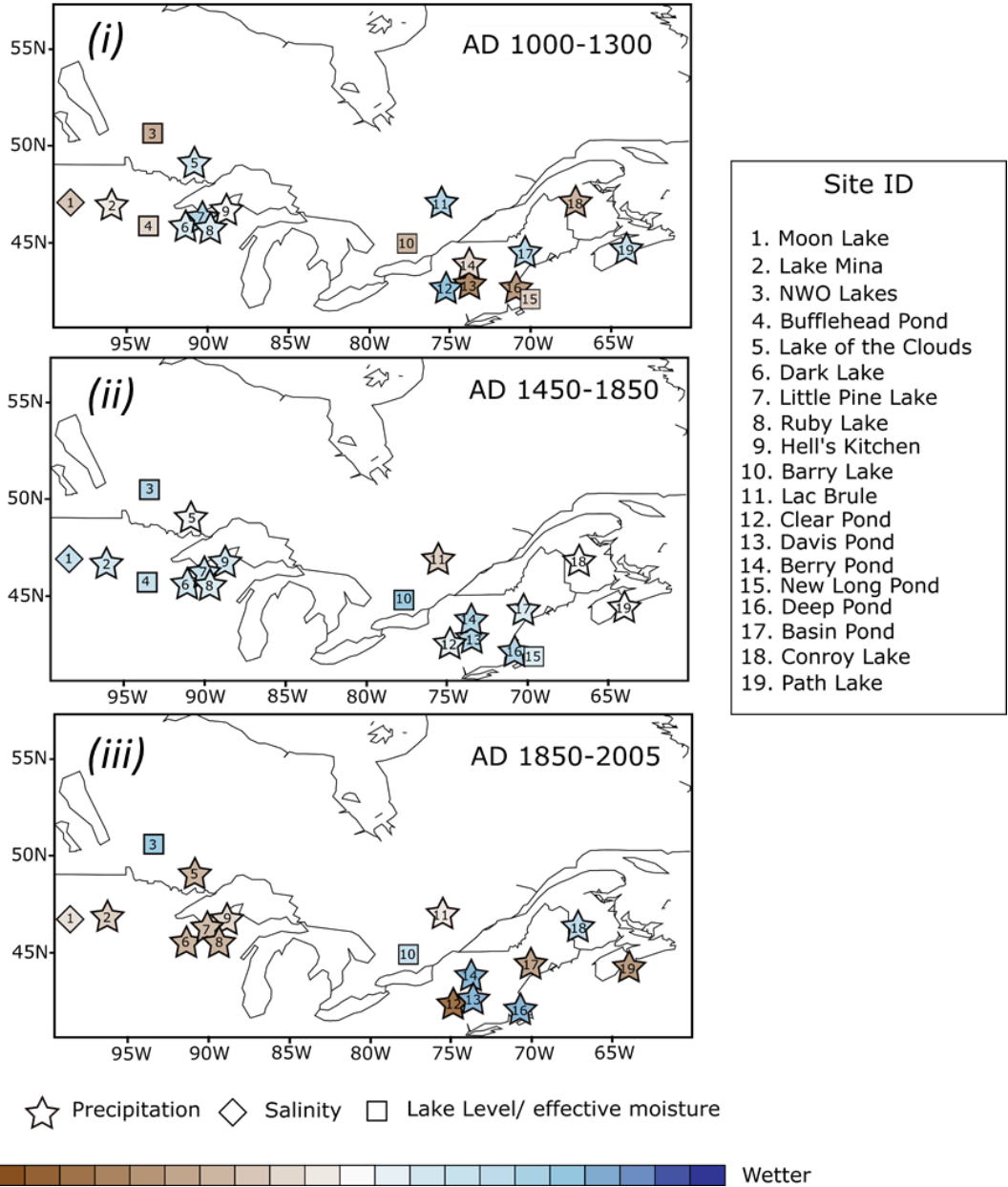


Figure 2.7 A regional view of hydroclimate across the (i) MCA (AD 1000-1350), (ii) LIA (AD 1450-1850) and (iii) the modern period (AD 1850-present). The sites shown here were lake records located between 40-55 °N and 60-100 °W and available from the National Oceanic and Atmospheric Administration (NOAA) paleoclimate database (<https://www.ncdc.noaa.gov/paleo-search/>). All records were averaged into three bins: AD 1000-1350, AD 1450-1850 and AD 1850-2005 and converted into z-scores, as described earlier. Shades of blue denote wetter-than-average conditions while shades of orange indicate more arid-than-average conditions. NWO stands for “northwestern Ontario”.

Table 2.1 A summary of data used to generate Figure 2.7. The sites shown here were (i) located between 40-55 °N and 60-100 °W and (ii) available from the National Oceanic and Atmospheric Administration (NOAA) paleoclimate database (<https://www.ncdc.noaa.gov/paleo-search/>).

Site ID	Main proxy used	Inferred variable	Source
1. Moon Lake	Diatom assemblages	Salinity	Laird et al., 2003
2. Lake Mina	Pollen assemblages	Effective moisture	St. Jacques et al., 2008
3. Northwestern Ontario (NWO)	Diatom assemblages	Lake level	Laird et al., 2012
4. Bufflehead Pond	Ground penetrating radar (GPR)	Lake level	Shuman et al., 2009
5. Lake of the Clouds	Pollen assemblages	Precipitation	Gajewski, 1987
6. Dark Lake	Pollen assemblages	Precipitation	Gajewski, 1987
7. Lake of the Clouds	Pollen assemblages	Precipitation	Gajewski, 1987
8. Ruby Lake	Pollen assemblages	Precipitation	Gajewski, 1987
9. Hell's Kitchen	Pollen assemblages	Precipitation	Gajewski, 1987
13. Barry Lake	$\delta^{18}\text{O}_{\text{marl}}$	Effective moisture/lake level	This study
14. Lac Brule	Pollen assemblages	Precipitation	Lafontaine-Boyer and Gajewski, 2014
16. Clear Pond	Pollen assemblages	Precipitation	Gajewski, 1988
17. Davis Pond	Ground penetrating radar (GPR)	Effective moisture/lake level	Newby et al., 2011
18. Berry Pond	Pollen assemblages	Precipitation	Whitehead, 1979
19. New Long Pond	Ground penetrating radar (GPR)	Effective moisture/lake level	Newby et al., 2009
20. Deep Pond	Ground penetrating radar (GPR)	Effective moisture/lake level	Marsicek et al., 2013
21. Basin Pond	Pollen assemblages	Precipitation	Gajewski, 1988
23. Conroy Lake	Pollen assemblages	Precipitation	Gajewski, 1987
24. Path Lake	Pollen assemblages	Precipitation	Neil et al., 2014

The fact that hydroclimate was heterogeneous during the MCA and modern periods is to be expected since the factors governing moisture are complex and often produce microclimates (Ljungqvist et al., 2020; Shinker, 2010). Furthermore, the hydroclimatic information recorded by each proxy in Figure 2.7 is slightly different. Records employing the

$\delta^{18}\text{O}_{\text{marl}}$ and pollen assemblages, for instance, generally reflect hydrologic changes across the growing season (usually defined as June, July and August), while records constructed using diatoms and ground penetrating radar (GPR) may integrate hydroclimatic variations across multiple seasons (Booth, 2007; Gasse et al., 1997).

Moreover, the records in Figure 2.7 not only reflect regional hydroclimatic variations but also factors in their immediate environment. The inference of salinity from diatoms and effective moisture from $\delta^{18}\text{O}_{\text{marl}}$, for instance, is influenced by the diverse controls on the hydrologic budget of lakes (Fritz, 2013; Talbot, 1990). Likewise, reconstructions of precipitation from pollen records may be confounded by biological interactions between taxa (*e.g.*, competition for nutrients) (Birks and Seppä, 2004). Lastly, inferences of lake level or effective moisture using GPR can be influenced by the mineralogy of the lake sediments (Smith and Jol, 1992).

The fact that the records of hydroclimate in Figure 2.7 record information at different times of the year, and are influenced by their local environment, makes it even more significant that, at times, these records agree. During the LIA, for instance, nearly all the sites in Figure 2.7 reflect wetter-than-average conditions. Widespread agreement across these records at this time provides strong evidence that these indicators recorded a regional increase in moisture availability that lasted many years.

I speculate that the position of the polar jet stream, a key driver of effective moisture in the Great Lakes region, influenced this relatively uniform increase in effective moisture during the LIA. The polar jet stream has occupied higher latitudes in the past (Kirby et al., 2002). It is therefore possible that the polar jet stream did not intersect the region during the LIA, resulting in more uniform delivery of moisture to the sites shown in Figure 2.7. In contrast, the polar jet stream's intersection of the region during the MCA and modern periods would cause moisture availability to differ between the western and the eastern halves of the region.

The Barry Lake hydroclimate record shows remarkable similarities with site 3 and site 25 shown on Figure 2.7. Variations in $\delta^{18}\text{O}_{\text{marl}}$, for instance, show similarities to a diatom-based reconstruction for northwestern Ontario lakes (Laird et al., 2012) (Fig. 2.8). This record, and $\delta^{18}\text{O}_{\text{marl}}$ from Barry Lake, suggest that lake levels were below average (indicating arid conditions) during the MCA, and above average (indicating wetter conditions) during the LIA. Although records from bogs tend to record decadal climatic trends rather than centennial trends, testate amoeba-derived water table depths at Saco Bog (Maine, USA) echo these findings. The fact that variations in $\delta^{18}\text{O}_{\text{marl}}$ from Barry Lake correspond with these other two hydroclimatic records suggests that the changes in effective moisture observed at Barry Lake are not simply a reflection of local hydrologic variations but are recording regional variations in atmospheric moisture.

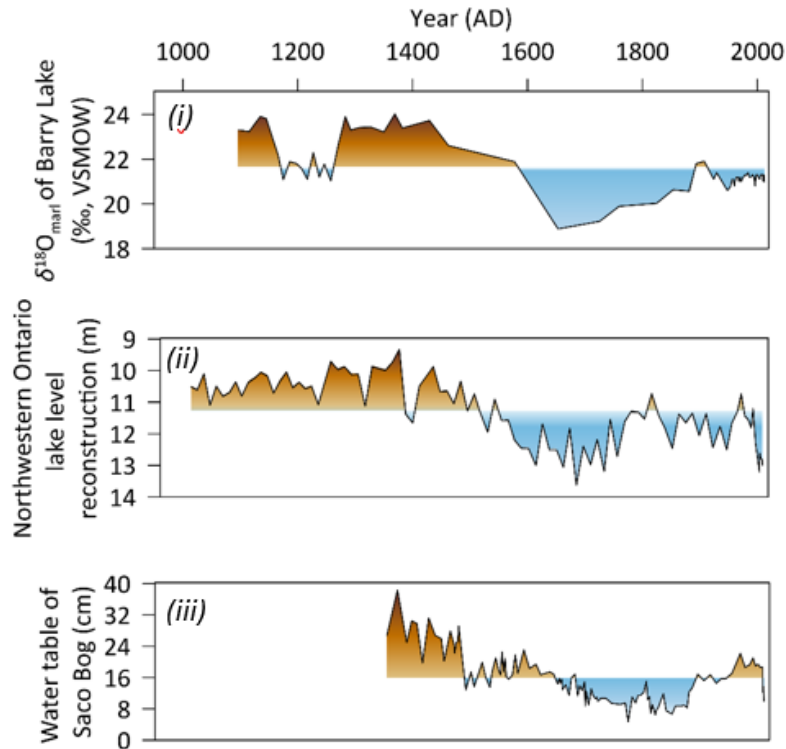


Figure 2.8 A comparison of (i) the $\delta^{18}\text{O}_{\text{marl}}$ record from BL-G17-01, (ii) a diatom-based reconstruction of lake level from lakes in northwestern Ontario (site 3 in Figure 2.7; Laird et al., 2012) and (iii) a reconstructed water table record from Saco Bog, Maine (site 25 in Figure 2.7), derived from testate amoebae (Clifford and Booth, 2013). Drier-than-average values are depicted in orange while wetter-than-average values are coloured blue.

2.4 Conclusions

Effective moisture at Barry Lake, southeastern Ontario, Canada, inferred mainly from $\delta^{18}\text{O}_{\text{marl}}$, has changed substantially over the past ~900 years, with more arid conditions during the MCA and wetter conditions during the LIA. The Barry Lake $\delta^{18}\text{O}_{\text{marl}}$ record is similar to other proxy records of lake level from northwestern Ontario, Canada (diatoms) and water table depths from Saco Bog, Maine, USA (testate amoebae), but different from hydroclimatic records at other sites, particularly during the MCA and modern period (AD 1850-2017). These comparisons indicate that hydroclimate has been more heterogeneous across the Great Lakes/St. Lawrence and northeastern USA during arid periods than during wetter periods, likely due to variations in the position of the polar jet stream. Effective moisture, as inferred from the Barry Lake record, remains within the range of natural

variation observed over the last millennium. Primary production in Barry Lake, as indicated by TOC-MAR, TN-MAR and calcite-MAR, was relatively insensitive to hydroclimatic change throughout the record. Inferences of primary production in the last 150 years are greater than the range of natural variation observed over the last millennium, despite only small changes in effective moisture since 1850. Therefore, shifts in effective moisture are unlikely to drive increases in primary production in small, dimictic lakes such as Barry Lake. Instead, the driver of the recent increase in primary production is likely related to ACW and/or land-use changes.

2.5 References

Appleby, P.G., Oldfield, F., 1978. The calculation of lead-210 dates assuming a constant rate of supply of unsupported ^{210}Pb to the sediment. *Catena* 5, 1–8.

[https://doi.org/10.1016/S03418162\(78\)80002-2](https://doi.org/10.1016/S03418162(78)80002-2)

Bai, J., Perron, P., 2002. Computation and analysis of multiple structural change models. *J. Appl. Econom.* 18, 1–22. <https://doi.org/10.1002/jae.659>

Beaudoin, A.B., Reasoner, M.A., 1992. Evaluation of differential pollen deposition and pollen focusing from three Holocene intervals in sediments from Lake O’Hara, Yoho National Park, British Columbia, Canada: intra-lake variability in pollen percentages, concentrations and influx. *Rev. Palaeobot. Palynol.* 75, 103–131.

[https://doi.org/10.1016/0034-6667\(92\)90152-7](https://doi.org/10.1016/0034-6667(92)90152-7)

Birks, H.J.B., Seppä, H., 2004. Pollen-based reconstructions of late-Quaternary climate in Europe Progress, problems, and pitfalls. *Acta Palaeobot.* 44, 317–334.

Blaauw, M., Christen, J.A., 2011. Flexible paleoclimate age-depth models using an autoregressive gamma process. *Bayesian Anal.* 6, 457–474.

<https://doi.org/10.1214/11BA618>

- Bonsal, B.R., Peters, D.L., Seglenieks, F., Rivera, A., Berg, A., 2019. Changes in freshwater availability across Canada, in: Bush, E., Lemmen, D.S. (Eds.), Canada's Changing Climate Report. Government of Canada, Ottawa, Canada, pp. 261.
- Booth, R.K., Jackson, S.T., Sousa, V.A., Sullivan, M.E., Minckley, T.A., Clifford, M.J., 2012. Multi-decadal drought and amplified moisture variability drove rapid forest community change in a humid region. *Ecology* 93, 219–226.
<https://doi.org/10.1890/11-1068.1>
- Booth, R.K., 2007. Testate amoebae as proxies for mean annual water-table depth in *Sphagnum*-dominated peatlands of North America. *J. Quat. Sci.* 23, 43–57.
<https://doi.org/10.1002/jqs.1114>
- Booth, R.K., Notaro, M., Jackson, S.T., Kutzbach, J.E., 2006. Widespread drought episodes in the western Great Lakes region during the past 2000 years: Geographic extent and potential mechanisms. *Earth Planet. Sci. Lett.* 242, 415–427.
<https://doi.org/10.1016/j.epsl.2005.12.028>
- Brahney, J., Ballantyne, A.P., Turner, B.L., Spaulding, S.A., Otu, M., Neff, J.C., 2014. Separating the influences of diagenesis, productivity and anthropogenic nitrogen deposition on sedimentary $\delta^{15}\text{N}$ variations. *Org. Geochem.* 75, 140–150.
<https://doi.org/10.1016/j.orggeochem.2014.07.003>
- Buhay, W.M., Edwards, T.W.D., 1995. Climate in southwestern Ontario, Canada, between AD 1610 and 1885 inferred from oxygen and hydrogen isotopic measurements of wood cellulose from trees in different hydrologic settings. *Quat. Res.* 44, 438–446.
<https://doi.org/10.1006/qres.1995.1089>
- Buhay, W.M., Edwards, T.W.D., 1993. Reconstruction of Little Ice Age climate in southwestern Ontario, Canada, from oxygen and hydrogen isotope ratios in tree rings. *Int. At. Energy Agency, Proc. Ser.* 329, 407–417.

- Clifford, M.J., Booth, R.K., 2013. Increased probability of fire during late Holocene droughts in northern New England. *Clim. Change*. 119, 693–704.
<https://doi.org/10.1007/s10584-013-0771-y>
- Cook, E.R., Seager, R., Heim, R.R., Vose, R.S., Herweijer, C., Woodhouse, C., 2009. Megadroughts in North America: placing IPCC projections of hydroclimatic change in a long-term palaeoclimate context. *J. Quat. Sci.* 25, 48–61.
<https://doi.org/10.1002/jqs.1303>
- Cook, E.R., Woodhouse, C.A., Eakin, C.M., Meko, D.H., Stahle, D.W., 2004. Long-term aridity changes in the western United States. *Science*. 306, 1015–1018.
<https://doi.org/10.1126/science.1102586>
- Cooper, S.R., Brush, G.S., 1993. A 2,500-year history of anoxia and eutrophication in Chesapeake Bay. *Estuaries* 16, 617–626. <https://doi.org/10.2307/1352799>
- Craig, H., 1965. The measurement of oxygen isotope paleotemperatures, in: Tongiorgi, E. (Ed.), *Stable Isotopes in Oceanographic Studies and Paleotemperatures*, first ed. Consiglio Nazionale delle Ricerche, Laboratorio de Geologia Nuclare, Pisa, pp. 161–182.
- Derrick, T.R., Bates, B.T., Dufek, J.S., 1994. Evaluation of time-series data sets using the Pearson product moment correlation coefficient. *Med. Sci. Sports Exerc.* 26, 919–928. <https://doi.org/10.1249/00005768-199407000-00018>
- Diefendorf, A.F., Patterson, W.P., Holmden, C., Mullins, H.T., 2008. Carbon isotopes of marl and lake sediment organic matter reflect terrestrial landscape change during the late Glacial and early Holocene (16,800 to 5,540 cal yr B.P.): A multiproxy study of lacustrine sediments at Lough Inchiquin, western Ireland. *J. Paleolimnol.* 39, 101–115. <https://doi.org/10.1007/s10933-0079099-9>

- Downing, J.A., Rath, L.C., 1988. Spatial patchiness in the lacustrine sedimentary environment. *Limnol. Oceanogr.* 33, 447–458.
<https://doi.org/10.4319/lo.1988.33.3.0447>
- Drummond, C.N., Patterson, W.P., Walker, J.C.G., 1995. Climatic forcing of carbon oxygen isotopic covariance in temperate-region marl lakes. *Geology* 23, 1031–1034. [https://doi.org/10.1130/00917613\(1995\)023<1031:cfocoi>2.3.co;2](https://doi.org/10.1130/00917613(1995)023<1031:cfocoi>2.3.co;2)
- Edwards, T.W.D., Fritz, P., 1986. Assessing meteoric water composition and relative humidity from ^{18}O and ^2H in wood cellulose: paleoclimatic implications for southern Ontario, Canada. *J. Appl. Geochem.* 1, 715–723.
[https://doi.org/10.1016/0883-2927\(86\)90093-4](https://doi.org/10.1016/0883-2927(86)90093-4)
- Ekdahl, E.J., Teranes, J.L., Guilderson, T.P., Turton, C.L., McAndrews, J.H., Wittkop, C.A., Stoermer, E.F., 2004. Prehistorical record of cultural eutrophication from Crawford Lake, Canada. *Geology* 32, 745–748. <https://doi.org/10.1130/G20496.1>
- Fritz, S.C., 2013. Salinity and climate reconstructions from continental lakes, in: Elias, S.A. and Mock, C.J. (Eds.) *Encyclopedia of Quaternary Science*, second ed. Newnes, Oxford, England, pp. 507–515. <https://doi.org/10.1016/B978-0-444-536433.00221-1>
- Fritz, S.C., Juggins, S., Battarbee, R.W., Engstrom, D.R., 1991. Reconstruction of past changes in salinity and climate using a diatom-based transfer function. *Nature* 352, 706–708. <https://doi.org/10.1038/352706a0>
- Gajewski, K., 1987. Climatic impacts on the vegetation of eastern North America during the past 2000 years. *Quat. Sci. Rev.* 68, 179–190. <https://doi.org/10.1007/BF00114719>
- Gajewski, K., 1988. Late Holocene climate changes in eastern North America estimated from pollen data. *Quat. Res.* 29, 255–262. [https://doi.org/10.1016/0033-5894\(88\)90034-8](https://doi.org/10.1016/0033-5894(88)90034-8)

- Gąsiorowski, M., Hercman, H., 2005. Recent sedimentation and eutrophication of Kruklin lake after artificial drop in water-level in the middle of 19th century. *Stud. Quat.* 22, 17–25.
- Gasse, F., Barker, P., Gell, P.A., Fritz, S.C., Chalié, F., 1997. Diatom-inferred salinity in palaeolakes: An indirect tracer of climate change. *Quat. Sci. Rev.* 16, 547–563. [https://doi.org/10.1016/S02773791\(96\)00081-9](https://doi.org/10.1016/S02773791(96)00081-9)
- Glew, J.R., Smol, J.P., Last, W.M., 2002. Sediment Core Collection and Extrusion, in: Smol, J.P., Last, W.M. (Eds.), *Tracking Environmental Change Using Lake Sediments*, first ed. Springer, Dordrecht, Netherlands, pp. 73–105. https://doi.org/10.1007/0-30647669-x_5
- Guilizzoni, P., Bonomi, G., Galanti, G., Ruggiu, D., 1983. Relationship between sedimentary pigments and primary production: Evidence from core analyses of twelve Italian lakes, in: Meriläinen, J., Huttunen, P., Battarbee, W. (Eds.), *Paleolimnology*, first ed. Springer Netherlands, Dordrecht, Netherlands, pp. 103–106. https://doi.org/10.1007/978-94-009-7290-2_17
- Hammarlund, D., Aravena, R., Barnekow, L., Buchardt, B., Possnert, G., 1997. Multi component carbon isotope evidence of early Holocene environmental change and carbon-flow pathways from a hard-water lake in northern Sweden. *J. Paleolimnol.* 18, 219–233. <https://doi.org/10.1023/A:1007953614927>
- Harris, D., Horwath, W. R., VanKessel, C., 2001. Acid fumigation of soils to remove carbonates prior to total organic carbon or carbon-13 isotopic analysis. *Soil Soc. Am. J.* 65, 1853–1856. <https://doi.org/10.2136/sssaj2001.1853>
- Harris, I., Jones, P.D., Osborn, T.J., Lister, D.H., 2014. Updated high-resolution grids of monthly climatic observations - the CRU TS3.10 Dataset. *Int. J. Climatol.* 34, 623–642. <https://doi.org/10.1002/joc.3711>

- Henderson, A.K., Shuman, B.N., 2009. Hydrogen and oxygen isotopic compositions of lake water in the western United States. *Bull. Geol. Soc. Am.* 121, 1179–1189. <https://doi.org/10.1130/B26441.1>
- Hilton, J., 1985. A conceptual framework for predicting the occurrence of sediment focusing and sediment redistribution in small lakes. *Limnol. Oceanogr.* 30, 1131–1143. <https://doi.org/10.4319/lo.1985.30.6.1131>
- Hladyniuk, R., Longstaffe, F.J., 2015. Paleoproductivity and organic matter sources in Late Quaternary Lake Ontario. *Palaeogeogr. Palaeoclimatol. Palaeoecol.* 435, 13–23. <https://doi.org/10.1016/j.palaeo.2015.05.026>
- Ho, J.C., Michalak, A.M., 2019. Exploring temperature and precipitation impacts on harmful algal blooms across continental U.S. lakes. *Limnol. Oceanogr.* 65, 1–19. <https://doi.org/10.1002/lno.11365>
- Hollander, D.J., McKenzie, J.A., 1991. CO₂ control on carbon-isotope fractionation during aqueous photosynthesis: A paleo-*p*CO₂ barometer. *Geology* 19, 929–932. [https://doi.org/10.1130/00917613\(1991\)019<0929:CCOCIF>2.3.CO;2](https://doi.org/10.1130/00917613(1991)019<0929:CCOCIF>2.3.CO;2)
- Hundey, E.J., Moser, K.A., Longstaffe, F.J., Michelutti, N., Hladyniuk, R., 2014. Recent changes in production in oligotrophic Uinta Mountain lakes, Utah, identified using paleolimnology. *Limnol. Oceanogr.* 59, 1987–2001. <https://doi.org/10.4319/lo.2014.59.6.1987>
- Hyodo, A., Longstaffe, F.J., 2011. The palaeoproductivity of ancient Lake Superior. *Quat. Sci. Rev.* 30, 2988–3000. <https://doi.org/10.1016/J.QUASCIREV.2011.07.004>
- Jasechko, S., Gibson, J.J., Edwards, T.W.D., 2014. Stable isotope mass balance of the Laurentian Great Lakes. *J. Great Lakes Res.* 40, 336–346. <https://doi.org/10.1016/j.jglr.2014.02.020>

- Kim, S.T., O'Neil, J.R., 1997. Equilibrium and nonequilibrium oxygen isotope effects in synthetic carbonates. *Geochim. Cosmochim. Acta.* 61, 3461–3475.
[https://doi.org/10.1016/S00167037\(97\)00169-5](https://doi.org/10.1016/S00167037(97)00169-5)
- Kirby, M., Patterson, W., Mullins, H., Burnett, A., 2002. Post-Younger Dryas climate interval linked to circumpolar vortex variability: Isotopic evidence from Fayetteville Green Lake, New York. *Clim. Dyn.* 19, 321–330.
<https://doi.org/10.1007/s00382-002-0227-y>
- Lafontaine-Boyer, K., Gajewski, K., 2014. Vegetation dynamics in relation to late Holocene climate variability and disturbance, Outaouais, Québec, Canada. *Holocene* 24, 1515–1526. <https://doi.org/10.1177/0959683614544054>
- Laird, K.R., Fritz, S.C., Grimm, E.C., Mueller, P.G., 2003. Moon Lake 11,000 year diatom inferred salinity data. *Papers in the Geosciences* 23.
<https://digitalcommons.unl.edu/geosciencefacpub/23>
- Laird, K.R., Haig, H.A., Ma, S., Kingsbury, M. V., Brown, T.A., Lewis, C.F.M., Oglesby, R.J., Cumming, B.F., 2012. Expanded spatial extent of the Medieval Climate Anomaly revealed in lake-sediment records across the boreal region in northwest Ontario. *Glob. Chang. Biol.* 18, 2869–2881.
<https://doi.org/10.1111/j.13652486.2012.02740.x>
- Lake, J.L., McKinney, R.A., Osterman, F.A., Pruell, R.J., Kiddon, J., Ryba, S.A., Libby, A.D., 2011. Stable nitrogen isotopes as indicators of anthropogenic activities in small freshwater systems. *Can. J. Fish. Aquat. Sci.* 58, 870–878.
<https://doi.org/10.1139/f01-038>
- Lemdahl, G., 2000. Late-glacial and Early Holocene insect assemblages from sites at different altitudes in the Swiss Alps – implications on climate and environment. *Palaeogeogr. Palaeoclimatol. Palaeoecol.* 159, 293–312.
[https://doi.org/10.1016/S0031-0182\(00\)00091-2](https://doi.org/10.1016/S0031-0182(00)00091-2)

- Le Moal, M., Gascuel-Oudou, C., Ménesguen, A., Souchon, Y., Étrillard, C., Levain, A., Moatar, F., Pannard, A., Souchu, P., Lefebvre, A., Pinay, G., 2019. Eutrophication: A new wine in an old bottle? *Sci. Total Environ.* 651, 1–11.
<https://doi.org/10.1016/j.scitotenv.2018.09.139>
- Li, H.C., Ku, T.L., 1997. $\delta^{13}\text{C}$ - $\delta^{18}\text{O}$ covariance as a paleohydrological indicator for closed basin lakes. *Palaeogr. Palaeoclimatol. Palaeoecol.* 133, 69–80.
[https://doi.org/10.1016/S0031-0182\(96\)00153-8](https://doi.org/10.1016/S0031-0182(96)00153-8)
- Li, Z., Xu, X., Ji, M., Wang, G., Han, R., Ma, J., Yan, X., Liu, J., 2018. Estimating sedimentary organic matter sources by multi-combined proxies for spatial heterogeneity in a large and shallow eutrophic lake. *J. Environ. Manage.* 224, 147–155. <https://doi.org/10.1016/j.jenvman.2018.07.017>
- Liu, Z., 2016. Stable isotope paleolimnology of Barry Lake, Ontario since AD ~1268. Electronic Thesis and Dissertation Repository 3497. <https://ir.lib.uwo.ca/etd/3497>
- Ljungqvist, F.C., Piermattei, A., Seim, A., Krusic, P.J., Büntgen, U., He, M., Kirilyanov, A. V., Luterbacher, J., Schneider, L., Seftigen, K., Stahle, D.W., Villalba, R., Yang, B., Esper, J., 2020. Ranking of tree-ring based hydroclimate reconstructions of the past millennium. *Quat. Sci. Rev.* 230, 106074.
<https://doi.org/10.1016/j.quascirev.2019.106074>
- Lowe, D.J., Green, J.D., Northcote, T.G., Hall, K.J., 1997. Holocene fluctuations of a meromictic lake in southern British Columbia. *Quat. Res.* 48, 100–113.
<https://doi.org/10.1006/qres.1997.1905>
- Ma, S., Laird, K.R., Kingsbury, M. V, Lewis, C.F.M., Cumming, B.F., 2013. Diatom-inferred changes in effective moisture during the late Holocene from nearshore cores in the southeastern region of the Winnipeg River Drainage Basin (Canada). *Holocene* 23, 568–578. <https://doi.org/10.1177/0959683612463103>

- Marsicek, J.P., Shuman, B., Brewer, S., Foster, D.R., Oswald, W.W., 2013. Moisture and temperature changes associated with the mid-Holocene *Tsuga* decline in the northeastern United States, *Quat. Sci. Rev.* 80, 129–142.
<https://doi.org/10.1016/j.quascirev.2013.09.001>
- McConnaughey, T.A., LaBaugh, J.W., Rosenberry, D. O, Striegl, R.G., Reddy, M.M., Schuster, P.F., Carter, V., 1994. Carbon budget for a groundwater-fed lake: Calcification supports summer photosynthesis. *Limnol. Oceanogr.* 39, 1319–1332.
<https://doi.org/10.4319/lo.1994.39.6.1319>
- Meyers, P.A., 1994. Preservation of elemental and isotopic source identification of sedimentary organic matter. *Chem. Geol.* 114, 289–302.
[https://doi.org/10.1016/0009-2541\(94\)90059-0](https://doi.org/10.1016/0009-2541(94)90059-0)
- Meyers, P.A., Ishiwatari, R., 1993. Lacustrine organic geochemistry – an overview of indicators of organic matter sources and diagenesis in lake sediments. *Org. Geochem* 20, 867–900. [https://doi.org/10.1016/0146-6380\(93\)90100-P](https://doi.org/10.1016/0146-6380(93)90100-P)
- Michelutti, N., Blais, J.M., Cumming, B.F., Paterson, A.M., Rühland, K., Wolfe, A.P., Smol, J.P., 2010. Do spectrally inferred determinations of chlorophyll *a* reflect trends in lake trophic status? *J. Paleolimnol.* 43, 205–217.
<https://doi.org/10.1007/s10933-009-9325-8>
- Murphy, D.H., Wilkinson, B.H., 1980. Carbonate deposition and facies distribution in a central Michigan marl lake. *Sedimentology* 27, 123–135.
<https://doi.org/10.1111/j.1365-3091.1980.tb01164.x>
- Naselli-Flores, L., 2003. Man-made lakes in Mediterranean semi-arid climate: the strange case of Dr. Deep Lake and Mr. Shallow Lake, *Hydrobiologia* 506, 13–21.
<https://doi.org/10.1023/B:HYDR.0000008550.34409.06>

- Neil, K., Gajewski, K., Betts, M., 2014. Human-ecosystem interactions in relation to Holocene environmental change in Port Joli Harbour, southwestern Nova Scotia, Canada. *Quat. Res.* 81, 203-212. <https://doi.org/10.1016/j.yqres.2014.01.001>
- Newby, P.E., Donnelly, J.P., Shuman, B.N., MacDonald, D., 2009. Evidence of centennial-scale drought from southeastern Massachusetts during the Pleistocene/Holocene transition. *Quat. Sci. Rev.* 28, 1675–1692. <https://doi.org/10.1016/j.quascirev.2009.02.020>
- Newby, P.E., Shuman, B.N., Donnelly, J.P., MacDonald, D., 2011. Repeated century-scale droughts over the past 13,000 yr near the Hudson River watershed, USA. *Quat. Res.* 75, 523-530. <https://doi.org/10.1016/j.yqres.2011.01.006>
- Özen, A., Karapinar, B., Kucuk, I., Jeppesen, E., Beklioglu, M., 2010. Drought-induced changes in nutrient concentrations and retention in two shallow Mediterranean lakes subjected to different degrees of management. *Hydrobiologia* 646, 61–72. <https://doi.org/10.1007/s10750-010-0179-x>
- Paquette, N., Gajewski, K., 2013. Climatic change causes abrupt changes in forest composition, inferred from a high-resolution pollen record, southwestern Quebec, Canada. *Quat. Sci. Rev.* 75, 169–180. <https://doi.org/10.1016/J.QUASCIREV.2013.06.007>
- Potůčková, A., Hájková, P., Žáčková, P., Petr, L., Grygar, T.M., Weiser, M., 2018. Spatiotemporal heterogeneity of the palaeoecological record in a large temperate palaeolake, Šúr, southwest Slovakia: Comparison of pollen, macrofossil and geochemical data. *Palaeogeogr. Palaeoclimatol. Palaeoecol.* 489, 52–63. <https://doi.org/10.1016/j.palaeo.2017.09.010>
- Reichwaldt, E.S., Ghadouani, A., 2012. Effects of rainfall patterns on toxic cyanobacterial blooms in a changing climate: Between simplistic scenarios and complex dynamics. *Water Res.* 46, 1372– 1393. <https://doi.org/10.1016/j.watres.2011.11.052>

- Reimer, P.J., Bard, E., Bayliss, A., Beck, J.W., Blackwell, P.G., Ramsey, C.B., Buck, C.E., Cheng, H., Edwards, R.L., Friedrich, M., Grootes, P.M., Guilderson, T.P., Hafliðason, H., Hajdas, I., Hatté, C., Heaton, T.J., Hoffmann, D.L., Hogg, A.G., Hughen, K.A., Kaiser, K.F., Kromer, B., Manning, S.W., Niu, M., Reimer, R.W., Richards, D.A., Scott, E.M., Southon, J.R., Staff, R.A., Turney, C.S.M., van der Plicht, J., 2013. IntCal13 and Marine13 Radiocarbon Age Calibration Curves 0–50,000 Years cal BP. *Radiocarbon* 55, 1869–1887.
https://doi.org/10.2458/azu_js_rc.55.16947
- Reinhardt, E.G., Little, M., Donato, S., Findlay, D., Krueger, A., Clark, C., Boyce, J., 2005. Arcellacean (thecamoebian) evidence of land-use change and eutrophication in Frenchman’s Bay, Pickering, Ontario. *Environ. Geol.* 47, 729–739.
<https://doi.org/10.1007/s00254-004-1213-y>
- Shinker, J.J., 2010. Visualizing spatial heterogeneity of western U.S. climate variability. *Earth Interact.* 14, 1–15. <https://doi.org/10.1175/2010EI323.1>
- Shuman, B., Henderson, A.K., Plank, C., Stefanova, I., Ziegler, S.S., 2009. Woodland-to forest transition during prolonged drought in Minnesota after ca. AD 1300. *Ecology* 90, 2792–2807. <https://doi.org/10.1890/08-0985.1>
- Smith, D.G., Jol, H.M., 1992. GPR results used to infer depositional processes of coastal spits in large lakes. *Spec. Pap. Geol. Surv. Finl.* 16, 169–177.
<https://doi.org/10.3997/2214-4609-PDB.303.22>
- St. Jacques, J.M., Cumming, B.F., Smol, J.P., 2008. A 900-year pollen-inferred temperature and effective moisture record from varved Lake Mina, west-central Minnesota, USA. *Quat. Sci. Rev.* 27, 781–796.
<https://doi.org/10.1016/j.quascirev.2008.01.005>
- Stevenson, M., 2019. Upper Canada (Ontario) Land Registry Records Research [WWW Document]. Ontario Genealogy. URL

<https://www.ontariogenealogy.com/canadacensusrecords/uppercanadaontarioensusreords851/northumberlandcountypioneersettlers/percytownship1851agrulturalcensus.pdf> (accessed 4.14.19).

Sun, M., Aller, R.C., Lee, C., 1991. Early diagenesis of chlorophyll-*a* in Long Island Sound sediments: a measure of carbon flux and particle reworking. *J. Mar. Res.* 49, 379–401. <https://doi.org/10.1357/002224091784995927>

Szymczak-Zyła, M., Kowalewska, G., Louda, J.W., 2011. Chlorophyll-*a* and derivatives in recent sediments as indicators of productivity and depositional conditions. *Mar. Chem.* 125, 39–48. <https://doi.org/10.1016/j.marchem.2011.02.002>

Szymczak-Zyła, M., Kowalewska, G., Louda, J.W., 2008. The influence of microorganisms on chlorophyll *a* degradation in the marine environment. *Limnol. Oceanogr.* 53, 851–862. <https://doi.org/10.4319/lo.2008.53.2.0851>

Talbot, M., 2001. Nitrogen isotopes in paleolimnology, in: Smol, J., Birks, H., Last, W. (Eds.), *Tracking Environmental Change Using Lake Sediments*, first ed. Springer Netherlands, Dordrecht, Netherlands, pp. 401–439.

Talbot, M.R., 1990. A review of the palaeohydrological interpretation of carbon and oxygen isotopic ratios in primary lacustrine carbonates. *Chem. Geol. Isot. Geosci. Sect.* 80, 261–279. [https://doi.org/10.1016/0168-9622\(90\)90009-2](https://doi.org/10.1016/0168-9622(90)90009-2)

Toms, J.D., Lesperance, M.L., 2003. Piecewise regression: a tool for identifying ecological thresholds. *Ecology* 84, 2034–2041. <https://doi.org/10.1890/02-0472>

Verburg, P., 2007. The need to correct for the Suess effect in the application of $\delta^{13}\text{C}$ in sediment of autotrophic Lake Tanganyika, as a productivity proxy in the Anthropocene. *J. Paleolimnol.* 37, 591–602. <https://doi.org/10.1007/s10933006-9056-z>

- Verrecchia, E.P., Verrecchia, K.E., 1994. Needle-fiber calcite: A critical review and a proposed classification. *J. Sediment Res.* 64, 650–664.
<https://doi.org/10.1306/d4267e332b26-11d78648000102c1865d>
- Wang, W., Lee, X., Xiao, W., Liu, S., Schultz, N., Wang, Y., Zhang, M., Zhao, L., 2018. Global lake evaporation accelerated by changes in surface energy allocation in a warmer climate. *Nat. Geosci.* 11, 410–414.
<https://doi.org/10.1038/s41561-018-0114-8>
- Whitehead, D.R., 1979. Late-glacial and postglacial vegetational history of the Berkshires, western Massachusetts. *Quat. Res.* 12, 333–357.
[https://doi.org/10.1016/0033-5894\(79\)90033-4](https://doi.org/10.1016/0033-5894(79)90033-4)
- Wiik, E., Bennion, H., Sayer, C.D., Willby, N.J., 2014. Chemical and biological responses of marl lakes to eutrophication. *Freshw. Rev.* 6, 35–62. <https://doi.org/10.1608/frj.6.2.630>
- Yu, S.Y., Berglund, B.E., Sandgren, P., Colman, S.M., 2007. Holocene organic carbon burial rates in the southeastern Swedish Baltic Sea. *Holocene* 17, 673–681.
<https://doi.org/10.1177/0959683607079001>
- Yuan, F., Linsley, B.K., Howe, S.S., 2006. Evaluating sedimentary geochemical lake-level tracers in Walker Lake, Nevada, over the last 200 years. *J. Paleolimnol.* 36, 37–54.
<https://doi.org/10.1007/s10933-006-0004-8>
- Yunev, O.A., Vedernikov, V.I., Basturk, O., Yilmaz, A., Kideys, A.E., Moncheva, S., Konovalov, S.K., 2002. Long-term variations of surface chlorophyll *a* and primary production in the open Black Sea. *Mar. Ecol. Prog. Ser.* 230, 11–28.
<https://doi.org/10.3354/meps230011>
- Zeileis, A., Kleiber, C., Krämer, W., Hornik, K., 2003. Testing and dating of structural changes in practice. *Comput. Stat. Data Anal.* 44, 109–123.

[https://doi.org/10.1016/S0167-9473\(03\)00030-6](https://doi.org/10.1016/S0167-9473(03)00030-6)

Zhang, X., Flato, G., Kirchmeier-Young, M., Vincent, L., Wan, H., Wang, X., Rong, R., Fyfe, J., Li, G., Kharin, V.V., 2019. Temperature and precipitation across Canada, in: Bush, E., Lemmen, D.S. (Eds.), *Canada's Changing Climate Report*. Government of Canada, Ottawa, Canada, pp. 117.

Chapter 3

3 Uncovering the linkages between effective moisture and the carbon dynamics of a small kettle lake in Ontario, Canada

3.1 Introduction

The carbon dynamics of lakes have changed dramatically across the last century (Deemer et al., 2016; Downing et al., 2003; Heathcote et al., 2015). Due to the influx of fertilizer-rich runoff to lakes, lakes are becoming more eutrophic (Le Moal et al., 2018). Eutrophication alters the carbon dynamics of lakes by increasing primary production (Le Moal et al., 2018). As primary production rises, bottom waters grow more anoxic (Heathcote and Downing, 2012). This enhanced anoxia improves organic matter (OM) preservation, increases carbon sequestration and stimulates methanogenesis (Beaulieu et al., 2019; Deemer et al., 2016; Pacheco et al., 2014). Compounding the problem of eutrophication is climate change, which amplifies the changes in carbon dynamics described above (Davidson et al., 2018; Jeppesen et al., 2015). This study focuses on *(i)* contextualizing these recent changes in carbon dynamics against a backdrop of paleoenvironmental change, and *(ii)* investigating the connections between climate change, OM source, carbon sequestration, primary production and methane oxidation. Understanding the drivers and magnitude of these changes in carbon dynamics is essential for predicting how carbon dioxide (CO₂) and methane (CH₄) emissions from lakes will change in future years.

Climate change can control the carbon dynamics of lakes in several ways.

Investigating the connections between climate change and the carbon dynamics of lakes is therefore complex. For this reason, this chapter is focused on one aspect of climate change: changes in effective moisture. Effective moisture is the net of water inputs to a lake (*i.e.*, surface/groundwater inlets and precipitation) minus water outputs (*i.e.*, surface/groundwater outlets and evaporative loss) (Tian et al., 2011). In the study region, central Ontario, changes in ocean surface temperatures often result in a change in the predominant wind patterns, which in turn alter the source and amount of atmospheric

moisture in the region, changing the effective moisture of lakes (Hilfinger IV et al., 2001). Thus, effective moisture is closely associated with climate change, particularly in hydrologically closed lakes that experience little local hydrologic change.

Several linkages between effective moisture and the carbon dynamics of lakes have been established in previous studies. For instance, effective moisture alters the carbon dynamics of lakes by controlling primary production. Some studies argue that primary production increases during periods of low effective moisture as limiting nutrients are concentrated (Gąsiorowski and Hercman, 2005; Özen et al., 2010; Yuan et al., 2006) and, in shallow lakes, vertical mixing is enhanced (Naselli-Flores, 2003). Others assert that primary production increases during periods of high effective moisture as surface flows carry soil nutrients to lakes, stimulating algal growth (Fritz et al., 1991; Ho and Michalak, 2019; Reichwaldt and Ghadouani, 2012). A second mechanism by which effective moisture can control the carbon dynamics of lakes is by influencing the sources of OM to lake sediments. Typically, the delivery of allochthonous OM to lake sediments increases during periods of high effective moisture (*i.e.*, wet periods) because surface flows carry allochthonous OM to lakes (Huguet et al., 2012). Some systems, however (*e.g.*, lakes with large catchments), receive inputs of terrestrial OM during periods of low effective moisture via atmospheric transport (Huguet et al., 2012). Effective moisture can also impact the types of vegetation that can survive in and around lakes, indirectly controlling OM sources to lakes. Periods of low effective moisture, for instance, decrease lake levels and favour the proliferation of submerged macrophytes (Lawniczak-Malińska et al., 2018). A third mechanism by which effective moisture can control the carbon dynamics of lakes is by regulating methane emissions from lakes. Lower lake levels reduce the hydrostatic pressure on sediments, encouraging the loss of methane directly to the atmosphere via ebullition (bubbling), reducing the amount of methane consumed by methane oxidizing bacteria (MOB) (Borrel et al., 2011; West et al., 2012). During periods of high effective moisture, however, evaporation of lake water slows. Consequently, ebullition (*i.e.*, bubbling) of methane slows, reducing methane emissions to the atmosphere (Beaulieu et al., 2018). Moreover, methane

slowly diffuses into the water column from the sediments where much of it is oxidized by MOB (Borrel et al., 2011).

Although it is well understood that the carbon dynamics of lakes have changed in the last ~100 years, few studies have focused on contextualizing these recent changes in carbon dynamics against a backdrop of paleoenvironmental change. This is problematic because, before one can assess the magnitude of these recent changes, the natural variability of lacustrine carbon dynamics must be understood. Understanding long-term variations in the carbon dynamics of lakes can also help researchers predict how the carbon dynamics of lakes will change in the future.

To help fill these gaps, this research focuses on reconstructing the carbon dynamics of a small kettle lake, Barry Lake, across the last millennium. The following aspects of the carbon cycle in Barry Lake are reconstructed: primary production/respiration, carbon sequestration, OM source and methane oxidation. These aspects of Barry Lake's carbon dynamics may be reconstructed using lake sediments and provide a window through which to view past changes in Barry Lake's carbon cycle. Barry Lake is an ideal lake to study the connections between climate change, eutrophication and the carbon cycle because it is sensitive to changes in climate and, like many small, temperate lakes, began to grow more productive after European settlement in AD ~1850 (Chapter 2). It is also hydrologically closed and sensitive to changes in atmospheric moisture (Chapter 2).

Effective moisture is reconstructed using the hydrogen isotope composition of the *n*-alkane C₁₇ ($\delta^2\text{H}_{\text{C17}}$) and the oxygen isotope composition of marl ($\delta^{18}\text{O}_{\text{marl}}$). The $\delta^2\text{H}_{\text{C17}}$ has been used previously as a proxy of $\delta^2\text{H}_{\text{water}}$ since C₁₇ originates from algae which inherit hydrogen from lake water (Sachse et al., 2012; Sessions, 2016). The efficacy of $\delta^{18}\text{O}_{\text{marl}}$ as an indicator of effective moisture was demonstrated in Chapter 2.

Carbon burial is estimated using the mass accumulation rate of total organic carbon (TOC-MAR). OM source is estimated using the abundances and carbon isotope ratios of *n*-alkanes ($\delta^{13}\text{C}_{n\text{-alkane}}$), which are straight-chained hydrocarbons derived from plant waxes.

Different groups of OM sources produce characteristic *n*-alkane chain length distributions: algae produce predominately C₁₅, C₁₇ and C₁₉ (Pu et al., 2009; Yu et al., 2016); mosses and submerged macrophytes produce predominantly C₂₁, C₂₃ and C₂₅ (Ficken et al., 2000), and semi-emergent and terrestrial plants produce predominantly C₂₇, C₂₉ and C₃₁ (Chevalier et al., 2015; Ficken et al., 2000). The values of $\delta^{13}\text{C}_{n\text{-alkane}}$ can help to differentiate algae and submerged macrophytes, which obtain carbon in the form of dissolved inorganic carbon (DIC), from semi-emergent macrophytes and terrestrial OM sources, which derive carbon from atmospheric carbon dioxide (Freimuth et al., 2017).

To better understand the past methane dynamics of Barry Lake, indicators of methane oxidation are analyzed to reconstruct abundances of methane oxidizing bacteria (MOB) in Barry Lake. These proxies include the mass accumulation rate, and the carbon isotope composition of, diploptene (diploptene-MAR and $\delta^{13}\text{C}_{\text{Diploptene}}$, respectively). Diploptene, also called hop-22(29)-ene and A'-Neogammancer-22(29)-ene, is found in ferns (Ageta et al., 1963), some mosses (Huang et al., 2010) and in the cell membranes of various aerobic bacteria (Hyun et al., 2014; Yamada et al., 1997). Three additional proxies are used to reconstruct the microbial dynamics of Barry Lake: the C₁₈-MAR; lupan-3-one-MAR; and $\epsilon_{\text{marl-TOC}}$, the fractionation between the carbon isotope ratios of total organic carbon ($\delta^{13}\text{C}_{\text{TOC}}$) and marl ($\delta^{13}\text{C}_{\text{marl}}$). Even and short-chained (<C₂₁) *n*-alkanes such as C₁₈ are thought to originate from microbial sources (Veloso et al., 2019; Wang et al., 2010; Yu et al., 2016). Lupan-3-one is a triterpene that originates from angiosperms (ten Haven et al., 1992). Previous studies have demonstrated its value as a biomarker for microbial degradation of terrigenous OM (Koller et al., 2001; López-Días et al., 2019; Orsini et al., 2015; ten Haven et al., 1992). Values of $\epsilon_{\text{marl-TOC}}$ have been reported to reflect inputs of chemoautotrophic bacteria, although they may also reflect allochthonous inputs of OM (Diefendorf et al., 2008; Hayes et al., 1999).

Three research questions guided this study. The first question is: How do changes in effective moisture across the last millennium influence the carbon dynamics of Barry Lake? Investigating how changes in effective moisture influence primary production/respiration,

carbon sequestration, OM sources and methane oxidation offers us insight into whether climate change is an important driver of carbon dynamics in Barry Lake. This chapter focuses on the last ~1000 years because this period contained three distinct climatic intervals: The Medieval Climate Anomaly (MCA) (AD 1000– 1300), the Little Ice Age (LIA) (AD 1450– 1850) and the modern period (AD 1850- present day). The MCA was characterized by low effective moisture (Booth et al., 2006). Effective moisture during the LIA was comparatively high (Buhay and Edwards, 1993). The modern period is characterized by European settlement and increased human impacts on lakes.

The second question is as follows: how do the carbon dynamics of Barry Lake in the last ~100 years compare with levels during the last ~1000 years? Understanding how these variables have changed across the last millennium allows us to contextualize any recent changes in the carbon dynamics of Barry Lake against a backdrop of natural variation. With the answers to these first two research questions in mind, a final research question was asked: how might the carbon dynamics of Barry Lake change in future years? Since Barry Lake is a small kettle lake, and such lakes are found in southern and central Ontario (Thorson, 2009), Quebec (Philibert et al., 2003), Michigan (Yansa et al., 2019), New York (Hilfinger IV et al., 2001) and Minnesota (Almquist-Jacobson et al., 1992), answering this question will be beneficial to scientists and lake managers working in these regions.

3.2 Materials and methods

3.2.1 Study area

Barry Lake (44°18'28"N, 77°55'17"W) is a kettle lake located in southeastern Ontario, Canada, 40 km north of Lake Ontario and 32 km east of Peterborough, Ontario (Fig. 1.2 in Chapter 1). Barry Lake, which has a bowl-like bathymetry, is ~7.6 m deep. The lake has two ephemeral inflows, derived from groundwater springs, and three ephemeral outflows. The area is characterized by hot, humid summers and cool, dry winters. The main water body is surrounded by a wetland. Adjacent to ~1/3 of the wetland is farmland. Floating (e.g.,

Nuphar sp.), semi-emerged (e.g., Typha sp.) and submerged (e.g., Chara sp., Potamogeton sp.) macrophytes are abundant around the shoreline of Barry Lake.

3.2.2 Core collection and sediment subsectioning

Four gravity cores, BL-G11-01, BL-G11-02, BL-G16-01 and BL-G17-01, were obtained from the deepest part of Barry Lake. Cores BL-G11-01 (41.5 cm) and BL-G11-02 (41.0 cm) were collected on November 6, 2011, while cores BL-G16-01 (55.5 cm) and BL-G17-01 (42.5 cm) were collected on November 26, 2016 and July 27, 2017, respectively. All cores were obtained using a Glew gravity corer (Glew et al., 2002). Upon collection, each core was visually inspected to ensure that the water-sediment interface was undisturbed. Immediately after collection, all cores were subsectioned into 0.5 cm intervals and individually sealed in Whirl-Pak bags. All samples were then freeze-dried. Next, shelly fauna were removed from the subsamples by hand-picking, and the remaining sediments were ground to <250 μm and then stored in a refrigerator at 4°C at *The University of Western Ontario*. Sample preparation methods and analyses of BL-G11-01 and BL-G17-01, including isotopic compositions of total organic carbon and total nitrogen ($\delta^{13}\text{C}_{\text{TOC}}$ and $\delta^{15}\text{N}_{\text{TN}}$, respectively), and TOC:TN, are reported in Chapter 2. Core BL-G16-01 was analyzed to determine $\delta^{13}\text{C}_{\text{TOC}}$, *n*-alkane abundances and carbon and hydrogen isotope compositions of *n*-alkanes ($\delta^{13}\text{C}_{n\text{-alkane}}$ and $\delta^2\text{H}_{n\text{-alkane}}$).

Since *n*-alkane analysis requires more sediment than available in individual, 0.5 cm subsections, subsamples from BL-G16-01 were recombined. To this end, ~0.5 g of dry, homogeneous sediment from each 0.5 cm interval was taken for total lipid extraction, followed by recombination of ten, stratigraphically consecutive 0.5 g samples. This approach resulted in a final sample resolution of 5 cm for the *n*-alkane analyses. Remaining sediment in each 0.5 cm interval was used for the bulk analysis of $\delta^{13}\text{C}_{\text{TOC}}$.

3.2.3 Analysis of sedimentary chlorophyll *a* and its derivatives (Chl-*a*_(s))

Sediments from BL-G17-01 were analyzed to determine the concentration of chlorophyll *a* and its derivatives using visible reflectance spectroscopy (VWRS), as detailed in Michelutti

et al. (2010). The 400– 2500 nm spectral range was measured for each 0.5 cm sediment interval using the spectroradiometer (Rapid Content Analyzer) at the Paleoecological Environmental Assessment and Research Laboratory (PEARL, Queen’s University). To determine the Chl- $a_{(s)}$ concentration, the area under the peak between 650– 700 nm was calculated. Then, a linear relationship, shown in Equation 2.1. (Chapter 2), was used to infer the concentration of Chl- $a_{(s)}$ (Michelutti et al., 2010).

3.2.4 Isotopic analysis of bulk sediment, marl and shelly fauna

The stable isotope results presented here use the δ - notation relative to the Vienna PDB standard (for C), AIR standard (for N) or Vienna SMOW standard (for O and H), as shown in Equation 1.2 (Chapter 1). The fractionation between $\delta^{13}C_{\text{marl}}$ and $\delta^{13}C_{\text{TOC}}$, a useful indicator, was calculated using Equation 3.1. For additional details regarding the isotopic analyses of bulk sediment and marl from BL-G11-01 and BL-G17-01, see Chapter 2. For sample preparation methods of all samples in Chapter 3, see Table C.1 in Appendix C.

Equation 3.1

$$\varepsilon_{\text{marl-TOC}} = 1000 * \left[\left(\frac{(1000 + \delta^{13}C_{\text{marl}})}{1000 + \delta^{13}C_{\text{TOC}}} \right) - 1 \right] (\text{in } \text{‰})$$

The $\delta^{13}C_{\text{TOC}}$ of BL-G16-01, which was used for core correlation, was analyzed at the Laboratory for Stable Isotope Science (LSIS) using a Costech Elemental Combustion system (EA) coupled to a Thermo Scientific™ Delta^{PLUS} XL™ isotope ratio mass spectrometer (IRMS) in continuous-flow (He) mode (EA-IRMS). The $\delta^{13}C_{\text{TOC}}$ of BL-G16-01 was calibrated to VPDB using USGS 41a (accepted values: $\delta^{13}C = +36.55 \text{‰}$; $\delta^{15}N = +47.55 \text{‰}$) and USGS 40 (accepted values: $\delta^{13}C = -26.39 \text{‰}$; $\delta^{15}N = -4.52 \text{‰}$). Internal standard keratin (MP Biomedicals Inc., Cat. No. 90211, Lot No. 9966H; $\delta^{13}C = -24.04 \text{‰}$) was used to monitor both analytical accuracy and precision. The average obtained for the keratin was $-24.20 \pm 0.09 \text{‰}$ ($n = 10$), which compares well with its accepted values and expected reproducibility. Sample duplicates were analyzed every 10 samples, with an average reproducibility of $\pm 0.16 \text{‰}$ ($n = 11$ sample pairs). The $\delta^{13}C_{\text{TOC}}$ of sediments deposited after AD 1850 were corrected for the

Suess Effect to account for the enrichment of atmospheric $^{12}\text{CO}_2$ caused by fossil fuel emissions (Verburg, 2007).

The $\delta^{13}\text{C}$ of the shelly fauna *Helisoma anceps* and *Pisidium* sp. from BL-G11-01 was analyzed at LSIS by reacting orthophosphoric acid at 90 °C using a Micromass Multiprep[®] autosampling device coupled to a VG Optima[®] dual-inlet IRMS. The $\delta^{13}\text{C}$ of shelly fauna was calibrated to VPDB using NBS-19 (accepted value: $\delta^{13}\text{C} = +1.95$ ‰) and LSVEC (accepted value: $\delta^{13}\text{C} = -46.6$ ‰). Laboratory standards Suprapur (accepted value: $\delta^{13}\text{C} = -35.6$ ‰) and WS-1 (accepted value: $\delta^{13}\text{C} = +0.76$ ‰), and international standard NBS-18 (accepted value: $\delta^{13}\text{C} = -5.0$ ‰), were used to evaluate accuracy and precision. The $\delta^{13}\text{C}$ of Suprapur, WS-1 and NBS-18 were as follows: -35.7 ± 0.1 ‰ ($n = 4$), $+0.8 \pm 0.0$ ‰ ($n = 2$), -5.0 ± 0.1 ‰ ($n = 11$), respectively. Duplicates were analyzed every 11 samples. The average reproducibility of duplicates for $\delta^{13}\text{C}$ was ± 0.23 ‰ ($n = 18$ pairs). Each shell sample was analyzed in 2-3 locations to capture the full range of $\delta^{13}\text{C}$ variability. For information regarding how $\delta^{13}\text{C}_{\text{DIC}}$ was estimated using the $\delta^{13}\text{C}$ of shelly fauna, see Table C.2 and Section C.2 in Appendix C.

3.2.5 Isotopic analysis of dissolved inorganic carbon (DIC) in modern waters

Five standards were used to calibrate samples to VPDB: three international standards (NBS-19, NBS-18 and LSVEC), and two laboratory standards (Suprapur and WS-1). Accepted values for these standards are reported above. NBS-18 and Suprapur were used to assess accuracy and precision of the measurements. The average $\delta^{13}\text{C}$ of NBS-18 was -5.11 ± 0.07 ‰ ($n = 5$) and the average $\delta^{13}\text{C}$ of Suprapur was -35.55 ± 0.03 ‰ ($n = 5$), which compares well with their accepted values. Duplicate samples were analyzed every 5 samples and had an average reproducibility of ± 0.03 ‰ ($n = 12$ pairs).

3.2.6 Extraction, identification and quantification of *n*-alkanes

For each 5 cm sample interval, 5 g of freeze dried, homogenous sediment was Soxhlet-extracted with 2:1 dichloromethane:methanol for 24 h to obtain a total lipid extract (TLE). Activated copper was then added to these extracts for 24 hours to reduce sulfur-containing

compounds. After this copper was removed, the TLEs were then (i) concentrated to 1 mL using a Buchi R-300 Rotavapor; (ii) spiked with 1 mL of 100 ng/ μ L 5 α -androstane; and (iii) purified by elution with hexane during silica gel column chromatography. Finally, *n*-alkane extracts were gently evaporated to dryness under nitrogen gas. As they evaporated, sample vials were partly submerged in an ice bath to minimize the evaporation of lower-chain *n*-alkanes. Immediately after drying, *n*-alkane extracts were redissolved in 50 μ L of hexane.

Identification and quantification of *n*-alkane abundances was performed using an Agilent 7890B gas chromatograph equipped with a flame ionization detector (GC-FID) in splitless mode. An Agilent HP-5 capillary column (30 m; 0.32 mm i.d.; 0.25 μ m film thickness) was used with helium flow rates set to 1 mL/min. The GC-FID temperature program used was 40 °C to 130 °C at 10 °C/min followed by 130 °C to 300 °C at 4 °C/min with a 10 min hold time. Each sample was analyzed in triplicate. Prior to each analytical session, external calibrations were conducted using a calibration mixture of *n*-alkanes (C₁₂-C₃₆) with known concentrations. Identification of *n*-alkanes was achieved through comparison of sample peaks with retention times of the peaks of this standard *n*-alkane mixture. Quantification of *n*-alkanes was achieved by integration of peak areas and those of the internal standard, 5 α -androstane.

The *n*-alkanes extracted from one *Charophyte* plant (*Chara*) were also analyzed. To do this, one *Chara* plant was freeze-dried and ground to a powder using a mortar and pestle. The extraction process was conducted according to the steps described above.

Absolute abundances of *n*-alkanes were used to calculate various indices used to interpret the *n*-alkane abundances. The formula for the carbon preference index (CPI, Equation 1.8 in Chapter 1) was used to assess the odd to even predominance of *n*-alkanes (Bray and Evans, 1961; Marzi et al., 1993). The abundance of C₂₀ was not included in this equation since C₂₀ sometimes coeluted with the internal standard, 5 α -androstane, and was often present in abundances too small to quantify. The degradation of *n*-alkanes is evaluated using the carbon preference index (CPI), the ratio of odd to even *n*-alkanes. CPI

values <1 are typically indicative of reworking of *n*-alkanes by microorganisms, while values ≥ 1 typically reflect fresh OM (Marzi et al., 1993).

The P_{aq} index represents the ratio of short- to long-chain *n*-alkanes. The original formula presented by Ficken et al. (2000) was adjusted for the purposes of this chapter such that the *n*-alkanes representing aquatic inputs are C_{17} and C_{19} , while the *n*-alkanes representing terrestrial inputs are C_{27} , C_{29} and C_{31} . This revised formula for P_{aq} is provided in Equation 1.9 in Chapter 1.

3.2.7 Isotopic analysis of *n*-alkanes

The $\delta^{13}C$ and δ^2H of *n*-alkanes ($\delta^{13}C_{n\text{-alkane}}$ and $\delta^2H_{n\text{-alkane}}$, respectively) were determined using a Thermo Scientific TraceTM 1310 GC-C-IRMS paired with a Thermo Scientific Delta VTM mass spectrometer. The GC oven temperature ramp, column dimensions and He flow rate were identical to those used for the GC-FID, and reactor temperatures were set to 1400 °C for hydrogen and 1000 °C for carbon modes, respectively. Samples were analyzed in at least duplicate for the analysis of $\delta^{13}C_{n\text{-alkane}}$ and at least triplicate for the analysis of $\delta^2H_{n\text{-alkane}}$. A standard mixture of *n*-alkanes (Mix A1, Arndt Schimmelmann, Indiana University) was analyzed at the beginning and end of every sequence. All but two of the *n*-alkanes in this standard mixture were used to generate a calibration curve while the remaining two *n*-alkanes in this mixture were used to monitor analytical accuracy and precision (C_{16} and C_{30} for measurement of $\delta^{13}C_{n\text{-alkane}}$ and C_{16} and C_{25} for the measurement of $\delta^2H_{n\text{-alkane}}$). The accepted $\delta^{13}C$ of C_{16} and C_{30} are -26.15 ‰ and -29.84 ‰, respectively. These values compare well with measured values of $\delta^{13}C_{C_{16}}$ (-26.17 ± 0.45 ‰ ($n=16$)) and $\delta^{13}C_{C_{30}}$ (-29.72 ± 0.44 ‰ ($n=16$)). The accepted δ^2H of C_{16} and C_{25} are -9.1 ‰ and -263 ‰, respectively. These values compare well with measurements of $\delta^2H_{C_{16}}$ (-6.4 ± 6.2 ‰ ($n=25$)), and measurements of $\delta^2H_{C_{25}}$ (-265 ± 5.8 ‰ ($n=25$)). Precision was also monitored by analyzing the average standard deviation of sample replicates. For the analysis of $\delta^{13}C_{n\text{-alkane}}$, the average standard deviation of sample replicates was ± 0.16 ‰ ($n=46$ replicates), while for analysis of $\delta^2H_{n\text{-alkane}}$, the average standard deviation of sample replicates was ± 3.0 ‰ ($n=9$ replicates).

3.2.8 Chronology

The age-depth model for BL-G16-01 was correlated with previously established age-depth models for BL-G17-01 by visual inspection and comparison of trends in $\delta^{13}\text{C}_{\text{TOC}}$. For additional details on the development of the age-depth models for BL-G17-01 and BL-G11-01, see Chapter 2. For additional details on the development of the age-depth model for BL-G16-01, see section C.3 in Appendix C.

3.3 Results

3.3.1 Chronology

The age-depth models for BL-G17-01 and BL-G16-01 are shown in Figure 3.1. Concentrations of ^{210}Pb follow a typical exponential curve, and the peak of ^{137}Cs occurs at 11.25 cm (AD 1966- 1967), confirming the ^{210}Pb model (Figure B.2 in Appendix B).

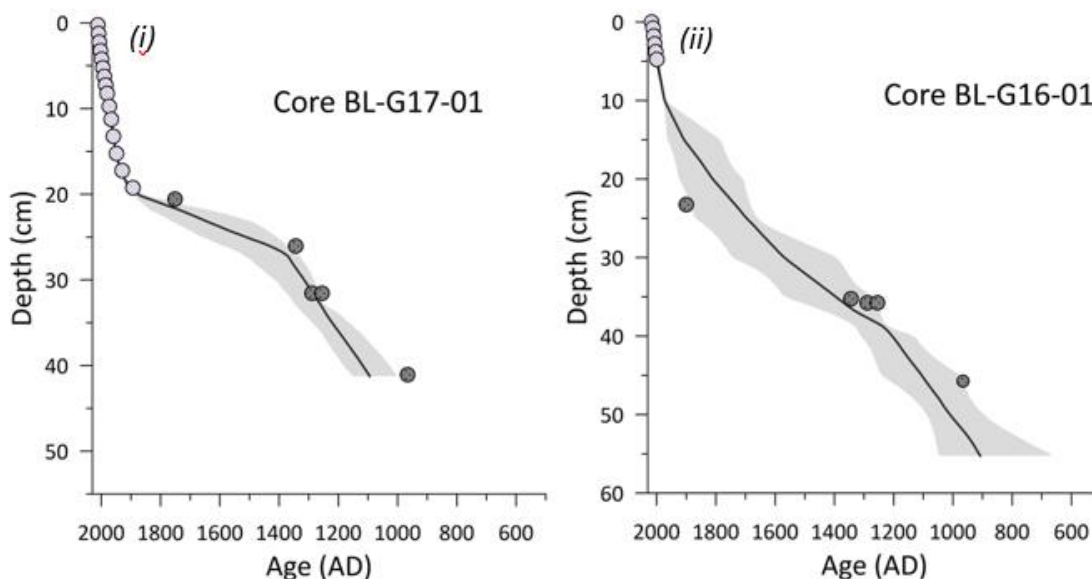


Figure 3.1 Age-depth model for BL-G17-01 (i) and BL-G16-01 (ii) generated using the R package “Bacon”. Light grey stippled circles represent ages obtained using ^{210}Pb dating whereas dark grey circles represent ^{14}C dates. Grey shading indicates the overall error associated with the age-depth model. Data used to generate the age-depth model for BL-G17-01 is provided in Chapter 2. More information about the age-depth model of BL-G16-01 is provided in Section C.3 in Appendix C.

Age-depth models were generated using the “Bacon” package in R (Blaauw and Christeny, 2011, R Core Development Team), which uses Bayesian statistics, IntCal13 (Reimer et al., 2013) and the calibration curves for each date to calculate sediment accumulation rates based on a gamma autoregressive process (Blaauw et al., 2011). All default settings were unchanged, except the model thickness was reduced to 1.5 to increase flexibility of the model, and maximum and minimum depths were specified. A surface (depth= 0) date of AD 2017.5 and AD 2016.9 was assigned for BL-G17-01 and BL-G16-01, respectively, to prevent extrapolation of the model into the future. Accumulation rates generated by Bacon were used to calculate total organic carbon mass accumulation rates (TOC-MAR) and chlorophyll *a* (Chl-*a*(s)-MAR).

3.3.2 Isotopic composition of biomarkers

The sediment cores have been divided into six intervals, from oldest (I) to youngest (VI), based on values of $\delta^{18}\text{O}_{\text{marl}}$ (Chapter 2; Figure 2.2). Reliable $\delta^2\text{H}$ measurements were possible only for the C_{17} *n*-alkane, due to low amplitudes or co-elution of other *n*-alkanes with compounds having similar retention times. The $\delta^2\text{H}$ of C_{17} in BL-G16-01 generally decreases upwards in the core and co-varies with $\delta^{18}\text{O}_{\text{marl}}$ in BL-G17-01 (Fig. 3.2). The $\delta^2\text{H}_{\text{C}_{17}}$ varies from ~ -230 to ~ -170 ‰.

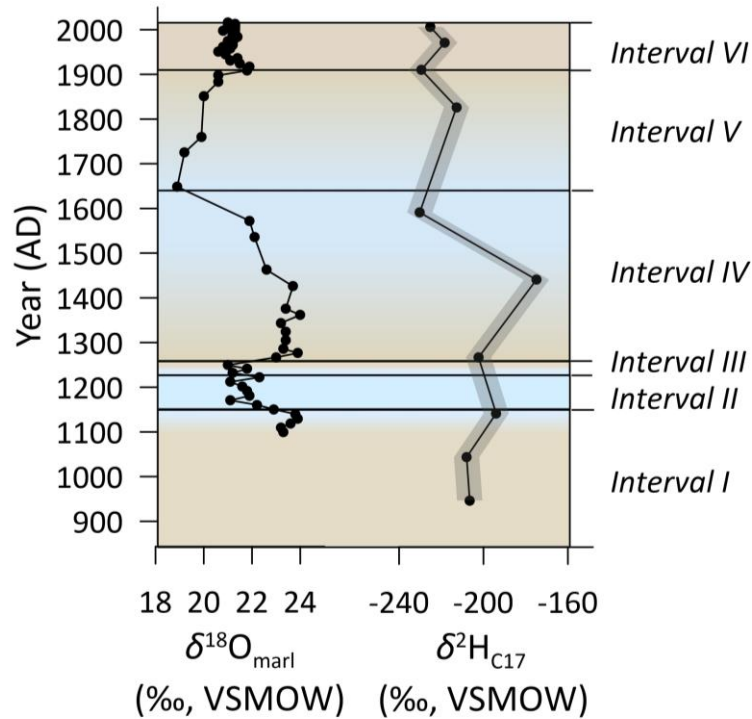


Figure 3.2 The $\delta^2\text{H}_{\text{C17}}$ from BL-G16-01 varies closely with $\delta^{18}\text{O}_{\text{marl}}$ from BL-G17-01, suggesting that both proxies respond to changes in effective moisture. The record is subdivided into six intervals based on variations in $\delta^{18}\text{O}_{\text{marl}}$. Brown shading indicates a dry period (defined by high $\delta^{18}\text{O}_{\text{marl}}$), whereas blue shading denotes a wet period (defined by low $\delta^{18}\text{O}_{\text{marl}}$). The grey shading around $\delta^2\text{H}_{\text{C17}}$ represents measurement error. Measurement error of $\delta^{18}\text{O}_{\text{marl}}$ is too low to visualize.

The $\delta^{13}\text{C}$ of *n*-alkanes and diploptene were also measured (Fig. 3.3). The $\delta^{13}\text{C}$ of all *n*-alkanes vary between -34 and -29 ‰. The $\delta^{13}\text{C}_{\text{C17}}$ and, to a lesser degree, the $\delta^{13}\text{C}_{\text{C21}}$ varies with $\delta^{13}\text{C}_{\text{marl}}$. In contrast, $\delta^{13}\text{C}_{\text{C19}}$ varies inversely with $\delta^{13}\text{C}_{\text{marl}}$. The $\delta^{13}\text{C}$ of C_{23} to C_{31} do not vary with $\delta^{13}\text{C}_{\text{marl}}$. The $\delta^{13}\text{C}_{\text{diploptene}}$ ranges from ~ -54 to -49 ‰ and decreases from *Interval I* to *Interval IV*. Trends in $\delta^{13}\text{C}_{\text{marl}}$ are described in Chapter 2.

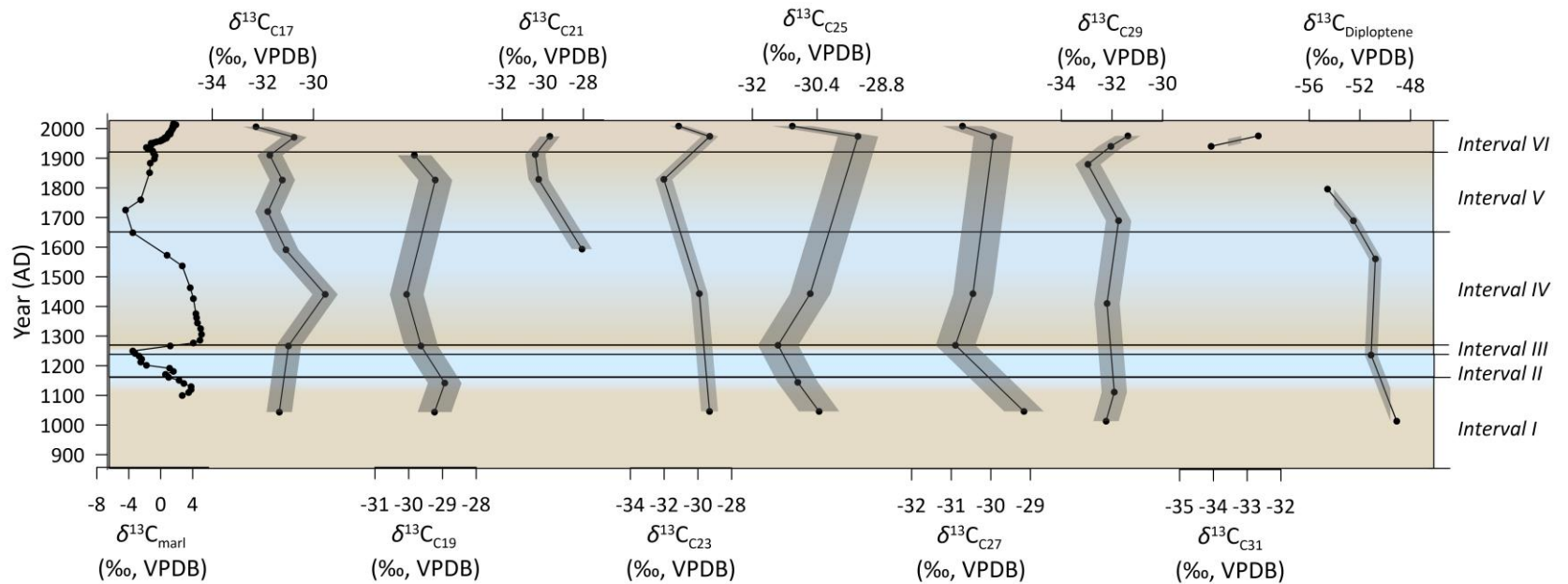


Figure 3.3 Carbon isotope ratios of diploptene and *n*-alkanes (BL-G16-01) compared with $\delta^{13}C_{marl}$ (BL-G17-01). The record is subdivided into six intervals based on variations in $\delta^{18}O_{marl}$. Brown shading indicates a dry period (defined by high $\delta^{18}O_{marl}$), whereas blue shading denotes a wet period (defined by low $\delta^{18}O_{marl}$). The grey shading around δ^2H_{C17} represents measurement error. Measurement error of $\delta^{18}O_{marl}$ is too low to visualize. After AD 1850, the $\delta^{13}C_{marl}$ and the $\delta^{13}C$ of each *n*-alkane were corrected for the Suess Effect, following Verburg (2007).

3.3.3 Mass accumulation rates and relative abundances of *n*-alkanes

The mass accumulation rates of each *n*-alkane show the same trends, reaching maximum values in AD ~1450 and AD ~1950, and minimum values around AD ~1250 and AD ~1600 (Fig. 3.4). C₁₉-MAR is similar in *Interval VI* compared to *Intervals I to Interval V*. The CPI of *n*-alkanes extracted from Barry Lake sediments increases from AD ~900–2017 (Fig. 3.4). CPI and P_{aq} do not covary, except for between AD ~900–1150. The *n*-alkane extracts from the single *Chara* plant analyzed consisted of mostly C₁₉ *n*-alkanes (Figure C.2 in Appendix C).

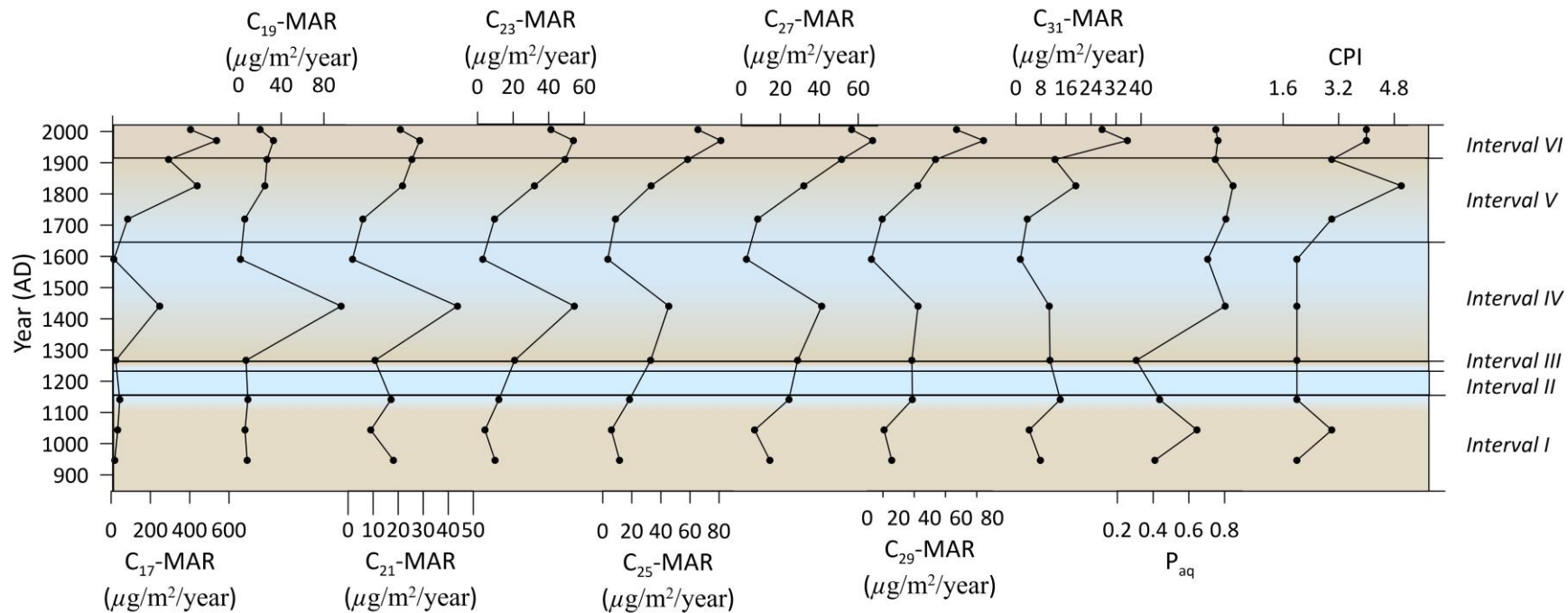


Figure 3.4 Mass accumulation rates, P_{aq} and CPI of n -alkanes. The record is subdivided into six intervals based on variations in $\delta^{18}\text{O}_{\text{marl}}$. Brown shading indicates a dry period (defined by high $\delta^{18}\text{O}_{\text{marl}}$), whereas blue shading denotes a wet period (defined by low $\delta^{18}\text{O}_{\text{marl}}$).

The relative abundances⁴ of C₂₃ to C₃₁ *n*-alkanes generally covary (Fig. 3.5), while the relative abundances of individual short chain *n*-alkanes are distinct. The relative abundance of C₁₇ generally increases upwards through entire core, with the exception of one decrease in the second half of *Interval I*. The relative abundance of C₁₉ changes little except for a large peak around AD ~1450. The relative abundance of C₂₁ is similar to C₁₉, except that C₂₁ abundances do not peak around AD ~1450.

⁴ Relative abundances represent the percent contribution of each *n*-alkane to the sediment organic matter (*e.g.*, if the relative abundance of C₂₃ is 25 %, this means that 25 % of the *n*-alkane mixture consists of C₂₃).

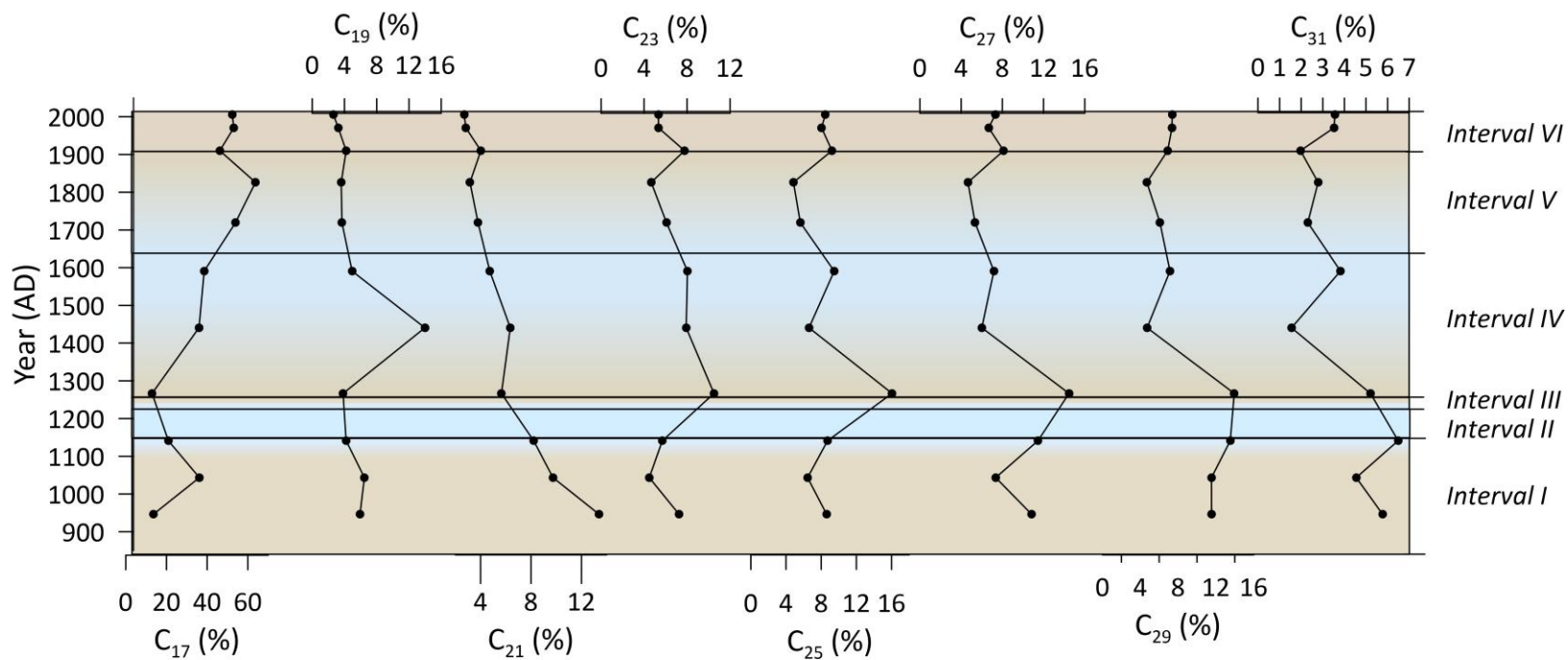


Figure 3.5 Relative abundances of *n*-alkanes. The record is subdivided into six intervals based on variations in $\delta^{18}\text{O}_{\text{marl}}$. Brown shading indicates a dry period (defined by high $\delta^{18}\text{O}_{\text{marl}}$), whereas blue shading denotes a wet period (defined by low $\delta^{18}\text{O}_{\text{marl}}$).

3.3.4 Isotopic and elemental ratios of bulk sediment from BL-G17-01

Chapter 2 provides a full description of the bulk sediment proxies measured in BL-G17-01. The TOC:TN follows similar yet muted variations compared with P_{aq} (Fig. 3.6 (ii)). The TOC:TN is significantly and directly correlated with $Chl-a_{(s)}$ -MAR (Table C.3 in Appendix C). TOC:TN is also significantly but inversely correlated with $\epsilon_{marl-TOC}$ (Table C.3 in Appendix C). The $\delta^{15}N_{TN}$ of BL-G17-01 is significantly correlated with TOC-MAR, TN-MAR, $Chl-a_{(s)}$ -MAR and calcite-MAR (Table C.3 in Appendix C). Trends in $Chl-a_{(s)}$ -TOC correlate significantly and directly with TOC-MAR (Table C.3 in Appendix C.; Fig. 3.6 (iii)).

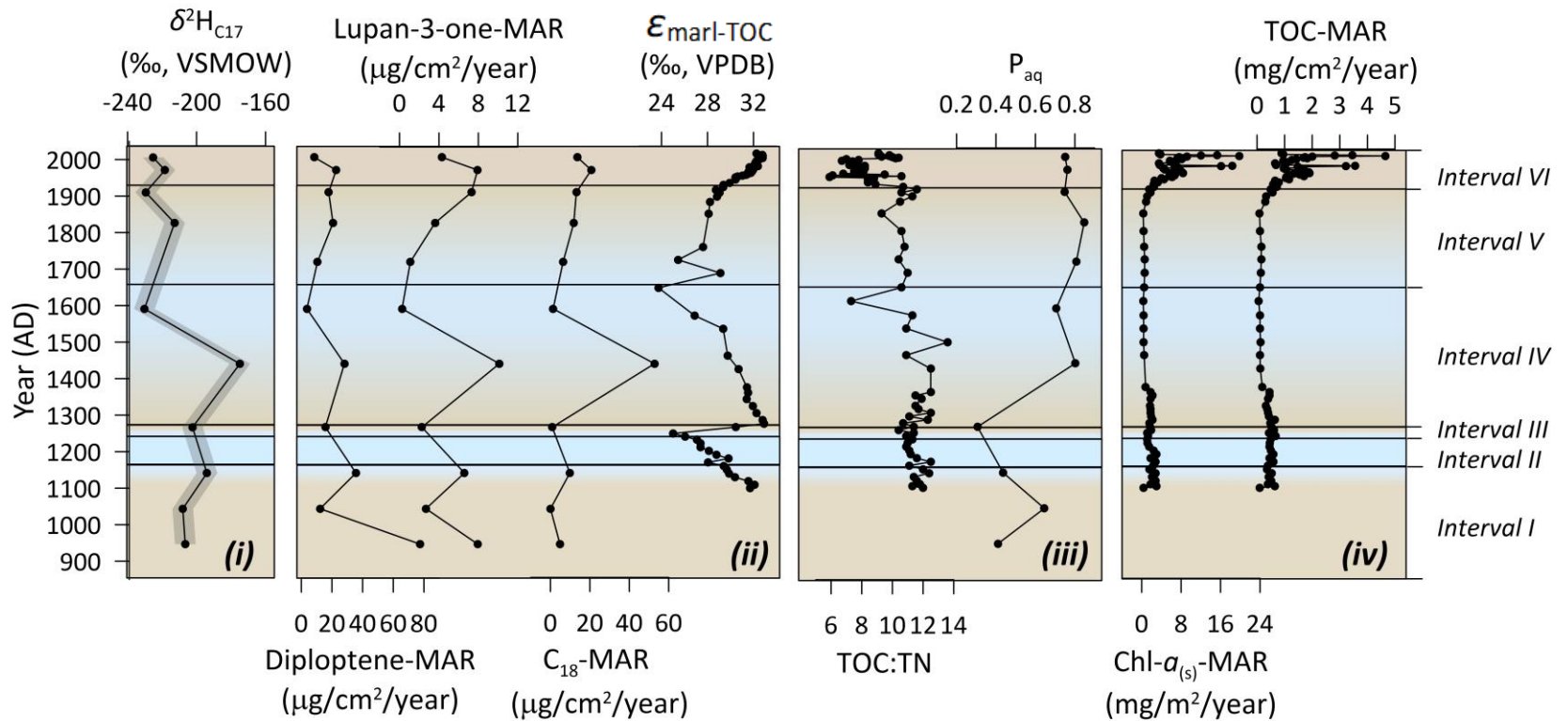


Figure 3.6 The (i) hydrogen isotopic composition of C_{17} compared with (ii) indicators of microbial abundance, (iii) OM source and (iv) primary production and carbon burial. The record is subdivided into six intervals based on variations in $\delta^{18}\text{O}_{\text{marl}}$. Brown shading indicates a dry period (defined by high $\delta^{18}\text{O}_{\text{marl}}$), whereas blue shading denotes a wet period (defined by low $\delta^{18}\text{O}_{\text{marl}}$).

3.3.5 Mass accumulation rates of diploptene, lupan-3-one and C₁₈, and trends in $\epsilon_{\text{marl-TOC}}$

The mass accumulation rate of diploptene follows a trend similar to $\delta^2\text{H}_{\text{C}_{17}}$, except at the beginning of *Interval I* (Fig. 3.6 (i)). At this time, values of diploptene-MAR are high (diploptene-MAR= $\sim 80 \mu\text{g}/\text{cm}^2/\text{year}$) relative to the rest of the record, while values of $\delta^2\text{H}_{\text{C}_{17}}$ are average (Fig. 3.6 (i)). The diploptene-MAR does not correspond with Chl- $a_{(s)}$ -MAR or TOC-MAR but is similar to P_{aq} (Fig. 3.6 (ii), (iii) and (iv)). The mass accumulation rates of lupan-3-one and C₁₈ are similar to $\delta^2\text{H}_{\text{C}_{17}}$ (Fig. 3.6 (i) and (ii)). Values of $\epsilon_{\text{marl-TOC}}$ also follow a similar pattern to diploptene-MAR and $\delta^2\text{H}_{\text{C}_{17}}$, except at the end of *Interval IV* when $\epsilon_{\text{marl-TOC}}$ continues to increase as $\delta^2\text{H}_{\text{C}_{17}}$ and diploptene-MAR decrease (Fig. 3.6 (i) and (ii)).

3.3.6 Carbon isotopic compositions of shelly fauna from BL-G11-01

Shelly fauna are present in the basal sections of BL-G17-01, from AD ~ 1080 – 1270 (*Interval I* to the beginning of *Interval III*) (Fig. 3.7). *Pisidium sp.* disappear from the record at the end of *Interval II*, in AD ~ 1230 . *Helisoma anceps* disappear from the record at the beginning of *Interval III*, in AD ~ 1270 . The inferred $\delta^{13}\text{C}_{\text{DIC}}$ from $\delta^{13}\text{C}_{\text{H. anceps}}$ and $\delta^{13}\text{C}_{\text{Pisidium}}$ is ~ 1 – 3 ‰ depleted in ^{13}C relative to the inferred $\delta^{13}\text{C}_{\text{DIC}}$ from $\delta^{13}\text{C}_{\text{marl}}$.

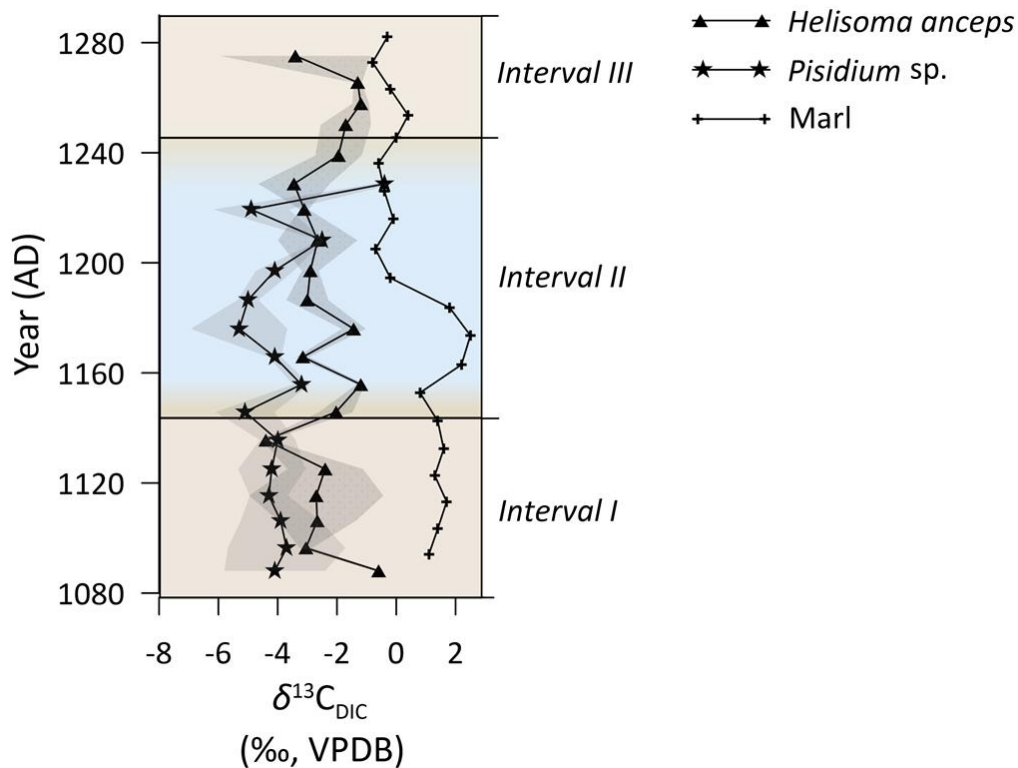


Figure 3.7 Estimates of the $\delta^{13}\text{C}_{\text{DIC}}$ based on measurements of the $\delta^{13}\text{C}_{\text{DIC}}$ of two shelly fauna (*Helisoma anceps* and *Pisidium* sp.), and marl. Shaded bars around *Helisoma anceps* and *Pisidium* sp. represent the variation of $\delta^{13}\text{C}$ present within a single shell. *Pisidium* sp. disappears from the sediment record around AD ~1230, while *Helisoma anceps* disappears from the record around AD ~1270. Brown shading indicates a dry period (defined by high $\delta^{18}\text{O}_{\text{marl}}$), whereas blue shading denotes a wet period (defined by low $\delta^{18}\text{O}_{\text{marl}}$). For more details regarding the estimation of $\delta^{13}\text{C}_{\text{DIC}}$, see Section C.2 in Appendix C.

3.4 Discussion

3.4.1 Identifying sources of OM in Barry Lake sediments using *n*-alkanes

One of the advantages of reconstructing OM source using *n*-alkanes, as opposed to TOC:TN, is that *n*-alkanes are more resistant to degradation (Eglinton and Eglinton, 2008). The following evidence suggests that the *n*-alkane record is well-preserved throughout the rest of the core: (i) increasing CPI towards the present (Fig. 3.4); (ii) a lack of covariation between P_{aq} and CPI after AD 1150 (Fig. 3.4); and (iii) close agreement between δ^2H_{C17} and $\delta^{18}O_{marl}$ (Fig. 3.1).

One section between AD ~900 and 1150, where P_{aq} and CPI vary directly, potentially exhibits signs of degradation (Fig. 3.4). Degradation of *n*-alkanes commonly occurs when microbes rework organic material. If microbes were altering OM, one would expect P_{aq} to decrease since microbes preferentially rework short-chain *n*-alkanes (Li et al., 2017). Yet decreases in P_{aq} can also indicate an influx of terrestrial OM to lake sediments (Ficken et al., 2000). How then can a pulse of terrestrial OM be differentiated from microbial degradation? Microbial reworking also results in a lowering of CPI (Marzi et al., 1993). For this reason, one can detect microbial reworking of *n*-alkanes by searching for periods when P_{aq} and CPI covary. Such covariance of P_{aq} and CPI was observed from AD ~900 to 1150. It is therefore likely that OM degraded at this time. High abundances of bacterial biomarkers (*i.e.*, diploptene, lupan-3-one, C_{18} -MAR and $\epsilon_{marl-TOC}$) prior to AD ~1150 further support this argument (Fig. 3.6 (i)). Caution will therefore be used when interpreting proxies extracted from sediments deposited between AD ~900 and 1150.

The $\delta^{13}C$ of C_{17} and C_{19} allow the sources of these *n*-alkanes to be characterized. As noted earlier, $\delta^{13}C_{C17}$ varies with $\delta^{13}C_{marl}$ (Fig. 3.3). Since $\delta^{13}C_{marl}$ closely reflects $\delta^{13}C_{DIC}$ (Diefendorf et al., 2008a), this pattern suggests that the organisms producing C_{17} also utilize DIC and represent OM produced in a fully aquatic environment. The C_{17} likely originated from planktonic algae. It is the most abundant *n*-alkane present in Barry Lake sediments and its abundance increases towards the present. The TOC:TN of the sediment approaches 8

towards the present (Fig. 3.6), confirming that the sediment is receiving inputs of OM from algae (Meyers and Ishiwatari, 1993). The close relationship between $\delta^{13}\text{C}_{21}$ and $\delta^{13}\text{C}_{\text{marl}}$ also suggests that this *n*-alkane originates from aquatic sources, but the $\delta^{13}\text{C}_{21}$ record is much more limited than for $\delta^{13}\text{C}_{17}$ (Fig. 3.3).

The contrasting behaviour of $\delta^{13}\text{C}_{\text{C19}}$, which varies inversely with $\delta^{13}\text{C}_{\text{marl}}$ (Fig. 3.3), shows that this *n*-alkane does not record $\delta^{13}\text{C}_{\text{DIC}}$. One explanation for this unexpected pattern is that the organism(s) producing this *n*-alkane utilized proton pumping during periods of low DIC availability. Proton pumping is the process by which some organisms, such as *Charophytes* (*Chara*), generate protons through the hydroxylation and formation of CO_2 (McConnaughey, 1991). It was expected that the availability of DIC would be lowest during arid periods, when DIC is lost to the atmosphere via outgassing of CO_2 (Andersen et al., 2019). Such outgassing would also lead to an increase in $\delta^{13}\text{C}_{\text{marl}}$. Proton pumping causes the biomass of organisms to become depleted of ^{12}C relative to $\delta^{13}\text{C}_{\text{DIC}}$ (McConnaughey, 1991). Accordingly, an organism utilizing proton pumping would produce *n*-alkanes depleted of ^{13}C during periods when $\delta^{13}\text{C}_{\text{marl}}$ is high. C_{19} is the predominant *n*-alkane produced by *Chara* in Barry Lake (Figure C.2 in Appendix C). The mass accumulation rate of C_{19} ($\text{C}_{19}\text{-MAR}$) will therefore be used to trace the contributions of *Chara* to the sediment OM.

A weak relationship between $\delta^{13}\text{C}_{\text{marl}}$ and the $\delta^{13}\text{C}$ of C_{23} to C_{31} suggests that these *n*-alkanes did not form in organisms that were dependent on DIC; instead, these *n*-alkanes likely originated from semi-emergent macrophytes and/or fully terrestrial sources. Previous studies have found that *n*-alkanes ranging from C_{27} to C_{31} originate from fully terrestrial sources whereas mid-chain *n*-alkanes (C_{23} to C_{25}) originate from semi-aquatic sources (Chevalier et al., 2015; Ficken et al., 2000). It will therefore be assumed that C_{23} and C_{25} originate from semi-emergent macrophytes while C_{27} , C_{29} and C_{31} originate from fully terrestrial sources such as trees.

3.4.2 Reconstructing MOB abundance and degradation using biomarker quantification and compound-specific isotopic analysis

Four proxies were used to reconstruct bacterial dynamics and the history of OM degradation in Barry Lake: (i) C₁₈-MAR, (ii) lupan-3-one-MAR, (iii) diploptene, and (iv) $\epsilon_{\text{marl-TOC}}$ (Fig. 3.6). The utility of C₁₈-MAR and lupan-3-one-MAR as indicators of microbial degradation has already been demonstrated in the literature (Koller et al., 2001; López-Días et al., 2019; Orsini et al., 2015; ten Haven et al., 1992; Veloso et al., 2019; Wang et al., 2010; Yu et al., 2016). The drivers of variation in diploptene-MAR and $\epsilon_{\text{marl-TOC}}$ must be examined more closely since they are controlled by multiple variables.

The origin of diploptene in Barry Lake can be deduced from its carbon isotopic composition. Groups of aerobic bacteria produce diploptene with characteristic carbon isotope compositions. In lacustrine environments, the following groups of aerobic bacteria produce diploptene: (i) methanotrophs ($\delta^{13}\text{C}_{\text{Diploptene}} \leq -38 \text{ ‰}$) (Aichner et al., 2010; Hyun et al., 2014; Naeher et al., 2014; Yamada et al., 1997), (ii) heterotrophic bacteria ($\delta^{13}\text{C} \approx -31 \text{ ‰}$) (Prahl et al., 1992); nitrifying bacteria ($\delta^{13}\text{C} \approx -31 \text{ ‰}$) (Elvert et al., 2001); and (iii) cyanobacteria ($\delta^{13}\text{C}_{\text{Diploptene}} \approx -25 \text{ ‰}$) (Hyun et al., 2014; Yamada et al., 1997). The low $\delta^{13}\text{C}_{\text{Diploptene}}$ in Barry Lake sediments ($\delta^{13}\text{C}_{\text{Diploptene}} = -56$ to -49 ‰ ; Fig. 3.3) strongly suggests that most of the diploptene throughout the entire record originates from methanotrophs (Aichner et al., 2010). Changes in the mass accumulation rates of diploptene (diploptene-MAR) are therefore interpreted to reflect shifts in the abundance of MOB. This interpretation is qualitative, as demonstrated by Davies et al. (2016). Yet, the diploptene flux varies closely with lupan-3-one-MAR and C₁₈-MAR (Fig. 3.6), which substantiates the claim of this chapter that variations in the diploptene flux reflect real changes in bacterial biomass.

Several lines of evidence suggest that the fourth proxy used here, $\epsilon_{\text{marl-TOC}}$, reflects bacterial activity. Values of $\epsilon_{\text{marl-TOC}}$ have been reported to reflect inputs of chemoautotrophic bacteria, although they may also reflect allochthonous inputs of OM (Diefendorf et al., 2008; Hayes et al., 1999). In the Barry Lake sediments, values of $\epsilon_{\text{marl-TOC}}$

range from ~23 to 32 ‰ (Fig. 3.6 (ii)). Hayes et al. (1999) proposed that values of $\epsilon_{\text{marl-TOC}}$ reflect variations in autochthonous sources: (i) >32 ‰ indicate significant inputs from chemoautotrophic bacteria (e.g., methanotrophs) (ii) 28 to 32 ‰ reflect lower inputs from chemoautotrophs or maximal fractionation of carbon isotopes by phytoplanktonic producers, and (iii) <28 ‰ reflect primarily phytoplanktonic producers with the reduction in primary fractionation a consequence of cell physiology and the growth environment. Diefendorf and Freimuth (2017) suggested that large values of $\epsilon_{\text{marl-TOC}}$ (~28 ‰) can be caused by inputs of refractory, terrestrial OM to the sediment, whereas smaller values (<28 ‰) are typical of a shift towards autochthonous inputs (Diefendorf et al., 2008).

Of these explanations, only the model proposed by Hayes et al. (1999) can plausibly explain the large $\epsilon_{\text{marl-TOC}}$ at Barry Lake. First, to my knowledge, no study has demonstrated that inputs of terrestrial OM can produce $\epsilon_{\text{marl-TOC}}$ as large as 32 ‰, which is observed in Barry Lake. Second, TOC:TN, a proxy of terrestrial OM input (Meyers and Ishiwatari, 1993), is significantly and inversely correlated with $\epsilon_{\text{marl-TOC}}$ (Table C.3 in Appendix C), suggesting that as the latter increased, allochthonous contributions decreased.

Only inputs of chemoautotrophic bacteria remain as a plausible explanation for the large values of $\epsilon_{\text{marl-TOC}}$ at Barry Lake. It follows that the diploptene flux should covary with $\epsilon_{\text{marl-TOC}}$ since diploptene originates from methanotrophs, a type of chemoautotrophic bacteria. Fluxes of lupan-3-one are likewise used to trace the degradation of terrigenous organic material in these sediments.

3.4.3 Reconstructing variations in primary production, carbon burial and effective moisture

Variations in primary production are reconstructed using Chl- $a_{(s)}$ -MAR, while carbon burial is estimated using TOC-MAR (Fig. 3.6 (iv)). The efficacy of Chl- $a_{(s)}$ -MAR as an indicator of primary production in Barry Lake is discussed in Chapter 2. The measurements of Chl- $a_{(s)}$ -MAR discussed here take into account the degradation products of Chl- $a_{(s)}$ (Michelutti et al., 2010). Variations in Chl- $a_{(s)}$ -MAR are therefore not the result of degradation. It is also

unlikely that TOC-MAR has degraded because it corresponds so closely with Chl- $a_{(s)}$ -MAR (Fig. 3.6 (iv); Table C.3 in Appendix C).

Trends in δ^2H_{C17} and $\delta^{18}O_{\text{marl}}$ were used to reconstruct shifts in effective moisture (Fig. 3.2). The sensitivity of $\delta^{18}O_{\text{marl}}$ in Barry Lake to effective moisture was detailed in Chapter 2. Briefly, $\delta^{18}O_{\text{marl}}$ reflects $\delta^{18}O_{\text{water}}$ and the temperature at which marl crystallizes. The $\delta^{18}O_{\text{water}}$ is controlled by effective moisture. The $\delta^{18}O_{\text{marl}}$ in Barry Lake appears to have been more sensitive to changes in effective moisture than temperature changes. For example, between AD 1250 and 1276, $\delta^{18}O_{\text{marl}}$ increased by 2.9 ‰. Without the influence of evaporation on $\delta^{18}O_{\text{lake water}}$, such an increase would require a rise in summer water temperatures of 14.5 °C (Kim and O'Neil, 1997). By comparison, average June, July and August temperatures derived from pollen assemblages in Clear Pond, New York (~345 km from Barry Lake) show that, between AD 1245 and AD 1285, temperatures increased by only 0.4 °C (Paquette and Gajewski, 2013). Variations in $\delta^{18}O_{\text{marl}}$ are therefore interpreted to reflect changes in effective moisture. Close variation between $\delta^{18}O_{\text{marl}}$ and δ^2H_{C17} confirms previous studies suggesting that δ^2H_{C17} is also a proxy of effective moisture (Sachse et al., 2012).

3.4.4 At Barry Lake, effective moisture exerts a stronger control on OM source than carbon availability or primary production

Throughout the entire record, trends in TOC-MAR correspond with Chl- $a_{(s)}$ -MAR, suggesting that carbon burial is largely controlled by primary production (Fig. 3.6 (iv); Table C.3 in Appendix C). This finding is unsurprising since most of the carbon in the sediment OM was supplied by aquatic sources, as indicated by low TOC:TN (Fig. 3.6 (iii)). The absence of a connection between primary production and effective moisture suggests that, in Barry Lake, changes in lake level do not affect the concentration of nutrients that limit primary production. This result also suggests that, during periods of high primary production, the introduction of nutrients to the lake via overland flow does not noticeably stimulate the growth of algae and macrophytes. See Chapter 2 for additional discussion of the relationship between primary production and effective moisture.

Trends in OM source, however, are associated with changes in effective moisture; throughout most of the record, trends in $\delta^2\text{H}_{\text{C17}}$ vary directly with trends in P_{aq} (Fig. 3.6 (iii)). This finding suggests that, throughout most of Barry Lake's history, periods of low effective moisture correspond with fewer inputs of allochthonous organic material whereas periods of high effective moisture correspond with greater inputs of allochthonous organic material. This result further suggests that terrestrial material is introduced to the lake via overland flow or the ephemeral inlets or that higher lake levels and subsequent flooding of the riparian zone are responsible for greater allochthonous inputs to the lake sediments during periods of high effective moisture.

Another important finding of this study is that, in the modern period (*Interval VI*), C_{19} -MAR and relative abundances of C_{19} are not markedly different than in *Intervals I to V* (Figs. 3.4 and 3.5). This result is interesting because it suggests that increased amounts of phytoplankton in *Interval VI*, indicated by rising C_{17} -MAR, have not noticeably altered populations of *Chara*. Rapid phytoplankton proliferation can shade out submerged macrophytes like *Chara*, causing them to disappear from the lake (Ozimek and Kowalczewski, 1984; Schwarz et al., 1996). It is possible that *Chara* has not been affected by this rapid growth of phytoplankton because it is more shade-tolerant than most other submerged macrophytes (Schwarz et al., 1996). It is also possible that the proliferation of phytoplankton in *Interval VI* has not substantially decreased light penetration of the water column. If *Chara* were to disappear from Barry Lake, the lake would likely undergo rapid eutrophication because *Chara* removes dissolved nutrients from the water column and sediments (Wiik et al., 2013) and may also co-precipitate phosphates with carbonates (Otsuki and Wetzel, 1972)

Trends in OM source are, however, associated with changes in effective moisture, particularly between AD 1150 (halfway through *Interval I*) and AD 1900 (halfway through *Interval IV*). Throughout this period, trends in $\delta^2\text{H}_{\text{C17}}$ vary directly with trends in P_{aq} . This finding suggests that, throughout most of Barry Lake's history, periods of low effective moisture correspond with fewer inputs of allochthonous organic material and periods of

high effective moisture correspond with greater inputs of allochthonous organic material. This result could indicate that terrestrial material is introduced to the lake via overland flow or through surface flows. Since Barry Lake has few surface flows, however, it is more likely that higher lake levels and subsequent flooding of the riparian zone are responsible for greater allochthonous inputs to lake sediments during periods of high effective moisture.

Why then do P_{aq} and δ^2H_{C17} vary independently at the beginning and end of the record? From AD ~900 to AD ~1150, P_{aq} and δ^2H_{C17} vary inversely, suggesting that inputs of allochthonous OM increase during periods of low effective moisture. This unexpected variation is most likely due to enhanced degradation throughout this portion of the record. Values of P_{aq} and δ^2H_{C17} disagree at one other time, however: around AD ~1950. At this time, P_{aq} is higher than expected based on the δ^2H_{C17} , suggesting that autochthonous inputs are higher than expected based on effective moisture. This irregularity could be the result of development around the lake which introduced limiting nutrients to the lake and increased algal production.

3.4.5 Effective moisture and OM source, rather than carbon availability or primary production, control MOB abundance at Barry Lake

Throughout the entire record, MOB abundance does not correspond with changes in primary production or carbon burial but generally corresponds with shifts in OM source (Fig. 3.6). This finding suggests that diploptene-MAR increases when the sediment consists of predominately autochthonous OM, as has been noted by Borrel et al. (2011). In short, MOB abundance may be influenced by OM source but appears insensitive to changes in carbon burial and primary production.

MOB abundances also vary closely with effective moisture, as indicated by covariation among diploptene-MAR, δ^2H_{C17} and $\delta^{18}O_{marl}$. The C_{18} -MAR, lupan-3-one-MAR and $\epsilon_{marl-TOC}$ also vary with δ^2H_{C17} (Fig. 3.6 (i) and (ii)), suggesting that effective moisture is an important control of bacterial abundance and OM degradation. Of note is that MOB abundance is high when effective moisture is low. High values of $\epsilon_{marl-TOC}$ also suggest that

contributions of biomass derived from chemoautotrophs to the sediment were high during arid periods. This observation is somewhat surprising since arid conditions lead to lower lake levels, and lower lake levels are generally thought to reduce the efficiency of methane oxidation by promoting methane loss by ebullition and plant-mediated transport (Bastviken et al., 2004).

I speculate that MOB abundance did not respond directly to changes in effective moisture but has responded instead to changes in temperature and dissolved oxygen (DO) concentration, which co-occur with shifts in effective moisture. Changes in effective moisture result in lake level fluctuations, which control DO concentrations (Naselli-Flores, 2003). MOB live within a narrow range of DO concentrations (Borrel et al., 2011). As a result, abrupt changes in DO can reduce MOB abundances and even cause these organisms to become dormant (Roslev and King, 1995).

One change in DO likely occurred in the Barry Lake record at the transition of *Interval II* to *Interval III*, a time when effective moisture rapidly decreases. At this time, the benthic bivalve *Pisidium* disappears, followed by the epifaunal gastropod *Helisoma anceps* (Fig. 3.7). The continued presence of marl throughout the record suggests that these shells did not dissolve. Rather, their disappearance likely reflects expanded hypolimnetic anoxia, which would limit the habitat available for shelly fauna. Diploptene-MAR increases at the end of *Interval II*, suggesting that expanded anoxia during arid periods might have accelerated methanogenesis, thereby stimulating methanotrophy and increasing MOB abundance. Close associations between hypolimnetic anoxia and diploptene-MAR have been previously demonstrated (Yamada et al., 1997).

However, previous research has also demonstrated that, when the lake levels of shallow lakes drop during periods of low effective moisture, stratification can break down, resulting in an increase in DO concentrations (Naselli-Flores, 2003). This appears to contradict the statements above. Yet, the data presented in this chapter suggest that Barry Lake was stratified during the transition between *Interval II* and *Interval III*. Continued

carbon isotopic separation between shelly fauna (which reside in the benthic or littoral zones) and marl (which is formed in the epilimnion) suggests the presence of two distinct pools of DIC during the transition from *Interval II* to *Interval III*. This finding is indicative of thermal stratification. How did Barry Lake remain stratified during this rapid decrease in effective moisture? Either (i) lake levels did not drop so low that stratification broke down and/or (ii) an increase in temperature strengthened thermal stratification, keeping the lake stratified in spite of a substantial decrease in lake level (Bartosiewicz et al., 2019; Zhang et al., 2015).

Since there is no paleotemperature reconstruction available from a site near Barry Lake, it cannot be said with certainty which explanation is correct. Changes in the predominant air mass reaching the Great Lakes region can drive simultaneous changes in temperature and moisture (Kirby et al., 2002). It is therefore possible that an increase in temperature occurred at the transition between *Interval II* and *Interval III* as effective moisture decreased. Also important to note is that rising temperatures stimulate methanogenesis, which can then lead to enhanced methane oxidation (Borrel et al., 2011). Increasing temperatures can therefore increase MOB abundance in two ways: (i) by strengthening thermal stratification and reducing DO concentrations in the hypolimnion, thereby creating a more favourable environment for methanogens; and (ii) accelerating methanogenesis by promoting bacterial activity and increasing reaction rates (Borrel et al., 2011).

In summary, the findings of this study suggest a link between climate change and MOB abundance. The exact connections between climate and MOB abundance, however, have yet to be determined.

3.4.6 Implications for greenhouse gas emissions from Barry Lake

The degree of carbon sequestration and primary production in modern Barry Lake is unprecedented across the entire record. These anomalous levels of carbon sequestration and primary production were not driven by variations in effective moisture. During *Interval*

VI, when carbon sequestration and primary production increased, levels of effective moisture were stable and were neither high nor low relative to the entire record. In Chapter 2, it was posited that recent changes in the carbon cycle at Barry Lake may be the result of human activity.

These findings offer an indication of how the greenhouse gas emissions from Barry Lake may have changed over time. Previous studies have determined that carbon burial by lakes is increasing due to human activity (Heathcote et al., 2015; Heathcote and Downing, 2012), and that lakes which undergo rapid increases in OM sequestration switch from becoming carbon dioxide sources to carbon dioxide sinks (Pacheco et al., 2014). I therefore speculate that, like these lakes, Barry Lake is now functioning as a carbon dioxide sink rather than a carbon dioxide source. It is unclear whether Barry Lake is a net source of methane to the atmosphere. The conditions that are observed in *Interval VI* (high primary production, anoxic bottom waters and rapid carbon burial) are often associated with enhanced methanogenesis (Borrel et al., 2011). Rapid methanogenesis can result in higher methane emissions if methane escapes the lake via ebullition or if methane oxidation does not keep up with methanogenesis (Borrel et al., 2011).

Since MOB abundances are closely linked to methane availability (Borrel et al., 2011), one would expect to observe high abundances of MOB in the modern period. Yet, MOB abundances are neither high nor low in the modern period relative to the rest of the record. The reason for this is unclear. One possibility is that methane oxidation is not keeping up with methane production, leading to greater methane emissions from the lake (Sepulveda-Jauregui et al., 2018). This possibility is alarming since methane is a more potent greenhouse gas than carbon dioxide. Over a 100-year period, methane is 28-36x more efficient at trapping longwave radiation than carbon dioxide (EPA, 2019). Lakes are an important source of methane to the atmosphere, producing 6-16 % of the world's atmospheric methane. (Bastviken et al., 2011).

Also possible is most methane oxidation in *Interval VI* was conducted by nitrogen-dependent anaerobic methane oxidation (n-damo), a process favoured over aerobic methane oxidation in nitrogen-rich environments (Shen et al., 2014). It was posited in Chapter 2 that increasing values of $\delta^{15}\text{N}_{\text{TN}}$ observed in *Interval VI* might be the result of fertilizer runoff from agricultural fields adjacent to Barry Lake. These fields were established around AD ~1850 (Stevenson, 2019), which is when $\delta^{15}\text{N}_{\text{TN}}$ began to increase. Such fertilizer inputs would create the nitrogen-rich environment favouring methane oxidation by n-damo bacteria (Shen et al., 2014). The microbes conducting n-damo are anaerobic, and therefore do not produce diploptene (Yamada et al., 1997). A rise in n-damo microbes could therefore explain the unexpectedly low MOB abundances in *Interval VI*. Next steps in this research should involve testing these ideas using microbiological assays to characterize the microbial communities in Barry Lake.

It is poorly understood whether anthropogenic climate change will lead to an increase or decrease in effective moisture across Canadian lakes (Bonsal et al., 2019). The findings in this study suggest that MOB abundance and OM source are most strongly controlled by climate, while primary production and carbon sequestration are more strongly controlled by other factors. If Barry Lake continues to behave like it did in previous years, it is likely that increases in effective moisture will enhance the delivery of allochthonous organic material to the lake. Increases in effective moisture, accompanied by rising water levels and cooler temperatures, may decrease abundances of MOB by weakening stratification and increasing DO concentrations, creating unfavourable conditions for MOB growth. Conversely, decreases in effective moisture would result in greater contributions of autochthonous organic carbon to the lake. Decreases in effective moisture, accompanied by lower water levels and warmer temperatures, may increase abundances of MOB by strengthening stratification and lowering DO concentrations, creating favourable conditions for MOB growth.

Since Barry Lake is a kettle lake, and such lakes are commonly found across southern and central Ontario (Thorson, 2009), Quebec (Philibert et al., 2003), Michigan (Yansa et al.,

2019), New York (Hilfinger IV et al., 2001) and Minnesota (Almquist-Jacobson et al., 1992), it is likely that these predictions are applicable to many other sites across eastern North America.

3.5 Conclusions

In this study, the relationships between effective moisture and the carbon dynamics of Barry Lake were explored. It was determined that trends in $\delta^2\text{H}_{\text{C17}}$ correspond well with the record of $\delta^{18}\text{O}_{\text{marl}}$ presented in Chapter 2. This finding supports previous studies that suggest that $\delta^2\text{H}_{\text{C17}}$ is a reliable indicator of effective moisture. The close associations between $\delta^{18}\text{O}_{\text{marl}}$ and $\delta^2\text{H}_{\text{C17}}$ also help confirm that the *n*-alkane record is generally well-preserved. Close variations between diploptene-MAR and three other indicators of microbial abundance, C_{18} -MAR, lupan-3-one and $\epsilon_{\text{marl-TOC}}$ were also identified. These results substantiate previous studies suggesting that diploptene-MAR is an indicator of MOB.

These proxies were used to determine that effective moisture and, to a lesser degree, OM source, exert a strong control on microbe abundance, including MOB abundance. Primary production and carbon burial are comparatively weak controls on microbe abundance. Of interest is that primary production and carbon burial are closely related to each other, but not to variations in effective moisture. Rather than varying with effective moisture, these variables remain constant until AD ~1850, after which they increase considerably. Since census records demonstrate that Europeans settled the land around Barry Lake around this time, I speculate that this sudden increase in primary production resulted from human activities, such as land use changes.

Lastly, it was determined how effective moisture and the carbon dynamics of Barry Lake varied in the modern period (*Interval VI*) relative to the rest of the record. It was determined that primary production and carbon burial were higher in the modern period than in previous years. Sudden increases in primary production combined with enhanced carbon burial are characteristic of lakes that have become carbon sinks (Pacheco et al., 2014). It is therefore possible that Barry Lake is also a carbon sink, although without further

measurements this cannot know this with certainty. High primary production, anoxic bottom waters and rapid carbon burial are also associated with enhanced methanogenesis. Yet, MOB abundances are not high relative to the rest of the record. Whether this means that methane oxidation in Barry Lake is failing to keep up with methane production, or whether methane oxidation is being conducted by microbes that do not produce diploptene is not yet known. If anthropogenic climate change causes effective moisture of Barry Lake to increase, the lake may begin receiving a greater proportion of allochthonous organic material and may experience lower abundances of MOB. A decrease in effective moisture would result in fewer inputs of allochthonous organic material and higher abundances of MOB.

3.6 References

- Ageta, H., Iwata, K., Yonezawa, K., 1963. Fern Constituents: Fernene and diploptene, triterpenoid hydrocarbons isolated from *Dryopteris crassirhizoma*. Nakai. Chem. Pharm. Bull. 11, 408–409. <https://doi.org/10.1248/cpb.11.408>
- Aichner, B., Wilkes, H., Herzsuh, U., Mischke, S., Zhang, C., 2010. Biomarker and compound-specific $\delta^{13}\text{C}$ evidence for changing environmental conditions and carbon limitation at Lake Koucha, eastern Tibetan Plateau. J. Paleolimnol. 43, 873–899. <https://doi.org/10.1007/s10933-009-9375-y>
- Almquist-Jacobson, H., Almendinger, J.E., Hobbie, S., 1992. Influence of terrestrial vegetation on sediment-forming processes in kettle lakes of west-central Minnesota. Quat. Res. 30, 103–116. [https://doi.org/10.1016/0033-5894\(92\)90033-F](https://doi.org/10.1016/0033-5894(92)90033-F)
- Andersen, M.R., Kragh, T., Martinsen, K.T., Kristensen, E., Sand-Jensen, K., 2019. The carbon pump supports high primary production in a shallow lake. Aquat. Sci. 81, 11. <https://doi.org/10.1007/s00027-019-0622-7>
- Bartosiewicz, M., Przytulska, A., Lapierre, J., Laurion, I., Lehmann, M.F., Maranger, R., 2019. Hot tops, cold bottoms: Synergistic climate warming and shielding effects

increase carbon burial in lakes. *Limnol. Oceanogr. Lett.* 4, 132–144.
<https://doi.org/10.1002/lol2.10117>

Bastviken, D., Cole, J., Pace, M., Tranvik, L., 2004. Methane emissions from lakes: Dependence of lake characteristics, two regional assessments, and a global estimate. *Global Biogeochem. Cycles* 18, 1–12.
<https://doi.org/10.1029/2004GB002238>

Bastviken, D., Tranvik, L.J., Downing, J.A., Crill, P.M., Enrich-Prast, A., 2011. Freshwater methane emissions offset the continental carbon sink. *Science* 331, 50.
<https://doi.org/10.1126/science.1196808>

Beaulieu, J.J., Balz, D.A., Birchfield, M.K., Harrison, J.A., Nietch, C.T., Platz, M.C., Squier, W.C., Waldo, S., Walker, J.T., White, K.M., Young, J.L., 2018. Effects of an experimental water-level drawdown on methane emissions from a eutrophic reservoir. *Ecosystems* 21, 657–674. <https://doi.org/10.1007/s10021-017-0176-2>

Beaulieu, J.J., DelSontro, T., Downing, J.A., 2019. Eutrophication will increase methane emissions from lakes and impoundments during the 21st century. *Nat. Commun.* 10, 1–5. <https://doi.org/10.1038/s41467-019-09100-5>

Blaauw, M., Christen, J.A., Christeny, J.A., 2011. Flexible paleoclimate age-depth models using an autoregressive gamma process. *Bayesian Anal.* 6, 457–474.
<https://doi.org/10.1214/11-BA618>

Bonsal, B.R., Peters, D.L., Seglenieks, F., Rivera, A., Berg, A., 2019. Changes in freshwater availability across Canada, in: Bush, E., Lemmen, D.S. (Eds.), *Canada's Changing Climate Report*. Government of Canada, Ottawa, Canada, pp. 261.

Booth, R.K., Notaro, M., Jackson, S.T., Kutzbach, J.E., 2006. Widespread drought episodes in the western Great Lakes region during the past 2000 years: Geographic extent and

potential mechanisms. *Earth Planet. Sci. Lett.* 242, 415–427.
<https://doi.org/10.1016/j.epsl.2005.12.028>

Borrel, G., Jézéquel, D., Biderre-Petit, C., Morel-Desrosiers, N., Morel, J.P., Peyret, P., Fonty, G., Lehours, A.C., 2011. Production and consumption of methane in freshwater lake ecosystems. *Res. Microbiol.* 162, 832–847.
<https://doi.org/10.1016/j.resmic.2011.06.004>

Bray, E.E., Evans, E.D., 1961. Distribution of *n*-paraffins as a clue to recognition of source beds. *Geochim. Cosmochim. Acta* 22, 2–15. [https://doi.org/10.1016/0016-7037\(61\)90069-2](https://doi.org/10.1016/0016-7037(61)90069-2)

Buhay, W.M., Edwards, T.W.D., 1993. Reconstruction of Little Ice Age climate in southwestern Ontario, Canada, from oxygen and hydrogen isotope ratios in tree rings. *Int. At. Energy Agency, Proc. Ser.* 329, 407–417.

Chevalier, N., Savoye, N., Dubois, S., Lama, M.L., David, V., Lecroart, P., Le Ménach, K., Budzinski, H., 2015. Precise indices based on *n*-alkane distribution for quantifying sources of sedimentary organic matter in coastal systems. *Org. Geochem.* 88, 69–77.
<https://doi.org/10.1016/j.orggeochem.2015.07.006>

Davidson, T.A., Audet, J., Jeppesen, E., Landkildehus, F., Lauridsen, T.L., Søndergaard, M., Syväranta, J., 2018. Synergy between nutrients and warming enhances methane ebullition from experimental lakes. *Nat. Clim. Chang.* 8, 156–160.
<https://doi.org/10.1038/s41558-017-0063-z>

Davies, K.L., Pancost, R.D., Edwards, M.E., Walter Anthony, K.M., Langdon, P.G., Torres, L.C., 2016. Diploptene $\delta^{13}\text{C}$ values from contemporary thermokarst lake sediments show complex spatial variation. *Biogeosciences* 13, 2611–2621.
<https://doi.org/10.5194/bg-13-2611-2016>

- Deemer, B.R., Harrison, J.A., Li, S., Beaulieu, J.J., Delsontro, T., Barros, N., Bezerra-Neto, J.F., Powers, S.M., Dos Santos, M.A., Vonk, J.A., 2016. Greenhouse gas emissions from reservoir water surfaces: A new global synthesis. *BioScience* 66, 949–964. <https://doi.org/10.1093/biosci/biw117>
- Diefendorf, A.F., Freimuth, E.J., 2017. Extracting the most from terrestrial plant-derived *n*-alkyl lipids and their carbon isotopes from the sedimentary record: A review. *Org. Geochem.* 103, 1–21. <https://doi.org/10.1016/j.orggeochem.2016.10.016>
- Diefendorf, A.F., Patterson, W.P., Holmden, C., Mullins, H.T., 2008. Carbon isotopes of marl and lake sediment organic matter reflect terrestrial landscape change during the late Glacial and early Holocene (16,800 to 5,540 cal yr B.P.): A multiproxy study of lacustrine sediments at Lough Inchiquin, western Ireland. *J. Paleolimnol.* 39, 101–115. <https://doi.org/10.1007/s10933-0079099-9>
- Downing, J.A., Rath, L.C., 1988. Spatial patchiness in the lacustrine sedimentary environment. *Limnol. Oceanogr.* 33, 447–458. <https://doi.org/10.4319/lo.1988.33.3.0447>
- Eglinton, T.I., Eglinton, G., 2008. Molecular proxies for paleoclimatology. *Earth Planet. Sci. Lett.* 275, 1–16. <https://doi.org/10.1016/j.epsl.2008.07.012>
- Elvert, M., Whiticar, M.J., Suess, E., 2001. Diploptene in varved sediments of Saanich Inlet: Indicator of increasing bacterial activity under anaerobic conditions during the Holocene. *Mar. Geol.* 174, 371–383. [https://doi.org/10.1016/S00253227\(00\)00161-4](https://doi.org/10.1016/S00253227(00)00161-4)
- EPA, 2019. Understanding Global Warming Potentials | Greenhouse Gas (GHG) Emissions [WWW Document]. URL <https://www.epa.gov/ghgemissions/understanding-global-warming-potentials> (accessed 2.19.20).

- Ficken, K.J., Li, B., Swain, D.L., Eglinton, G., 2000. An *n*-alkane proxy for the sedimentary input of submerged/floating freshwater aquatic macrophytes. *Org. Geochem.* 31, 745–749. [https://doi.org/10.1016/S0146-6380\(00\)00081-4](https://doi.org/10.1016/S0146-6380(00)00081-4)
- Freimuth, E.J., Diefendorf, A.F., Lowell, T. V., 2017. Hydrogen isotopes of *n*-alkanes and *n*-alkanoic acids as tracers of precipitation in a temperate forest and implications for paleorecords. *Geochim. Cosmochim. Acta* 206, 166–183. <https://doi.org/10.1016/j.gca.2017.02.027>
- Fritz, S.C., Juggins, S., Battarbee, R.W., Engstrom, D.R., 1991. Reconstruction of past changes in salinity and climate using a diatom-based transfer function. *Nature* 352, 706–708. <https://doi.org/10.1038/352706a0>
- Gąsiorowski, M., Hercman, H., 2005. Recent sedimentation and eutrophication of Kruklin lake after artificial drop in water-level in the middle of 19th century. *Stud. Quat.* 22, 17–25.
- Glew, J.R., Smol, J.P., Last, W.M., 2002. Sediment core collection and extrusion, in: Smol, J.P., Last, W.M. (Eds.), *Tracking Environmental Change Using Lake Sediments*, first ed. Springer, Dordrecht, pp. 73–105. https://doi.org/10.1007/0-30647669-x_5
- Hayes, J.M., Strauss, H., Kaufman, A.J., 1999. The abundance of ^{13}C in marine organic matter and isotopic fractionation in the global biogeochemical cycle of carbon during the past 800 Ma. *Chem. Geol.* 161, 103–125. [https://doi.org/10.1016/S0009-2541\(99\)00083-2](https://doi.org/10.1016/S0009-2541(99)00083-2)
- Heathcote, A.J., Anderson, N.J., Prairie, Y.T., Engstrom, D.R., Del Giorgio, P.A., 2015. Large increases in carbon burial in northern lakes during the Anthropocene. *Nat. Commun.* 10016. <https://doi.org/10.1038/ncomms10016>

- Heathcote, A.J., Downing, J.A., 2012. Impacts of eutrophication on carbon burial in freshwater lakes in an intensively agricultural landscape. *Ecosystems* 15, 60–70. <https://doi.org/10.1007/s10021-011-9488-9>
- Hilfinger IV, M.F., Mullins, H.T., Burnett, A., Kirby, M.E., 2001. A 2500-year sediment record from Fayetteville Green Lake, New York: evidence for anthropogenic impacts and historic isotope shift. *J. Paleolimnol.* 26, 293–305. <https://doi.org/10.1023/A:1017560300681>
- Ho, J.C., Michalak, A.M., 2019. Exploring temperature and precipitation impacts on harmful algal blooms across continental U.S. lakes. *Limnol. Oceanogr.* 1–18. <https://doi.org/10.1002/lno.11365>
- Huang, X., Wang, C., Xue, J., Meyers, P.A., Zhang, Ze, Tan, K., Zhang, Zhiqi, Xie, S., 2010. Occurrence of diploptene in moss species from the Dajiuhu Peatland in southern China. *Org. Geochem.* 41, 321–324. <https://doi.org/10.1016/j.orggeochem.2009.09.008>
- Huguet, C., Fietz, S., Moraleda, N., Litt, T., Heumann, G., Stockhecke, M., Anselmetti, F.S., Sturm, M., 2012. A seasonal cycle of terrestrial inputs in Lake Van, Turkey. *Environ. Sci. Pollut. Res.* 19, 3628–3635. <https://doi.org/10.1007/s11356-012-0948-3>
- Hyun, S., Bahk, J.J., Yim, U.H., Uchida, M., Nam, S., Woo, K.S., 2014. Carbon isotope variations in diploptene for methane hydrate dissociation during the last glacial episode in the Japan Sea/East Sea. *Geochem. J.* 48, 287–297. <https://doi.org/10.2343/geochemj.2.0305>
- Jeppesen, E., Brucet, S., Naselli-Flores, L., Papastergiadou, E., Stefanidis, K., Nöges, T., Nöges, P., Attayde, J.L., Zohary, T., Coppens, J., Bucak, T., Menezes, R.F., Freitas, F.R.S., Kernan, M., Søndergaard, M., Beklioglu, M., 2015. Ecological impacts of global warming and water abstraction on lakes and reservoirs due to changes in

water level and related changes in salinity. *Hydrobiologia* 750, 201–227.
<https://doi.org/10.1007/s10750-014-2169-x>

Kim, S.T., O'Neil, J.R., 1997. Equilibrium and nonequilibrium oxygen isotope effects in synthetic carbonates. *Geochim. Cosmochim. Acta* 61, 3461–3475.
[https://doi.org/10.1016/S0016-7037\(97\)00169-5](https://doi.org/10.1016/S0016-7037(97)00169-5)

Kirby, M., Patterson, W., Mullins, H., Burnett, A., 2002. Post-Younger Dryas climate interval linked to circumpolar vortex variability: Isotopic evidence from Fayetteville Green Lake, New York. *Clim. Dyn.* 19, 321–330.
<https://doi.org/10.1007/s00382-002-0227-y>

Koller, J., Baumer, U., Mania, D., 2001. High-tech in the middle Palaeolithic: Neandertal manufactured pitch identified. *Eur. J. Archaeol.* 4, 385–397.
<https://doi.org/10.1179/eja.2001.4.3.385>

Lawniczak-Malińska, A., Ptak, M., Celewicz, S., Choiński, A., 2018. Impact of lake morphology and shallowing on the rate of overgrowth in hard-water eutrophic lakes. *Water* 10, 1827. <https://doi.org/10.3390/w10121827>

Le Moal, M., Gascuel-Oudou, C., Ménesguen, A., Souchon, Y., Étrillard, C., Levain, A., Moatar, F., Pannard, A., Souchu, P., Lefebvre, A., Pinay, G., 2018. Eutrophication: A new wine in an old bottle? *Sci. Total Environ.* 651, 1–11.
<https://doi.org/10.1016/j.scitotenv.2018.09.139>

Li, R., Fan, J., Xue, J., Meyers, P.A., 2017. Effects of early diagenesis on molecular distributions and carbon isotopic compositions of leaf wax long chain biomarker *n* alkanes: Comparison of two one-year-long burial experiments. *Org. Geochem.* 104, 8–18. <https://doi.org/10.1016/j.orggeochem.2016.11.006>

- López-Días, Borrego, Blanco, Bechtel, Püttmann, 2019. Significance of the high abundance of pentacyclic triterpenyl and hopenyl acetates in *Sphagnum* peat bogs from Northern Spain. *Quaternary* 2, 1–26. <https://doi.org/10.3390/quat2030030>
- Marzi, R., Torkelson, B.E., Olson, R.K., 1993. A revised carbon preference index. *Org. Geochem.* 20, 1303–1306. [https://doi.org/10.1016/0146-6380\(93\)90016-5](https://doi.org/10.1016/0146-6380(93)90016-5)
- McConnaughey, T., 1991. Calcification in *Chara corallina*: CO₂ hydroxylation generates protons for bicarbonate assimilation. *Limnol. Oceanogr.* 36, 619–628. <https://doi.org/10.4319/lo.1991.36.4.0619>
- Meyers, P.A., Ishiwatari, R., 1993. Lacustrine organic geochemistry: an overview of indicators of organic matter sources and diagenesis in lake sediments. *Org. Geochem* 20, 867–900. [https://doi.org/10.1016/0146-6380\(93\)90100-P](https://doi.org/10.1016/0146-6380(93)90100-P)
- Michelutti, N., Blais, J.M., Cumming, B.F., Paterson, A.M., Rühland, K., Wolfe, A.P., Smol, J.P., 2010. Do spectrally inferred determinations of chlorophyll *a* reflect trends in lake trophic status? *J. Paleolimnol.* 43, 205–217. <https://doi.org/10.1007/s10933-009-9325-8>
- Naeher, S., Niemann, H., Peterse, F., Smittenberg, R.H., Zigah, P.K., Schubert, C.J., 2014. Tracing the methane cycle with lipid biomarkers in Lake Rotsee (Switzerland). *Org. Geochem.* 66, 174–181. <https://doi.org/10.1016/j.orggeochem.2013.11.002>
- Naselli-Flores, L., 2003. Man-made lakes in Mediterranean semi-arid climate: the strange case of Dr. Deep Lake and Mr. Shallow Lake, *Hydrobiologia* 506, 13–21. <https://doi.org/10.1023/B:HYDR.00000008550.34409.06>
- Otsuki, A., Wetzel, R.G., 1972. Coprecipitation of phosphate with carbonates in a marl lake. *Limnol. Oceanogr.* 17, 763–767. <https://doi.org/10.4319/lo.1972.17.5.0763>
- Özen, A., Karapinar, B., Kucuk, I., Jeppesen, E., Beklioglu, M., 2010. Drought-induced changes in nutrient concentrations and retention in two shallow Mediterranean

- lakes subjected to different degrees of management. *Hydrobiologia* 646, 61–72.
<https://doi.org/10.1007/s10750-010-0179-x>
- Ozimek, T., Kowalczewski, A., 1984. Long-term changes of the submerged macrophytes in eutrophic lake Mikołajskie (North Poland). *Aquat. Bot.* 19, 1–11.
[https://doi.org/10.1016/0304-3770\(84\)90002-0](https://doi.org/10.1016/0304-3770(84)90002-0)
- Pacheco, F.S., Roland, F., Downing, J.A., 2014. Eutrophication reverses whole-lake carbon budgets. *Int. Waters* 4, 41–48. <https://doi.org/10.5268/IW-4.1.614>
- Paquette, N., Gajewski, K., 2013. Climatic change causes abrupt changes in forest composition, inferred from a high-resolution pollen record, southwestern Quebec, Canada. *Quat. Sci. Rev.* 75, 169–180.
<https://doi.org/10.1016/J.QUASCIREV.2013.06.007>
- Philibert, A., Prairie, Y.T., Carcaillet, C., 2003. 1200 years of fire impact on biogeochemistry as inferred from high resolution diatom analysis in a kettle lake from the *Picea mariana*-moss domain (Quebec, Canada). *J. Paleolimnol.* 30, 167–181.
<https://doi.org/10.1023/A:1025526200880>
- Prahl, F.G., Hayes, J.M., Xie, T.M., 1992. Diploptene: An Indicator of terrigenous organic carbon in Washington coastal sediments. *Limnol. Oceanogr.* 37, 1290–1299.
<https://doi.org/10.4319/lo.1992.37.6.1290>
- Pu, Y., Zhang, H., Lei, G., Chang, F., Yang, M., Huang, X., 2009. *n*-alkane distribution coupled with organic carbon isotope composition in the shell bar section, Qarhan paleolake, Qaidam basin, NE Tibetan Plateau. *Front. Earth Sci. China* 3, 327–335.
<https://doi.org/10.1007/s11707-009-0044-2>
- R Core Development Team, 2020. R: A Language and Environment for Statistical Computing.

- Reichwaldt, E.S., Ghadouani, A., 2012. Effects of rainfall patterns on toxic cyanobacterial blooms in a changing climate: Between simplistic scenarios and complex dynamics. *Water Res.* 46, 1372–1393. <https://doi.org/10.1016/j.watres.2011.11.052>
- Reimer, P.J., Bard, E., Bayliss, A., Beck, J.W., Blackwell, P.G., Ramsey, C.B., Buck, C.E., Cheng, H., Edwards, R.L., Friedrich, M., Grootes, P.M., Guilderson, T.P., Hafliðason, H., Hajdas, I., Hatté, C., Heaton, T.J., Hoffmann, D.L., Hogg, A.G., Hughen, K.A., Kaiser, K.F., Kromer, B., Manning, S.W., Niu, M., Reimer, R.W., Richards, D.A., Scott, E.M., Southon, J.R., Staff, R.A., Turney, C.S.M., van der Plicht, J., 2013. IntCal13 and Marine13 radiocarbon age calibration curves 0–50,000 years cal BP. *Radiocarbon* 55, 1869–1887. https://doi.org/10.2458/azu_js_rc.55.16947
- Roslev, P., King, G.M., 1995. Aerobic and anaerobic starvation metabolism in methanotrophic bacteria. *Appl. Environ. Microbiol.* 61, 1563–1570. <https://doi.org/10.1128/aem.61.4.1563-1570.1995>
- Sachse, D., Billault, I., Bowen, G.J., Chikaraishi, Y., Dawson, T.E., Feakins, S.J., Freeman, K.H., Magill, C.R., McInerney, F.A., van der Meer, M.T.J., Polissar, P., Robins, R.J., Sachs, J.P., Schmidt, H.-L., Sessions, A.L., White, J.W.C., West, J.B., Kahmen, A., 2012. Molecular Paleohydrology: Interpreting the Hydrogen-Isotopic Composition of Lipid Biomarkers from Photosynthesizing Organisms. *Annu. Rev. Earth Planet. Sci.* 40, 221–249. <https://doi.org/10.1146/annurev-earth-042711105535>
- Schwarz, A.M., Hawes, I., Howard-Williams, C., 1996. The role of photosynthesis/light relationships in determining lower depth limits of Characeae in South Island, New Zealand lakes. *Freshw. Biol.* 35, 69–80. <https://doi.org/10.1046/j.13652427.1996.00481.x>

- Sepulveda-Jauregui, A., Hoyos-Santillan, J., Martinez-Cruz, K., Walter Anthony, K.M., Casper, P., Belmonte-Izquierdo, Y., Thalasso, F., 2018. Eutrophication exacerbates the impact of climate warming on lake methane emission. *Sci. Total Environ.* 636, 411–419. <https://doi.org/10.1016/j.scitotenv.2018.04.283>
- Sessions, A.L., 2016. Factors controlling the deuterium contents of sedimentary hydrocarbons. *Org. Geochem.* 96, 43–64. <https://doi.org/10.1016/j.orggeochem.2016.02.012>
- Shen, L. D, Wu, H. S, Gao, Z. G, 2014. Distribution and environmental significance of nitrite dependent anaerobic methane-oxidising bacteria in natural ecosystems. *Appl. Microbiol. Biotechnol.* 99, 133–142. <https://doi.org/10.1007/s00253-014-6200-y>
- Stevenson, M., 2019. Upper Canada (Ontario) Land Registry Records Research [WWW Document]. Ontario Genealogy. URL <https://www.ontariogenealogy.com/canadacensusrecords/uppercanadaontarioensusrecords1851/northumberlandcountypioneersettlers/percytownship1851agriculturalcensus.pdf> (accessed 4.14.19).
- ten Haven, H.L., Peakman, T.M., Rullkötter, J., 1992. Δ^2 -Triterpenes: Early intermediates in the diagenesis of terrigenous triterpenoids. *Geochim. Cosmochim. Acta* 56, 1993–2000. [https://doi.org/10.1016/0016-7037\(92\)90325-D](https://doi.org/10.1016/0016-7037(92)90325-D)
- Tian, J., Nelson, D., Hu, F.D., 2011. How well do sediment indicators record past climate? An evaluation using annually laminated sediments. *J Paleolimnol* 45, 73–84. <https://doi.org/10.1007/s10933-010-9481-x>
- Thorson, R.M., 2009. Beyond Walden: The Hidden History of America's Kettle Lakes and Ponds. Walker and Company, New York, United States, pp. 6.
- Veloso, M.G., Dick, D.P., da Costa, J.B, Bayer, C., 2019. Cropping systems including

legume cover crops favour mineral–organic associations enriched with microbial metabolites in no-till soil. *Soil Res.* 57, 851–858.

<https://doi.org/10.1071/SR19144>

Verburg, P., 2007. The need to correct for the Suess effect in the application of $\delta^{13}\text{C}$ in sediment of autotrophic Lake Tanganyika, as a productivity proxy in the Anthropocene. *J. Paleolimnol.* 37, 591–602.

<https://doi.org/10.1007/s10933006-9056-z>

Wang, Yongli, Fang, X., Zhang, T., Li, Y., Wu, Y., He, D., Wang, Youxiao, 2010. Predominance of even carbon-numbered *n*-alkanes from lacustrine sediments in Linxia Basin, NE Tibetan Plateau: Implications for climate change. *Appl. Geochemistry* 25, 1478–1486.

<https://doi.org/10.1016/j.apgeochem.2010.07.002>

West, W.E., Coloso, J.J., Jones, S.E., 2012. Effects of algal and terrestrial carbon on methane production rates and methanogen community structure in a temperate lake sediment. *Freshw. Biol.* 57, 949–955.

<https://doi.org/10.1111/j.13652427.2012.02755.x>

Wiik, E., Bennion, H., Sayer, C.D., Willby, N.J., 2013. Chemical and biological responses of marl lakes to eutrophication. *Freshw. Rev.* 6, 35–62.

<https://doi.org/10.1608/frj-6.2.630>

Yamada, K., Ishiwatari, R., Matsumoto, K., Naraoka, H., 1997. $\delta^{13}\text{C}$ records of diploptene in the Japan Sea sediments over the past 25 kyr. *Geochem. J.* 31, 315–321.

<https://doi.org/10.2343/geochemj.31.315>

Yansa, C.H., Fulton, A.E. II, Schaetzl, R.J., Kettle, J.M., Arbogast, A.F., 2019. Interpreting basal sediments and plant fossils in kettle lakes: insights from Silver Lake, Michigan, USA.

Can. J. Earth Sci. 57, 292–305. <https://doi.org/10.1139/cjes-2018-0338>

Yu, Y., Li, Y., Guo, Z., Zou, H., 2016. Distribution and sources of *n*-alkanes in surface sediments of Taihu Lake, China. Arch. Environ. Prot. 42, 49–55.

<https://doi.org/10.1515/aep-2016-0006>

Yuan, F., Linsley, B.K., Howe, S.S., 2006. Evaluating sedimentary geochemical lake-level tracers in Walker Lake, Nevada, over the last 200 years. J. Paleolimnol. 36, 37–54.

<https://doi.org/10.1007/s10933-006-0004-8>

Zhang, Y., Wu, Z., Liu, M., He, J., Shi, K., Zhou, Y., Wang, M., Liu, X., 2015. Dissolved oxygen stratification and response to thermal structure and long-term climate change in a large and deep subtropical reservoir (Lake Qiandaohu, China). Water Res. 75, 249–258. <https://doi.org/10.1016/j.watres.2015.02.052>

Chapter 4

4 Estimating source apportionment of organic matter (OM) to alpine lake sediments using bulk and compound-specific stable isotopic analysis

4.1 Introduction

Paleolimnology provides scientists the opportunity to reconstruct past environments in areas where long-term monitoring is not available. One of the benefits of using lake sediments to investigate paleoenvironments is that lakes incorporate signals from terrestrial and aquatic systems, as well as the atmosphere, allowing scientists to paint a holistic picture of environmental change. Yet, the integration of these three signals in lake sediments can also complicate paleoenvironmental interpretations because it is not always clear whether proxies are reflecting conditions within or outside of the lake. The use of tracers (*e.g.*, biomarkers) offers the potential for researchers to accurately identify organic matter (OM) sources to lakes and lake sediments and interpret sedimentary records (Chevalier et al., 2015; Mead et al., 2005). Identification of OM sources, however, requires knowledge of the distinct “fingerprints” of each source.

Several proxies for OM source have been developed to improve estimates of source apportionment of the sediment OM, including carbon and nitrogen isotope compositions ($\delta^{13}\text{C}_{\text{TOC}}$ and $\delta^{15}\text{N}_{\text{TN}}$) (Meyers, 1994; Meyers and Ishiwatari, 1993; Tenzer et al., 1997), and total organic carbon to total nitrogen ratios (TOC:TN) (Meyers and Ishiwatari, 1993) of the sediment OM. The relative abundances and carbon and hydrogen isotope compositions of *n*-alkanes ($\delta^{13}\text{C}_{n\text{-alkane}}$ and $\delta^2\text{H}_{n\text{-alkane}}$) from the sediment OM are also indicators of OM source (Chevalier et al., 2015; Cooper et al., 2015; Mead et al., 2005). To use these proxies to identify OM source, however, baseline studies of the isotopic, elemental and *n*-alkane characteristics of modern sources of OM (*e.g.*, vegetation, lichen and algae) are required.

Such studies are necessary for the accurate identification of OM source and paleoenvironmental reconstructions from lake sediments.

Existing baseline studies of the isotopic, elemental and *n*-alkane characteristics of modern sources of OM to lakes are focused on low-elevation, temperate environments (e.g., Bush and McInerney, 2013; Chevalier et al., 2015; Chikaraishi and Naraoka, 2007, 2003; Cooper et al., 2015; Hedges et al., 1985; Mead et al., 2005; Meyers, 1990). This is problematic for researchers studying lakes in remote, alpine areas. Although limited, research concerning mountainous regions suggests that the $\delta^{13}\text{C}_{\text{TOC}}$, $\delta^{15}\text{N}_{\text{TN}}$, TOC:TN, $\delta^{13}\text{C}_{n\text{-alkane}}$, $\delta^2\text{H}_{n\text{-alkane}}$ and *n*-alkane abundances of plants in these environments differ from those in low-elevation, temperate environments (Bresson et al., 2009; Feakins et al., 2016; Körner et al., 1991, 1988; Luo et al., 2011; Polissar et al., 2009; Townsend-Small et al., 2005; Wu et al., 2017). The $\delta^{13}\text{C}_{\text{TOC}}$ and $\delta^{13}\text{C}_{n\text{-alkane}}$ of alpine plants, for instance, are typically higher than in low-elevation, temperate plants due to increased aridity and lower partial pressures of carbon dioxide ($p\text{CO}_2$) at high elevations (Körner et al., 1991; Wei and Jia, 2009; Wu et al., 2017). Likewise, the $\delta^2\text{H}_{n\text{-alkane}}$ of alpine plants are lower than low-elevation plants as a function of the lower $\delta^2\text{H}$ of precipitation at high elevations (Luo et al., 2011; Polissar et al., 2009). The TOC:TN and $\delta^{15}\text{N}_{\text{TN}}$ of alpine plants also differ from low-elevation plants because of nitrogen limitation in alpine regions (Michelsen et al., 1998; Talbot and Lærdal, 2000; Tossavainen et al., 2019). Alpine plants also tend to produce fewer long-chain *n*-alkanes than their low-elevation counterparts, perhaps as an adaptation to survive at lower temperatures (Feakins et al., 2016). Additional baseline studies of the $\delta^{13}\text{C}_{\text{TOC}}$, $\delta^{15}\text{N}_{\text{TN}}$, TOC:TN, $\delta^{13}\text{C}_{n\text{-alkane}}$ and $\delta^2\text{H}_{n\text{-alkane}}$ of modern OM sources at high elevations are therefore needed to improve the accuracy of source apportionment studies of remote, alpine environments.

This study of the $\delta^{13}\text{C}_{\text{TOC}}$, $\delta^{15}\text{N}_{\text{TN}}$, TOC:TN, $\delta^{13}\text{C}_{n\text{-alkane}}$, $\delta^2\text{H}_{n\text{-alkane}}$ and *n*-alkane abundances of modern sources of OM to lakes in the Uinta Mountains, Utah (USA) was initiated to provide such baseline data for paleoenvironmental studies in a climatically sensitive region (Leonard, 2007; Petersky et al., 2019). This baseline will support future

paleoenvironmental studies in such regions; it also offers us the opportunity to explore the isotope systematics and *n*-alkane characteristics of modern OM sources growing in this extreme environment. For instance, measurements of $\delta^{13}\text{C}_{n\text{-alkane}}$ and $\delta^2\text{H}_{n\text{-alkane}}$ are used to calculate fundamental parameters such as the carbon isotope fractionation associated with *n*-alkane synthesis (ϵ_{bulk} ⁵), and the apparent hydrogen isotope fractionation between $\delta^2\text{H}_{n\text{-alkane}}$ and $\delta^2\text{H}$ of source water (ϵ_{water}). Modern measurements of $\delta^{13}\text{C}_{n\text{-alkane}}$ are used to calculate the carbon isotope fractionation between the $\delta^{13}\text{C}$ of modern CO_2 and $\delta^{13}\text{C}_{n\text{-alkane}}$, $\epsilon_{\text{atm-n-alkane}}$. Likewise, the hydrogen isotope fractionation between the $\delta^2\text{H}$ of modern precipitation and the $\delta^2\text{H}_{n\text{-alkane}}$ is calculated. These fractionation factors can then be used to estimate the $\delta^{13}\text{C}$ of ancient CO_2 ($\delta^{13}\text{C}_{\text{CO}_2}$) and $\delta^2\text{H}$ of precipitation ($\delta^2\text{H}_{\text{precipitation}}$), respectively. Estimating $\delta^{13}\text{C}_{\text{CO}_2}$ and $\delta^2\text{H}_{\text{precipitation}}$ is helpful for contextualizing recent excursions of $\delta^{13}\text{C}_{\text{CO}_2}$ and $\delta^2\text{H}_{\text{precipitation}}$ caused by climate change.

This database of $\delta^{13}\text{C}_{n\text{-alkane}}$ measurements is also helpful for improving our understanding of the factors driving variation in $\epsilon_{\text{atm-n-alkane}}$ among different groups of potential OM sources. This fractionation is the sum of two smaller fractionations: $\epsilon_{\text{atm-TOC}}$ (the carbon isotope fractionation between atmospheric CO_2 and total organic carbon of the potential OM source) and ϵ_{bulk} , (the carbon isotope fractionation between TOC and the *n*-alkane synthesized from that TOC) (Diefendorf and Freimuth, 2017). Commonly, it is assumed that $\epsilon_{\text{atm-TOC}}$ is mostly controlled by environmental factors, like aridity, while ϵ_{bulk} is controlled by genetics (Diefendorf and Freimuth, 2017). However, so little is known about the fractionations associated with *n*-alkane synthesis that it is unclear if variations in ϵ_{bulk} among groups also respond to environmental influences (*e.g.*, temperature) (Diefendorf et al., 2010; Diefendorf and Freimuth, 2017). Identifying the controls on these two fractionation factors should allow researchers to correct for factors like environmental variation that might obscure estimates of $\delta^{13}\text{C}_{\text{CO}_2}$. Since the plants sampled for this chapter

⁵ ϵ_{bulk} is the fractionation between the $\delta^{13}\text{C}_{n\text{-alkane}}$ and the $\delta^{13}\text{C}$ of bulk plant tissue.

grew in similar climates at similar elevations, one would expect any variation observed among groups to reflect phylogenetic differences. This chapter therefore investigates whether the variation in ϵ_{bulk} observed among different potential sources of OM reflect phylogenetic variations.

Given this background, the overall purpose of this research is twofold: (i) to establish a baseline of $\delta^{13}\text{C}_{\text{TOC}}$, $\delta^{15}\text{N}_{\text{TN}}$, TOC:TN, $\delta^{13}\text{C}_{n\text{-alkane}}$, $\delta^2\text{H}_{n\text{-alkane}}$, ϵ_{bulk} and ϵ_{water} of probable OM sources to Uinta Mountain lakes; and (ii) to explore the drivers of variation in these proxies. This database of TOC:TN, $\delta^{13}\text{C}_{\text{TOC}}$, $\delta^{15}\text{N}_{\text{TN}}$, relative abundances of *n*-alkanes, $\delta^{13}\text{C}_{n\text{-alkane}}$, $\delta^2\text{H}_{n\text{-alkane}}$, ϵ_{bulk} and ϵ_{water} are used to address five questions: (i) How distinct are the $\delta^{13}\text{C}_{\text{TOC}}$, $\delta^{15}\text{N}_{\text{TN}}$ and TOC:TN of various OM sources to Uinta Mountain sediments? (ii) How distinct are the relative abundances and isotopic compositions of *n*-alkanes from semi-emergent macrophytes, lichen, mosses and terrestrial plants? (iii) What are the probable OM sources to sediments from the centre of the lake⁶, and sediments in the littoral zone? (iv) What was the $\delta^{13}\text{C}_{\text{CO}_2}$ and $\delta^2\text{H}_{\text{precipitation}}$ in the Uinta Mountain study sites around AD ~1400? Finally, (v) how does ϵ_{bulk} differ between semi-emergent macrophytes, lichen, mosses and terrestrial plants and are these variations consistent with phylogenetic differences between groups?

By addressing questions (i) and (ii), this chapter evaluates which proxies are most useful for differentiating between probable sources of OM to Uinta Mountain lake sediments and establish best practices for interpreting these proxies in remote, alpine regions. Answering question (iii) demonstrates how these proxies can be used for source apportionment. By addressing question (iv), reconstructions of $\epsilon_{\text{CO}_2\text{-}n\text{-alkane}}$ in alpine areas are improved. Addressing question (v) clarifies the extent of phylogenetic control on $\delta^{13}\text{C}_{n\text{-}}$

⁶Unless otherwise specified, the term “sediments from the center of the lake” refers to sediments that have accumulated at the deepest part of the lake, here assumed to be the center of the lake.

alkane. In summary, this research provides vital baseline data for future paleoenvironmental studies of alpine lakes, while also investigating the isotopic and *n*-alkane systematics of modern sources of OM growing in the Uinta Mountains.

4.2 Materials and methods

4.2.1 Study area

The Uinta Mountains are an east-west trending range of mountains that stretches from the northeastern part of Utah (40°-41° N, 109°-111° west) to northeastern Colorado (Fig. 1.4 in Chapter 1). The mountain range reaches elevations over 4000 m above sea level and contains hundreds of lakes with minimal exposure to direct human activity. Quartzite, sandstone and shale dominate the bedrock geology. Multiple glacial events have led to the formation of cirques, U-shaped valleys, and many glacial lakes in the Uinta Mountains (Munroe et al., 2007).

The following high elevation (> 3000 m.a.s.l.), oligotrophic/mesotrophic lakes in the Uinta Mountains were selected as sampling locations: Denise Lake, Taylor Lake, Upper Carrol Lake and East Carrol Lake (Fig. 1.3 in Chapter 1). Lakes were selected to maximize variation in their depth and lake to catchment area ratios (Table 4.1). This chapter maximizes variation in these variables because lakes with different lake morphometries and catchment size tend to receive different sources of OM. Deep alpine lakes, for instance, tend to receive greater OM inputs from submerged macrophytes than shallow alpine lakes because the macrophyte growth in shallow alpine lakes is limited by ice scouring of the littoral zone (Ballesteros et al., 1989). Lakes with high catchment area:lake ratios tend to receive greater inputs of allochthonous OM than lakes with low catchment area:lake ratios (Toming et al., 2013). Exploring the OM sources of lakes with different depths and catchment area:lake ratios increases the chances of capturing the full range of variation in the sediment OM, and sources of OM to these sediments.

Table 4.1 Summary characteristics of the four study lakes. Adapted with permission from Hundey et al., 2014. The trophic status of each lake was determined by Hundey et al. (2014).

Lake name	Latitude (°N)	Longitude (°W)	Elevation (m a.s.l)	Lake depth (m)	Lake area (ha)	Catchment area (ha)	Stratifies	Secchi depth (m)	Trophic status	Headwater lake?	Hydrologic connectivity
Denise	40.77	110.09	3399	2.4	1.1	391.9	No	To bottom	Oligo	Yes	Several inflows and outflows
Taylor	40.79	110.09	3414	9.7	9.0	349.9	Yes	3.4	Oligo-meso	Yes	Several inflows and outflows
Upper Carrol	40.72	110.35	3395	13.8	11.6	316.1	Yes	4.7	Oligo-meso	Yes	Several inflows and outflows
East Carrol	40.72	110.35	3423	5.5	3.4	35.1	No	3.3	Oligo-meso	Yes	Intermittent inflow and an outflow

Denise and East Carrol Lake are shallow (2.4 and 5 m, respectively) while Taylor and Upper Carrol Lake are deeper (~10 m). Taylor and Upper Carrol Lake experience thermal stratification in the summer months; Denise and East Carrol Lake do not stratify. Taylor and Upper Carrol lakes have permanent inflows, while Denise and East Carrol lakes have intermittent inflows.

The dominant tree species at these sites is Engelmann spruce (*Picea engelmanni*), which adopts a krummholz formation at high altitudes, meaning that its growth is stunted by factors such as continual exposure to cold temperatures and wind, frost damage and nutrient limitation (Körner, 2003). Other common species at these high elevation sites include the sedge *Carex aquatilis*; the shrubs *Betula glandulosa*, *Salix glauca* and *Salix plantifolia*; and various species of mosses and lichen.

There are two precipitation regimes in the Uinta Mountains: a summer wet/winter dry regime that dominates the eastern Uinta Mountains and a summer dry/winter wet regime that dominates the western Uinta Mountains (Munroe, 2003). Due to orographic effects, precipitation typically increases with elevation (MacDonald and Tingstad, 2007). Although climatic data are not available for each study site, all the study lakes are located at similar elevations (Table 4.1) in the eastern Uinta Mountains. One would therefore expect climate to be similar among these four sites.

4.2.2 Sample collection and storage

Samples of potential OM sources were collected from Taylor and Denise lakes in May 2014, July 2015 and September 2016. Samples from Upper Carrol and East Carrol lakes were collected in July 2015. In this chapter, “potential OM sources” are defined as photosynthetic organisms and lichen located within the catchment of each lake, particularly those sources growing next to or within the lake. To aid in this investigation, these probable OM sources were divided into groups. Terrestrial plants and semi-emergent macrophytes were classified based on their growth form and functional group. Algae and submerged macrophytes were classified according to whether the organism had roots, stems and leaves (submerged

macrophyte), or was missing these plant parts (algae). Using these guidelines, the following groups of OM sources were established: (i) algae; (ii) broadleaf deciduous shrubs; (iii) mosses; (iv) semi-emergent macrophytes; (v) coniferous krummholz trees; (vi) lichen; (vii) herbaceous perennials; (viii) submerged macrophytes and (ix) graminoids (Fig. 4.1). Although semi-emergent macrophytes and the other graminoids are closely related (both are *Carex* sp.), semi-emergent macrophytes are treated separately. This is because semi-emergent macrophytes grow in water, which, as discussed later, affects their nitrogen and hydrogen isotope systematics.

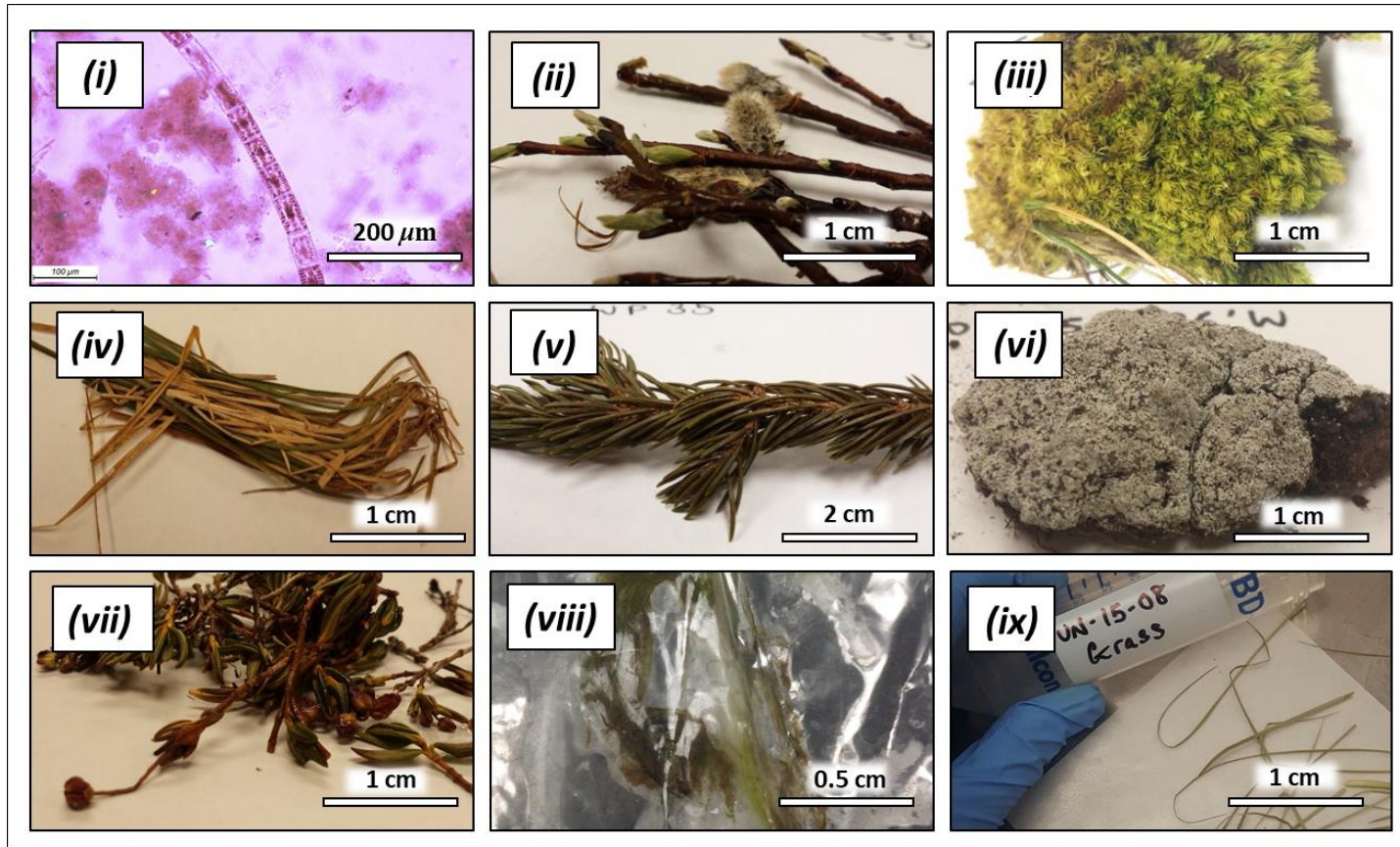


Figure 4.1 Photos of potential sources of OM in sediments: (i) algae, (ii) broadleaf deciduous shrubs, (iii) moss, (iv) semi-emergent macrophytes, (v) coniferous krummholz trees, (vi) lichen, (vii) herbaceous perennials, (viii) submergent macrophytes, and (ix) graminoids.

Terrestrial plants and semi-emergent macrophytes were gathered opportunistically around the perimeter of each lake, except when an area was not accessible. Abundant plant species were collected in greater quantities than scarce species to reflect the actual community composition around each lake. Species closer to the lake were collected in greater abundances because those species are more likely to enter the lake and influence the isotopic composition of the lake sediment.

Wherever possible, entire organisms (*e.g.*, lichen, moss) were sampled to account for intraspecies variability. Only mature tissue was sampled since very young tissue tends to be enriched in ^{13}C relative to mature tissue (Leavitt and Long, 1982), and it is unlikely that newly emerging tissues are significant contributors of OM to the sediment. For each tree and shrub, samples were collected from the bottom, middle and top of the plant to account for intraspecies variation in $\delta^{13}\text{C}$ and canopy effects (Broadmeadow and Griffiths, 1993; Schleser, 1992). Needles, broadleaves and woody twigs (collected from trees and shrubs) were analyzed separately to investigate the isotopic variation among different plant tissues. Except when examining variations between tissues, isotopic and elemental compositions of plants parts from the same plant were averaged together and treated as one datapoint. Senesced and fresh tissues from *Carex aquatilis* were collected to facilitate the comparison of the isotopic and elemental compositions of senesced tissue with fresh tissue.

Benthic algae scrapes were collected from rocks near the shore using a toothbrush. The benthic algae were scraped into scintillation vials and promptly frozen for later analysis. Planktonic algae samples were collected from Taylor and Upper Carrol lakes using a vertical plankton tow net. Samples were not collected from East Carrol Lake because the water was so turbid that the net became clogged.

To collect the algae samples, the tow net was lowered to the deepest part of the lake and retrieved quickly. The algae collected in the net were rinsed out with lake water and emptied into several 250 mL amber Nalgene bottles. The samples were promptly frozen for later analysis. Submergent macrophytes (and at Denise Lake also littoral algae) were

collected opportunistically from each lake using a reaching/grabber tool from a float tube. All submerged macrophytes that were sampled were rooted. Once collected, the macrophytes were stored in Whirlpak bags. All samples of living tissue were frozen soon after collection and remained frozen until analysis. Samples of surficial sediments from the littoral zone of each lake were placed into WhirlPak bags and were immediately frozen until they could be freeze-dried at *The University of Western Ontario*.

Collection of waters from the four study lakes took place in July 2008– 2015. Pre-cleaned polyethylene 1 L amber Nalgene bottles were filled to maximum capacity (to avoid headspace) from a depth of 0.5 m below the surface. Waters were then transferred to a cooler and were promptly refrigerated at 4 °C. Waters designated for oxygen and hydrogen isotope analysis were left unfiltered and were stored in a 4 °C refrigerator at *The University of Western Ontario*. Samples used for the analysis of TN and TP were frozen. Samples designated for analysis of dissolved inorganic carbon (DIC) and dissolved inorganic nitrogen (DIN) were filtered and frozen. Samples designated for the analysis of nutrients were sent to Chesapeake Biological Laboratory in Maryland. The analytical protocols of the Chesapeake Biological Laboratory are available from <http://nasl.cbl.umces.edu/>.

Finally, a Glew gravity corer (Glew et al., 2002) was used to collect one 30-cm gravity core from the centre of Taylor Lake in September 2016. Upon collection, the core was visually inspected to ensure that the water-sediment interface was undisturbed. Immediately after collection, the core was subsectioned into 0.5 cm intervals. Each interval of sediment was individually sealed in a Whirl-Pak bag. All sediment samples were then freeze-dried. One sample from the bottom of the core was used in this thesis.

4.2.3 Determination of nutrient limitation in the Uinta Mountain study lakes

Water chemistry results were used to determine whether each lake was phosphorous- or nitrogen-limited, or co-limited. First, the mass ratio of DIN:TP was calculated. These DIN:TP mass ratios were then used to classify nutrient limitation in each lake according to the

following thresholds: DIN:TP < 1.5 indicates nitrogen-limitation; DIN:TP = 1.5– 3.4 represents co-limitation; and DIN:TP > 3.4 indicates phosphorous-limitation (Bergström, 2010).

4.2.4 Dissolved oxygen measurements

Measurements of dissolved oxygen from all four lakes were obtained using an In Situ Inc.® TROLL 9500 Multiparameter Probe Hydrolab® and a YSI Multiparameter Probe. Measurements were obtained from every metre, or every half-metre, of the lake. The measurements were obtained between 2008 and 2015, with most measurements occurring in July.

4.2.5 Analyses of carbon and nitrogen isotope ratios of bulk organic material

The $\delta^{13}\text{C}_{\text{TOC}}$, $\delta^{15}\text{N}_{\text{TN}}$ and TOC:TN of eight groups of probable OM sources were analyzed: algae, submerged macrophytes, semi-emergent macrophytes, broadleaf deciduous shrubs, herbaceous perennials, coniferous krummholz trees, lichen, mosses and graminoids. The $\delta^{13}\text{C}_{\text{TOC}}$, $\delta^{15}\text{N}_{\text{TN}}$ and TOC:TN of surficial sediments (the upper 0- 0.5 cm of sediment from the lake bottom) collected from the center of each study lake (Denise, Taylor, Upper Carrol and East Carrol lakes) was previously reported by Hundey et al. (2014). The analyses of $\delta^{13}\text{C}_{\text{TOC}}$, $\delta^{15}\text{N}_{\text{TN}}$ and TOC:TN of these surficial sediments were conducted in the same laboratory and following the same procedures as the analyses of the $\delta^{13}\text{C}_{\text{TOC}}$, $\delta^{15}\text{N}_{\text{TN}}$ and TOC:TN of probable OM sources. The interpretations in this chapter also refer to the $\delta^{13}\text{C}_{\text{TOC}}$ and $\delta^{15}\text{N}_{\text{TN}}$ of surficial sediments from the four study lakes, reported in Hundey et al. (2014). These data were included in the present study to improve our understanding of which probable sources of OM were important components of the sediment OM.

The amounts of total organic carbon (%TOC) and total nitrogen (%TN) in OM sources were analyzed concurrently with $\delta^{13}\text{C}_{\text{TOC}}$ and $\delta^{15}\text{N}_{\text{TN}}$ at LSIS using a Costech Elemental Combustion system (EA) coupled to a Thermo Scientific™ Delta^{PLUS} XL™ isotope ratio mass spectrometer (IRMS) in continuous-flow (He) mode (EA-IRMS). The %TOC and %TN data from these analyses were used to calculate elemental TOC:TN ratios (Meyers, 1994). Two

standards, USGS 40 (accepted values: %TOC= 40.7 %; %TN= 9.52 %) and USGS 41 (accepted values: %TOC= +40.7 %; %TN= 9.52 %) were used to generate calibration curves for %TOC and %TN measurements. After March 3, 2018, USGS 41 was replaced with USGS 41a (accepted values: %TOC= 40.7 %; %TN= 9.52 %). The internal standard keratin (MP Biomedicals Inc., Cat. No. 90211, Lot No. 9966H; average values: %TOC= 48.14 %; TN= 15.10 %) was used to evaluate precision and accuracy of carbon and nitrogen contents. The average %TOC and %TN of keratin was calculated by averaging over 1050 analyses of keratin at LSIS. The measured average values obtained in the present study of 46.88 ± 2.38 % ($n= 68$) for %TOC and 14.8 ± 0.46 % ($n= 54$) for %TN compare well with the accepted values. Duplicates were analyzed every ~11 samples and had an average reproducibility of ± 1.63 % ($n= 15$ sample pairs) for %TOC and ± 0.03 % ($n= 15$ sample pairs) for %TN.

Values of $\delta^{13}\text{C}_{\text{TOC}}$ and $\delta^{15}\text{N}_{\text{TN}}$ were measured in separate analytical sessions. The $\delta^{13}\text{C}_{\text{TOC}}$ and $\delta^{15}\text{N}_{\text{TN}}$ of plants were calibrated to VPDB and AIR using USGS 40 (accepted values: $\delta^{13}\text{C}= -26.29$ ‰; $\delta^{15}\text{N}= -4.52$ ‰) and USGS 41 (accepted values: $\delta^{13}\text{C}= +37.63$ ‰; $\delta^{15}\text{N}= +47.57$ ‰). For samples analyzed after March 3, 2018 date, USGS 41 was replaced by USGS 41a (accepted values: $\delta^{13}\text{C}= +37.55$ ‰; $\delta^{15}\text{N}= +47.55$ ‰). In addition to USGS 40 and USGS 41, internal standard keratin (MP Biomedicals Inc., Cat. No. 90211, Lot No. 9966H; $\delta^{13}\text{C}= +24.04$ ‰; $\delta^{15}\text{N}= +6.35$ ‰) was analyzed to monitor analytical accuracy and precision. In the present study, the measured $\delta^{13}\text{C}$ of keratin was -24.05 ± 0.10 ‰ ($n= 69$) and $+6.36 \pm 0.13$ ‰ ($n= 55$) for $\delta^{15}\text{N}$, which compare well with expected values. Sample duplicates were analyzed every ~10 samples and yielded an average reproducibility of ± 0.06 ‰ ($n= 15$ sample pairs) for $\delta^{13}\text{C}$ and ± 0.05 ‰ ($n= 15$ sample pairs) for $\delta^{15}\text{N}$.

The carbon isotope compositions of modern sediments from the centre of each lake (Hundey et al., 2014) were not corrected for the Suess Effect since these sediments were all deposited within the last decade. If one corrected these sediments for the Suess Effect, their $\delta^{13}\text{C}_{\text{TOC}}$ would increase by 0.4 ‰, which is near measurement error and would not alter the interpretations presented in this chapter (Verburg, 2007).

4.2.6 Extraction, identification and quantification of *n*-alkanes

Except for submerged macrophytes, *n*-alkanes could be extracted from all groups of probable OM samples groups in sufficient amounts. The sample amounts for submerged macrophytes were too limited. There was also insufficient algal material for this analysis. From each sample of probable OM sources, 0.5 g of tissue was used for *n*-alkane extraction. From the sediment core, 15 g of sediment from the very bottom of the core (~29–30 cm) was used for *n*-alkane extraction. All samples were Soxhlet extracted with 2:1 dichloromethane:methanol for 24 h to obtain a total lipid extract (TLE). Activated copper was then added to these extracts for 24 hours to reduce sulfur-containing compounds. After the copper was removed, the TLEs were then (i) concentrated to 1 mL using a Buchi R-300 Rotavapor; (ii) spiked with 1 mL of 100 ng/ μ L 5 α -androstane; and (iii) purified by elution with hexane during silica gel column chromatography. Finally, the *n*-alkane extracts were gently evaporated to dryness under nitrogen gas. Sample vials were partly submerged in an ice bath to minimize the evaporation of lower-chain *n*-alkanes. Immediately after drying, *n*-alkane extracts were redissolved in 50 μ L of hexane.

Identification and quantification of *n*-alkane abundances was performed using an Agilent 7890B gas chromatograph equipped with a flame ionization detector (GC-FID) in splitless mode. An Agilent HP-5 capillary column (30 m; 0.32 mm i.d.; 0.25 μ m film thickness) was used with helium flow rates set to 1 mL/min. The GC-FID temperature program utilized was as follows: 40 to 130 °C at 10 °C/min followed by 130 to 300 °C at 4 °C/min with a 10 min hold time. Each sample was analyzed in triplicate. Prior to each analytical session, external calibrations were conducted using a calibration mixture of *n*-alkanes (C₁₂-C₃₆) with known concentrations. Identification of *n*-alkanes was achieved through comparison of sample peaks with retention times of the peaks of this standard *n*-alkane mixture. Quantification of *n*-alkanes was achieved by integration of peak areas and those of the internal standard, 5 α -androstane.

4.2.7 Analyses of carbon and hydrogen isotope ratios of *n*-alkanes

The $\delta^{13}\text{C}$ and $\delta^2\text{H}$ of *n*-alkanes ($\delta^{13}\text{C}_{n\text{-alkane}}$ and $\delta^2\text{H}_{n\text{-alkane}}$, respectively) were determined using a Thermo Scientific™ Trace™ 1310 GC-C-IRMS paired to a Thermo Scientific™ Delta V™ IRMS in continuous-flow (He) mode. The GC oven temperature ramp, column dimensions and He flow rate were identical to those used for the GC-FID. Reactor temperatures were set to 1400 °C for hydrogen and 1000 °C for carbon modes, respectively. When analyzing $\delta^{13}\text{C}_{n\text{-alkane}}$, all samples were analyzed at least twice. When analyzing $\delta^2\text{H}_{n\text{-alkane}}$, all samples were analyzed at least three times. A standard mixture of *n*-alkanes (Mix A1, Arndt Schimmelmann, Indiana University) was analyzed at the beginning and end of every sequence. All but two of the *n*-alkanes in this standard mixture (C_{17} to C_{29}) were used to generate a calibration curve while the remaining two *n*-alkanes in this mixture (C_{16} and C_{30}) were used to monitor analytical accuracy and precision. The accepted $\delta^{13}\text{C}$ and $\delta^2\text{H}$ of C_{16} are -26.15‰ and -9.1‰ , respectively. These values compare well with measurements of $\delta^{13}\text{C}_{\text{C}_{16}}$ ($-26.06 \pm 0.35\text{‰}$ ($n=25$)), $\delta^2\text{H}_{\text{C}_{16}}$ ($-6.39 \pm 2.9\text{‰}$ ($n=19$)). The accepted $\delta^{13}\text{C}$ and $\delta^2\text{H}$ of C_{30} are -29.84‰ and -213.6‰ , respectively. These values compare well with measurements of $\delta^{13}\text{C}_{\text{C}_{30}}$ ($-29.95 \pm 0.30\text{‰}$ ($n=25$)) and $\delta^2\text{H}_{\text{C}_{30}}$ ($-207.18 \pm 6.78\text{‰}$). Precision was also monitored using the average standard deviation of sample replicates. For the analysis of $\delta^{13}\text{C}_{n\text{-alkane}}$, the average standard deviation of sample replicates was ± 0.29 ($n=121$ pairs), while for analysis of $\delta^2\text{H}_{n\text{-alkane}}$, the average standard deviation of sample replicates was ± 2.04 ($n=54$ triplicate analyses). The $\delta^{13}\text{C}_{n\text{-alkane}}$ of littoral sediments were not corrected for the Suess Effect; previous research suggests that they are unlikely more than 10 years old (Hundey et al., 2014).

4.2.8 Analyses of hydrogen and oxygen isotope ratios of lake waters

The $\delta^2\text{H}_{\text{water}}$ and $\delta^{18}\text{O}_{\text{water}}$ were measured at LSIS using a Thermo Scientific™ GasBench® II connected to a Thermo Scientific™ Delta^{plus} XL continuous-flow isotope ratio mass spectrometer (CF-IRMS) and a heater block equipped with a CombiPal® autosampler. The CO_2 -equilibration method was used to measure $\delta^{18}\text{O}_{\text{water}}$ (Epstein and Mayeda, 1953). For the analysis of $\delta^{18}\text{O}$, 1 mL of water was injected into septum-sealed glass vials and then

flushed with CO₂ for five minutes. Samples were then equilibrated with the CO₂ for 24 hours at 35 °C in the GasBench® heater block, after which and the CO₂ was automatically transported to the IRMS using the autosampler. Four internal standards, which had been previously calibrated to the internationally accepted VSMOW-SLAP scale (Coplen, 1994), were measured regularly throughout the analytical session, including LSD (accepted value: $\delta^{18}\text{O} = -22.57 \text{ ‰}$), MID (accepted value: $\delta^{18}\text{O} = -13.08 \text{ ‰}$), EDT (accepted value: $\delta^{18}\text{O} = -7.27 \text{ ‰}$) and Heaven (accepted value: -0.27 ‰). LSD and Heaven were used to generate the calibration curve and had average standard deviations of $\pm 0.27 \text{ ‰}$ ($n = 8$) and $\pm 0.07 \text{ ‰}$ ($n = 12$), respectively. MID and EDT were used to evaluate the accuracy and precision of the calibration and had average values of $-13.1 \pm 0.10 \text{ ‰}$ ($n = 8$) and $-7.3 \text{ ‰} \pm 0.14$ ($n = 22$), respectively, which compare well with accepted values. Duplicate samples had an average standard deviation of $\pm 0.34 \text{ ‰}$ ($n = 7$ sample pairs).

The H₂-equilibration method was used to measure $\delta^2\text{H}_{\text{water}}$. First, 1 mL of water was pipetted into a glass vial and a reusable platinum catalyst stuck was added to each vial. Half of the catalyst length was submerged in the water. Next, the vial was septum-sealed and capped and flushed with 3 % H₂ in He for five minutes prior to isotopic analysis. Last, the waters were equilibrated in He at 35 °C for at least 30 minutes using the GasBench® heater block and then were automatically transported to the IRMS using the autosampler. Four internal standards, which were previously calibrated to the VSMOW-SLAP scale (Coplen, 1994) were measured regularly throughout the analytical session, including LSD (accepted $\delta^2\text{H} = -161.8 \text{ ‰}$), MID (accepted $\delta^2\text{H} = -108.1 \text{ ‰}$), EDT ($\delta^2\text{H} = -56.0 \text{ ‰}$) and Heaven ($\delta^2\text{H} = +88.7 \text{ ‰}$). LSD and Heaven were used to generate the calibration curve and had an average reproducibility (standard deviations) of $\pm 2.1 \text{ ‰}$ ($n = 8$) and $\pm 1.50 \text{ ‰}$ ($n = 12$), respectively. MID and EDT were used to evaluate the accuracy and precision of the calibration and had average values of $-107 \pm 2.7 \text{ ‰}$ ($n = 8$) and $-55.1 \pm 1.1 \text{ ‰}$ ($n = 22$), respectively, which compares well with accepted values. Duplicate samples had an average standard deviation of $\pm 1.1 \text{ ‰}$ ($n = 7$ sample pairs).

4.2.9 Data treatment and calculations

Standard Bayesian ellipses, generated using the R package SIBER (Jackson and Parnell, 2020; R Core Development Team 2020), were used to evaluate overlap of the $\delta^{13}\text{C}_{\text{TOC}}$ and $\delta^{15}\text{N}_{\text{TN}}$ of probable OM sources (Jackson et al., 2011; Parnell et al., 2013). Standard predictive ellipses contain ~40 % of the data, and are used to describe bivariate data in the same way that standard deviation is used to describe univariate data (Batschelet, 1981). Such ellipses are useful because they are insensitive to changes in sample size, particularly when the small sample size correction in SIBER is applied (Syväranta et al., 2013). These ellipses were used to estimate the distribution of $\delta^{13}\text{C}_{\text{TOC}}$ and $\delta^{15}\text{N}_{\text{TN}}$ of groups of OM sources that would occur if one continued obtaining and analyzing samples.

In order to generate a standard predictive ellipse, each group of probable OM sources must contain at least eight points. For this reason, ellipses were not generated for graminoids or herbaceous perennials. To increase sample sizes, the submerged and semi-emergent macrophytes were grouped together. The correction detailed in Jackson et al. (2011) was applied to all ellipses to mitigate bias caused by small sample sizes. The four samples of surficial sediment from the centre of the lake from Hundey et al. (2014) were plotted together with these ellipses. In a separate plot, the $\delta^{13}\text{C}_{\text{TOC}}$ and $\delta^{15}\text{N}_{\text{TN}}$ of the surficial sediments were adjusted to account for degradation under aerobic conditions. This correction was made by shifting the $\delta^{13}\text{C}_{\text{TOC}}$ of these sediments upward by 1.6 ‰ (Lehmann et al., 2002) and the $\delta^{15}\text{N}_{\text{TN}}$ of these sediments downward by 2 ‰ (Brahney et al., 2014). For additional information on this correction, see Section D.1 in Appendix D. For the R code for Bayesian ellipses, see Subsection D.2.1 in Appendix D.

In order to evaluate which *n*-alkanes are the most useful for differentiating between OM source, the relative abundance of *n*-alkanes extracted from some groups of probable OM sources were analyzed using principal component analysis (PCA). PCA was conducted in the R package Vegan (Oksanen, 2013; R Core Development Team 2020). Since *n*-alkanes could not be extracted from algae, submerged macrophytes or sediments from the centre of the lake, these groups were not included in the PCA. The relative abundances of *n*-

alkanes extracted from littoral sediments were used in lieu of sediments in the centre of the lake. Data were not normalized prior to creating the PCA because all data were measured in the same units and across the same scale. The ellipses, which were also generated using Vegan, are non-Bayesian and represent the bimodal standard deviation of data from each subgroup. Ellipses were not generated for *n*-alkanes extracted from moss and lichen because the sample sizes of these groups were too small. For the R code used to generate this PCA, see Subsection D.2.2 in Appendix D.

Groups of probable OM sources were also compared using frequentist (non-Bayesian) statistical approaches. The *p*-values obtained from these tests are reported in Tables D.1 to D.4 in Appendix D. Student t-tests were used to compare groups that were normally distributed. When data were not normally distributed, groups were compared using nonparametric tests such as Kruskal-Wallis tests or, for pairwise comparison, pairwise Wilcoxon tests. All statistical tests were conducted in R (R Core Development Team, 2020). Tests were considered significant when $p \leq 0.01$.

Several calculations were used to assist in interpreting the *n*-alkane data. The average chain length (ACL), a weighted average of the abundance of each *n*-alkane, was used to characterize OM sources. The equation for ACL is given in Equation 1.7 (Chapter 1), where C_n is the concentration of each *n*-alkane with *n* carbon atoms (Bush and McInerney, 2013). The carbon preference index (CPI), a measure of *n*-alkane preservation, was calculated using Equation 1.8 (Chapter 1), revised from Bray and Evans (1961) and Marzi et al. (1993) to reflect the *n*-alkane chain lengths present in Uinta Mountain sediments.

The biosynthetic fractionation factor associated with *n*-alkane synthesis. Equation 1.10 (Chapter 1) was used to calculate the carbon isotope fractionation between *n*-alkanes and bulk organic tissue, while Equation 1.11 (Chapter 2) is used to calculate the hydrogen isotope fractionation between associated *n*-alkanes and source water. Measurements of the $\delta^2\text{H}$ of the study lakes was used as source water for semi-emergent macrophytes (Table D.5 in Appendix D). For terrestrial plants, the $\delta^2\text{H}$ of precipitation was estimated by

averaging the $\delta^2\text{H}$ of inflows. Surface waters can be used to estimate $\delta^2\text{H}$ of precipitation if the water has not been subject to evaporation (Henderson and Shuman, 2009). Inflows should be less evaporated than lake waters (Gat et al., 1994), so the $\delta^2\text{H}$ of inflows are ideal for estimating the $\delta^2\text{H}$ of precipitation.

The modern carbon isotope fractionation between $\delta^{13}\text{C}_{\text{CO}_2}$ and $\delta^{13}\text{C}_{\text{C}_{23}}$, or $\epsilon_{\text{atm-C}_{23}}$, was calculated using the measurements of $\delta^{13}\text{C}_{\text{C}_{23}}$ of coniferous krummholz trees, and the $\delta^{13}\text{C}$ of modern carbon dioxide (-8.4‰) (Equation 4.1). The C_{23} *n*-alkane was used because, as explained in the discussion, C_{23} is mostly produced by a single OM source: coniferous krummholz trees. The fact that one potential source of OM produces most of the C_{23} means that one does not need to estimate the proportional contribution of C_{23} from different plants/lichen. Another advantage of choosing an *n*-alkane derived from coniferous krummholz trees is that these trees have a high water use efficiency (Sachse et al., 2012), meaning that their $\delta^{13}\text{C}_{n\text{-alkane}}$ tend to be less affected by changes in aridity than other potential sources. Equation 4.1 was then used to calculate $\delta^{13}\text{C}_{\text{CO}_2}$. Sediments from the bottom of a ~ 30 cm sediment core were used for this purpose. Although these sediments were not dated, previously dated cores from Taylor Lake suggest that sediments this deep were deposited around AD ~ 1400 .

$$\text{Equation 4.1} \quad \epsilon_{\text{atm-}n\text{-alkane}} = 1000 * \left[\left(\frac{1000 + \delta^{13}\text{C}_{\text{atm}}}{1000 + \delta^{13}\text{C}_{n\text{-alkane}}} \right) - 1 \right] (\text{in ‰})$$

Values of ϵ_{water} were used to calculate the $\delta^2\text{H}$ of ancient precipitation. This time, C_{23} could not be used because concentrations of C_{23} in coniferous krummholz trees were too low to obtain accurate measurements of $\delta^2\text{H}_{n\text{-alkane}}$. Instead, C_{25} was used. As explained later, semi-emergent macrophytes produce little C_{25} relative to the other potential sources of OM in sediments. Semi-emergent macrophytes utilize lake water, or a mixture of lake water and precipitation, and as such, one would not expect their *n*-alkanes to record the $\delta^2\text{H}$ of precipitation. It was therefore important to focus on an *n*-alkane produced exclusively by terrestrial plants. These investigations revealed that mosses, broadleaf deciduous shrubs and herbaceous perennials produce C_{25} . To simplify these calculations, it

was assumed that these three sources contribute equal amounts of C₂₅ to sediments from the centre of the lake. The ϵ_{water} calculated for these sources is similar, varying only by ± 16 ‰, which limits any error arising from this assumption. Values of ϵ_{water} of these sources were then averaged to obtain an average separation between $\delta^2\text{H}_{n\text{-alkane}}$ and $\delta^2\text{H}_{\text{precipitation}}$ for the C₂₅ *n*-alkane. Finally, the $\delta^2\text{H}_{\text{precipitation}}$ was calculated using Equation 4.2.

$$\text{Equation 4.2} \quad \epsilon_{\text{water}} = 1000 * \left[\left(\frac{(1000 + \delta^2\text{H}_{n\text{-alkane}})}{1000 + \delta^2\text{H}_{\text{water}}} \right) - 1 \right] \text{ (in ‰)}$$

To aid in interpreting ϵ_{bulk} and ϵ_{water} , a phylogenetic tree was generated using the PhyloT tool at <https://phylot.biobyte.de/>. This tool generates phylogenetic trees based on the National Center for Biotechnology Information (NCBI) taxonomy. The NCBI database (<https://www.ncbi.nlm.nih.gov/>) was also used to determine which probable sources of OM to Uinta Mountain lakes were angiosperms, gymnosperms, monocotyledons (monocots) and/or dicotyledons (dicots). Only terrestrial and semi-aquatic organisms were used to create the tree because this phylogenetic tree is used to help interpret variation in *n*-alkane data, and *n*-alkanes could only be extracted from terrestrial and semi-aquatic sources. The taxa names used to generate this tree are shown in Table D.6 in Appendix D. The genus of each organism, except for lichen, was identified with high confidence. For the purposes of this study an exact identification of the lichen sample was not necessary since it is the only organism in Table D.6 that is not a plant. Hence, lichen must be more distantly related to the other OM sources than they are to one another. Figures D.1 and D.2 in Appendix D show the resulting phylogenetic tree. A simplified version of this tree, shown in Figure D.3, was ultimately used in the following discussion of *n*-alkanes. The purpose of simplifying this tree was to emphasize the relationships among groups of OM sources rather than the relationships between species.

4.3 Results

4.3.1 Water chemistry and dissolved oxygen in the four study lakes

Previous research showed that nutrient-limitation in the Uinta Mountains varies spatially and temporally, probably as a result of low concentrations of nitrogen and phosphorous (Hundey et al., 2014). At the time of sampling, these data show that Denise Lake was nitrogen-limited in 2012 but phosphorous-limited in 2015 (Table 4.2). Taylor Lake was phosphorous-limited or co-limited in 2011, nitrogen-limited in 2012 and phosphorous-limited in 2015. Upper Carrol Lake was co-limited in 2012 and phosphorous-limited in 2015, while East Carrol was phosphorous-limited in 2012 and 2015. All four lakes usually have well-oxygenated water columns (Figure D.4 in Appendix D) and low concentrations of dissolved inorganic carbon during the summer months (Table D.7 in Appendix D).

Table 4.2 Summary of nutrient measurements for water from the four Uinta Mountain lakes examined in this study and their N:P relationships. Bold text represents N limitation (DIN:TP <1.5), italic text represents uncertain limitation (DIN:TP= 1.5- 3.4), and underlined text represents P limitation (DIN:TP > 3.4). Limitation thresholds were taken from Bergström (2010). Data collected from before 2015 are from Hundey et al. (2014) (used with permission).

Lake	Date	DIN ($\mu\text{g L}^{-1}$)	TN ($\mu\text{g L}^{-1}$)	TP ($\mu\text{g L}^{-1}$)	DIN:TP mass ratio
Denise	Jul 2011	N/A	230	9.5	N/A
Denise	Jun 2012	10.8	150	13.2	0.8
Denise	Sep 2012	12.7	470	29.3	0.4
Denise	Jul 2015	53.6	210	4.5	<u>11.9</u>
Taylor	Jul 2011	139.0	240	15.4	<u>9.0</u>
Taylor	Sep 2011	28.0	210	11.0	2.5
Taylor	Jun 2012	17.0	190	18.5	0.9
Taylor	Sep 2012	9.7	220	10.8	0.9
Taylor	Jul 2015	39.4	340	6.9	<u>5.7</u>
Upper Carrol	May 2012	28.3	270	16.4	1.7
Upper Carrol	Jul 2015	23.1	190	5.4	<u>4.3</u>
East Carrol	May 2012	28.0	130	6.7	<u>4.2</u>
East Carrol	Jul 2015	70.2	270	12.5	<u>5.6</u>

4.3.2 Isotopic and elemental analyses of bulk sediments and tissues

Measurements of $\delta^{13}\text{C}_{\text{TOC}}$ and $\delta^{15}\text{N}_{\text{TN}}$ in potential sources of OM in Uinta Mountain lake sediments, and sediments from the centre of each study lake, are shown in Figure 4.2. Several tests were conducted to ensure that the measurements of $\delta^{13}\text{C}_{\text{TOC}}$, $\delta^{15}\text{N}_{\text{TN}}$ and TOC:TN from small tissue samples were appropriately characterizing the variation in isotopic and elemental compositions of subgroups. There was no significant difference in the $\delta^{13}\text{C}_{\text{TOC}}$, $\delta^{15}\text{N}_{\text{TN}}$ or TOC:TN of senesced versus fresh tissue (Fig. D.5 in Appendix D), broadleaves versus woody tissue (Fig. D.6 in Appendix D), or needles versus woody tissue (Fig. D.7 in Appendix D). There were also no significant differences in the $\delta^{13}\text{C}_{\text{TOC}}$ or $\delta^{15}\text{N}_{\text{TN}}$ of *Salix* leaves sampled from Taylor Lake versus East Carrol Lake (Fig. D.8 in Appendix D).

Significant differences were observed, however, in the TOC:TN of fresh *Salix* leaves sampled from Taylor Lake versus East Carrol Lake. For additional details regarding these comparisons, see Section D.7 in Appendix D.

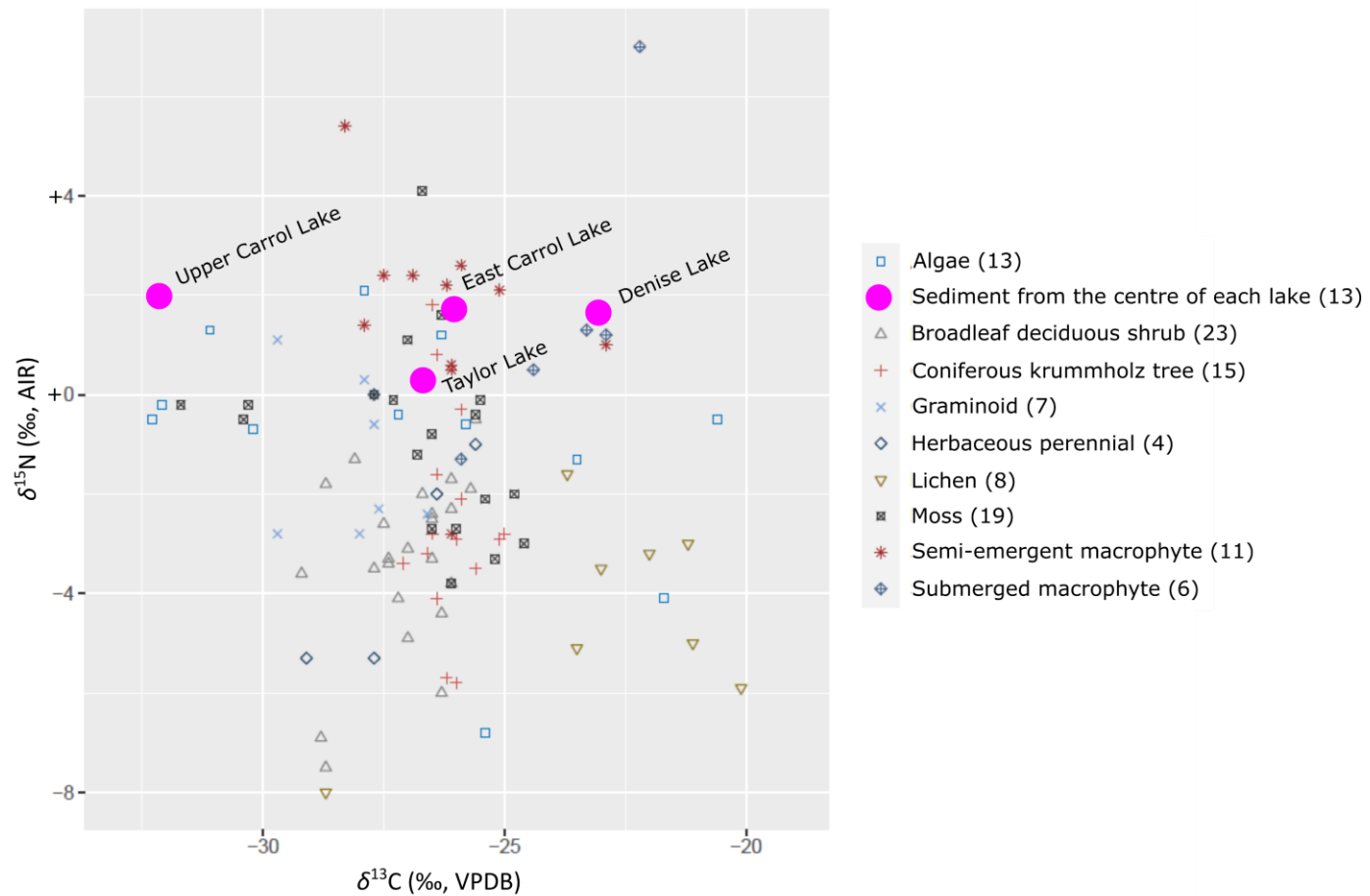


Figure 4.2 Scatter plot showing the $\delta^{13}\text{C}_{\text{TOC}}$ and $\delta^{15}\text{N}_{\text{TN}}$ of potential sources of OM captured by surficial sediments at the center of each study lake.

There was no significant difference in $\delta^{13}\text{C}_{\text{TOC}}$ between groups (Table D.1 in Appendix D); however, there were some significant differences in $\delta^{15}\text{N}_{\text{TN}}$ (Table D.2 in Appendix D). The $\delta^{15}\text{N}_{\text{TN}}$ of moss was significantly different than the $\delta^{15}\text{N}_{\text{TN}}$ of broadleaf deciduous shrubs. Likewise, the $\delta^{15}\text{N}_{\text{TN}}$ of semi-emergent macrophytes was significantly different than the $\delta^{15}\text{N}_{\text{TN}}$ of broadleaf deciduous shrubs. The $\delta^{15}\text{N}_{\text{TN}}$ of submerged macrophytes was significantly different than the $\delta^{15}\text{N}_{\text{TN}}$ of broadleaf deciduous shrubs. Finally, the $\delta^{15}\text{N}_{\text{TN}}$ of semi-emergent macrophytes was significantly different than the $\delta^{15}\text{N}_{\text{TN}}$ of coniferous krummholz trees. Lichen had the highest mean $\delta^{13}\text{C}_{\text{TOC}}$ (mean $\delta^{13}\text{C}_{\text{TOC}} = -22.9$ ‰), followed by submerged macrophytes (mean $\delta^{13}\text{C}_{\text{TOC}} = -24.4$ ‰), coniferous krummholz trees (mean $\delta^{13}\text{C}_{\text{TOC}} = -26.1$ ‰), semi-emergent macrophytes (mean $\delta^{13}\text{C}_{\text{TOC}} = -26.3$ ‰), algae (mean $\delta^{13}\text{C}_{\text{TOC}} = -27.0$ ‰), broadleaf deciduous shrubs (mean $\delta^{13}\text{C}_{\text{TOC}} = -27.1$ ‰), herbaceous perennials (mean $\delta^{13}\text{C}_{\text{TOC}} = -27.2$ ‰) and graminoids (mean $\delta^{13}\text{C}_{\text{TOC}} = -28.2$ ‰).

Semi-emergent and submerged macrophytes exhibit the highest mean $\delta^{15}\text{N}_{\text{TN}}$ of all groups (mean $\delta^{15}\text{N}_{\text{TN}} = +1.6$ ‰ and $+1.5$ ‰, respectively). Intermediate values of $\delta^{15}\text{N}_{\text{TN}}$ were measured for mosses (mean $\delta^{15}\text{N}_{\text{TN}} = -0.8$ ‰), algae (mean $\delta^{15}\text{N}_{\text{TN}} = -0.9$ ‰) and graminoids (mean $\delta^{15}\text{N}_{\text{TN}} = -1.4$ ‰). The lowest mean $\delta^{15}\text{N}_{\text{TN}}$ were obtained for coniferous trees (mean $\delta^{15}\text{N}_{\text{TN}} = -2.6$ ‰), broadleaf deciduous shrubs (mean $\delta^{15}\text{N}_{\text{TN}} = -3.3$ ‰), herbaceous perennials (mean $\delta^{15}\text{N}_{\text{TN}} = -3.4$ ‰) and lichen (mean $\delta^{15}\text{N}_{\text{TN}} = -4.4$ ‰).

The Bayesian ellipse characterizing the $\delta^{13}\text{C}_{\text{TOC}}$ and $\delta^{15}\text{N}_{\text{TN}}$ of algae overlaps with all other ellipses (Fig. 4.3 (i)). The ellipses characterizing the $\delta^{13}\text{C}_{\text{TOC}}$ and $\delta^{15}\text{N}_{\text{TN}}$ of moss, broadleaf deciduous shrubs, coniferous krummholz trees, macrophytes (both submerged and semi-emerged) and surficial sediments from the centre of the lake overlap. The ellipse characterizing the $\delta^{13}\text{C}_{\text{TOC}}$ and $\delta^{15}\text{N}_{\text{TN}}$ of lichen overlaps with algae, but no other ellipse. The $\delta^{13}\text{C}_{\text{TOC}}$ and $\delta^{15}\text{N}_{\text{TN}}$ of surficial sediments from the centre of the lake overlap with the $\delta^{13}\text{C}_{\text{TOC}}$ and $\delta^{15}\text{N}_{\text{TN}}$ of semi-emergent macrophytes, submerged macrophytes, moss, graminoids and coniferous krummholz trees (Figure 4.3 (i)). The $\delta^{13}\text{C}_{\text{TOC}}$ and $\delta^{15}\text{N}_{\text{TN}}$ of surficial sediments from the centre of the lake do not overlap with the $\delta^{13}\text{C}_{\text{TOC}}$ and $\delta^{15}\text{N}_{\text{TN}}$ of herbaceous

perennials, broadleaf deciduous shrubs or lichen. Figure 4.3 (ii) is the same as Figure 4.3 (i) except the $\delta^{13}\text{C}_{\text{TOC}}$ and $\delta^{15}\text{N}_{\text{TN}}$ of sediments have been shifted to account for degradation under oxic conditions, as described in Section D.1 in Appendix D. Following this correction, the $\delta^{13}\text{C}_{\text{TOC}}$ and $\delta^{15}\text{N}_{\text{TN}}$ of sediments overlap with the isotopic compositions of algae, mosses, macrophytes and coniferous krummholz trees.

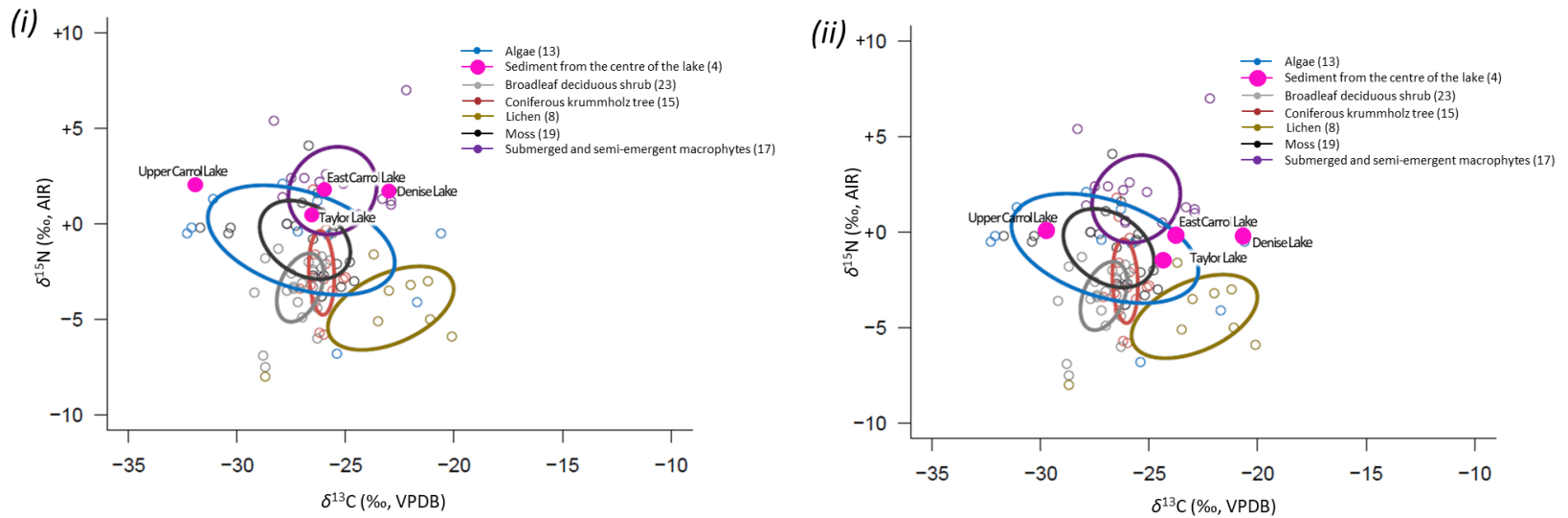


Figure 4.3 Standard Bayesian ellipses generated from the $\delta^{13}\text{C}_{\text{TOC}}$ and $\delta^{15}\text{N}_{\text{TN}}$ of probable OM sources sampled from the Uinta Mountain study sites. Graminoids and herbaceous perennials were excluded from this analysis due to their low sample size (<8 samples per group). Submerged and semi-emergent macrophytes were combined into one group because these groups have similar isotopic compositions. **(i)** – Measured $\delta^{13}\text{C}_{\text{TOC}}$ and $\delta^{15}\text{N}_{\text{TN}}$ of OM sources and sediments from the center of the lakes. **(ii)** – The $\delta^{13}\text{C}_{\text{TOC}}$ and $\delta^{15}\text{N}_{\text{TN}}$ of sediments from the center of the lake have been corrected for the influence of degradation (see text).

The highest mean TOC:TN was measured for coniferous krummholz trees (mean TOC:TN= 59), followed by graminoids (mean TOC:TN= 46), broadleaf deciduous shrubs (mean TOC:TN= 42), semi-emergent macrophytes (mean TOC:TN= 42), moss (mean TOC:TN= 32), herbaceous perennials (mean TOC:TN= 30), Lichen (mean TOC:TN= 28), submerged macrophytes (mean TOC:TN= 15), algae (mean TOC:TN= 15), and surficial sediments from the centre of the lake (mean TOC:TN= 9) (Figure 4.4). The TOC:TN of some groups of OM sources were significantly different from one another. For instance, the TOC:TN of algae was significantly different from the TOC:TN of broadleaf deciduous shrubs, as well as the TOC:TN of moss. The TOC:TN of sediments from the centre of the lake were significantly different than the TOC:TN of broadleaf deciduous shrubs. The TOC:TN of submerged macrophytes differed significantly from the TOC:TN of broadleaf deciduous shrubs, as well as moss. Finally, when algae, submerged macrophytes and sediments from the centre of the lake were grouped, their TOC:TN were significantly different from all other OM sources.

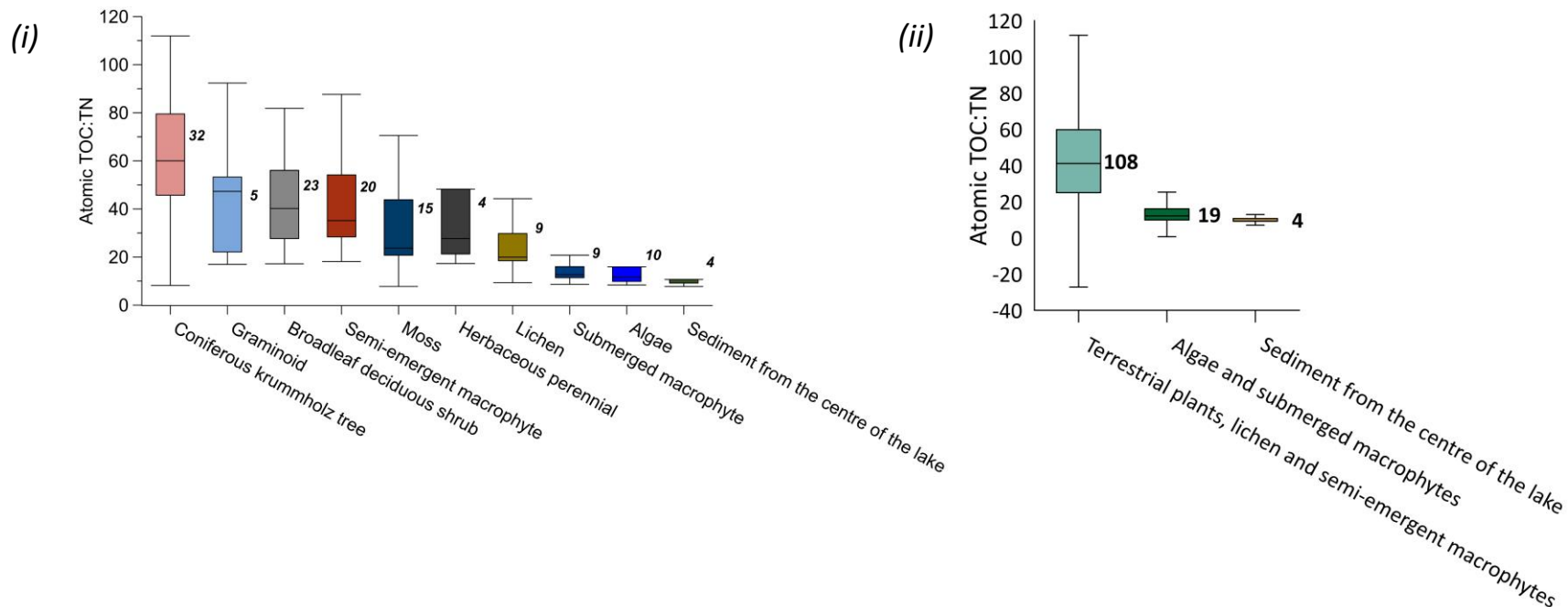


Figure 4.4 Atomic TOC:TN ratios of probable OM sources and surficial sediments from the center of the lake. (i): the TOC:TN of all probable sources of OM to the Uinta Mountain lakes. **(ii):** the TOC:TN of terrestrial plants, lichen and semi-emergent macrophytes; algae and submerged macrophytes; and sediments from the centre of the lake (Hundey et al., 2014). Each coloured box represents 50 % of the data clustered around the mean. Tails extending above and below these boxes represent the interquartile range of the data. Bold numbers represent the sample size of each group.

4.3.3 Relative and absolute abundances of *n*-alkanes extracted from probable OM sources and littoral sediments

Approximately 25 % of the *n*-alkanes produced by coniferous krummholz trees consist of C₂₃, the predominant *n*-alkane produced by this group (Figure 4.5). Mosses produced mainly C₂₅ (~30 %) and C₂₉ (~28 %). The *n*-alkane C₂₇ is most abundant in broadleaf deciduous shrubs (~35 %), semi-emergent macrophytes (~28 %) and littoral sediments (~18 %). Graminoids, herbaceous perennials and lichen all produced greater abundances of long-chain *n*-alkanes (\geq C₂₇) than short and mid-chain *n*-alkanes ($<$ C₂₇). Lichen produced almost exclusively C₂₉ and C₃₁, while graminoids and herbaceous perennials produced a more uniform distribution of *n*-alkanes.

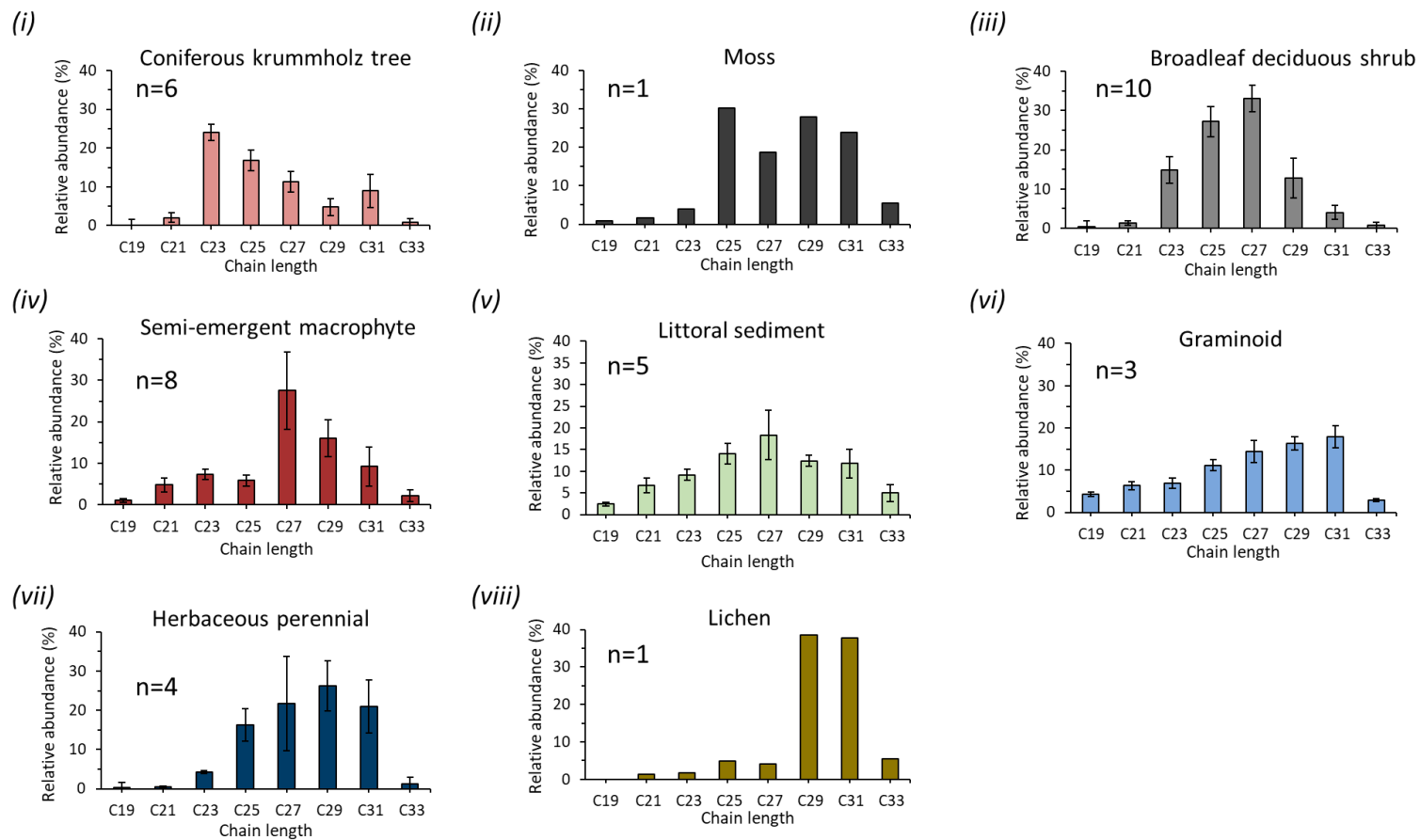


Figure 4.5 Average relative abundances of *n*-alkanes extracted from (i) coniferous krummholz trees, (ii) mosses, (iii) broadleaf deciduous shrubs, (iv) semi-emergent macrophytes, (v) littoral sediments, (vi) graminoids, (vii) herbaceous perennials and (viii) lichen. Error bars represent the standard error of the mean.

The results of PCA (Figs. 4.6 and 4.7) show that the *n*-alkanes of coniferous krummholz trees plot close to the C₂₃ eigenvector, indicating that they are distinct from other groups in having higher abundances of this *n*-alkane (Figs. 4.6 and 4.7). The other groups (*i.e.*, herbaceous perennials, graminoids, broadleaf deciduous shrubs and semi-emergent macrophytes) all overlap with each other but are distinct from the coniferous krummholz trees by having higher abundances of longer chain lengths (C₂₇, C₂₉ and C₃₁). The semi-emergent macrophytes samples fall into two groups that are differentiated by either high or low abundances of C₂₇. The littoral sediments plot at the intersection of all eigenvectors and overlap with the graminoid, semi-emergent macrophyte and broadleaf deciduous shrubs ellipse.

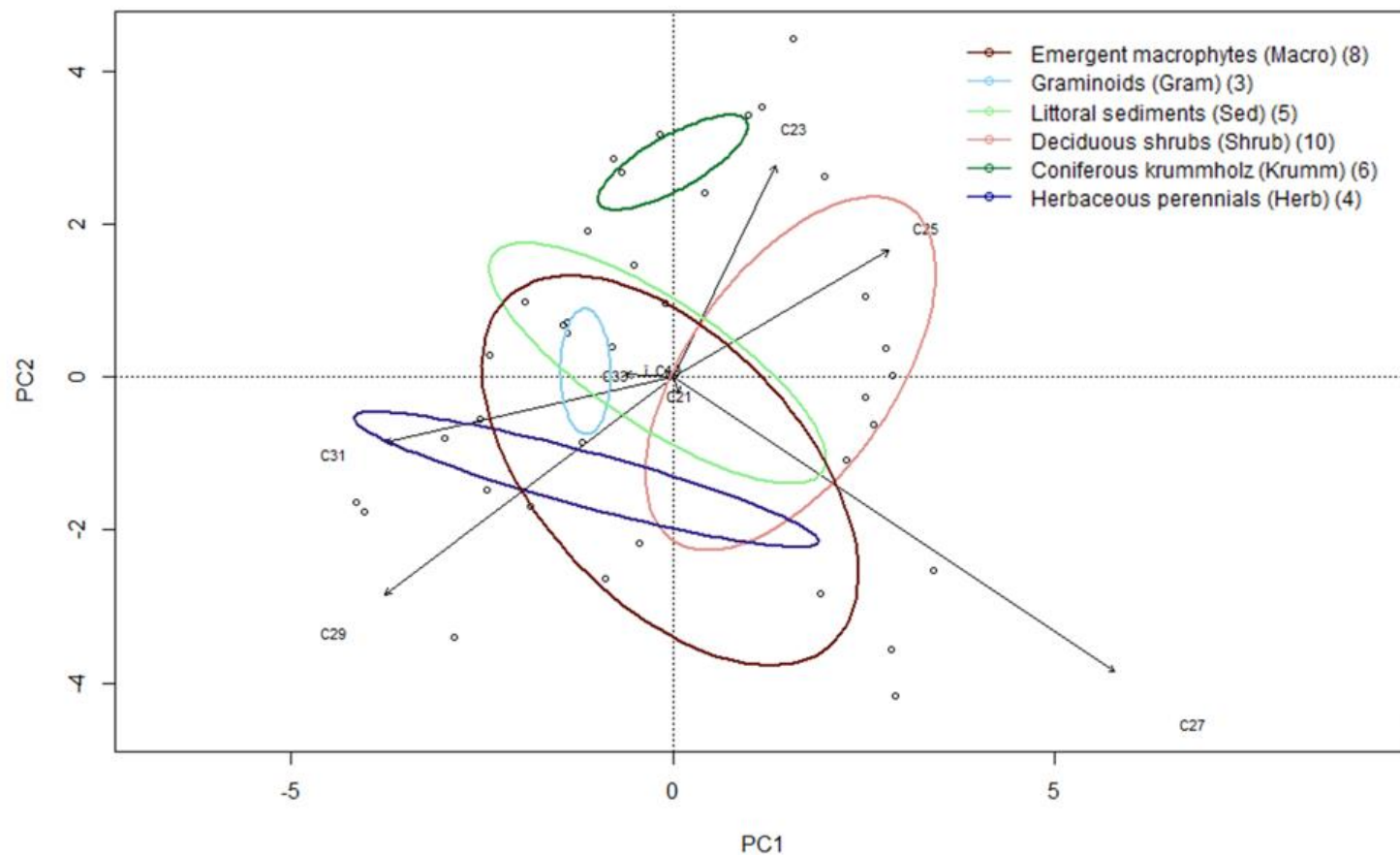


Figure 4.6 PCA generated using the relative abundances of *n*-alkanes extracted from semi-emergent macrophytes, graminoids, littoral sediments, broadleaf deciduous shrubs, herbaceous perennials, moss and lichen. Samples are represented as points surrounded by non-Bayesian ellipses that represent the bimodal standard deviation of each group. Eigenvectors represent odd chain lengths of *n*-alkanes. Lichen and moss samples are not surrounded by an ellipse due to their small sample sizes.

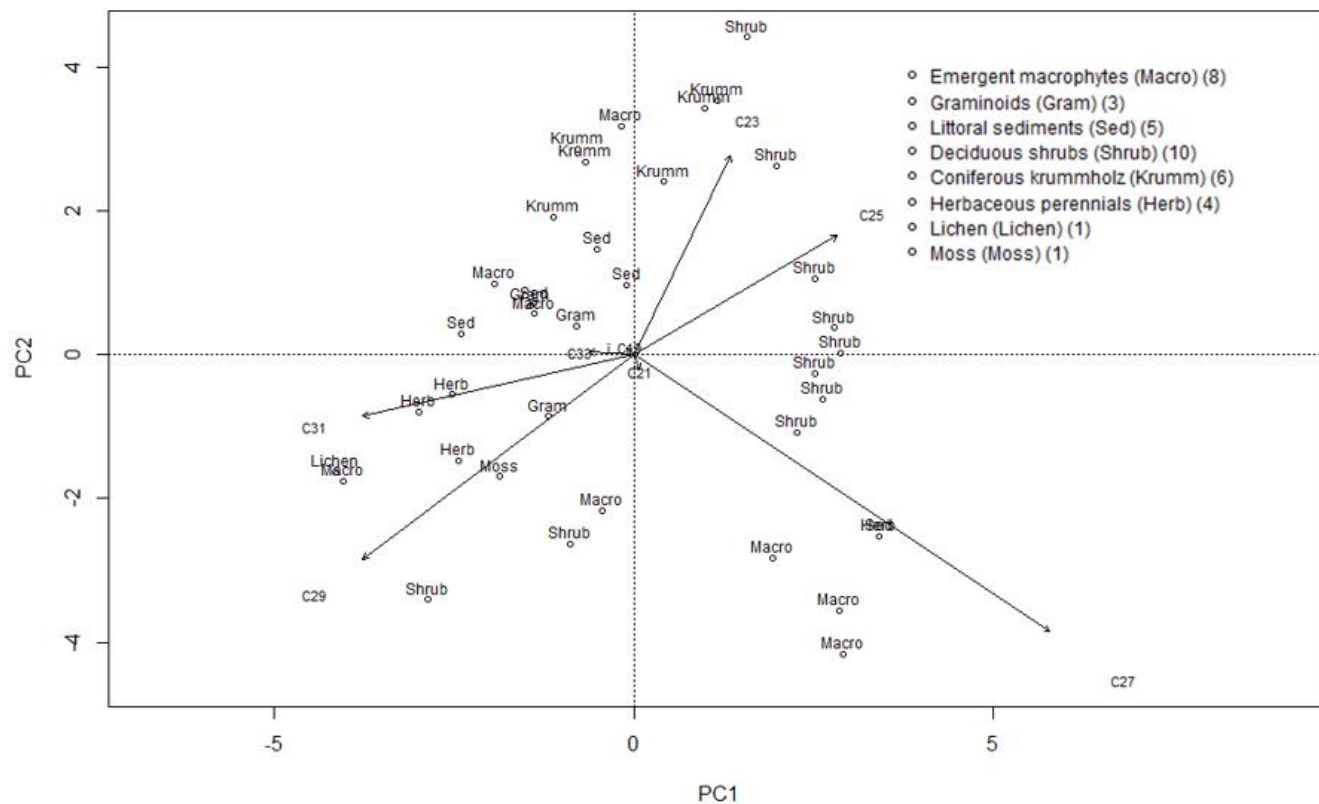


Figure 4.7 The same PCA as in Figure 4.7, but points are labelled and ellipses have been removed for clarity. By noting the proximity of samples to the tip of each eigenvector, one can deduce the relative abundance of chain lengths produced by each group of possible OM sources. For instance, shrubs plot near the tip of the C₂₅ eigenvector, indicating that they produce high relative abundances of C₂₅. Groups of potential OM sources that overlap produce similar relative abundances of *n*-alkanes, while groups that plot separately produce unique relative abundances of *n*-alkanes. This plot demonstrates that broadleaf deciduous shrubs and coniferous krummholz trees produce unique distributions of *n*-alkanes.

Lichen have the highest ACL (ACL= 29), followed by moss (ACL= 28), herbaceous perennials (mean ACL= 28), semi-emergent macrophytes (mean ACL= 27), graminoids (mean ACL= 27), littoral sediments (mean ACL= 26), broadleaf deciduous shrubs (mean ACL= 26) and coniferous krummholz trees (mean ACL= 25) (Fig. 4.8 (i)). Broadleaf deciduous shrubs and herbaceous perennials produced the widest range of *n*-alkane abundances, ranging from ~100-1200 $\mu\text{g/g}$ for broadleaf deciduous shrubs and ~150-1150 $\mu\text{g/g}$ for herbaceous perennials. Graminoids, littoral sediments and coniferous krummholz trees produced the lowest abundances of *n*-alkanes (>100 $\mu\text{g/g}$). Mosses, semi-emergent macrophytes and lichen produced *n*-alkanes with intermediate abundances, ranging from ~50– 500 $\mu\text{g/g}$ (Fig. 4.8 (ii)). Broadleaf deciduous shrubs produced *n*-alkanes with the highest mean CPI (mean CPI= 9), but also the most widely varying CPI (CPI= <1 to ~17) (Fig. 4.8 (iii)). The mean CPI of the remaining groups are, in descending order: lichen (7), herbaceous perennials (5), mosses (5), semi-emergent macrophytes (4), graminoids (3), littoral sediments (2) and coniferous krummholz trees (1).

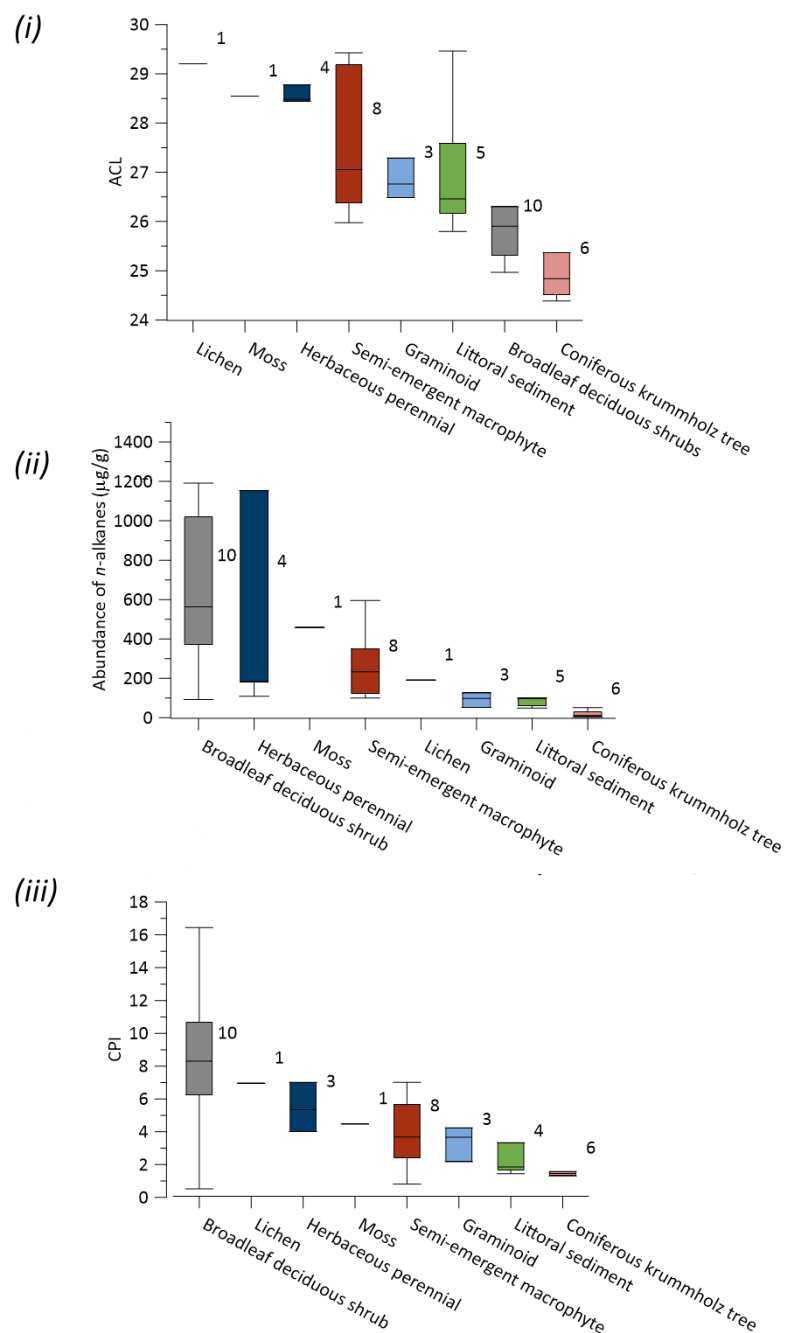


Figure 4.8 Variations in (i) average chain length (ACL), (ii) absolute abundances of n-alkanes, and (iii) carbon preference index (CPI) of potential OM sources that may have contributed to the littoral sediments. Potential OM sources to littoral sediments include: lichen, mosses, herbaceous perennials, semi-emergent macrophytes, graminoids, broadleaf deciduous shrubs and coniferous krummholz trees. *n*-Alkanes could not be extracted from algae or submerged macrophytes. These potential sources of OM were sampled from a subset of plants analyzed to determine $\delta^{13}\text{C}_{\text{TOC}}$, $\delta^{15}\text{N}_{\text{TN}}$ and TOC:TN. Littoral sediments consisted of one sediment sample per lake.

4.3.4 Carbon and hydrogen isotopic compositions of *n*-alkanes extracted from probable OM sources and littoral sediments

Littoral sediments exhibit the highest $\delta^{13}\text{C}_{n\text{-alkane}}$, followed by coniferous krummholz trees (Fig. 4.9 (i)). Lichen, semi-emergent macrophytes, mosses, graminoids and broadleaf deciduous shrubs produce *n*-alkanes with lower $\delta^{13}\text{C}_{n\text{-alkane}}$ that overlap. The $\delta^{13}\text{C}_{n\text{-alkane}}$ of littoral sediments overlaps most closely with the $\delta^{13}\text{C}_{n\text{-alkane}}$ of coniferous trees and, to a lesser degree, herbaceous perennials. The $\delta^2\text{H}_{n\text{-alkane}}$ of potential sources of OM in sediments also exhibit a high degree of overlap (Fig. 4.9 (ii)). The $\delta^2\text{H}_{n\text{-alkane}}$ of C_{27} *n*-alkanes produced by semi-emergent macrophytes plot below other potential sources of OM in sediments. The analytical error associated with this measurement is high relative to the other measurements. After correcting the $\delta^{13}\text{C}_{n\text{-alkane}}$ data for the effect of senescence, the $\delta^{13}\text{C}_{n\text{-alkane}}$ of littoral sediments overlaps with the $\delta^{13}\text{C}_{n\text{-alkane}}$ of broadleaf deciduous shrubs (Fig. 4.9 (iii)). The calculated values of $\epsilon_{\text{atm-}n\text{-alkane}}$ range from 19 to 29 ‰ (Fig. 4.9 (iv)). The calculation of $\delta^{13}\text{C}_{\text{CO}_2}$ (using the $\delta^{13}\text{C}_{\text{C}_{23}}$ from sediment and $\epsilon_{\text{CO}_2\text{-}n\text{-alkane}}$) revealed that the $\delta^{13}\text{C}_{\text{CO}_2}$ in AD ~1400 was -6.3 ± 0.4 ‰.

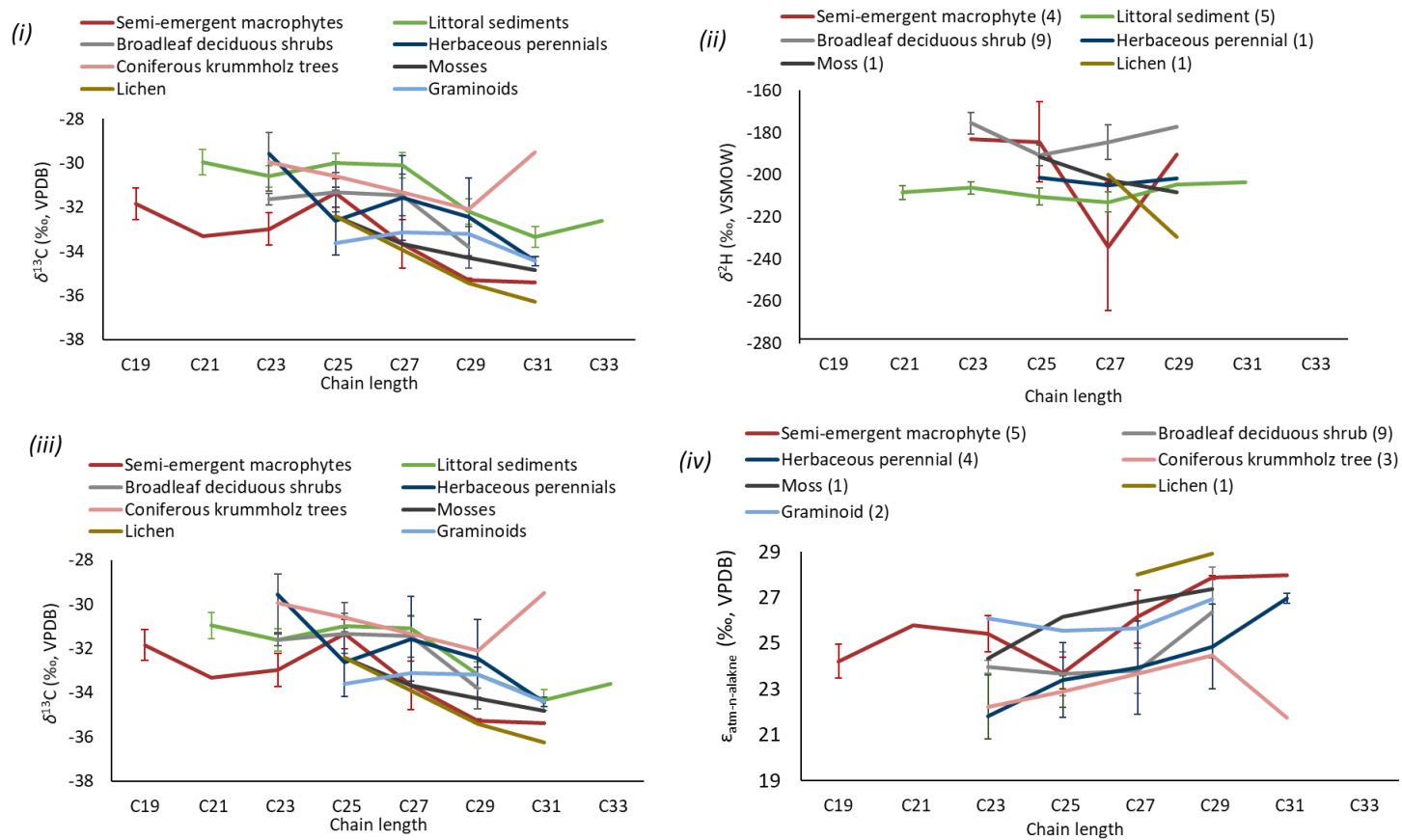


Figure 4.9 Variations in (i) $\delta^{13}\text{C}_{n\text{-alkane}}$, (ii) $\delta^2\text{H}_{n\text{-alkane}}$, (iii) $\delta^{13}\text{C}_{n\text{-alkane}}$ (corrected for the effect of senescence) and (iv) $\epsilon_{\text{atm-}n\text{-alkane}}$ of C₁₉ to C₃₃ n -alkanes extracted from semi-emergent macrophytes, littoral sediments, coniferous krummholz trees, lichen, moss, graminoids and herbaceous perennials sampled around Uinta Mountain lakes. Error bars represent the standard error of the mean. Sample sizes represent the number of organisms analyzed. Sample sizes of individual n -alkanes may differ from this total sample size.

Lichen are genetically distant from mosses, coniferous krummholz trees, semi-emergent macrophytes, graminoids, broadleaf deciduous shrubs and herbaceous perennials (Fig. 4.10). Mosses, which are nonvascular plants, are genetically distinct from vascular plants (coniferous krummholz trees, semi-emergent macrophytes, graminoids, broadleaf deciduous shrubs (Fig. 4.10). The ϵ_{bulk}^7 of lichen is the largest of all the groups of OM sources (Fig. 4.11 (i)), followed by mosses. The ϵ_{bulk} of gymnosperms is smaller than that of angiosperms (Fig. 4.11 (ii)). Among angiosperms, the ϵ_{bulk} of dicotyledonous plants (dicots; flowering angiosperms) is smaller than the ϵ_{bulk} of monocotyledonous plants (monocots; non-flowering angiosperms) (Fig. 4.11 (iii)).

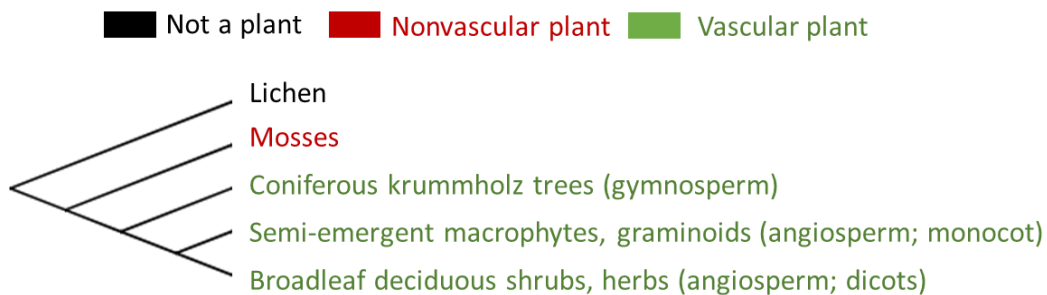


Figure 4.10 A phylogenetic tree representing the phylogenetic relationships between OM sources. The phylogenetic tree shown in panel (ii) was generated using the PhyloT tool at <https://phylot.biobyte.de/>. Semi-emergent macrophytes and other graminoids are classified as monocots, a type of non-flowering angiosperm, while broadleaf deciduous shrubs and herbaceous perennials (herbs) are classified as dicots, or flowering angiosperms.

⁷ ϵ_{bulk} is the carbon isotope fractionation between an *n*-alkane and the bulk tissue of the plant.

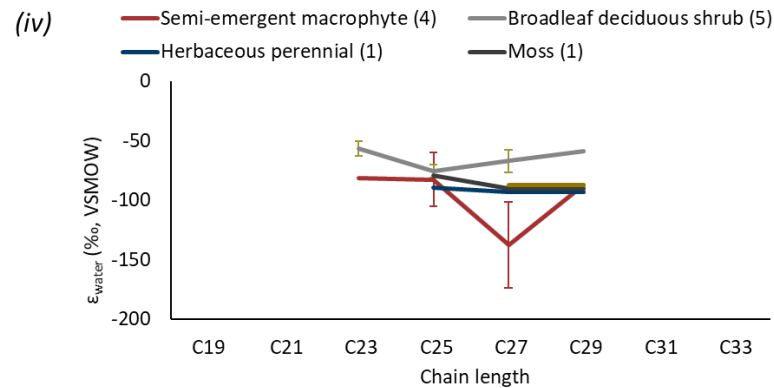
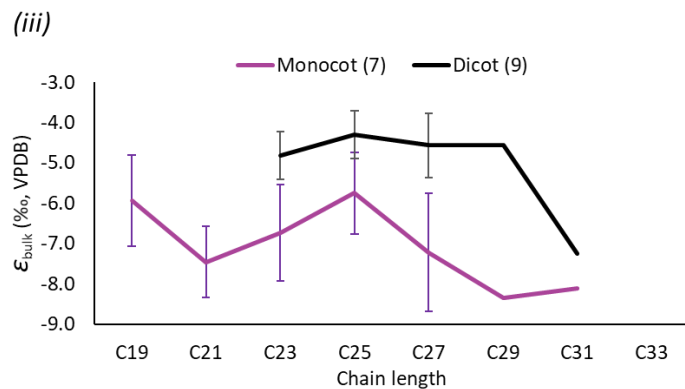
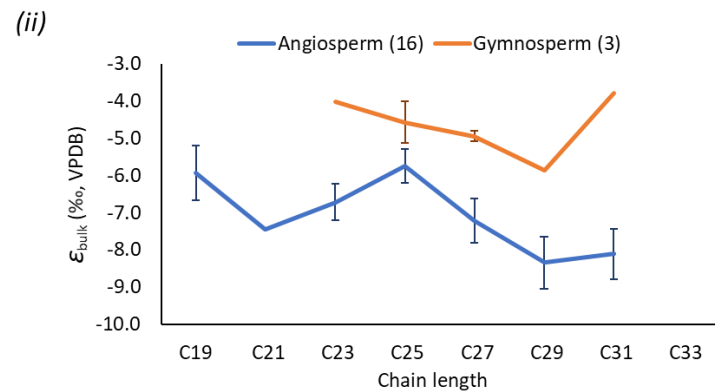
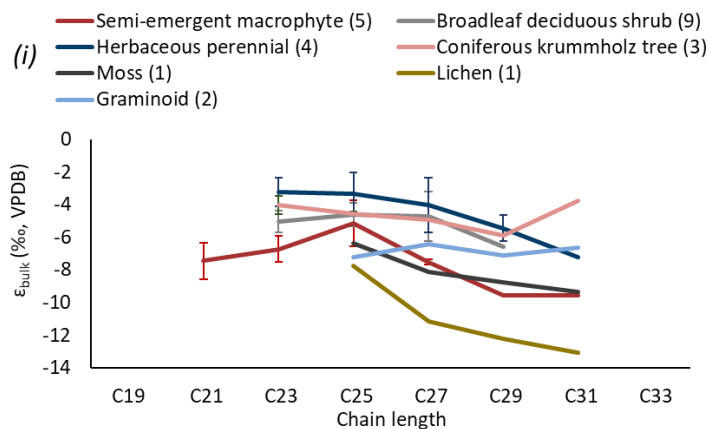


Figure 4.11 Variations in (i) ϵ_{bulk} from terrestrial/semi-aquatic OM sources; (ii) ϵ_{bulk} from angiosperms and gymnosperms; (iii) ϵ_{bulk} from monocots and dicots; and (iv) ϵ_{water} from terrestrial/semi-aquatic OM sources. Error bars represent the standard error of the mean. Sample sizes represent the number of organisms analyzed. Sample sizes of individual n -alkanes may differ from this total sample size.

Measurements of $\delta^2\text{H}_{n\text{-alkane}}$ were obtained for semi-emergent macrophytes, broadleaf deciduous shrubs, herbaceous perennials, mosses, lichen and littoral sediments (Fig. 4.9 (ii)). Accurate measurements of $\delta^2\text{H}_{n\text{-alkane}}$ could only be made for C_{23} to C_{29} n -alkanes. Broadleaf deciduous shrubs produced n -alkanes with the most consistently high $\delta^2\text{H}_{n\text{-alkane}}$. Semi-emergent macrophytes produced n -alkanes with $\delta^2\text{H}_{n\text{-alkane}}$ that ranged from high to low. Littoral sediments, herbaceous perennials, moss and lichen produced n -alkanes with $\delta^2\text{H}$ that fell between those of broadleaf deciduous shrubs and semi-emergent macrophytes. The $\delta^2\text{H}_{n\text{-alkane}}$ of littoral sediments correspond most closely with the $\delta^2\text{H}_{n\text{-alkane}}$ of semi-emergent macrophytes, mosses and herbaceous perennials. Broadleaf deciduous shrubs exhibit the smallest ϵ_{water} ⁸. The ϵ_{water} of the remaining sources of OM (semi-emergent macrophytes, lichen, mosses and herbaceous perennials) overlap for all chain lengths except for C_{27} . The ϵ_{water} of C_{27} produced by macrophytes is large relative to the other OM sources. The calculation of $\delta^2\text{H}_{\text{precipitation}}$ (using $\delta^2\text{H}_{\text{C}_{25}}$ from sediment and ϵ_{water}) revealed that the $\delta^2\text{H}_{\text{precipitation}}$ around AD ~1400 was -139 ± 10 ‰.

4.4 Discussion

4.4.1 Estimating sources of OM using TOC:TN, $\delta^{13}\text{C}_{\text{TOC}}$ and $\delta^{15}\text{N}_{\text{TN}}$

The results of this study indicate that the best indicator of OM source in lake sediments is TOC:TN. The TOC:TN suggests that aquatic organisms are the primary sources of OM to sediments from the centre of Uinta Mountain lakes (Fig. 4.4). The TOC:TN of OM sources is controlled by the macromolecular composition of tissues (Szpak et al., 2013). Woody terrestrial plants, such as coniferous krummholz trees, exhibit relatively high mean TOC:TN because these organisms are rich in carbon-containing compounds such as cellulose and lignin (Meyers and Ishiwatari, 1993). Conversely, aquatic organisms such as submerged macrophytes and algae exhibit the lowest mean TOC:TN as they are rich in nitrogen-

⁸ ϵ_{water} is the hydrogen isotope fractionation between the n -alkane and its source water.

containing compounds like proteins (Meyers and Ishiwatari, 1993). Hence, the TOC:TN of Uinta Mountain sediments is useful for differentiating between allochthonous (terrestrial) and autochthonous (aquatic) sources of OM. Nonetheless, care should be taken when interpreting the TOC:TN of sediments receiving large OM inputs from sources like lichen, which can have low TOC:TN in the range of submerged macrophytes and algae (Fig. 4.4).

Values of $\delta^{13}\text{C}_{\text{TOC}}$ and $\delta^{15}\text{N}_{\text{TN}}$ are less useful for determining the source of OM in Uinta Mountain lake sediments. The $\delta^{13}\text{C}_{\text{TOC}}$ of surficial lake sediments overlap with every probable OM source shown in Figure 4.2. The $\delta^{13}\text{C}_{\text{TOC}}$ of probable sources of OM to the Uinta Mountain lakes display a high degree of overlap (Fig. 4.2), and there is no significant difference in the $\delta^{13}\text{C}_{\text{TOC}}$ among groups (Table D.1 in Appendix D).

Lichen exhibit the highest mean $\delta^{13}\text{C}_{\text{TOC}}$ of all groups (Fig. 4.2). Lichen are composite organisms comprising a fungus and a photobiont (algae). The $\delta^{13}\text{C}_{\text{TOC}}$ of lichen depend on the species of photobiont. Lichen with cyanobacteria as the photobiont tend to have $\delta^{13}\text{C}_{\text{TOC}}$ between -23 and -14 ‰, while lichen with green algae as the photobiont exhibit $\delta^{13}\text{C}_{\text{TOC}}$ between -35 and -17 ‰ (Huiskes et al., 2007; Lange et al., 1988; Lee et al., 2009). Some lichen growing in the Uinta Mountains had $\delta^{13}\text{C}$ of ~ -27 ‰, and hence these plants must use green algae as the photobiont. Submerged macrophytes have the second highest mean $\delta^{13}\text{C}_{\text{TOC}}$. The $\delta^{13}\text{C}_{\text{TOC}}$ of submerged macrophytes depends largely on the $\delta^{13}\text{C}_{\text{TOC}}$ of dissolved inorganic carbon (DIC) in the surrounding water (LaZerte and Szalados, 1982). The $\delta^{13}\text{C}_{\text{DIC}}$ of waters, and therefore submerged macrophytes, can increase in response to primary production in $^{12}\text{CO}_2$ -limiting environments (Hollander and McKenzie, 1991).

Coniferous krummholz trees, semi-emergent macrophytes, algae, broadleaf deciduous shrubs, herbaceous perennials and graminoids all exhibited mean $\delta^{13}\text{C}_{\text{TOC}}$ that fell within ± 1 ‰ of -27 ‰, the typical $\delta^{13}\text{C}$ of organisms utilizing the C_3 pathway of carbon fixation (Deines, 1980). Among vascular, terrestrial plants, water use efficiency plays an important role in modulating $\delta^{13}\text{C}_{\text{TOC}}$ around -27 ‰ (Farquhar and Lloyd, 1993).

Although algae also utilize C₃ photosynthesis, they exhibit a wide range of $\delta^{13}\text{C}_{\text{TOC}}$. Algae that obtain DIC in the form of CO₂ typically have $\delta^{13}\text{C}_{\text{TOC}} \approx -27 \text{‰}$ (Fogel and Cifuentes, 1993). The $\delta^{13}\text{C}_{\text{TOC}}$ of algae utilizing CO₂ can become lower than -27‰ in environments where ¹²CO₂ is not limiting. Under such conditions, algae will preferentially utilize ¹²C-rich CO₂, driving down their $\delta^{13}\text{C}_{\text{TOC}}$ (Hollander and McKenzie, 1991). Some algae, however, have adapted to obtain DIC in the form of HCO₃⁻, particularly when CO₂ is limiting. Such algae produce $\delta^{13}\text{C}_{\text{TOC}} \approx -20 \text{‰}$ (Fogel and Cifuentes, 1993). It is unsurprising that algae utilizing HCO₃⁻ live in the Uinta Mountain lakes because these lakes are situated in quartzite bedrock, rather than carbonate-rich bedrocks. Moreover, productivity in these lakes are low. Due to the bedrock geology of these lakes, and limited productivity, DIC concentrations in the lake are low (Table D.7 in Appendix D). Mosses from these lakes also have a mean $\delta^{13}\text{C}$ of $\sim -27 \text{‰}$ and exhibit a wide range of $\delta^{13}\text{C}_{\text{TOC}}$. Their $\delta^{13}\text{C}_{\text{TOC}}$ are so variable because they lack stomata. Instead CO₂ availability, and consequently $\delta^{13}\text{C}_{\text{TOC}}$, depends on the thickness of water coating their leaves (Rice, 2000; Rundel et al., 1979; Szpak et al., 2013).

Surficial sediments from the centre of each lake exhibit relatively high $\delta^{15}\text{N}_{\text{TN}}$ that overlap with the $\delta^{15}\text{N}_{\text{TN}}$ of algae, semi-emergent macrophytes, submerged macrophytes, moss, graminoids and coniferous krummholz trees. Among the probable sources of OM to the Uinta Mountain study lakes, the $\delta^{15}\text{N}_{\text{TN}}$ of all sources exhibit less overlap than $\delta^{13}\text{C}_{\text{TOC}}$. Semi-emergent and submerged macrophytes exhibit the highest mean $\delta^{15}\text{N}_{\text{TN}}$ of all groups. Previous studies have also noted high $\delta^{15}\text{N}_{\text{TN}}$ in these plants (Cloern et al., 2002; Delong and Thorp, 2006; Molina et al., 2011). The high $\delta^{15}\text{N}_{\text{TN}}$ is most likely related to assimilation of dissolved inorganic nitrogen (DIN) in lacustrine sediments (Cloern et al., 2002). The $\delta^{15}\text{N}$ of such DIN can increase due to nitrification/denitrification in the littoral zone (Cline and Kaplan, 1975). The semi-emergent macrophytes can also have high $\delta^{15}\text{N}_{\text{TN}}$ due to their deep rooting depths, which allows access to soils/littoral sediments enriched in ¹⁵N (Kielland, 1997). Soils/littoral sediments tend to become enriched in ¹⁵N with depth because degradation results in the preferential loss of ¹⁴N (Natlhoffer and Fry, 1988). All of the semi-emergent macrophytes analyzed in this study consist of *Carex* sp., which are known to have deep rooting depths.

Intermediate values of $\delta^{15}\text{N}_{\text{TN}}$ were measured for mosses, graminoids and algae. It is unclear why the $\delta^{15}\text{N}_{\text{TN}}$ of moss is higher than the $\delta^{15}\text{N}_{\text{TN}}$ of lichen. These organisms are thought to obtain nitrogen from similar sources and therefore typically have similar $\delta^{15}\text{N}_{\text{TN}}$ (Kielland, 1997). That said, some mosses in nitrogen-stressed environments, such as the boreal forest and tundra, have evolved the ability to fix atmospheric N_2 , causing the $\delta^{15}\text{N}_{\text{TN}}$ of their tissues to approach 0 ‰, which is the average $\delta^{15}\text{N}_{\text{TN}}$ of atmospheric N_2 (Rousk et al., 2014). The $\delta^{15}\text{N}_{\text{TN}}$ of some Uinta Mountain mosses also have an average $\delta^{15}\text{N}_{\text{TN}}$ of ~ 0 ‰, which may suggest that they also fix N_2 . It is also uncertain why the $\delta^{15}\text{N}_{\text{TN}}$ of graminoids is higher than that of other terrestrial, vascular plants, such as herbaceous perennials. The higher-than-expected mean $\delta^{15}\text{N}_{\text{TN}}$ of graminoids suggests that these plants are accessing an unidentified source of ^{15}N , perhaps due to deep rooting depths.

Algae in the Uinta Mountains produce the widest range of $\delta^{15}\text{N}_{\text{TN}}$. The foremost control on algal $\delta^{15}\text{N}_{\text{TN}}$ is the $\delta^{15}\text{N}$ of dissolved inorganic nitrogen (DIN) of the water body (Cloern et al., 2002). This $\delta^{15}\text{N}_{\text{DIN}}$ can be modified by primary production, respiration, nitrification and denitrification and fertilizer inputs (Talbot, 2001). Even within one lake, however, the $\delta^{15}\text{N}_{\text{TN}}$ of algae may vary considerably depending on the strategies that algae use to obtain nitrogen, and the isotopic fractionations that occur as this nitrogen is assimilated by the algae (Fogel and Cifuentes, 1993). The wide range of $\delta^{15}\text{N}_{\text{TN}}$ observed among Uinta Mountain algae suggests that algae in these nutrient-poor lakes must utilize a variety of strategies to obtain nitrogen.

The lowest $\delta^{15}\text{N}_{\text{TN}}$ were measured in lichen, coniferous krummholz trees, broadleaf deciduous shrubs and herbaceous perennials. Previous studies have also measured lichen with low $\delta^{15}\text{N}_{\text{TN}}$ relative to plants (Huiskes et al., 2007; Lee et al., 2009; Szpak et al., 2013; Wang and Wooller, 2006). Wang and Wooller (2006) determined that some lichen may have low $\delta^{15}\text{N}$ as a result of uptake of atmospheric ammonia. Uptake of atmospheric ammonia ($\text{NH}_3(\text{g})$) can lower the $\delta^{15}\text{N}_{\text{TN}}$ of lichen as the $\delta^{15}\text{N}$ of ammonia ranges from -8 to -1 ‰ (Tozer et al., 2005). It is likely that coniferous krummholz trees, broadleaf deciduous shrubs and herbaceous perennials have low $\delta^{15}\text{N}_{\text{TN}}$ relative to the other groups because these

plants obtain nitrogen through mycorrhizal relationships (Hobbie and Colpaert, 2003; Hobbie and Ouimette, 2009). Terrestrial plants in alpine areas typically form symbiotic relationships with fungi to obtain nitrogen (Körner, 2003). This nitrogen is depleted of ^{15}N relative to soil nitrogen, and therefore lowers the overall $\delta^{15}\text{N}_{\text{TN}}$ of the plant (Michelsen et al., 1998).

Although $\delta^{13}\text{C}_{\text{TOC}}$ and $\delta^{15}\text{N}_{\text{TN}}$ are less useful for identifying source of OM in Uinta Mountain lake sediments relative to TOC:TN, Bayesian analysis of $\delta^{13}\text{C}_{\text{TOC}}$ and $\delta^{15}\text{N}_{\text{TN}}$ can provide additional useful information. Using Bayesian ellipses, it was determined that the most likely sources of OM to sediments in the centre of the lake are algae, submerged and semi-emerged macrophytes, mosses and coniferous krummholz trees (Fig. 4.3). When considered with the TOC:TN data, these proxies point towards algae and submerged macrophytes as the most important sources of OM in sediments from the centre of each Uinta Mountain study lake.

In addition to exploring the variations in TOC:TN, $\delta^{13}\text{C}_{\text{TOC}}$ and $\delta^{15}\text{N}_{\text{TN}}$ among groups, the variation in TOC:TN, $\delta^{13}\text{C}_{\text{TOC}}$ and $\delta^{15}\text{N}_{\text{TN}}$ within groups and between study sites was also characterized (Section D.7 in Appendix D). With one exception, no significant differences were observed between plant parts, senesced versus fresh tissues, or plants growing in different study sites. This finding suggests that the small tissue samples collected from each organism capture most of the variation in TOC:TN, $\delta^{13}\text{C}_{\text{TOC}}$ and $\delta^{15}\text{N}_{\text{TN}}$ present in the entire organism. A significant difference was observed between the TOC:TN of *Salix sp.* (a species of broadleaf deciduous shrub) growing around Taylor and East Carrol lakes. This is likely due to differences in the availability of soil nitrogen between sites (Turner, 1977), as described more fully in Subsection D.7.1 of Appendix D.

4.5 Estimating the sources of OM to sediments from the littoral zone of Uinta Mountain lakes

Due to sampling constraints associated with working in a remote area, the sample sizes of algae, submerged macrophytes and sediments from the centre of the lake were too small

for *n*-alkane analysis. This section therefore focuses on semi-emergent macrophytes, coniferous krummholz trees, mosses, lichen, graminoids, broadleaf deciduous shrubs, herbaceous perennials and surficial sediments from the littoral zone.

Figures 4.6 and 4.7 demonstrate that the relative abundances of *n*-alkanes extracted from littoral sediments correspond most closely with those extracted from semi-emergent macrophytes, graminoids and broadleaf deciduous shrubs. This finding suggests that, of the organisms sampled, emergent macrophytes, graminoids and broadleaf deciduous shrubs likely contribute the most OM to littoral sediments. This makes sense since these groups would be most proximal to the littoral zone of the lake.

These findings do not, however, match well with the probable sources of OM suggested by the $\delta^{13}\text{C}_{n\text{-alkane}}$ and $\delta^2\text{H}_{n\text{-alkane}}$ measurements (Fig. 4.9). The $\delta^{13}\text{C}_{n\text{-alkane}}$ of littoral sediments overlaps most closely with the $\delta^{13}\text{C}_{n\text{-alkane}}$ of coniferous krummholz trees and, to a lesser degree, herbaceous perennials (Fig. 4.9 (i)). The $\delta^2\text{H}_{n\text{-alkane}}$ overlaps most closely with the $\delta^2\text{H}_{n\text{-alkane}}$ of semi-emergent macrophytes, mosses and herbaceous perennials (the $\delta^2\text{H}_{n\text{-alkane}}$ of coniferous krummholz trees could not be measured) (Fig. 4.9 (ii)). There are two possible reasons why the $\delta^{13}\text{C}_{n\text{-alkane}}$ and $\delta^2\text{H}_{n\text{-alkane}}$ may not correspond with the relative abundance data for the *n*-alkanes. One possibility is that the original *n*-alkanes abundances and isotopic signatures of the littoral sediments have been affected by degradation. The CPI of these sediments, however, is ≥ 1 (Fig. 4.8 (iii)), suggesting that these *n*-alkanes are well-preserved (Marzi et al., 1993). The most likely reason for the discordance between the relative abundance and isotopic records is that leaf senescence exerts different influences on the relative abundances of *n*-alkanes and the isotopic compositions of those *n*-alkanes.

Although fresh OM may be delivered directly to littoral sediments, it is more likely that tissues from terrestrial organisms will senesce before being transported to sediments. Senescence greatly reduces the absolute abundance of *n*-alkanes in fresh tissues, but does not noticeably affect the relative abundances of *n*-alkanes in these tissues (Bush and McInerney, 2013). Senescence can, however, increase the $\delta^{13}\text{C}_{n\text{-alkane}}$ of tissues. Tu et al.

(2004) found that senescence resulted in a ~ 1 ‰ increase in the $\delta^{13}\text{C}_{n\text{-alkane}}$ of plant tissues. To adjust for this effect, the $\delta^{13}\text{C}_{n\text{-alkane}}$ of littoral sediments, which are comprised of senesced tissues, were reduced by 1 ‰. This adjustment results in the $\delta^{13}\text{C}_{n\text{-alkane}}$ of littoral sediments overlapping with broadleaf deciduous shrubs from C_{23} to C_{29} (Fig. 4.9 (iii)).

The effect of senescence on $\delta^2\text{H}_{n\text{-alkane}}$ is more poorly understood than the effect on $\delta^{13}\text{C}_{n\text{-alkane}}$. Previous studies have noted a difference between the $\delta^2\text{H}_{n\text{-alkane}}$ of fresh foliar tissue and leaf litter (Zech et al., 2011). The prevailing driver of this difference in $\delta^2\text{H}_{n\text{-alkane}}$ and $\delta^2\text{H}_{\text{leaf litter}}$ is a change in the $\delta^2\text{H}$ of source water (Sachse et al., 2009). In the summer months, the $\delta^2\text{H}$ of source water is higher than during the winter months (Dansgaard, 1964). Since n -alkanes have a turnover time on the order of weeks, the n -alkanes produced in the summer months exhibit a $\delta^2\text{H}_{n\text{-alkane}}$ that is higher than that of the n -alkanes produced around the time of leaf senescence (Sachse et al., 2009). This could explain why the $\delta^2\text{H}_{n\text{-alkane}}$ of littoral sediments is 20 to 30 ‰ lower than the $\delta^2\text{H}_{n\text{-alkane}}$ of broadleaf deciduous shrubs, the predominant source of OM as indicated by relative abundances of n -alkanes and $\delta^{13}\text{C}_{n\text{-alkane}}$.

Together, the relative abundances of n -alkanes and corrected trends in $\delta^{13}\text{C}_{n\text{-alkane}}$ point towards broadleaf deciduous trees as the predominant source of OM to littoral sediments. This interpretation is complicated, however, by the fact that broadleaf deciduous shrubs also produce the highest mean abundance of n -alkanes of any terrestrial/semi-aquatic source of OM (Fig. 4.8 (ii)). It is therefore unclear whether broadleaf deciduous shrubs are really the most important source of n -alkanes to littoral sediments, or if they are simply overrepresented in the sediment record.

One method of accounting for variations in the absolute abundance of n -alkanes is to include absolute abundances of n -alkanes as a concentration dependency, or a weighting factor, in a stable isotope mixing model. Such models, such as Stable Isotope Mixing Model in R (Simmr), estimate the proportional contributions of each probable OM source to sediments (Parnell and Inger, 2020; R Core Development Team, 2020). In order to use stable

isotope mixing models, however, the $\delta^{13}\text{C}_{n\text{-alkane}}$ and/or $\delta^2\text{H}_{n\text{-alkane}}$ of each probable source of OM must be unique (Parnell et al., 2013). Given the overlap in $\delta^{13}\text{C}_{n\text{-alkane}}$ and $\delta^2\text{H}_{n\text{-alkane}}$ between probable sources of OM, this approach cannot be used to estimate source apportionment to littoral sediments in the Uinta Mountains. This high degree of overlap between the n -alkanes of C_3 plants has previously been observed in other ecosystems (Cooper et al., 2015).

This section therefore highlights two limitations associated with using relative abundances of n -alkanes, and $\delta^{13}\text{C}_{n\text{-alkane}}$ and $\delta^2\text{H}_{n\text{-alkane}}$, in source apportionment studies: (i) sources of OM to lake sediments produce different concentrations of n -alkanes, and so are not equally represented in the sediment record and (ii) values of $\delta^{13}\text{C}_{n\text{-alkane}}$ and $\delta^2\text{H}_{n\text{-alkane}}$ do not always differ substantially between groups, especially in alpine environments.

4.6 Unique characteristics of OM at high elevations

Previous studies have determined that the isotopic, molecular and elemental composition of probable OM sources to lakes differ in cold, alpine environments from more commonly studied warm, temperate environments (Körner et al., 1991; Luo et al., 2011; Polissar et al., 2009; Wei and Jia, 2009; Wu et al., 2017). Since there are many competing factors controlling $\delta^{13}\text{C}_{\text{TOC}}$, $\delta^{13}\text{C}_{n\text{-alkane}}$ and $\delta^2\text{H}_{n\text{-alkane}}$ (Diefendorf et al., 2008; Sachse et al., 2012), the effect of elevation on the $\delta^{13}\text{C}_{\text{TOC}}$, $\delta^{13}\text{C}_{n\text{-alkane}}$ and $\delta^2\text{H}_{n\text{-alkane}}$ measurements presented in this study cannot be isolated. It is possible, however, to compare measurements of TOC:TN and relative abundances of n -alkanes from the Uinta Mountains with those from predominately temperate, low-elevation sites. Compared to $\delta^{13}\text{C}_{\text{TOC}}$, $\delta^{13}\text{C}_{n\text{-alkane}}$, $\delta^2\text{H}_{n\text{-alkane}}$, these latter proxies are controlled by fewer factors and are easier to interpret.

These measurements of TOC:TN of algae and submerged macrophytes, for instance, are higher than expected based on previous studies. In most low-elevation, temperate lakes, a TOC:TN ≤ 10 reflects inputs of algae and submerged macrophytes; a TOC:TN between 11 and 19 reflects a mixture of terrestrial and aquatic inputs; and a TOC:TN ≥ 20 reflects predominately terrestrial inputs (Meyers and Ishiwatari, 1993). In the Uinta

Mountains, however, fresh algae and submerged macrophytes have a TOC:TN that ranges between 8 and 15 (Fig. 4.4). Such higher values can occur in nitrogen-stressed environments (Hillebrand and Sommer, 1999), which lower the protein content, and therefore increase the TOC:TN, of algae to > 10 (Talbot and Lærdal, 2000; Tossavainen et al., 2019). At times (particularly before AD 2015), the Uinta Mountain study lakes were nitrogen-limited or co-limited, supporting this idea (Table 4.2). This finding suggests that paleolimnologists studying nutrient-poor, alpine lakes should not assume that sediments with a TOC:TN between 10 and 15 are indicative of mixed inputs of terrestrial and aquatic OM. Rather, such values can reflect mostly aquatic inputs of OM.

The ACL of *n*-alkanes from Uinta Mountain plants are lower than the ACL reported in the literature for similar organisms. Measurements reported in this chapter demonstrate that coniferous krummholz trees produce *n*-alkanes with a mean ACL of ~25 (Fig. 4.8 (i)). Approximately 25 % of the *n*-alkanes produced by these trees consist of C₂₃, an alkane generally associated with submergent macrophytes and mosses (Ficken et al., 2000). Coniferous trees with a normal growth form are not normally high producers of C₂₃; rather, they produce *n*-alkanes with a mean ACL of ~29 (Bush and McInerney, 2013). Broadleaf shrubs and subshrubs growing in the Uinta Mountains also produce *n*-alkanes with a lower ACL than expected for terrestrial plants. These plants produce *n*-alkanes with a mean ACL of ~26. Most of the plants in this functional group consist of dwarf *Betula* and *Salix* species. Yet, the literature suggests that *Betula* sp. produce *n*-alkanes with a mean ACL of ~29 and *Salix* sp. at low-elevations produce mainly C₂₉ and C₃₁ *n*-alkanes (Yang and Huang, 2003). Plants growing at high elevations have been shown to produce *n*-alkanes with a lower ACL than plants growing at lower elevations, perhaps because shorter-chain *n*-alkanes offer plants an advantage in cooler climates (Guo et al., 2016). Longer chain lengths confer an advantage on plants growing in warmer climates because they help improve moisture retention (Shepherd and Griffiths, 2006). The mean ACL of Uinta Mountain sediments is ~26.5, which is comparable with the ACL of surficial sediment from other remote alpine lakes: 27.8 (Pu et al., 2017), ~28 (Zhang et al., 2020), ~27.5 (Pu et al., 2018), ~27 (Street et al., 2013).

Measurements of the CPI and absolute abundance of *n*-alkanes from the Uinta Mountain plants analyzed here correspond with previous studies (Fig. 4.8). A wide range of CPI was observed across the organisms sampled for this research, even though senesced tissue was avoided during sampling (Fig. 4.8 (iii)). With the exception of one sample of broadleaf deciduous shrubs, all samples had $CPI \geq 1$, supporting previous studies that such a value is indicative of fresh organic material (Marzi et al., 1993). The littoral sediments also had a CPI indicative of fresh organic material, which was surprising considering that the four study lakes have oxygenated hypolimnia throughout most of the year (Figure D.4. in Appendix D), and oxygen contributes to OM degradation (Lehmann et al., 2002). Previous studies of alpine lakes have also measured $CPI \geq 1$ in surficial sediments (Aichner et al., 2010; Pu et al., 2018, 2017; Zhang et al., 2020). This finding suggests that, at least in surficial sediments, *n*-alkane signatures in alpine lakes tend to be well-preserved. As reported in previous studies (Bush and McInerney, 2013; Zech et al., 2012), this research identified significantly fewer *n*-alkanes in coniferous krummholz trees relative to the other sources of OM. This finding could mean that their respective *n*-alkane distributions are underrepresented in the sediment record. Previous research also found that broadleaf deciduous shrubs produce the highest amount of *n*-alkanes (Bush and McInerney, 2013), which is also evident in the Uinta Mountains.

4.6.1 Investigating the ϵ_{bulk}^9 , $\epsilon_{\text{atm-}n\text{-alkane}}^{10}$ and $\epsilon_{\text{water}}^{11}$ of sources of OM to Uinta Mountain lakes

Although the data for *n*-alkanes from this study proved challenging to use for source apportionment, they remain useful for other applications. For instance, they can be used to improve estimates of ancient $\delta^{13}\text{C}_{\text{CO}_2}$ (Diefendorf and Freimuth, 2017). Using the estimates of $\epsilon_{\text{atm-C}_{23}}$ from coniferous krummholz trees, and the $\delta^{13}\text{C}_{\text{C}_{23}}$ of sediments from AD ~1400, it

⁹ ϵ_{bulk} is the fractionation between $\delta^{13}\text{C}_{n\text{-alkane}}$ and $\delta^{13}\text{C}$ of bulk plant tissue.

¹⁰ $\epsilon_{\text{atm-}n\text{-alkane}}$ is the fractionation between $\delta^{13}\text{C}_{\text{CO}_2}$ and $\delta^{13}\text{C}_{n\text{-alkane}}$.

¹¹ ϵ_{water} is the fractionation between $\delta^2\text{H}_{n\text{-alkane}}$ and $\delta^2\text{H}$ of source water.

was determined that the $\delta^{13}\text{C}_{\text{atm}}$ during AD ~ 1400 was -6.3 ± 0.4 ‰. This estimate overlaps with -6.4 ± 0.02 ‰, the commonly accepted $\delta^{13}\text{C}$ of pre-industrial CO_2 (Dombrosky, 2020). This brief test provides convincing evidence that the database of $\epsilon_{\text{atm-n-alkane}}$ presented in this chapter is useful for reconstructing $\delta^{13}\text{C}_{\text{CO}_2}$. Modern values of $\epsilon_{\text{atm-n-alkane}}$ are rare in the literature and are especially sparse for alpine environments.

This database of $\delta^{13}\text{C}_{n\text{-alkane}}$ measurements is also helpful for improving our understanding of the factors driving variation in $\epsilon_{\text{atm-n-alkane}}$ among different groups of potential OM sources. Since the plants sampled for this research grew in similar climates at similar elevations, one would expect any variation observed among groups to reflect phylogenetic differences. To test this idea, it was first ensured that there were not any systematic differences in ϵ_{bulk} of plants of the same species growing in different sites. To accomplish this task, the ϵ_{bulk} of broadleaf deciduous shrubs (*Salix* sp. and *Betula* sp.) sampled from East Carrol, Upper Carrol and Taylor lakes were compared (Figure D.9 in Appendix D). These samples were collected in the same month. This comparison revealed a high degree of overlap among the ϵ_{bulk} of shrubs from different sites, suggesting that environmental differences between sites are not an important control on ϵ_{bulk} in this system.

Next, it was investigated whether phylogenetic differences between groups could explain variations in ϵ_{bulk} . A phylogenetic tree showing the genetic similarities among the groups of OM sources is shown in Figure 4.10. After regrouping the OM sources into evolutionary lineages commonly examined in the literature (*i.e.*, lichen, mosses, angiosperms, gymnosperms, monocots and dicots), it was determined that the ϵ_{bulk} of gymnosperms is smaller than that of angiosperms, as also observed by Diefendorf et al. (2011) (Fig. 4.11 (ii)). It was also determined that the ϵ_{bulk} of dicotyledonous plants (dicots; flowering angiosperms) is smaller than the ϵ_{bulk} of monocotyledonous plants (monocots; non-flowering angiosperms), as previously noted by Eley et al. (2016) (Fig. 4.11 (iii)). Together, these findings seem to support a phylogenetic control on ϵ_{bulk} . It was also determined that the ϵ_{bulk} of lichen is distinct from all other groups (Fig. 4.11 (i)). This finding

is unsurprising considering lichen are not plants, and as such, are most distantly related to the other groups of terrestrial/semi-aquatic sources of OM (Fig. 4.10).

Based on these results, one might expect average ϵ_{bulk} to differ in accordance with the phylogenetic relationships shown in Figure 4.10. Yet, Figure 4.11 (i) shows that, aside from lichen, the ϵ_{bulk} of OM sources overlap. Moreover, the ϵ_{bulk} of mosses, which are nonvascular plants and evolved via a different evolutionary pathway than vascular plants, exhibit ϵ_{bulk} that overlap with the vascular plants. Since only one moss sample was analyzed, it is possible that this value is not representative of all mosses in the Uinta Mountains. It is also possible, however, that phylogenetic differences are not the most important control on ϵ_{bulk} in this system, or that this research has failed to account for differences in microclimate within sites. In summary, phylogenetic relationships were useful for explaining some, but not all, of the variation in ϵ_{bulk} in this system.

The ϵ_{water} of semi-emergent macrophytes, broadleaf deciduous shrubs, herbaceous perennials, mosses and lichen was also measured. One trend that emerges from these data is that broadleaf deciduous shrubs exhibit the smallest ϵ_{water} of the groups shown in Figure 4.11 (iv). A previous comparison of the ϵ_{water} of shrubs, trees, forbs, C₃ graminoids and C₄ graminoids also revealed that shrubs exhibited the smallest ϵ_{water} (Sachse et al., 2012). This could be a function of water use efficiency and/or a small biosynthetic fractionation factor associated with *n*-alkane synthesis (Diefendorf et al., 2015; Diefendorf and Freimuth, 2017). Plants with low water-use efficiencies tend to become enriched in ²H as ¹H is preferentially lost to the atmosphere during periods when stomata are open, resulting in a smaller fractionation between the $\delta^2\text{H}_{n\text{-alkane}}$ and $\delta^2\text{H}$ of source water (Sachse et al., 2012). The ϵ_{water} of the remaining sources of OM (semi-emergent macrophytes, lichen, mosses and herbaceous perennials) overlap for all chain lengths except for C₂₇. When considering C₂₇, the ϵ_{water} of semi-emergent macrophytes is larger than any of the other groups. Given that the error on this measurement is high relative to the other measurements, is also possible that this result is due to analytical error. Values of ϵ_{water} can be added to the $\delta^2\text{H}$ of sedimentary *n*-alkanes to calculate the $\delta^2\text{H}$ of paleowaters.

To demonstrate the utility of this dataset of ϵ_{water} , the $\delta^2\text{H}$ of past precipitation around the Uinta Mountain study lakes was estimated. This estimate focused on a sediment sample from the bottom of an undated core from Taylor Lake. Comparisons of this core with dated cores from Hundey et al. (2014) suggest that this sample was likely deposited AD ~ 1400 . I estimate that the $\delta^2\text{H}$ of precipitation at this time was $-139 \pm 10 \text{ ‰}$, which is slightly lower than -126 ‰ , the $\delta^2\text{H}$ of modern inflows to Uinta Mountain lakes. This preliminary finding suggests that climate in the Uinta Mountains may have been cooler in AD ~ 1400 compared to today (Dansgaard, 1964). It is also possible that the source of water vapour differed in the past relative to today (Dansgaard, 1964). A full reconstruction of the $\delta^2\text{H}$ of past precipitation for the Uinta Mountains will be generated in future studies.

4.7 Conclusion

The most important contribution of this study is its provision of a novel, modern baseline of TOC:TN, $\delta^{13}\text{C}_{\text{TOC}}$, $\delta^{15}\text{N}_{\text{TN}}$, $\delta^{13}\text{C}_{n\text{-alkane}}$, $\delta^2\text{H}_{n\text{-alkane}}$, ϵ_{bulk} , $\epsilon_{\text{atm-}n\text{-alkane}}$ and ϵ_{water} of potential OM sources in Uinta Mountain lake sediments. This baseline helps fill a current knowledge gap concerning the carbon, nitrogen and hydrogen isotope compositions of organisms growing in high-elevation sites. The study also explores the drivers of variation in proxy values among different groups of plants/algae and assesses the efficacy of these proxies for unique identification of the OM contained in high alpine lake sediments. Identifying OM sources in sediment is critical for the accurate interpretation of paleoenvironmental proxies. Without an understanding of OM source, it is unclear if proxies in the sediment are reflecting conditions inside or outside of the lake (Meyers, 1994).

The study has also demonstrated some strengths and several limitations associated with using these proxies for OM source identification in alpine areas. In the Uinta Mountains, TOC:TN and $\delta^{15}\text{N}_{\text{TN}}$ were more useful than $\delta^{13}\text{C}_{\text{TOC}}$ for differentiating among OM sources. Using a combination of TOC:TN, $\delta^{15}\text{N}_{\text{TN}}$ and $\delta^{13}\text{C}_{\text{TOC}}$, it was determined that algae and submerged macrophytes are currently the most important sources of OM to Uinta Mountain lake sediments. This finding is good news for isotope-based paleolimnological investigations that rely on aquatic OM.

An attempt was made to use relative abundances and isotopic compositions of *n*-alkanes to trace the OM sources contributing to littoral sediments. These results were inconclusive because of: (i) the unequal abundance of *n*-alkanes produced by different OM sources, and (ii) overlap in the $\delta^2\text{H}_{n\text{-alkane}}$ and $\delta^{13}\text{C}_{n\text{-alkane}}$ among different sources. These findings suggest that, in alpine regions dominated by C_3 plants, *n*-alkanes can be poor tracers of the sources of terrestrial and semi-aquatic OM delivered to lake sediments. They also suggest that paleolimnologists should avoid extracting cores from the littoral zone of the lake, unless one is seeking a mixed aquatic-terrestrial OM signal.

Nonetheless, the $\delta^{13}\text{C}_{n\text{-alkane}}$ and $\delta^2\text{H}_{n\text{-alkane}}$ were useful for several other applications in this system. It was possible, for instance, able to estimate the $\delta^{13}\text{C}_{\text{CO}_2}$ and $\delta^2\text{H}_{\text{precipitation}}$ in the Uinta Mountains around AD ~1400. These estimates of $\delta^{13}\text{C}_{\text{CO}_2}$ correspond with estimates of $\delta^{13}\text{C}_{\text{CO}_2}$ in previous studies, emphasizing the accuracy of this technique. The estimates of $\delta^2\text{H}_{\text{precipitation}}$ presented in this chapter show that $\delta^2\text{H}_{\text{precipitation}}$ was slightly lower around AD ~1400 than at present. This preliminary result suggests that temperatures around the study lakes might be warmer today than in the past, and/or that the predominant source of water vapour has changed (Dansgaard, 1964).

These measurements of $\delta^{13}\text{C}_{n\text{-alkane}}$ and $\delta^2\text{H}_{n\text{-alkane}}$ were also useful for calculating the ϵ_{bulk} and ϵ_{water} of different groups of terrestrial and semi-aquatic plants and algae from the Uinta Mountain lake localities. This dataset demonstrated that phylogenetic differences do not explain all of the variation in ϵ_{bulk} among groups of potential OM sources. This finding is important because it suggests that environmental factors may exert a greater influence on ϵ_{bulk} and, consequently, estimates of $\delta^{13}\text{C}_{\text{CO}_2}$ than previously thought. The measurements of ϵ_{water} presented in this chapter revealed substantial overlap among semi-emergent macrophytes, lichen, mosses and herbaceous perennials. Future research should be focused on improving our understanding of the factors controlling ϵ_{water} .

In summary, this study has provided a useful baseline of isotopic proxies in a remote, alpine setting. The work has also presented a few examples of how these proxies can be used to reconstruct paleoenvironmental change in such extreme environments.

4.8 References

- Aichner, B., Herzsuh, U., Wilkes, H., 2010. Influence of aquatic macrophytes on the stable carbon isotopic signatures of sedimentary organic matter in lakes on the Tibetan Plateau. *Org. Geochem.* 41, 706–718.
<https://doi.org/10.1016/j.orggeochem.2010.02.002>
- Ballesteros, E., Gacia, E., Camarero, L., 1989. Composition, distribution et biomasse des communautés de macrophytes benthiques d'un lac alpin des Pyrénées centrales: Le lac Baciver (Espagne). *Ann. Limnol.* 25, 177–184.
<https://doi.org/10.1051/limn/1989017>
- Batschelet, E., 1981. Circular statistics in biology, in: Sibson, R., Cohen, J.E. (Eds.) *Mathematics in Biology*. Academic Press, Cambridge, United States.
- Bergström, A.K., 2010. The use of TN:TP and DIN:TP ratios as indicators for phytoplankton nutrient limitation in oligotrophic lakes affected by N deposition. *Aquat. Sci.* 72, 277–281. <https://doi.org/10.1007/s00027-010-0132-0>
- Brahney, J., Ballantyne, A.P., Turner, B.L., Spaulding, S.A., Otu, M., Neff, J.C., 2014. Separating the influences of diagenesis, productivity and anthropogenic nitrogen deposition on sedimentary $\delta^{15}\text{N}$ variations. *Org. Geochem.* 75, 140–150.
<https://doi.org/10.1016/j.orggeochem.2014.07.003>
- Bray, E.E., Evans, E.D., 1961. Distribution of *n*-paraffins as a clue to recognition of source beds. *Geochim. Cosmochim. Acta* 22, 2–15.
[https://doi.org/10.1016/00167037\(61\)90069-2](https://doi.org/10.1016/00167037(61)90069-2)

- Bresson, C.C., Kowalski, A.S., Kremer, A., Delzon, S., 2009. Evidence of altitudinal increase in photosynthetic capacity: Gas exchange measurements at ambient and constant CO₂ partial pressures. *Ann. For. Sci.* 66, 505–505.
<https://doi.org/10.1051/forest/2009027>
- Broadmeadow, M.S.J., Griffiths, H., 1993. Carbon isotope discrimination and the coupling of CO₂ fluxes within forest canopies, in: *Stable Isotopes and Plant Carbon-Water Relations*. Elsevier Inc., Amsterdam, Netherlands, pp. 109–129.
<https://doi.org/10.1016/b978-008-091801-3.50015-5>
- Bush, R.T., McInerney, F.A., 2013. Leaf wax *n*-alkane distributions in and across modern plants: Implications for paleoecology and chemotaxonomy. *Geochim. Cosmochim. Acta* 117, 161–179. <https://doi.org/10.1016/j.gca.2013.04.016>
- Chevalier, N., Savoye, N., Dubois, S., Lama, M.L., David, V., Lecroart, P., Le Ménach, K., Budzinski, H., 2015. Precise indices based on *n*-alkane distribution for quantifying sources of sedimentary organic matter in coastal systems. *Org. Geochem.* 88, 69–77.
<https://doi.org/10.1016/j.orggeochem.2015.07.006>
- Chikaraishi, Y., Naraoka, H., 2007. $\delta^{13}\text{C}$ and δD relationships among three *n*-alkyl compound classes (*n*-alkanoic acid, *n*-alkane and *n*-alkanol) of terrestrial higher plants. *Org. Geochem.* 38, 198–215. <https://doi.org/10.1016/j.orggeochem.2006.10.003>
- Chikaraishi, Y., Naraoka, H., 2003. Compound-specific D–C analyses of *n*-alkanes extracted from terrestrial and aquatic plants. *Phytochemistry* 63, 361–371.
[https://doi.org/10.1016/S0031-9422\(02\)00749-5](https://doi.org/10.1016/S0031-9422(02)00749-5)
- Cline, J.D., Kaplan, I.R., 1975. Isotopic fractionation of dissolved nitrate during denitrification in the eastern tropical north Pacific Ocean. *Mar. Chem.* 3, 271–299. [https://doi.org/10.1016/0304-4203\(75\)90009-2](https://doi.org/10.1016/0304-4203(75)90009-2)

- Cloern, J.E., Canuel, E.A., Harris, D., 2002. Stable carbon and nitrogen isotope composition of aquatic and terrestrial plants of the San Francisco Bay estuarine system. *Limnol. Oceanogr.* 47, 713–729.
<https://doi.org/10.4319/lo.2002.47.3.0713>
- Cooper, R.J., Pedentchouk, N., Hiscock, K.M., Disdle, P., Krueger, T., Rawlins, B.G., 2015. Apportioning sources of organic matter in streambed sediments: An integrated molecular and compound-specific stable isotope approach. *Sci. Total Environ.* 520, 187–197. <https://doi.org/10.1016/j.scitotenv.2015.03.058>
- Coplen, T.B., 1994. Reporting of stable hydrogen, carbon, and oxygen isotopic abundances: (Technical Report). *Pure Appl. Chem.* 66, 273–276.
<https://doi.org/10.1351/pac199466020273>
- Dansgaard, W., 1964. Stable isotopes in precipitation. *Tellus* 16, 436–468.
<https://doi.org/10.3402/tellusa.v16i4.8993>
- Deines, P., 1980. The isotopic composition of reduced organic carbon, in: Fritz, P. (Ed.) *The Terrestrial Environment*, first ed. Elsevier Inc., Amsterdam, Netherlands, pp. 329–406. <https://doi.org/10.1016/b978-0-444-417800.50015-8>
- Delong, M.D., Thorp, J.H., 2006. Significance of instream autotrophs in trophic dynamics of the Upper Mississippi River. *Oecologia* 147, 76–85.
<https://doi.org/10.1007/s00442005-0241-y>
- Diefendorf, A.F., Freeman, K.H., Wing, S.L., Graham, H. V., 2011. Production of *n*-alkyl lipids in living plants and implications for the geologic past. *Geochim. Cosmochim. Acta* 75, 7472–7485. <https://doi.org/10.1016/j.gca.2011.09.028>
- Diefendorf, A.F., Freimuth, E.J., 2017. Extracting the most from terrestrial plant-derived *n* alkyl lipids and their carbon isotopes from the sedimentary record: A review. *Org. Geochem.* 103, 1–21. <https://doi.org/10.1016/j.orggeochem.2016.10.016>

- Diefendorf, A.F., Leslie, A.B., Wing, S.L., 2015. Leaf wax composition and carbon isotopes vary among major conifer groups. *Geochim. Cosmochim. Acta* 170, 145–156.
<https://doi.org/10.1016/j.gca.2015.08.018>
- Diefendorf, A.F., Mueller, K.E., Wing, S.L., Koch, P.L., Freeman, K.H., 2010. Global patterns in leaf ^{13}C discrimination and implications for studies of past and future climate. *Proc. Natl. Acad. Sci. U.S.A.* 107, 5738–5743.
<https://doi.org/10.1073/pnas.0910513107>
- Diefendorf, A.F., Patterson, W.P., Holmden, C., Mullins, H.T., 2008. Carbon isotopes of marl and lake sediment organic matter reflect terrestrial landscape change during the late Glacial and early Holocene (16,800 to 5,540 cal yr B.P.): A multiproxy study of lacustrine sediments at Lough Inchiquin, western Ireland. *J. Paleolimnol.* 39, 101–115. <https://doi.org/10.1007/s10933-007-9099-9>
- Dombrosky, J., 2020. A ~1000-year ^{13}C Suess correction model for the study of past ecosystems. *Holocene* 30, 474–478. <https://doi.org/10.1177/0959683619887416>
- Eley, Y., Dawson, L., Pedentchouk, N., 2016. Investigating the carbon isotope composition and leaf wax *n*-alkane concentration of C3 and C4 plants in Stiffkey saltmarsh, Norfolk, UK. *Org. Geochem.* 96, 28–42.
<https://doi.org/10.1016/j.orggeochem.2016.03.005>
- Epstein, S., Mayeda, T., 1953. Variation of O^{18} content of waters from natural sources. *Geochim. Cosmochim. Acta.* 4, 213–224.
[https://doi.org/10.1016/0016-7037\(53\)90051-9](https://doi.org/10.1016/0016-7037(53)90051-9)
- Farquhar, G.D., Lloyd, J., 1993. Carbon and oxygen isotope effects in the exchange of carbon dioxide between terrestrial plants and the atmosphere, in: Ehleringer, J.R., Hall, A.E., Farquhar, G.D. (Eds.), *Stable Isotopes and Plant-Carbon-Water Relations*, first ed. Elsevier Inc., Amsterdam, Netherlands, pp. 47–70.
<https://doi.org/10.1016/C2009-0-03312-1>

- Feakins, S.J., Peters, T., Wu, M.S., Shenkin, A., Salinas, N., Girardin, C.A.J., Bentley, L.P., Blonder, B., Enquist, B.J., Martin, R.E., Asner, G.P., Malhi, Y., 2016. Production of leaf wax *n*-alkanes across a tropical forest elevation transect. *Org. Geochem.* 100, 89–100. <https://doi.org/10.1016/j.orggeochem.2016.07.004>
- Ficken, K.J., Li, B., Swain, D.L., Eglinton, G., 2000. An *n*-alkane proxy for the sedimentary input of submerged/floating freshwater aquatic macrophytes. *Org. Geochem.* 31, 745–749. [https://doi.org/10.1016/S0146-6380\(00\)00081-4](https://doi.org/10.1016/S0146-6380(00)00081-4)
- Fogel, M.L., Cifuentes, L.A., 1993. Isotope fractionation during primary production, in: Eglinton, G., Murphy, M.T.J. (Eds.) *Organic Geochemistry*, first ed. Springer US, New York City, United States, pp. 73–94. https://doi.org/10.1007/978-1-4615-2890-6_3
- Gat, J.R., Bowser, C.J., Kendall, C., 1994. The contribution of evaporation from the Great Lakes to the continental atmosphere: estimate based on stable isotope data. *Geophys. Res. Lett.* 21, 557–560. <https://doi.org/10.1029/94GL00069>
- Glew, J.R., Smol, J.P., Last, W.M., 2002. Sediment Core Collection and Extrusion, in: Smol, J.P., Last, W.M. (Eds.), *Tracking Environmental Change Using Lake Sediments*. Springer, Dordrecht, pp. 73–105. https://doi.org/10.1007/0-30647669-x_5
- Guo, N., Gao, J., He, Y., Guo, Y., 2016. *Compositae* Plants Differed in Leaf Cuticular Waxes between High and Low Altitudes. *Chem. Biodivers.* 13, 710–718. <https://doi.org/10.1002/cbdv.201500208>
- Hedges, J.I., Cowie, G.L., Ertel, J.R., James Barbour, R., Hatcher, P.G., 1985. Degradation of carbohydrates and lignins in buried woods. *Geochim. Cosmochim. Acta* 49, 701–711. [https://doi.org/10.1016/0016-7037\(85\)90165-6](https://doi.org/10.1016/0016-7037(85)90165-6)

- Henderson, A.K., Shuman, B.N., 2009. Hydrogen and oxygen isotopic compositions of lake water in the western United States. *Bull. Geol. Soc. Am.* 121, 1179–1189. <https://doi.org/10.1130/B26441.1>
- Hillebrand, H., Sommer, U., 1999. The nutrient stoichiometry of benthic microalgal growth: Redfield proportions are optimal. *Limnol. Oceanogr.* 44, 440–446. <https://doi.org/10.4319/lo.1999.44.2.0440>
- Hobbie, E.A., Colpaert, J. V., 2003. Nitrogen availability and colonization by mycorrhizal fungi correlate with nitrogen isotope patterns in plants. *New Phytol.* 157, 115–126. <https://doi.org/10.1046/j.1469-8137.2003.00657.x>
- Hobbie, E.A., Ouimette, A.P., 2009. Controls of nitrogen isotope patterns in soil profiles. *Biogeochemistry*. <https://doi.org/10.1007/s10533-009-9328-6>
- Hollander, D.J., McKenzie, J.A., 1991. CO₂ control on carbon-isotope fractionation during aqueous photosynthesis: A paleo-*p*CO₂ barometer. *Geology* 19, 929–932. [https://doi.org/10.1130/0091-7613\(1991\)019<0929:CCOCIF>2.3.CO;2](https://doi.org/10.1130/0091-7613(1991)019<0929:CCOCIF>2.3.CO;2)
- Huiskes, A.H.L., Boschker, H.T.S., Lud, D., Moerdijk-Poortvliet, T.C.W., 2007. Stable isotope ratios as a tool for assessing changes in carbon and nutrient sources in Antarctic terrestrial ecosystems, in: *Plants and Climate Change*. Springer Netherlands, pp. 79–88. https://doi.org/10.1007/978-1-4020-4443-4_6
- Hundey, E.J., Moser, K.A., Longstaffe, F.J., Michelutti, N., Hladyniuk, R., 2014. Recent changes in production in oligotrophic Uinta Mountain lakes, Utah, identified using paleolimnology. *Limnol. Oceanogr.* 59, 1987–2001. <https://doi.org/10.4319/lo.2014.59.6.1987>
- Jackson, A.L., Inger, R., Parnell, A.C., Bearhop, S., 2011. Comparing isotopic niche widths among and within communities: SIBER - Stable Isotope Bayesian Ellipses in R. *J. Anim. Ecol.* 80, 595–602. <https://doi.org/10.1111/j.1365-2656.2011.01806.x>

- Jackson, A.L., Parnell, A., 2020. SIBER: Stable isotope Bayesian ellipses in R. R Project.
- Kielland, K., 1997. Role of free amino acids in the nitrogen economy of arctic cryptogams. *Ecoscience* 4, 75–79.
<https://doi.org/10.1080/11956860.1997.11682379>
- Körner, C., 2003. *Alpine Plant Life*, second ed. Springer-Verlag Berlin Heidelberg, Berlin.
<https://doi.org/10.1007/978-3-642-18970-8>
- Körner, C., Farquhar, G.D., Roksandic, Z., 1988. A global survey of carbon isotope discrimination in plants from high altitude. *Oecologia* 74, 623–632.
<https://doi.org/10.1007/BF00380063>
- Körner, C., Farquhar, G.D., Wong, S.C., 1991. Carbon isotope discrimination by plants follows latitudinal and altitudinal trends. *Oecologia* 88, 30–40.
<https://doi.org/10.1007/BF00328400>
- Lange, O.L., Green, T.G.A., Ziegler, H., 1988. Water status related photosynthesis and carbon isotope discrimination in species of the lichen genus *Pseudocyphellaria* with green or blue-green photobionts and in photosymbiodemes. *Oecologia* 75, 494–501. <https://doi.org/10.1007/BF00776410>
- LaZerte, B.D., Szalados, J.E., 1982. Stable carbon isotope ratio of submerged freshwater macrophytes. *Limnol. Oceanogr.* 27, 413–418.
<https://doi.org/10.4319/lo.1982.27.3.0413>
- Leavitt, S.W., Long, A., 1982. Evidence for $^{13}\text{C}/^{12}\text{C}$ fractionation between tree leaves and wood. *Nature* 298, 742–744. <https://doi.org/10.1038/298742a0>
- Lee, Y. Il, Lim, H.S., Yoon, H. Il, 2009. Carbon and nitrogen isotope composition of vegetation on King George Island, maritime Antarctic. *Polar Biol.* 32, 1607–1615.
<https://doi.org/10.1007/s00300-009-0659-5>

- Lehmann, M.F., Bernasconi, S.M., Barbieri, A., Mckenzie, J.A., 2002. Preservation of organic matter and alteration of its carbon and nitrogen isotope composition during simulated and *in situ* early sedimentary diagenesis. *Geochim. Cosmochim. Acta* 66, 3573–3584.
- Leonard, E., 2007. Modeled patterns of Late Pleistocene glacier inception and growth in the Southern and Central Rocky Mountains, USA: sensitivity to climate change and paleoclimatic implications. *Quat. Sci. Rev.* 26, 2152–2166.
<https://doi.org/10.1016/j.quascirev.2007.02.013>
- Luo, P., Peng, P., Gleixner, G., Zheng, Z., Pang, Z., Ding, Z., 2011. Empirical relationship between leaf wax *n*-alkane δD and altitude in the Wuyi, Shennongjia and Tianshan Mountains, China: Implications for paleoaltimetry. *Earth Planet. Sci. Lett.* 301, 285–296. <https://doi.org/10.1016/j.epsl.2010.11.012>
- MacDonald, G.M., Tingstad, A.H., 2007. Recent and multicentennial precipitation variability and drought occurrence in the Uinta Mountains region, Utah. *Arct. Antarct. Alp. Res.* 39, 549–555.
[https://doi.org/10.1657/1523-0430\(06-070\)\[MACDONALD\]2.0.CO;2](https://doi.org/10.1657/1523-0430(06-070)[MACDONALD]2.0.CO;2)
- Marzi, R., Torkelson, B.E., Olson, R.K., 1993. A revised carbon preference index. *Org. Geochem.* 20, 1303–1306. [https://doi.org/10.1016/0146-6380\(93\)90016-5](https://doi.org/10.1016/0146-6380(93)90016-5)
- Mead, R., Xu, Y., Chong, J., Jaffé, R., 2005. Sediment and soil organic matter source assessment as revealed by the molecular distribution and carbon isotopic composition of *n*-alkanes. *Org. Geochem.* 36, 363–370.
<https://doi.org/10.1016/j.orggeochem.2004.10.003>
- Meyers, P.A., 1994. Preservation of elemental and isotopic source identification of sedimentary organic matter. *Chem. Geol.* 114, 289–302.
[https://doi.org/10.1016/0009-2541\(94\)90059-0](https://doi.org/10.1016/0009-2541(94)90059-0)

- Meyers, P.A., 1990. Impacts of late Quaternary fluctuations in water level on the accumulation of sedimentary organic matter in Walker Lake, Nevada. *Palaeogeogr. Palaeoclimatol. Palaeoecol.* 78, 229–240.
[https://doi.org/10.1016/00310182\(90\)90216-T](https://doi.org/10.1016/00310182(90)90216-T)
- Meyers, P.A., Ishiwatari, R., 1993. Lacustrine organic geochemistry – an overview of indicators of organic matter sources and diagenesis in lake sediments. *Org. Geochem* 20, 867–900. [https://doi.org/10.1016/0146-6380\(93\)90100-P](https://doi.org/10.1016/0146-6380(93)90100-P)
- Michelsen, A., Quarmby, C., Sleep, D., Jonasson, S., 1998. Vascular plant ¹⁵N natural abundance in heath and forest tundra ecosystems is closely correlated with presence and type of mycorrhizal fungi in roots. *Oecologia* 115, 406–418.
<https://doi.org/10.1007/s004420050535>
- Molina, C.I., Gibon, F.M., Oberdorff, T., Dominguez, E., Pinto, J., Marín, R., Roulet, M., 2011. Macroinvertebrate food web structure in a floodplain lake of the Bolivian Amazon. *Hydrobiologia* 663, 135–153.
<https://doi.org/10.1007/s10750-010-0565-4>
- Munroe, J.S., 2003. Holocene timberline and palaeoclimate of the northern Uinta Mountains, northeastern Utah, USA. *Holocene* 13, 175–185.
<https://doi.org/10.1191/0959683603hl600rp>
- Munroe, J., 2007. Exploring relationships between watershed properties and Holocene loss on-ignition records in high-elevation lakes, southern Uinta Mountains, Utah, USA. *Arc. Antarct. Alp. Res.* 39, 556–565.
[https://doi.org/10.1657/1523-0430\(06-096\)\[MUNROE\]2.0.CO;2](https://doi.org/10.1657/1523-0430(06-096)[MUNROE]2.0.CO;2)
- Natelhoffer, K.J., Fry, B., 1988. Controls on natural nitrogen-15 and carbon-13 abundances in forest soil organic matter. *Soil Sci. Am. J.* 52, 1633–1640.
<https://doi.org/10.2136/sssaj1988.03615995005200060024x>

- Oksanen, J., 2013. Vegan: ecological diversity. R Project.
- Tu, N.T.T., Derenne, S., Largeau, C., Bardoux, G., Mariotti, A., 2004. Diagenesis effects on specific carbon isotope composition of plant *n*-alkanes. *Org. Geochem.* 35, 317–329. <https://doi.org/10.1016/j.orggeochem.2003.10.012>
- Parnell, A.C., Phillips, D.L., Bearhop, S., Semmens, B.X., Ward, E.J., Moore, J.W., Jackson, A.L., Grey, J., Kelly, D.J., Inger, R., 2013. Bayesian stable isotope mixing models. *Environmetrics* 24, 387–399. <https://doi.org/10.1002/env.2221>
- Parnell, A., Inger, R., 2020. Simmr: Stable isotope mixing models in R. R Project.
- Petersky, R.S., Shoemaker, K.T., Weisberg, P.J., Harpold, A.A., 2019. The sensitivity of snow ephemerality to warming climate across an arid to montane vegetation gradient. *Ecohydrology* 12, e2060. <https://doi.org/10.1002/eco.2060>
- Polissar, P.J., Freeman, K.H., Rowley, D.B., McInerney, F.A., Currie, B.S., 2009. Paleoaltimetry of the Tibetan Plateau from D/H ratios of lipid biomarkers. *Earth Planet. Sci. Lett.* 287, 64–76. <https://doi.org/10.1016/j.epsl.2009.07.037>
- Pu, Y., Jia, J., Cao, J., 2018. The aliphatic hydrocarbon distributions of terrestrial plants around an alpine lake: a pilot study from Lake Ximencuo, Eastern Qinghai-Tibet Plateau. *Front. Earth Sci.* 12, 600–610. <https://doi.org/10.1007/s11707-017-0685-5>
- Pu, Y., Wang, C., Meyers, P.A., 2017. Origins of biomarker aliphatic hydrocarbons in sediments of alpine Lake Ximencuo, China. *Palaeogeogr. Palaeoclimatol. Palaeoecol.* 475, 106–114. <https://doi.org/10.1016/J.PALAEO.2017.03.011>
- R Core Development Team, 2020. R: A Language and Environment for Statistical Computing.

- Rice, S.K., 2000. Variation in carbon isotope discrimination within and among Sphagnum species in a temperate wetland. *Oecologia* 123, 1–8.
<https://doi.org/10.1007/s004420050983>
- Rousk, K., Jones, D.L., DeLuca, T.H., 2014. Exposure to nitrogen does not eliminate N₂ fixation in the feather moss *Pleurozium schreberi* (Brid.) Mitt. *Plant Soil* 374, 513–521. <https://doi.org/10.1007/s11104-013-1908-5>
- Rundel, P.W., Stichler, W., Zander, R.H., Ziegler, H., 1979. Carbon and hydrogen isotope ratios of bryophytes from arid and humid regions. *Oecologia* 44, 91–94.
<https://doi.org/10.1007/BF00346404>
- Sachse, D., Billault, I., Bowen, G.J., Chikaraishi, Y., Dawson, T.E., Feakins, S.J., Freeman, K.H., Magill, C.R., McInerney, F.A., van der Meer, M.T.J., Polissar, P., Robins, R.J., Sachs, J.P., Schmidt, H.-L., Sessions, A.L., White, J.W.C., West, J.B., Kahmen, A., 2012. Molecular paleohydrology: Interpreting the hydrogen-isotopic composition of lipid biomarkers from photosynthesizing organisms. *Annu. Rev. Earth Planet. Sci.* 40, 221–249. <https://doi.org/10.1146/annurev-earth-042711105535>
- Sachse, D., Kahmen, A., Gleixner, G., 2009. Significant seasonal variation in the hydrogen isotopic composition of leaf-wax lipids for two deciduous tree ecosystems (*Fagus sylvatica* and *Acer pseudoplatanus*). *Org. Geochem.* 40, 732–742.
<https://doi.org/10.1016/j.orggeochem.2009.02.008>
- Schleser, G.H., 1992. $\delta^{13}\text{C}$ Pattern in a forest tree as an indicator of carbon transfer in trees. *Ecology* 73, 1922–1925. <https://doi.org/10.2307/1940045>
- Shepherd, T., Griffiths, D.W., 2006. The effects of stress on plant cuticular waxes. *New Phytol.* 171, 469–499. <https://doi.org/10.1111/j.1469-8137.2006.01826.x>

- Street, J.H., Anderson, R.S., Rosenbauer, R.J., Paytan, A., 2013. *n*-Alkane evidence for the onset of wetter conditions in the Sierra Nevada, California (USA) at the mid late Holocene transition, ~3.0ka. *Quat. Res. (United States)* 79, 14–23.
<https://doi.org/10.1016/j.yqres.2012.09.004>
- Syväranta, J., Lensu, A., Marjomäki, T.J., Oksanen, S., Jones, R.I., 2013. An empirical evaluation of the utility of convex hull and standard ellipse areas for assessing population niche widths from stable isotope data. *PLoS One* 8, e56094.
<https://doi.org/10.1371/journal.pone.0056094>
- Szpak, P., White, C.D., Longstaffe, F.J., Millaire, J.-F., Vásquez Sánchez, V.F., 2013. Carbon and nitrogen isotopic survey of northern Peruvian plants: Baselines for paleodietary and paleoecological studies. *PLoS One* 8, e53763.
<https://doi.org/10.1371/journal.pone.0053763>
- Talbot, M., 2001. Nitrogen isotopes in paleolimnology, in: Smol, J., Birks, H., Last, W. (Eds.), *Tracking Environmental Change Using Lake Sediments*, first ed. Springer Netherlands, pp. 401–439.
- Talbot, M.R., Lærdal, T., 2000. The Late Pleistocene - Holocene palaeolimnology of Lake Victoria, East Africa, based upon elemental and isotopic analyses of sedimentary OM. *J. Paleolimnol.* 23, 141–164. <https://doi.org/10.1023/A:1008029400463>
- Tenzer, G.E., Meyers, P.A., Knoop, P., 1997. Sources and distribution of organic and carbonate carbon in surface sediments of Pyramid Lake, Nevada. *J. Sediment. Res.* 67, 884–890.
<https://doi.org/10.1306/D4268667-2B26-11D78648000102C1865D>
- Toming, K., Tuvikene, L., Vilbaste, S., Agasild, H., Viik, M., Kisand, A., Feldmann, T., Martma, T., Jones, R.I., Nõges, T., 2013. Contributions of autochthonous and allochthonous sources to dissolved organic matter in a large, shallow, eutrophic lake

with a highly calcareous catchment. *Limnol. Oceanogr.* 58, 1259–1270.
<https://doi.org/10.4319/lo.2013.58.4.1259>

Tossavainen, M., Ilyass, U., Ollilainen, V., Valkonen, K., Ojala, A., Romantschuk, M., 2019. Influence of long-term nitrogen limitation on lipid, protein and pigment production of *Euglena gracilis* in photoheterotrophic cultures. *PeerJ* 7, e6624.
<https://doi.org/10.7717/peerj.6624>

Townsend-Small, A., McClain, M.E., Brandes, J.A., 2005. Contributions of carbon and nitrogen from the Andes Mountains to the Amazon River: Evidence from an elevational gradient of soils, plants, and river material. *Limnol. Oceanogr.* 50, 672–685. <https://doi.org/10.4319/lo.2005.50.2.0672>

Tozer, W.C., Hackell, D., Miers, D.B., Silvester, W.B., 2005. Extreme isotopic depletion of nitrogen in New Zealand lithophytes and epiphytes; the result of diffusive uptake of atmospheric ammonia? *Oecologia* 144, 628–635.
<https://doi.org/10.1007/s00442-005-0098-0>

Tu, T.T.N., Derenne, S., Largeau, C., Bardoux, G., Mariotti, A., 2004. Diagenesis effects on specific carbon isotope composition of plant *n*-alkanes. *Org. Geochem.* 35, 317–329.
<https://doi.org/10.1016/j.orggeochem.2003.10.012>

Turner, J., 1977. Effect of nitrogen availability on nitrogen cycling in a douglas-fir stand. *For. Sci.* 23, 307–316. <https://doi.org/10.1093/forestscience/23.3.307>

Verburg, P., 2007. The need to correct for the Suess effect in the application of $\delta^{13}\text{C}$ in sediment of autotrophic Lake Tanganyika, as a productivity proxy in the Anthropocene. *J. Paleolimnol.* 37, 591–602. <https://doi.org/10.1007/s10933-006-9056-z>

- Wang, Y., Wooller, M., 2006. The stable isotopic (C and N) composition of modern plants and lichens from northern Iceland: with ecological and paleoenvironmental implications. *Jökull* 56, 27–38.
- Wei, K., Jia, G., 2009. Soil *n*-alkane $\delta^{13}\text{C}$ along a mountain slope as an integrator of altitude effect on plant species $\delta^{13}\text{C}$. <https://doi.org/10.1029/2009GL038294>
- Wu, M.S., Feakins, S.J., Martin, R.E., Shenkin, A., Bentley, L.P., Blonder, B., Salinas, N., Asner, G.P., Malhi, Y., 2017. Altitude effect on leaf wax carbon isotopic composition in humid tropical forests. *Geochim. Cosmochim. Acta* 206, 1–17. <https://doi.org/10.1016/j.gca.2017.02.022>
- Yang, H., Huang, Y., 2003. Preservation of lipid hydrogen isotope ratios in Miocene lacustrine sediments and plant fossils at Clarkia, northern Idaho, USA. *Org. Geochem.* 34, 413–423. [https://doi.org/10.1016/S0146-6380\(02\)00212-7](https://doi.org/10.1016/S0146-6380(02)00212-7)
- Zech, M., Pedentchouk, N., Buggle, B., Leiber, K., Kalbitz, K., Marković, S.B., Glaser, B., 2011. Effect of leaf litter degradation and seasonality on D/H isotope ratios of *n*-alkane biomarkers. *Geochim. Cosmochim. Acta* 75, 4917–4928. <https://doi.org/10.1016/j.gca.2011.06.006>
- Zech, M., Rass, S., Buggle, B., Löscher, M., Zöller, L., 2012. Reconstruction of the late Quaternary paleoenvironments of the Nussloch loess paleosol sequence, Germany, using *n*-alkane biomarkers. *Quat. Res. (United States)* 78, 226–235. <https://doi.org/10.1016/j.yqres.2012.05.006>
- Zhang, Y., Yu, J., Su, Y., Du, Y., Liu, Z., 2020. A comparison of *n*-alkane contents in sediments of five lakes from contrasting environments. *Org. Geochem.* 139, 103943. <https://doi.org/10.1016/j.orggeochem.2019.103943>

Chapter 5

5 Strengths and limitations of stable isotopic proxies of environmental change from lake sediment archives

5.1 Introduction

This thesis has demonstrated the many applications of stable isotope proxies as indicators of paleoenvironmental change in lacustrine systems. Chapters 2 and 3 focused on a low-elevation, temperate lake. In Chapter 4, the focus of the thesis shifted to four remote, alpine lakes. In this chapter, findings from these two regions are compared to assess the strengths and limitations of stable isotope proxies of paleoenvironmental change in temperate and alpine environments. This comparison is vital because it will show whether proxies from alpine lakes can be interpreted similarly to proxies from low-elevation, temperate lakes.

Since there are no endogenic carbonates in the Uinta Mountain lakes, this chapter focuses on the carbon ($\delta^{13}\text{C}_{\text{TOC}}$) and nitrogen ($\delta^{15}\text{N}_{\text{TN}}$) isotope compositions of sediment organic matter (OM). These isotopes are commonly used to reconstruct variations in primary production (*e.g.*, Hladyniuk and Longstaffe, 2015; Hundey et al., 2014; Hyodo and Longstaffe, 2011; Meyers and Lallier-Vergès, 1999; Wolfe et al., 1996).

A comprehensive understanding of the long-term variations in primary production is a precursor for assessing whether a lake is growing more eutrophic due to human activities. While many proxies, such as sedimentary chlorophyll-*a* ($\text{Chl-}a_{(s)}$), can also be used to reconstruct variations in primary production (Michelutti et al., 2010), stable isotopes provide information about multiple aspects of paleoenvironmental change. In addition to reflecting variations in primary production, the $\delta^{13}\text{C}_{\text{TOC}}$ and $\delta^{15}\text{N}_{\text{TN}}$ of lake sediments are sensitive to other factors, including changes in the source of OM to lake sediments (Meyers,

1994; Meyers and Lallier-Vergès, 1999) and OM degradation (Gälman et al., 2009; Lehmann et al., 2002; Meyers and Ishiwatari, 1993).

The fact that stable isotope ratios record multiple in-lake processes makes them uniquely useful tools for paleoenvironmental research. Values of $\delta^{13}\text{C}_{\text{TOC}}$ and $\delta^{15}\text{N}_{\text{TN}}$ increase in response to rising primary production because photosynthetic organisms preferentially incorporate ^{12}C and ^{14}N , enriching the DIC- and DIN-pools in ^{13}C and ^{15}N , respectively (Hollander and McKenzie, 1991). A rise in $\delta^{15}\text{N}_{\text{TN}}$ could also, however, reflect inputs of organic fertilizer ($\delta^{15}\text{N} = +6$ to $+30$ ‰) and/or denitrification (Hornibrook et al., 2000; Meyers and Ishiwatari, 1993; Talbot, 2001). Increases in $\delta^{13}\text{C}_{\text{TOC}}$ could also result from a shift in OM inputs from plants utilizing carbon dioxide (CO_2) ($\delta^{13}\text{C}_{\text{TOC}} \approx -27$ ‰) to plants utilizing bicarbonate (HCO_3^-) ($\delta^{13}\text{C} \approx -20$ ‰) (Fogel and Cifuentes, 1993). In lakes with a pH of between 6 and 9.5 (*i.e.*, Barry Lake and the Uinta Mountain lakes), HCO_3^- is more readily available than CO_2 (Wetzel, 2001); however, CO_2 requires less energy to assimilate than HCO_3^- . It therefore only becomes advantageous for submerged macrophytes to take up HCO_3^- when concentrations of CO_2 are low (Fogel and Cifuentes, 1993).

The fact that these proxies are sensitive to so many factors, however, also makes them difficult to interpret. In order to accurately reconstruct variations in primary production, for instance, one must ensure that the sediment OM is well-preserved and correctly identify the source(s) of OM present in the sediment (Meyers, 1994; Meyers and Ishiwatari, 1993). Fulfilling these two criteria is complicated when working in extreme environments, such as alpine lakes. Under aerobic conditions, sediments are susceptible to oxidative degradation as well as degradation by aerobic heterotrophic bacteria (Meyers and Ishiwatari, 1993). Low-elevation, temperate lakes, by comparison, typically develop anoxic bottom water during the summer months, which can slow the rate of oxidative degradation (Lehmann et al., 2002). Under anaerobic conditions, one would expect degradation to result in a decrease in $\delta^{13}\text{C}_{\text{TOC}}$ and TOC:TN, and an increase in $\delta^{15}\text{N}_{\text{TN}}$, when interpreting the core from the past to the present (Table 5.1) (Gälman et al., 2009, 2008; Lehmann et al., 2002). Under aerobic conditions, degradation typically causes an increase in $\delta^{13}\text{C}_{\text{TOC}}$ and TOC:TN,

and no overall change to TOC:TN, towards the present (Gälman et al., 2009, 2008; Lehmann et al., 2002) (Table 5.1).

Table 5.1 A summary of how $\delta^{13}\text{C}_{\text{TOC}}$, $\delta^{15}\text{N}_{\text{TN}}$ and TOC:TN degrade under aerobic and anaerobic conditions. Degradation trends are typically described as a change in the original isotopic value of the sediment that occurs with age. This table also reports how this change manifests in a sediment core (e.g., an increase of $\delta^{13}\text{C}$ with sediment age looks like a decrease in $\delta^{13}\text{C}$ when the core is interpreted from the past/bottom to the present/top).

Proxy	Degradation under aerobic conditions	Source	Degradation under anaerobic conditions	Source
$\delta^{13}\text{C}_{\text{TOC}}$	Decrease by 1.6 ‰ with age; looks like an increase towards the present	Lehmann et al., 2002	Increase by 0.4– 1.5 ‰ with age; looks like a decrease towards the present	Gälman et al., 2009
$\delta^{15}\text{N}_{\text{TN}}$	Fluctuations but no overall change	Lehmann et al., 2002	Decrease by 3 ‰ with age; looks like an increase towards the present	Lehmann et al., 2002
TOC:TN	Decrease by 1– 2 with age; looks like an increase towards the present	Lehmann et al., 2002	Increase by 2; looks like a decrease towards the present	Gälman et al., 2008

Alpine lakes tend to be more well-oxygenated than lakes at lower elevations (Jacobsen and Dangles, 2017). Proxies derived from the sediment OM, such as $\delta^{13}\text{C}_{\text{TOC}}$ and $\delta^{15}\text{N}_{\text{TN}}$, are therefore less likely to be well-preserved in aerobic alpine waters than in anoxic, temperate waters (Lehmann et al., 2002). Moreover, alpine lakes tend to receive a greater proportion of their OM from terrestrial sources (Wolfe et al., 2003), meaning that the $\delta^{13}\text{C}_{\text{TOC}}$ and $\delta^{15}\text{N}_{\text{TN}}$ of their sediment reflects environmental conditions in the terrestrial environment rather than in-lake conditions. This can make reconstructing in-lake conditions challenging in alpine areas.

The purpose of this chapter is to compare the controls on $\delta^{13}\text{C}_{\text{TOC}}$ and $\delta^{15}\text{N}_{\text{TN}}$ of alpine and temperate lake sediments to advance our interpretive framework for these proxies. The first comparison focuses on the sources of OM supplied to sediments from alpine lakes in the Uinta Mountains (Utah, USA) versus Barry Lake, a low-elevation, temperate lake (Ontario, Canada). Next, the relative preservation of OM in the Uinta Mountain lakes versus Barry Lake is evaluated. Recent trends in primary production in the

Uinta Mountain lakes (Hundey et al., 2014) are then compared with those from Barry Lake. Gaining an understanding of how and when primary production changed in alpine lakes compared with temperate lakes is essential for assessing the ubiquity of anthropogenic impacts on freshwater systems.

5.2 Materials and methods

5.2.1 Study area

This study focuses on a group of alpine lakes in the Uinta Mountains, Utah (USA), and one temperate lake, Barry Lake, in Ontario (Canada) (Figs. 1.2 and 1.4 in Chapter 1). The four Uinta Mountain lakes were selected to maximize variation in depth and lake to catchment:area ratios, for reasons described in Chapter 4. Denise and East Carrol lakes are shallow (2.4 m and 5.5 m deep, respectively), while Taylor and East Carrol lakes are deeper (9.7 m and 13.8 m deep, respectively). Lake depth is important in determining a lake's mixing regime: in the Uinta Mountains, lakes with depths between 0- 6 m are continuously mixed, whereas lakes > 8 m are dimictic (Ngai, 2014). Denise and East Carrol lakes do not stratify and are permanently oxygenated. Taylor and Upper Carrol lakes have permanent inflows, while Denise and East Carrol lakes have intermittent inflows. The water columns of all four lakes are fully oxygenated throughout most of the year; however, Taylor and Upper Carrol lakes undergo thermal stratification and dysoxia in the summer months.

The dominant tree species at these sites is Engelmann spruce (*Picea engelmanni*), which adopts a krummholz formation at high altitudes, meaning that its growth is stunted by continual exposure to fierce, freezing winds. Other common species at these high elevation sites include the sedge *Carex aquatilis*; the prostrate shrubs *Betula glandulosa*, *Salix glauca* and *Salix plantifolia*; and various species of mosses and lichen.

Barry Lake (44°18'28"N, 77°55'17"W) is a kettle lake located in southeastern Ontario, Canada, 40 km north of Lake Ontario and 32 km east of Peterborough, Ontario. Barry Lake has a bowl-like bathymetry and is ~7.6 m deep at its centre. Barry Lake stratifies and develops an anoxic hypolimnion during the summer months. The lake has two

ephemeral inflows, likely derived from groundwater springs, and three ephemeral outflows. The area is characterized by hot, humid summers and cool, drier winters. The main water body is surrounded by wetland, and adjacent to the wetland is farmland. Floating (*e.g.*, *Nuphar* sp.), semi-emerged (*e.g.*, *Typha* sp.) and submerged (*e.g.*, *Chara* sp., *Potamogeton* sp.) macrophytes are abundant at Barry Lake.

5.2.2 Sample collection from the Uinta Mountain lakes

Samples of modern vegetation were collected from Taylor and Denise lakes in May 2014, July 2015 and September 2016. Samples from Upper Carrol and East Carrol lakes were collected in July 2015. The vegetation samples collected included: (i) algae; (ii) broadleaf deciduous shrubs; (iii) mosses; (iv) semi-emergent macrophytes; (v) coniferous krummholz trees; (vi) lichen; (vii) herbaceous perennials; (viii) submergent macrophytes, and (ix) graminoids (Fig. 4.1 in Chapter 4). For more information on these collections, see Chapter 4.

Collection of water samples from the four study lakes took place in July 2015. Precleaned polyethylene 1 L amber Nalgene bottles were filled to maximum capacity (to avoid headspace) from a depth of 0.5 m below the surface. Waters were then transferred to a cooler and were promptly refrigerated at 4 °C. Waters designated for isotopic analysis were left unfiltered and were stored in a 4 °C refrigerator at the University of Western Ontario. Samples designated for analysis of dissolved inorganic carbon (DIC) were filtered, frozen and sent to Chesapeake Biological Laboratory in Maryland for analysis. The Chesapeake Biological Laboratory Protocols are available from <http://nasl.cbl.umces.edu/>. For methods regarding the collection of surficial samples from the Uinta Mountain lakes and one core from Taylor Lake, see Chapter 4. Measurements of pH were made at each lake using an Insitu 9500 Multiparameter Probe Hydrolab. For more details regarding these measurements, see Table E.1 in Appendix E.

5.2.3 Sample collection from Barry Lake

Samples of modern vegetation were collected from Barry Lake in July 2017 and August 2018 following similar protocols used in the Uinta Mountains. Modern vegetation was gathered

opportunistically from around the perimeter of each lake, except when an area was not traversable. Abundant plant species were collected in greater quantities than scarce species to reflect the actual community composition around each lake. Species closer to the lake were collected in greater abundances because those species are more likely to enter the lake and influence the isotopic composition of OM contained in the lake sediment. These OM samples were divided into the following eight subgroups: (i) algae (*e.g.*, unknown species of green algae), (ii) floating macrophytes (*e.g.*, *Nuphar* sp.); (iii) submerged macrophytes (*e.g.*, *Chara* sp. and *Potamogeton* sp.); (iv) semi-emergent macrophytes (*e.g.*, *Typha* sp.), and (v) broadleaf deciduous plants (*e.g.*, *Salix* sp.) (Fig. 5.1). Four sediment cores (BL-G16-01, BL-G17-01, BL-G11-01 and BL-G11-02) were collected from the deepest part of Barry Lake using a Glew gravity corer (Glew et al., 2002). For more information about these cores, see Chapter 2. The pH of Barry Lake waters was characterized using a YSI Multisensor Probe. For more details, see Table E.1 in Appendix E.

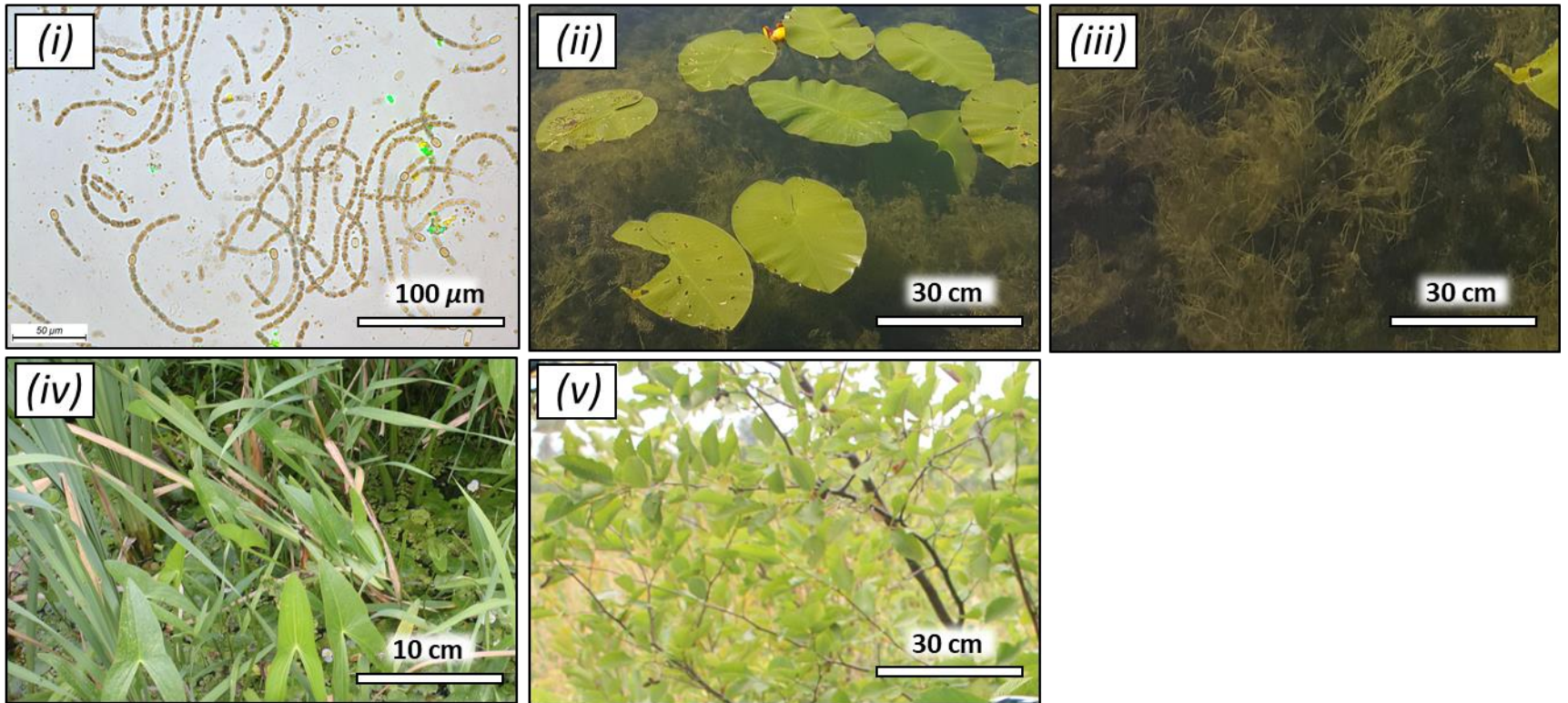


Figure 5.1 Photos of vegetation subgroups from Barry Lake: (i) algae (1000x magnification), (ii) floating macrophytes, (iii) submerged macrophytes, (iv) semi-emergent macrophytes, and (v) broadleaf deciduous plants.

5.2.4 Chronology of cores collected from Barry Lake

The ^{210}Pb and ^{137}Cs measurements were made at the LANSET Laboratory (Ottawa, Canada). A constant rate of supply (CRS) model was used to calculate the ^{210}Pb dates as it accounts for variations in sedimentation rates (Appleby and Oldfield, 1978). AMS dates were established at The A.E. Lalonde Laboratory (Ottawa, Canada). Age-depth models were generated using the “Bacon” package in R (Blaauw and Christeny, 2011), which uses Bayesian statistics, IntCal13 (Reimer et al., 2013) and the calibration curves for each date to calculate sediment accumulation rates based on a gamma autoregressive process (Blaauw and Christen, 2011). For more information, see Chapter 2.

5.2.5 Extraction, identification and quantification of *n*-alkanes in sediments of the Uinta Mountain lakes and Barry Lake

For methods regarding *n*-alkane extraction from sediments, see chapters 3 and 4.

5.2.6 Analyses of carbon and nitrogen isotope ratios of modern vegetation and sediment core BL-G17-01 from Barry Lake, and modern vegetation from the Uinta Mountains

For methods, and details on precision and accuracy, regarding the analyses of $\delta^{13}\text{C}_{\text{TOC}}$, $\delta^{15}\text{N}_{\text{TN}}$, %TOC and %TN of sediments from Barry Lake, and details on precision and accuracy, see chapters 2 and 3. For methods, and details on precision and accuracy, regarding the analyses of $\delta^{13}\text{C}_{\text{TOC}}$, $\delta^{15}\text{N}_{\text{TN}}$, %TOC and %TN of plants and sediments from the Uinta Mountains, and details on precision and accuracy, see Chapter 4.

The following methods pertain to the analysis of modern plants from Barry Lake, which have not been reported elsewhere in this thesis. The amounts of total organic carbon (%TOC) and total nitrogen (%TN) in OM sources were analyzed concurrently with $\delta^{13}\text{C}_{\text{TOC}}$ and $\delta^{15}\text{N}_{\text{TN}}$ at LSIS using a Costech Elemental Combustion system (EA) coupled to a Thermo ScientificTM Delta^{PLUS} XLTM isotope ratio mass spectrometer (IRMS) in continuous-flow (He)

mode (EA-IRMS). The %TOC and %TN data from these analyses were used to calculate elemental TOC:TN ratios (Meyers, 1994). Two standards, USGS 40 (accepted values: %TOC= 40.7 %; %TN= 9.52 %) and USGS 41a (accepted values: %TOC= 40.7 %; %TN= 9.52 %) were used to generate calibration curves for %TOC and %TN measurements. The internal standard keratin (MP Biomedicals Inc., Cat. No. 90211, Lot No. 9966H; average values: %TOC= 48.14 %; TN= 15.10 %) was used to evaluate precision and accuracy of carbon and nitrogen contents. The average %TOC and %TN of keratin was calculated by averaging over 1050 analyses of keratin at LSIS. The measured average value of 47.38 ± 2.14 % ($n= 114$) compares well with its accepted values for %TOC, and the measured average value of 14.85 ± 0.42 % ($n= 88$) compares well with its accepted values for %TN. Duplicates were analyzed every ~11 samples and had average reproducibilities of ± 1.05 % ($n= 35$ sample pairs) for %TOC and ± 0.04 % ($n= 34$ sample pairs) for %TN.

Values of $\delta^{13}\text{C}_{\text{TOC}}$ and $\delta^{15}\text{N}_{\text{TN}}$ were measured in separate analytical sessions to generate reliable amplitudes. The $\delta^{13}\text{C}_{\text{TOC}}$ and $\delta^{15}\text{N}_{\text{TN}}$ of plants were calibrated to VPDB and AIR using USGS 40 (accepted values: $\delta^{13}\text{C}_{\text{USGS 40}} = -26.39$ ‰; $\delta^{15}\text{N}_{\text{USGS 40}} = -4.52$ ‰) and USGS 41a (accepted values: $\delta^{13}\text{C}_{\text{USGS 41a}} = +36.55$ ‰; $\delta^{15}\text{N}_{\text{USGS 41a}} = +47.55$ ‰). In addition to USGS 40 and USGS 41a, internal standard keratin (MP Biomedicals Inc., Cat. No. 90211, Lot No. 9966H; $\delta^{13}\text{C}_{\text{keratin}} = -24.04$ ‰; $\delta^{15}\text{N}_{\text{keratin}} = +6.35$ ‰) was analyzed to monitor analytical accuracy and precision. The measured $\delta^{13}\text{C}$ of keratin was -24.06 ± 0.15 ‰ ($n= 115$) and $+6.39 \pm 0.12$ ‰ ($n= 89$) for $\delta^{15}\text{N}_{\text{keratin}}$, which compare well with expected values. Sample duplicates were analyzed approximately every 10 samples and yielded average reproducibilities of ± 0.07 ‰ ($n=35$ sample pairs) for $\delta^{13}\text{C}_{\text{TOC}}$ and ± 0.05 ‰ ($n=34$ sample pairs) for $\delta^{15}\text{N}_{\text{TN}}$.

5.2.7 Analysis of sedimentary chlorophyll *a* and its derivatives (Chl- $a_{(s)}$) in Barry Lake sediment core BL-G17-01

Sediments from BL-G17-01 were analyzed to determine the concentration of sedimentary chlorophyll *a* and its derivatives using visible reflectance spectroscopy (VWRS), as detailed in Michelutti et al. (2010). For more information regarding these analyses, see Chapter 2.

5.2.8 Data treatment and calculations

Standard Bayesian ellipses, generated using the R package SIBER (Jackson and Parnell, 2020; R Core Development Team, 2020), were used to evaluate overlap between different subgroups of vegetation (Jackson et al., 2011; Parnell et al., 2013). For more details on the creation of Bayesian ellipses, see Chapter 4. Only OM sources common to the Uinta Mountains and Barry Lake were included in this analysis. Although algae are present at both sites, too few algae samples were collected from Barry Lake to generate a Bayesian ellipse, and so algae from both sites were also omitted from the analyses in this chapter.

Groups of probable OM sources were also compared using frequentist (*i.e.*, non-Bayesian) statistical approaches. Groups were compared using nonparametric tests such as Kruskal-Wallis tests or, for pairwise comparison, pairwise Wilcoxon tests. Tests were considered significant when $p \leq 0.01$ (Table E.2 in Appendix E).

The odd-over-even predominance of *n*-alkanes was calculated using a modified Carbon Preference Index (CPI) (Bray and Evans, 1961). The equation for CPI is shown in Equation 1.8 in Chapter 1. Values of $CPI > 1$ are indicative of good OM preservation (Marzi et al., 1993)

5.3 Results

5.3.1 Dissolved inorganic carbon (DIC) concentrations in modern Uinta Mountain lake waters

The concentrations of DIC in Taylor Denise, Upper Carrol and East Carrol lake were as follows: 1.21 mg C/L, 1.22 mg C/L, 1.12 mg C/L and 1.48 mg C/L, respectively.

5.3.2 The CPI of *n*-alkanes extracted from surficial sediments from the Uinta Mountains lakes and Barry Lake

The CPI of *n*-alkanes extracted from surficial sediments in Taylor, Denise and East Carrol lakes is 5, 2 and 3, respectively. The CPI extracted from sediments at the bottom of one 30 cm gravity core from Taylor Lake was 3. The CPI of *n*-alkanes extracted from surficial sediments in Barry Lake is 9. The CPI of *n*-alkanes extracted from sediments at the bottom of core BL-G17-01 was 2.

5.3.3 Carbon and nitrogen isotope compositions, and elemental ratios, of modern vegetation around the Uinta Mountain lakes and Barry Lake

Only groups of OM source common at both sites were investigated. At the Uinta Mountain lakes, the broadleaf deciduous plant ellipse has a $\delta^{13}\text{C}_{\text{TOC}}$ that ranges from ~ -28 to -26 ‰ and a $\delta^{15}\text{N}_{\text{TN}}$ that ranges from -5 to -3 ‰ (Fig. 5.2 (i)). At Barry Lake, the broadleaf deciduous plant ellipse exhibits a $\delta^{13}\text{C}_{\text{TOC}}$ that ranges from ~ -30 to -29 ‰ and a $\delta^{15}\text{N}_{\text{TN}}$ that ranges from ~ -3 ‰ to $+3$ ‰ (Fig. 5.2 (ii)). At the Uinta Mountain lakes, the semi-emergent macrophyte ellipse exhibits a $\delta^{13}\text{C}_{\text{TOC}}$ that ranges from ~ -27 to -24 ‰ and a $\delta^{15}\text{N}_{\text{TN}}$ that ranges from -1 to $+3$ ‰. At Barry Lake, the semi-emergent macrophytes ellipse has a $\delta^{13}\text{C}_{\text{TOC}}$ that ranges from ~ -29 to -25 ‰ and a $\delta^{15}\text{N}_{\text{TN}}$ that ranges from ~ -4 to $+4$. At the Uinta Mountain lakes, the submerged macrophytes ellipse has a $\delta^{13}\text{C}_{\text{TOC}}$ that ranges from ~ -26 to -23 ‰ and a $\delta^{15}\text{N}_{\text{TN}}$ that ranges from ~ -1 to $+4$ ‰. At Barry Lake, the submerged macrophytes ellipse has a $\delta^{13}\text{C}_{\text{TOC}}$ that ranges from ~ -27 to -15 ‰ and a $\delta^{15}\text{N}_{\text{TN}}$ that ranges from ~ -4 to $+4$.

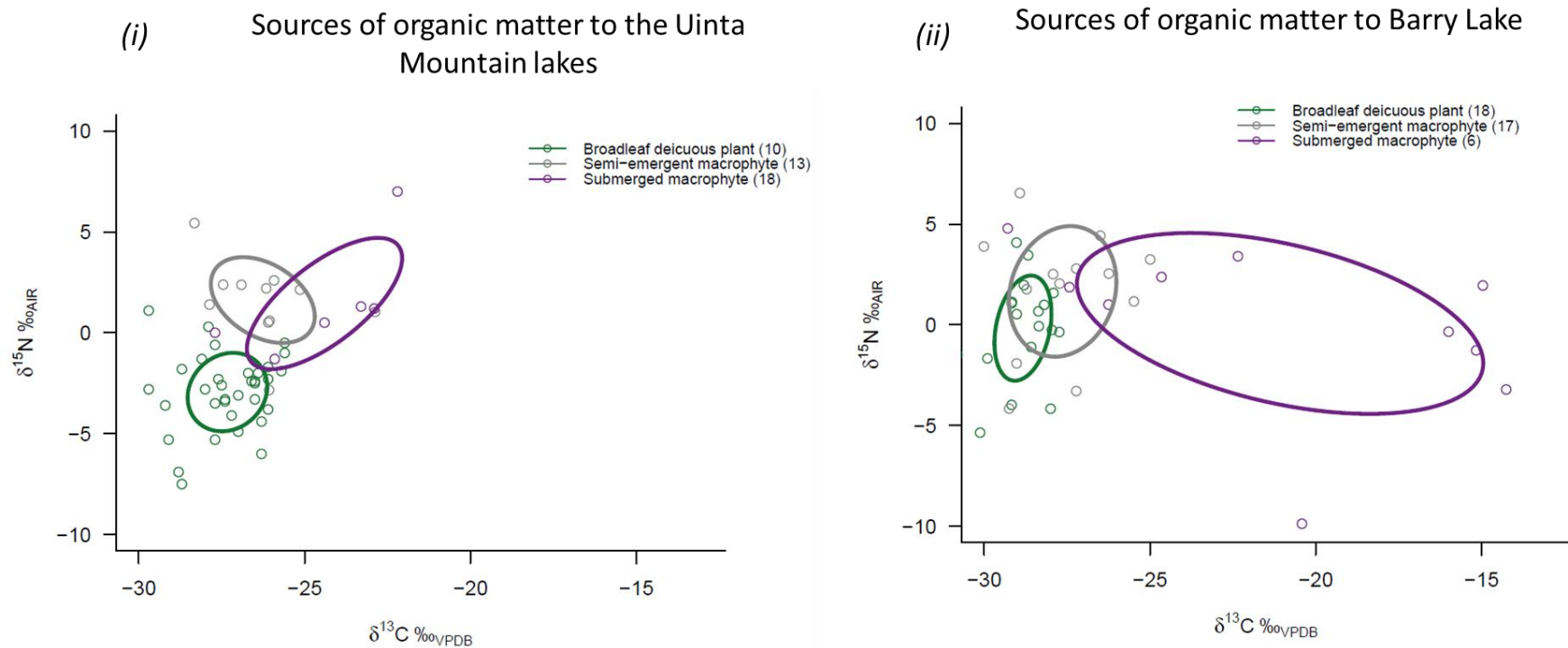


Figure 5.2 40 % standard predictive ellipses surrounding the $\delta^{15}\text{N}_{\text{TN}}$ and $\delta^{13}\text{C}_{\text{TOC}}$ of probable sources to (i) the Uinta Mountain lakes, and (ii) Barry Lake. Only groups of OM sources common to the two sites were included in these plots. Algae are found at both sites, but too few algae samples from Barry Lake were analyzed to include in this figure.

The $\delta^{13}\text{C}_{\text{TOC}}$ of semi-emergent macrophytes from the Uinta Mountains and Barry Lake are not significantly different (for p -values, see Table E.2 in Appendix E) as is also the case for $\delta^{15}\text{N}_{\text{TN}}$. The $\delta^{15}\text{N}_{\text{TN}}$ and $\delta^{13}\text{C}_{\text{TOC}}$ of submerged macrophytes from Barry Lake are not significantly different from the $\delta^{15}\text{N}_{\text{TN}}$ and $\delta^{13}\text{C}_{\text{TOC}}$ of submerged macrophytes from the Uinta Mountains. The $\delta^{13}\text{C}_{\text{TOC}}$ and $\delta^{15}\text{N}_{\text{TN}}$ of broadleaf deciduous shrubs growing in the Uinta Mountains, however, are significantly different than the $\delta^{13}\text{C}_{\text{TOC}}$ and $\delta^{15}\text{N}_{\text{TN}}$ of broadleaf deciduous plants growing at Barry Lake. In the Uinta Mountains and Barry Lake, submerged macrophytes exhibit a wider range of $\delta^{13}\text{C}_{\text{TOC}}$ than semi-emergent macrophytes and broadleaf deciduous shrubs.

5.3.4 Comparison of isotopic compositions, elemental ratios and Chl- $a_{(s)}$ -MAR of lake sediment records from Barry Lake to Uinta Mountains

At Barry Lake, Chl- $a_{(s)}$ -MAR remains relatively constant between 0 and 1 mg/m²/year from AD 1100–1850 (Fig. 5.3 (i)). From AD 1850–2017, it increases to 24 mg/m²/year.

Throughout the entire core, TOC:TN fluctuates between 8 and 12. From AD ~1100–1350, the $\delta^{13}\text{C}_{\text{TOC}}$ fluctuates between ~ -29.0 and -25.5 ‰ (Fig. 5.3 (i)). From AD ~1350–1600, the $\delta^{13}\text{C}_{\text{TOC}}$ remains constant. From AD ~1600–1950, the $\delta^{13}\text{C}_{\text{TOC}}$ decreases from ~ -25.5 to -31.0 ‰. From AD ~1950–2017, the $\delta^{13}\text{C}_{\text{TOC}}$ increases to ~ -29.5 ‰. From AD ~1100–1900, $\delta^{15}\text{N}_{\text{TN}}$ remains constant. From AD ~2000–2017, $\delta^{15}\text{N}_{\text{TN}}$ increases by ~4 ‰.

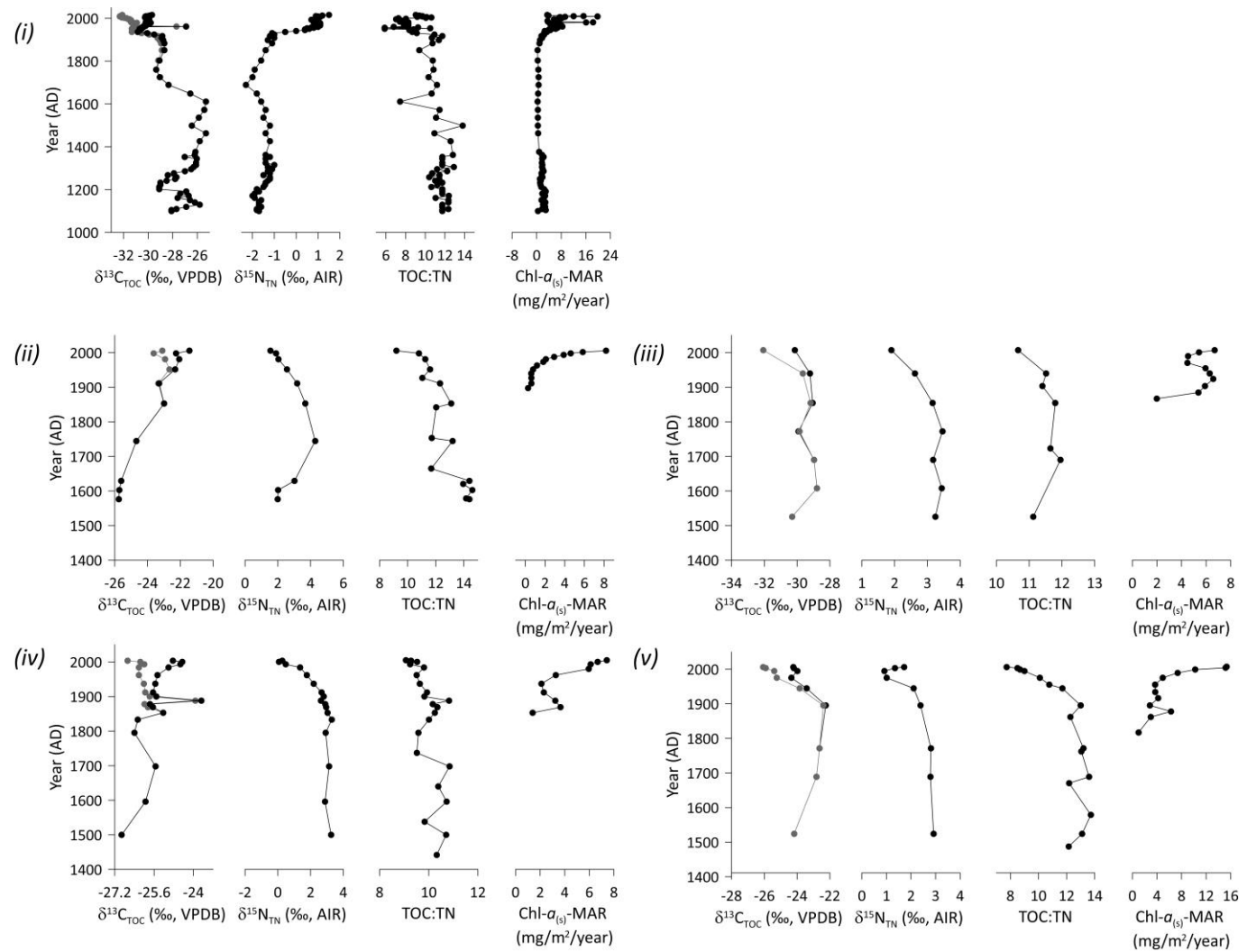


Figure 5.3 The $\delta^{13}\text{C}_{\text{TOC}}$, $\delta^{15}\text{N}_{\text{TN}}$, TOC:TN and Chl- $\alpha_{(s)}$ -MAR of sediment cores collected from (i) Barry Lake, (ii) Denise Lake, (iii) Upper Carrol Lake, (iv) Taylor Lake, and (v) East Carrol Lake. Data for plots (ii) to (v) is from Hundey et al. (2014). For plots of $\delta^{13}\text{C}_{\text{TOC}}$, grey lines represent uncorrected data while black lines represent data corrected for the Suess Effect (Verberg, 2007)

Among all the Uinta Mountain lakes, Chl- $a_{(s)}$ -MAR increases between AD 1900–2000, with the most rapid increases occurring after AD 1950 (Hundey et al., 2014). From AD 1900–2000, the Chl- $a_{(s)}$ -MAR of Denise Lake increases from ~ 0 to $9 \text{ mg/m}^2/\text{year}$ (Hundey et al., 2014) (Fig. 5.3 (ii)). The Chl- $a_{(s)}$ -MAR of Upper Carrol Lake increases from ~ 2 to $7 \text{ mg/m}^2/\text{year}$ (Fig. 5.3 (iii)). The Chl- $a_{(s)}$ -MAR of Taylor Lake increases from ~ 1 to $8 \text{ mg/m}^2/\text{year}$ (Fig. 5.3 (iv)). The Chl- $a_{(s)}$ -MAR of East Carrol Lake increases from ~ 0 to $16 \text{ mg/m}^2/\text{year}$ (Hundey et al., 2014) (Fig. 5.3 (v)). The TOC:TN of all lakes decrease throughout the entire record: the TOC:TN of Denise Lake decreases from ~ 15 to ~ 9 ; the TOC:TN of Upper Carrol lake decreases from ~ 11 to ~ 10.8 ; the TOC:TN of Taylor Lake decreases from ~ 11 to ~ 9 ; and the TOC:TN of East Carrol lake decreases from ~ 12 to ~ 7 (Hundey et al., 2014). The $\delta^{15}\text{N}_{\text{TN}}$ of all lakes decrease across the entire record: the $\delta^{15}\text{N}_{\text{TN}}$ of Denise Lake decreases from $\sim +2$ to $+1.6 \text{ ‰}$; the $\delta^{15}\text{N}_{\text{TN}}$ of Upper Carrol lake decreases from $\sim +3.2$ to $+2 \text{ ‰}$; the $\delta^{15}\text{N}_{\text{TN}}$ of Taylor Lake decreases from $\sim +3.2$ to 0 ‰ ; and the $\delta^{15}\text{N}_{\text{TN}}$ of East Carrol Lake decreases from $\sim +2.8$ to $+2 \text{ ‰}$. Between AD ~ 1550 –2000, $\delta^{13}\text{C}_{\text{TOC}}$ of Denise Lake increases from -26 ‰ to $\sim -21 \text{ ‰}$. The $\delta^{13}\text{C}_{\text{TOC}}$ of Upper Carrol lake fluctuates between -30.4 ‰ and -28.8 ‰ throughout the entire record. Between AD ~ 1500 –2000, $\delta^{13}\text{C}_{\text{TOC}}$ of Taylor Lake decreases from -27.2 ‰ to $\sim -24 \text{ ‰}$. The $\delta^{13}\text{C}_{\text{TOC}}$ of East Carrol Lake increases from AD 1500–1900 and then decreases from AD 1900–2000 (Hundey et al., 2014). The percentage of planktonic diatoms varies more closely with $\delta^{13}\text{C}_{\text{TOC}}$ at Denise and Taylor Lakes than at East Carrol or Upper Carrol lakes (Hundey et al., 2014).

5.4 Discussion

5.4.1 OM is well preserved in Barry Lake and in the Uinta Mountain lakes

Lack of alteration is a prerequisite for using $\delta^{13}\text{C}_{\text{TOC}}$ and $\delta^{15}\text{N}_{\text{TN}}$ in lacustrine sediments to reconstruct primary production. Since isotopic proxies tend to be better preserved in anoxic environments (Lehmann et al., 2002), one would expect to observe a higher degree of preservation in anoxic Barry Lake than in the Uinta Mountain lakes, which are usually aerobic (Fig. E.1 in Appendix E). These analyses revealed that the sediments from all lakes

have likely retained their original OM isotopic signatures. It is possible that the sediments from Barry Lake and the Uinta Mountain lakes have been altered somewhat by degradation; however, it is unlikely that such degradation completely overprinted the original isotopic signatures of sediments from these lakes.

Previous studies have identified variations in the $\delta^{13}\text{C}_{\text{TOC}}$, $\delta^{15}\text{N}_{\text{TN}}$ and TOC:TN that commonly appear in degrading sediment (Brahney et al., 2014; Gälman et al., 2009b, 2008; Lehmann et al., 2002) (Table 5.1). Unfortunately, identical variations can be caused by factors other than degradation, such as increasing primary production (Brahney et al., 2014) or inputs of dissolved inorganic nitrogen (DIN) from fertilizers (Hundey et al., 2014). To help distinguish variations caused by degradation versus primary production, one can examine variations in Chl- $a_{(s)}$ -MAR, an indicator of primary production. The measurements of Chl- $a_{(s)}$ -MAR discussed here take into account the degradation products of Chl- $a_{(s)}$ (Michelutti et al., 2010). Variations in Chl- $a_{(s)}$ -MAR are therefore not the result of degradation. The CPI of surficial sediments were also measured, which can provide additional information about OM preservation (Marzi et al., 1993).

Since the water column of Barry Lake is typically anoxic in the hypolimnion (Fig. E.1 in Appendix E), the OM of Barry Lake sediments is susceptible to degradation by anaerobic microbes such as methanogens (Borrel et al., 2011). Values of $\delta^{13}\text{C}_{\text{TOC}}$ fluctuate throughout the core but increase towards the top of the core, where one would expect anaerobic degradation to be most intense. This variation is inconsistent with degradation under anaerobic conditions. Values of $\delta^{15}\text{N}_{\text{TN}}$ are unchanging throughout the core and then increase towards the top of the core, while values of TOC:TN decrease towards the top of the core. These variations in $\delta^{15}\text{N}_{\text{TN}}$ and TOC:TN are indicative of degradation under anaerobic conditions. Yet, concurrent rises in Chl- $a_{(s)}$ -MAR with $\delta^{13}\text{C}_{\text{TOC}}$ and $\delta^{15}\text{N}_{\text{TN}}$ suggest that these increases might also reflect increasing primary production. Rising primary production also increases the amount of algae being delivered to the sediment, reducing TOC:TN (Meyers and Ishiwatari, 1993). CPI values of Barry Lake sediment suggest that recent and ~1000-year old sediments are well-preserved (CPI= 2– 9) (Chapter 3). Thus, while

degradation may be contributing to the trends in $\delta^{13}\text{C}_{\text{TOC}}$, $\delta^{15}\text{N}_{\text{TN}}$ and TOC:TN observed at Barry Lake, it is unlikely that the original isotopic compositions and elemental ratios of the sediment OM have been completely overprinted by degradation.

Degradation under aerobic conditions, which one would expect to occur in the Uinta Mountain lakes, typically leads to an increase in $\delta^{13}\text{C}_{\text{TOC}}$ and TOC:TN towards the present (Gälman et al., 2009, 2008; Lehmann et al., 2002). Trends in $\delta^{15}\text{N}_{\text{TN}}$ during aerobic degradation fluctuate but experience no net change. Upper Carrol and East Carrol lakes display none of these characteristic variations. Furthermore, the surficial sediments of East Carrol lakes had a CPI of 3, indicating good OM preservation. The CPI of surficial sediments of Upper Carrol lake were not measured. It is therefore likely that variations in $\delta^{13}\text{C}_{\text{TOC}}$, $\delta^{15}\text{N}_{\text{TN}}$ and TOC:TN in Upper Carrol and East Carrol lakes are reflecting real environmental variations rather than only reflecting OM degradation. This finding supports previous work by Brahney et al. (2014), which suggests that variations in $\delta^{13}\text{C}_{\text{TOC}}$, $\delta^{15}\text{N}_{\text{TN}}$ and TOC:TN of alpine lakes are preserved, even if sediments have undergone some OM degradation.

Taylor and Denise lakes exhibit one sign of degradation under aerobic conditions: increasing $\delta^{13}\text{C}_{\text{TOC}}$ towards the present. Trends in $\delta^{15}\text{N}_{\text{TN}}$ and TOC:TN at these lakes are not indicative of degradation. As in Barry Lake, increases in $\delta^{13}\text{C}_{\text{TOC}}$ at Taylor and Denise Lake can be explained as a response to increasing primary production in these lakes. As shown in Figure 5.3, Chl- $a_{(s)}$ -MAR, an indicator of primary production, is increasing in all four study lakes. While one would ordinarily expect $\delta^{15}\text{N}_{\text{TN}}$ to increase in response to primary production, here $\delta^{15}\text{N}_{\text{TN}}$ decreases towards the present due to inputs of nitrates (Hundey et al., 2016). The CPI at these lakes is 5 and 2, respectively, indicating that the OM of these lakes is well preserved at the surface (Marzi et al., 1993). CPI was also measured at the bottom of a core from Taylor Lake. At the bottom of this core, CPI was 3, suggesting that the sediments were well-preserved downcore. These measurements favour the interpretation that $\delta^{13}\text{C}_{\text{TOC}}$, $\delta^{15}\text{N}_{\text{TN}}$ and TOC:TN in Taylor and Denise lakes are reflecting changes in primary production and nitrate inputs rather than exclusively reflecting OM degradation under aerobic conditions.

One question remains: if primary production is increasing in Upper Carrol and East Carrol lakes, why is $\delta^{13}\text{C}_{\text{TOC}}$ in these lakes decreasing? It is possible that the $\delta^{13}\text{C}_{\text{TOC}}$ of sediments from these lakes are not increasing like in Denise and Taylor Lakes because ^{12}C -rich DIC is not limited in these systems (Hollander and McKenzie, 1991). This possibility is unlikely, however, because DIC concentrations in these lakes are so low (Table D.7 in Appendix D). One would therefore expect even modest amounts of primary production to cause ^{12}C -rich DIC to become limiting, as described in the next section. Another possibility is that the low $\delta^{13}\text{C}_{\text{TOC}}$ in Upper Carrol and East Carrol lakes reflects a change in algal community composition (Hundey et al., 2014). A shift from predominately benthic to planktonic algae could lower $\delta^{13}\text{C}_{\text{TOC}}$ because benthic algae tend to exhibit higher $\delta^{13}\text{C}_{\text{TOC}}$ than planktonic algae (France, 1995). This behaviour occurs because turbulent waters in the epilimnion disrupt the surface tension around planktonic algae, allowing them to more efficiently discriminate against ^{13}C (France, 1995). A comparison of the relative abundance of planktonic diatoms with $\delta^{13}\text{C}_{\text{TOC}}$ of the sediment demonstrates that lower values of $\delta^{13}\text{C}_{\text{TOC}}$ at Denise and Taylor lakes correspond with a higher relative abundance of planktonic diatoms (Hundey et al., 2014). This relationship, however, is weaker at East Carrol and Upper Carrol lakes. In summary, it remains unclear why the $\delta^{13}\text{C}_{\text{TOC}}$ of East Carrol and Upper Carrol lake are not increasing in the same way as Taylor and Denise lakes.

5.4.2 The $\delta^{13}\text{C}_{\text{TOC}}$ and $\delta^{15}\text{N}_{\text{TN}}$ of potential OM sources present in Uinta Mountain lakes and Barry Lake sediments are similar

The Uinta Mountain study lakes, and Barry Lake, receive most of their OM from autochthonous sources, suggesting that the $\delta^{13}\text{C}_{\text{TOC}}$ and $\delta^{15}\text{N}_{\text{TN}}$ of these sediments can be used to reconstruct in-lake conditions (Diefendorf et al., 2008; Kendall, 1998; Talbot, 2001). Downcore analyses of TOC:TN of the Uinta Mountain lakes by Hundey et al. (2014) show variations from 9 (minimum TOC) to 15 (maximum TOC) which, according to the baseline of OM sources established in Chapter 4, corresponds with the TOC:TN of autochthonous sources. In Chapter 3, it was established that, across the last ~600 years, Barry Lake sediments have derived most of their OM from planktonic algae.

A comparison of the $\delta^{13}\text{C}_{\text{TOC}}$ and $\delta^{15}\text{N}_{\text{TN}}$ of submerged macrophytes around the Uinta Mountain lakes and Barry Lake reveal interesting variations between the two sites that may be useful to future studies of source apportionment (Fig. 5.2). At Barry Lake, the wide range in $\delta^{13}\text{C}_{\text{TOC}}$ of submerged macrophytes suggests that some submerged macrophytes are taking up bicarbonate (HCO_3^-) instead of carbon dioxide (CO_2) (Fogel and Cifuentes, 1993). Species utilizing CO_2 exhibit a $\delta^{13}\text{C}_{\text{TOC}}$ that is typically ~ -27 ‰, while the $\delta^{13}\text{C}_{\text{TOC}}$ of species utilizing HCO_3^- is > -20 ‰ (Fogel and Cifuentes, 1993). These values correspond with the measured $\delta^{13}\text{C}_{\text{TOC}}$ of submerged macrophytes from Barry Lake.

It is well understood why some organisms take up CO_2 while others take up HCO_3^- . In lakes with a pH between 6 and 9, such as Barry Lake (Table E.1 in Appendix E), HCO_3^- is more abundant than CO_2 (Wetzel, 2001). During periods of intense primary production, CO_2 is removed from the DIC pool by photosynthesis and sedimentation (Fogel and Cifuentes, 1993; Maberly, 2008). If this process continues, it may become more beneficial for species to utilize the abundant yet energetically costly form of DIC, HCO_3^- , over the less abundant but energetically cheap form of DIC, CO_2 (Fogel and Cifuentes, 1993). Not all species, however, have evolved the protein necessary to utilize HCO_3^- (Yoshioka, 1997). It is therefore likely that the wide range in $\delta^{13}\text{C}_{\text{TOC}}$ of submerged macrophytes in Barry Lake is the result of some macrophytes utilizing CO_2 and others utilizing HCO_3^- .

In the Uinta Mountain lakes, most of the submerged macrophyte samples exhibited $\delta^{13}\text{C}_{\text{TOC}}$ higher than -27 ‰, the typical $\delta^{13}\text{C}_{\text{TOC}}$ of aquatic plants that take up CO_2 (Fogel and Cifuentes, 1993). This finding suggests that, in the Uinta Mountain lakes, submerged macrophytes assimilate some HCO_3^- . If some macrophytes are assimilating HCO_3^- , then concentrations of CO_2 must be very low (Barlett et al., 2006). How can this be, if primary production is low in the Uinta Mountains? Unlike Barry Lake, which is situated in carbonate bedrock and is DIC-rich, the Uinta Mountains are situated in insoluble quartzite bedrock so is DIC-poor (Table D.7 in Appendix D). Within this small DIC pool, concentrations of CO_2 are especially low because the pH of the Uinta Mountain lakes typically falls between 6 and 7 (Table E.2 in Appendix E), indicating that HCO_3^- is the dominant form of DIC (Wetzel, 2001).

Thus, even though primary production in the Uinta Mountains is less than at Barry Lake, CO₂ concentrations in the water column are likely smaller, so even modest amounts of primary production can favour HCO₃⁻ uptake by submerged macrophytes.

It was surprising that the $\delta^{13}\text{C}_{\text{TOC}}$ of semi-aquatic plants from the Uinta Mountains and Barry Lake are not significantly different (Table E.1, Appendix E) because previous studies have suggested that the $\delta^{13}\text{C}_{\text{TOC}}$ of terrestrial, semi-aquatic and fully aquatic organisms growing at high elevations is typically enriched in ¹³C relative to vegetation growing at lower elevations due to lower ambient partial pressures of CO₂ ($p\text{CO}_2$) (Körner et al., 1988; Liu et al., 2007). This phenomenon is debated, however, as many argue that alpine plants adapt to lower ambient CO₂ and therefore do not have higher $\delta^{13}\text{C}_{\text{TOC}}$ at high elevations (Farquhar et al., 1989; Seibt et al., 2008). The similar $\delta^{13}\text{C}_{\text{TOC}}$ of semi-aquatic plants from the Uinta Mountains compared with semi-aquatic plants from Barry Lake support the hypothesis that plants at high elevations adapt to lower $p\text{CO}_2$ and, as such, do not have unusually high $\delta^{13}\text{C}_{\text{TOC}}$.

Unlike the semi-aquatic plants, the $\delta^{13}\text{C}_{\text{TOC}}$ of broadleaf deciduous shrubs in the Uinta Mountains are significantly higher than the $\delta^{13}\text{C}_{\text{TOC}}$ of broadleaf deciduous plants at Barry Lake (Table E.1, Appendix E). This finding seems to support the assertion that plants at higher elevations have higher $\delta^{13}\text{C}_{\text{TOC}}$ than plants growing at lower elevations. Yet, this is unlikely because semi-emergent macrophytes in the Uinta Mountains and Barry Lake exhibit similar $\delta^{13}\text{C}_{\text{TOC}}$. Instead, higher $\delta^{13}\text{C}_{\text{TOC}}$ of broadleaf deciduous shrubs in the Uinta Mountains could be the result of (i) greater aridity in this environment (e.g., Hartman and Danin, 2010) and/or (ii) species- or genus-specific differences in the $\delta^{13}\text{C}_{\text{TOC}}$ of broadleaf deciduous shrubs growing in the Uinta Mountains and broadleaf deciduous plants growing around Barry Lake (e.g., Gebrekirstos et al., 2011).

Option (i) is a more likely explanation than option (ii) because the majority of plants sampled in both groups consist of *Salix* sp., and so it is unlikely that genetic differences in $\delta^{13}\text{C}_{\text{TOC}}$ are a strong driver of variation in this dataset. Relative humidity in the Uinta

Mountains typically varies between 35 and 75 % in the summer months but may drop to near 10 % on a clear day (Hayward, 1952). Relative humidity around Barry Lake, by comparison, typically ranges from 50 to 100 % in the summer (Environment and Climate Change Canada, 2020). Water stress causes terrestrial plants to close their stomata to conserve water, which reduces discrimination against ^{13}C and increases $\delta^{13}\text{C}_{\text{TOC}}$ of the plant (Lloyd and Farquhar, 1994). Since semi-aquatic plants live in the water for at least part of the year, it is unsurprising that they are less water stressed than the terrestrial plants. Thus, differences between the $\delta^{13}\text{C}_{\text{TOC}}$ of terrestrial plants in the Uinta Mountains and Barry Lake may be the result of higher aridity in the Uinta Mountains.

The $\delta^{15}\text{N}_{\text{TN}}$ of submergent macrophytes and semi-emergent macrophytes are not significantly different between the Uinta Mountains and Barry Lake (Table E.1, Appendix E). This result was surprising since one would expect the $\delta^{15}\text{N}$ of DIN in the Uinta Mountain lakes to be substantially lower than the $\delta^{15}\text{N}$ of DIN at Barry Lake. The Uinta Mountains are receiving inputs of atmospheric nitrates, which exhibit a $\delta^{15}\text{N}$ of ~ 0 ‰ (Hundey et al., 2016). Consequently, the dissolved inorganic nitrogen (DIN) of these lakes exhibit a low $\delta^{15}\text{N}_{\text{TN}}$ of $\sim +0$ to $+3$ ‰ (Hundey et al., 2016). Since Barry Lake is more productive than the Uinta Mountain lakes, has anoxic bottom waters that promote denitrification, and may be receiving inputs of organic fertilizers (chapters 2 and 3), one would expect the $\delta^{15}\text{N}$ of its DIN, and the $\delta^{15}\text{N}_{\text{TN}}$ of submergent macrophytes taking up this DIN, to be far higher (Talbot, 2001). It is unclear why submergent macrophytes from Barry Lake have a mean $\delta^{15}\text{N}_{\text{TN}}$ that is so similar to the Uinta Mountain lakes. One possible explanation is that, in recent years, farmers have switched from organic to inorganic fertilizers, or that Barry Lake is also being affected by the atmospheric deposition of nitrates. In theory, such a change could drive down the $\delta^{15}\text{N}_{\text{DIN}}$ of lake water but not yet appear in the sediment record. Another explanation is that many of the species sampled from Barry Lake are nitrogen fixers, which usually have a $\delta^{15}\text{N}_{\text{TN}}$ of ~ 0 ‰ (Talbot, 2001).

The $\delta^{15}\text{N}_{\text{TN}}$ of broadleaf deciduous shrubs from the Uinta Mountains is significantly different from the $\delta^{15}\text{N}_{\text{TN}}$ of broadleaf deciduous plants sampled at Barry Lake (Table E.1 in

Appendix E). The lower $\delta^{15}\text{N}_{\text{TN}}$ of terrestrial OM sources in the Uinta Mountains could be the result of many terrestrial species obtaining nitrogen through mycorrhizal associations (Hobbie and Colpaert, 2003). Such associations are particularly common in alpine areas (Körner, 2003). It is also possible that atmospheric deposition of nitrates have lowered the $\delta^{15}\text{N}_{\text{TN}}$ of soil nitrate, resulting in lower $\delta^{15}\text{N}_{\text{TN}}$ of plants utilizing that nitrate (Bourgeois et al., 2019).

5.4.3 Recent increases in primary production in the Uinta Mountain lakes and Barry Lake are not recorded by $\delta^{13}\text{C}_{\text{TOC}}$ or $\delta^{15}\text{N}_{\text{TN}}$

Rising $\text{Chl-}a_{(s)\text{-MAR}}$ at all sites suggests that the Uinta Mountain lakes and Barry Lake are experiencing an increase in primary production (chapters 2 and 3; Hundey et al., 2014). Given that these lacustrine sediments record in-lake conditions and are well-preserved, one would expect $\delta^{13}\text{C}_{\text{TOC}}$ and $\delta^{15}\text{N}_{\text{TN}}$ to increase at all sites in response to this rise in primary production (Hollander and McKenzie, 1991; Meyers and Ishiwatari, 1993). Yet, these trends are not observed at every site. In the Uinta Mountains, $\delta^{13}\text{C}_{\text{TOC}}$ increases in only two of the four study lakes, even though primary production increases at all four sites. Likewise, $\delta^{15}\text{N}_{\text{TN}}$ decreases at all four sites instead of increasing as expected giving the observed increases in primary production.

At Barry Lake, $\delta^{13}\text{C}_{\text{TOC}}$ and $\delta^{15}\text{N}_{\text{TN}}$ are also poor proxies of primary production. As described in Chapter 2, the $\delta^{13}\text{C}_{\text{TOC}}$ of sediment at Barry Lake records at least two variables: primary production and effective moisture. Of note is that the $\delta^{13}\text{C}_{\text{TOC}}$ of sediments from Barry Lake only records the large increase in primary production that is most intense after AD 1900 (Chapter 2). It does not record more subtle variations in primary production that occur before AD 1900 (Chapter 2). Instead, values of $\delta^{13}\text{C}_{\text{TOC}}$ are more strongly influenced by fluctuations in effective moisture (Chapter 2). Variations in $\delta^{15}\text{N}_{\text{TN}}$ from Barry Lake sediments correspond more closely with $\text{Chl-}a_{(s)\text{-MAR}}$ (Fig. 5.4 (v)). It is unclear, however, if this increase in $\delta^{15}\text{N}_{\text{TN}}$ after AD 1850 is the result of increased primary production (Hyodo and Longstaffe, 2011; Talbot, 2001), agricultural runoff (Lake et al., 2011), denitrification (Hornibrook et al., 2000; Talbot, 2001) or a combination of these factors.

In summary, while the $\delta^{13}\text{C}_{\text{TOC}}$ and $\delta^{15}\text{N}_{\text{TN}}$ of the sediment OM are at times sensitive to primary production, they are often influenced by other factors. The $\delta^{13}\text{C}_{\text{TOC}}$ and $\delta^{15}\text{N}_{\text{TN}}$ of lake sediments should therefore not be used as indicators of primary production except if other indicators of primary production, like Chl- $a_{(s)}$ -MAR or diatom assemblages, are also evaluated.

5.4.4 Are there anthropogenic drivers of recent increases in primary production in the Uinta Mountain lakes and Barry Lake?

Hundey et al. (2014) evaluated the history of primary production in the Uinta Mountain study lakes using Chl- $a_{(s)}$ -MAR and diatom assemblages. In Chapter 2, the history of primary production at Barry Lake was evaluated using several proxies, including the mass accumulation rates of sedimentary chlorophyll- a (Chl- $a_{(s)}$ -MAR). These reconstructions demonstrate that primary production increased in the Uinta Mountain lakes around AD ~1950 (Hundey et al., 2014) and in Barry Lake at AD ~1850. The timing of these increases in primary production in the Uinta Mountain lakes and Barry Lake suggests that human impacts are responsible for promoting the growth of algae and/or aquatic plants at these sites.

Hundey et al. (2016) demonstrated that recent increases in primary production in the Uinta Mountain lakes are the result of atmospheric fertilization from remote agricultural fields, which intensified around AD ~1950. The cause of recent increases in primary production in Barry Lake remain unclear but may also be related to nitrogen pollution from agricultural fields. Census records suggest that European agriculture began near Barry Lake at AD ~1850 (Stevenson, 2019), when Chl- $a_{(s)}$ began to increase. Previous studies have attributed sharp increases in primary production to the advent of European agriculture since European settlers manured their fields, and runoff containing manure can stimulate primary production (Cooper and Brush, 1993; Reinhardt et al., 2005). Inputs of manure could explain the rising $\delta^{15}\text{N}_{\text{TN}}$ at Barry Lake. Manure has a $\delta^{15}\text{N}_{\text{TN}}$ of +6 to +30 ‰ (Lake et al., 2011), and so even small inputs of organic fertilizer could drive the 4 ‰

increase in $\delta^{15}\text{N}_{\text{TN}}$ observed at Barry Lake. Yet, this increase could also be caused by other factors, as explained earlier.

At both sites it is unclear if anthropogenic climate warming (ACW) has contributed to these increases in primary production. In theory, alpine lakes such as the Uinta Mountain lakes should be more sensitive to climate warming than low-elevation lakes such as Barry Lake (Beniston, 2003). In alpine areas, warming can increase primary production by lengthening the growing season and ice-free season, enhancing nutrient cycling, changing thermal properties and increasing nutrients in the catchment (Rühland et al., 2008). Yet, variations in temperature from the area do not correspond with trends in $\text{Chl-}a_{(s)}$ measured in the Uinta Mountain study lakes (Hundey et al., 2014). This finding suggests that, if climate warming is increasing primary production in the Uinta Mountain study lakes, it is not the only factor driving this increase (Hundey et al., 2014). More recent research on subalpine lakes from the Uinta Mountains, however, shows stronger connections between primary production and ACW. Using breakpoint analysis, Sia et al. (2020) revealed similarities between the instrumental temperature record and increases in the $\text{Chl-}a_{(s)}$ content of subalpine lakes in the Uinta Mountains. It is therefore possible that increasing temperatures are influencing productivity of the Uinta Mountain study lakes.

It is similarly unclear if ACW contributed to rising primary production in Barry Lake. In Chapter 2, this possibility was investigated by comparing the instrumental record with trends in $\text{Chl-}a_{(s)}$ (Figs. 2.5 and 2.6 in Chapter 2). These comparisons revealed that, from AD 1900- 2017, mean June-July-August (JJA) temperatures and $\text{Chl-}a_{(s)}\text{-MAR}$ increased. Mean annual temperatures also increased with $\text{Chl-}a_{(s)}\text{-MAR}$ across this period. Yet, higher frequency variations in $\text{Chl-}a_{(s)}\text{-MAR}$ did not correspond with variations in annual temperature or JJA temperature, suggesting that rising temperatures are not the only factor driving increased primary production at Barry Lake. As in the Uinta Mountains, ACW is likely one of several factors responsible for the observed increase in primary production. Regardless of the exact driver of primary production at these sites, it is evident from these

comparisons that human impacts on lakes are ubiquitous, increasing the primary production of remote alpine lakes as well as low-elevation, temperate sites.

5.5 Conclusion

This chapter demonstrated that the $\delta^{13}\text{C}_{\text{TOC}}$ and $\delta^{15}\text{N}_{\text{TN}}$ of the sediment are sensitive to factors other than primary production. Caution should therefore be exercised when using these proxies to reconstruct primary production. This investigation also revealed important differences between alpine and temperate lakes that must be considered when interpreting $\delta^{13}\text{C}_{\text{TOC}}$ and $\delta^{15}\text{N}_{\text{TN}}$ of the sediment. It was observed that submerged macrophytes at Barry Lake exhibited a wider range of $\delta^{13}\text{C}_{\text{TOC}}$ than submerged macrophytes in the Uinta Mountains. However, substantial overlap occurred in the $\delta^{13}\text{C}_{\text{TOC}}$ and $\delta^{15}\text{N}_{\text{TN}}$ of various vegetation types that are potential OM sources for the Uinta Mountain lakes, as well as for Barry Lake. As such, it is equally challenging to utilize carbon and nitrogen isotopes to uniquely identify OM sources at both sites. Good OM preservation was observed in all five study lakes. One notable similarity between these two systems is that both are becoming more productive. The fact that the Uinta Mountain lakes and Barry Lake experienced unprecedented increases in primary production in the last ~150 years speaks to the ubiquity of human impacts on lakes.

5.6 References

Appleby, P.G., Oldfield, F., 1978. The calculation of lead-210 dates assuming a constant rate of supply of unsupported ^{210}Pb to the sediment. *Catena* 5, 1–8.

[https://doi.org/10.1016/S0341-8162\(78\)80002-2](https://doi.org/10.1016/S0341-8162(78)80002-2)

Bartlett, S., Mitra, M., Moroney, J., 2006. CO_2 concentrating mechanisms, in: Wise, R.R., Hooper, J.K. (Eds.) *The Structure and Function of Plastids*, first ed. Springer, Berlin, Germany, pp. 253–271.

Beniston, M., 2003. Climatic change in mountain regions: A review of possible impacts, in: Diaz, H.F. (Ed.). *Climate Variability and Change in High Elevation Regions: Past,*

Present and Future, first ed. Springer, Dordrecht, pp. 5–31.
https://doi.org/10.1007/978-94-015-1252-7_2

Blaauw, M., Christen, J.A., 2011. Flexible paleoclimate age-depth models using an autoregressive gamma process. *Bayesian Anal.* 6, 457–474
<https://doi.org/10.1214/11-BA618>

Borrel, G., Jézéquel, D., Biderre-Petit, C., Morel-Desrosiers, N., Morel, J.P., Peyret, P., Fonty, G., Lehours, A.C., 2011. Production and consumption of methane in freshwater lake ecosystems. *Res. Microbiol.* 162, 832–847.
<https://doi.org/10.1016/j.resmic.2011.06.004>

Bourgeois, I., Clément, J.C., Caillon, N., Savarino, J., 2019. Foliar uptake of atmospheric nitrate by two dominant subalpine plants: insights from in situ triple-isotope analysis. *New Phytol.* 223, 1784–1794. <https://doi.org/10.1111/nph.15761>

Brahney, J., Ballantyne, A.P., Turner, B.L., Spaulding, S.A., Otu, M., Neff, J.C., 2014. Separating the influences of diagenesis, productivity and anthropogenic nitrogen deposition on sedimentary $\delta^{15}\text{N}$ variations. *Org. Geochem.* 75, 140–150.
<https://doi.org/10.1016/j.orggeochem.2014.07.003>

Bray, E.E., Evans, E.D., 1961. Distribution of *n*-paraffins as a clue to recognition of source beds. *Geochim. Cosmochim. Acta* 22, 2–15. [https://doi.org/10.1016/0016-7037\(61\)90069-2](https://doi.org/10.1016/0016-7037(61)90069-2)

Cooper, S.R., Brush, G.S., 1993. A 2,500-year history of anoxia and eutrophication in Chesapeake Bay. *Estuaries* 16, 617–626. <https://doi.org/10.2307/1352799>

Diefendorf, A.F., Patterson, W.P., Holmden, C., Mullins, H.T., 2008. Carbon isotopes of marl and lake sediment OM reflect terrestrial landscape change during the late Glacial and early Holocene (16,800 to 5,540 cal yr B.P.): A multiproxy study of

lacustrine sediments at Lough Inchiquin, western Ireland. *J. Paleolimnol.* 39, 101–115. <https://doi.org/10.1007/s10933-007-9099-9>

Environment and Climate Change Canada, 2020. Relative Humidity - Annual data for Ontario [WWW Document]. URL https://peterborough.weatherstats.ca/charts/relative_humidity-hourly.html (accessed 5.6.20).

Farquhar, G.D., Ehleringer, J.R., Hubick, K.T., 1989. Carbon isotope discrimination and photosynthesis. *Annu. Rev. Plant Physiol. Plant Mol. Biol.* 40, 503–537. <https://doi.org/10.1146/annurev.pp.40.060189.002443>

Fogel, M.L., Cifuentes, L.A., 1993. Isotope fractionation during primary production, in: Eglinton, G., Murphy, M.T.J. (Eds.) *Organic Geochemistry*, first ed. Springer US, New York City, United States, pp. 73–94. https://doi.org/10.1007/978-1-4615-2890-6_3

France, R.L., 1995. Carbon-13 enrichment in benthic compared to planktonic algae: foodweb implications. *Mar. Ecol. Prog. Ser.* 124, 307–312. <https://doi.org/10.3354/meps124307>

Gälman, V., Rydberg, J., Bigler, C., 2009. Decadal diagenetic effects on $\delta^{13}\text{C}$ and $\delta^{15}\text{N}$ studied in varved lake sediment. *Limnol. Oceanogr.* 54, 917–924. <https://doi.org/10.4319/lo.2009.54.3.0917>

Gälman, V., Rydberg, J., De-Luna, S.S., Bindler, R., Renberg, I., 2008. Carbon and nitrogen loss rates during aging of lake sediment: Changes over 27 years studied in varved lake sediment. *Limnol. Oceanogr.* 53, 1076–1082. <https://doi.org/10.4319/lo.2008.53.3.1076>

Gebrekirstos, A., van Noordwijk, M., Neufeldt, H., Mitlöhner, R., 2011. Relationships of stable carbon isotopes, plant water potential and growth: An approach to asses

water use efficiency and growth strategies of dry land agroforestry species. *Trees Struct. Funct.* 25, 95–102. <https://doi.org/10.1007/s00468-010-0467-0>

Glew, J.R., Smol, J.P., Last, W.M., 2002. Sediment core collection and extrusion, in: Smol, J.P., Last, W.M. (Eds.), *Tracking Environmental Change Using Lake Sediments*. Springer, Dordrecht, pp. 73–105. https://doi.org/10.1007/0-30647669-x_5

Hartman, G., Danin, A., 2010. Isotopic values of plants in relation to water availability in the Eastern Mediterranean region. *Oecologia* 162, 837–852. <https://doi.org/10.1007/s00442-009-1514-7>

Hayward, C.L., 1952. Alpine biotic communities of the Uinta Mountains, Utah. *Ecol. Monogr.* 22, 93–120. <https://doi.org/10.2307/1943513>

Hladyniuk, R., Longstaffe, F.J., 2015. Paleoproductivity and organic matter sources in Late Quaternary Lake Ontario. *Palaeogeogr. Palaeoclimatol. Palaeoecol.* 435, 13–23. <https://doi.org/10.1016/j.palaeo.2015.05.026>

Hobbie, E.A., Colpaert, J. V., 2003. Nitrogen availability and colonization by mycorrhizal fungi correlate with nitrogen isotope patterns in plants. *New Phytol.* 157, 115–126. <https://doi.org/10.1046/j.1469-8137.2003.00657.x>

Hollander, D.J., McKenzie, J.A., 1991. CO₂ control on carbon-isotope fractionation during aqueous photosynthesis: A paleo-*p*CO₂ barometer. *Geology* 19, 929. [https://doi.org/10.1130/0091-7613\(1991\)019<0929:CCOCIF>2.3.CO;2](https://doi.org/10.1130/0091-7613(1991)019<0929:CCOCIF>2.3.CO;2)

Hornibrook, E.R.C., Longstaffe, F.J., Fyfe, W.S., 2000. Evolution of stable carbon isotope compositions for methane and carbon dioxide in freshwater wetlands and other anaerobic environments. *Geochim. Cosmochim. Acta* 64, 1013–1027. [https://doi.org/10.1016/S0016-7037\(99\)00321-X](https://doi.org/10.1016/S0016-7037(99)00321-X)

Hundey, E.J., Moser, K.A., Longstaffe, F.J., Michelutti, N., Hladyniuk, R., 2014. Recent changes in production in oligotrophic Uinta Mountain lakes, Utah, identified

using paleolimnology. *Limnol. Oceanogr.* 59, 1987–2001.
<https://doi.org/10.4319/lo.2014.59.6.1987>

Hundey, E.J., Russell, S.D., Longstaffe, F.J., Moser, K.A., 2016. Agriculture causes nitrate fertilization of remote alpine lakes. *Nat. Commun.* 7, 10571.
<https://doi.org/10.1038/ncomms10571>

Hyodo, A., Longstaffe, F.J., 2011. The palaeoproductivity of ancient Lake Superior. *Quat. Sci. Rev.* 30, 2988–3000. <https://doi.org/10.1016/j.quascirev.2011.07.004>

Jackson, A.L., Inger, R., Parnell, A.C., Bearhop, S., 2011. Comparing isotopic niche widths among and within communities: SIBER - Stable Isotope Bayesian Ellipses in R. *J. Anim. Ecol.* 80, 595–602. <https://doi.org/10.1111/j.1365-2656.2011.01806.x>

Jackson, A.L., Parnell, A., 2020. SIBER: Stable isotope Bayesian ellipses in R. R Project.

Jacobsen, D., Dangles, O., 2017. *Ecology of High Altitude Waters*, first ed. Oxford University Press, New York, NY.

Kendall, C., 1998. Tracing nitrogen sources and cycling in catchments, in: McDonnell, J.J., Kendall, C. (Eds.), *Isotope Tracers in Catchment Hydrology*, first ed. Elsevier Science, Philadelphia, United States, pp. 519–576.
<https://doi.org/10.1016/B978-0-444-81546-0.50023-9>

Körner, C., 2003. *Alpine Plant Life*, second ed. Springer-Verlag Berlin Heidelberg, Berlin, Germany. <https://doi.org/10.1007/978-3-642-18970-8>

Körner, C., Farquhar, G.D., Roksandic, Z., 1988. A global survey of carbon isotope discrimination in plants from high altitude. *Oecologia* 74, 623–632.
<https://doi.org/10.1007/BF00380063>

Lake, J.L., McKinney, R.A., Osterman, F.A., Pruett, R.J., Kiddon, J., Ryba, S.A., Libby, A.D., 2011. Stable nitrogen isotopes as indicators of anthropogenic activities in small

freshwater systems. *Can. J. Fish. Aquat. Sci.* 58, 870–878.
<https://doi.org/10.1139/f01-038>

Lehmann, Moritz F., Bernasconi, S.M., Barbieri, A., McKenzie, J.A., 2002. Preservation of organic matter and alteration of its carbon and nitrogen isotope composition during simulated and *in situ* early sedimentary diagenesis. *Geochim. Cosmochim. Acta* 66, 3573–3584. [https://doi.org/10.1016/S0016-7037\(02\)00968-7](https://doi.org/10.1016/S0016-7037(02)00968-7)

Liu, G., Li, M., An, L., 2007. The environmental significance of stable carbon isotope composition of modern plant leaves in the northern Tibetan Plateau, China. *Arct. Antarct. Alp. Res.* 39, 678–681.
[https://doi.org/10.1657/1523-0430\(07-505\)\[LIU-G\]2.0.CO;2](https://doi.org/10.1657/1523-0430(07-505)[LIU-G]2.0.CO;2)

Lloyd, J., Farquhar, G.D., 1994. ¹³C discrimination during CO₂ assimilation by the terrestrial biosphere. *Oecologia* 99, 201–215. <https://doi.org/10.1007/BF00627732>

Maberly, S.C., 2008. Diel, episodic and seasonal changes in pH and concentrations of inorganic carbon in a productive lake. *Freshw. Biol.* 35, 579–598.
<https://doi.org/10.1111/j.1365-2427.1996.tb01770.x>

Marzi, R., Torkelson, B.E., Olson, R.K., 1993. A revised carbon preference index. *Org. Geochem.* 20, 1303–1306. [https://doi.org/10.1016/0146-6380\(93\)90016-5](https://doi.org/10.1016/0146-6380(93)90016-5)

Meyers, P.A., 1994. Preservation of elemental and isotopic source identification of sedimentary organic matter. *Chem. Geol.* 114, 289–302.
[https://doi.org/10.1016/0009-2541\(94\)90059-0](https://doi.org/10.1016/0009-2541(94)90059-0)

Meyers, P.A., Ishiwatari, R., 1993. Lacustrine organic geochemistry: an overview of indicators of organic matter sources and diagenesis in lake sediments. *Org. Geochem* 20, 867–900. [https://doi.org/10.1016/0146-6380\(93\)90100-P](https://doi.org/10.1016/0146-6380(93)90100-P)

- Meyers, P.A., Lallier-Vergès, E., 1999. Lacustrine sedimentary organic matter records of Late Quaternary paleoclimates. *J. Paleolimnol.* 21, 345–372.
<https://doi.org/https://doi.org/10.1023/A:1008073732192>
- Michelutti, N., Blais, J.M., Cumming, B.F., Paterson, A.M., Rühland, K., Wolfe, A.P., Smol, J.P., 2010. Do spectrally inferred determinations of chlorophyll *a* reflect trends in lake trophic status? *J. Paleolimnol.* 43, 205–217.
<https://doi.org/10.1007/s10933-009-9325-8>
- Ngai, S., 2014. Potential Effects of Changing Climate on the Physical, Chemical, and Biological Characteristics of Alpine Lakes, Uinta Mountains, Utah, USA. The University of Western Ontario. Electronic Thesis and Dissertation Repository. 2521. <https://ir.lib.uwo.ca/etd/2521>
- Parnell, A.C., Phillips, D.L., Bearhop, S., Semmens, B.X., Ward, E.J., Moore, J.W., Jackson, A.L., Grey, J., Kelly, D.J., Inger, R., 2013. Bayesian stable isotope mixing models. *Environmetrics* 24, 387–399. <https://doi.org/10.1002/env.2221>
- Reimer, P.J., Bard, E., Bayliss, A., Beck, J.W., Blackwell, P.G., Ramsey, C.B., Buck, C.E., Cheng, H., Edwards, R.L., Friedrich, M., Grootes, P.M., Guilderson, T.P., Hafliðason, H., Hajdas, I., Hatté, C., Heaton, T.J., Hoffmann, D.L., Hogg, A.G., Hughen, K.A., Kaiser, K.F., Kromer, B., Manning, S.W., Niu, M., Reimer, R.W., Richards, D.A., Scott, E.M., Southon, J.R., Staff, R.A., Turney, C.S.M., van der Plicht, J., 2013. IntCal13 and Marine13 Radiocarbon Age Calibration Curves 0 50,000 Years cal BP. *Radiocarbon* 55, 1869–1887.
https://doi.org/10.2458/azu_js_rc.55.16947
- Reinhardt, E.G., Little, M., Donato, S., Findlay, D., Krueger, A., Clark, C., Boyce, J., 2005. Arcellacean (thecamoebian) evidence of land-use change and eutrophication in Frenchman’s Bay, Pickering, Ontario. *Environ. Geol.* 47, 729–739.
<https://doi.org/10.1007/s00254-004-1213-y>

- Rühland, K., Paterson, A.M., Smol, J.P., 2008. Hemispheric-scale patterns of climate related shifts in planktonic diatoms from North American and European lakes. *Glob. Chang. Biol.* 14, 2740–2754.
<https://doi.org/10.1111/j.13652486.2008.01670.x>
- Seibt, U., Rajabi, A., Griffiths, H., Berry, J.A., 2008. Carbon isotopes and water use efficiency: Sense and sensitivity. *Oecologia.* 155, 441.
<https://doi.org/10.1007/s00442-0070932-7>
- Sia, M.E., Doyle, R.M., Moser, K.A., 2020. Recent trends in mountain algal production: evaluating the response to fish stocking relative to regional environmental stressors. *Lake Reserv. Manag.* 36, In press. 10.1080/10402381.2020.1814462
- Stevenson, M., 2019. Upper Canada (Ontario) Land Registry Records Research [WWW Document]. Ontario Genealogy. URL
<https://www.ontariogenealogy.com/canadacensusrecords/uppercanadaontarioensusrecords1851/northumberlandcountypioneersettlers/percytownship1851agriculturalcensus.pdf> (accessed 4.14.19).
- Talbot, M., 2001. Nitrogen isotopes in paleolimnology, in: Smol, J., Birks, H., Last, W. (Eds.), *Tracking Environmental Change Using Lake Sediments*, first ed. Springer Netherlands, pp. 401–439.
- Wetzel, R., 2001. *Limnology: Lake and River Ecosystems*, third ed. Academic Press, San Diego, United States.
- Wolfe, A.P., Van Gorp, A.C., Baron, J.S., 2003. Recent ecological and biogeochemical changes in alpine lakes of Rocky Mountain National Park (Colorado, USA): a response to anthropogenic nitrogen deposition. *Geobiology* 1, 153–168.
- Wolfe, B.B., Edwards, T.W.D., Aravena, R., MacDonald, G.M., 1996. Rapid Holocene hydrologic change along boreal treeline revealed by $\delta^{13}\text{C}$ and $\delta^{18}\text{O}$ in organic lake

sediments, Northwest Territories, Canada. *J. Paleolimnol.* 15, 171–181.
<https://doi.org/10.1007/bf00196779>

Yoshioka, T., 1997. Phytoplanktonic carbon isotope fractionation: equations accounting for CO₂-concentrating mechanisms. *J. Plankton Res.* 19, 1455–1476.
<https://doi.org/DOI 10.1093/plankt/19.10.1455>

6 Conclusion

This research focused on investigating the isotope systematics of one warm, low-elevation temperate lake (Barry Lake, Ontario, Canada) and four cold, high-elevation alpine lakes (Uinta Mountains, Utah, United States). At Barry Lake, several aspects of the lake's carbon cycle were reconstructed across the last millennium (Chapters 2 and 3). This investigation allowed us to showcase the strengths of stable isotope science as a tool in paleolimnology, and to contextualize recent changes in the carbon dynamics of Barry Lake against a backdrop of environmental variation. In the Uinta Mountains, modern baselines of the carbon and nitrogen isotope systematics, and *n*-alkane characteristics, of potential sources of OM in lake sediments were established (Chapter 4). This investigation established the foundations for future isotopic studies in this region and offered important insights into how the interpretation of isotopic proxies differs between commonly studied, low-elevation lakes and understudied remote, alpine lakes (Chapter 5). This concluding chapter will focus on summarizing the key findings of chapters 2-5 and identifying the overall contributions of this thesis to the fields of paleolimnology and stable isotope science. Suggestions for future work are also presented at the end of this chapter.

6.1 Key findings of this thesis

6.1.1 Carbon dynamics at Barry Lake today are unique in the last ~1000 years

In chapters 2 and 3, the carbon dynamics of Barry Lake were explored. The findings of this research show that the carbon dynamics of Barry Lake differ in the modern (AD 1850–2017) period from the Medieval Climate Anomaly (MCA) (AD 1000– 1350) and the Little Ice Age (LIA) (AD 1450– 1850). Primary production and carbon burial are significantly higher in the modern period than during the MCA and LIA (Chapter 2). The lake also receives more of its OM from autochthonous sources in the modern period than during the MCA or LIA (Chapter 3). I speculate that the high levels of carbon sequestration in modern Barry Lake mean that it is a carbon dioxide (CO₂) sink. This is similar to other lakes that have undergone increases

in primary production and carbon sequestration in the modern period. While modern Barry Lake is not eutrophic, further increases in primary production could threaten the health of the lake. Excessive algae growth can lead to fish kills, increased toxicity, foul odors and decreased biodiversity. Care should therefore be taken to limit primary production in Barry Lake and other small sinkhole lakes in southern Ontario. Small lakes often receive little attention compared to larger lakes like the Great Lakes; however, the species richness of small lakes exceeds that of large lakes by up to six orders of magnitude (Downing et al., 2006). Small lakes also contain higher densities of fish, and produce more methane per lake area, than large lakes (Downing et al., 2006). Given the outsized importance of small lakes as habitat and greenhouse gas emitters, it is critical that human impacts on these lakes are minimized.

6.1.2 Human impacts contribute to recent changes to the carbon cycle at Barry Lake and in the Uinta Mountains

The fact that the Uinta Mountain lakes and Barry Lake have experienced similar increases in primary production, despite being in entirely different environments, emphasizes the ubiquity of human impacts on lacustrine systems. The investigations in chapters 2 and 3 revealed that Barry Lake is experiencing increases in primary production similar to those observed in the Uinta Mountains. Primary production is increasing in the Uinta Mountain lakes due to nitrate fertilization (Hundey et al., 2016). Although one recent study suggested that anthropogenic climate warming (ACW) might be increasing the primary production of subalpine lakes in the Uinta Mountains (Sia et al., 2020), Hundey et al. (2014) determined that ACW was not the initial driver of increased primary production in alpine lakes in this region (Hundey et al., 2014). At Barry Lake it was also determined that recent increases in primary production were more likely the result of fertilizer inputs and/or land use changes than ACW or changes in effective moisture (Chapter 2).

6.1.3 Methane oxidation in Barry Lake is closely associated with changes in dissolved oxygen and temperature that co-occur with effective moisture

While MOB abundances were insensitive to increases in carbon sequestration and increased inputs of autochthonous OM sources, they were closely associated with changes in effective moisture. Of interest is that MOB abundances increased during periods of low effective moisture, which is opposite to what one would expect in light of previous research (Borrel et al., 2011). In Chapter 3, it was therefore speculated that MOB abundances are responding to decreases in dissolved oxygen (DO) concentrations, and increases in temperature, which often co-occur with decreases in effective moisture. ACW is expected to change small lakes by warming surface waters (Bartosiewicz et al., 2019), strengthening thermal stratification (Bartosiewicz et al., 2019), lowering DO concentrations in the hypolimnion (Zhang et al., 2015) and lowering effective moisture (Bonsal et al., 2019). The research in Chapter 3 suggests that such changes would increase MOB abundances in Barry Lake, potentially increasing rates of methane oxidation. In theory, higher rates of methane oxidation could help mitigate methane emissions from Barry Lake.

Of note is that inferred microbial abundances in the modern period fell within the range of values inferred for the last ~1000 years (Chapter 3). This finding was surprising because increased carbon sequestration, enhanced delivery of labile carbon to the sediment OM, and warmer temperatures related to ACW are all known to increase microbial abundances (Borrel et al., 2011). It is therefore unclear why the inferred microbial abundances in the modern period are not higher. Especially interesting was that the inferred MOB abundances, indicated by mass accumulation rates of the triterpene diploptene, were not especially high in the modern period (Chapter 3). This finding suggests that either *(i)* a shift occurred in the microbial composition such that the predominant oxidizers of methane do not produce diploptene, and/or *(ii)* methane oxidation is not keeping up with methanogenesis. If the latter possibility is true, Barry Lake may be a net source of methane, an important greenhouse gas, to the atmosphere.

6.1.4 Baselines of $\epsilon_{n\text{-alkane-atm}}$ and ϵ_{water} can be used to calibrate estimates of ancient $\delta^{13}\text{C}_{\text{CO}_2}$ and $\delta^2\text{H}_{\text{precipitation}}$ in the Uinta Mountains

Chapter 4 established baselines of $\delta^{13}\text{C}_{\text{TOC}}$, $\delta^{15}\text{N}_{\text{TN}}$, TOC:TN, $\delta^{13}\text{C}_{n\text{-alkane}}$, $\delta^2\text{H}_{n\text{-alkane}}$, ϵ_{bulk} , $\epsilon_{n\text{-alkane-atm}}$ and ϵ_{water} for potential sources of OM in Uinta Mountain lake sediments. These baselines help fill a current knowledge gap concerning the carbon, nitrogen and hydrogen isotope compositions of organisms growing in high-elevation sites. As demonstrated in Chapter 4, values of $\epsilon_{n\text{-alkane-atm}}$ (the carbon isotope fractionation between n -alkanes and atmospheric CO_2) and ϵ_{water} (the hydrogen isotope fractionation between n -alkanes and source water) can be used to reconstruct ancient $\delta^{13}\text{C}_{\text{CO}_2}$ and $\delta^2\text{H}_{\text{precipitation}}$. These fractionation factors will therefore be of great use to the community of paleolimnologists working in the Uinta Mountains, and other nearby high-elevation sites.

6.1.5 Isotopic compositions of n -alkanes and bulk sediments must be interpreted differently in low-elevation environments than in remote, high-elevation environments

In Chapter 5, proxy records from Barry Lake were compared with those from the Uinta Mountain lakes. One similarity between the two sites is that the $\delta^{13}\text{C}_{\text{TOC}}$ and $\delta^{15}\text{N}_{\text{TN}}$ of the sediment OM were well preserved. This finding substantiates the use of these proxies as indicators of paleoenvironmental change. Although $\delta^{13}\text{C}_{\text{TOC}}$ and $\delta^{15}\text{N}_{\text{TN}}$ of the sediment OM were well preserved, caution should be exercised when using these proxies to reconstruct primary production. It was demonstrated that the $\delta^{13}\text{C}_{\text{TOC}}$ and $\delta^{15}\text{N}_{\text{TN}}$ of the sediment are sensitive to many factors in addition to primary production (Chapter 5).

The investigations in chapters 4 and 5 revealed differences between the isotopic proxies of Uinta Mountain and Barry Lake sediments, and sources of OM in these sediments. Chapter 4 showed that, while n -alkanes have been successfully used as tracers of OM source in temperate areas, they may be challenging to use as tracers of OM source in alpine areas. Challenges arise because (i) alpine lakes are commonly surrounded by coniferous trees, which produce few n -alkanes; and (ii) because the vegetation growing in

alpine regions is dominated by C₃ plants, which commonly produce *n*-alkanes with indistinguishable isotopic compositions.

The comparisons of Barry Lake and the Uinta Mountains also revealed important differences between alpine and low-elevation, temperate lakes that must be considered when interpreting $\delta^{13}\text{C}_{\text{TOC}}$ and $\delta^{15}\text{N}_{\text{TN}}$ of the sediment. It was observed that submerged macrophytes at Barry Lake exhibited a wider range of $\delta^{13}\text{C}_{\text{TOC}}$ than submerged macrophytes in the Uinta Mountains. However, substantial overlap occurred in the $\delta^{13}\text{C}_{\text{TOC}}$ and $\delta^{15}\text{N}_{\text{TN}}$ of various vegetation types that are potential OM sources for the Uinta Mountain lakes, as well as for Barry Lake. As such, it is equally challenging to utilize carbon and nitrogen isotopes to uniquely identify OM sources at both sites.

6.2 Suggestions for future research

6.2.1 Confirming the cause of increased primary production in Barry Lake beginning in AD ~1850

While it was speculated in this thesis that recent increases in primary production at Barry Lake were caused by human impacts, the exact cause of this increase needs to be confirmed. Understanding the cause of increased primary production at Barry Lake will clarify how managers of the lake can mitigate further increases in primary production. As a first step, modern waters from Barry Lake could be analyzed to determine the coliform bacteria content of the water. Coliform bacteria are present in the feces of all warm-blooded animals (Craun et al., 1997), so a high coliform bacteria count could confirm that the lake is receiving inputs of organic fertilizer from nearby agricultural fields. To identify when organic fertilizer first entered the lake, one could measure the abundance of fecal biomarkers such as sterols and stanols contained in a sediment core (Engels et al., 2018; Vane et al., 2010). A coeval increase in sterols and stanols with Chl-*a*_(s)-MAR, and the other proxies of primary production at Barry Lake, would provide convincing evidence that runoff from agricultural fields caused the observed increase in primary production.

6.2.2 Characterizing the greenhouse gas fluxes to and from modern Barry Lake

The net greenhouse gas emissions from Barry Lake should be quantified to assess whether the lake is a source or sink of CO₂ and CH₄. Such measurements would confirm whether modern Barry Lake is behaving as a CO₂ sink and CH₄ source, as suggested in this thesis. Of interest to many researchers is whether lakes undergoing eutrophication are becoming net sources of “CO₂-equivalents” to the atmosphere (Grasset et al., 2020). CO₂-equivalents account for the fact that CH₄ is, over a timescale of 100 years, 34 times more potent as a greenhouse gas than CO₂ (Myhre et al., 2013). A CO₂-equivalent balance, as presented by Grasset et al. (2020), would be useful for Barry Lake because it would show whether the lake is helping to mitigate climate warming, or contributing to climate warming. In temperate latitudes, the overwhelming majority of lakes are small (> 0.1 km²) (Downing et al., 2006). It is therefore likely that the results of this thesis are applicable to most temperate lakes. Small lakes are likely more important than large lakes as contributors to, and regulators of, the global carbon cycle (Read and Rose, 2013). It is therefore vital that scientists understand how net carbon emissions from such small lakes have changed due to ACW.

While previous studies have calculated CO₂-equivalent balances, these studies have not paired these data with paleoenvironmental records (*e.g.*, Grasset et al., 2020; Jansen et al., 2019). If one were to construct a CO₂-equivalent balance for Barry Lake, it could be interpreted using the reconstructions of primary production, methane oxidation, carbon burial, OM source and OM degradation presented in this thesis (Chapter 3). To begin, one could identify the relationships between net CO₂ and CH₄ fluxes and other aspects of the carbon cycle at Barry Lake (*e.g.*, primary production, respiration, OM source, carbon sequestration, methane oxidation). If these relationships were clarified, one could then use the proxy record established in this thesis to estimate how fluxes of CO₂ and CH₄ changed during the MCA and LIA. This information would shed light on how small, temperate lakes have contributed to global carbon emissions over time.

6.2.3 Identifying and enumerating the community MOB and methanogens living in Barry Lake

Additional work at Barry Lake should also focus on microbiological assays, which could be used to characterize the community of methanotrophs and MOB living in Barry Lake. With this information, it would be easier to understand why methane oxidation at Barry Lake is not anomalously high in the modern period. As detailed in Chapter 3, a change in the MOB community could explain this discrepancy. Characterizing the MOB community in Barry Lake would clarify whether this explanation is accurate. Characterizing the methanogen community would also be beneficial. Of interest to researchers is whether, in a warming world, abundances of methanogens are growing at a faster rate than abundances of MOB. If this were the case at Barry Lake, methane might be being produced at a faster rate than it can be oxidized, resulting in net methane emissions from the lake.

6.2.4 Concurrent monitoring of diploptene abundances, dissolved oxygen concentrations and temperature

Concurrent monitoring of MOB abundance, diploptene abundances, dissolved oxygen concentrations and temperature at Barry Lake would help to clarify the relationship between climate change and methane oxidation. In Chapter 3, a clear relationship was identified between $\delta^{18}\text{O}_{\text{marl}}$ and $\delta^2\text{H}_{\text{C}_{17}}$, indicators of effective moisture, and diploptene-MAR, an indicator of methane oxidation. Yet, this relationship was opposite to trends described in the literature. It was therefore speculated that MOB abundance was responding, not to changes in effective moisture, but to changes in dissolved oxygen and temperature that occur concurrently with shifts in effective moisture. To test this theory, one could regularly monitor dissolved oxygen and temperature in Barry Lake, as well as diploptene abundances of sediments sampled from sediment traps. Understanding the connections between climate and diploptene abundances is critical for estimating how methane oxidation changed over the last millennium.

The results of this monitoring study could also be compared with CH_4 fluxes and microbiological assays to clarify the relationships between diploptene, MOB abundance and

CH₄ emissions. These findings would further strengthen the arguments made in Chapter 3 that diploptene-MAR is a proxy for methane oxidation in Barry Lake.

6.2.5 Estimating changes in $\delta^{13}\text{C}_{\text{CO}_2}$ and $\delta^2\text{H}_{\text{precipitation}}$ in the Uinta Mountains using the fractionation factors established in Chapter 4

In Chapter 4, it was demonstrated that one can estimate the $\delta^{13}\text{C}$ of ancient CO₂ and the $\delta^2\text{H}$ of ancient precipitation using (i) downcore measurements of *n*-alkane abundances; (ii) downcore measurements of the $\delta^{13}\text{C}_{n\text{-alkane}}$ and $\delta^2\text{H}_{n\text{-alkane}}$ of the sediment OM; and (iii) the fractionation factors established in Chapter 4. Future studies should make additional downcore measurements of *n*-alkane abundances and their isotopic compositions so that changes in $\delta^{13}\text{C}_{\text{CO}_2}$ and $\delta^2\text{H}_{\text{precipitation}}$ can be estimated.

In the Uinta Mountains, a ~1000-year record of $\delta^{13}\text{C}_{\text{CO}_2}$ could be used to calibrate a regional Suess effect correction for the Uinta Mountains. The Suess effect is a ~2 ‰ lowering of the $\delta^{13}\text{C}$ of atmospheric CO₂ that began around AD 1850 upon the advent of fossil fuel burning (Dombrosky, 2020). Modern Suess effect corrections (*e.g.*, Dombrosky, 2020; Verburg, 2007) are calibrated using measurements of $\delta^{13}\text{C}_{\text{CO}_2}$ from Antarctic ice cores. Yet, previous studies have demonstrated that $\delta^{13}\text{C}_{\text{atm}}$ is heterogenous across the globe, suggesting that regional Suess effect corrections may be needed. The $\delta^{13}\text{C}_{\text{atm}}$ at 60 °N, for instance, is generally 0.2 ‰ more negative than at 60 °S; this effect is most likely due to the anthropogenic burning of fossil fuels occurring at northern latitudes (Keeling et al., 1989). More concerning is that the $\delta^{13}\text{C}_{\text{atm}}$ in major cities is more negative than the global average due to inputs of CO₂ from vehicle exhaust and other sources of local fossil fuel burning. The $\delta^{13}\text{C}_{\text{atm}}$ above Paris, for instance is ~1 ‰ lower than the global average (Widory and Javoy, 2003). The Uinta Mountains are located to the east of nine oil refineries, which could in theory alter the $\delta^{13}\text{C}_{\text{CO}_2}$ in these mountains. For these reasons, a regional Suess effect correction for the Uinta Mountains could improve the accuracy of paleoenvironmental interpretations in this area.

Estimates of $\delta^2\text{H}_{\text{precipitation}}$ could be useful for investigating whether anthropogenic climate warming has altered atmospheric circulation patterns in the Uinta Mountains. First, estimates of $\delta^2\text{H}_{\text{precipitation}}$ from sediments <100 years old should be compared with instrumental records of precipitation, temperature, relative humidity and PDSI to establish the controls of $\delta^2\text{H}_{\text{precipitation}}$. With this understanding, one can interpret variations in $\delta^2\text{H}_{\text{precipitation}}$ downcore. Variations in $\delta^2\text{H}_{\text{precipitation}}$ are likely to reflect changes (i) in the source of atmospheric moisture, (ii) effective moisture, (iii) temperature; (iv) snowmelt; or (v) a combination of these factors (Dansgaard, 1964; Sachse et al., 2012). Inferred $\delta^2\text{H}_{\text{precipitation}}$ could therefore improve our understanding of how changes in climate, including ACW, have affected the hydrology of Uinta Mountain lakes. This information could also provide an indication into how the hydrology of these lakes may change in the future.

6.3 References

- Bartosiewicz, M., Przytulska, A., Lapierre, J., Laurion, I., Lehmann, M.F., Maranger, R., 2019. Hot tops, cold bottoms: Synergistic climate warming and shielding effects increase carbon burial in lakes. *Limnol. Oceanogr. Lett.* 4, 132–144.
<https://doi.org/10.1002/lol2.10117>
- Bonsal, B.R., Peters, D.L., Seglenieks, F., Rivera, A., Berg, A., 2019. Changes in freshwater availability across Canada, in: Bush, E., Lemmen, D.S. (Eds.), *Canada's Changing Climate Report*. Government of Canada, Ottawa, Canada, pp. 261.
- Borrel, G., Jézéquel, D., Biderre-Petit, C., Morel-Desrosiers, N., Morel, J.P., Peyret, P., Fonty, G., Lehours, A.C., 2011. Production and consumption of methane in freshwater lake ecosystems. *Res. Microbiol.* 162, 832–847.
<https://doi.org/10.1016/j.resmic.2011.06.004>
- Craun, G.F., Berger, P.S., Calderon, R.L., 1997. Coliform bacteria and waterborne disease outbreaks. *J. Am. Water Work. Assoc.* 89, 96–104.
<https://doi.org/10.1002/j.1551-8833.1997.tb08197.x>

- Dansgaard, W., 1964. Stable isotopes in precipitation. *Tellus* 16, 436–468.
<https://doi.org/10.3402/tellusa.v16i4.8993>
- Dombrosky, J., 2020. A ~1000-year ¹³C Suess correction model for the study of past ecosystems. *Holocene* 30, 474–478. <https://doi.org/10.1177/0959683619887416>
- Downing, J.A., Prairie, Y.T., Cole, J.J., Duarte, C.M., Tranvik, L.J., Striegl, R.G., McDowell, W.H., Kortelainen, P., Caraco, N.F., Melack, J.M., Middelburg, J.J., 2006. The global abundance and size distribution of lakes, ponds, and impoundments. *Limn. Oceanogr.* 51, 2388–2397. <https://doi.org/10.4319/lo.2006.51.5.2388>
- Engels, S., van Oostrom, R., Cherli, C., Dungait, J.A.J., Jansen, B., van Aken, J.M., van Geel, B., Visser, P.M., 2018. Natural and anthropogenic forcing of Holocene lake ecosystem development at Lake Uddelermeer (The Netherlands). *J. Paleolimnol.* 59, 329–347. <https://doi.org/10.1007/s10933-017-0012-x>
- Grasset, C., Sobek, S., Scharnweber, K., Moras, S., Villwock, H., Andersson, S., Hiller, C., Nydahl, A.C., Chaguaceda, F., Colom, W., Tranvik, L.J., 2020. The CO₂-equivalent balance of freshwater ecosystems is non-linearly related to productivity. *Glob. Chang. Biol.* 26, 5705–5715. <https://doi.org/10.1111/gcb.15284>
- Jansen, J., Thornton, B.F., Jammet, M.M., Wik, M., Cortés, A., Friborg, T., MacIntyre, S., Crill, P.M., 2019. Climate-sensitive controls on large spring emissions of CH₄ and CO₂ From northern lakes. *J. Geophys. Res. Biogeosciences* 124, 2379–2399.
<https://doi.org/10.1029/2019JG005094>
- Keeling, C.D., Bacastow, R.B., Carter, A.F., Piper, S.C., Whorf, T.P., Heimann, M., Mook, W.G., Roeloffzen, H., 1989. A three-dimensional model of atmospheric CO₂ transport based on observed winds: 1. Analysis of observational data., in: Peterson, D.H. (Ed.), *Aspects of Climate Variability in the Pacific and the Western Americas*. American Geophysical Union, Washington, pp. 165–236.

- Myhre, G., Shindell, D., Pongratz, J., 2013. Anthropogenic and natural radiative forcing, in: Climate Change 2013 the Physical Science Basis: Working Group I Contribution to the Fifth Assessment Report of the Intergovernmental Panel on Climate Change. Cambridge University Press, pp. 659–740.
<https://doi.org/10.1017/CBO9781107415324.018>
- Read, J.S., Rose, K.C., 2013. Physical responses of small temperate lakes to variation in dissolved organic carbon concentrations. *Limn. Oceanogr.* 58, 921–931.
<https://doi.org/10.4319/lo.2013.58.3.0921>
- Sachse, D., Billault, I., Bowen, G.J., Chikaraishi, Y., Dawson, T.E., Feakins, S.J., Freeman, K.H., Magill, C.R., McInerney, F.A., van der Meer, M.T.J., Polissar, P., Robins, R.J., Sachs, J.P., Schmidt, H.-L., Sessions, A.L., White, J.W.C., West, J.B., Kahmen, A., 2012. Molecular paleohydrology: Interpreting the hydrogen-isotopic composition of lipid biomarkers from photosynthesizing organisms. *Annu. Rev. Earth Planet. Sci.* 40, 221–249.
<https://doi.org/10.1146/annurev-earth-042711105535>
- Sia, M.E., Doyle, R.M., Moser, K.A., 2020. Recent trends in mountain algal production: evaluating the response to fish stocking relative to regional environmental stressors. *Lake Reserv. Manag.* 36, In press. 10.1080/10402381.2020.1814462
- Vane, C.H., Kim, A.W., McGowan, S., Leng, M.J., Heaton, T.H.E., Kendrick, C.P., Coombs, P., Yang, H., Swann, G.E.A., 2010. Sedimentary records of sewage pollution using faecal markers in contrasting peri-urban shallow lakes. *Sci. Total Environ.* 409, 345–356. <https://doi.org/10.1016/j.scitotenv.2010.09.033>
- Verburg, P., 2007. The need to correct for the Suess effect in the application of $\delta^{13}\text{C}$ in sediment of autotrophic Lake Tanganyika, as a productivity proxy in the Anthropocene. *J. Paleolimnol.* 37, 591–602. <https://doi.org/10.1007/s10933-006-9056-z>

Widory, D., Javoy, M., 2003. The carbon isotope composition of atmospheric CO₂ in Paris. *Earth Planet. Sci. Lett.* 215, 289–298. [https://doi.org/10.1016/S001821X\(03\)00397-2](https://doi.org/10.1016/S001821X(03)00397-2)

Zhang, Y., Wu, Z., Liu, M., He, J., Shi, K., Zhou, Y., Wang, M., Liu, X., 2015. Dissolved oxygen stratification and response to thermal structure and long-term climate change in a large and deep subtropical reservoir (Lake Qiandaohu, China). *Water Res.* 75, 249–258. <https://doi.org/10.1016/j.watres.2015.02.052>

Appendix A: Data tables

Table A.1 $\delta^{13}\text{C}_{\text{DIC}}$ of modern waters collected from Barry Lake. From Liu (2016).

Sample ID	Station number	Approximate Depth of collection (m)	$\delta^{13}\text{C}_{\text{DIC}}$ (‰, VPDB)	Number of replicates	Duplicate $\delta^{13}\text{C}_{\text{DIC}}$ (‰, VPDB)	SD of replicates (‰, VPDB)
1-2-B	1	6.5	-4.9			
1-3-B	1	6.5	-5			
1-4-B	1	6.5	-5.2			
2-2-B	2	6.5	-6.6			
2-3-B	2	6.5	-3.4			
2-4-B	2	6.5	-6.3			
3-1-B	3	6.5	-4.5			
3-2-B	3	6.5	-4.6			
3-3-B	3	6.5	-4.5			
1-2-M	1	3.5	-5.2			
1-3-M	1	3.5	-5.1			
1-4-M	1	3.5	-5.1			
2-2-M	2	3.5	-3.6			
2-3-M	2	3.5	-3.6			
2-4-M	2	3.5	-3.7			
3-1-M	3	3.5	-4.6			
3-2-M	3	3.5	-4.6			
3-3-M	3	3.5	-4.6			
1-1-T	1	0.3	-5.3	1	-5.3	0.01
1-2-T	1	0.3	-5.2			
1-2-T	1	0.3	-5.1			
1-4-T	1	0.3	-5.2			
2-1-T	2	0.3	-2.4	1	-2.4	0.01
2-2-T	2	0.3	-3.4			
2-3-T	2	0.3	-3.5	1	-3.4	0.05
2-4-T	2	0.3	-3.5			
3-1-T	3	0.3	-4.6			
3-2-T	3	0.3	-4.6			
3-3-T	3	0.3	-4.6			
3-4-T	3	0.3	-4			

Table A.2 Values of $\delta^{13}\text{C}_{\text{TOC}}$, $\delta^{15}\text{N}_{\text{TN}}$, %TOC, %TN and TOC:TN from BL-G11-01. From Liu (2016).

Midpoint (cm)	Year AD	$\delta^{13}\text{C}_{\text{TOC}}$ ‰, VPDB	$\delta^{13}\text{C}_{\text{TOC}}$ ‰, VPDB	No. of replicates	SD of replicates ‰, VPDB	$\delta^{15}\text{N}_{\text{TN}}$ ‰, AIR	No. of replicates	SD of replicates ‰, AIR	TOC %	No. of replicates	SD TOC %	TN %	No. of replicates	SD of replicates %	TOC:TN
0.25	2016														
0.75	2013	+1.9	-0.2			+1.3			27.4	1	0.14	1.9			17.1
1.25	2011	+1.6	-0.5			+1.4			14.1			1.9			8.6
1.75	2010	+1.7	-0.3			+1.2			14.6			2.0			8.7
2.25	2009	+1.8	-0.2			+1.3			15.0			2.0			8.9
2.75	2007	+1.7	-0.2			+1.2			14.6			2.0			8.6
3.25	2005	+1.5	-0.3			+1.1	2	0.05	13.9			2.0			8.0
3.75	2004	+1.7	-0.1			+1.0			14.3			1.9			8.6
4.25	2002	+1.5	-0.2			+0.9			14.1			1.9			8.4
4.75	2000	+1.4	-0.2			+1.0			13.3			1.9			8.1
5.25	1998								15.0						
5.75	1996	+1.4	-0.1			+1.0	2	0.04	13.6	2	0.27	1.9			8.2
6.25	1993	+1.3	-0.1			+1.0			13.3			1.8			8.6
6.75	1991	+1.4	-0.1	1	0.01	+1.0	1	0.09	13.0			1.7			8.8
7.25	1988	+1.2	-0.0			+1.0			13.2			2.			7.0
7.75	1984	+1.1	-0.0			+1.0			12.1			1.9			7.4
8.25	1981	+1.1	-0.0			+1.2			12.1			1.7			8.3
8.75	1980	+1.1	-0.0			+1.3			12.3	1	0.44	1.8	1	0.02	7.9
9.25	1978	+1.0	-0.0			+1.1			12.0			1.6			8.5
9.75	1976	+1.0	-0.0			+1.0			12.0			1.6			8.6
10.25	1974	+0.9	-0.0			+1.1			12.4			1.6	1	0	8.9
10.75	1972	+0.7	-0.2			+1.5			11.9			1.7			8.2
11.25	1969	+0.9	+0.1			+1.2			11.6			1.5			8.9
11.75	1967	+0.9	+0.1			+1.4			11.5			1.5			9.1
12.25	1965	+0.8	+0.0			+1.4			11.4			1.4			9.2
12.75	1963	+0.8	+0.1	1	0.03	+1.2	1	0.05	10.8			1.5			8.6
13.25	1962	+0.9	+0.2			+1.6			10.5	1	0.23	1.4			8.4
13.75	1960	+0.7	+0.0			+1.6			10.1			1.4			8.4
14.25	1958	+0.7	+0.1			+1.7			10.2			1.4			8.6
14.75	1955	+0.6	+0.0			+1.7			10.4			1.4			8.5

*Corrected for the Suess Effect according to Verburg (2007).

Midpoint (cm)	Year AD	$\delta^{13}\text{C}_{\text{TOC}^*}$ ‰, VPDB	$\delta^{13}\text{C}_{\text{TOC}}$ ‰, VPDB	No. of replicates	SD of replicates ‰, VPDB	$\delta^{15}\text{N}_{\text{TN}}$ ‰, AIR	No. of replicates	SD of replicates ‰, AIR	TOC %	No. of replicates	SD TOC %	TN %	No. of replicates	SD of replicates %	TOC:TN
15.25	1953	+0.5	-0.1			+1.8			9.9			1.4			8.4
15.75	1951	+0.6	-0.0			+1.9			10.7	2	0.43	1.4			8.8
16.25	1948	+0.4	-0.1			+1.8			10.1	1	0.03	1.4	1	0.00	8.2
16.75	1945	+0.3	-0.2			+1.7			11.2			1.5			8.8
17.25	1941	+0.1	-0.3			+1.7			11.6			1.5			8.8
17.75	1936	+0.2	-0.2			+1.6			12.2			1.6			9.1
18.25	1931	-0.1	-0.4			+1.5			11.9			1.6			8.7
18.75	1924	-0.1	-0.4			+1.4			11.8			1.6			8.4
19.25	1917	-0.3	-0.6	1	0.01	+1.3	1	0.09	12.5			1.6			8.9
19.75	1909	-0.6	-0.8			+1.1			13.1			1.7			9.0
20.25	1898	-0.7	-0.9			+0.9			13.9			1.7			9.5
20.75	1883	-0.8	-0.9	1	0.01	+1.0	2	0.07	13.7			1.7			9.4
21.25	1851	-0.8	-0.8			+0.7			13.3			1.7			9.1
21.75	1803	-1.0	-0.9			+0.5	2	0.05	13.5			1.7			9.3
22.25	1760	-0.8	-0.7			+0.3			13.6			1.7			9.3
22.75	1725	-0.7	-0.7			+0.4	2	0.38	14.1			1.8			9.3
23.25	1689	-0.1	-0.1			-0.4			16.2			2.0			9.4
23.75	1648	+0.1	+0.1			-0.9	2	0.03	19.8			2.4			9.5
24.25	1611	-0.2	-0.2			-1.4			27.1			3.1			10.1
24.75	1572	+5.1	+5.1			-1.3	2	0.09	30.4			3.4			10.3
25.25	1536	+2.4	+2.4			-1.2			27.4			3.1	1	0.00	10.4
25.75	1498	+2.6	+2.6			-1.1	2	0.04	25.6			2.9			10.3
26.25	1463	+3.2	+3.2			-1.1			23.4			2.8			9.9
26.75	1426	+4.1	+4.1			-1.1			23.2			2.8			9.8
27.25	1397	+3.6	+3.6	1	0.00	-1.0			23.8			2.8			10.1
27.75	1376	+3.1	+3.1			-0.9			25.5			2.9			10.1
28.25	1362	+2.7	+2.7			-1.0	2	0.03	28.3			3.2			10.3
28.75	1352	+2.2	+2.2			-0.8			28.7			3.3			10.0
29.25	1344	+0.9	+0.9			-0.8			30.3			3.4			10.3
29.75	1334	-0.1	-0.1			-0.8			31.6			3.5			10.5

*Corrected for the Suess Effect according to Verburg (2007).

Midpoint (cm)	Year AD	$\delta^{13}\text{C}_{\text{TOC}^*}$ ‰, VPDB	$\delta^{13}\text{C}_{\text{TOC}}$ ‰, VPDB	No. of replicates	SD of replicates ‰, VPDB	$\delta^{15}\text{N}_{\text{TN}}$ ‰, AIR	No. of replicates	SD of replicates ‰, AIR	TOC %	No. of replicates	SD TOC %	TN %	No. of replicates	SD of replicates %	TOC:TN
30.75	1315	+0.1	+0.1			-1.0			33.3	1	0.04	3.6			10.7
31.25	1305	+0.6	+0.6			-1.1			32.5			3.7			10.4
31.75	1295	+0.7	+0.7			-1.2			30.8			3.6			9.9
32.25	1286	+0.2	+0.2			-1.4			31.4			3.8			9.7
32.75	1276	+0.8	+0.8			-1.4			31.4			3.7			9.8
33.25	1267	+1.4	+1.4			-1.2			31.1			3.6			10.1
33.75	1258	+1.0	+1.0	1	0.00	-1.2	1	0.04	30.8	1	0.14	3.6	1	0.00	10.1
34.25	1250	+0.4	+0.4			-1.3			30.4			3.6			10.0
34.75	1241	+0.6	+0.6			-1.3			30.6	1	0.89	3.5			10.1
35.25	1232	+0.9	+0.9			-1.5			26.6			3.1			10.0
35.75	1222	+0.3	+0.3	1	0.49	-1.6	2	0.28	26.0			3.2			9.5
36.25	1212	+0.8	+0.8			-1.8			23.8			3.1			9.0
36.75	1202	+2.8	+2.8			-1.8			17.9			2.4			8.7
37.25	1191	+3.5	+3.5			-1.5			15.5			2.1			8.6
37.75	1181	+3.2	+3.2			-1.8			15.4			2.1			8.7
38.25	1171	+1.8	+1.8			-1.7			17.1			2.3			8.8
38.75	1161	+2.4	+2.4			-1.6			17.4			2.3			8.9
39.25	1151	+2.6	+2.6			-1.4			17.8			2.4			8.6
39.75	1140	+2.3	+2.3			-1.9			18.5			2.5			8.4
40.25	1129	+2.7	+2.7	1	0.05	-1.9	1	0.00	22.7	3	0.67	3.0	1	0.00	8.8
40.75	1119	+2.4	+2.4			-1.7			23.3			3.2			8.6
41.25	1109	+2.1	+2.1	1	0.02	-1.8	1	0.11	21.0			2.8	1	0.00	8.8

*Corrected for the Suess Effect according to Verburg (2007).

Table A.3 Values of $\delta^{13}\text{C}_{\text{marl}}$, $\delta^{18}\text{O}_{\text{marl}}$ and %calcite from BL-G11-01. From Liu (2016).

Midpoint (cm)	Year AD	$\delta^{13}\text{C}_{\text{marl}}$ ‰, VPDB	$\delta^{13}\text{C}_{\text{marl}}$ ‰, VPDB	No. of rep- licates	SD of replicates ‰, VPDB	$\delta^{18}\text{O}_{\text{marl}}$ ‰, VSMOW	No. of rep- licates	SD of rep- licates ‰, AIR	Mid- point (cm)	Year AD	$\delta^{13}\text{C}_{\text{marl}}$ ‰, VPDB	$\delta^{13}\text{C}_{\text{marl}}$ ‰, VPDB	No. of replicates	SD of replicates ‰, VPDB	$\delta^{18}\text{O}_{\text{marl}}$ ‰, VSMOW
0.25	2011								0.25	2011					
0.75	2011	+1.9	-0.2			+21.3			0.75	2011	+1.9	-0.2			+21.3
1.25	2010	+1.6	-0.5			+21.0			1.25	2010	+1.6	-0.5			+21.0
1.75	2008	+1.7	-0.3			+21.3			1.75	2008	+1.7	-0.3			+21.3
2.25	2007	+1.8	-0.2			+21.3			2.25	2007	+1.8	-0.2			+21.3
2.75	2005	+1.7	-0.2			+21.2			2.75	2005	+1.7	-0.2			+21.2
3.25	2003	+1.5	-0.3			+21.2			3.25	2003	+1.5	-0.3			+21.2
3.75	2002	+1.7	-0.1			+21.3			3.75	2002	+1.7	-0.1			+21.3
4.25	2000	+1.5	-0.2			+21.2			4.25	2000	+1.5	-0.2			+21.2
4.75	1997	+1.4	-0.2			+21.3			4.75	1997	+1.4	-0.2			+21.3
5.25	1994								5.25	1994					
5.75	1993	+1.4	-0.1			+21.3			5.75	1993	+1.4	-0.1			+21.3
6.25	1991	+1.3	-0.1			+21.3			6.25	1991	+1.3	-0.1			+21.3
6.75	1986	+1.4	+0.1			+21.3			6.75	1986	+1.4	+0.1			+21.3
7.25	1983	+1.2	+0.0			+21.3			7.25	1983	+1.2	+0.0			+21.3
7.75	1981	+1.1	+0.0			+21.3			7.75	1981	+1.1	+0.0			+21.3
8.25	1979	+1.1	+0.0			+21.3			8.25	1979	+1.1	+0.0			+21.3
8.75	1978	+1.1	+0.0			+21.3			8.75	1978	+1.1	+0.0			+21.3
9.25	1976	+1.0	+0.0			+21.4			9.25	1976	+1.0	+0.0			+21.4
9.75	1973	+1.0	+0.0			+21.4			9.75	1973	+1.0	+0.0			+21.4
10.25	1971	+0.9	+0.0			+21.3			10.25	1971	+0.9	+0.0			+21.3
10.75	1969	+0.7	-0.2			+21.3			10.75	1969	+0.7	-0.2			+21.3
11.25	1967	+0.9	+0.1			+21.4			11.25	1967	+0.9	+0.1			+21.4
11.75	1965	+0.9	+0.1			+21.3			11.75	1965	+0.9	+0.1			+21.3
12.25	1963	+0.8	+0.0			+21.4			12.25	1963	+0.8	+0.0			+21.4
12.75	1961	+0.8	+0.1			+21.5			12.75	1961	+0.8	+0.1			+21.5
13.25	1959	+0.9	+0.2			+21.4			13.25	1959	+0.9	+0.2			+21.4
13.75	1957	+0.7	+0.0	1	0.01	+21.4	1	0.00	13.75	1957	+0.7	+0.0	1	0.01	+21.4
14.25	1955	+0.7	+0.1			+21.5			14.25	1955	+0.7	+0.1			+21.5
14.75	1952	+0.6	+0.0			+21.4			14.75	1952	+0.6	+0.0			+21.4

*Corrected for the Suess Effect according to Verburg (2007).

Midpoint (cm)	Year AD	$\delta^{13}\text{C}_{\text{marl}}^*$ ‰, VPDB	$\delta^{13}\text{C}_{\text{marl}}$ ‰, VPDB	No. of replicates	SD of replicates ‰, VPDB	$\delta^{18}\text{O}_{\text{marl}}$ ‰, VSMOW	No. of replicates	SD of replicates ‰, AIR	Midpoint (cm)	Year AD	$\delta^{13}\text{C}_{\text{marl}}^*$ ‰, VPDB	$\delta^{13}\text{C}_{\text{marl}}$ ‰, VPDB	No. of replicates	SD of replicates ‰, VPDB	$\delta^{18}\text{O}_{\text{marl}}$ ‰, VSMOW
15.25	1949.9								15.25	1949.9					
15.75	1946.9	+1.9	-0.2			+21.3			15.75	1946.9	+1.9	-0.2			+21.3
16.25	1943	+1.6	-0.5			+21.0			16.25	1943	+1.6	-0.5			+21.0
16.75	1938.6	+1.7	-0.3			+21.3			16.75	1938.6	+1.7	-0.3			+21.3
17.25	1933.6	+1.8	-0.2			+21.3			17.25	1933.6	+1.8	-0.2			+21.3
17.75	1927.9	+1.7	-0.2			+21.2			17.75	1927.9	+1.7	-0.2			+21.2
18.25	1920.7	+1.5	-0.3			+21.2			18.25	1920.7	+1.5	-0.3			+21.2
18.75	1912.6	+1.7	-0.1			+21.3			18.75	1912.6	+1.7	-0.1			+21.3
19.25	1902.6	+1.5	-0.2			+21.2			19.25	1902.6	+1.5	-0.2			+21.2
19.75	1890.5	+1.4	-0.2			+21.3			19.75	1890.5	+1.4	-0.2			+21.3
20.25	1863.5								20.25	1863.5					
20.75	1822.9	+1.4	-0.1			+21.3			20.75	1822.9	+1.4	-0.1			+21.3
21.25	1783.8	+1.3	-0.1			+21.3			21.25	1783.8	+1.3	-0.1			+21.3
21.75	1742.8	+1.4	+0.1			+21.3			21.75	1742.8	+1.4	+0.1			+21.3
22.25	1707	+1.2	+0.0			+21.3			22.25	1707	+1.2	+0.0			+21.3
22.75	1672.5	+1.1	+0.0			+21.3			22.75	1672.5	+1.1	+0.0			+21.3
23.25	1639.1	+1.1	+0.0			+21.3			23.25	1639.1	+1.1	+0.0			+21.3
23.75	1603.3	+1.1	+0.0			+21.3			23.75	1603.3	+1.1	+0.0			+21.3
24.25	1569.2	+1.0	+0.0			+21.4			24.25	1569.2	+1.0	+0.0			+21.4
24.75	1530.4	+1.0	+0.0			+21.4			24.75	1530.4	+1.0	+0.0			+21.4
25.25	1492.9	+0.9	+0.0			+21.3			25.25	1492.9	+0.9	+0.0			+21.3
25.75	1451.7	+0.7	-0.2			+21.3			25.75	1451.7	+0.7	-0.2			+21.3
26.25	1418.3	+0.9	+0.1			+21.4			26.25	1418.3	+0.9	+0.1			+21.4
26.75	1389.7	+0.9	+0.1			+21.3			26.75	1389.7	+0.9	+0.1			+21.3
27.25	1369.3	+0.8	+0.0			+21.4			27.25	1369.3	+0.8	+0.0			+21.4
27.75	1360.4	+0.8	+0.1			+21.5			27.75	1360.4	+0.8	+0.1			+21.5
28.25	1351.2	+0.9	+0.2			+21.4			28.25	1351.2	+0.9	+0.2			+21.4
28.75	1341.1	+0.7	+0.0	1	0.01	+21.4	1	0.00	28.75	1341.1	+0.7	+0.0	1	0.01	+21.4
29.25	1330.9	+0.7	+0.1			+21.5			29.25	1330.9	+0.7	+0.1			+21.5
29.75	1320.2	+0.6	+0.0			+21.4			29.75	1320.2	+0.6	+0.0			+21.4

*Corrected for the Suess Effect according to Verburg (2007).

Midpoint (cm)	Year AD	$\delta^{13}\text{C}_{\text{marl}}^*$ ‰, VPDB	$\delta^{13}\text{C}_{\text{marl}}$ ‰, VPDB	No. of replicates	SD of replicates ‰, VPDB	$\delta^{18}\text{O}_{\text{marl}}$ ‰, VSMOW	No. of replicates	SD of replicates ‰, AIR	Midpoint (cm)	Year AD	$\delta^{13}\text{C}_{\text{marl}}^*$ ‰, VPDB	$\delta^{13}\text{C}_{\text{marl}}$ ‰, VPDB	No. of replicates	SD of replicates ‰, VPDB	$\delta^{18}\text{O}_{\text{marl}}$ ‰, VSMOW
30.25	1310.6	-0.2	+0.2			+22.0			30.25	1310.6	+0.2	+0.2			+22.0
30.75	1301.1	-0.1	+0.1			+22.1			30.75	1301.1	+0.1	+0.1			+22.1
31.25	1291.9	-0.6	+0.6			+21.9			31.25	1291.9	+0.6	+0.6			+21.9
31.75	1282.1	-0.7	+0.7	1	0.19	+21.8	1	0.10	31.75	1282.1	+0.7	+0.7	1	0.19	+21.8
32.25	1272.8	-0.2	+0.2			+21.7			32.25	1272.8	+0.2	+0.2			+21.7
32.75	1263.1	-0.8	+0.8			+22.0			32.75	1263.1	+0.8	+0.8			+22.0
33.25	1253.6	-1.4	+1.4			+22.3			33.25	1253.6	+1.4	+1.4			+22.3
33.75	1245.5	-1.0	+1.0	1	0.07	+23.1	1	0.12	33.75	1245.5	+1.0	+1.0	1	0.07	+23.1
34.25	1236.2	-0.4	+0.4			+23.0			34.25	1236.2	+0.4	+0.4			+23.0
34.75	1226	-0.6	+0.6			+22.6			34.75	1226	+0.6	+0.6			+22.6
35.25	1215.9	-0.9	+0.9			+22.8			35.25	1215.9	+0.9	+0.9			+22.8
35.75	1205	-0.3	+0.3			+22.7			35.75	1205	+0.3	+0.3			+22.7
36.25	1194.5	-0.8	+0.8			+23.1			36.25	1194.5	+0.8	+0.8			+23.1
36.75	1183.7	-2.8	+2.8	1	0.44	+23.9	1	0.71	36.75	1183.7	+2.8	+2.8	1	0.44	+23.9
37.25	1173.6	-3.5	+3.5	1	0.09	+23.7	1	0.04	37.25	1173.6	+3.5	+3.5	1	0.09	+23.7
37.75	1163	-3.2	+3.2			+23.7			37.75	1163	+3.2	+3.2			+23.7
38.25	1152.8	-1.8	+1.8	1	0.06	+22.9	1	0.07	38.25	1152.8	+1.8	+1.8	1	0.06	+22.9
38.75	1142.5	-2.4	+2.4			+23.4			38.75	1142.5	+2.4	+2.4			+23.4
39.25	1132.4	-2.6	+2.6			+23.5			39.25	1132.4	+2.6	+2.6			+23.5
39.75	1122.7	-2.3	+2.3			+23.0			39.75	1122.7	+2.3	+2.3			+23.0
40.25	1113.2	-2.7	+2.7	1	1.77	+22.8	1	0.39	40.25	1113.2	+2.7	+2.7	1	1.77	+22.8
40.75	1103.4	-2.4	+2.4			+23.1			40.75	1103.4	+2.4	+2.4			+23.1
41.25	1094.1	-2.1	+2.1	1	0.01	+22.8	1	0.04	41.25	1094.1	+2.1	+2.1	1	0.01	+22.8

*Corrected for the Suess Effect according to Verburg (2007).

Table A.4 Mass accumulation rates from BL-G11-01. From Liu et al. (2016).

Midpoint (cm)	Year (AD)	Accumulation rate (cm/year)	Sedimentation rate (mg/cm ² /year)	TOC-MAR (mg/cm ² /year)	TN-MAR (mg/cm ² /year)	calcite-MAR (mg/cm ² /year)
0.25	2011	0.6	18.8			
0.75	2011	0.6	22.0			
1.25	2010	0.4	14.1	1.9	0.3	5.2
1.75	2008	0.4	19.6	2.9	0.4	6.3
2.25	2007	0.2	10.9	1.6	0.2	3.9
2.75	2005	0.2	11.7	1.7	0.2	4.0
3.25	2003	0.4	17.9	2.5	0.4	6.3
3.75	2002	0.4	22.3	3.2	0.4	8.5
4.25	2000	0.1	5.9	0.8	0.1	2.2
4.75	1997	0.1	8.7	1.2	0.2	2.7
5.25	1994	0.5	17.9			
5.75	1993	0.4	23.1	3.1	0.4	9.0
6.25	1991	0.1	4.3	0.6	0.1	1.4
6.75	1986	0.1	7.4	1.0	0.1	2.6
7.25	1983	0.2	7.8	1.0	0.2	2.7
7.75	1981	0.2	13.9	1.7	0.3	4.6
8.25	1979	0.8	40.3	4.9	0.7	15.3
8.75	1978	0.8	55.5	6.8	1	19.4
9.25	1976	0.2	10.6	1.3	0.2	3.5
9.75	1973	0.2	5.7	0.7	0.1	1.8
10.25	1971	0.2	15.9	2.0	0.3	5.2
10.75	1969	0.2	16.3	1.9	0.3	4.9
11.25	1967	0.2	11.0	1.3	0.2	3.6
11.75	1965	0.2	17.8	2.1	0.3	5.9
12.25	1963	0.3	19.7	2.2	0.3	6.5
12.75	1961	0.3	21.7	2.3	0.3	7.8
13.25	1959	0.3	9,1	1.0	0.1	3.0
13.75	1957	0.2	16.1	1.6	0.2	4.8
14.25	1955	0.2	14.4	1.5	0.3	5.0
14.75	1952	0.2	15.0	1.6	0.2	4.7

Midpoint (cm)	Year (AD)	Accumulation rate (cm/year)	Sedimentation rate (mg/cm ² /year)	TOC-MAR (mg/cm ² /year)	TN-MAR (mg/cm ² /year)	calcite-MAR (mg/cm ² /year)
15.25	1949.9	0.2	5.8	0.6	0.1	
15.75	1946.9	0.2	11.4	1.2	0.2	3.5
16.25	1943	0.1	7.7	0.8	0.1	2.0
16.75	1938.6	0.1	8.3	0.9	0.1	1.9
17.25	1933.6	0.1	3.0	0.3	0.0	0.7
17.75	1927.9	0.1	6.0	0.7	0.1	0.8
18.25	1920.7	0.1	3.5	0.4	0.1	0.4
18.75	1912.6	0.1	4.1	0.5	0.1	0.3
19.25	1902.6	0.0	2.0	0.3	0.0	0.0
19.75	1890.5	0.0	2.7	0.3	0.0	0.0
20.25	1863.5	0.0	0.7	0.1	0.0	0.0
20.75	1822.9	0.0	0.9	0.1	0.0	
21.25	1783.8	0.0	1.0	0.1	0.0	0.0
21.75	1742.8	0.0	0.8	0.1	0.0	0.0
22.25	1707	0.0	0.4	0.1	0.0	0.0
22.75	1672.5	0.0	0.4	0.1	0.0	0.0
23.25	1639.1	0.0	0.4	0.1	0.0	0.0
23.75	1603.3	0.0	0.4	0.1	0.0	0.0
24.25	1569.2	0.0	0.4	0.1	0.0	0.0
24.75	1530.4	0.0	0.3	0.1	0.0	0.0
25.25	1492.9	0.0	0.4	0.1	0.0	0.0
25.75	1451.7	0.0	0.2	0.1	0.0	0.0
26.25	1418.3	0.0	0.7	0.2	0.0	0.2
26.75	1389.7	0.0	0.5	0.1	0.0	0.2
27.25	1369.3	0.0	2.0	0.5	0.1	0.6
27.75	1360.4	0.1	1.4	0.4	0.0	0.3
28.25	1351.2	0.0	1.4	0.4	0.1	0.2
28.75	1341.1	0.0	1.6	0.4	0.0	0.1
29.25	1330.9	0.0	1.6	0.5	0.0	0.1
29.75	1320.2	0.0	1.4	0.4	0.0	0.1

Midpoint (cm)	Year (AD)	Accumulation rate (cm/year)	Sedimentation rate (mg/cm ² /year)	TOC-MAR (mg/cm ² /year)	TN-MAR (mg/cm ² /year)	calcite-MAR (mg/cm ² /year)
30.25	1311	0.1	2.0	0.7	0.1	0.0
30.75	1301	0.0	1.3	0.4	0.0	0.1
31.25	1292	0.0	1.7	0.6	0.1	0.1
31.75	1282	0.0	1.6	0.5	0.1	0.1
32.25	1273	0.1	1.5	0.5	0.1	0.3
32.75	1263	0.0	1.8	0.6	0.1	0.1
33.25	1254	0.0	1.6	0.5	0.1	0.2
33.75	1245	0.1	3.1	1.0	0.1	0.3
34.25	1236	0.0	1.8	0.6	0.1	0.1
34.75	1226	0.0	1.7	0.5	0.1	
35.25	1216	0.0	1.9			
35.75	1205	0.0	2.6	0.7	0.1	0.8
36.25	1194	0.0	2.4	0.6	0.1	0.8
36.75	1184	0.0	3.0	0.5	0.1	1.2
37.25	1174	0.0	3.1	0.5	0.1	1.8
37.75	1163	0.0	3.3	0.5	0.1	2.0
38.25	1153	0.0	3.0	0.5	0.1	1.2
38.75	1142	0.0	2.6	0.5	0.1	1.7
39.25	1132	0.0	2.9	0.5	0.1	1.6
39.75	1123	0.0	2.0	0.4	0.1	1.3
40.25	1113	0.0	2.7	0.6	0.1	0.9
40.75	1103	0.0	0.6	0.1	0.0	0.2
41.25	1094	0.1				

Table A.5 Minerology, magnetic susceptibility (MS) and grain size analysis of BL-G11-01 (Liu, 2016). Minerology was determined using powder x-ray diffraction (pXRD) and as a byproduct of isotope analysis.

Midpoint (cm)	Year AD	Determined via pXRD			Determined via pXRD			Grain size (μm)	MS (SI units)
		% Quartz	% Quartz	% Calcite	%Quartz*	% Calcite**	% Aragonite***		
0.25	2011	21	79	0					2
0.75	2011	18	82	0					1
1.25	2010	18	82	0	37	28	35	5.85	2
1.75	2008	16	84	0	32	29	38		0
2.25	2007	18	82	0	36	30	34		2
2.75	2005	18	82	0	34	29	36		1
3.25	2003	19	81	0	35	28	37		2
3.75	2002	18	82	0	38	29	33		2
4.25	2000	18	82	0	37	28	35		2
4.75	1997	18	82	0	31	27	42		2
5.25	1994								1
5.75	1993	17	83	0	39	27	34	5.3	1
6.25	1991	22	78	0	33	27	40		1
6.75	1986	17	83	0	35	26	39		1
7.25	1983	26	74	0	34	26	40		1
7.75	1981	23	77	0	33	24	43		2
8.25	1979	23	78		38	24	38		2
8.75	1978	25	75	0	35	25	41		2
9.25	1976	24	76	0	33	24	44		2
9.75	1973	23	77	0	31	24	45		2
10.25	1971	26	74	0	33	25	42		2
10.75	1969	25	75	0	30	24	46	5.2	2
11.25	1967	26	74	0	33	23	43		2
11.75	1965	27	73	0	33	23	44		2
12.25	1963	27	73	0	33	23	44		2
12.75	1961	25	75	0	36	22	43		2

*% Quartz is calculated by subtracting %calcite and %organics from 100 %.

**% Calcite was determined as a byproduct of isotope analysis. %

***% Organics was estimated by multiplying %TOC by 2 (see text).

Midpoint (cm)	Year AD	Determined via pXRD			Determined via pXRD			Grain size (μm)	MS (SI units)
		% Quartz	% Quartz	% Calcite	%Quartz*	% Calcite**	% Aragonite***		
13.25	1959	27	73	0	33	21	46		2
13.75	1957	30	70	0	30	20	49		3
14.25	1955	25	75	0	35	20	44		3
14.75	1952	25	75	0	31	21	49		3
15.25	1949.9	24	76	0					3
15.75	1946.9	31	69	0	31	21	48		4
16.25	1943	43	57	0	26	20	54		4
16.75	1938.6	34	66	0	23	22	55		4
17.25	1933.6	43	57	0	22	23	55	5.02	5
17.75	1927.9	48	52	0	13	24	63		5
18.25	1920.7	50	50	0	11	24	65		7
18.75	1912.6	62	38	0	7	24	59	4.05	7
19.25	1902.6	66	34	0	0	25	75		10
19.75	1890.5	75	25	0	1	26	73		7
20.25	1863.5	75	25	0	1	28	72	3.65	6
20.75	1822.9	73	27	0					9
21.25	1783.8	75	25	0	0	27	73		13
21.75	1742.8	71	29	0	0	27	73	3.56	5
22.25	1707	73	27	0	2	27	71		6
22.75	1672.5	70	30	0	2	28	70		3
23.25	1639.1	61	39	0	4	32	64	3.46	4
23.75	1603.3	49	51	0	3	40	57		1
24.25	1569.2	62	38	0	4	54	42	4.51	0
24.75	1530.4	35	65	0	4	61	36		0
25.25	1492.9	22	78	0	5	55	40	4.75	0
25.75	1451.7	21	79	0	18	51	31		0
26.25	1418.3	15	85	0	26	47	27		0
26.75	1389.7	10	90	0	29	46	25	3.49	0
27.25	1369.3	12	88	0	31	48	21		0
27.75	1360.4	16	84	0	18	51	31		0

*% Quartz is calculated by subtracting %calcite and %organics from 100 %.

**% Calcite was determined as a byproduct of isotope analysis. %

***% Organics was estimated by multiplying %TOC by 2 (see text).

Midpoint (cm)	Year AD	Determined via pXRD			Determined via pXRD			Grain size (μm)	MS (SI units)
		% Quartz	% Quartz	% Calcite	%Quartz*	% Calcite**	% Aragonite***		
28.25	1351.2	22	78	0	16	57	28		1
28.75	1341.1	25	75	0	8	57	34	5	0
29.25	1330.9	29	71	0	8	61	32		0
29.75	1320.2	34	66	0	4	63	33		0
30.25	1310.6	24	76	0	0	69	31		0
30.75	1301.1	24	76	0	6	67	28	8.66	0
31.25	1291.9	21	79	0	5	65	30		0
31.75	1282.1	13	80	7	7	62	31	6.85	0
32.25	1272.8	13	78	9	22	63	15		0
32.75	1263.1	14	86	0	8	63	29		0
33.25	1253.6	17	75	8	10	62	27		0
33.75	1245.5	14	76	10	11	62	27	6.48	0
34.25	1236.2	9	84	7	8	62	30		0
34.75	1226	9	91	0				6.72	0
35.25	1215.9	8	84	8					0
35.75	1205	10	80	10	32	52	16	6.08	0
36.25	1194.5	5	87	8	36	48	17		0
36.75	1183.7	0	96	4	41	36	23		0
37.25	1173.6	0	98	2	57	31	12	3.51	0
37.75	1163	0	98	2	61	31	9		0
38.25	1152.8	0	96	4	41	34	25		0
38.75	1142.5	3	97	0	64	35	1	3.74	0
39.25	1132.4	0	94	6	56	36	8		0
39.75	1122.7	0	93	7	63	37	0		0
40.25	1113.2	0	93	7	34	46	19	4.91	0
40.75	1103.4	4	89	7	32	47	21	4.03	0
41.25	1094.1	0	93	7	58	42	0		0

*% Quartz is calculated by subtracting %calcite and %organics from 100 %.

**% Calcite was determined as a biproduct of isotope analysis. %

***% Organics was estimated by multiplying %TOC by 2 (see text).

Table A.6 Values of $\delta^{13}\text{C}_{\text{marl}}$ and $\delta^{18}\text{O}_{\text{marl}}$ of shelly fauna from BL-G11-01. From Liu (2016).

Mid-point (cm)	Year AD	$\delta^{13}\text{C}_{\text{Helisoma}}$ ‰, VPDB	No. of rep- licates	SD of replicates ‰, VPDB	$\delta^{13}\text{C}_{\text{Pisidium}}$ ‰, VPDB	No. of rep- licates	SD of replicates ‰, VPDB	$\delta^{18}\text{O}_{\text{Helisoma}}$ ‰, VSMOW	No. of rep- licates	SD of replicates ‰, VSMOW	$\delta^{18}\text{O}_{\text{Pisidium}}$ ‰, VSMOW	No. of rep- licates	SD of replicates ‰, VSMOW
31.75	1282	-3.1	1	2.5				+22.7	1	0.4			
32.25	1273	-1.0	1	0.1				+23.4	1	0.6			
32.75	1263	-1.0	1	0.4				+25.6	1	0.2			
33.25	1254	-1.4	1	0.8				+23.2	1	0.1			
33.75	1245	-1.7	1	0.8	+1.9	2	0.3	+23.1	1	1.0	+23.7	2	0.4
34.25	1236	-3.2	1	1.2				+23.5	1	0.8			
34.75	1226	-2.8	1	0.1	-1.5	1	1.3	+23.7	1	0.1	+24.3	1	0.6
35.25	1216	-2.4	1	1.3	-0.1	1	0.1	+22.8	1	0.1	+25.7	1	1.7
35.75	1205	-2.6	1	0.3	-2.1	1	0.6	+23.2	1	0.1	+23.9	1	0.1
36.25	1194	-2.8	1	0.8	-2.8	1	0.4	+23.9	1	0.6	+23.4	1	1.1
36.75	1184	-1.1	2	0.5	-2.0	2	1.3	+24.2	2	0.7	+24.8	2	0.5
37.25	1174	-2.9	1	0.2	-1.5	1	0.2	+22.6	1	1.1	+23.0	1	0.1
37.75	1163	-0.9	1	0.1	-0.5	1	0.3	+23.1	1	0.0	+25.1	1	0.5
38.25	1153	-1.7	2	0.6	-2.0	1	1	+23.2	2	1.0	+23.4	1	0.9
38.75	1142	-4.1	1	0.1	-1.4	2	0.6	+24.4	1	0.2	+23.4	2	0.8
39.25	1132	-2.1	1	1.3	-0.9	1	1.1	+23.3	1	0.6	+24.6	1	0.6
39.75	1123	-2.4	1	2.3	-1.4	2	0.6	+23.1	1	0.2	+23.2	2	0.6
40.25	1113	-2.4	2	1.3	-0.5	1	1.3	+22.8	2	0.3	+23.0	1	1.1
40.75	1103	-2.9	1	0.2	+0.2	1	2	+22.9	1	0.6	+23.1	1	1.0
41.25	1094	-0.3	1	0.1	-0.4	1	1.7	+23.4	1	0.4	+23.1	1	2.3

Table A.7 Values of $\delta^{13}\text{C}_{\text{TOC}}$, $\delta^{15}\text{N}_{\text{TN}}$, %TOC, %TN and TOC:TN from BL-G17-01.

Midpoint (cm)	Year AD	$\delta^{13}\text{C}_{\text{TOC}}^*$ ‰, VPDB	$\delta^{13}\text{C}_{\text{TOC}}$ ‰, VPDB	No. of replicates	SD of replicates ‰, VPDB	$\delta^{15}\text{N}_{\text{TN}}$ ‰, AIR	No. of replicates	SD of replicates ‰, AIR	TOC %	No. of replicates	SD TOC %	TN %	No. of replicates	SD of replicates %	TOC:TN
0.25	2016	-29.7	-32.1			+1.5			20			2.6			9.0
0.75	2013	-29.9	-32.1			+1.2			20			2.5			9.4
1.25	2011	-30.0	-32.2			+0.9			19			2.3			9.7
1.75	2010	-30.2	-32.3			+0.9			19			2.4			9.3
2.25	2009	-30.2	-32.3			+1.0			19			2.3			9.7
2.75	2007	-30.2	-32.2			+1.1			18			2.3			9.2
3.25	2005	-30.1	-32.0			+0.9			19			2.2			10.1
3.75	2004	-30.3	-32.1			+0.9			19			2.1			10.6
4.25	2002	-30.1	-31.9	1	0.05	+0.9			18	1	0.30	2.1			10.1
4.75	2000	-30.0	-31.7			+0.9			13			2.1			7.3
5.25	1998	-30.0	-31.7			+0.9			13			1.9			8.0
5.75	1996	-29.9	-31.5			+1.0			12			2			7.0
6.25	1993	-30.0	-31.5			+0.7			12			1.9			7.4
6.75	1991	-29.9	-31.4			+1.0			12			1.9			7.4
7.25	1988	-30.1	-31.5			+1.0			12			1.8			7.8
7.75	1984	-30.1	-31.4			+0.9			12			1.9			7.4
8.25	1982	-30.2	-31.4			+0.8			12			1.7			8.3
8.75	1980	-30.1	-31.3	1	0.04	+1.0	1	0.10	12	1	0.11	1.8	1	0.00	7.8
9.25	1979	-29.8	-30.9			+0.9	1	0.10	12			1.8	1	0.12	7.8
9.75	1977	-30.0	-31.1			+1.1			12			1.8			7.8
10.25	1974	-30.1	-31.1			+1.0			12			1.7			8.3
10.75	1972	-30.2	-31.2			+1.1			12			1.8			7.8
11.25	1969	-30.2	-31.1			+0.9			12			1.7			8.3
11.75	1967	-30.2	-31.1			+1.1			12			1.8			7.8
12.25	1965	-30.2	-31.0			+0.9			12			1.7			8.3
12.75	1963	-30.4	-31.2			+1.0			13			1.9			8.0
13.25	1962	-26.9	-27.7	1	0.06	+0.8			13	1	0.51	1.9			8.0
13.75	1960	-30.4	-31.1			+1.0			11			1.9			6.8
14.25	1958	-30.5	-31.2			+0.7			15			1.9			9.3
14.75	1955	-30.6	-31.3			+0.8			10			2			5.9

*Corrected for the Suess Effect according to Verburg (2007).

Mid-point (cm)	Year AD	$\delta^{13}\text{C}_{\text{TOC}}^*$ ‰, VPDB	$\delta^{13}\text{C}_{\text{TOC}}$ ‰, VPDB	No. of rep- licates	SD of rep- licates ‰, VPDB	$\delta^{15}\text{N}_{\text{TN}}$ ‰, AIR	No. of replicates	SD of rep- licates ‰, AIR	TOC %	No. of rep-licates	SD TOC %	TN %	No. of rep- licates	SD of rep- licates %	TOC:TN
15.25	1953	-30.5	-31.2			+0.5			17			1.9			10.5
15.75	1951	-30.7	-31.3			+0.6			10			2			5.9
16.25	1948	-30.7	-31.3			+0.4			15			2			8.8
16.75	1945	-30.7	-31.3			+0.4			15			2.1			8.4
17.25	1941	-30.8	-31.3			+0.0			15			2			8.8
17.75	1936	-30.8	-31.3			-0.5	1	0.02	17			2.3	1	0.02	8.7
18.25	1931	-30.1	-30.5			-1.1	1	0.17	21			2.7	1	0.02	9.1
18.75	1924	-29.5	-29.9			-1.0			27			2.9			10.9
19.25	1917	-28.8	-29.2			-1.2			31			3.1			11.7
19.75	1909	-28.9	-29.2			-1.0			30			3.3			10.7
20.25	1898	-28.8	-29.1			-1.3			32			3.3			11.4
20.75	1883	-28.7	-28.9			-1.1			32			3.5			10.7
21.25	1851	-28.7	-28.9			-1.4			28			3.5			9.4
21.75	1803	-29.1	-29.2			-1.6			33			3.6			10.8
22.25	1760	-29.3	-29.3			-1.9			36			3.9			10.8
22.75	1725	-29.1	-29.0			-2.0			37			4.2			10.3
23.25	1689	-28.3	-28.3			-2.3			41			4.3			11.2
23.75	1648	-26.6	-26.6			-1.8			39			4.3			10.6
24.25	1611	-25.3	-25.3			-1.6			26			4.1			7.4
24.75	1572	-25.4	-25.4			-1.4			39			4			11.4
25.25	1536	-25.9	-25.9			-1.5			35			3.7			11.1
25.75	1498	-26.4	-26.4			-1.2			40			3.4			13.8
26.25	1463	-25.3	-25.3	1	0.10	-1.4			27	1	1.5	2.9			10.9
26.75	1426	-25.8	-25.8			-1.2	1	0.01	30			2.8	1	0.01	12.6
27.25	1397														
27.75	1376	-26.2	-26.2						26						
28.25	1362	-26.2	-26.2			-1.4	1	0.05	24			2.2	1	0.01	12.8
28.75	1352	-27.0	-27.0	1	0.40	-1.2			22	1	0.6	2.2			11.7
29.25	1344	-26.0	-26.0			-1.4			21			2.1			11.7
29.75	1334														
30.25	1325	-26.1	-26.1			-1.4			19			1.9			11.7

*Corrected for the Suess Effect according to Verburg (2007).

Midpoint (cm)	Year AD	$\delta^{13}\text{C}_{\text{TOC}}^*$ ‰, VPDB	$\delta^{13}\text{C}_{\text{TOC}}$ ‰, VPDB	No. of replicates	SD of replicates ‰, VPDB	$\delta^{15}\text{N}_{\text{TN}}$ ‰, AIR	No. of replicates	SD of replicates ‰, AIR	TOC %	No. of replicates	SD TOC %	TN %	No. of replicates	SD of replicates %	TOC:TN
30.75	1315	-26.1	-26.1			-1.0			20			2.0			11.7
31.25	1305	-26.3	-26.3			-1.3			22			2.0			12.9
31.75	1295	-26.5	-26.5			-1.1			21			2.2			11.2
32.25	1286	-27.0	-27.0			-1.3			25			2.4			12.2
32.75	1276	-27.9	-27.9			-1.2			31			3.4			10.7
33.25	1267	-28.4	-28.4			-1.5			40			4.1			11.5
33.75	1258	-27.7	-27.7			-1.2			39			4.4			10.4
34.25	1250	-27.8	-27.8			-1.2			37			3.8			11.4
34.75	1241	-28.5	-28.5			-1.3			30			3.2			11.0
35.25	1232	-29.0	-29.0	1	0.14	-1.4			26	1	0.56	2.6			11.7
35.75	1222	-29.0	-29.0			-1.4	1	0.04	22			2.3	1	0.05	11.2
36.25	1212	-29.1	-29.1			-1.5			19			2.1			10.6
36.75	1202	-29.1	-29.1			-1.8			18			1.8			11.7
37.25	1191	-26.9	-26.9			-1.7			20			2.0			11.7
37.75	1181	-27.4	-27.4	1	0.03	-1.9			18	1	0.12	1.8			11.7
38.25	1171	-26.7	-26.7			-2.0			19			1.8			12.4
38.75	1161	-27.6	-27.6			-1.9			16			1.7			11.0
39.25	1151	-26.6	-26.6			-1.6			20			1.9			12.4
39.75	1140	-26.2	-26.2			-1.7			20			1.9			12.4
40.25	1129	-25.8	-25.8			-1.7	1	0.02	17			1.7	1	0.09	11.7
40.75	1119	-26.9	-26.9			-1.6			17			1.7			11.7
41.25	1109	-27.7	-27.7			-1.8			20			1.9			12.4
41.75	1104	-28.1	-28.1			-1.8			20			2.0			11.7
42.25	1100	-28.1	-28.1			-1.7			20			2.0			11.7

*Corrected for the Suess Effect according to Verburg (2007).

Table A.8 Mass accumulation rates and TOC:TN from BL-G17-01.

Midpoint (cm)	Year (AD)	Accumulation rate (cm/year)	Sedimentation rate (mg/cm ² /year)	TOC-MAR (mg/cm ² /year)	TN-MAR (mg/cm ² /year)	Calcite-MAR (mg/cm ² /year)	Chl- <i>a</i> _(s) -MAR (mg/m ² /year)
0.25	2016	0.2	4.4	0.9	0.1	0.6	3.5
0.75	2013	0.2	4.7	0.9	0.1	0.6	3.8
1.25	2011	0.6	18.2	3.4	0.4	2.8	15.3
1.75	2010	0.5	14.8	2.8	0.4	3.2	12.0
2.25	2009	0.3	24.5	4.7	0.6	5.0	19.8
2.75	2007	0.3	11.1	2.0	0.3	2.4	9.2
3.25	2005	0.3	9.1	1.7	0.2	1.4	7.6
3.75	2004	0.3	8.9	1.7	0.2	2.1	7.3
4.25	2002	0.2	10.1	1.8	0.2		8.3
4.75	2000	0.3	11.0	1.4	0.2		8.1
5.25	1998	0.2	9.7	1.3	0.2		7.0
5.75	1996	0.2	7.9	0.9	0.2	1.6	5.7
6.25	1993	0.2	8.1	1.0	0.1	1.9	5.8
6.75	1991	0.2	9.2	1.1	0.2	1.8	6.2
7.25	1988	0.1	5.5	0.6	0.1	0.8	3.5
7.75	1984	0.1	5.7	0.7	0.1	1.3	3.7
8.25	1982	0.5	29.6	3.5	0.5	6.1	18.4
8.75	1980	0.5	26.8	3.2	0.5	4.7	16.1
9.25	1979	0.2	12.3	1.5	0.2	1.9	7.2
9.75	1977	0.2	12.5	1.5	0.2	2.3	6.7
10.25	1974	0.2	8.1	1.0	0.1	1.1	4.4
10.75	1972	0.2	8.8	1.0	0.2	1.6	4.7
11.25	1969	0.3	14.4	1.7	0.2	1.8	7.8
11.75	1967	0.2	13.1	1.6	0.2	2.0	7.1
12.25	1965	0.2	13.3	1.6	0.2	1.5	7.3
12.75	1963	0.3	14.5	1.9	0.3	1.5	8.2
13.25	1962	0.3	14.6	1.9	0.3	0.7	8.4
13.75	1960	0.2	12.1	1.3	0.2	0.7	6.7
14.25	1958	0.2	10.3	1.5	0.2	0.6	5.7
14.75	1955	0.2	11.5	1.1	0.2	0.4	6.7

Midpoint (cm)	Year (AD)	Accumulation rate (cm/year)	Sedimentation rate (mg/cm ² /year)	TOC-MAR (mg/cm ² /year)	TN-MAR (mg/cm ² /year)	Calcite-MAR (mg/cm ² /year)	Chl- <i>a</i> _(s) -MAR (mg/m ² /year)
15.25	1953	0.3	10.0	1.7	0.2	0.2	5.6
15.75	1951	0.2	10.6	1.1	0.2	0.2	6.2
16.25	1948	0.2	7.0	1.0	0.1		4.0
16.75	1945	0.2	7.7	1.2	0.2		4.5
17.25	1941	0.1	4.4	0.7	0.1		2.6
17.75	1936	0.1	4.7	0.8	0.1	0.1	3.3
18.25	1931	0.1	2.8	0.6	0.1	0.1	2.4
18.75	1924	0.1	2.7	0.7	0.1	0.2	2.5
19.25	1917	0.1	1.6	0.5	0.0	0.1	1.5
19.75	1909	0.1	1.9	0.6	0.1	0.1	1.8
20.25	1898	0.0	1.0	0.3	0.0	0.0	1.1
20.75	1883	0.0	0.9	0.3	0.0	0.0	0.9
21.25	1851	0.0	0.3	0.1	0.0	0.0	0.3
21.75	1803	0.0	0.3	0.1	0.0	0.0	0.4
22.25	1760	0.0	0.4	0.1	0.0	0.0	0.5
22.75	1725	0.0	0.4	0.1	0.0	0.0	0.6
23.25	1689	0.0	0.3	0.1	0.0		0.6
23.75	1648	0.0	0.3	0.1	0.0	0.0	0.5
24.25	1611	0.0	0.2	0.1	0.0		0.3
24.75	1572	0.0	0.3	0.1	0.0	0.0	0.4
25.25	1536	0.0	0.3	0.1	0.0	0.0	0.4
25.75	1498	0.0	0.3	0.1	0.0		0.4
26.25	1463	0.0	0.4	0.1	0.0	0.1	0.5
26.75	1426	0.0	0.4	0.1	0.0	0.1	
27.25	1397	0.0					
27.75	1376	0.0	0.7	0.2		0.2	0.8
28.25	1362	0.0	1.9	0.4	0.0	0.7	1.8
28.75	1352	0.0	2.0	0.4	0.0		2.2
29.25	1344	0.0	1.9	0.4	0.0	0.5	1.8
29.75	1334	0.0					
30.25	1325	0.0	1.7	0.3	0.0	0.6	1.7
30.75	1315	0.0	1.8	0.4	0.0		1.8

Midpoint (cm)	Year (AD)	Accumulation rate (cm/year)	Sedimentation rate (mg/cm ² /year)	TOC-MAR (mg/cm ² /year)	TN-MAR (mg/cm ² /year)	Calcite-MAR (mg/cm ² /year)	Chl- <i>a</i> _(s) -MAR (mg/m ² /year)
31.25	1305	0.0	1.8	0.4	0.0	0.7	1.8
31.75	1295	0.0	2.0	0.4	0.0		1.9
32.25	1286	0.1	2.6	0.6	0.1	0.7	2.2
32.75	1276	0.0	1.6	0.5	0.1	0.3	1.6
33.25	1267	0.0	1.3	0.5	0.1	0.0	1.7
33.75	1258	0.1	1.6	0.6	0.1		1.9
34.25	1250	0.0	1.2	0.4	0.0	0.1	1.1
34.75	1241	0.1	2.2	0.7	0.1	0.6	1.3
35.25	1232	0.0	1.9	0.5	0.0	0.4	1.1
35.75	1222	0.0	2.1	0.5	0.0	0.9	1.2
36.25	1212	0.0	2.4	0.5	0.1	1.0	1.5
36.75	1202	0.0	2.8	0.5	0.1	1.7	2.4
37.25	1191	0.0	3.0	0.6	0.1		3.0
37.75	1181	0.0	2.5	0.5	0.0	1.3	1.8
38.25	1171	0.0	3.1	0.6	0.1	1.0	2.8
38.75	1161	0.0	2.5	0.4	0.0	1.3	2.3
39.25	1151	0.0	1.8	0.4	0.0	0.6	1.6
39.75	1140	0.0	2.6	0.5	0.1	1.4	2.8
40.25	1129	0.0	2.5	0.4	0.0	1.0	2.1
40.75	1119	0.0	3.0	0.5	0.1	1.6	2.8
41.25	1109	0.0	1.9	0.4	0.0	0.8	1.8
41.75	1104	0.0	3.2	0.6	0.1		3.0
42.25	1100	0.1	0.5	0.1	0.0		0.4

Table A.9 Values of $\delta^{13}\text{C}_{\text{marl}}$, $\delta^{18}\text{O}_{\text{marl}}$ and %calcite from BL-G17-01.

Midpoint cm	Year AD	$\delta^{13}\text{C}_{\text{marl}}$ * ‰, VPDB	$\delta^{13}\text{C}_{\text{marl}}$ ‰, VPDB	No. of replicates	SD of replicates ‰, VPDB	$\delta^{18}\text{O}_{\text{marl}}$ ‰, VSMOW	No. of replicates	SD of replicates ‰, AIR
0.25	2016	+1.6	-0.8			+21.0		
0.75	2013	+1.9	-0.4			+21.3		
1.25	2011	+1.7	-0.5			+21.0		
1.75	2010	+1.6	-0.5			+21.3		
2.25	2009	+1.6	-0.5			+21.3		
2.75	2007	+1.5	-0.5			+21.3		
3.25	2005	+1.6	-0.4			+21.1		
3.75	2004	+1.5	-0.4			+21.2		
4.25	2002	+1.5	-0.3			+21.3		
4.75	2000	+1.5	-0.2			+21.3		
5.25	1998	+1.4	-0.3			+20.8		
5.75	1996	+1.4	-0.2	1	0.00	+21.2	1	0.00
6.25	1993	+1.3	-0.2			+21.3		
6.75	1991	+1.3	-0.1			+21.2		
7.25	1988	+1.2	-0.2			+21.2		
7.75	1984	+1.0	-0.2			+21.4		
8.25	1982	+1.2	-0.0			+21.3		
8.75	1980	+1.1	-0.1			+21.3		
9.25	1979	+0.9	-0.2			+21.2		
9.75	1977							
10.25	1974	+0.8	-0.2	1	0.02	+21.0	1	0.02
10.75	1972	+0.8	-0.2	1	0.04	+21.2	1	0.05
11.25	1969	+0.5	-0.4			+21.0		
11.75	1967	+0.7	-0.2			+21.2		
12.25	1965	+0.4	-0.4			+21.2		
12.75	1963	+0.4	-0.4			+21.1		
13.25	1962	+0.1	-0.7			+20.8		
13.75	1960	+0.1	-0.7			+21.1		
14.25	1958	-0.1	-0.8			+21.1		
14.75	1955	-0.5	-1.2			+20.8		

*Corrected for the Suess Effect according to Verburg (2007).

Midpoint cm	Year AD	$\delta^{13}\text{C}_{\text{marl}}^*$ ‰, VPDB	$\delta^{13}\text{C}_{\text{marl}}$ ‰, VPDB	No. of replicates	SD of replicates ‰, VPDB	$\delta^{18}\text{O}_{\text{marl}}$ ‰, VSMOW	No. of replicates	SD of replicates ‰, AIR
15.25	1953	-0.8	-1.5	1	0.34	+20.7	1	0.33
15.75	1951	-1.2	-1.8			+20.6		
16.25	1948							
16.75	1945	-1.2	-1.8			+20.9		
17.25	1941							
17.75	1936	-1.8	-2.3			+21.4		
18.25	1931	-1.6	-2.1	1	0.20	+21.1	1	0.10
18.75	1924	-1.0	-1.4			+21.5		
19.25	1917	-0.9	-1.3	1	0.02	+21.9	1	1.13
19.75	1909	-0.7	-1.0			+21.8		
20.25	1898	-0.8	-1.1			+20.6		
20.75	1883	-1.3	-1.6			+20.6		
21.25	1851	-1.4	-1.6			+20.0		
21.75	1803							
22.25	1760	-2.5	-2.5			+19.9		
22.75	1725	-4.4	-4.4			+19.2		
23.25	1689							
23.75	1648	-3.5	-3.5			+18.9		
24.25	1611							
24.75	1572	+0.8	+0.8			+21.9		
25.25	1536	+2.7	+2.7			+22.1		
25.75	1498							
26.25	1463	+3.7	+3.7			+22.6		
26.75	1426	+4.1	+4.1			+23.7		
27.25	1397							
27.75	1376	+4.4	+4.4			+23.4		
28.25	1362	+4.5	+4.5			+24.0		
28.75	1352							
29.25	1344	+4.6	+4.6			+23.2		
29.75	1334							
30.25	1325	+5.0	+5.0	1	0.27	+23.4	1	0.14
30.75	1315							

*Corrected for the Suess Effect according to Verburg (2007).

Midpoint cm	Year AD	$\delta^{13}\text{C}_{\text{marl}}^*$ ‰, VPDB	$\delta^{13}\text{C}_{\text{marl}}$ ‰, VPDB	No. of replicates	SD of replicates ‰, VPDB	$\delta^{18}\text{O}_{\text{marl}}$ ‰, VSMOW	No. of replicates	SD of replicates ‰, AIR
31.25	1305	+5.1	+5.1			+23.4		
31.75	1295							
32.25	1286	+4.9	+4.9			+23.3		
32.75	1276	+4.1	+4.1			+23.9		
33.25	1267	+1.2	+1.2			+23.0		
33.75	1258							
34.25	1250	-3.5	-3.5	1	0.02	+21.0	1	0.04
34.75	1241	-3.2	-3.2			+21.8		
35.25	1232	-2.7	-2.7	1	0.11	+21.2	1	0.59
35.75	1222	-2.4	-2.4			+22.3		
36.25	1212	-2.5	-2.5			+21.1		
36.75	1202	-1.8	-1.8			+21.6		
37.25	1191	+1.1	+1.1			+21.8		
37.75	1181	+1.6	+1.6			+21.9		
38.25	1171	+0.6	+0.6			+21.1		
38.75	1161	+1.0	+1.0	1	0.22	+22.2	1	0.05
39.25	1151	+2.3	+2.3			+22.9		
39.75	1140	+2.9	+2.9			+23.8		
40.25	1129	+3.8	+3.8	1	0.19	+23.9	1	0.08
40.75	1119	+3.8	+3.8			+23.6		
41.25	1109	+3.5	+3.5			+23.2		
41.75	1104							
42.25	1100	+2.7	+2.7			+23.3		

*Corrected for the Suess Effect according to Verburg (2007).

Table A.10 Minerology, magnetic susceptibility (MS) and grain size analysis of BL-G11-01 (Liu, 2016). Minerology was determined using powder x-ray diffraction (pXRD) and as a byproduct of isotope analysis.

Midpoint (cm)	Year AD	Determined via pXRD			Determined via pXRD			MS (SI units)	Chl- <i>a</i> (s) (mg/g)
		% Quartz	% Quartz	% Calcite	%Quartz*	% Calcite**	% Aragonite***		
0.25	2016				46	14	40	0.0	0.03951
0.75	2013				47	13	40	-0.3	0.040884
1.25	2011				46	16	38	0.3	0.042561
1.75	2010				40	22	38	0.0	0.041059
2.25	2009				42	20	38	0.3	0.040953
2.75	2007				42	22	36	-0.7	0.042031
3.25	2005				46	16	38	1.0	0.042118
3.75	2004				38	24	38	1.0	0.041812
4.25	2002						36	-0.3	0.041527
4.75	2000						26	0.0	0.037457
5.25	1998						26	0.0	0.036674
5.75	1996				56	20	24	0.0	0.036343
6.25	1993				53	23	24	0.0	0.03635
6.75	1991				57	19	24	0.0	0.034065
7.25	1988				62	14	24	0.0	0.032846
7.75	1984				54	22	24	-0.3	0.032408
8.25	1982				55	21	24	0.0	0.031551
8.75	1980				59	17	24	0.0	0.03052
9.25	1979				60	16	24	0.0	0.029731
9.75	1977				58	18	24	1.0	0.027116
10.25	1974				63	13	24	0.0	0.02742
10.75	1972				58	18	24	-0.3	0.027437
11.25	1969				64	12	24	0.0	0.027807
11.75	1967				60	16	24	0.3	0.027759
12.25	1965				64	12	24	0.7	0.027859
12.75	1963				64	10	26	1.0	0.028675
13.25	1962				69	5	26	0.7	0.029239
13.75	1960				72	6	22	0.0	0.028457
14.25	1958				64	6	30	0.0	0.027998

*% Quartz is calculated by subtracting %calcite and %organics from 100 %.

**% Calcite was determined as a byproduct of isotope analysis. %

***% Organics was estimated by multiplying %TOC by 2 (see text).

Midpoint (cm)	Year AD	Determined via pXRD			Determined via pXRD			MS (SI units)	Chl- $\alpha_{(s)}$ (mg/g)
		% Quartz	% Quartz	(SI units)	(mg/g)	% Calcite**	% Aragonite***		
14.75	1955				77	3	20	0.3	0.029851
15.25	1953	71	23	6	64	2	34	0.0	0.028732
15.75	1951				78	2	20	0.7	0.02987
16.25	1948						30	0.0	0.029269
16.75	1945						30	0.0	0.029368
17.25	1941						30	-0.3	0.030767
17.75	1936				64	2	34	0.0	0.036336
18.25	1931				55	3	42	-0.7	0.04452
18.75	1924				40	6	54	-0.7	0.04694
19.25	1917				34	4	62	0.0	0.048725
19.75	1909				33	7	60	-0.7	0.04869
20.25	1898				33	3	64	-1.3	0.052766
20.75	1883				31	5	64	-1.0	0.049396
21.25	1851				40	4	56	-1.0	0.048154
21.75	1803						66	-1.0	0.053733
22.25	1760				25	3	72	-0.3	0.063332
22.75	1725				23	3	74	-0.3	0.074877
23.25	1689	38	61	0			82	-0.7	0.095904
23.75	1648				20	2	78	-1.0	0.087279
24.25	1611						52	-0.7	0.074339
24.75	1572				18	4	78	-0.7	0.069162
25.25	1536				22	8	70	0.0	0.063701
25.75	1498						80	0.0	0.0597
26.25	1463				24	22	54	-0.7	0.058436
26.75	1426				11	29	60	-0.7	
27.25	1397							0.0	
27.75	1376				18	30	52		0.054262
28.25	1362				16	36	48	0.0	0.047904
28.75	1352						44	-1.3	0.055216
29.25	1344				31	27	42	0.0	0.047389

*% Quartz is calculated by subtracting %calcite and %organics from 100 %.

**% Calcite was determined as a biproduct of isotope analysis. %

***% Organics was estimated by multiplying %TOC by 2 (see text).

Midpoint (cm)	Year AD	Determined via pXRD			Determined via pXRD			MS (SI units)	Chl- $a_{(s)}$ (mg/g)
		% Quartz	% Quartz	(SI units)	(mg/g)	% Calcite**	% Aragonite***		
29.75	1334								0.036357
30.25	1325				28	34	38	-2.0	0.051612
30.75	1315						40	-2.3	0.050063
31.25	1305				20	36	44	-2.7	0.049243
31.75	1295						42	-3.0	0.048419
32.25	1286				23	27	50	-3.0	0.044036
32.75	1276				19	19	62	-1.0	0.05178
33.25	1267	28	72	0	17	3	80	-0.3	0.064222
33.75	1258						78	-1.0	0.059592
34.25	1250				17	9	74	-1.0	0.045115
34.75	1241				15	25	60	-2.0	0.030042
35.25	1232				25	23	52	-1.0	0.030488
35.75	1222				12	44	44	-1.7	0.030192
36.25	1212				22	40	38	-1.7	0.032144
36.75	1202				2	62	36	-1.7	0.043528
37.25	1191						40	-2.0	0.050213
37.75	1181				12	52	36	-1.0	0.036858
38.25	1171				29	33	38	-1.0	0.044866
38.75	1161				14	54	32	-1.0	0.047568
39.25	1151				25	35	40	-1.7	0.04524
39.75	1140				8	52	40	-1.7	0.053811
40.25	1129				26	40	34	-1.3	0.041849
40.75	1119				15	51	34	-1.7	0.046039
41.25	1109				20	40	40	-1.3	0.047279
41.75	1104						40	-1.7	0.046365
42.25	1100						40	-1.3	0.044309

*% Quartz is calculated by subtracting %calcite and %organics from 100 %.

**% Calcite was determined as a biproduct of isotope analysis. %

***% Organics was estimated by multiplying %TOC by 2 (see text)

Table A.11 Mass accumulation rates of odd-chain *n*-alkanes extracted from BI-G16-01.

Midpoint (cm)	Year (AD)	C ₁₇ -MAR (µg/m ² /year)	C ₁₉ -MAR (µg/m ² /year)	C ₂₁ -MAR (µg/m ² /year)	C ₂₃ -MAR (µg/m ² /year)	C ₂₅ -MAR (µg/m ² /year)	C ₂₇ -MAR (µg/m ² /year)	C ₂₉ -MAR (µg/m ² /year)	C ₃₁ -MAR (µg/m ² /year)
3	2005	404	20	21	41	65	57	57	28
8	1981	537	33	29	54	81	67	74	36
13	1960	293	27	25	49	58	51	44	12
18	1919	438	25	22	32	33	32	32	19
23	1799	84	6	6	9	9	8	9	4
28	1599	14	2	2	3	3	3	3	1
33	1392	247	96	44	54	45	41	32	11
38	1219	23	7	11	21	33	29	28	11
43	1112	43	9	17	12	18	24	29	14
48	1013	33	6	9	4	6	7	11	4
53	929	18	8	18	10	12	15	16	8

Table A.12 Mass accumulation rates of even-chain *n*-alkanes, diploptene and lupan-3-one extracted from BI-G16-01.

Midpoint (cm)	Year (AD)	C ₁₈ (µg/m ² /year)	C ₂₂ (µg/m ² /year)	C ₂₄ (µg/m ² /year)	C ₂₆ (µg/m ² /year)	C ₂₈ (µg/m ² /year)	C ₃₀ (µg/m ² /year)	Diploptene (µg/m ² /year)	Lupan-3-one (µg/m ² /year)
3	2005	14	14	13	15	19	4	8	4
8	1981	21	21	15	20	17	4	23	8
13	1960	13	17	14	15	8	4	18	7
18	1919	12	10	8	11	9	2	21	4
23	1799	6	4	4	4	1	1	11	1
28	1599	1	1	1	1	0	0	4	0
33	1392	53	27	16	17	0	0	28	10
38	1219	1	7	7	12	4	2	16	2
43	1112	10	4	4	17	7	1	36	7
48	1013	0	2	1	7	1	1	12	3
53	929	5	3	3	14	3	0	77	8

Table A.13 Hydrogen isotope ratios of C₁₇ from BL-G16-01.

Midpoint (cm)	$\delta^2\text{H}_{\text{C}_{17}}$	Number of replicates	SD of replicates
3	-55	4	1.8
8	-42	3	6.0
13	-53	3	1.4
18	-37	3	2.1
23			
28	-51	3	1.4
33	-22	2	7.1
38	-27	3	3.5
43	-15	3	2.3
48	-31	3	5.2
53	-27	1	N/A

Table A.14 Carbon isotope ratios of C₁₇ and C₁₉ from BL-G16-01.

Midpoint (cm)	Year (AD)	$\delta^{13}\text{C}_{\text{C}_{17}}$ (‰, VPDB)	$\delta^{13}\text{C}_{\text{C}_{17}^*}$ (‰, VPDB)	No. of replicates	SD of replicates (‰, VPDB)	$\delta^{13}\text{C}_{\text{C}_{19}}$ (‰, VPDB)	$\delta^{13}\text{C}_{\text{C}_{19}^*}$ (‰, VPDB)	No. of replicates	SD of replicates (‰, VPDB)
3	2005	-32.3	-30.2	3	0.05				
8	1981	-30.8	-29.4	2	0.02				
13	1960	-31.7	-30.9	2	0.04	-29.8	-29.0	2	-29.0
18	1919	-31.2	-30.7	2	0.20	-29.2	-28.7	4	-28.7
23	1799	-31.8	-31.8	2	0.12				
28	1599	-31.1	-31.1	2	0.06				
33	1392	-29.5	-29.5	2	0.27	-30.1	-30.1	2	-30.1
38	1219	-31.0	-31.0	2	0.22	-29.6	-29.6	3	-29.6
43	1112					-28.9	-28.9	2	-28.9
48	1013	-31.4	-31.4	2	0.09	-29.2	-29.2	2	-29.2
53	929								

*Corrected for the Suess Effect according to Verburg (2007).

Table A.15 Carbon isotope ratios of C₂₁ and C₂₃ from BL-G16-01.

Midpoint (cm)	Year (AD)	$\delta^{13}\text{C}_{\text{C}21}$ (‰, VPDB)	$\delta^{13}\text{C}_{\text{C}21}^*$ (‰, VPDB)	No. of replicates	SD of replicates (‰, VPDB)	$\delta^{13}\text{C}_{\text{C}23}$ (‰, VPDB)	$\delta^{13}\text{C}_{\text{C}23}^*$ (‰, VPDB)	No. of replicates	SD of replicates (‰, VPDB)
3	2005					-31.1	-29.1	2	
8	1981	-29.7	-28.3	2	0.16	-29.3	-28.0	2	0.09
13	1960	-30.4	-29.5	2	0.00				0.11
18	1919	-30.2	-29.7	3	0.06	-32.0	-31.5	4	
23	1799								0.27
28	1599	-28.1	-28.1	2	0.13				
33	1392					-29.9	-29.9	2	
38	1219								0.28
43	1112								
48	1013					-29.3	-29.3	2	
53	929								0.28

*Corrected for the Suess Effect according to Verburg (2007).

Table A.16 Carbon isotope ratios of C₂₅ and C₂₇ from BL-G16-01.

Midpoint (cm)	Year (AD)	$\delta^{13}\text{C}_{\text{C}25}$ (‰, VPDB)	$\delta^{13}\text{C}_{\text{C}25}^*$ (‰, VPDB)	No. of replicates	SD of replicates (‰, VPDB)	$\delta^{13}\text{C}_{\text{C}27}$ (‰, VPDB)	$\delta^{13}\text{C}_{\text{C}27}^*$ (‰, VPDB)	No. of replicates	SD of replicates (‰, VPDB)
3	2005	-31.0	-29.0	2	0.03	-30.7	-28.7	2	0.07
8	1981	-29.4	-28.1	2	0.16	-29.9	-28.6	2	
13	1960								
18	1919								
23	1799								
28	1599								
33	1392	-30.6	-30.6	2	0.46	-30.4	-30.4	2	0.30
38	1219	-31.4	-31.4	3	0.09	-30.9	-30.9	3	0.12
43	1112	-30.9	-30.9	2	0.10				
48	1013	-30.4	-30.4	2	0.38	-29.2	-29.2	2	0.21
53	929								

*Corrected for the Suess Effect according to Verburg (2007).

Table A.17 Carbon isotope ratios of C₂₉ and C₃₁ from BL-G16-01.

Midpoint (cm)	Year (AD)	$\delta^{13}\text{C}_{\text{C}_{29}}$ (‰, VPDB)	$\delta^{13}\text{C}_{\text{C}_{29}^*}$ (‰, VPDB)	No. of replicates	SD of replicates (‰, VPDB)	$\delta^{13}\text{C}_{\text{C}_{31}}$ (‰, VPDB)	$\delta^{13}\text{C}_{\text{C}_{31}^*}$ (‰, VPDB)	No. of replicates	SD of replicates (‰, VPDB)
3	2005	-31.4	-29.3	2	0.14	-32.7	-30.6	2	0.26
8	1981	-32.0	-30.7	3	0.24	-34.1	-32.7	2	0.08
13	1960	-33.0	-32.1	2	0.06				
18	1919								
23	1799	-31.7	-31.7	2	0.05				
28	1599								
33	1392	-32.2	-32.2	2	0.34				
38	1219								
43	1112	-31.9	-31.9	2	0.11				
48	1013	-32.2	-32.2	2	0.30				
53	929								

*Corrected for the Suess Effect according to Verburg (2007).

Table A.18 Carbon isotope ratios of diploptene and lupan-3-one from BL-G16-01.

Midpoint (cm)	Year (AD)	$\delta^{13}\text{C}_{\text{Diploptene}}$ (‰, VPDB)	$\delta^{13}\text{C}_{\text{Diploptene}^*}$ (‰, VPDB)	No. of replicates	SD of replicates (‰, VPDB)	$\delta^{13}\text{C}_{\text{Lupan-3-one}}$ (‰, VPDB)	$\delta^{13}\text{C}_{\text{Lupan-3-one}^*}$ (‰, VPDB)	No. of replicates	SD of replicates (‰, VPDB)
3	2005								
8	1981								
13	1960								
18	1919	-54.5	-54.0	1	N/A	-41.6		2	0.3
23	1799	-52.5	-52.5	1	N/A	-40.0		1	N/A
28	1599	-50.8	-50.8	2	0.35	-36.0		1	N/A
33	1392								
38	1219	-51.1	-51.1	1	N/A				
43	1112								
48	1013	-49.1	-49.1	1	N/A	-36.0		2	0.1
53	929								

*Corrected for the Suess Effect according to Verburg (2007).

Table A.19 Relative abundances of odd-chain *n*-alkanes extracted from BL-G16-01.

Midpoint (cm)	Year (AD)	C ₁₇ (%)	C ₁₉ (%)	C ₂₁ (%)	C ₂₃ (%)	C ₂₅ (%)	C ₂₇ (%)	C ₂₉ (%)	C ₃₁ (%)
3	2005	52	3	3	5	8	7	7	4
8	1981	53	3	3	5	8	7	7	4
13	1960	46	4	4	8	9	8	7	2
18	1919	64	4	3	5	5	5	5	3
23	1799	54	4	4	6	6	5	6	2
28	1599	39	5	5	8	9	7	7	4
33	1392	36	14	6	8	7	6	5	2
38	1219	13	4	6	11	16	14	14	5
43	1112	21	4	8	6	9	11	14	6
48	1013	36	6	10	4	6	7	12	5
53	929	14	6	13	7	9	11	12	6

Table A.20 Relative abundances of even-chain *n*-alkanes extracted from BL-G16-01.

Midpoint (cm)	Year (AD)	C ₁₈ (%)	C ₂₂ (%)	C ₂₄ (%)	C ₂₆ (%)	C ₂₈ (%)	C ₃₀ (%)
3	2005	2	2	2	2	2	0
8	1981	2	2	2	2	2	0
13	1960	2	3	2	2	1	1
18	1919	2	1	1	2	1	0
23	1799	4	3	2	2	1	1
28	1599	4	3	3	4	1	1
33	1392	8	4	2	3	0	0
38	1219	1	4	4	6	2	1
43	1112	5	2	2	8	3	1
48	1013	0	2	2	8	1	1
53	929	4	2	2	11	2	0

Table A.21 Absolute abundances of odd-chain *n*-alkanes extracted from BI-G16-01.

Midpoint (cm)	Year (AD)	C ₁₇ (μg/g)	C ₁₉ (μg/g)	C ₂₁ (μg/g)	C ₂₃ (μg/g)	C ₂₅ (μg/g)	C ₂₇ (μg/g)	C ₂₉ (μg/g)	C ₃₁ (μg/g)
3	2005	6	0	0	1	1	1	1	0
8	1981	7	0	0	1	1	1	1	0
13	1960	3	0	0	1	1	1	0	0
18	1919	6	0	0	0	0	0	0	0
23	1799	7	0	0	1	1	1	1	0
28	1599	6	1	1	1	2	1	1	1
33	1392	7	3	1	2	1	1	1	0
38	1219	2	1	1	2	3	3	3	1
43	1112	5	1	2	1	2	3	3	2
48	1013	5	1	1	1	1	1	2	1
53	929	2	1	2	1	1	1	2	1

Table A.22 Absolute abundances of even-chain *n*-alkanes, diploptene and lupan-3-one extracted from BI-G16-01.

Midpoint (cm)	Year (AD)	C ₁₈ (μg/g)	C ₂₂ (μg/g)	C ₂₄ (μg/g)	C ₂₆ (μg/g)	C ₂₈ (μg/g)	C ₃₀ (μg/g)	Diploptene (μg/g)	Lupan-3-one (μg/g)
3	2005	0	0	0	0	0	0	0	0
8	1981	0	0	0	0	0	0	0	0
13	1960	0	0	0	0	0	0	0	0
18	1919	0	0	0	0	0	0	0	0
23	1799	1	0	0	0	0	0	1	0
28	1599	1	1	1	1	0	0	2	0
33	1392	2	1	0	0	0	0	1	0
38	1219	0	1	1	1	0	0	1	0
43	1112	1	0	0	2	1	0	4	1
48	1013	0	0	0	1	0	0	2	0
53	929	0	0	0	1	0	0	7	1

Table A.23 Indices calculated using relative abundances of *n*-alkanes extracted from BL-G16-01.

Midpoint (cm)	Year (AD)	P _{aq}	CPI	ACL
3	2005	0.2	4	21
8	1981	0.2	4	20
13	1960	0.3	3	21
18	1919	0.1	5	19
23	1799	0.2	3	20
28	1599	0.3	2	21
33	1392	0.2	2	20
38	1219	0.6	2	24
43	1112	0.4	2	23
48	1013	0.2	3	22
53	929	0.4	2	24

Table A.24 Values of $\delta^{13}\text{C}_{\text{TOC}}$ and %TOC from modern OM sources to Uinta Mountain lakes. Conif. tree = coniferous krummholz tree; Herb = herbaceous perennial; B.D. shrub = broadleaf deciduous shrub; S.E. macro = semi-emergent macrophyte; Unk = unknown; Litt sed = littoral sediment; Sub macro = submergent macrophyte.

Carbon datasheet	Nitrogen datasheet	Sample ID	Site	Group	Genus	Plant Part
CF-C14-01	CF-NO-15-01	1A-Terrplant-Needles	East Carrol	Conif. tree	<i>Picea</i>	Needle
CF-C14-01	CF-NO-15-01	1B-Terrplant-Branches	East Carrol	Conif. tree	<i>Picea</i>	Branch
CF-C14-01	CF-NO-15-01	2B-Terrplant-Branches	Upper Carrol	Conif. tree	<i>Picea</i>	Branch
CF-C14-01	CF-NO-15-02	2A-Terrplant-Needles	Upper Carrol	Conif. tree	<i>Picea</i>	Needle
CF-C14-01	CF-NO-15-01	3A-Terrplant-Needles	Taylor	Conif. tree	<i>Picea</i>	Needle
CF-C14-01	CF-NO-15-01	3B-Terrplant-Branches	Taylor	Conif. tree	<i>Picea</i>	Branch
CF-C14-01	CF-NO-15-01	4A-Terrplant-Needles	Taylor	Conif. tree	<i>Picea</i>	Needle
CF-C14-01	CF-NO-15-01	4B-Terrplant-Branches	Taylor	Conif. tree	<i>Picea</i>	Branch
CF-C14-01	CF-NO-15-01	5A-Terrplant-Needles	Walkup	Conif. tree	<i>Picea</i>	Needle
CF-C14-01	CF-NO-15-01	5B-Terrplant-Branches	Walkup	Conif. tree	<i>Picea</i>	Branch
CF-C14-01	CF-NO-15-01	6B-Terrplant-Leaves	Bluebell Pass	Herb	<i>Kalmia</i>	Green leaf
CF-C14-01	CF-NO-17-02	6A-Terrplant-Branches	Bluebell Pass	Herb	<i>Kalmia</i>	Branch
CF-C14-01	CF-NO-15-01	7B-Terrplant-Branches	Taylor	B. D. shrub	<i>Salix</i>	Branch
CF-C14-01	CF-NO-15-02	7A-Terrplant-Greenleaves	Taylor	B. D. shrub	<i>Salix</i>	Green leaf
CF-C14-01	CF-NO-15-01	8B-Terrplant-Stem	Taylor	B. D. shrub	<i>Salix</i>	Branch
CF-C14-01	CF-NO-17-02	8A-Terrplant-Leaves	Taylor	B. D. shrub	<i>Salix</i>	Green leaf
CF-C14-01	CF-NO-15-01	9B-Terrplant-S. glauca	Walkup	B. D. shrub	<i>Salix</i>	
CF-C14-01	CF-NO-15-01	9A-Terrplant-Stem	Walkup	B. D. shrub	<i>Salix</i>	Branch
CF-C14-01	CF-NO-17-02	10-Terrplant-Entire	Taylor	B. D. shrub	<i>Salix</i>	N/A
CF-C14-01	CF-NO-15-01	11C-Terrplant-Stem	Upper Carrol	B. D. shrub	<i>Salix</i>	Branch
CF-C14-01	CF-NO-15-02	11B-Terrplant-Brownleaves	Upper Carrol	B. D. shrub	<i>Salix</i>	Brown leaf
CF-C14-01	CF-NO-15-02	11A-Terrplant-Greenleaves	Upper Carrol	B. D. shrub	<i>Salix</i>	Green leaf
CF-C14-01	CF-NO-15-01	12A-Terrplant-Seeds	Taylor	B. D. shrub	<i>Salix</i>	Seed
CF-C14-01	CF-NO-15-01	12B-Terrplant-Stem	Upper Carrol	B. D. shrub	<i>Salix</i>	Stem
CF-C14-01	CF-NO-15-02	13A-Macrophyte-Greenleaves	Upper Carrol	S.E. macro	<i>Salix</i>	Green leaf
CF-C14-01	CF-NO-15-02	13B-Macrophyte-Greenleaves	Upper Carrol	S.E. macro	<i>Salix</i>	Green leaf
CF-C14-01	CF-NO-15-02	14-Macrophyte-Greenleaves	Upper Carrol	S.E. macro	<i>Salix</i>	Green leaf
CF-C14-01	CF-NO-15-01	15A-Terrplant-Greenleaves	Walkup	Graminoid	<i>Unk.</i>	Green leaf
CF-C14-01	CF-NO-15-01	15B-Terrplant-Brownleaves	Walkup	Graminoid	<i>Unk.</i>	Brown leaf
CF-C14-01	CF-NO-15-01	16B-Terrplant-Stem	Upper Carrol	B. D. shrub	<i>Betula</i>	Branch

Carbon datasheet	Nitrogen datasheet	Sample ID	Site	Group	Genus	Plant Part
CF-C14-01	CF-NO-15-02	16A-Terrplant-Greenleaves	Upper Carrol	B. D. shrub	<i>Betula</i>	Green leaf
CF-C14-01	CF-NO-15-01	17B-Terrplant-Seeds	Taylor	B. D. shrub	<i>Salix</i>	Seed
CF-C14-01	CF-NO-15-01	17C-Terrplant-Branches	Taylor	B. D. shrub	<i>Salix</i>	Branch
CF-C14-01	CF-NO-17-02	17A-Terrplant-Greenleaves	Taylor	B. D. shrub	<i>Salix</i>	Green leaf
CF-C14-01	CF-NO-15-02	18-Terrplant-Entire	Denise	Moss	<i>Unk.</i>	N/A
CF-C14-01	CF-NO-15-02	19-Terrplant-Entire	Taylor	Lichen	<i>Unk.</i>	N/A
CF-C14-01	CF-NO-15-01	20-Terrplant-Entire	Taylor	Herb	<i>Vaccinium</i>	N/A
CF-C14-01	CF-NO-15-01	21-Terrplant-Entire	Taylor	Moss	<i>Unk.</i>	N/A
CF-C15-01	CF-NO-15-02	22C-Macrophyte-Greenleaves	Taylor	S.E. macro	<i>Carex</i>	Green leaf
CF-C15-01	CF-NO-15-02	22D-Macrophyte-Brownleaves	Taylor	S.E. macro	<i>Carex</i>	Brown leaf
CF-C15-01	CF-NO-15-02	22E-Macrophyte-Roots	Denise	S.E. macro	<i>Carex</i>	Roots
CF-C15-01	CF-NO-15-02	23D-Macrophyte-Brownleaves	Denise	S.E. macro	<i>Carex</i>	Brown leaf
CF-C15-01	CF-NO-15-02	24D-Macrophyte-Brownleaves	Upper Carrol	S.E. macro	<i>Carex</i>	Brown leaf
CF-C15-01	CF-NO-15-02	24C-Macrophyte-Greenleaves	Upper Carrol	S.E. macro	<i>Carex</i>	Green leaf
CF-C15-01	CF-NO-17-02	25-Soil	No Name	Soil		N/A
CF-C15-01	CF-NO-15-02	26-Soil	East Carrol	Soil		N/A
CF-C15-01	CF-NO-15-02	27-Soil	Upper Carrol	Soil		N/A
CF-C15-01	CF-NO-15-02	29-Soil	Denise	Soil		N/A
CF-C15-01	CF-NO-15-02	30-Littoral Sediment	Taylor	Littoral sed		N/A
CF-C17-03	CF-NO-17-01	32_Submacrophyte_14-UN-32	Walkup	Sub. macro		N/A
CF-C17-03	CF-NO-17-01	33_Algae_15-UN-07	Denise	Algae	<i>Unk.</i>	N/A
CF-C17-03	CF-NO-17-01	35_Algae_15-UN-08	Taylor	Algae	<i>Unk.</i>	N/A
CF-C17-03	CF-NO-17-01	36_Algae_14-UN-08	Taylor	Algae	<i>Unk.</i>	N/A
CF-C17-03	CF-NO-17-01	37_Algae_15-UN-55	Upper Carrol	Algae	<i>Unk.</i>	N/A
CF-C17-03	CF-NO-17-01	38_Algae_14-UN-08	Taylor	Algae	<i>Unk.</i>	N/A
CF-C17-03	CF-NO-17-01	39_Algae_15-UN-55	Upper Carrol	Algae	<i>Unk.</i>	N/A
CF-C16-02	CF-NO-16-01	40A_15-UN-56_Conif_Krumm	East Carrol	Conif. tree	<i>Picea</i>	Needle
CF-C16-02	CF-NO-16-01	40B_15-UN-56_Conif_Krumm	East Carrol	Conif. tree	<i>Picea</i>	Needle
CF-C16-02	CF-NO-16-01	41A_15-UN-56_Conif_Krumm	East Carrol	Conif. tree	<i>Picea</i>	Needle
CF-C16-02	CF-NO-16-01	41B_15-UN-56_Conif_Krumm	East Carrol	Conif. tree	<i>Picea</i>	Needle

Carbon datasheet	Nitrogen datasheet	Sample ID	Site	Group	Genus	Plant Part
CF-C16-02	CF-NO-16-01	42A_15-UN-56_Lichen	East Carrol	Lichen	<i>Unk.</i>	N/A
CF-C16-02	CF-NO-16-01	42B_15-UN-56_Lichen	East Carrol	Lichen	<i>Unk.</i>	N/A
CF-C16-02	CF-NO-16-01	43A_15-UN-56_Emerg_macro	East Carrol	S.E. macro	<i>Carex</i>	Green leaf
CF-C16-02	CF-NO-16-01	43B_15-UN-56_Emerg_macro	East Carrol	S.E. macro	<i>Carex</i>	Brown leaf
CF-C16-02	CF-NO-16-01	44A_15-UN-55_Conif_Krumm	Upper Carrol	Conif. tree	<i>Picea</i>	Needle
CF-C16-02	CF-NO-16-01	44B_15-UN-55_Conif_Krumm	Upper Carrol	Conif. tree	<i>Picea</i>	Branch
CF-C16-02	CF-NO-16-01	45A_15-UN-56_Decid_Shrub	East Carrol	B. D. shrub	<i>Salix</i>	Green leaf
CF-C16-02	CF-NO-16-01	45B_15-UN-56_Decid_Shrub	East Carrol	B. D. shrub	<i>Salix</i>	Branch
CF-C16-02	CF-NO-16-01	46A_15-UN-56_Decid_Shrub	East Carrol	B. D. shrub	<i>Salix</i>	Green leaf
CF-C16-02	CF-NO-16-01	46B_15-UN-56_Decid_Shrub	East Carrol	B. D. shrub	<i>Salix</i>	Branch
CF-C16-02	CF-NO-16-01	47A_15-UN-56_Conif_Krumm	East Carrol	Conif. tree	<i>Picea</i>	Needle
CF-C16-02	CF-NO-16-01	47B_15-UN-56_Conif_Krumm	East Carrol	Conif. tree	<i>Picea</i>	Branch
CF-C16-02	CF-NO-16-01	48A_15-UN-55_Herb_Shrub	Upper Carrol	Herb	<i>Unk.</i>	Green leaf
CF-C16-02	CF-NO-16-01	48B_15-UN-55_Herb_Shrub	Upper Carrol	Herb	<i>Unk.</i>	Stem
CF-C16-02	CF-NO-16-01	49A_15-UN-56_Conif_Krumm	East Carrol	Conif. tree	<i>Picea</i>	Green leaf
CF-C16-02	CF-NO-16-01	49B_15-UN-56_Conif_Krumm	East Carrol	Conif. tree	<i>Picea</i>	Branch
CF-C16-02	CF-NO-16-01	50A_15-UN-56_Decid_Shrub	East Carrol	B. D. shrub	<i>Betula</i>	Green leaf
CF-C16-02	CF-NO-16-01	50B_15-UN-56_Decid_Shrub	East Carrol	B. D. shrub	<i>Betula</i>	Branch
CF-C16-02	CF-NO-16-01	51A_15-UN-56_Decid_Shrub	East Carrol	B. D. shrub	<i>Salix</i>	Green leaf
CF-C16-02	CF-NO-16-01	51B_15-UN-56_Decid_Shrub	East Carrol	B. D. shrub	<i>Salix</i>	Branch
CF-C16-02	CF-NO-16-01	52A_15-UN-56_Lichen	East Carrol	Lichen	<i>Unk.</i>	N/A
CF-C16-02	CF-NO-16-01	53A_15-UN-56_Decid_Shrub	East Carrol	B. D. shrub	<i>Salix</i>	Green leaf
CF-C16-02	CF-NO-16-01	54A_15-UN-56_Decid_Shrub	East Carrol	B. D. shrub	<i>Salix</i>	Branch
CF-C16-02	CF-NO-16-01	55A_15-UN-55_Decid_Shrub	Upper Carrol	B. D. shrub	<i>Betula</i>	Green leaf
CF-C16-02	CF-NO-16-01	55B_15-UN-55_Decid_Shrub	Upper Carrol	B. D. shrub	<i>Betula</i>	Branch
CF-C16-02	CF-NO-16-01	56A_15-UN-55_Conif_Krumm	Upper Carrol	Conif. tree	<i>Picea</i>	Needle
CF-C16-02	CF-NO-16-01	56B_15-UN-55_Conif_Krumm	Upper Carrol	Conif. tree	<i>Picea</i>	Branch
CF-C16-02	CF-NO-16-01	57A_15-UN-55_Decid_Shrub	Upper Carrol	B. D. shrub	<i>Salix</i>	Green leaf
CF-C16-02	CF-NO-16-01	57B_15-UN-55_Decid_Shrub	Upper Carrol	B. D. shrub	<i>Salix</i>	Branch
CF-C16-02	CF-NO-16-01	58A_15-UN-55_Decid_Shrub	Upper Carrol	B. D. shrub	<i>Salix</i>	Branch

Carbon datasheet	Nitrogen datasheet	Sample ID	Site	Group	Genus	Plant Part
CF-C16-02	CF-NO-16-01	58B_15-UN-55_Decid_Krumm	Upper Carrol	B. D. shrub	<i>Salix</i>	Leaf
CF-C16-02	CF-NO-16-01	59A_15-UN-55_Conif_Krumm	Upper Carrol	Conif. tree	<i>Picea</i>	Branch
CF-C16-02	CF-NO-16-01	59B_15-UN-55_Conif_Krumm	Upper Carrol	Conif. tree	<i>Picea</i>	Needle
CF-C16-02	CF-NO-16-02	61A_15-UN-55_Conif_Krumm	Upper Carrol	Conif. tree	<i>Picea</i>	Needle
CF-C16-02	CF-NO-16-02	61B_15-UN-55_Conif_Krumm	Upper Carrol	Conif. tree	<i>Picea</i>	Branch
CF-C16-02	CF-NO-16-02	62A_15-UN-55_Emerg_Macro	Upper Carrol	S.E. Macro	<i>Carex</i>	Green leaf
CF-C16-02	CF-NO-16-02	63A_15-UN-55_Decid_Krumm	Upper Carrol	B. D. shrub	<i>Salix</i>	Green leaf
CF-C16-02	CF-NO-16-02	63B_15-UN-55_Decid_Krumm	Upper Carrol	B. D. shrub	<i>Salix</i>	Branch
CF-C16-02	CF-NO-16-02	63C_15-UN-55_Decid_Krumm	Upper Carrol	B. D. shrub	<i>Salix</i>	Seed
CF-C16-02	CF-NO-16-02	64A_15-UN-55_Conif_Krumm	Upper Carrol	Conif. tree	<i>Picea</i>	Needle
CF-C16-02	CF-NO-16-02	64B_15-UN-55_Conif_Krumm	Upper Carrol	Conif. tree	<i>Picea</i>	Branch
CF-C16-02	CF-NO-16-02	65A_15-UN-55_Emerg_Macro	Upper Carrol	S.E. Macro	<i>Salix</i>	Green leaf
CF-C16-02	CF-NO-16-02	65B_15-UN-55_Emerg_Macro	Upper Carrol	S.E. Macro	<i>Salix</i>	Brown leaf
CF-C16-02	CF-NO-16-02	66A_15-UN-55_Emerg_Macro	Upper Carrol	S.E. Macro	<i>Salix</i>	Green leaf
CF-C16-02	CF-NO-16-02	66B_15-UN-55_Emerg_Macro	Upper Carrol	S.E. Macro	<i>Salix</i>	Brown leaf
CF-C16-02	CF-NO-16-02	67A_15-UN-55_Herb_Shrub	Upper Carrol	Herb	<i>Unk.</i>	Green leaf
CF-C16-02	CF-NO-16-02	67B_15-UN-55_Herb_Shrub	Upper Carrol	Herb	<i>Unk.</i>	Flower
CF-C16-02	CF-NO-16-02	67C_15-UN-55_Herb_Shrub	Upper Carrol	Herb	<i>Unk.</i>	Moss
CF-C16-02	CF-NO-16-02	68A_15-UN-55_Moss	Upper Carrol	Moss	<i>Unk.</i>	N/A
CF-C16-02	CF-NO-16-02	69A_15-UN-55_Moss	Upper Carrol	Moss	<i>Unk.</i>	N/A
CF-C16-02	CF-NO-16-02	70A_15-UN-55_Moss	Upper Carrol	Moss	<i>Unk.</i>	N/A
CF-C16-02	CF-NO-16-02	71A_15-UN-55_Moss	Upper Carrol	Moss	<i>Unk.</i>	N/A
CF-C16-02	CF-NO-16-02	71B_15-UN-55_Moss	Upper Carrol	Moss	<i>Unk.</i>	N/A
CF-C16-02	CF-NO-16-02	72A_15-UN-55_Decid_Krumm	Upper Carrol	Conif. tree	<i>Picea</i>	Green leaf
CF-C16-03	CF-NO-17-02	72B_15-UN-55_Decid_Krumm	Upper Carrol	Conif. tree	<i>Picea</i>	Branch
CF-C16-03	CF-NO-17-02	73A_15-UN-55_Conif_Krumm	Upper Carrol	Conif. tree	<i>Picea</i>	Needle
CF-C16-03	CF-NO-17-02	73B_15-UN-55_Conif_Krumm	Upper Carrol	Conif. tree	<i>Picea</i>	Branch
CF-C16-03	CF-NO-17-02	74A_15-UN-55_Emerg_Macro	Upper Carrol	S.E. Macro	<i>Carex</i>	Green leaf
CF-C16-03	CF-NO-17-02	74B_15-UN-56_Emerg_Macro	Upper Carrol	S.E. Macro	<i>Carex</i>	Brown leaf
CF-C17-03	CF-NO-17-02	76A_Herb_15-UN-08	Taylor	Herb	<i>Castilleja</i>	Stem

Carbon datasheet	Nitrogen datasheet	Sample ID	Site	Group	Genus	Plant Part
CF-C17-03	CF-NO-17-01	77_Shrub_15-UN-08	Taylor	B. D. shrub	<i>Salix</i>	Green leaf
CF-C17-03	CF-NO-17-01	78_Herb_15-UN-08	Taylor	Herb	<i>Castilleja</i>	Green leaf
CF-C17-03	CF-NO-17-02	79A_Herb_15-UN-08	Taylor	Herb	<i>Dasiphora</i>	Green leaf
CF-C17-03	CF-NO-17-02	79B_Herb_15-UN-08	Taylor	Herb	<i>Dasiphora</i>	Green leaf
CF-C17-03	CF-NO-17-01	80A_Terrgrass_15-UN-08	Taylor	Graminoid	<i>Unk.</i>	N/A
CF-C17-03	CF-NO-17-01	81A_Terrgrass_15-UN-08	Taylor	Graminoid	<i>Unk.</i>	Green leaf
CF-C17-03	CF-NO-17-01	81B_Terrgrass_15-UN-08	Taylor	Graminoid	<i>Unk.</i>	Brown leaf
CF-C17-03	CF-NO-17-01	82_Lichen_15-UN-08	Taylor	Lichen	<i>Unk.</i>	N/A
CF-C18-01	CF-NO-18-01	83A_17-UN-07_Sub_Mac	Denise	Sub macro	<i>Unk.</i>	Green leaf
CF-C18-01	CF-NO-18-01	83B_17-UN-07_Sub_Mac	Denise	Sub macro	<i>Unk.</i>	Root
CF-C18-01	CF-NO-18-01	84_17-UN-08_Sub_Mac	Taylor	Sub macro	<i>Unk.</i>	N/A
CF-C18-01	CF-NO-18-01	85_17-UN-Sharlee_Algae	Sharlee	Algae	<i>Unk.</i>	N/A
CF-C18-01	CF-NO-18-01	86A_17-UN-07_Sub_Mac	Denise	Sub macro	<i>Unk.</i>	Green leaf
CF-C18-01	CF-NO-18-01	86B_17-UN-07_Sed	Denise	Litt sed	N/A	Root
CF-C18-01	CF-NO-18-01	87_15-UN-07_Moss	Denise	Moss	<i>Unk.</i>	N/A
CF-C18-01	CF-NO-18-01	88_18-UN-07_Moss	Denise	Moss	<i>Unk.</i>	N/A
CF-C18-01	CF-NO-18-01	89_17-UN-08_Lichen	Taylor	Lichen	<i>Unk.</i>	N/A
CF-C18-01	CF-NO-18-01	90_16-UN-08_Lichen	Taylor	Lichen	<i>Unk.</i>	N/A
CF-C18-01	CF-NO-18-01	91_15-UN-07_Moss	Denise	Moss	<i>Unk.</i>	N/A
CF-C18-01	CF-NO-18-01	92_15-UN-07_Lichen	Denise	Lichen	<i>Unk.</i>	N/A
CF-C18-01	CF-NO-18-01	93_15-UN-07_Sub_Moss	Denise	Moss	<i>Unk.</i>	N/A
CF-C18-01	CF-NO-18-01	94_15-UN-07_Sub_Moss	Denise	Moss	<i>Unk.</i>	N/A
CF-C18-01	CF-NO-18-01	95_15-UN-Reader_Algae	Reader	Algae	<i>Unk.</i>	N/A
CF-C18-01	CF-NO-18-01	96_15-UN-55_Sub_Mac	Upper Carrol	Sub macro	<i>Unk.</i>	N/A
CF-C18-01	CF-NO-18-01	97_16-UN-32_Algae	Walkup	Algae	<i>Unk.</i>	N/A
CF-C18-01	CF-NO-18-01	98_15-UN-07_Sub_Moss	Denise	Sub macro	<i>Unk.</i>	N/A
CF-C18-01	CF-NO-18-01	99_15-UN-07_Sub_Moss	Denise	Sub macro	<i>Unk.</i>	N/A
CF-C18-01	CF-NO-18-01	100_15-UN-07_Sub_Mac	Denise	Sub macro	<i>Unk.</i>	N/A
CF-C18-01	CF-NO-18-01	101_15-UN-07_SubMoss	Denise	Sub macro	<i>Unk.</i>	N/A
CF-C18-01	CF-NO-18-01	102_15-UN-07_Algae	Denise	Algae	<i>Unk.</i>	N/A

Carbon datasheet	Nitrogen datasheet	Sample ID	Site	Group	Genus	Plant Part
CF-C18-01	CF-NO-18-01	103_15-UN-07_Algae	Denise	Algae	Unk.	Green leaf
CF-C18-01	CF-NO-18-01	104A_17-UN-07_Sub_Macro	Denise	Sub. macro	Unk.	Root
CF-C18-01	CF-NO-18-01	104B_17-UN-07_Sed	Denise	Littoral sed	Unk.	N/A
CF-C18-01	CF-NO-18-01	106_16-UN-08_Lichen	Taylor	Lichen	Unk.	Green leaf
CF-C18-01	CF-NO-18-01	107-A_17-UN-07_Sub_Macro	Denise	Sub. macro	Unk.	Root
CF-C18-01	CF-NO-18-01	107-B_17-UN-07_Sub_Macro	Denise	Sub. macro	Unk.	N/A
CF-C18-07	CF-NO-18-06	132A_17-UN-08_Green_Moss	Taylor	Moss	Unk.	N/A
CF-C18-07	CF-NO-18-06	132B_17-UN-08_Brown_Moss	Taylor	Moss	Unk.	N/A
CF-C18-07	CF-NO-18-06	133A_17-UN-07_Grass	Denise	Graminoid	Unk.	Green leaf
CF-C18-07	CF-NO-18-06	133B_17-UN-07_Terr soil >300 nm	Denise	Soil	N/A	N/A
CF-C18-07	CF-NO-18-06	133C_17-UN-07_Roots	Denise	N/A	Unk.	Root
CF-C18-08	CF-NO-18-06	133D_17-UN-07_Terr_Soil <300 nm	Denise	Soil	N/A	N/A
CF-C18-07	CF-NO-18-06	134A_17-UN-07_Green Moss	Denise	Moss	Unk.	Green top
CF-C18-07	CF-NO-18-06	134B_17-UN-07_Brown Moss	Denise	Moss	Unk.	Brown bottom
CF-C18-07	CF-NO-18-06	134C_17-UN-07_Terr_Soil <300 nm	Denise	Soil	N/A	N/A
CF-C18-07	CF-NO-18-06	135C_17-UN-07_Terr_Soil <300 nm	Denise	Soil	N/A	N/A
CF-C18-07	CF-NO-18-06	135A_17-UN-07_Grass	Denise	Graminoid	Unk.	Green leaf
CF-C18-07	CF-NO-18-06	135B_17-UN-07_Terr Soil >300 nm	Denise	Soil	Unk.	N/A
CF-C18-07	CF-NO-18-06	137C_17-UN-07_Terr_Soil <300 nm	Denise	Soil	Unk.	N/A
CF-C18-07	CF-NO-18-06	138C_17-UN-07_Terr_Soil <300 nm	Denise	Soil	Unk.	N/A
CF-C18-07	CF-NO-18-06	139C_17-UN-07_Terr_Soil <300 nm	Denise	Soil	Unk.	N/A
CF-C18-08	CF-NO-18-07	141A_15-UN-07_Sub_Macro	Denise	Sub. macro	Unk.	Green leaf
CF-C18-08	CF-NO-18-07	148A_17-UN-07_Moss	Denise	Moss	Unk.	N/A
CF-C18-08	CF-NO-18-07	148B_17-UN-07_Graminoid	Denise	Graminoid	Unk.	Green leaf
CF-C18-08	CF-NO-18-07	149A_17-UN-07_Graminoid	Denise	Graminoid	Unk.	Green leaf
CF-C18-08	CF-NO-18-07	149B_17-UN-07_Soil	Denise	Soil	N/A	N/A
CF-C18-08	CF-NO-18-07	151A_17-UN-07_Algae	Denise	Algae	Unk.	N/A
CF-C18-08	CF-NO-18-07	152_16-UN-08_Algae	Taylor	Algae	Unk.	N/A
CF-C18-08	CF-NO-18-07	153_17-UN-07_Algae	Denise	Algae	Unk.	N/A
CF-C18-08	CF-NO-18-07	155_17-UN-07_Algae	Denise	Algae	Unk.	N/A

Table A.25 Values of $\delta^{13}\text{C}_{\text{TOC}}$, $\delta^{15}\text{N}_{\text{TN}}$, %TOC and %TN from modern OM sources to Uinta Mountains lakes. Avg: average of plant parts.

Sample ID	$\delta^{13}\text{C}_{\text{TOC}}$ (‰, VPDB)	No. of replicates	SD (‰, VPDB)	Avg (‰, VPDB)	$\delta^{15}\text{N}_{\text{TN}}$ (‰, AIR)	No. of replicates	SD (‰, AIR)	Avg (‰, AIR)	TOC (%)	No. of replicates	SD (%)	Avg (%)	TN (%)	No. of replicates	SD (%)	Avg (%)
1A-Terrplant-Needles	-26.3			-26.0	-5.5			-5.8	52			52	1			1
1B-Terrplant-Branches	-25.7	1	0.00		-6.2	1	0.07		52	1	1.4		1	1	0.00	
2B-Terrplant-Branches	-26.4			-26.4	-1.9			-1.6	53			51	1			1
2A-Terrplant-Needles	-26.5				-1.4				50				1			
3A-Terrplant-Needles	-25.9			-26.5	+0.9			+1.8	51			50	1			2
3B-Terrplant-Branches	-27.2				+2.7				49				2			
4A-Terrplant-Needles	-26.5			-26.2	-5.2			-5.7	50			45	1			1
4B-Terrplant-Branches	-26.0				-6.2				41				1			
5A-Terrplant-Needles	-25.7			-25.9	-1.2			-2.1	50			53	1			1
5B-Terrplant-Branches	-26.0				-2.9				56				1			
6B-Terrplant-Leaves	-28.0	1	0.01	-27.7	-3.8			-3.5	51	1	0.1	52	2			1
6A-Terrplant-Branches	-27.4				-3.3				52				1			
7B-Terrplant-Branches	-28.7			-29.2	-4.4			-3.6	48			49	1			1
7A-Terrplant-Greenleaves	-29.8				-2.8				50				1			
8B-Terrplant-Stem	-27.1			-27.5	-3.4			-2.6	50			50	1			1
8A-Terrplant-Leaves	-27.8				-1.8				50				1			
9B-Terrplant-S. glauca	-27.2	1	0.05	-26.3	-5.0	1	0.02	-4.4	52	1	1.7	51	2	1	0.02	3
9A-Terrplant-Stem	-25.5				-3.8				50				4			
10-Terrplant-Entire	-28.7				-1.8				51				1			
11C-Terrplant-Stem	-28.3			-27.4	-4.5			-3.4	34			45	1			2
11B-Terrplant-Brownleaves	-28.1				-2.9				51				1			
11A-Terrplant-Greenleaves	-25.9				-2.8				49				4			
12A-Terrplant-Seeds	-25.7			-26.3	-5.3			-6.0	44			48	4			2
12B-Terrplant-Stem	-26.9				-6.7				52				1			
13A-Macrophyte-Greenleaves	-28.3			-28.3	+4.7			+5.4	46			46	2			2
13B-Macrophyte-Greenleaves	-28.4	1	0.02		+6.1	1	0.04		46	1	1.0		1	1	0.028	
14-Macrophyte-Greenleaves	-25.9				+2.6				47				2			
15A-Terrplant-Greenleaves	-26.7			-26.6	-1.9			-2.4	46			44	3			2
15B-Terrplant-Brownleaves	-26.4				-2.8				42				1			
16B-Terrplant-Stem	-27.4			-26.8	-2.7			-2.2	56			54	1			2

Sample ID	$\delta^{13}\text{C}_{\text{TOC}}$ (‰, VPDB)	No. of replicates	SD (‰, VPDB)	Avg (‰, VPDB)	$\delta^{15}\text{N}_{\text{TN}}$ (‰, AIR)	No. of replicates	SD (‰, AIR)	Avg. (‰, AIR)	TOC (%)	No. of replicates	SD (%)	Avg (%)	TN (%)	No. of replicates	SD (%)	Avg (%)
16A-Terrplant-Greenleaves	-26.1				-1.7				53				4			
17B-Terrplant-Seeds	-26.9			-26.7	-1.3			-2.0	47			50	1			1
17C-Terrplant-Branches	-26.3				-2.9				53				1			
17A-Terrplant-Greenleaves	-26.9				-1.9				50				1			
18-Terrplant-Entire	-25.4				-2.1				45				1			
19-Terrplant-Entire	-23.0				-3.5				35				1			
20-Terrplant-Entire	-27.2				-4.1				46				1			
21-Terrplant-Entire	-24.6				-3.0				44				1			
22C-Macrophyte-Greenleaves	-27.5			-27.9	+1.1			+1.4	43			43	1			1
22D-Macrophyte-Brownleaves	-27.3				+0.7				44				1			
22E-Macrophyte-Roots	-28.7	1	0.03		+2.4				42	1	0.1		1			
23D-Macrophyte-Brownleaves	-25.1				+2.1				45				1			
24D-Macrophyte-Brownleaves	-27.2			-27.5	+2.0			+2.4	81			63	1			1
24C-Macrophyte-Greenleaves	-27.7				+2.8				45				2			
25-Soil	-24.9				+3.7				1				0			
26-Soil	-28.6				-0.5	1	0.01		35				2	1	0.01	
27-Soil	-25.8				+2.2				4				0			
29-Soil	-23.6				+1.5				16				2			
30-Littoral Sediment	-26.7	1	0.03		-0.1				17	1	0.1		1			
32_Submacrophyte_14-UN-32	-22.2				+7.0				38				3			
33_Algae_15-UN-07	-10.5				-1.3				19				2			
35_Algae_15-UN-08	-31.1				+1.3				25				2			
36_Algae_14-UN-08	-26.3	1	0.12		+1.2				38	1	1.8		3			
37_Algae_15-UN-55	-32.1				-0.2				31				1			
38_Algae_14-UN-08	-20.6				-0.5				25				3			
39_Algae_15-UN-55	-32.3				-0.5	1	0.02		32				1	1	0.01	
40A_15-UN-56_Conif_Krumm	-26.9			-26.4	+0.8			+0.8	48			48	6			8
40B_15-UN-56_Conif_Krumm	-25.9				+0.9				49				10			
41A_15-UN-56_Conif_Krumm	-25.8			-25.9	+0.8			-0.3	46			47	7			4
41B_15-UN-56_Conif_Krumm	-26.0				-1.3				47				2			

Sample ID	$\delta^{13}\text{C}_{\text{TOC}}$ (‰, VPDB)	No. of replicates	SD (‰, VPDB)	Avg (‰, VPDB)	$\delta^{15}\text{N}_{\text{TN}}$ (‰, AIR)	No. of replicates	SD (‰, AIR)	Avg (‰, AIR)	TOC (%)	No. of replicates	SD (%)	Avg (%)	TN (%)	No. of replicates	SD (%)	Avg (%)
42A_15-UN-56_Lichen	-22.5			-23.7	-3.0			-1.6	37			22	1			1
42B_15-UN-56_Lichen	-24.9				-0.1				8				1			
43A_15-UN-56_Emerg_macro	-27.1			-26.1	-6.4			-2.8	84			66	3			2
43B_15-UN-56_Emerg_macro	-25.1				+0.7				48				1			
44A_15-UN-55_Conif_Krumm	-25.0			-25.0	-2.1			-2.8	48			49	1			1
44B_15-UN-55_Conif_Krumm	-25.1				-3.6				49				1			
45A_15-UN-56_Decid_Shruh	-26.7			-27.0	-2.7			-3.1	46			47	3			2
45B_15-UN-56_Decid_Shruh	-27.4				-3.5				47				1			
46A_15-UN-56_Decid_Shruh	-28.9			-28.8	-6.8			-6.9	46			46	2			2
46B_15-UN-56_Decid_Shruh	-28.8				-7.0				47				1			
47A_15-UN-56_Conif_Krumm	-26.4			-26.4	-3.4			-4.1	47			49	1			1
47B_15-UN-56_Conif_Krumm	-26.5				-4.8				51				1			
48A_15-UN-55_Herb_Shruh	-28.7			-29.1	-4.7			-5.3	50			49	2			1
48B_15-UN-55_Herb_Shruh	-29.4				-5.8				48				1			
49A_15-UN-56_Conif_Krumm	-26.2	1	0.04	-26.5	-2.3	1	0.01	-2.8	47	1	0.0	48	2	1	0.0	1
49B_15-UN-56_Conif_Krumm	-26.8				-3.3				50				1			
50A_15-UN-56_Decid_Shruh	-27.0			-27.0	-4.7			-4.9	46			48	3			2
50B_15-UN-56_Decid_Shruh	-26.9				-5.1				51				1			
51A_15-UN-56_Decid_Shruh	-28.6			-28.7	-7.0			-7.5	46			47	2			2
51B_15-UN-56_Decid_Shruh	-28.7				-8.0				47				1			
52A_15-UN-56_Lichen	-26.1				-2.3				38				1			
53A_15-UN-56_Decid_Shruh	-27.4				-3.3				47				3			
54A_15-UN-56_Decid_Shruh	-26.5				-3.3				47				3			
55A_15-UN-55_Decid_Shruh	-26.2			-26.5	+0.7			+0.5	46			50	3			2
55B_15-UN-55_Decid_Shruh	-26.9	1	0.28		+0.3	1	0.06		54	1	4.7		1	1	0.0	0
56A_15-UN-55_Conif_Krumm	-27.0			-27.1	-2.9			-3.4	47			48	1			1
56B_15-UN-55_Conif_Krumm	-27.2				-4.0				49				1			
57A_15-UN-55_Decid_Shruh	-25.4			-25.7	-1.2			-1.9	47			47	3			2
57B_15-UN-55_Decid_Shruh	-25.9				-2.7				47				2			
58A_15-UN-55_Decid_Shruh	-26.0			-26.1	-4.1			-3.8	48			48	3			2

Sample ID	$\delta^{13}\text{C}_{\text{TOC}}$ (‰, VPDB)	No. of replicates	SD (‰, VPDB)	Avg (‰, VPDB)	$\delta^{15}\text{N}_{\text{TN}}$ (‰, AIR)	No. of replicates	SD (‰, AIR)	Avg (‰, AIR)	TOC (%)	No. of replicates	SD (%)	Avg (%)	TN (%)	No. of replicates	SD (%)	Avg (%)
58B_15-UN-55_Decid_Krumm	-26.3				-3.5				48				1			
59A_15-UN-55_Conif_Krumm	-25.4			-25.6	-3.5			-3.5	48			49	1			1
59B_15-UN-55_Conif_Krumm	-25.8				-3.5				50				1			
61A_15-UN-55_Conif_Krumm	-26.1			-26.0	-2.2			-2.9	48			49	1			1
61B_15-UN-55_Conif_Krumm	-25.9				-3.6				50				1			
62A_15-UN-55_Emerg_Macro	-26.1				+0.6				42				2			
63A_15-UN-55_Decid_Krumm	-26.8			-26.5	-2.3			-2.4	47			47	3			2
63B_15-UN-55_Decid_Krumm	-26.5				-3.2				48				1			
63C_15-UN-55_Decid_Krumm	-26.1				-1.6				45				2			
64A_15-UN-55_Conif_Krumm	-25.3			-25.1	-2.0			-2.9	47			48	1			1
64B_15-UN-55_Conif_Krumm	-24.9				-3.8				48				1			
65A_15-UN-55_Emerg_Macro	-26.1			-26.2	+2.2			+2.2	43			46	3			2
65B_15-UN-55_Emerg_Macro	-26.2	1	0.08		+2.2	1	0.09		50	1	12.4		2	1	0.06	
66A_15-UN-55_Emerg_Macro	-26.8			-26.9	+2.1			+2.4	43			42	3			2
66B_15-UN-55_Emerg_Macro	-27.0				+2.7				42				2			
67A_15-UN-55_Herb_Shruh	-29.5			-27.7	-7.1			-5.3	49			46	2			2
67B_15-UN-55_Herb_Shruh	-28.5				-5.3				49				2			
67C_15-UN-55_Herb_Shruh	-25.1				-3.5				42				1			
68A_15-UN-55_Moss	-26.1				-3.8				42				1			
69A_15-UN-55_Moss	-25.2				-3.3				40				1			
70A_15-UN-55_Moss	-26.0	1	0.01		-2.7				40	1	0.3		1			
71A_15-UN-55_Moss	-25.1			-26.5	-3.5	1	0	-2.7	40			39	2	1	0.00	2
71B_15-UN-55_Moss	-27.9				-1.9				37				2			
72A_15-UN-55_Decid_Krumm	-26.5			-26.5	-2.4			-2.5	46			49	3			2
72B_15-UN-55_Decid_Krumm	-26.5				-2.7	1	0.15		51				1	1	0.19	
73A_15-UN-55_Conif_Krumm	-26.1			-26.6	-3.0			-3.2	45			47	1			1
73B_15-UN-55_Conif_Krumm	-27.1				-3.4				50				2			
74A_15-UN-55_Emerg_Macro	-26.4			-26.1	+0.5			+0.5	44			44	1			1
74B_15-UN-56_Emerg_Macro	-25.8				+0.6				43				1			
76A_Herb_15-UN-08	-25.6				-1.0				40				3			

Sample ID	$\delta^{13}\text{C}_{\text{TOC}}$ (‰, VPDB)	No. of replicates	SD (‰, VPDB)	Avg (‰, VPDB)	$\delta^{15}\text{N}_{\text{TN}}$ (‰, AIR)	No. of replicates	SD (‰, AIR)	Avg (‰, AIR)	TOC (%)	No. of replicates	SD (%)	Avg (%)	TN (%)	No. of replicates	SD (%)	Avg (%)
77_Shrub_15-UN-08	-25.6				-0.5				64				1			
78_Herb_15-UN-08	-26.4				-2.0				39				2			
79A_Herb_15-UN-08	-28.3			-28.1	-0.9	1	0.05	-1.3	45			45	3	1	0.04	2
79B_Herb_15-UN-08	-28.0				-1.8				44				1			
80A_Terrgrass_15-UN-08	-28.0				-2.8				41				1			
81A_Terrgrass_15-UN-08	-28.4			-27.6	-1.5			-2.3	41			41	2			1
81B_Terrgrass_15-UN-08	-26.9				-3.1				40				1			
82_Lichen_15-UN-08	-23.5	1	0.02		-5.1				22	1	0.2		1			
83A_17-UN-07_Sub_Mac	-23.3			-22.9	+0.9			+1.0	38			24	4			2
83B_17-UN-07_Sub_Mac	-22.5				+1.1				11				1			
84_17-UN-08_Sub_Mac	-26.3				+1.6				39				2			
85_17-UN-08_Sharlee_Algae	-21.7				-4.1				39				3			
86A_17-UN-07_Sub_Mac	-22.9			-22.9	+1.3			+1.2	25			21	3			2
86B_17-UN-07_Sed	-23.0				+1.1				17				2			
87_15-UN-07_Moss	-24.8				-2.0				41				1			
88_18-UN-07_Moss	-26.7				+4.1				40				2			
89_17-UN-08_Lichen	-21.2	1	0.03		-3.0	1	0.08		41	1	0.1		1	1	0.00	
90_16-UN-08_Lichen	-20.1				-5.9				26				2			
91_15-UN-07_Moss	-27.3				-0.1				30				2			
92_15-UN-07_Lichen	-22.0				-3.2				43				1			
93_15-UN-07_Sub_Moss	-26.5				-0.8				33				2			
94_15-UN-07_Sub_Moss	-27.0				+1.1				37				2			
95_15-UN-Reader_Algae	-27.9				+2.1				15				2			
96_15-UN-55_Sub_Mac	-27.7				+0.0				33				5			
97_16-UN-32_Algae	-25.4				-6.8				15				2			
98_15-UN-07_Sub_Moss	-30.3	1	0.15		-0.2	1	0.03		31	1	0.1		2	1	0.03	
99_15-UN-07_Sub_Moss	-31.7				-0.2				37				2			
100_15-UN-07_Sub_Mac	-27.7				+0.0				32				2			
101_15-UN-07_SubMoss	-30.4				-0.5				38				1			
102_15-UN-07_Algae	-27.2				-0.4				35				3			

Sample ID	$\delta^{13}\text{C}_{\text{TOC}}$ (‰, VPDB)	No. of replicates	SD (‰, VPDB)	Avg (‰, VPDB)	$\delta^{15}\text{N}_{\text{TN}}$ (‰, AIR)	No. of replicates	SD (‰, AIR)	Avg (‰, AIR)	TOC (%)	No. of replicates	SD (%)	Avg (%)	TN (%)	No. of replicates	SD (%)	Avg (%)
103_15-UN-07_Algae	-25.8				-0.6				31				4			
104A_17-UN-07_Sub_Macro	-24.9			-24.4	+0.0			+0.5	36			25	4			2
104B_17-UN-07_Sed	-24.0				+1.0				14				1			
106_16-UN-08_Lichen	-21.1				-5.0				39				10			
107-A_17-UN-07_Sub_Macro	-23.3			-23.3	+2.9			+1.3	26			22	3			3
107-B_17-UN-07_Sub_Macro	-23.4				-0.4				19				2			
132A_17-UN-08_Green_Moss	-25.1			-25.6	-0.7			-0.4	41			40	1			1
132B_17-UN-08_Brown_Moss	-26.1				+0.0				39				1			
133A_17-UN-07_Grass	-28.5	1	0.00	-27.9	-0.1			+0.3	40	1	0.6	38	1			1
133B_17-UN-07_Terr soil >300 nm	-27.6				+0.6				32				2			
133C_17-UN-07_Roots	-27.8				+0.2				43				1			
133D_17-UN-07_Terr_Soil <300 nm					+2.9								2			
134A_17-UN-07_Green Moss	-25.3			-25.5	+1.8	1	0.06	+1.0	41			35	1	1	0.06	1
134B_17-UN-07_Brown Moss	-25.2				-0.6				38				1			
134C_17-UN-07_Terr_Soil <300 nm	-25.9				+1.7	1	0.03		26				1	1	0.01	
135C_17-UN-07_Terr_Soil <300 nm	-27.5			-27.7	-0.3			-0.6	34			38	2			1
135A_17-UN-07_Grass	-27.8				+0.1				43				1			
135B_17-UN-07_Terr Soil >300 nm	-27.6				-1.7				38				2			
137C_17-UN-07_Terr_Soil <300 nm	-25.8				+3.6				10				1			
138C_17-UN-07_Terr_Soil <300 nm	-26.1				+0.9				21				1			
139C_17-UN-07_Terr_Soil <300 nm	-24.9				+4.5				9				1			
141A_15-UN-07_Sub_Macro	-25.9				-1.3				31				3			
148A_17-UN-07_Moss	-26.8				-1.2				41				2			
148B_17-UN-07_Graminoid	-29.7				-2.8				44				1			
149A_17-UN-07_Graminoid	-29.7				+1.1				43				2			
149B_17-UN-07_Soil	-28.3				+0.0				39				1			
151A_17-UN-07_Algae	-23.5				-1.3				36				6			
152_16-UN-08_Algae	-30.2	1	0.17		-0.7	1	0.07		32	1	1.2		2	1	0.11	
153_17-UN-07_Algae	-22.7								28							
155_17-UN-07_Algae	-23.1								28							
156A_17-UN-07_Algae	-23.4								26							
156B_17-UN-07_Sediment	-22.7								15							

Table A.26 Values of $\delta^{13}\text{C}_{\text{TOC}}$, $\delta^{15}\text{N}_{\text{TN}}$, %TOC and %TN from modern OM sources to Uinta Mountains lakes. Avg: average of plant parts.

Sample ID	TOC:TN	Avg. of plant parts
1A-Terrplant-Needles	78	94
1B-Terrplant-Branches	110	
2B-Terrplant-Branches	53	57
2A-Terrplant-Needles	61	
3A-Terrplant-Needles	56	41
3B-Terrplant-Branches	25	
4A-Terrplant-Needles	82	81
4B-Terrplant-Branches	80	
5A-Terrplant-Needles	46	76
5B-Terrplant-Branches	107	
6B-Terrplant-Leaves	34	47
6A-Terrplant-Branches	60	
7B-Terrplant-Branches	43	49
7A-Terrplant-Greenleaves	56	
8B-Terrplant-Stem	81	72
8A-Terrplant-Leaves	62	
9B-Terrplant-S. glauca	39	26
9A-Terrplant-Stem	13	
10-Terrplant-Entire	65	
11C-Terrplant-Stem	39	40
11B-Terrplant-Brownleaves	66	
11A-Terrplant-Greenleaves	16	
12A- Terrplant-Seeds	15	45
12B-Terrplant-Stem	76	
13A-Macrophyte-Greenleaves	28	35
13B-Macrophyte-Greenleaves	42	
14-Macrophyte-Greenleaves	25	
15A-Terrplant-Greenleaves	17	32
15B-Terrplant-Brownleaves	47	
16B-Terrplant-Stem	81	49
16A-Terrplant-Greenleaves	17	
17B-Terrplant-Seeds	94	82
17C-Terrplant-Branches	71	
17A-Terrplant-Greenleaves	80	
18-Terrplant-Entire	45	
19-Terrplant-Entire	34	
20-Terrplant-Entire	57	
21-Terrplant-Entire	53	
22C-Macrophyte-Greenleaves	40	57
22D-Macrophyte-Brownleaves	88	
22E-Macrophyte-Roots	44	
23D-Macrophyte-Brownleaves	69	
24D-Macrophyte-Brownleaves	95	63
24C-Macrophyte-Greenleaves	31	

Sample ID	TOC:TN	Avg. of plant parts
25-Soil	14	
26-Soil	22	
27-Soil	19	
29-Soil	11	
30-Littoral Sediment	16	
32_Submacrophyte_14-UN-32	15	
33_Algae_15-UN-07	11	
35_Algae_15-UN-08	16	
36_Algae_14-UN-08	15	
37_Algae_15-UN-55	26	
38_Algae_14-UN-08	11	
39_Algae_15-UN-55	30	
40A_15-UN-56_Conif_Krumm	10	8
40B_15-UN-56_Conif_Krumm	5	
41A_15-UN-56_Conif_Krumm	8	17
41B_15-UN-56_Conif_Krumm	25	
42A_15-UN-56_Lichen	44	31
42B_15-UN-56_Lichen	18	
43A_15-UN-56_Emerg_macro	39	41
43B_15-UN-56_Emerg_macro	44	
44A_15-UN-55_Conif_Krumm	63	77
44B_15-UN-55_Conif_Krumm	90	
45A_15-UN-56_Decid_Shrub	17	28
45B_15-UN-56_Decid_Shrub	38	
46A_15-UN-56_Decid_Shrub	24	48
46B_15-UN-56_Decid_Shrub	72	
47A_15-UN-56_Conif_Krumm	46	67
47B_15-UN-56_Conif_Krumm	89	
48A_15-UN-55_Herb_Shrub	32	48
48B_15-UN-55_Herb_Shrub	65	
49A_15-UN-56_Conif_Krumm	26	56
49B_15-UN-56_Conif_Krumm	87	
50A_15-UN-56_Decid_Shrub	17	31
50B_15-UN-56_Decid_Shrub	46	
51A_15-UN-56_Decid_Shrub	23	44
51B_15-UN-56_Decid_Shrub	65	
52A_15-UN-56_Lichen	56	
53A_15-UN-56_Decid_Shrub	20	
54A_15-UN-56_Decid_Shrub	19	
55A_15-UN-55_Decid_Shrub	18	38
55B_15-UN-55_Decid_Shrub	58	
56A_15-UN-55_Conif_Krumm	51	56
56B_15-UN-55_Conif_Krumm	62	
57A_15-UN-55_Decid_Shrub	16	25

Sample ID	TOC:TN	Avg. of plant parts
25-Soil	14	
26-Soil	22	
27-Soil	19	
29-Soil	11	
30-Littoral Sediment	16	
32_Submacrophyte_14-UN-32	15	
33_Algae_15-UN-07	11	
35_Algae_15-UN-08	16	
36_Algae_14-UN-08	15	
37_Algae_15-UN-55	26	
38_Algae_14-UN-08	11	
39_Algae_15-UN-55	30	
40A_15-UN-56_Conif_Krumm	10	8
40B_15-UN-56_Conif_Krumm	5	
41A_15-UN-56_Conif_Krumm	8	17
41B_15-UN-56_Conif_Krumm	25	
42A_15-UN-56_Lichen	44	31
42B_15-UN-56_Lichen	18	
43A_15-UN-56_Emerg_macro	39	41
43B_15-UN-56_Emerg_macro	44	
44A_15-UN-55_Conif_Krumm	63	77
44B_15-UN-55_Conif_Krumm	90	
45A_15-UN-56_Decid_Shruh	17	28
45B_15-UN-56_Decid_Shruh	38	
46A_15-UN-56_Decid_Shruh	24	48
46B_15-UN-56_Decid_Shruh	72	
47A_15-UN-56_Conif_Krumm	46	67
47B_15-UN-56_Conif_Krumm	89	
48A_15-UN-55_Herb_Shruh	32	48
48B_15-UN-55_Herb_Shruh	65	
49A_15-UN-56_Conif_Krumm	26	56
49B_15-UN-56_Conif_Krumm	87	
50A_15-UN-56_Decid_Shruh	17	31
50B_15-UN-56_Decid_Shruh	46	
51A_15-UN-56_Decid_Shruh	23	44
51B_15-UN-56_Decid_Shruh	65	
52A_15-UN-56_Lichen	56	
53A_15-UN-56_Decid_Shruh	20	
54A_15-UN-56_Decid_Shruh	19	
55A_15-UN-55_Decid_Shruh	18	38
55B_15-UN-55_Decid_Shruh	58	
56A_15-UN-55_Conif_Krumm	51	56
56B_15-UN-55_Conif_Krumm	62	
57A_15-UN-55_Decid_Shruh	16	25
57B_15-UN-55_Decid_Shruh	33	

Sample ID	TOC:TN	Avg. of plant parts
58A_15-UN-55_Decid_Shrub	21	40
58B_15-UN-55_Decid_Krumm	59	
59A_15-UN-55_Conif_Krumm	60	66
59B_15-UN-55_Conif_Krumm	72	
61A_15-UN-55_Conif_Krumm	60	64
61B_15-UN-55_Conif_Krumm	68	
62A_15-UN-55_Emerg_Macro	25	
63A_15-UN-55_Decid_Krumm	19	35
63B_15-UN-55_Decid_Krumm	64	
63C_15-UN-55_Decid_Krumm	21	
64A_15-UN-55_Conif_Krumm	65	77
64B_15-UN-55_Conif_Krumm	90	
65A_15-UN-55_Emerg_Macro	18	25
65B_15-UN-55_Emerg_Macro	31	
66A_15-UN-55_Emerg_Macro	18	24
66B_15-UN-55_Emerg_Macro	31	
67A_15-UN-55_Herb_Shrub	32	34
67B_15-UN-55_Herb_Shrub	27	
67C_15-UN-55_Herb_Shrub	43	
68A_15-UN-55_Moss	41	
69A_15-UN-55_Moss	69	
70A_15-UN-55_Moss	39	
71A_15-UN-55_Moss	27	24
71B_15-UN-55_Moss	20	
72A_15-UN-55_Decid_Krumm	17	31
72B_15-UN-55_Decid_Krumm	44	
73A_15-UN-55_Conif_Krumm	60	44
73B_15-UN-55_Conif_Krumm	29	
74A_15-UN-55_Emerg_Macro	63	58
74B_15-UN-56_Emerg_Macro	54	
76A_Herb_15-UN-08	17	
77_Shrub_15-UN-08	58	
78_Herb_15-UN-08	21	
79A_Herb_15-UN-08	21	34
79B_Herb_15-UN-08	46	
80A_Terrgrass_15-UN-08	53	
81A_Terrgrass_15-UN-08	22	57
81B_Terrgrass_15-UN-08	92	
82_Lichen_15-UN-08	25	
83A_17-UN-07_Sub_Mac	12	12
83B_17-UN-07_Sub_Mac	12	
84_17-UN-08_Sub_Mac	21	
85_17-UN-Sharlee_Algae	13	
86A_17-UN-07_Sub_Mac	9	11
86B_17-UN-07_Sed	12	

Sample ID	TOC:TN	Avg. of plant parts
88_18-UN-07_Moss	24	
89_17-UN-08_Lichen	50	
90_16-UN-08_Lichen	18	
91_15-UN-07_Moss	19	
92_15-UN-07_Lichen	44	
93_15-UN-07_Sub_Moss	20	
94_15-UN-07_Sub_Moss	23	
95_15-UN-Reader_Algae	8	
96_15-UN-55_Sub_Mac	8	
97_16-UN-32_Algae	9	
98_15-UN-07_Sub_Moss	21	
99_15-UN-07_Sub_Moss	24	
100_15-UN-07_Sub_Mac	18	
101_15-UN-07_SubMoss	38	
102_15-UN-07_Algae	13	
103_15-UN-07_Algae	10	
104A_17-UN-07_Sub_Macro	12	12
104B_17-UN-07_Sed	13	
106_16-UN-08_Lichen	5	
107-A_17-UN-07_Sub_Macro	9	10
107-B_17-UN-07_Sub_Macro	11	
132A_17-UN-08_Green_Moss	34	35
132B_17-UN-08_Brown_Moss	37	
133A_17-UN-07_Grass	49	49
133B_17-UN-07_Terr soil >300 nm	18	
133C_17-UN-07_Roots	81	
133D_17-UN-07_Terr_Soil <300 nm		
134A_17-UN-07_Green Moss	33	34
134B_17-UN-07_Brown Moss	47	
134C_17-UN-07_Terr_Soil <300 nm	22	
135C_17-UN-07_Terr_Soil <300 nm	20	35
135A_17-UN-07_Grass	55	
135B_17-UN-07_Terr Soil >300 nm	29	
137C_17-UN-07_Terr_Soil <300 nm	15	
138C_17-UN-07_Terr_Soil <300 nm	17	
139C_17-UN-07_Terr_Soil <300 nm	15	
141A_15-UN-07_Sub_Macro	14	
148A_17-UN-07_Moss	30	
148B_17-UN-07_Graminoid	56	
149A_17-UN-07_Graminoid	25	
149B_17-UN-07_Soil	32	
151A_17-UN-07_Algae	6	
152_16-UN-08_Algae	15	

Table A.27 Additional information about foliar tissue from which n-alkanes are extracted. Conif. tree = coniferous krummholz tree; Herb = herbaceous perennial; B.D. shrub = broadleaf deciduous shrub; S.E. macro = semi-emergent macrophyte; Unk = unknown; Litt sed = littoral sediment; Sub macro = submergent macrophyte; Sub sed = submerged sed.

<i>n</i> -Alkane sample ID	Size fraction (μm)	Group	Genus	Site	Water source	Foliar $\delta^{13}\text{C}_{\text{TOC}}$ (‰, VPDB)	Foliar $\delta^{15}\text{N}_{\text{TN}}$ (‰, AIR)	Foliar TOC (%)	Foliar TN (%)	Foliar TOC:TN
14A		S.E. macro	<i>Carex</i>	Upper Carrol	Lake water	-25.9	+3.1	47.0	2.2	24.9
22C		S.E. macro	<i>Carex</i>	Taylor	Lake water	-27.5	+1.3	43.2	1.1	45.5
65A		S.E. macro	<i>Carex</i>	Upper Carrol	Lake water	-26.1	+1.9	42.6	2.6	18.8
24C		S.E. macro	<i>Carex</i>	Upper Carrol	Lake water	-27.7	+2.3	44.6	1.6	32.1
66A		S.E. macro	<i>Carex</i>	Upper Carrol	Lake water	-26.1	+1.9	42.6	2.6	18.8
23D		S.E. macro	<i>Carex</i>	Denise	Lake water	-25.1	+2.1	45.2	0.8	69.1
43B		S.E. macro	<i>Carex</i>	East Carrol	Lake water	-25.1	+0.7	47.5	1.3	43.6
62A		S.E. macro	<i>Carex</i>	Upper Carrol	Lake water	-26.1	+0.6	41.6	2.0	24.6
Core sediment 15g		Sub sed	N/A	Taylor	N/A	Not analyzed				
Core sediment 10g		Sub sed	N/A	Taylor	N/A	Not analyzed				
Core sediment 5g		Sub sed	N/A	Taylor	N/A	Not analyzed				
Littoral sediment		Litt sed	N/A	East Carrol	N/A	-28.6	-0.7	34.9	1.7	24.1
Littoral sediment		Litt sed	N/A	Taylor	N/A	-25.7	+4.1	3.7	0.3	14.2
Littoral sediment	>250	Litt sed	N/A	Taylor	N/A	-26.7	-0.1	16.7	1.1	17.2
Littoral sediment	<250	Litt sed	N/A	Taylor	N/A	-26.7	-0.1	16.7	1.1	17.2
Littoral sediment	>250	Litt sed	N/A	Denise	N/A	-23.6	+1.6	16.4	1.6	12.0
Littoral sediment	<250	Litt sed	N/A	Denise	N/A	-23.6	+1.6	16.4	1.6	12.0
77A		B.D. shrub	<i>Salix</i>	Taylor	Precipitation	-25.6	-2.2	63.8	2.6	29.2
53A		B.D. shrub	<i>Salix</i>	East Carrol	Precipitation	-27.4	-3.3	46.9	2.6	21.0
54A		B.D. shrub	<i>Salix</i>	East Carrol	Precipitation	-26.5	-3.3	47.2	2.8	19.4
63A		B.D. shrub	<i>Salix</i>	Upper Carrol	Precipitation	-26.8	-2.2	47.3	2.8	19.9
45A		B.D. shrub	<i>Salix</i>	East Carrol	Precipitation	-26.7	-2.8	45.9	3.0	18.0
46A		B.D. shrub	<i>Salix</i>	East Carrol	Precipitation	-28.9	-6.8	46.0	2.3	23.8
57A		B.D. shrub	<i>Salix</i>	Upper Carrol	Precipitation	-25.4	-1.0	47.2	3.2	17.2
55A		B.D. shrub	<i>Betula</i>	East Carrol	Precipitation	-26.2	+0.9	46.3	3.0	18.2
50A		B.D. shrub	<i>Betula</i>	East Carrol	Precipitation	-27.0	-4.8	45.6	3.1	17.1
72A		B.D. shrub	<i>Betula</i>	Upper Carrol	Precipitation	-26.5	-2.4	46.4	3.1	17.3
58A		B.D. shrub	<i>Salix</i>	Upper Carrol	Precipitation	-26.0	-4.1	47.8	2.7	20.6

<i>n</i> -Alkane sample ID	Size fraction (μm)	Group	Genus	Site	Water source	Foliar δ ¹³ C _{TOC} (‰, VPDB)	Foliar δ ¹⁵ N _{TN} (‰, AIR)	Foliar TOC (%)	Foliar TN (%)	Foliar TOC:TN
78A		Herb	<i>Unk.</i>	Taylor	Precipitation	-26.4	-2.0	39.5	2.2	21.3
79A		Herb	<i>Unk.</i>	Taylor	Precipitation	-28.3	-0.9	45.3	2.5	21.3
76B		Herb	<i>Unk.</i>	Taylor	Precipitation	-28.3	-0.9	45.3	2.5	21.3
76A		Herb	<i>Unk.</i>	Taylor	Precipitation	-25.6	-1.0	39.8	2.7	17.3
59A		Conif. tree	<i>Picea</i>	Upper Carrol	Precipitation	-25.8	-3.1	49.8	0.8	73.4
47A		Conif. tree	<i>Picea</i>	East Carrol	Precipitation	-26.4	-3.5	47.1	1.1	50.2
40A		Conif. tree	<i>Picea</i>	East Carrol	Precipitation	-26.9	+0.8	47.5	5.6	9.8
41A		Conif. tree	<i>Picea</i>	East Carrol	Precipitation	-25.8	+0.8	46.4	6.6	8.2
56A		Conif. tree	<i>Picea</i>	Upper Carrol	Precipitation	-27.0	-2.9	46.8	1.1	50.6
5A		Conif. tree	<i>Picea</i>	Walkup	Precipitation	-25.7	-0.8	49.9	1.3	45.8
Moss		Moss	<i>Unk.</i>	Upper Carrol	Precipitation	-25.7				
82A		Lichen	<i>Unk.</i>	Taylor	Precipitation	-23.5	-5.1	22.6	1.1	24.9
81A		Graminoid	<i>Unk.</i>	Taylor	Precipitation	-28.4	-1.5	41.3	2.2	22.1
81B		Graminoid	<i>Unk.</i>	Taylor	Precipitation	-26.9	-3.1	39.8	0.5	92.9
80A		Graminoid	<i>Unk.</i>	Taylor	Precipitation	-28.0	-2.8	40.8	0.9	53.4

Table A.28 Relative abundances of *n*-alkanes extracted from modern sources to Uinta Mountain lakes, and Uinta Mountain lake sediments.

<i>n</i> -Alkane sample ID	C ₁₉ %	C ₂₁ %	C ₂₃ %	C ₂₅ %	C ₂₇ %	C ₂₉ %	C ₃₁ %	C ₃₃ %
14A	2	0	14	13	4	0	0	0
22C	0	0	4	7	6	21	0	8
65A	2	9	8	4	60	7	2	0
24C	0	0	9	8	6	14	22	7
66A	0	8	6	3	63	9	2	0
23D	0	11	6	5	28	28	6	0
43B	1	2	2	2	5	39	37	0
62A	3	9	8	5	50	10	5	2
Core sediment 15g	2	9	11	15	17	17	11	3
Core sediment 10g	3	14	12	13	14	15	11	2
Core sediment 5g	3	12	13	14	13	14	10	2
Littoral sediment	1	6	9	10	10	15	16	8
Littoral sediment	1	2	5	6	8	13	32	17
Littoral sediment	<i>Not analyzed</i>							
Littoral sediment	4	5	9	13	16	8	6	5
Littoral sediment	4	6	11	13	11	9	8	2
Littoral sediment	0	0	4	29	57	8	1	0
77A	0	0	0	0	0	0	0	0
53A	0	1	12	39	39	5	1	0
54A	1	2	10	30	43	6	2	0
63A	0	1	8	30	42	12	2	0
45A	0	0	13	34	42	4	1	0
46A	1	0	1	2	18	49	20	1
57A	0	6	25	48	12	2	1	0
55A	1	1	28	23	38	3	1	0
50A	1	1	36	25	28	3	2	0
72A	0	1	14	27	42	4	4	0
58A	0	1	2	14	26	39	7	1
78A	0	0	4	29	57	8	1	0
79A	1	1	5	14	9	29	29	0
76B	1	0	4	12	13	36	24	3
76A	0	1	5	11	7	33	30	2
59A	8	6	20	9	4	6	6	4
47A	0	6	23	12	6	10	7	0
40A	0	0	30	18	15	0	0	0
41A	0	0	27	26	21	0	27	0
56A	0	0	28	24	15	0	0	0
5A	0	0	17	12	7	12	14	0
MOSS	1	2	4	7	19	28	24	5
82A	0	1	2	3	4	39	38	5
81A	3	8	9	11	15	14	13	3
81B	5	8	9	15	10	17	20	3
80A	5	5	5	10	19	20	20	3

Table A.29 Absolute abundances of *n*-alkanes extracted from modern sources to Uinta Mountain lakes, and Uinta Mountain lake sediments.

<i>n</i> -Alkane sample ID	C ₁₉ (µg/g)	C ₂₁ (µg/g)	C ₂₃ (µg/g)	C ₂₅ (µg/g)	C ₂₇ (µg/g)	C ₂₉ (µg/g)	C ₃₁ (µg/g)	C ₃₃ (µg/g)
14A	4	0	36	32	10	122	16	0
22C	0	0	5	9	7	25	40	10
65A	5	20	18	9	128	15	4	0
24C	0	0	4	4	3	7	11	3
66A	0	27	21	10	205	29	5	0
23D	0	13	8	6	34	34	7	0
43B	8	9	15	14	28	233	220	0
62A	10	30	29	16	175	35	18	6
Core sediment 15g	0	1	2	2	2	2	2	0
Core sediment 10g	0	2	2	2	2	3	2	0
Core sediment 5g	1	4	4	4	4	4	3	1
Littoral sediment	1	3	4	5	5	7	8	4
Littoral sediment	11	38	72	87	121	202	492	260
Littoral sediment	<i>Not analyzed</i>							
Littoral sediment	2	2	4	6	7	4	3	2
Littoral sediment	4	6	10	12	11	8	7	2
Littoral sediment	0	0	42	331	662	87	11	0
77A	0	0	0	0	0	0	0	0
53A	0	7	123	395	398	52	8	0
54A	9	12	77	231	335	50	14	0
63A	0	14	92	362	500	146	22	0
45A	0	0	6	16	20	2	0	0
46A	0	2	6	11	91	241	98	3
57A	102	21	25	55	38	16	14	0
55A	3	8	160	130	217	15	7	0
50A	2	3	94	65	73	7	5	0
72A	0	5	52	101	155	16	15	0
58A	0	5	9	76	147	215	39	4
78A	0	0	42	331	662	87	11	0
79A	1	2	10	27	18	56	54	5
76B	2	0	7	21	24	64	44	5
76A	0	1	5	12	7	35	32	3
59A	2	2	6	3	1	2	2	1
47A	0	3	12	6	3	5	4	0
40A	0	0	3	2	2	0	0	0
41A	0	0	1	1	1	0	0	0
56A	0	1	6	5	3	0	0	0
5A	0	0	2	1	1	1	2	0
MOSS	4	8	18	30	85	128	110	25
82A	8	0	4	5	8	74	68	11
81A	2	4	5	6	8	7	7	1
81B	5	8	9	15	10	17	20	2
80A	6	7	7	13	23	25	26	4

Table A.30 Carbon isotope ratios of C₁₉ and C₂₁ extracted from OM sources to Uinta Mountain lakes.

<i>n</i> -Alkane sample ID	$\delta^{13}\text{C}_{19}$ (‰, VPDB)	No. of replicates	SD of replicates (‰, VPDB)	ϵ_{bulk} (‰, VPDB)	$\delta^{13}\text{C}_{21}$ (‰, VPDB)	No. of replicates	SD of replicates (‰, VPDB)	ϵ_{bulk} (‰, VPDB)
14A								
22C								
65A								
24C								
66A	-31.1	2	0.79	-5.2				
23D								
43B								
62A	-32.5	2	0.09	-6.7	-33.3	2	0.39	-7.5
Core sediment 15g	-28.5	2	0.13		-33.2	2	0.05	
Core sediment 10g	-27.9	2	0.18		-29.4	2	0.55	
Core sediment 5g	-27.9	2	0.18		-33.1	2	4.77	
Littoral sediment					-31.1	2	0.17	
Littoral sediment					-30.5	2	0.26	
Littoral sediment								
Littoral sediment					-28.4	2	0.22	
Littoral sediment					-29.9	2	0.01	
77A								
53A								
54A								
63A								
45A								
46A								
57A								
55A								
50A								
72A								
58A								
78A								
79A								
76B								
76A								
59A								
47A								
40A								
41A								
56A								
5A								
MOSS								
82A								
81A								
81B								
80A								

Table A.31 Carbon isotope ratios of C₂₃ and C₂₅ extracted from OM sources to Uinta Mountain lakes.

<i>n</i> -Alkane sample ID	$\delta^{13}\text{C}_{23}$ (‰, VPDB)	No. of replicates	SD of replicates (‰, VPDB)	ϵ_{bulk} (‰, VPDB)	$\delta^{13}\text{C}_{25}$ (‰, VPDB)	No. of replicates	SD of replicates (‰, VPDB)	ϵ_{bulk} (‰, VPDB)
14A					-30.5	2	0.40	-4.7
22C	-30.8	2	0.00	-3.3	-30.6	2	0.06	-3.1
65A	-33.6	2	0.38	-7.7	-31.2	2	0.67	-5.3
24C								
66A	-33.7	2	0.49	-7.8	-30.5	2	0.30	-4.5
23D								
43B								
62A	-33.9	2	0.25	-8.0	-33.9	2	0.11	-8.1
Core sediment 15g	-28.1	2	0.02		-28.3	2	0.06	
Core sediment 10g	-29.2	2	1.31		-29.6	2	0.83	
Core sediment 5g	-28.9	2	0.79		-28.9	2	0.03	
Littoral sediment	-31.8	2	0.03		-31.8	2	0.07	
Littoral sediment	-31.0	2	0.12		-30.8	2	0.05	
Littoral sediment					-29.3	2	0.40	
Littoral sediment	-29.6	2	1.20		-29.6	2	0.04	
Littoral sediment	-30.1	2	0.05		-29.9	2	0.10	
77A					-27.9	2	0.11	-2.4
53A	-31.3	2	0.01	-4.0	-29.9	2	0.01	-2.5
54A	-31.8	2	0.36	-5.4	-29.8	2	0.03	-3.4
63A	-31.0	2	0.16	-4.3	-30.5	2	0.14	-3.8
45A	-31.9	2	0.12	-5.4	-32.0	2	0.04	-5.5
46A					-37.5	2	0.11	-8.9
57A								
55A	-30.6	2	0.13	-4.6	-30.1	2	0.17	-4.0
50A	-32.0	2	0.12	-5.2	-32.2	2	0.06	-5.4
72A	-32.7	2	0.16	-6.4	-32.1	2	0.17	-5.7
58A								
78A	-29.6	2	0.06	-3.2	-28.0	2	0.02	-1.6
79A					-32.6	2	0.27	-4.4
76B					-32.6	2	0.25	-4.0
76A								
59A								-4.0
47A	-28.6	2	0.01	-2.3	-29.9	2	1.84	-4.0
40A								
41A								
56A								
5A	-31.3	2	0.60	-5.7	-31.2	2	1.26	-5.7
MOSS					-32.0	2		-6.4
82A					-32.4	2		-7.8
81A								
81B								-8.7
80A					-33.6	2	0.51	-5.8

Table A.32 Carbon isotope ratios of C₂₇ and C₂₉ extracted from OM sources to Uinta Mountain lakes.

<i>n</i> -Alkane sample ID	$\delta^{13}\text{C}_{27}$ (‰, VPDB)	No. of replicates	SD of replicates (‰, VPDB)	ϵ_{bulk} (‰, VPDB)	$\delta^{13}\text{C}_{29}$ (‰, VPDB)	No. of replicates	SD of replicates (‰, VPDB)	ϵ_{bulk} (‰, VPDB)
14A	-32.7	2	0.56	-7.0	-35.4	2	0.33	-9.7
22C	-29.9	2	0.07	-2.4				
65A	-35.3	2	0.00	-9.5				
24C								
66A	-36.0	2	0.99	-10.1				
23D								
43B								
62A	-34.5	2	0.14	-8.6	-35.2	2	0.1	-9.4
Core sediment 15g	-28.0	2	0.02		-30.2	2	0.02	
Core sediment 10g	-29.0	2	0.37		-30.6	2	0.40	
Core sediment 5g	-28.5	2	0.31		-30.7	2	0.32	
Littoral sediment	-32.0	2	0.13		-33.7	2	0.11	
Littoral sediment	-31.3	2	0.10		-32.1	2	0.16	
Littoral sediment	-29.5	2	0.38		-31.8	2	0.36	
Littoral sediment	-30.0	2	0.53		-33.2	2	1.35	
Littoral sediment	-29.2	2	0.09		-30.4	2	0.01	
77A	-27.4	2	0.09	-1.9				
53A	-31.2	2	0.07	-3.8	-31.7	2	0.25	-4.4
54A	-30.1	2	0.12	-3.7				
63A	-30.8	2	0.00	-4.1	-30.6	2	0.23	-3.9
45A	-32.4	2	0.14	-5.9	-34.1	2	1.41	-7.6
46A	-37.8	2	0.01	-9.2	-39.0	2	0.08	-10.4
57A								
55A	-29.5	2	0.21	-3.4				
50A	-31.5	2	0.02	-4.6				
72A	-32.3	2	0.18	-6.0				
58A								
78A	-27.7	2	0.09	-1.4	-27.2	2	0.25	-0.8
79A	-33.2	2	0.16	-5.1	-34.5	2	0.10	-6.4
76B	-33.8	2	0.14	-5.6	-34.0	2	0.24	-5.8
76A					-34.1	2	0.01	-8.7
59A								
47A	-31.3	2	0.20	-5.1	-32.1	2	0.10	-5.9
40A								
41A								
56A								
5A				-4.8				
MOSS	-33.7	2	0.33	-8.1	-34.3	2	0.08	-8.8
82A				-11.1	-35.4	2	0.08	-12.2
81A								
81B				-7.6				-8.9
80A	-33.1	2	0.07	-5.3	-33.2	2	0.08	-5.4

Table A.33 Carbon isotope ratios of C₃₁ and C₃₃ extracted from OM sources to Uinta Mountain lakes.

<i>n</i> -Alkane sample ID	$\delta^{13}\text{C}_{31}$ (‰, VPDB)	No. of replicates	SD of replicates (‰, VPDB)	ϵ_{bulk} (‰, VPDB)	$\delta^{13}\text{C}_{33}$ (‰, VPDB)	No. of replicates	SD of replicates (‰, VPDB)	ϵ_{bulk} (‰, VPDB)
14A								
22C								
65A								
24C								
66A								
23D								
43B								
62A	-35.4	2	0.22	-9.6				
Core sediment 15g	-31.3	2	0.06		-30.5	2	0.13	
Core sediment 10g								
Core sediment 5g	-31.7	2	0.12					
Littoral sediment	-34.3	2	0.48		-33.8	2	0.00	
Littoral sediment	-32.0	2	0.05		-31.4	2	0.10	
Littoral sediment								
Littoral sediment	-33.5	2	0.07					
Littoral sediment	-33.6	2	0.08					
77A								
53A								
54A								
63A								
45A								
46A								
57A								
55A								
50A								
72A								
58A								
78A								
79A	-34.8	2	0.19	-6.7				
76B	-34.3	2	0.35	-6.2				
76A	-34.1	2	0.02	-8.8				
59A								
47A								
40A								
41A	-29.5	2	0.20	-3.8				
56A								
5A								
MOSS	-34.8	2	0.01	-9.4				
82A	-36.3	2	0.01	-13.1				
81A								
81B								
80A	-34.4	2	0.43	-6.6				

Table A.34 Hydrogen isotope ratios of C₁₉ and C₂₁ extracted from OM sources to Uinta Mountain lakes.

<i>n</i> -Alkane sample ID	$\delta^2\text{H}_{\text{C}_{19}}$ (‰, VPDB)	No. of replicates	SD of replicates (‰, VPDB)	ϵ_{water} (‰, VSMOW)	$\delta^2\text{H}_{\text{C}_{21}}$ (‰, VPDB)	No. of replicates	SD of replicates (‰, VPDB)	ϵ_{water} (‰, VSMOW)
14A								
22C								
65A								
24C								
66A								
23D								
43B								
62A								
Core sediment 15g								
Core sediment 10g								
Core sediment 5g								
Littoral sediment					-208	3	5.7	
Littoral sediment								
Littoral sediment								
Littoral sediment								
Littoral sediment								
77A								
53A								
54A								
63A								
45A								
46A								
57A								
55A								
50A								
72A								
58A								
78A								
79A								
76B								
76A								
59A								
47A								
40A								
41A								
56A								
5A								
MOSS								
82A								
81A								
81B								
80A								

Table A.35 Hydrogen isotope ratios of C₁₉ and C₂₁ extracted from OM sources to Uinta Mountain lakes.

<i>n</i> -Alkane sample ID	$\delta^2\text{H}_{\text{C}_{23}}$ (‰, VPDB)	No. of replicates	SD of replicates (‰, VPDB)	ϵ_{water} (‰, VSMOW)	$\delta^2\text{H}_{\text{C}_{25}}$ (‰, VPDB)	No. of replicates	SD of replicates (‰, VPDB)	ϵ_{water} (‰, VSMOW)
14A								
22C	-183	3	2.09	-81	-184	3	0.70	-83
65A								
24C								
66A								
23D								
43B								
62A								
Core sediment 15g	-209	3	4.44		-205	3	1.48	
Core sediment 10g					-209	3	2.30	
Core sediment 5g								
Littoral sediment	-203	3	6.68		-208	3	3.29	
Littoral sediment					-222	3	2.77	
Littoral sediment								
Littoral sediment								
Littoral sediment								
77A					-192	3	3.60	-89
53A	-188	3	0.83	-70	-203	3	0.67	-89
54A					-199	3	2.07	-83
63A					-211	3	4.26	-98
45A	-153	3	5.11	-31	-196	3	2.78	-80
46A								
57A								
55A	-181	3	0.75	-63	-177	3	0.37	-58
50A	-180	3	0.59	-62	-172	3	0.43	-53
72A					-175	3	1.31	-56
58A								
78A					-201	3	0.24	-86
79A								
76B								
76A								
59A								
47A								
40A								
41A								
56A								
5A								
MOSS					-191	3	2.80	-75
82A								
81A								
81B								
80A					-217	3	1.05	-104

Table A.36 Hydrogen isotope ratios of C₂₇ and C₂₉ extracted from OM sources to Uinta Mountain lakes.

<i>n</i> -Alkane sample ID	$\delta^2\text{H}_{\text{C}_{27}}$ (‰, VPDB)	No. of replicates	SD of replicates (‰, VPDB)	ϵ_{water} (‰, VSMOW)	$\delta^2\text{H}_{\text{C}_{29}}$ (‰, VPDB)	No. of replicates	SD of replicates (‰, VPDB)	ϵ_{water} (‰, VSMOW)
14A	-247	3	0.33	-154	-221	3	1.91	-124
22C	-177	3	0.88	-71	-160	3	3.39	-52
65A	-257	3	1.35	-165				
24C								
66A	-255	3	0.50	-162				
23D								
43B								
62A								
Core sediment 15g	-206	3	0.13		-199	3	1.02	
Core sediment 10g	-207	3	2.91		-201	3	0.03	
Core sediment 5g								
Littoral sediment								
Littoral sediment	-221	3	1.31		-214	3	3.10	
Littoral sediment								
Littoral sediment								
Littoral sediment								
77A	-198	3	1.62	-83	-191	3	2.57	-75
53A	-182	3	0.28	-64	-171	3	2.65	-51
54A	-185	3	0.49	-67	-175	3	3.63	-56
63A	-203	3	3.35	-88	-201	3	4.19	-86
45A	-207	3	1.99	-92				
46A	-176	3	1.20	-57	-183	3	0.80	-65
57A								
55A	-176	3	0.87	-58				
50A	-164	3	0.76	-43				
72A	-171	3	1.69	-52	-143	3	4.21	-20
58A								
78A	-205	3	0.38	-90	-202	3	1.55	-86
79A								
76B								
76A								
59A								
47A								
40A								
41A								
56A								
5A								
MOSS	-202	3	2.01	-87	-208	3	2.10	-94
82A	-200	3	0.37	-84	-229	3	0.63	-118
81A								
81B								
80A								

Table A.37 Hydrogen isotope ratios of C₃₁ and C₃₃ extracted from OM sources to Uinta Mountain lakes.

<i>n</i> -Alkane sample ID	$\delta^2\text{H}_{\text{C}_{31}}$ (‰, VPDB)	No. of replicates	SD of replicates (‰, VPDB)	ϵ_{water} (‰, VSMOW)	$\delta^2\text{H}_{\text{C}_{33}}$ (‰, VPDB)	No. of replicates	SD of replicates (‰, VPDB)	ϵ_{water} (‰, VSMOW)
14A								
22C								
65A								
24C								
66A								
23D								
43B								
62A								
Core sediment 15g								
Core sediment 10g								
Core sediment 5g								
Littoral sediment	-203	3	8.63					
Littoral sediment								
Littoral sediment								
Littoral sediment								
Littoral sediment								
Littoral sediment								
77A								
53A								
54A								
63A								
45A								
46A								
57A								
55A								
50A								
72A								
58A								
78A								
79A								
76B								
76A								
59A								
47A								
40A								
41A								
56A								
5A								
MOSS								
82A								
81A								
81B								
80A								

Table A.38 Oxygen isotope ratios of Uinta Mountain lake waters.

Sample ID	Site	Year	Source of water	Type of water	$\delta^{18}\text{O}$ (‰, VSMOW)	No. of replicates	SD of replicates (‰, VPDB)
14-UN-08	Taylor	2014	Middle of lake	Lake water	-14.8		
15-UN-08	Taylor	2015	Middle of lake	Lake water	-14.7	1	0.35
15-UN-55	Upper Carrol	2015	Middle of lake	Lake water	-13.7		
15-UN-56	East Carrol	2015	Middle of lake	Lake water	-12.4		
15-UN-07	Denise	2015	Middle of lake	Lake water	-14.4		
14-UN-07_INA	Denise	2014	Inlet	Lake water	-14.7		
14-UN-07_INB	Denise	2014	Inlet	Lake water	-16.4		
14-UN-07	Denise	2014	Middle of lake	Lake water	-16.4		
09-UN-58 IN1A	Bluebell Pass	2009	Inlet	Lake water	-17.1	1	0.02
12-UN-08	Taylor	2012	Middle of lake	Lake water	-18.0		
12-UN-57	No Name	2012	Middle of lake	Lake water	-16.1		
12-UN-58	Bluebell Pass	2012	Middle of lake	Lake water	-16.5		
12-UN-56	East Carrol	2012	Middle of lake	Lake water	-14.5		
09-UN-55	Upper Carrol	2009	Middle of lake	Lake water	-15.9		
12-UN-55	Upper Carrol	2012	Middle of lake	Lake water	-16.6		
09-UN-56	East Carrol	2009	Middle of lake	Lake water	-13.4		
08-UN-08-IN2	Taylor	2008	Inlet	Lake water	-17.5		
08-UN-08-IN10	Taylor	2008	Inlet	Lake water	-19.4		
08-UN-32	Walkup	2008	Middle of lake	Lake water	-16.7		
08-UN-58-IN1B	Bluebell Pass	2008	Inlet	Lake water	-16.5	1	0.94
09-UN-56-IN1B	East Carrol	2009	Inlet	Lake water	-14.9		
09-UN-08-IN2	Taylor	2009	Inlet	Lake water	-15.0		
09-UN-55-IN1A	Upper Carrol	2009	Inlet	Lake water	-16.0		
08-UN-57	No Name	2008	Middle of lake	Lake water	-12.5	1	0.06
09-UN-07	Denise	2009	Middle of lake	Lake water	-15.6		
09-UN-58 SNOW	Bluebell Pass	2009	Unknown	Snow	-18.6		
08-UN-56-IN1	East Carrol	2008	Inlet	Lake water	-16.3		
09-UN-08-IN1B	Taylor Lake	2009	Inlet	Lake water	-17.9		
08-UN-07-IN	Denise Lake	2008	Inlet	Lake water	-17.6		
09-UN-08-IN3	Taylor Lake	2009	Inlet	Lake water	-15.0		
09-UN-55-IN1B	Upper Carrol	2009	Inlet	Lake water	-15.6		
08-UN-58	Bluebell Pass	2008	Middle of lake	Lake water	-14.8	1	0.01
09-UN-86	?	2009	Middle of lake	Lake water	-16.7		
09-UN-58-IN1C	Bluebell Pass	2009	Inlet	Lake water	-16.4		
08-UN-58-IN1A	Bluebell Pass	2008	Inlet	Lake water	-16.6		
09-UN-08 SNOW	Taylor Lake	2009	Unknown	Snow	-18.4		
08-UN-08-IN1A	Taylor Lake	2008	Inlet	Lake water	-23.5		
09-UN-58-IN1B	Bluebell Pass	2009	Inlet	Lake water	-16.5		
09-UN-07-IN1	Denise	2009	Inlet	Lake water	-16.1		
08-UN-86	?	2008	Middle of lake	Lake water	-17.6		
08-UN-55	Upper Carrol	2008	Middle of lake	Lake water	-15.3		
08-UN-08-IN1C	Taylor	2008	Inlet	Lake water	-19.4		
08-UN-08-IN3	Taylor	2008	Inlet	Lake water	-19.9		

Sample ID	Site	Year	Source of water	Type of water	$\delta^{18}\text{O}$ (‰, VSMOW)	No. of replicates	SD of replicates (‰, VPDB)
08-UN-55-IN1	Upper Carrol	2008	Inlet	Lake water	-16.4		
09-UN-08-IN1C	Taylor	2009	Inlet	Lake water	-17.8		
09-UN-56-IN1A	East Carrol	2009	Inlet	Lake water	-14.2	1	1.02
09-UN-08-IN1A	Taylor	2009	Inlet	Lake water	-17.9		
08-UN-08-1N1B	Taylor	2008	Inlet	Lake water	-21.8	1	0.01

Table A.39 Hydrogen isotope ratios of Uinta Mountain lake waters

Sample ID	Site	Year	Source of water	Type of water	$\delta^2\text{H}$ (‰, VSMOW)	No. of replicates	SD of replicates (‰, VPDB)
14-UN-08	Taylor	2014	Middle of lake	Lake water	-108		
15-UN-08	Taylor	2015	Middle of lake	Lake water	-104	1	2.01
15-UN-55	Upper Carrol	2015	Middle of lake	Lake water	-95		
15-UN-56	East Carrol	2015	Middle of lake	Lake water	-95		
15-UN-07	Denise	2015	Middle of lake	Lake water	-97		
14-UN-07_INA	Denise	2014	Inlet	Lake water	-104		
14-UN-07_INB	Denise	2014	Inlet	Lake water	-125		
14-UN-07	Denise	2014	Middle of lake	Lake water	-123		
09-UN-58 IN1A	Bluebell Pass	2009	Inlet	Lake water	-120	1	0.47
12-UN-08	Taylor	2012	Middle of lake	Lake water	-130		
12-UN-57	No Name	2012	Middle of lake	Lake water	-121		
12-UN-58	Bluebell Pass	2012	Middle of lake	Lake water	-122		
12-UN-56	East Carrol	2012	Middle of lake	Lake water	-107		
09-UN-55	Upper Carrol	2009	Middle of lake	Lake water	-114		
12-UN-55	Upper Carrol	2012	Middle of lake	Lake water	-119		
09-UN-56	East Carrol	2009	Middle of lake	Lake water	-102		
08-UN-08-IN2	Taylor	2008	Inlet	Lake water	-126		
08-UN-08-IN10	Taylor	2008	Inlet	Lake water	-143		
08-UN-32	Walkup	2008	Middle of lake	Lake water	-125		
08-UN-58-IN1B	Bluebell Pass	2008	Inlet	Lake water	-120	1	1.21
09-UN-56-IN1B	East Carrol	2009	Inlet	Lake water	-106		
09-UN-08-IN2	Taylor	2009	Inlet	Lake water	-107		
09-UN-55-IN1A	Upper Carrol	2009	Inlet	Lake water	-115		
08-UN-57	No Name	2008	Middle of lake	Lake water	-103	1	0.58
09-UN-07	Denise	2009	Middle of lake	Lake water	-119		
09-UN-58 SNOW	Bluebell Pass	2009	Unknown	Snow	-139		
08-UN-56-IN1	East Carrol	2008	Inlet	Lake water	-116		
09-UN-08-IN1B	Taylor Lake	2009	Inlet	Lake water	-129		
08-UN-07-IN	Denise Lake	2008	Inlet	Lake water	-131		
09-UN-08-IN3	Taylor Lake	2009	Inlet	Lake water	-106		
09-UN-55-IN1B	Upper Carrol	2009	Inlet	Lake water	-114		
08-UN-58	Bluebell Pass	2008	Middle of lake	Lake water	-115	1	0.58
09-UN-86	?	2009	Middle of lake	Lake water	-124		
09-UN-58-IN1C	Bluebell Pass	2009	Inlet	Lake water	-119		
08-UN-58-IN1A	Bluebell Pass	2008	Inlet	Lake water	-119		
09-UN-08 SNOW	Taylor Lake	2009	Unknown	Snow	-139		
08-UN-08-IN1A	Taylor Lake	2008	Inlet	Lake water	-181		
09-UN-58-IN1B	Bluebell Pass	2009	Inlet	Lake water	-119		
09-UN-07-IN1	Denise	2009	Inlet	Lake water	-122		
08-UN-86	?	2008	Middle of lake	Lake water	-133		
08-UN-55	Upper Carrol	2008	Middle of lake	Lake water	-114		
08-UN-08-IN1C	Taylor	2008	Inlet	Lake water	-142		
08-UN-08-IN3	Taylor	2008	Inlet	Lake water	-147		

Sample ID	Site	Year	Source of water	Type of water	$\delta^2\text{H}$ (‰, VSMOW)	No. of replicates	SD of replicates (‰, VPDB)
08-UN-55-IN1	Upper Carrol	2008	Inlet	Lake water	-120		
09-UN-08-IN1C	Taylor	2009	Inlet	Lake water	-129		
09-UN-56-IN1A	East Carrol	2009	Inlet	Lake water	-105	1	2.11
09-UN-08-IN1A	Taylor	2009	Inlet	Lake water	-129		
08-UN-08-1N1B	Taylor	2008	Inlet	Lake water	-163	1	0.45

Appendix B: Supplementary methods for Chapter 2

Table B.1 Sample preparation methods in Chapter 2.

Core(s)	Analyses	Sample preparation
BL-G11-01 and BL-G17-01	$\delta^{13}\text{C}_{\text{TOC}}$, $\delta^{15}\text{N}_{\text{TN}}$, %TOC, %TN	Sediments were freeze dried, ground and sieved to $<300\ \mu\text{m}$. Then, sediments designated for the analysis of $\delta^{13}\text{C}_{\text{TOC}}$ and %TOC underwent acid fumigation following Harris et al. (2014) prior to analysis. Fractions analyzed to determine $\delta^{15}\text{N}_{\text{TN}}$ and %TN were not acid-fumigated.
	$\delta^{13}\text{C}_{\text{marl}}$ and $\delta^{18}\text{O}_{\text{marl}}$ of sediments	Samples were inspected for mollusc shells and shell fragments, which were removed by hand-picking prior to further processing. The remaining sediment was freeze-dried, ground using a Wig-L-Bug [®] for 1.5 minutes, and then sieved to $<300\ \mu\text{m}$.
BL-G17-01 only	AMS dating	Woody fragments, shelly fauna and charcoal fragments were hand-picked, while bulk sediment samples were freeze-dried, ground and sieved to $<300\ \mu\text{m}$. At the A.E. Lalonde AMS Laboratory (Ottawa, Canada), woody and charcoal fragments were treated with an acid-alkali-acid (AAA) wash. Shelly fauna were treated with pre-etch and digestion. Bulk sediments were treated with an acid wash only.
BL-G11-02 only	^{210}Pb dating	Sediment samples from BL-G11-02 were dated using ^{210}Pb techniques on 20 dried and ground samples between 0 cm and 30.75 cm core depth. Sediment samples were transferred, still frozen, to the Laboratory for the Analysis of Natural and Synthetic Environmental Toxins (LANSET), at the University of Ottawa, for ^{210}Pb dating. Keeping the samples frozen allowed for the accurate determination of wet weights and porosity.
BL-G11-01, BL-G17-01 and BL-G11-02	Magnetic susceptibility	Samples from BL-G11-02 and BL-G17-01 were freeze-dried. Samples from BL-G11-01 were not freeze-dried (<i>i.e.</i> , were analyzed wet).

B.1 Additional details regarding the creation of the age-depth model

To calculate the height of sediment deposited during the 5.6 years between collection of BL-G11-01 and BL-G17-01, a plot of age versus depth was created using dates generated via ^{210}Pb dating of BL-G11-02. The equation of a cubic polynomial fitted to these data was used to determine that ~ 0.69 cm of sediment had been deposited during this time (Fig. B.1); this offset was used to adjust inputs to the “Bacon” models (Table B.2). For BL-G11-01, the depths associated with the ^{210}Pb dates were unchanged since these dates were measured in BL-G11-02 and then correlated to BL-G11-01. Depths associated with ^{14}C dates in BL-G11-01, however, were decreased by 0.69 cm since ^{14}C dates were determined using material from the BL-G17-01 core. Likewise, depths associated with the ^{210}Pb dates were increased by 0.69 cm for BL-G17-01 because they were determined using sediments from BL-G11-02. Each of the age models (one for BL-G11-01 and one for BL-G17-01) generated accumulation rates in cm/year which were multiplied by bulk dry density (mg/cm^3) to obtain accumulation rates in $\text{mg}/\text{cm}^2/\text{year}$.

Table B.2 Calibrated and uncalibrated AMS ¹⁴C (BL-G17-01) and ²¹⁰Pb dates (BL-G11-02). Depths of BL-G17-01 are in parentheses. Depths from BL-G17-01 are 0.69 cm lower than those of BL-G11-01 to account for the 5.6-year difference between collection of the cores.

Dating method	ID	Depth in core (cm)	Dated material	Uncalibrated age (¹⁴ C yr AD)	Calibrated age (AD)	Error
Surface of BL-G17-01		0	N/A		2017.5	0.0010
²¹⁰ Pb		0.25 (0.94)	Bulk sediment		2012	0.0028
		1.25 (1.94)			2010	0.0185
		2.25 (2.94)			2007	0.0245
		3.25 (3.94)			2003	0.0222
		4.25 (4.94)			1999	0.0265
		5.25 (5.94)			1995	0.0636
		6.25 (6.94)			1990	0.1065
		7.25 (8.94)			1985	0.1515
		8.25 (9.59)			1980	0.2015
		9.75 (10.44)			1973	0.2992
		11.25 (11.94)			1967	0.3983
		13.25 (13.94)			1959	0.5628
		15.25 (15.94)			1949	0.8503
		17.25 (17.94)			1930	1.7384
	19.25 (19.94)		1893	5.7728		
¹⁴ C (AMS)	UOC-7781	20.56 (21.25)	Wood	1751	1650-1684 (23.8 %) 1733-1807 (51.6 %) 1929 (20.0 %)	26
	UOC-7782	26.06 (26.75)	Bulk sediment	1344	1296- 1405 (95.4 %)	26
	UOC-7338	31.56 (32.25)	Charcoal	1289	1280- 1317 (47.5 %); 1353-1389 (47.9 %)	22
	UOC-7339	31.56 (32.25)	Shell fragments	1255	1268- 1302 (82.9 %); 1366- 1383 (12.5 %)	22
	UOC-7783	41.06 (41.75)	Shell fragments	966	994- 1052 (51.9 %); 1080- 1152 (43.5 %)	26

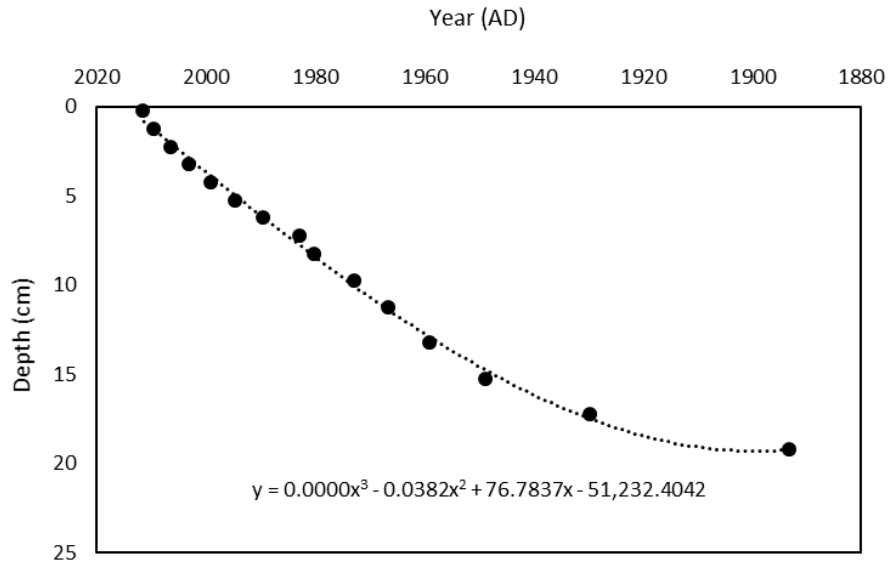


Figure B.1 Estimate of the sedimentation rate of Barry Lake from AD 1900– 2017.

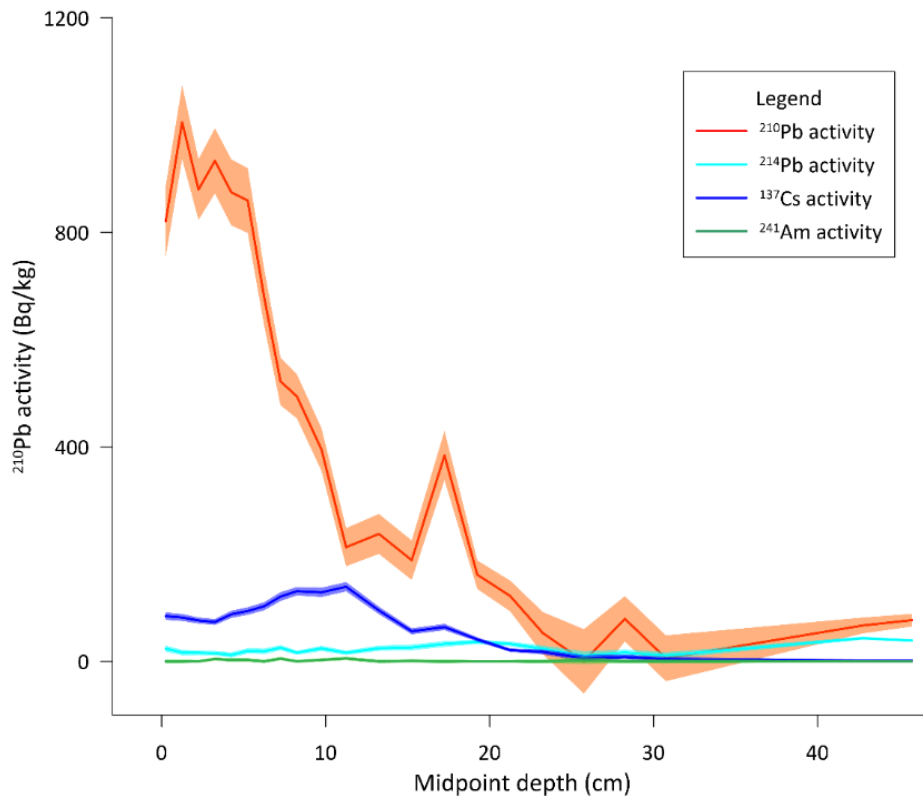


Figure B.2 Downcore activity of ^{210}Pb , ^{214}Pb , ^{137}Cs and ^{241}Am in core BL-G11-01. Shading represents the error associated with each measurement.

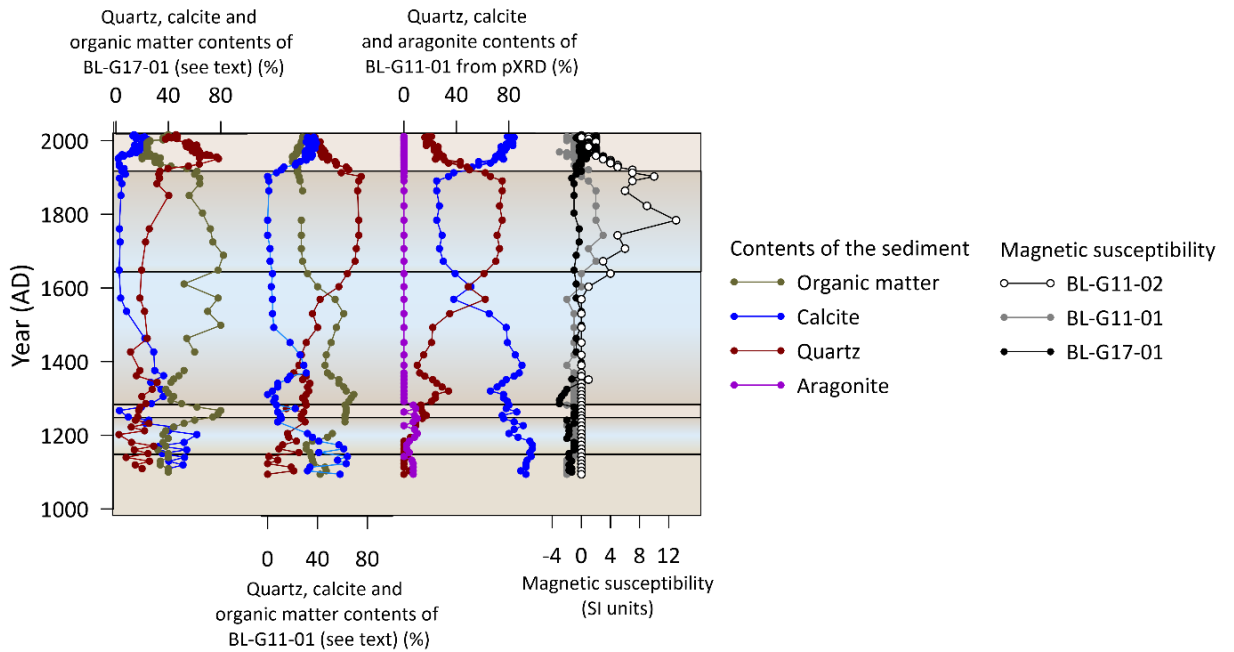


Figure B.3 Age (depth) dependent variation (from left to right) in: *(i)* quartz, calcite and OM contents of BL-G17-01 and BL-G11-01 (see text), *(ii)* quartz, calcite and aragonite contents of BL-G11-01 determined by powder x-ray diffraction (pXRD) (normalized to 100%), and *(iii)* magnetic susceptibility of BL-G17-01 (black), BL-G11-01 (grey) and BL-G11-02 (white). Time periods shaded blue are interpreted to be wetter than average, whereas yellow shading denotes drier periods.

Table B.3 The Pearson correlation coefficient (*r*) between two variables, and associated *p*-values. All variables are derived from BL-G17-01 (see text). Values of $\delta^{13}\text{C}_{\text{TOC}}$ and $\delta^{13}\text{C}_{\text{marl}}$ were Suess-corrected prior to these tests according to Verburg (2007).

Year (AD)	Variable1	Variable2	<i>r</i>	<i>p</i> -value	Significant at <i>p</i> < 0.01?
1100-2017	Calcite-MAR	TOC-MAR	0.848	< 0.00001	Yes
1100-2017	Calcite-MAR	TN-MAR	0.836	< 0.00001	Yes
1100-2017	Calcite-MAR	Chl- <i>a</i> (_s)-MAR	0.882	< 0.00001	Yes
1100-2017	Calcite-MAR	$\delta^{18}\text{O}_{\text{marl}}$	-0.063	0.62	No
1100-2017	$\delta^{18}\text{O}_{\text{marl}}$	TOC-MAR	-0.274	0.02	No
1100-2017	$\delta^{18}\text{O}_{\text{marl}}$	TN-MAR	-3.086	0.01	No
1100-2017	$\delta^{18}\text{O}_{\text{marl}}$	Chl- <i>a</i> (_s)-MAR	-0.255	0.03	No
1100-2017	$\delta^{18}\text{O}_{\text{marl}}$	$\delta^{13}\text{C}_{\text{marl}}$	0.759	<0.00001	Yes
1100-2017	$\delta^{18}\text{O}_{\text{marl}}$	$\delta^{13}\text{C}_{\text{TOC}}$	0.759	<0.00001	Yes
1100-2017	$\delta^{13}\text{C}_{\text{marl}}$	TOC-MAR	-0.201	0.09	No
1100-2017	$\delta^{13}\text{C}_{\text{marl}}$	TN-MAR	-0.157	0.20	No
1100-2017	$\delta^{13}\text{C}_{\text{marl}}$	Chl- <i>a</i> (_s)-MAR	0.0899	0.46	No
1100-2017	$\delta^{13}\text{C}_{\text{marl}}$	calcite-MAR	-0.006	0.96	No
1100-2017	$\delta^{13}\text{C}_{\text{TOC}}$	TOC-MAR	-0.587	< 0.00001	Yes
1100-2017	$\delta^{13}\text{C}_{\text{TOC}}$	TN-MAR	-0.631	<0.00001	Yes
1100-2017	$\delta^{13}\text{C}_{\text{TOC}}$	Chl- <i>a</i> (_s)-MAR	-0.571	<0.00001	Yes
1100-2017	$\delta^{13}\text{C}_{\text{TOC}}$	calcite-MAR	-0.372	<0.0025	Yes
1100-2017	$\delta^{15}\text{N}_{\text{TN}}$	TOC-MAR	0.717	<0.00001	Yes
1100-2017	$\delta^{15}\text{N}_{\text{TN}}$	TN-MAR	0.777	< 0.00001	Yes
1100-2017	$\delta^{15}\text{N}_{\text{TN}}$	Chl- <i>a</i> (_s)-MAR	0.559	< 0.00001	Yes
1100-2017	$\delta^{15}\text{N}_{\text{TN}}$	calcite-MAR	0.508	0.00002	Yes
1100-1900	$\delta^{13}\text{C}_{\text{TOC}}$	TOC-MAR	-0.169	0.29	No
1100-1900	$\delta^{13}\text{C}_{\text{TOC}}$	TN-MAR	-0.202	0.21	No
1100-1900	$\delta^{13}\text{C}_{\text{TOC}}$	Chl- <i>a</i> (_s)-MAR	0.101	0.53	No
1100-1900	$\delta^{13}\text{C}_{\text{TOC}}$	calcite-MAR	0.004	0.98	No
1950-2017	$\delta^{18}\text{O}_{\text{marl}}$	TOC-MAR	0.195	0.30	No
1950-2017	$\delta^{18}\text{O}_{\text{marl}}$	TN-MAR	0.153	0.43	No
1950-2017	$\delta^{18}\text{O}_{\text{marl}}$	Chl- <i>a</i> (_s)-MAR	0.223	0.24	No
1950-2017	$\delta^{18}\text{O}_{\text{marl}}$	calcite-MAR	0.550	0.0036	Yes

B.2 References for Appendix B.

Harris, David, Horwath, William R., VanKessel, C., 2001. Acid fumigation of soils to total organic carbon. *Soil Soc. Am. J.* 65, 1853–1856.

Verburg, P., 2007. The need to correct for the Suess effect in the application of $\delta^{13}\text{C}$ in sediment of autotrophic Lake Tanganyika, as a productivity proxy in the Anthropocene. *J. Paleolimnol.* 37, 591–602.

Appendix C: Supplementary methods for Chapter 3

C.1 Sample preparation methods

Table C.1 Sample preparation methods.

Source of sample	Analyses	Sample preparation
Core BL-G16-01	$\delta^{13}\text{C}_{\text{TOC}}$	Sediments were freeze dried, ground and sieved to $<300\ \mu\text{m}$. Then, samples underwent acid fumigation following Harris et al. (2014) prior to analysis.
Core BL-G11-01	$\delta^{13}\text{C}$ of shelly fauna	First, the shells were placed in an ultrasonic bath filled with distilled water. The shells were ultrasonicated for 5 minutes. Then, they were rinsed in distilled water and air-dried. Under a microscope, the shells were cleaned of any detritus adhering to the inside or outside of the shell. Approximately 0.09 mg of the cleaned shell sample was then weighed into a reaction vessel, sealed with silicone septa and placed in the GasBench [®] heating block at 90 °C. A double-bore needle was then pushed through the septa into the vial. Next, the vial was evacuated with He and orthophosphoric acid was dispensed onto the sample. Samples and acid were left to react for 12 minutes. The evolved CO ₂ was then passed through a trap to remove water and cryogenically collected using an external cold finger. Finally, the gas was transferred to the IRMS for isotopic analysis.
Modern water	$\delta^{13}\text{C}_{\text{DIC}}$	For samples, five drops of 100 % concentrated orthophosphoric acid was added to the bottom of the glass vials, which were septum-sealed and flushed with He for 5 minutes. Using a syringe, 1 mL of sample was injected into the flushed vial. The vials then reacted in the GasBench heater block at 35 °C overnight prior to isotopic measurements. 0.25 mg of each standard was weighed into the bottom of a clean, oven-baked vial, and the vial was placed in a horizontal position. Concentrated (100 %) orthophosphoric acid was then added to the top of the vial such that the acid was separated from the standard. A septum cap was then attached to the vial and tightened. Next, the vial was flushed with He for 5 minutes at room temperature and turned upright, allowing the acid to react with the standard powder. The vial was then immediately placed in the GasBench [®] heating block overnight to react at 35 °C. The gas produced from standards and samples were then transported automatically to the IRMS using an autosampler.

C.2 Calculating $\delta^{13}\text{C}_{\text{DIC}}$ from $\delta^{13}\text{C}_{\text{Pisidium}}$, $\delta^{13}\text{C}_{H. anceps}$ and $\delta^{13}\text{C}_{\text{marl}}$

The $\delta^{13}\text{C}_{\text{marl}}$ was converted to an estimated $\delta^{13}\text{C}_{\text{DIC}}$ by subtracting 1 ‰ to account for the temperature-insensitive carbon isotope fractionation between calcite and DIC (Romanek et al., 1992). Estimating the $\delta^{13}\text{C}_{\text{DIC}}$ using $\delta^{13}\text{C}_{\text{Pisidium}}$ and $\delta^{13}\text{C}_{H. anceps}$ was more complicated for three reasons: (i) *H. anceps* is an air-breathing gastropod, (ii) the $\delta^{13}\text{C}$ of both shells must be corrected for vital effects, and (iii) the estimated $\delta^{13}\text{C}_{\text{DIC}}$ must account for the fractionation between aragonite and DIC.

Although Fritz and Poplawski (1974) found that aquatic gastropods such as *H. anceps* grown under different $\delta^{13}\text{C}_{\text{DIC}}$ conditions precipitate their shells in close to carbon isotope equilibrium with DIC, McConnaughey et al. (1997) demonstrated that the carbon used by freshwater gastropods includes both metabolic carbon (10 %) and DIC (>90 %). Since metabolic carbon in freshwater gastropods originates from food and respired carbon that has much lower $\delta^{13}\text{C}$ than DIC (McConnaughey et al., 1997), $\delta^{13}\text{C}_{H. anceps}$ and $\delta^{13}\text{C}_{\text{Pisidium}}$ were corrected for vital effects before being used to estimate $\delta^{13}\text{C}_{\text{DIC}}$. Von Grafenstein et al. (1999) established a vital effect correction of -0.2 ‰ for *Pisidium* species. No vital effect has, to my knowledge, been reported for *H. anceps*.

A vital effect correction is especially needed for *H. anceps* since this species breathes air, which may result in its shell containing an especially high amount of metabolic carbon (Shanahan et al., 2005). Accordingly, one was estimated in the absence of an established value. First, the expected $\delta^{13}\text{C}$ of *H. anceps* was calculated, assuming that it precipitated its shell in carbon isotope equilibrium with the surrounding DIC (*i.e.*, if there was no vital effect). To perform this calculation, the average $\delta^{13}\text{C}_{\text{DIC}}$ of modern Barry Lake waters ($\delta^{13}\text{C}_{\text{DIC}} = -3.8$ ‰), and the fractionation between aragonite and bicarbonate ($\epsilon_{\text{aragonite-HCO}_3^-} = 2.7 \pm 0.6$) (Mook et al., 1974), was used. The calculated $\delta^{13}\text{C}_{H. anceps}$ was then compared with the observed $\delta^{13}\text{C}_{H. anceps}$ to determine a vital effect for each shell sample. Finally, the estimated vital effects for each modern shell were averaged to obtain a vital effect of $+2.4$

‰. After correcting the measured $\delta^{13}\text{C}_{H. anceps}$ for this average vital effect, $\delta^{13}\text{C}_{\text{DIC}}$ was estimated using $\varepsilon_{\text{aragonite-HCO}_3^-} = 2.7 \pm 0.6$ ‰.

Table C.2 Calculated vital effects using the measured $\delta^{13}\text{C}_{\text{DIC}}$ of modern waters, and the $\delta^{13}\text{C}$ of modern *H. anceps* shells.

Modern $\delta^{13}\text{C}_{H. anceps}$ (‰, VPDB)	Modern $\delta^{13}\text{C}_{\text{DIC}}$ (‰, VPDB)	Expected $\delta^{13}\text{C}$ if <i>H. anceps</i> precipitated in equilibrium (‰, VPDB)*	Vital effect (‰, VPDB)	Average vital effect (‰, VPDB)
-3.0	-3.8	-1.1	+1.9	+2.4 ‰
-3.8	-3.8	-1.1	+2.7	
-3.6	-3.8	-1.1	+2.5	
-4.2	-3.8	-1.1	+3.1	
-3.1	-3.8	-1.1	+2.0	

C.3 Additional details regarding the calculation of the age-depth model

In order to transfer the age-depth model from BL-G17-01 to BL-G16-01, trends in $\delta^{13}\text{C}_{\text{TOC}}$ from each core were visually correlated (Fig. C.1). Following correlation, the radiocarbon and ^{210}Pb dates used to generate the age-depth model for BL-G17-01 could be matched with depths from BL-G16-01. These dates and corresponding depths were then input into the software Bacon (Blaauw and Christeny, 2011, R Core Development Team), to generate the age-depth model shown for BL-G16-01 in Figure 3.1. Some ^{210}Pb dates from the age-depth model of BL-G17-01 were not matched with depths from BL-G16-01, or used to create the age-depth model for BL-G16-01; their exclusion improved the correlation between trends in BL-G17-01 and BL-G16-01.

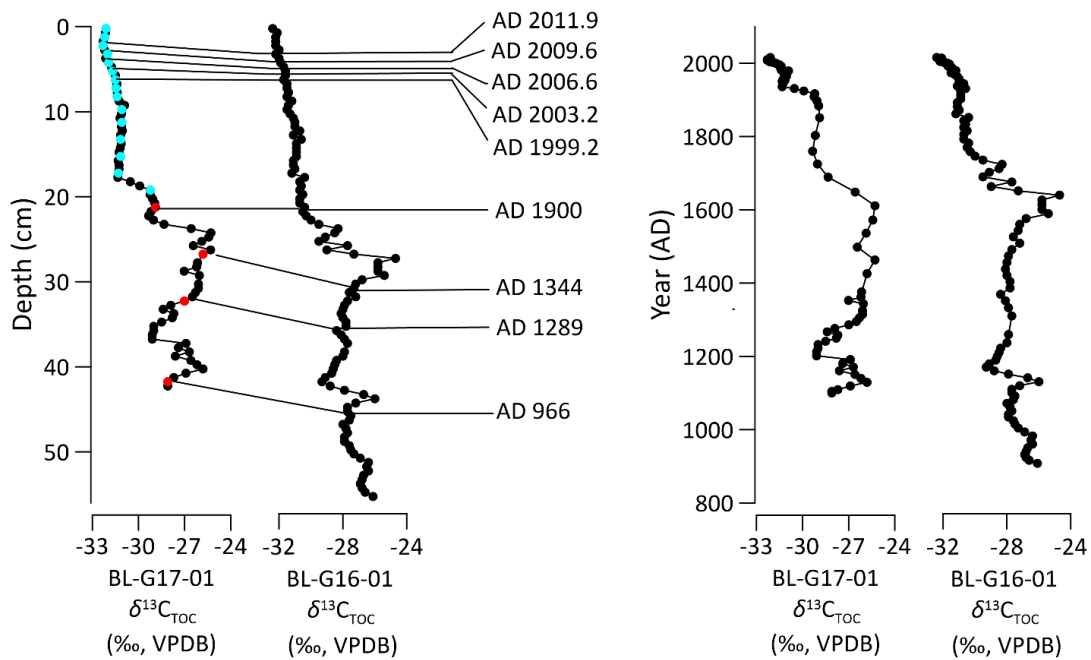


Figure C.1 Plots of depth (left) and year (right) versus $\delta^{13}\text{C}_{\text{TOC}}$ from BL-G17-01 and BL-G16-01. Cores BL-17-01 and BL-G16-01 were visually correlated so that a number of ^{210}Pb (blue dots) and AMS (red dots) dates from BL-G17-01 could be matched with depths from BL-G16-01. These ages, and new depths, were used to generate the age-depth model for BL-G16-01 shown in Figure 3.1. This new age-depth model, and the age-depth model for BL-G17-01, were used to create the plot of year versus $\delta^{13}\text{C}_{\text{TOC}}$ shown to the right.

C.4 Statistical comparisons of variables

Table C.3 Statistical comparisons of variables.

Variable1	Variable2	Pearson correlation (<i>r</i>)	<i>p</i> -value	Significant at <i>p</i> < 0.01?
TOC:TN	ε _{marl} -TOC	-0.370	0.0019	Yes
δ ¹⁵ N	TOC-MAR	0.717	<0.00001	Yes
δ ¹⁵ N	TN-MAR	0.777	<0.00001	Yes
δ ¹⁵ N	Chl-a(s)-MAR	0.559	<0.00001	Yes
δ ¹⁵ N	calcite-MAR	0.508	0.00002	Yes
TOC-MAR	Chl-a(s)-MAR	0.983	<0.00001	Yes

C.5 Analysis of the *n*-alkanes extracted from modern *Chara* in Barry Lake

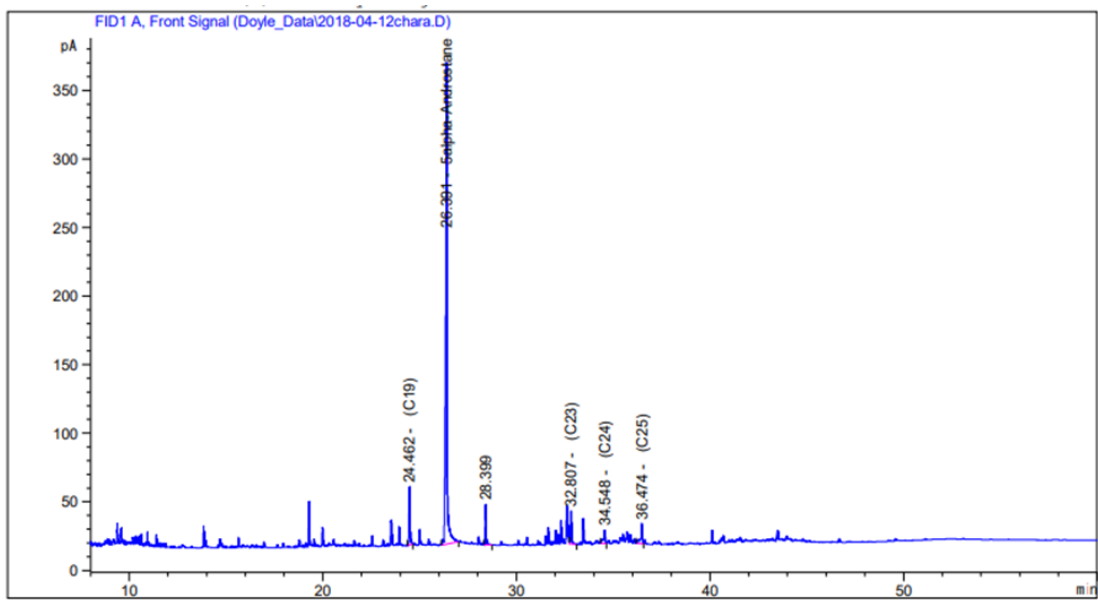


Figure C.2 Chromatograph depicting the *n*-alkanes contained in modern *Chara*. *Chara* in Barry Lake produce predominately C₁₉ *n*-alkanes.

C.6 References for Appendix C

- Blaauw, M., Christen, J.A., Christeny, J.A., 2011. Flexible paleoclimate age-depth models using an autoregressive gamma process. *Bayesian Anal.* 6, 457–474.
<https://doi.org/10.1214/11-BA618>
- Fritz, P., Poplawski, S., 1974. ^{18}O and ^{13}C in the shells of freshwater molluscs and their environments. *Earth Planet. Sci. Lett.* 24, 91–98. [https://doi.org/10.1016/0012-821X\(74\)90012-0](https://doi.org/10.1016/0012-821X(74)90012-0)
- Harris, David, Horwath, William R., VanKessel, C., 2001. Acid fumigation of soils to total organic carbon. *Soil Soc. Am. J.* 65, 1853–1856.
- McConnaughey, T.A., Burdett, J., Whelan, J.F., Paull, C.K., 1997. Carbon isotopes in biological carbonates: Respiration and photosynthesis. *Geochim. Cosmochim. Acta* 61, 611–622. [https://doi.org/10.1016/S0016-7037\(96\)00361-4](https://doi.org/10.1016/S0016-7037(96)00361-4)
- Mook, W.G., Bommerson, J.C., Staverman, W.H., 1974. Carbon isotope fractionation between dissolved bicarbon and gaseous carbon dioxide. *Earth Planet. Sci. Lett.* 22, 169–176.
- R Core Development Team, 2020. *R: A Language and Environment for Statistical Computing.*
- Romanek, C.S., Grossman, E.L., Morse, J.W. Carbon isotopic fractionation in synthetic aragonite and calcite: Effects of temperature and precipitation rate. *Geochim. Cosmochim. Acta* 56, 419–430. [https://doi.org/10.1016/0016-7037\(92\)90142-6](https://doi.org/10.1016/0016-7037(92)90142-6)
- Shanahan, T., Pigati, J., Dettman, D., Quade, J., 2005. Isotopic variability in the aragonite shells of freshwater gastropods living in springs with nearly constant temperature and isotopic composition. *Geochim. Cosmochim. Acta* 69, 3949–3966.

Von Grafenstein, U., Erlenkeuser, H., Trimborn, P., 1999. Oxygen and carbon isotopes in modern fresh-water ostracod valves: assessing vital offsets and autecological effects of interest for palaeoclimate studies. *Palaeogeogr. Palaeoclimatol. Palaeoecol.* 148, 133–152.

Appendix D: Supplementary methods for Chapter 4

D.1 More details regarding correcting $\delta^{13}\text{C}_{\text{TOC}}$ and $\delta^{15}\text{N}_{\text{TN}}$ for the effects of degradation

The $\delta^{13}\text{C}_{\text{TOC}}$ and $\delta^{15}\text{N}_{\text{TN}}$ of sediments are susceptible to degradation when the water column is fully oxygenated. The $\delta^{13}\text{C}_{\text{TOC}}$ and $\delta^{15}\text{N}_{\text{TN}}$ of these sediments were therefore corrected to account for this degradation. Lehmann et al. (2002) determined using microcosm experiments that, under oxygenated conditions, the $\delta^{13}\text{C}_{\text{TOC}}$ of surficial sediments tend to decrease by ~ 1.6 ‰. After this initial decrease, $\delta^{13}\text{C}_{\text{TOC}}$ of sediments stabilizes (Lehmann et al., 2002). The $\delta^{13}\text{C}_{\text{TOC}}$ of surficial sediments were therefore corrected by increasing the $\delta^{13}\text{C}_{\text{TOC}}$ by 1.6 ‰. Brahney et al. (2014) found that, when the water column is fully oxygenated, the $\delta^{15}\text{N}_{\text{TN}}$ of sediments tends to increase by 2 ‰. The $\delta^{15}\text{N}_{\text{TN}}$ of surficial sediments was therefore corrected by reducing the $\delta^{15}\text{N}_{\text{TN}}$ by 2 ‰.

D.2 R code used in Chapter 4

D.2.1 Example of code for generating Bayesian ellipses

`#load file (can also do this through "tools --> load dataset") and name it`

```
data6 <- read.csv("C:/Users/rebec/Desktop/Uinta Mountains/R  
plots/RMD_TEST1/data6.csv")
```

`#load the SIBER package to R`

```
library(SIBER)
```

`#now set colour palette`

```
palette(c("#CD534CFF", "#868686FF", "#712286", "#3B3B3BFF", "#8F7700FF", "#0073C2FF", "#  
8F7700FF", "#3B3B3BFF", "#A73030FF", "#4A6990FF"))
```

```
#specify arguments for your community-level hulls, likewise line width, colour type, line depth
community.hulls.args <- list(col = 1, lty = 1, lwd = 1)
```

```
#do the same for your group-level ellipses. Note that for the ellipses,
```

```
#you can switch between probability-based orbitals and maximum area orbitals by entering
a p-value
```

```
#if you enter p=NULL your ellipses will become maximum area orbital
```

```
group.ellipses.args <- list(n = 100, p.interval = .40, lty= 1, lwd = 3, small.sample = T)
```

```
#do the same for your group-level hulls
```

```
group.hull.args <- list(lty = 2, col = "grey20")
```

```
#set margins with mar and oma functions. Mar changes position of figure,
```

```
#oma changes outside margins. Set oma to 0,0,0,0 if you want the maximum space.
```

```
par(mar=c(4.5,5.5,8,10), oma=c(0,0,0,0))
```

```
#name plot and plot the siber object named earlier. ax.pad causes orbitals to become bigger
or smaller. #hulls can be set to TRUE (T) or FALSE (F). The same goes for ellipses. bty
changes whether a box #appears around graph. IMPORTANT: iso.order must be set to 1,2 or
the plot will not work. It is a glitch #in SIBER. if iso.order is set to 1,2 SIBER will put the first
column variables on the x-axis and the second #column variables on the y axis. Use
expression function for fancy delta symbol for label.
```

```
data6 <- createSiberObject(data6)
```

```
plot6 <- plotSiberObject(data6,
  ax.pad = 1,
  hulls = F, community.hulls.args,
  ellipses = T, group.ellipses.args,
  group.hulls = F, group.hull.args,
  bty = "L",
  iso.order = c(1,2),
  x.limits = c(-35,-10),
  y.limits = c(-10,10),
```

```

xlab = c({delta}^13*C~'\u2030'[VPDB]),
las = 1,
pch = c(2, 1),
ylab = expression({delta}^15*N~'\u2030'[AIR])

```

```
#Add legend using locator
```

```

legend(locator(1),c("Algae (13)", "Benthic sediment (4)", "Broadleaf deciduous shrub
(23)", "Coniferous krummholz tree (15)", "Lichen (8)", "Moss (19)", "All macrophytes (17)"),
col=c("#0073C2FF", "#375623", "#868686FF", "#CD534CFF",
"#8F7700FF", "#3B3B3BFF", "#712286"),
pch=c(1, 16, 1, 1, 1, 1, 1), lty = c(1), cex = (0.75), bty = "n", xpd = TRUE)

```

D.2.2 R code for Principal Components Analysis (PCA) with Non-Bayesian Standard Ellipses

```
#Load Tidyverse package
```

```
library("tidyverse")
```

```
#Load Vegan package
```

```
library("vegan")
```

```
#Set working directory and read in data
```

```
setwd("C:/Users/rebec/Desktop")
```

```
data <- read_csv("C:/Users/rebec/Desktop/ACL_PCA.csv")
```

```
#Generate PCA
```

```
data.pca <- princomp(data[, -7])
```

```
biplot(data.pca)
```

```
#Plot PCA
```

```
my.rda <- rda(data[, -7], scale = FALSE, lwd = 2, col=c("black"))
```

```
biplot(my.rda)
```

```

biplot(my.rda,
display = c("sites", "species"),
type = c("text",
"points"), col= c("black"))

```

```
#Add labels
```

```

ordilabel(my.rda, display = c("sites"),
labels = c("Moss", "Lichen",
"Macro", "Macro", "Macro"),

```

```

"Macro","Macro","Macro",
"Macro","Macro",
"Gram","Gram","Gram",
"Shrub","Shrub","Shrub","Shrub",
"Shrub","Shrub","Shrub","Shrub",
"Herb","Herb","Herb","Herb",
"Krum","Krum","Krum","Krum",
"Krum","Krum"), cex = 0.4, font = 1,
border = NA, fill = NA, pos=4, offset=0.25)

```

#Add 40% standard ellipses (the standard deviation of bimodal data is the same as a 40 % standard ellipse)

```

ordiellipse(my.rda,group = data$Subgroup, kind="sd",
col = c("#DF918D","#7AA6DCFF","#003C67FF",
"green","dark red","dark red","dark grey","black"),
lty=c(1, 2, 1, 1, 1, 1, 1), label=FALSE, lwd=2)

```

#Add legend

```

legend(locator(1),c("Semi-emergent macrophyte (Macro)","Graminoid (Gram)",
"Coniferous krummholz tree (Krumm)",
"Broadleaf deciduous shrub (Shrub)","Herbaceous perennial (Herb)"),
col=c("dark red","#7AA6DCFF","pink","#868686FF",
"#003C67FF","#999933","#003C67FF"),
pch=c(1), lty = c(1,2,1,1,1,1,1,1), cex = (0.5), bty = "n", xpd = TRUE)

```

D.3 Results of statistical tests

Table D.1 Pairwise Wilcoxon tests of $\delta^{13}\text{C}_{\text{TOC}}$ of potential sources of OM in Uinta Mountain sediments. Significant p -values are shown in red. Sample sizes are showed in brackets.

	Algae (13)	Sediment from the centre of the lake (4)	Broadleaf deciduous shrub (23)	Coniferous krummholz tree (15)	Graminoid (7)	Herbaceous perennial (4)	Lichen (8)	Moss (19)	Semi-emergent macrophyte (11)
Benthic sediment (4)	1.00								
Broadleaf deciduous shrub (23)	1.00	1.00							
Coniferous krummholz tree (15)	1.00	1.00	0.16						
Graminoid (7)	1.00	1.00	1.00	0.02					
Herbaceous perennial (4)	1.00	1.00	1.00	1.00	1.00				
Lichen (8)	1.00	1.00	0.06	0.18	0.41	1.00			
Moss (19)	1.00	1.00	1.00	1.00	1.00	1.00	0.07		
Semi-emergent macrophyte (11)	1.00	1.00	1.00	1.00	0.56	1.00	0.66	1.00	
Submerged macrophyte (6)	1.00	1.00	0.37	1.00	0.45	1.00	1.00	1.00	1.00

Table D.2 Pairwise Wilcoxon tests of $\delta^{15}\text{N}_{\text{TN}}$ of OM sources. Significant *p*-values are shown in red. Sample sizes are shown in brackets.

	Algae (13)	Sediment from the centre of the lake (4)	Broadleaf deciduous shrub (23)	Coniferous krummholz tree (15)	Graminoid (7)	Herbaceous perennial (4)	Lichen (8)	Moss (19)	Semi-emergent macrophyte (11)
Benthic sediment (4)	1.00								
Broadleaf deciduous shrub (23)	0.05	0.09							
Coniferous krummholz tree (15)	1.00	0.48	1.00						
Graminoid (7)	1.00	1.00	1.00	1.00					
Herbaceous perennial (4)	1.00	1.00	1.00	1.00	1.00				
Lichen (8)	0.22	0.18	1.00	1.00	0.29	1.00			
Moss (19)	1.00	0.53	0.01	0.79	1.00	1.00	0.04		
Semi-emergent macrophyte (11)	0.25	1.00	0.00	0.01	0.38	0.48	0.02	0.09	
Submerged macrophyte (6)	1.00	1.00	0.01	0.26	1.00	1.00	0.03	1.00	1.00

Table D.3 Pairwise Wilcoxon tests of TOC:TN of potential OM sources. Significant *p*-values are shown in red. Sample sizes are shown in brackets.

	Algae (13)	Sediment from the centre of the lakes (4)	Broadleaf deciduous shrub (23)	Coniferous krummholz tree (15)	Graminoid (7)	Herbaceous perennial (4)	Lichen (8)	Moss (19)	Semi-emergent macrophyte (11)
Benthic sediment (4)	1.00								
Broadleaf deciduous shrub (23)	0.00	0.01							
Coniferous krummholz tree (15)	0.01	0.28	0.79						
Graminoid (7)	0.04	0.27	1.00	1.00					
Herbaceous perennial (4)	0.81	1.00	1.00	1.00	1.00				
Lichen (8)	0.68	1.00	1.00	0.72	1.00	1.00			
Moss (19)	0.01	0.11	1.00	0.16	1.00	1.00	1.00		
Semi-emergent macrophyte (11)	0.08	0.07	1.00	1.00	1.00	1.00	1.00	1.00	
Submerged macrophyte (6)	1.00	1.00	0.00	0.05	0.05	0.43	0.90	0.01	0.05

Table D.4 Other statistical comparisons among groups. Significant *p*-values are shown in red.

Group 1	Group 2	Test	<i>p</i> -value
Absolute abundance of coniferous krummholz trees	Absolute abundance of broadleaf deciduous shrubs	Student t-test	0.01
Absolute abundance of coniferous krummholz trees	Absolute abundance of semi-emergent macrophytes	Student t-test	0.00
Absolute abundance of coniferous krummholz trees	Absolute abundance of graminoids	Student t-test	0.02
TOC:TN of terrestrial source of OM	TOC:TN of algae and submerged macrophytes	Kruskal-Wallis test	0.00

D.4 Hydrogen isotope composition of lake water and inflows

Table D.5 Hydrogen isotope composition of lake waters and inflows from the Uinta Mountains. Standard deviations represent the reproducibility of replicate analyses.

Lake	Site of sample collection	Date of sample collection	$\delta^2\text{H}$ (‰, VSMOW)	SD (‰)
Taylor	Middle of Lake	2015	-108	14
	Middle of Lake	2015	-104	
	Middle of Lake	2012	-130	
	Inflow	2008	-126	
	Inflow	2008	-143	
	Inflow	2009	-129	
	Inflow	2009	-107	
	Inflow	2009	-106	
	Inflow	2008	-181	
	Inflow	2009	-129	
	Inflow	2008	-164	
Denise	Middle of Lake	2015	-97	14
	Middle of Lake	2014	-123	
	Middle of Lake	2009	-119	
	Inflow	2014	-104	
	Inflow	2014	-125	
	Inflow	2008	-132	
	Inflow	2009	-122	
Upper Carrol	Middle of Lake	2015	-95	11
	Middle of Lake	2008	-114	
	Middle of Lake	2009	-114	
	Middle of Lake	2012	-119	
	Inflow	2009	-115	
	Inflow	2009	-114	
East Carrol	Middle of Lake	2015	-95	6
	Middle of Lake	2009	-102	
	Middle of Lake	2012	-107	
	Inflow	2009	-106	
	Inflow	2008	-116	

D.5 Generating a phylogenetic tree

Table D.6 Summary of the information used to generate the phylogenetic tree in the following figure.

Identification	Group	Confidence in identification	Confidence in species identification
<i>Aspicilia supertegens</i>	Lichen	Low	Low
<i>Aulacomnium palustre</i>	Moss	High	Low
<i>Picea engelmannii</i>	Coniferous krummholz tree	High	High
<i>Carex aquatilis</i>	Semi-emergent macrophytes	High	High
<i>Carex sp.</i>	Terrestrial graminoids	High	Low
<i>Castilleja occidentalis</i>	Herbaceous perennial	High	Low
<i>Kalmia polifolia</i>	Herbaceous perennial	High	Low
<i>Salix planifolia</i>	Broadleaf deciduous shrub	High	High
<i>Betula glandulosa</i>	Broadleaf deciduous shrub	High	High
<i>Dasiphora fruticosa</i>	Herbaceous perennial	High	Low

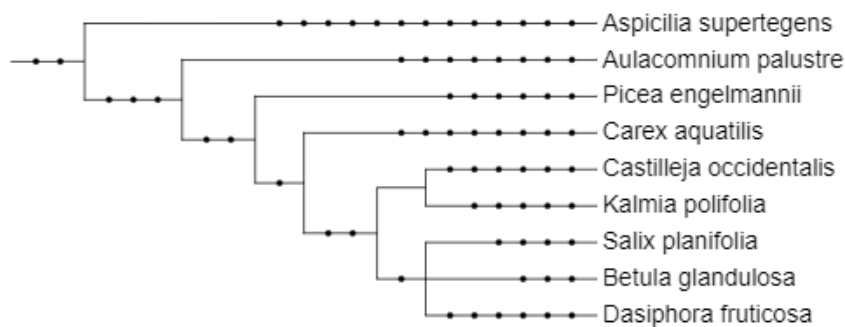


Figure D.1 This phylogenetic tree was generated using the PhyloT tool at <https://phylot.biobyte.de/>. Only terrestrial and semi-aquatic organisms were used to create the tree because it is used to help interpret variation in n-alkane data. Because of sample size limitations, n-alkanes could only be extracted from terrestrial and semi-aquatic plant samples.

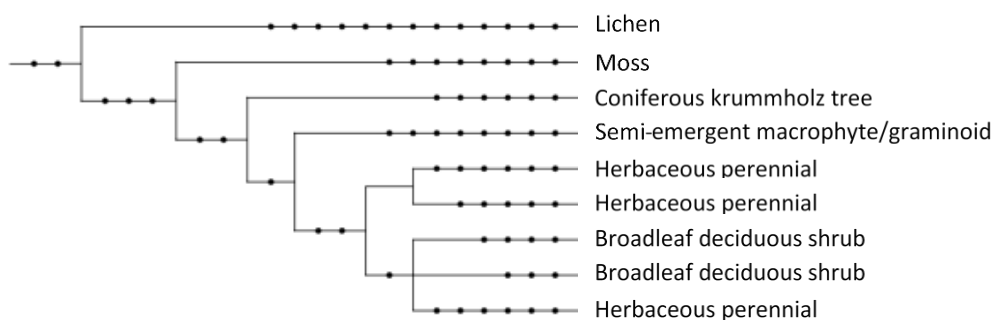


Figure D.2 The same tree as shown in Figure D.1, except that species names have been replaced by their group names.

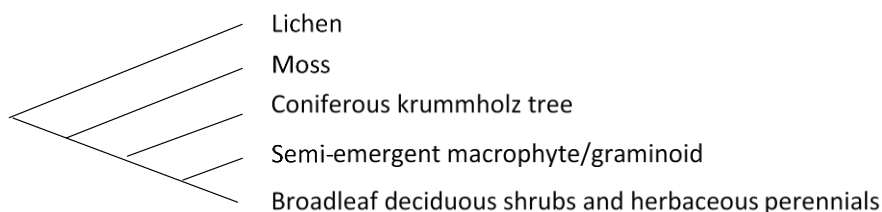


Figure D.3 Simplified phylogenetic tree used in the main text of Chapter 4.

D.6 Dissolved oxygen (DO) and dissolved inorganic carbon (DIC) for the four study lakes

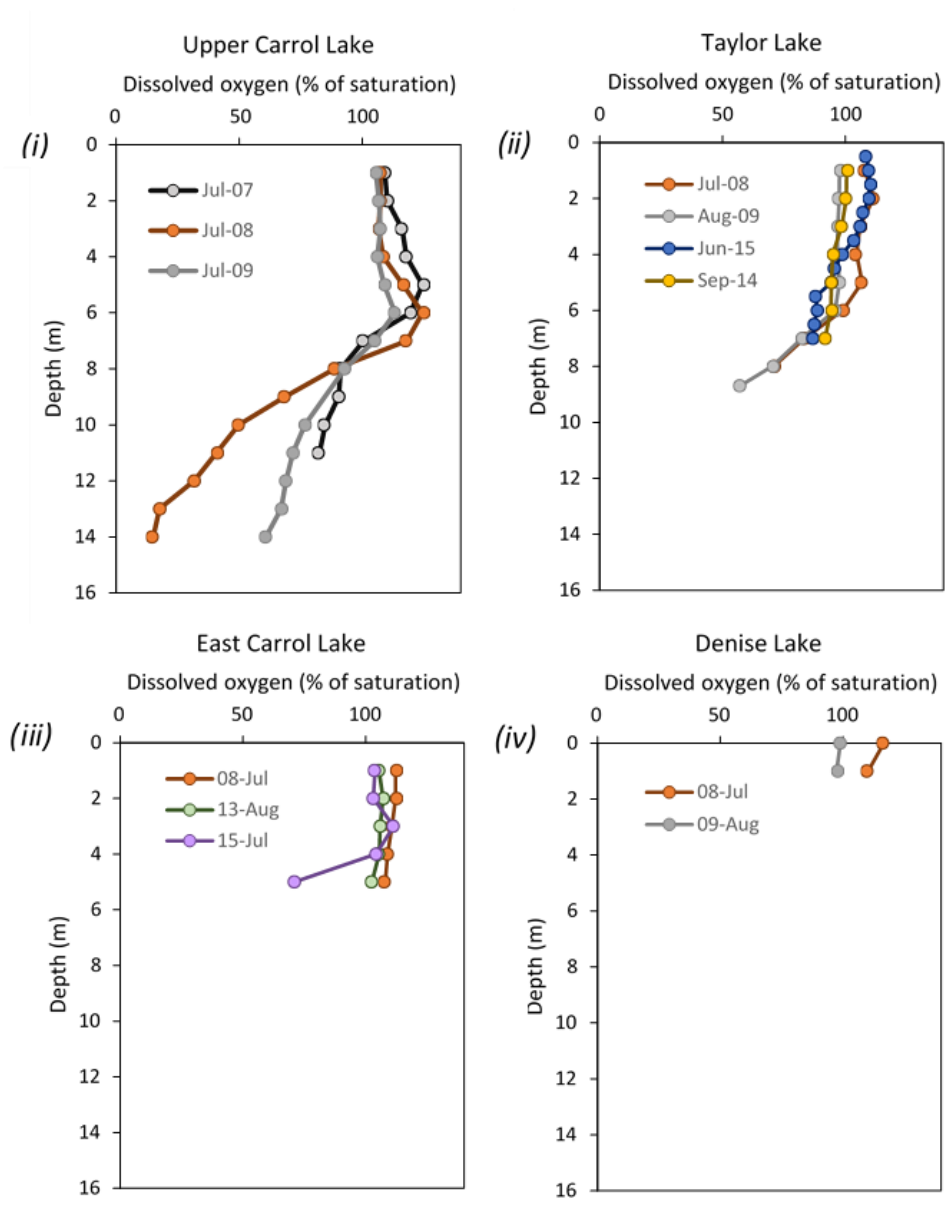


Figure D.4 Dissolved oxygen concentrations for (i) Upper Carrol Lake, (ii) Taylor Lake, (iii) East Carrol Lake, and (iv) Denise Lake. Numbers in the legend (e.g., Jul-16) refer to the year of collection (July 2016).

Table D.7 Concentrations of DIC from the Uinta Mountain study lakes.

Lake	Sample Date	DIC (mg C/L)
Taylor	July 2015	1.21
Denise	July 2015	1.22
Upper Carrol	July 2015	1.12
East Carrol	July 2015	1.48

D.7 How well do the samples presented in Chapter 4 capture the variation in $\delta^{13}\text{C}_{\text{TOC}}$, $\delta^{15}\text{N}_{\text{TN}}$ and TOC:TN present around the study lakes?

Several tests were conducted to ensure that the measurements of $\delta^{13}\text{C}$, $\delta^{15}\text{N}$ and TOC:TN from small tissue samples were appropriately characterizing the variation in isotopic and elemental compositions of subgroups. No significant difference in the $\delta^{13}\text{C}$, $\delta^{15}\text{N}$ or TOC:TN of senesced versus fresh tissue (Fig. D.5), broadleaves versus woody tissue (Fig. D.6) or needles versus woody tissue (Fig. D.7) was detected. This investigation was conducted since it is unclear if broadleaf deciduous shrubs and coniferous krummholz trees are contributing only senesced foliar tissue to the sediment OM or if they are also contributing fresh and/or woody tissue. Ultimately, this distinction is not important since no significant differences were detected between the $\delta^{13}\text{C}$, $\delta^{15}\text{N}$ or TOC:TN of woody tissue compared with needles.

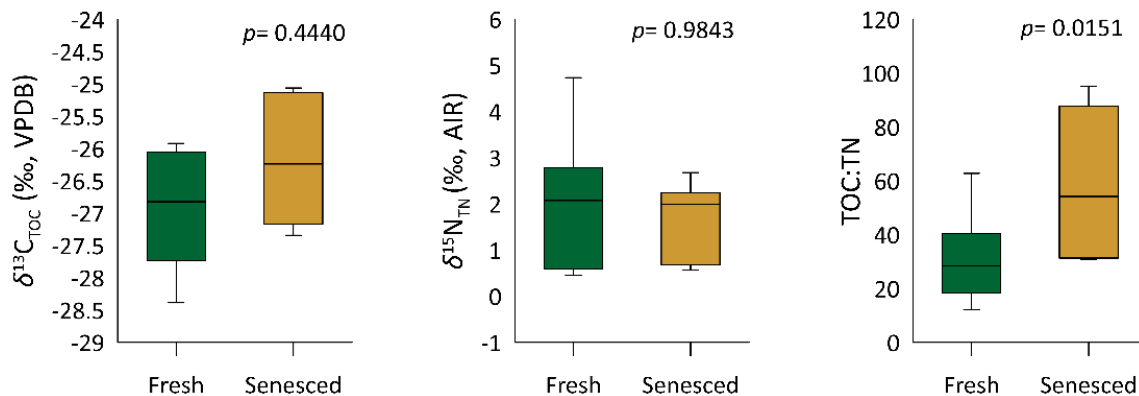


Figure D.5 Comparison of the isotopic and elemental compositions of fresh (11 samples) versus senescing (7 samples) leaves from *Carex aquatilis*. There is no significant difference in the $\delta^{13}\text{C}$ (left), $\delta^{15}\text{N}$ (middle) and TOC:TN (right) of fresh versus senesced material.

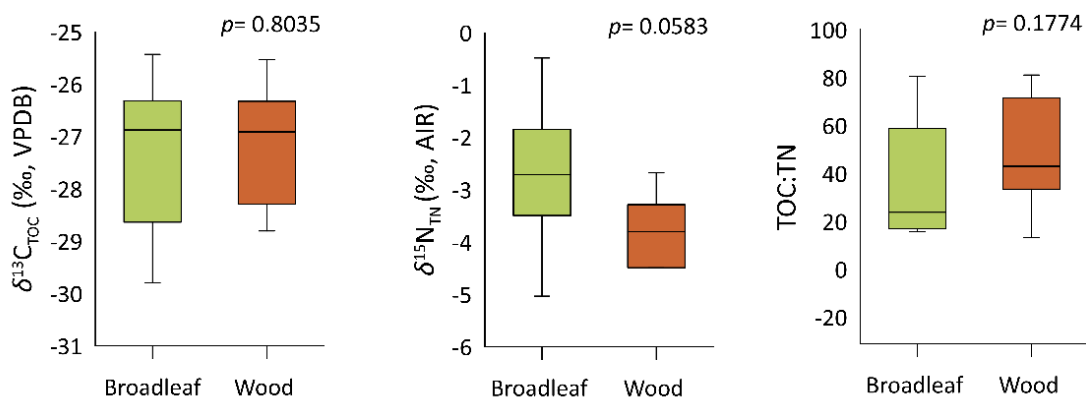


Figure D.6 A comparison of the isotopic and elemental compositions of broadleaves (15 samples) and woody tissue (13 samples) from deciduous shrubs. There are no significant differences in the $\delta^{13}\text{C}$ (left), $\delta^{15}\text{N}$ (middle) or TOC:TN of broadleaves and woody tissue from deciduous shrubs.

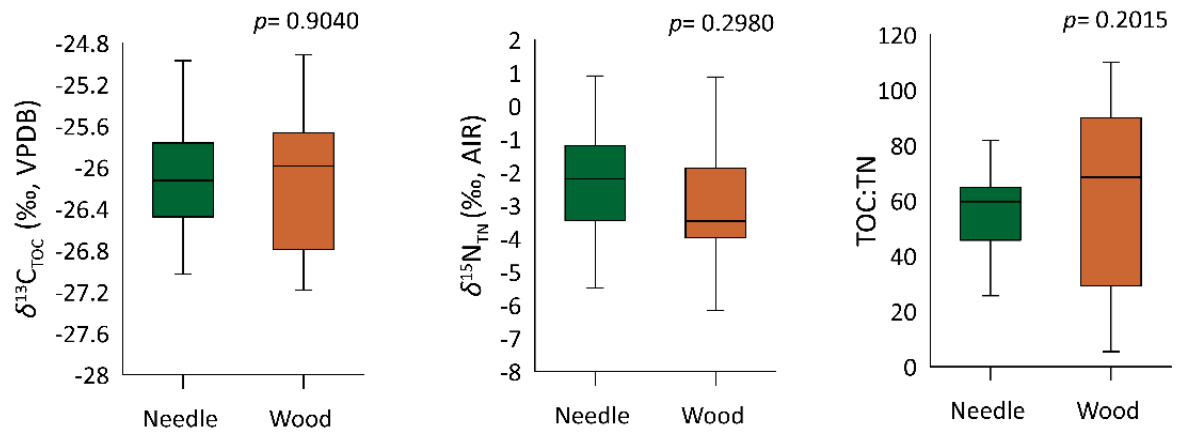


Figure D.7 A comparison of the isotopic and elemental compositions of needles (15 samples) and woody tissue (15 samples) from coniferous krummholz trees. There are no significant differences in the $\delta^{13}\text{C}$ (left), $\delta^{15}\text{N}$ (middle) or TOC:TN of needles and woody tissue from coniferous krummholz trees.

D.7.1 More details regarding comparisons in $\delta^{13}\text{C}_{\text{TOC}}$, $\delta^{15}\text{N}_{\text{TN}}$ and TOC:TN

It is surprising that no differences in the isotopic and elemental compositions of senesced versus fresh leaves were detected. Prior studies have determined that the $\delta^{15}\text{N}$ of senesced tissues is lower than fresh tissues due to loss of chlorophyll-*a* and preferential breakdown of amino acids (Inglett and Reddy, 2006; Keskitalo et al., 2005). Conversely, the $\delta^{13}\text{C}$ of senesced leaves is generally higher than fresh leaves because (i) the stomata of leaves undergoing senescence are unable to close, meaning that they cannot actively discriminate against ^{13}C and (ii) plants relocate isotopically light compounds from older, senescing tissue towards the rhizome, leaving the senesced leaves enriched in ^{13}C (Kao et al., 2002; Welker et al., 2003). This relocation also causes the TOC:TN ratio of senesced tissues to increase relative to fresh tissues (Welker et al., 2003). It is possible that, upon additional sampling, these differences in the isotopic and elemental composition of senesced versus fresh tissue would emerge. I speculate, however, that similarities in the $\delta^{13}\text{C}$, $\delta^{15}\text{N}$ and TOC:TN of fresh versus senesced tissue may be caused by the sharing of nutrients between juvenile and mature *Carex* plants via underground rhizomes, as has been previously reported by Welker et al. (2003).

It was also surprising that no significant differences were observed in $\delta^{13}\text{C}$, $\delta^{15}\text{N}$ and TOC:TN of foliar tissue compared with woody twigs. Typically, the $\delta^{15}\text{N}$ of woody twigs is lower than that of foliar tissue. One reason why the $\delta^{15}\text{N}$ of woody twigs is lower than foliar tissue is that ^{14}N is preferentially extracted from senesced tissues, which causes foliar tissues to become enriched in ^{15}N (Gebauer and Schulze, 1991). Conversely, so-called “photosynthetic tissues”, such as green broadleaves, needles and stems, are more depleted of ^{13}C than non-photosynthetic tissues, such as woody twigs, because ^{12}C is preferentially used for photosynthesis (Szpak et al., 2013). The literature also suggests that foliar tissues contain less cellulose and lignin than woody tissues and therefore have lower TOC:TN (Ma et al., 2018). In a large baseline study of arctic plants, however, Tahmasebi et al. (2017) also did not detect systematic differences in the $\delta^{15}\text{N}$ of foliar tissue and other plant parts, which they attributed to confounding factors such as differences in microhabitat, mycorrhizal

associations and root morphology. Since the nitrogen systematics of arctic regions are similar to alpine regions (Burpee and Saros, 2020), it is likely that such factors are also obscuring differences in the $\delta^{15}\text{N}$ of foliar tissue and woody twigs in the Uinta Mountains.

Tahmasebi et al. (2007) did detect significantly lower $\delta^{13}\text{C}$ of foliar tissue compared with other plant parts. That no such differences were detected suggests that plants in the Uinta Mountains are unable to fully discriminate against ^{12}C , perhaps because of aridity. Plants in arid environments typically produce foliar tissue that is enriched in ^{13}C relative to foliar tissue formed in wetter environments. In arid environments many plants have adapted to conserve water by closing their stomata for longer periods, resulting in decreased discrimination against ^{12}C (Lloyd and Farquhar, 1994). Since the relative humidity in the Uinta Mountains is low, often dropping to $\sim 10\%$ on a clear day (Hayward, 1952), it is likely that plants growing in these mountains have adapted to minimize water loss, causing their leaves to become enriched in ^{13}C . It is unclear why no significant differences were detected between the TOC:TN of foliar tissue and twigs. I speculate that the nitrogen content of broadleaves and needles is lower than expected due to nitrogen stress. Previous studies have demonstrated that the TOC:TN of foliar tissue is highly dependent on nitrogen availability (Lü et al., 2012). It is also possible that further sampling would reveal significant differences in the TOC:TN of foliar and woody tissues.

No significant differences were observed in the $\delta^{13}\text{C}$ or $\delta^{15}\text{N}$ of fresh *Salix* leaves between those sampled at Taylor Lake and those sampled at East Carrol Lake (Fig. D.8), which was unsurprising given that both sites are located at similar altitudes (3414 m.a.s.l. and 3423 m.a.s.l, respectively) and in the same climate regime. Significant differences were detected, however, in the TOC:TN of *Salix* sp. between the two sites, perhaps due to differences in nitrogen availability. Nonetheless, broadleaf shrubs growing at both sites had TOC:TN far above the TOC:TN of aquatic sources. Thus, this discrepancy did not affect our ability to distinguish between fully aquatic and fully terrestrial OM sources using TOC:TN.

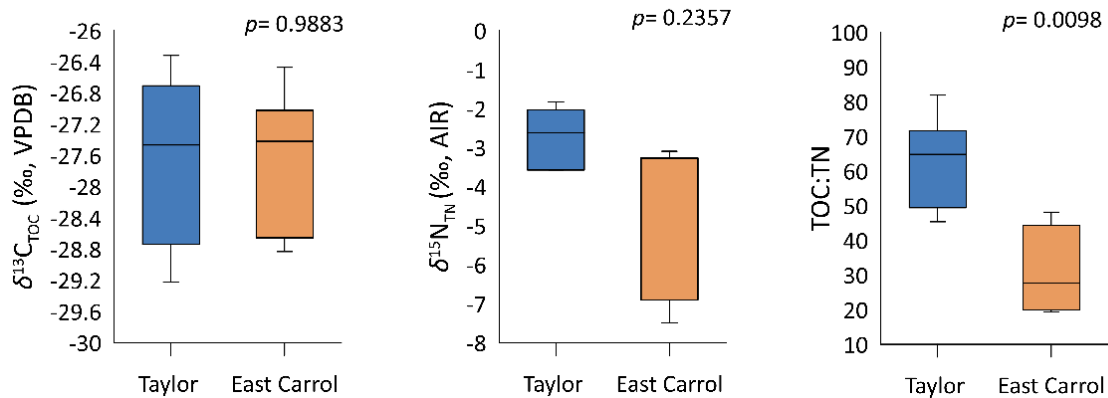


Figure D.8 A comparison of the isotopic and elemental compositions of *Salix* sp. leaves from Taylor Lake (5 samples) and East Carrol Lake (5 samples). There is no significant difference in the $\delta^{13}\text{C}_{\text{TOC}}$ (left) and $\delta^{15}\text{N}_{\text{TN}}$ (middle) of *Salix* from Taylor Lake and East Carrol Lake. There is a significant difference in the TOC:TN of *Salix* from Taylor Lake and East Carrol Lake.

D.8 Comparing the ϵ_{bulk} of broadleaf deciduous trees sampled from East Carrol, Upper Carrol and Taylor lakes

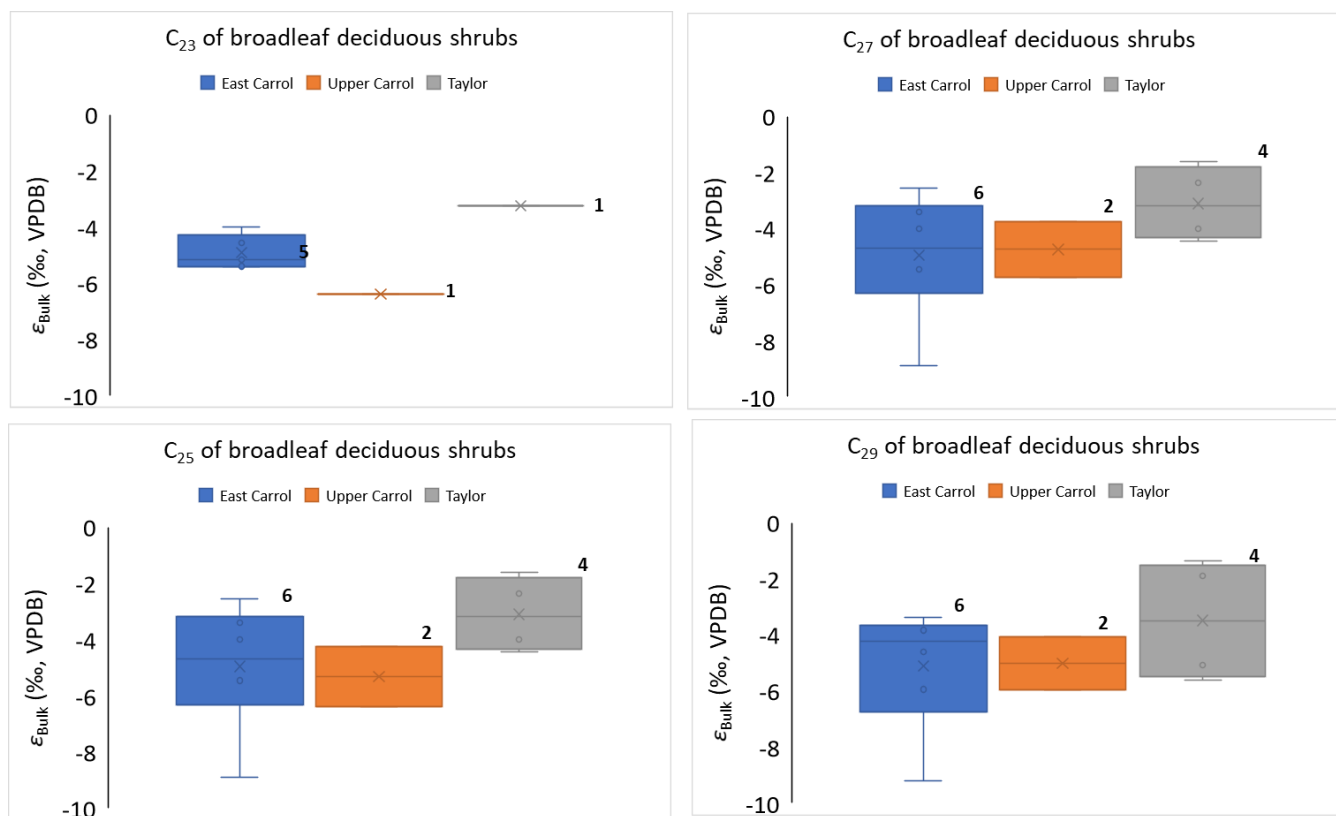


Figure D.9 Comparing the ϵ_{bulk} of broadleaf deciduous shrubs (*Salix* sp. and *Betula* sp.) across three of the four study lakes. (i) the ϵ_{bulk} of C₂₃. (ii) the ϵ_{bulk} of C₂₅. (iii) the ϵ_{bulk} of C₂₇. (iv) the ϵ_{bulk} of C₂₉. Broadleaf deciduous shrubs were not sampled from Denise Lake. Numbers beside the boxplots represent the sample size.

D.9 References for Appendix D

- Brahney, J., Ballantyne, A.P., Turner, B.L., Spaulding, S.A., Otu, M., Neff, J.C., 2014. Separating the influences of diagenesis, productivity and anthropogenic nitrogen deposition on sedimentary $\delta^{15}\text{N}$ variations. *Org. Geochem.* 75, 140–150. <https://doi.org/10.1016/j.orggeochem.2014.07.003>
- Burpee, B.T., Saros, J.E., 2020. Cross-ecosystem nutrient subsidies in Arctic and alpine lakes: implications of global change for remote lakes. *Environ. Sci. Process. Impacts.* <https://doi.org/10.1039/c9em00528e>
- Gebauer, G., Schulze, E.D., 1991. Carbon and nitrogen isotope ratios in different compartments of a healthy and a declining *Picea abies* forest in the Fichtelgebirge, NE Bavaria. *Oecologia* 87, 198–207. <https://doi.org/10.1007/BF00325257>
- Hayward, C.L., 1952. Alpine biotic communities of the Uinta Mountains, Utah. *Ecol. Monogr.* 22, 93–120. <https://doi.org/10.2307/1943513>
- Inglett, P.W., Reddy, K.R., 2006. Investigating the use of macrophyte stable C and N isotopic ratios as indicators of wetland eutrophication: Patterns in the P-affected Everglades. *Limnol. Oceanogr.* 51, 2380–2387. <https://doi.org/10.4319/lo.2006.51.5.2380>
- Kao, W.Y., Tsai, H.C., Shih, C.N., Tsai, T.T., Handley, L.L., 2002. Nutrient contents, $\delta^{13}\text{C}$ and $\delta^{15}\text{N}$ during leaf senescence in the mangrove, *Kandelia candel* (L.) Druce. *Bot. Bull. Acad. Sin.* 43, 277–282. <https://doi.org/10.7016/BBAS.200210.0277>
- Keskitalo, J., Bergquist, G., Gardeström, P., Jansson, S., 2005. A cellular timetable of autumn senescence. *Plant Physiol.* 139, 1635–1648. <https://doi.org/10.1104/pp.105.066845>

- Lehmann, M.F., Bernasconi, S.M., Barbieri, A., McKenzie, J.A., 2002. Preservation of organic matter and alteration of its carbon and nitrogen isotope composition during simulated and *in situ* early sedimentary diagenesis. *Geochim. Cosmochim. Acta* 66, 3573–3584. [https://doi.org/10.1016/S0016-7037\(02\)00968-7](https://doi.org/10.1016/S0016-7037(02)00968-7)
- Lloyd, J., Farquhar, G.D., 1994. ^{13}C discrimination during CO_2 assimilation by the terrestrial biosphere. *Oecologia* 99, 201–215. <https://doi.org/10.1007/BF00627732>
- Lü, X.T., Kong, D.L., Pan, Q.M., Simmons, M.E., Han, X.G., 2012. Nitrogen and water availability interact to affect leaf stoichiometry in a semi-arid grassland. *Oecologia* 168, 301–310. <https://doi.org/10.1007/s00442-011-2097-7>
- Ma, S., He, F., Tian, D., Zou, D., Yan, Z., Yang, Y., Zhou, T., Huang, K., Shen, H., Fang, J., 2018. Variations and determinants of carbon content in plants: A global synthesis. *Biogeosciences* 15, 693–702. <https://doi.org/10.5194/bg-15-693-2018>
- Szpak, P., White, C.D., Longstaffe, F.J., Millaire, J.-F., Vásquez Sánchez, V.F., 2013. Carbon and nitrogen isotopic survey of northern Peruvian plants: Baselines for paleodietary and paleoecological studies. *PLoS One* 8, e53763. <https://doi.org/10.1371/journal.pone.0053763>
- Tahmasebi, F., Longstaffe, F.J., Zazula, G., Bennett, B., 2017. Nitrogen and carbon isotopic dynamics of subarctic soils and plants in southern Yukon Territory and its implications for paleoecological and paleodietary studies. *PLoS One* 12, e0183016. <https://doi.org/10.1371/journal.pone.0183016>
- Welker, J.M., Jónsdóttir, I.S., Fahnestock, J.T., 2003. Leaf isotopic ($\delta^{13}\text{C}$ and $\delta^{15}\text{N}$) and nitrogen contents of *Carex* plants along the Eurasian Coastal Arctic: Results from the Northeast Passage expedition. *Polar Biol.* 27, 29–37. <https://doi.org/10.1007/s00300-003-0562-4>

Appendix E: Supplementary Methods for Chapter 5

E.1 Statistical tests and water chemistry measurements

Table E.1 Measurements of pH of waters from the Uinta Mountain lakes and Barry Lake.

Lake	Date of measurement	pH
Taylor	Fall 2017	6.64
Taylor	Spring 2018	5.87
Taylor	Spring 2019	7.34
Taylor	Fall 2012	6.77
Upper Carrol	Spring 2015	6.67
East Carrol	Spring 2015	7.28
Barry Lake	Summer 2016	7.89
Barry Lake	Fall 2016	7.58
Barry Lake	Summer 2018	7.90
Barry Lake	Fall 2018	7.88

Table E.2 The p -values from two-tailed t-tests (normally distributed data) or Kruskal-Wallis tests (non-parametric data). Statistically significant p -values ($p < 0.01$) are shown in red.

Isotope	Variable1	Variable2	Test	p -value	Significant at $p < 0.01$?
$\delta^{13}\text{C}_{\text{TOC}}$	Submerged macrophytes from Barry Lake	Submerged macrophytes from the Uinta Mountains	Two-tailed t-test	0.12	No
$\delta^{15}\text{N}_{\text{TN}}$	Submerged macrophytes from Barry Lake	Submerged macrophytes from Barry Lake	Kruskal-Wallis test	1	No
$\delta^{13}\text{C}_{\text{TOC}}$	Semi-emergent macrophytes from Barry Lake	Semi-emergent macrophytes from the Uinta Mountains	Two-tailed t-test	0.04	No
$\delta^{15}\text{N}_{\text{TN}}$	Semi-emergent macrophytes from Barry Lake	Semi-emergent macrophytes from the Uinta Mountains	Two-tailed t-test	0.97	No
$\delta^{13}\text{C}_{\text{TOC}}$	Broadleaf deciduous shrubs from Barry Lake	Broadleaf deciduous shrubs from the Uinta Mountains	Kruskal-Wallis test	<0.00	Yes
$\delta^{15}\text{N}_{\text{TN}}$	Broadleaf deciduous shrubs from Barry Lake	Broadleaf deciduous shrubs from the Uinta Mountains	Kruskal-Wallis test	<0.00	Yes

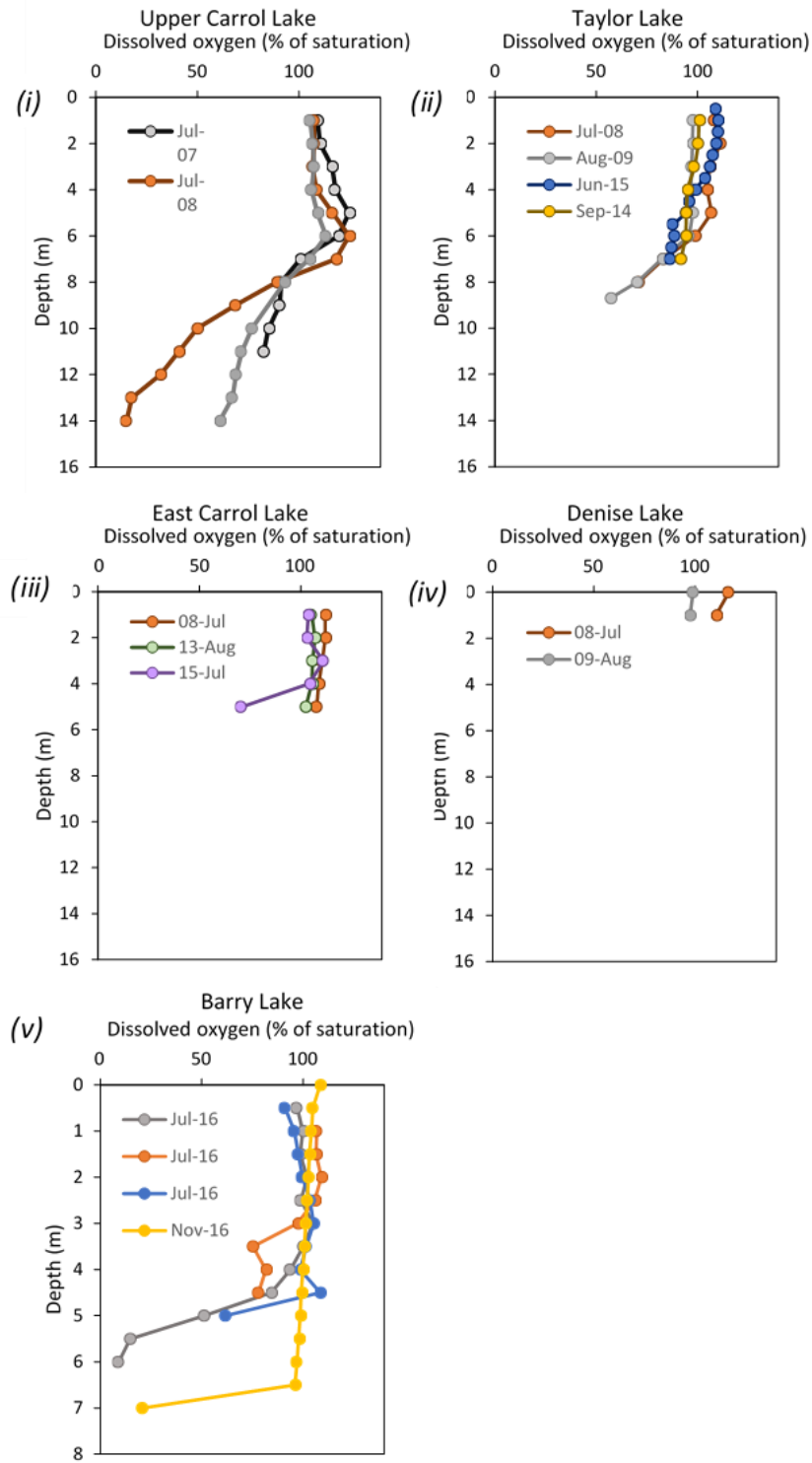


Figure E.1 Measurements of dissolved oxygen concentrations from (i) Upper Carrol Lake, (ii) Taylor Lake, (iii) East Carrol Lake, (iv) Denise Lake, and (v) Barry Lake. Numbers in the legend (e.g., Jul-16) refer to the year of collection (July 2016).

Appendix F: Technical Memorandum for Analyzing the $\delta^{13}\text{C}$ and $\delta^2\text{H}$ of *n*-Alkanes

F.1 Analysis of $\delta^{13}\text{C}_{n\text{-alkane}}$

1. If a new type of column is installed, and/or at the beginning of every analytical session (*i.e.*, once per every three-week period of continuous analysis) users should:
 - 1.1 Start with instrument conditions in standby mode (Delta V IRMS source off, needle valve closed, backflush on, injection port and oven temperatures 40-50 °C, and reactor temperature 0-500 °C).
 - 1.2 Check for large leaks. Check the flow of helium (He) on the screen above the He tank. The number should read around 1 mL/min. If the flow is much higher than this, tighten fittings to remove leak. If the number is around 1 mL/min, you can move to the next step.
 - 1.3 Bake the column according to the following method: Temperature₁ = 40 °C, Time₁ = 1.0 min, Ramp₁ = 15.0 °C/min, Temperature₂ = 315.0 °C, Time₂ = 720.0 mins, Ramp₂ = 15.0 °C/min, T₃ = 40.0 °C. While the column is baking, you can oxidize the column by right-clicking on the oxidation column and choosing the option “oxidation”. Make sure that the oxygen gas cylinder is turned on. The room might start to smell strange (like something is burning) during baking of the column – this is normal.
 - 1.4 Evaluate He flow through the Trace GC-C-IRMS system using a flow detector at the measure point. Check that flow is directed towards the measure point by looking at the diagram in the Acquisition window of the Isodat software. Check that He is flowing through the instrument (*i.e.*, that there is no blockage). If the new column has a different inner diameter than the older column, the flow may differ from

expected – this is normal and will be corrected later. If there is no flow present than the column should be reinstalled. If some flow is present, follow the next steps.

- 1.5 Check for large leaks. Before turning on the Delta V IRMS to check for small leaks, users must first search for large leaks. First, check the flow rate of helium on the screen above the He tank. The Trace generally uses 1 mL/min (backflush off) to 1.5 mL/min (backflush on) of He. If the screen above the He tank shows a higher number than this, the Trace may have developed a substantial leak. Such leaks can be detected using the He detector kept in the drawer labelled “He detector” in the Bird Wing. The straight union connecting the siliflow valve to the column is a common source of leaks. After large leaks are eliminated, small leaks can be identified and fixed.
- 1.6 If no large leaks are found, turn up the combustion reactor temperature to 1030 °C by right-clicking on the number below the combustion reactor on the schematic on Isodat. Select “edit” and type “1030”.
- 1.7 Once the reactor is up to temperature, search for small leaks by first evaluating Ar backgrounds. To do this, right-click on the second collector cup, click “jump to”, and type “40”. Peak centre on Ar by clicking on the peak centre icon. You may need to introduce some air into the Delta V to do this; if so, ask Li for help. Turn off all sources of air to the Delta V IRMS and allow backgrounds to stabilize. Ar backgrounds should be less than 100 mV with the backflush off. If Ar backgrounds are lower than this, skip to step 6. If Ar backgrounds are higher than this, follow the remaining directions in step 5 as there may be a leak in the Trace.
- 1.8 Next, turn on the Delta V IRMS by first slowly opening the needle valve (ask Li to help with this) and then turning on the source (do not turn on the source before opening the needle valve as the sudden rush of air could blow the filament). Under

the Instrument Control window, peak centre on Ar, as described in the previous step. Next, initiate a scan by selecting “scan” in the upper, left-hand corner of the Isodat Acquisition window. A line will appear across the screen representing the Ar background in mV.

1.9 Spray all joints in the oven, and on the left-hand side of the Trace, with a gentle flow of Ar from a pure Ar tank. Be careful that the flow of Ar from this tank is not too high; it should be just fast enough that you can feel it on the palm of one’s hand if held near the source of the flow. Be sure to spray each joint for at least 30 second before moving on to the next joint as it takes this long for gas to flow through the Trace and into the Delta V IRMS. Since Ar is lighter than air, it will tend to rise as you spray. Thus, you should spray the highest joints first and move towards the lowest joints. If a leak is present, a distinct Ar peak (usually 5000- 10 000 mV) will be observed on the screen.

1.10 Inject air into the Trace while the Delta V IRMS is scanning for Ar (mass 40). This test will help identify any blockages and will allow you to evaluate the response of the machine to varying amounts of gas. To do this, first make sure that the oven is not following any method. To check this, navigate to the “Oven” settings in “Instrument Control” on the Trace touch screen. If any values have been entered for “Ramp1”, delete them. Click the green “Standby” triangle at the bottom of the screen to ready the Trace for injection. Then measure out 2 μL of air using an air-tight syringe (check if the syringe is air-tight by injecting some air into a beaker of water – you should see bubbling). Inject the air into the Trace and click “Start” (the green triangle). After 200-300 s a peak should be observed on the screen as the Ar in the injected air passes through the Delta V IRMS. Repeat this process using 3 μL , and 4 μL . You should observe larger peaks each time (Table F.1). A plot of amount of air injected (in μL) versus peak height (in mV) should be linear.

Table F.1 Expected response in mV after injecting Ar into the Trace – Delta V IRMS system while the combustion reactor is in use.

Amount of air injected (μL)	Expected response (mV)
2	1600
4	3000
8	5000

1.11 Calibrate flow. On the Trace touch screen, navigate to the “Diagnostics” menu and select the front column. Using the schematic in the Acquisition window in the Isodat software, direct He flow to the measure point. Measure He flow using a flow meter. Type the “actual flow” into the touch screen. The Trace will automatically calculate the “real” column dimensions of the new column, adjusting the flow rate so that the actual flow matches the theoretical flow.

1.12 Evaluate linearity Delta V using the CO₂_zero sequence. The linearity should be <0.3 ‰.

2. Every day, users should:

2.1 Test stability of the Delta V IRMS using the CO₂_zero sequence. For stability tests, the $\delta^{13}\text{C}$ of repeated reference pulses should have a standard deviation of less than 0.3 ‰.

2.2 Record gas backgrounds. The background of H₂O must be less than 2000 mV with the backflush off. In the drier winter months, H₂O backgrounds are generally less than 500 mV. The background of CO₂ is generally <10 across all cups with the backflush off. Remember to turn on the ref gas to peak centre on CO₂. The background of Ar should be less than 100 mV with the backflush off. Higher values could indicate a leak.

- 2.3 Inject a standard mixture of *n*-alkanes from Indiana University (A or B series) at the beginning and end of each analytical session. Before analyzing samples, these raw values should be plotted against calibrated values. The correlation (r^2 value) of the raw and calibrated values should be ~ 0.98 or higher. Be sure to use the calibrated values on the sheet provide with the standard and not calibrated values listed online as the $\delta^{13}\text{C}$ of batches change frequently.
- 2.4 Inject samples 2-3 times and monitor reproducibility using the lab notebook. The standard deviation between sample duplicates should be $< 0.3\text{ ‰}$. Previous tests have demonstrated that sample peak heights should fall between 2000 and 10 000 mV to maintain a standard deviation $\sim 0.3\text{ ‰}$ (Fig. F.1). If sample peaks are too high or too low, try changing the sample dilution. If this does not work, you must concentrate/dilute the sample. You can inject manually by setting the Isolink method to “none” in your sample sequence, or you can program the Isolink autosampler to inject samples for you. Ask Li to help you with this. If you choose to use the autosampler, be sure that your sample vial contains at least $\sim 50\ \mu\text{L}$ of hexane, or the arm will not pick up the sample.

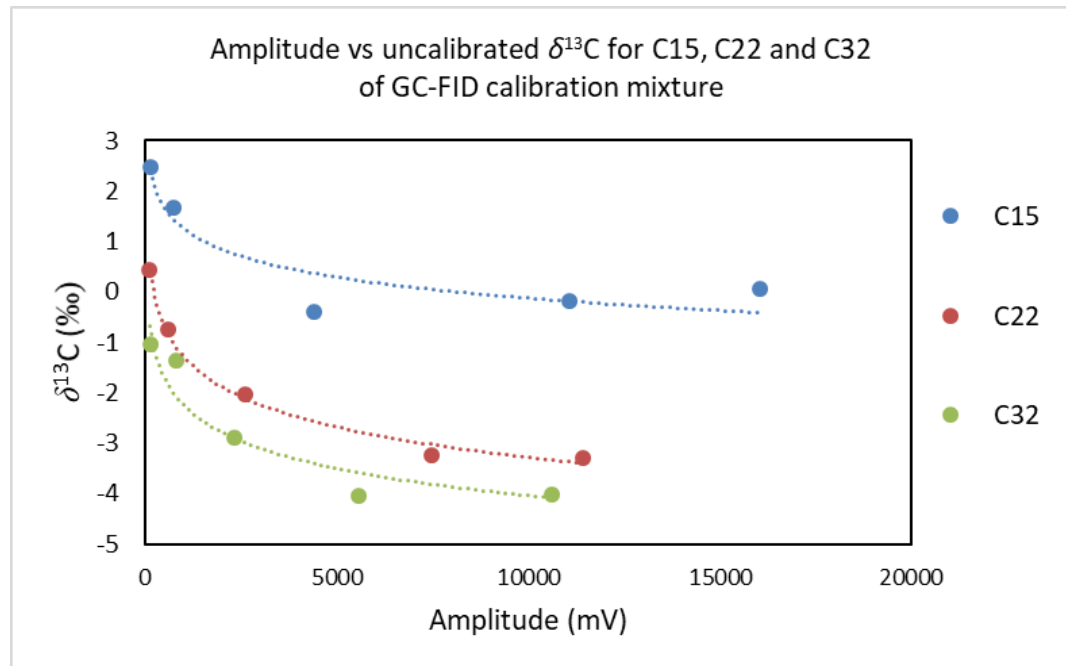


Figure F.1 Evaluating the linearity of the Trace-Delta V IRMS system by injecting the same mixture at different concentrations. These results indicate that samples should be analyzed between ~2000 to 10 000 mV to maintain a sample error of $\sim\pm 0.3$ ‰. Note that $\delta^{13}\text{C}$ is not yet relative to VPDB.

2.5 Complete a smaller oxidation every third injection by clicking the oxidation checkbox in the sample sequence. Three subsequent injections of the same mixture produced a standard deviation of 0.36 ‰, which is close to overall sample error. Four injections of the same mixture produced a standard deviation of 1.85 ‰, which is far above sample error. Therefore, oxidizing after every three injections is recommended. After each smaller oxidation the following sample may be erroneous. To avoid this problem, inject another compound (*e.g.*, GC-FID calibration mixture or 5 α -androstane) immediately after each oxidation. The values of this extra compound may not be accurate, so should be discarded.

2.6 Finish each analytical session by injecting the *n*-alkane standard mixture from Indiana University. Again, the r^2 between calibrated and raw values should be ~ 0.98 or higher. At the end of the day, turn on the backflush and set the sample dilution to 100 %.

3. At the end of each analytical session (*e.g.*, three-week period), users should:

3.1 Put the Trace in standby mode by right-clicking the combustion reactor icon in the Isodat software and clicking “Standby”. Doing this will automatically cool the injection port, oven, and reactor, and will turn the backflush on. Slowly close the needle valve on the Delta V IRMS (ask Li to help with this) and then turn off the source. Close gas tanks that are not in use.

3.2 Input all calibration data from each analytical session into one excel spreadsheet. Calculate the precision and accuracy of each peak within this standard mixture. These values offer a clearer understanding of overall error.

F.2 Analysis of $\delta^2\text{H}_{n\text{-alkane}}$

4. If a new column is installed, or at the beginning of an analytical session (*e.g.*, three-week session), complete the following steps. Differences relative to the last section are highlighted in **bold**.

4.1 Start with instrument conditions in standby mode (Delta V IRMS source off, needle valve closed, backflush on, injection port and oven temperatures 40-50 °C, and reactor temperature 0-500 °C).

4.2 Check for large leaks. Check the flow of helium on the screen above the He tank. The number should read around 1 mL/min. If the flow is much higher than this, tighten fittings to remove leak. If the number is around 1 mL/min, you can move to the next step.

4.3 Bake the column according to the following method: Temperature₁ = 40 °C, Time₁ = 1.0 min, Ramp₁ = 15.0 °C/min, Temperature₂ = 315.0 °C, Time₂ = 720.0 mins, Ramp₂

= 15.0 °C/min, T₃ – 40.0 °C. While the column is baking, you can oxidize the column by right-clicking on the oxidation column and choosing the option “oxidation”. Make sure that the oxygen gas cylinder is turned on. The room might start to smell strange (like something is burning) during baking of the column – this is normal.

4.4 Evaluate He flow through the Trace GC-C-IRMS system using a flow detector at the measure point. Check that flow is directed towards the measure point by looking at the diagram in the Acquisition window of the Isodat software. Check that He is flowing through the instrument (*i.e.*, that there is no blockage). If the new column has a different inner diameter than the older column, the flow may differ from expected – this is normal and will be corrected later. If there is no flow present than the column should be reinstalled. If some flow is present, follow the next steps.

4.5 Check for large leaks. Before turning on the Delta V IRMS to check for small leaks, users must first search for large leaks. First, check the flow rate of helium on the screen above the He tank. The Trace generally uses 1 mL/min (backflush off) to 1.5 mL/min (backflush on) of He. If the screen above the He tank shows a higher number than this, the Trace may have developed a substantial leak. Such leaks can be detected using the He detector kept in the drawer labelled “He detector” in the Bird Wing. The straight union connecting the siliflow valve to the column is a common source of leaks. After large leaks are eliminated, small leaks can be identified and fixed.

4.6 If no large leaks are found, turn up the reduction/HTC reactor temperature to 1430 °C by right-clicking on the number below the reduction reactor on the schematic on Isodat. Select “edit” and type “1430”.

4.7 Once the reactor is up to temperature, search for small leaks by first evaluating Ar backgrounds. To do this, right-click on the second collector cup, click “jump to”, and

type "40". Peak centre on Ar by clicking on the peak centre icon (PIC). You may need to introduce some air into the Delta V to do this; if so, ask Li for help. Turn off all sources of air to the Delta V IRMS and allow backgrounds to stabilize. Ar backgrounds should be less than 100 mV with the backflush off. If Ar backgrounds are lower than this, skip to step 6. If Ar backgrounds are higher than this, follow the remaining directions in step 5 as there may be a leak in the Trace.

4.8 Next, turn on the Delta V IRMS by first slowly opening the needle valve (ask Li to help with this) and then turning on the source (do not turn on the source and then open the needle valve as the sudden rush of air could blow the filament). Under the Instrument Control window, peak centre on Ar, as described in the previous step. Next, initiate a scan by selecting "scan" in the upper, left-hand corner of the Isodat Acquisition window. A line will appear across the screen representing the Ar background in mV.

4.9 Spray all joints in the oven, and on the left-hand side of the Trace, with a gentle flow of Ar from a pure Ar tank. Be careful that the flow of Ar from this tank is not too high; it should be just fast enough that you can feel it on the palm of your hand if you hold your hand near the source of the flow. Be sure to spray each joint for at least 1 minute before moving on to the next joint as it takes at least 60 seconds for gas to flow through the Trace and into the Delta V IRMS. Since Ar is lighter than air, it will tend to rise as you spray. Thus, you should spray the highest joints first and move towards the lowest joints. If a leak is present, a distinct Ar peak (usually 5000-10 000 mV) will be observed on the screen.

4.10 Inject air into the Trace while the Delta V IRMS is scanning for Ar (mass 40). This test will help identify any blockages and will allow you to evaluate the response of the machine to varying amounts of gas. To do this, first make sure that the oven is not following any method. To check this, navigate to the "Oven" settings in

“Instrument Control” on the Trace touch screen. If any values have been entered for “Ramp1”, delete them. Click the green “Standby” triangle at the bottom of the screen to ready the Trace for injection. Then measure out 1 μL of air using an air-tight syringe (check if the syringe is air-tight by injecting some air into a beaker of water – you should see bubbling). Inject the air into the Trace and click “Start” (the green triangle).

After 200-300 s a peak should be observed on the screen as the Ar in the injected air passes through the Delta V IRMS (Table F.2). Repeat this process using 2 μL , 3 μL , and 4 μL . You should observe larger peaks each time (Table F.2). A plot of amount of air injected (in μL) versus peak height (in mV) should be linear.

Table F.2 Expected response in mV after injecting Ar into the Trace – Delta V IRMS system while the reduction/HTC reactor is in use.

Amount of air injected (μL)	Expected response (mV)
2	1600
4	3000
8	5000

4.11 Calibrate flow. On the Trace touch screen, navigate to the “Diagnostics” menu and select “front column”. Using the schematic in the Acquisition window in the Isodat software, direct He flow to the measure point. Measure He flow using a flow meter. Type the “actual flow” into the touch screen. The Trace will automatically calculate the “real” column dimensions of the new column, adjusting the flow rate so that the actual flow matches the theoretical flow.

4.12 Turn on the hydrogen tank and evaluate stability and linearity of the Delta V using the H2_zero sequence. The stability should be within 3 ‰ and the linearity (expressed here as an H₃ correction) should be within 0.3.

5. One per day, users should:

5.1 Test stability and linearity of the Delta V IRMS by running the “H2Zero” sequence.

This sequence will evaluate the stability and H₃ correction, a measure of linearity.

Write down the H₃ correction in the lab notebook.

5.2 Record gas backgrounds. The background of H₂O must be less than 2000 mV with the backflush off. In the drier winter months, H₂O backgrounds are generally less than 500 mV. The background of Ar should be less than 100 mV with the backflush off. Higher values could indicate a leak.

5.3 Inject a standard mixture of *n*-alkanes from Indiana University (A or B series) at the beginning and end of each analytical session. Before analyzing samples, these raw values should be plotted against calibrated values. The correlation (r^2 value) of the raw and calibrated values should be ~ 0.98 or higher. Be sure to use the calibrated values on the sheet provide with the standard and not calibrated values listed online as the $\delta^2\text{H}$ of batches change frequently.

5.4 Inject samples 3 times and monitor reproducibility using the lab notebook. The standard deviation between sample triplicates should be $<3\%$. Previous tests have demonstrated that sample peak heights should fall between 2000 and 10 000 mV to maintain a standard deviation $\sim 3\%$. It is normal that sample peaks are much lower for analysis of $\delta^2\text{H}$ than for analysis of $\delta^{13}\text{C}$. If sample peaks are too high or too low, try changing the sample dilution. If this does not work, you must concentrate/dilute the sample. You can inject manually by setting the Isolink method to “none” in your sample sequence, or you can program the Isolink autosampler to inject samples for you. Ask Li to help you with this. If you choose to use the autosampler, be sure that your sample vial contains at least $\sim 50\ \mu\text{L}$ of

hexane, or the arm will not pick up the sample. If you leave the Trace to analyze overnight, be sure to leave a conspicuous note indicating that the machine is still running.

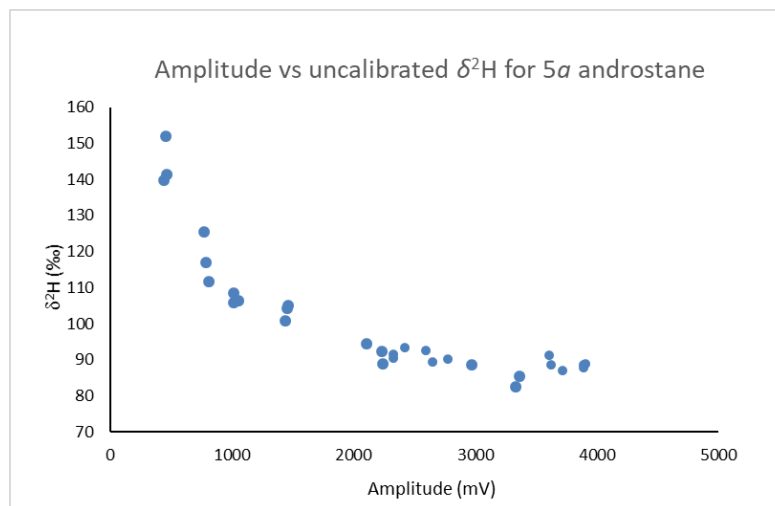


Figure F.2 Evaluating the linearity of the Trace-Delta V IRMS system by injecting the same mixture at different concentrations. These results indicate that samples should be analyzed between ~2000 to 10 000 mV to maintain a sample error of $\sim \pm 3$ ‰.

5.5 Inject hexane after every third or fourth injection (*i.e.*, after each triplicate, or standard + triplicate) to ensure that the pyrolysis reaction goes to completion. Injections of the same standard have demonstrated that after three injections the standard deviation between samples increases above 3 ‰, the sample error. Be sure to use the designated hexane injection method, as this method allows hexane to enter the reactor (it is usually removed by the backflush). Inject X μL of hexane to condition the reactor.

5.6 Finish each analytical session by injecting the *n*-alkane standard mixture from Indiana University. Again, the r^2 between calibrated and raw values should be ~ 0.98 or higher. At the end of the day, turn on the backflush and set the sample dilution to 100 %. Be sure to turn off the hydrogen tank at the end of the day.

Check the screen of the other computer to ensure that the Univector is not in use before turning off the hydrogen.

F.3 The impact of sample preparation on $\delta^2\text{H}_{n\text{-alkane}}$

Since hydrogen is easily influenced by isotopic exchange and evaporation, it was tested whether chromatography and evaporation caused the $\delta^2\text{H}_{n\text{-alkane}}$ to change beyond error (± 3 ‰). Samples of pure 5α -androstane were purified using liquid-to-liquid chromatography as usual but were purposefully left to evaporate under the dry N_2 stream for an extra five minutes after the samples had entirely dried. The $\delta^2\text{H}$ of the resulting 5α -androstane showed no evidence of fractionation as a result of this sample preparation. 5α -androstane is a branched molecule so should be even more susceptible fractionation by evaporation than n -alkanes. It is possible, however, that lower chain n -alkanes (C_{15} to C_{19}) may be influenced by evaporation, so care should be taken to ensure that n -alkane mixtures are not left to dry under the N_2 stream for longer than is needed.

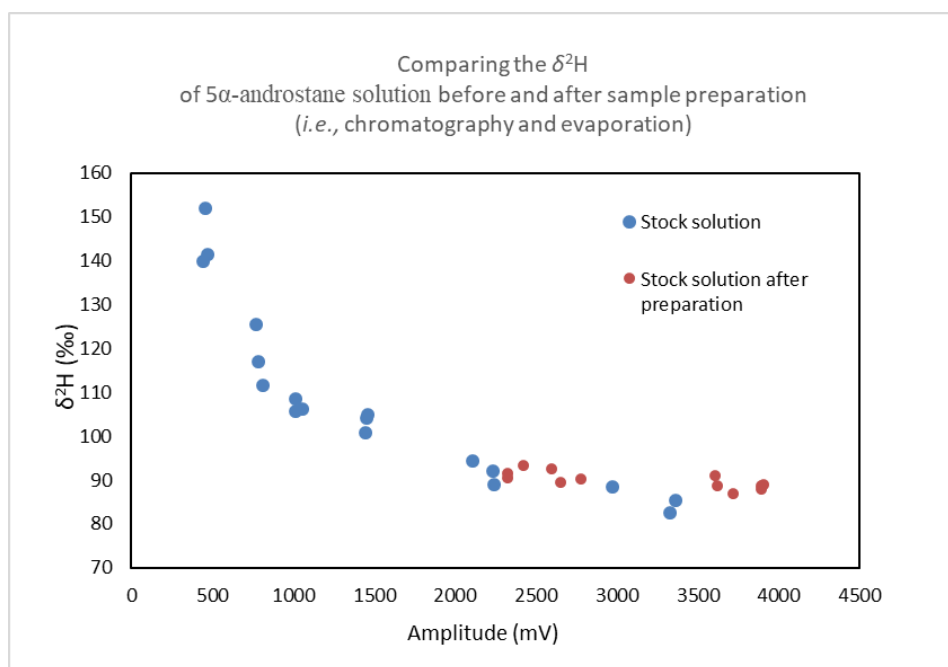


Figure F.3 This plot shows that evaporation and chromatography do not alter the $\delta^2\text{H}$ of the standard 5α -androstane.

Appendix G: Published Manuscript Reprint Permissions

OXFORD UNIVERSITY PRESS LICENSE
TERMS AND CONDITIONS
Dec 20, 2020

This Agreement between Western University -- Rebecca Doyle ("You") and Oxford University Press ("Oxford University Press") consists of your license details and the terms and conditions provided by Oxford University Press and Copyright Clearance Center.

License Number	4973281130816
License date	Dec 20, 2020
Licensed content publisher	Oxford University Press
Licensed content publication	BioScience
Licensed content title	Carbon Isotopes in Photosynthesis: Fractionation techniques may reveal new aspects of carbon dynamics in plants
Licensed content author	O'Leary, Marion H.
Licensed content date	May 1, 1988
Type of Use	Thesis/Dissertation
Institution name	
Title of your work	Reconstructing carbon dynamics of alpine and temperate zone lakes using stable isotopic analysis
Publisher of your work	The University of Western Ontario
Expected publication date	Dec 2020
Permissions cost	0.00 CAD
Value added tax	0.00 CAD
Total	0.00 CAD
Title	Reconstructing carbon dynamics of alpine and temperate zone lakes using stable isotopic analysis
Institution name	The University of Western Ontario
Expected presentation date	Dec 2020
Portions	2
Requestor location	The University of Western Ontario 1151 Richmond St. LONDON, ON N6A 3K7 Canada Attn: Rebecca Doyle
Publisher Tax ID	GB125506730
Total	0.00 CAD
Terms and Conditions	

STANDARD TERMS AND CONDITIONS FOR REPRODUCTION OF MATERIAL FROM AN OXFORD UNIVERSITY PRESS JOURNAL

1. Use of the material is restricted to the type of use specified in your order details.
2. This permission covers the use of the material in the English language in the following territory: world. If you have requested additional permission to translate this material, the terms and conditions of this reuse will be set out in clause 12.
3. This permission is limited to the particular use authorized in (1) above and does not allow you to sanction its use elsewhere in any other format other than specified above, nor does it apply to quotations, images, artistic works etc that have been reproduced from other sources which may be part of the material to be used.
4. No alteration, omission or addition is made to the material without our written consent. Permission must be re-cleared with Oxford University Press if/when you decide to reprint.
5. The following credit line appears wherever the material is used: author, title, journal, year, volume, issue number, pagination, by permission of Oxford University Press or the sponsoring society if the journal is a society journal. Where a journal is being published on behalf of a learned society, the details of that society must be included in the credit line.
6. For the reproduction of a full article from an Oxford University Press journal for whatever purpose, the corresponding author of the material concerned should be informed of the proposed use. Contact details for the corresponding authors of all Oxford University Press journal contact can be found alongside either the abstract or full text of the article concerned, accessible from www.oxfordjournals.org Should there be a problem clearing these rights, please contact journals.permissions@oup.com
7. If the credit line or acknowledgement in our publication indicates that any of the figures, images or photos was reproduced, drawn or modified from an earlier source it will be necessary for you to clear this permission with the original publisher as well. If this permission has not been obtained, please note that this material cannot be included in your publication/photocopies.
8. While you may exercise the rights licensed immediately upon issuance of the license at the end of the licensing process for the transaction, provided that you have disclosed complete and accurate details of your proposed use, no license is finally effective unless and until full payment is received from you (either by Oxford University Press or by Copyright Clearance Center (CCC)) as provided in CCC's Billing and Payment terms and conditions. If full payment is not received on a timely basis, then any license preliminarily granted shall be deemed automatically revoked and shall be void as if never granted. Further, in the event

that you breach any of these terms and conditions or any of CCC's Billing and Payment terms and conditions, the license is automatically revoked and shall be void as if never granted. Use of materials as described in a revoked license, as well as any use of the materials beyond the scope of an unrevoked license, may constitute copyright infringement and Oxford University Press reserves the right to take any and all action to protect its copyright in the materials.

9. This license is personal to you and may not be sublicensed, assigned or transferred by you to any other person without Oxford University Press's written permission.

10. Oxford University Press reserves all rights not specifically granted in the combination of (i) the license details provided by you and accepted in the course of this licensing transaction, (ii) these terms and conditions and (iii) CCC's Billing and Payment terms and conditions.

11. You hereby indemnify and agree to hold harmless Oxford University Press and CCC, and their respective officers, directors, employees and agents, from and against any and all claims arising out of your use of the licensed material other than as specifically authorized pursuant to this license.

12. Other Terms and Conditions:

v1.4

Questions? customer care@copyright.com or +1-855-239-3415 (toll free in the US) or +1-978-646-2777.

JOHN WILEY AND SONS LICENSE
TERMS AND CONDITIONS

Dec 20, 2020

This Agreement between Western University -- Rebecca Doyle ("You") and John Wiley and Sons ("John Wiley and Sons") consists of your license details and the terms and conditions provided by John Wiley and Sons and Copyright Clearance Center.

License Number	4973290612056
License date	Dec 20, 2020
Licensed Content Publisher	John Wiley and Sons
Licensed Content Publication	Limnology and Oceanography
Licensed Content Title	Recent changes in production in oligotrophic Uinta Mountain lakes, Utah, identified using paleolimnology
Licensed Content Author	R. Hladyniuk, N. Michelutti, F. J. Longstaffe, et al
Licensed Content Date	Oct 12, 2014
Licensed Content Volume	59
Licensed Content Issue	6
Licensed Content Pages	15
Type of use	Dissertation/Thesis
Requestor type	University/Academic
Format	Print and electronic
Portion	Figure/table
Number of figures/tables	3
Will you be translating?	No
Title	Reconstructing carbon dynamics of alpine and temperate zone lakes using stable isotopic analysis
Institution name	The University of Western Ontario
Expected presentation date	Dec 2020
Portions	Table 1, Table 2, Figure 1 The University of Western Ontario 1151 Richmond St.
Requestor Location	LONDON, ON N6A 3K7 Canada Attn: Rebecca Doyle
Publisher Tax ID	EU826007151
Total	0.00 CAD
Terms and Conditions	

TERMS AND CONDITIONS

This copyrighted material is owned by or exclusively licensed to John Wiley & Sons, Inc. or one of its group companies (each a "Wiley Company") or handled on behalf of a society with which a Wiley Company has exclusive publishing rights in relation to a particular work (collectively "WILEY"). By clicking "accept" in connection with completing this licensing transaction, you agree that the following terms and conditions apply to this transaction (along with the billing and payment terms and conditions established by the Copyright Clearance Center Inc., ("CCC's Billing and Payment terms and conditions"), at the time that you opened your RightsLink account (these are available at any time at <http://myaccount.copyright.com>).

Terms and Conditions

- The materials you have requested permission to reproduce or reuse (the "Wiley Materials") are protected by copyright.
- You are hereby granted a personal, non-exclusive, non-sub licensable (on a stand-alone basis), non-transferable, worldwide, limited license to reproduce the Wiley Materials for the purpose specified in the licensing process. This license, **and any CONTENT (PDF or image file) purchased as part of your order**, is for a one-time use only and limited to any maximum distribution number specified in the license. The first instance of republication or reuse granted by this license must be completed within two years of the date of the grant of this license (although copies prepared before the end date may be distributed thereafter). The Wiley Materials shall not be used in any other manner or for any other purpose, beyond what is granted in the license. Permission is granted subject to an appropriate acknowledgement given to the author, title of the material/book/journal and the publisher. You shall also duplicate the copyright notice that appears in the Wiley publication in your use of the Wiley Material. Permission is also granted on the understanding that nowhere in the text is a previously published source acknowledged for all or part of this Wiley Material. Any third party content is expressly excluded from this permission.
- With respect to the Wiley Materials, all rights are reserved. Except as expressly granted by the terms of the license, no part of the Wiley Materials may be copied, modified, adapted (except for minor reformatting required by the new Publication), translated, reproduced, transferred or distributed, in any form or by any means, and no derivative works may be made based on the Wiley Materials without the prior permission of the respective copyright owner. **For STM Signatory Publishers clearing permission under the terms of the [STM Permissions Guidelines](#) only, the terms of the license are extended to include subsequent editions and for editions in other languages, provided such editions are for the**

work as a whole in situ and does not involve the separate exploitation of the permitted figures or extracts, You may not alter, remove or suppress in any manner any copyright, trademark or other notices displayed by the Wiley Materials. You may not license, rent, sell, loan, lease, pledge, offer as security, transfer or assign the Wiley Materials on a stand-alone basis, or any of the rights granted to you hereunder to any other person.

- The Wiley Materials and all of the intellectual property rights therein shall at all times remain the exclusive property of John Wiley & Sons Inc, the Wiley Companies, or their respective licensors, and your interest therein is only that of having possession of and the right to reproduce the Wiley Materials pursuant to Section 2 herein during the continuance of this Agreement. You agree that you own no right, title or interest in or to the Wiley Materials or any of the intellectual property rights therein. You shall have no rights hereunder other than the license as provided for above in Section 2. No right, license or interest to any trademark, trade name, service mark or other branding ("Marks") of WILEY or its licensors is granted hereunder, and you agree that you shall not assert any such right, license or interest with respect thereto
- NEITHER WILEY NOR ITS LICENSORS MAKES ANY WARRANTY OR REPRESENTATION OF ANY KIND TO YOU OR ANY THIRD PARTY, EXPRESS, IMPLIED OR STATUTORY, WITH RESPECT TO THE MATERIALS OR THE ACCURACY OF ANY INFORMATION CONTAINED IN THE MATERIALS, INCLUDING, WITHOUT LIMITATION, ANY IMPLIED WARRANTY OF MERCHANTABILITY, ACCURACY, SATISFACTORY QUALITY, FITNESS FOR A PARTICULAR PURPOSE, USABILITY, INTEGRATION OR NON-INFRINGEMENT AND ALL SUCH WARRANTIES ARE HEREBY EXCLUDED BY WILEY AND ITS LICENSORS AND WAIVED BY YOU.
- WILEY shall have the right to terminate this Agreement immediately upon breach of this Agreement by you.
- You shall indemnify, defend and hold harmless WILEY, its Licensors and their respective directors, officers, agents and employees, from and against any actual or threatened claims, demands, causes of action or proceedings arising from any breach of this Agreement by you.
- IN NO EVENT SHALL WILEY OR ITS LICENSORS BE LIABLE TO YOU OR ANY OTHER PARTY OR ANY OTHER PERSON OR ENTITY FOR ANY SPECIAL, CONSEQUENTIAL, INCIDENTAL, INDIRECT, EXEMPLARY OR PUNITIVE DAMAGES, HOWEVER CAUSED, ARISING OUT OF OR IN CONNECTION WITH THE DOWNLOADING, PROVISIONING, VIEWING OR USE OF THE MATERIALS REGARDLESS OF THE FORM OF ACTION, WHETHER FOR BREACH OF CONTRACT, BREACH OF WARRANTY, TORT, NEGLIGENCE, INFRINGEMENT OR OTHERWISE (INCLUDING, WITHOUT LIMITATION, DAMAGES BASED ON LOSS OF PROFITS, DATA, FILES, USE, BUSINESS OPPORTUNITY

OR CLAIMS OF THIRD PARTIES), AND WHETHER OR NOT THE PARTY HAS BEEN ADVISED OF THE POSSIBILITY OF SUCH DAMAGES. THIS LIMITATION SHALL APPLY NOTWITHSTANDING ANY FAILURE OF ESSENTIAL PURPOSE OF ANY LIMITED REMEDY PROVIDED HEREIN.

- Should any provision of this Agreement be held by a court of competent jurisdiction to be illegal, invalid, or unenforceable, that provision shall be deemed amended to achieve as nearly as possible the same economic effect as the original provision, and the legality, validity and enforceability of the remaining provisions of this Agreement shall not be affected or impaired thereby.
- The failure of either party to enforce any term or condition of this Agreement shall not constitute a waiver of either party's right to enforce each and every term and condition of this Agreement. No breach under this agreement shall be deemed waived or excused by either party unless such waiver or consent is in writing signed by the party granting such waiver or consent. The waiver by or consent of a party to a breach of any provision of this Agreement shall not operate or be construed as a waiver of or consent to any other or subsequent breach by such other party.
- This Agreement may not be assigned (including by operation of law or otherwise) by you without WILEY's prior written consent.
- Any fee required for this permission shall be non-refundable after thirty (30) days from receipt by the CCC.
- These terms and conditions together with CCC's Billing and Payment terms and conditions (which are incorporated herein) form the entire agreement between you and WILEY concerning this licensing transaction and (in the absence of fraud) supersedes all prior agreements and representations of the parties, oral or written. This Agreement may not be amended except in writing signed by both parties. This Agreement shall be binding upon and inure to the benefit of the parties' successors, legal representatives, and authorized assigns.
- In the event of any conflict between your obligations established by these terms and conditions and those established by CCC's Billing and Payment terms and conditions, these terms and conditions shall prevail.
- WILEY expressly reserves all rights not specifically granted in the combination of (i) the license details provided by you and accepted in the course of this licensing transaction, (ii) these terms and conditions and (iii) CCC's Billing and Payment terms and conditions.

- This Agreement will be void if the Type of Use, Format, Circulation, or Requestor Type was misrepresented during the licensing process.
- This Agreement shall be governed by and construed in accordance with the laws of the State of New York, USA, without regards to such state's conflict of law rules. Any legal action, suit or proceeding arising out of or relating to these Terms and Conditions or the breach thereof shall be instituted in a court of competent jurisdiction in New York County in the State of New York in the United States of America and each party hereby consents and submits to the personal jurisdiction of such court, waives any objection to venue in such court and consents to service of process by registered or certified mail, return receipt requested, at the last known address of such party.

WILEY OPEN ACCESS TERMS AND CONDITIONS

Wiley Publishes Open Access Articles in fully Open Access Journals and in Subscription journals offering Online Open. Although most of the fully Open Access journals publish open access articles under the terms of the Creative Commons Attribution (CC BY) License only, the subscription journals and a few of the Open Access Journals offer a choice of Creative Commons Licenses. The license type is clearly identified on the article.

The Creative Commons Attribution License

The [Creative Commons Attribution License \(CC-BY\)](#) allows users to copy, distribute and transmit an article, adapt the article and make commercial use of the article. The CC-BY license permits commercial and non-

Creative Commons Attribution Non-Commercial License

The [Creative Commons Attribution Non-Commercial \(CC-BY-NC\)License](#) permits use, distribution and reproduction in any medium, provided the original work is properly cited and is not used for commercial purposes.(see below)

Creative Commons Attribution-Non-Commercial-NoDerivs License

The [Creative Commons Attribution Non-Commercial-NoDerivs License](#) (CC-BY-NC-ND) permits use, distribution and reproduction in any medium, provided the original work is properly cited, is not used for commercial purposes and no modifications or adaptations are made. (see below)

Use by commercial "for-profit" organizations

Use of Wiley Open Access articles for commercial, promotional, or marketing purposes requires further explicit permission from Wiley and will be subject to a fee.

Further details can be found on Wiley Online

Library <http://olabout.wiley.com/WileyCDA/Section/id-410895.html>

Other Terms and Conditions:

v1.10 Last updated September 2015

Questions? customercare@copyright.com or +1-855-239-3415 (toll free in the US) or +1-978-646-2777.

Curriculum Vitae

Name: Rebecca M. Doyle

Post-secondary Education and Degrees: *The University of Western Ontario*
London, Ontario, Canada
2011– 2015 B.Sc. (Hons.)

The University of Western Ontario
London, Ontario, Canada
2015– 2016 (M.Sc. upgraded to Ph.D.)

The University of Western Ontario
London, Ontario, Canada
2017– 2021 Ph.D.

Honours and Awards: Western Scholarship of Excellence 2011
Western Green Award 2014
Dean’s Entrance Scholarship 2015
NSERC Canada Graduate Scholarship (Master’s) 2016-2017
NSERC Canada Graduate Scholarship (Doctoral) 2017-2020
Environment & Sustainability Travel Award 2016, 2018
Environment & Sustainability Award of Excellence 2016, 2018
Sumac Travel Award 2019

Related Work Experience: Research Assistant, Biotron Centre for Experimental Climate Change Research, *The University of Western Ontario*, Summer 2014

Teaching Assistant, multiple courses, Department of Geography, *The University of Western Ontario*, 2015-2019

Lecturer, Geography 1300B: Introduction to the Physical Environment, Winter 2021

Publications: Sia, M.E., **Doyle, R.M.**, Moser, K.A. (2020) Does fish stocking affect primary production? Results from a paleolimnological investigation in the Uinta Mountains, Utah. *Journal of Lake and Reservoir Management*. In press.
<https://doi.org/10.1080/10402381.2020.1814462>